FUNGAL BIOTECHNOLOGY

EDITED BY: Song Yang, Fred O. Asiegbu, Peng Fu, Fernando Rodrigues, Wenhai Xiao and Mingwen Zhao
PUBLISHED IN: Frontiers in Microbiology

frontiers Research Topics

About Frontiers

Frontiers is more than just an open-access publisher of scholarly articles: it is a pioneering approach to the world of academia, radically improving the way scholarly research is managed. The grand vision of Frontiers is a world where all people have an equal opportunity to seek, share and generate knowledge. Frontiers provides immediate and permanent online open access to all its publications, but this alone is not enough to realize our grand goals.

Frontiers Journal Series

The Frontiers Journal Series is a multi-tier and interdisciplinary set of open-access, online journals, promising a paradigm shift from the current review, selection and dissemination processes in academic publishing. All Frontiers journals are driven by researchers for researchers; therefore, they constitute a service to the scholarly community. At the same time, the Frontiers Journal Series operates on a revolutionary invention, the tiered publishing system, initially addressing specific communities of scholars, and gradually climbing up to broader public understanding, thus serving the interests of the lay society, too.

Dedication to Quality

Each Frontiers article is a landmark of the highest quality, thanks to genuinely collaborative interactions between authors and review editors, who include some of the world's best academicians. Research must be certified by peers before entering a stream of knowledge that may eventually reach the public - and shape society; therefore, Frontiers only applies the most rigorous and unbiased reviews.

Frontiers revolutionizes research publishing by freely delivering the most outstanding research, evaluated with no bias from both the academic and social point of view. By applying the most advanced information technologies, Frontiers is catapulting scholarly publishing into a new generation.

What are Frontiers Research Topics?

Frontiers Research Topics are very popular trademarks of the Frontiers Journals Series: they are collections of at least ten articles, all centered on a particular subject. With their unique mix of varied contributions from Original Research to Review Articles, Frontiers Research Topics unify the most influential researchers, the latest key findings and historical advances in a hot research area! Find out more on how to host your own Frontiers Research Topic or contribute to one as an author by contacting the Frontiers Editorial Office: frontiersin.org/about/contact

FUNGAL BIOTECHNOLOGY

Topic Editors:
Song Yang, Qingdao Agricultural University, China
Fred O. Asiegbu, University of Helsinki, Finland
Peng Fu, Ocean University of China, China
Fernando Rodrigues, University of Minho, Portugal
Wenhai Xiao, Tianjin University, China
Mingwen Zhao, Nanjing Agricultural University, China

Table of Contents

Antiproliferative Sorbicillinoids From the Deep-Sea-Derived *Penicillium allii-sativi*

Chun-Lan Xie[1,2†], Duo Zhang[1†], Ting Lin[1], Zhi-Hui He[2], Qing-Xiang Yan[2], Qi Cai[1], Xiao-Kun Zhang[1]*, Xian-Wen Yang[2]* and Hai-Feng Chen[1]*

[1]School of Pharmaceutical Sciences, Xiamen University, Xiamen, China, [2]Key Laboratory of Marine Biogenetic Resources, Third Institute of Oceanography, Ministry of Natural Resources, Xiamen, China

Two new (**1**–**2**) and three known (**3**–**5**) sorbicillinoids were isolated from the deep-sea-derived fungus *Penicillium allii-sativi* MCCC 3A00580. Compounds **1** and **2**, named sorbicatechols C and D, were two new hybrid dihydrosorbillinoids. Their structures were established mainly by spectroscopic analyses and electronic circular dichroism (ECD) calculations. All five isolates were tested for antiproliferative activities against four tumor cell lines of MCF-7, HT-29, HuH-7, and LNCap. Compounds **2** and **5** inhibited HT-29 cells in a good dose-dependent manner. Mechanism investigation uncovered that they could significantly induce cell cycle G2-M phase arresting by increasing the protein levels of p-H3 and cyclin B1.

Keywords: deep-sea, fungi, sorbicillinoids, cell cycle, cytotoxicities

INTRODUCTION

Sorbicillinoids are hexaketide metabolites that possess complex and highly oxygenated frameworks. Structurally, they can be divided into four groups: monomeric, dimeric, trimeric, and hybrid sorbicillinoids (Harned and Volp, 2011; Meng et al., 2016). The unique structural features of the sorbicillinoids make them attractive candidates for developing new pharmaceutical and agrochemical agents (Abe et al., 2000, 2001; Fahad et al., 2013; Meng et al., 2019; Kahlert et al., 2020). Up to now, around 100 sorbicillinoids have been reported from fungi, especially marine *Penicillium* (Meng et al., 2016). During our ongoing search for structurally novel and biologically interesting secondary metabolites from deep-sea-derived microorganisms (Yang et al., 2013; Niu et al., 2017, 2020; Xie et al., 2019a), the rice static fermentation extract of *Penicillium allii-sativi* MCCC 3A00580 exhibited potent *in vitro* antitumor activity. Previously, three meroterpenoids were obtained and andrastones A showed significant inhibitory effect against HepG2 tumor cells by activating caspase-3 and regulating the transcriptional activation function of RXRα (Xie et al., 2019b). Further investigation on this strain led to the discovery of two new and three known sorbicillinoid derivates (**Figure 1**). Structurally, compounds **1** and **2** are two novel hybrid dihydrosorbicillinoids. All isolates were tested for antiproliferative bioactivities, compounds **2** and **5** could inhibit HT-29 tumor cells in a good dose-dependent manner. Herein, we report the isolation, structures, and bioactivities of these compounds.

FIGURE 1 | Compounds **1–5** from *Penicillium allii-sativi* MCCC 3A00580.
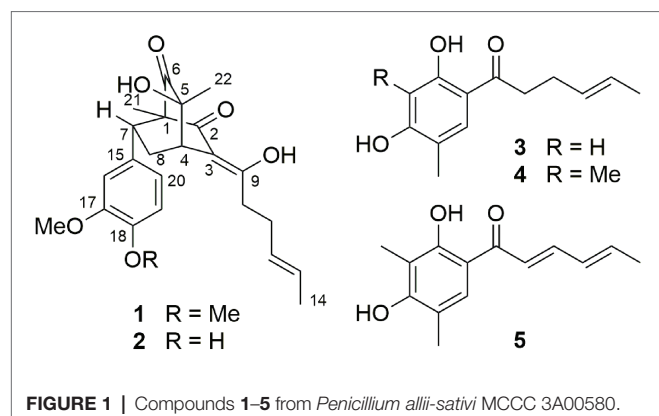
MATERIALS AND METHODS

General Experimental Procedures

The NMR spectra were recorded on a Bruker 400 MHz spectrometer using TMS as an internal standard. The high resolution electrospray ionization mass spectroscopy (HRESIMS) spectra were measured on a Waters Xevo G2 Q-TOF (Waters) mass spectrometer. Optical rotations were measured with an Anton Paar MCP100 polarimeter. Electronic circular dichroism (ECD) spectra were measured on a JASCO J-715 spectropolarimeter. TLC and column chromatography (CC) were performed on plates precoated with silica gel GF254 (10–40 μm) or over silica gel (200–300 mesh, Qingdao Marine Chemical Factory). Chromatography was performed using Sephadex LH-20 (18–110 μm, Amersham Pharmacia Biotech AB), and octadecylsilane (ODS) silica gel (50 μm, Daiso). The preparative and semipreparative HPLC were performed on an Agilent Technologies 1,260 infinity instrument equipped with the DAD detector. Anti-β-actin (Cat. 4970S), anti-p-H3 (Cat. 3,377), and anti-Cyclin B1 (Cat. 12231S) antibodies were all purchased from Cell Signaling Technology (Boston, MA, United States).

Fermentation, Extraction, and Isolation

Penicillium allii-sativi was isolated from the western Pacific Ocean (−4,302 m). The identification and fermentation of the fungus were reported previously (Xie et al., 2019b). As a result, a defatted extract (60.4 g) was obtained, which was subjected to CC over silica gel with gradient CH_2Cl_2-MeOH to get eight fractions (Fr.1–Fr.8). Fraction Fr.3 (5.5 g) was further purified by CC on ODS using a gradient H_2O-MeOH to yield three subfractions (Fr.3.1–Fr.3.3). Compounds **1** (23.2 mg) and **2** (4.5 mg) were obtained from subfraction Fr.3.2 (211.4 mg) by repeated CC over silica gel CC (PE-EtOAc, 3:1) and Sephadex LH-20 (MeOH). While compound **3** (4.4 mg) was obtained from subfraction Fr.3.3 (150.6 mg) by CC over silica gel (CH_2Cl_2-MeOH, 50:1) and Sephadex LH-20 (MeOH). Fraction Fr.8 (15 g) was subjected subsequently to CC over ODS (MeOH-H_2O: 5%→100%) and silica gel (CH_2Cl_2-MeOH, 30:1) to get compounds **4** (20.3 mg) and **5** (16.5 mg).
Sorbicatechol C (1): yellow oil; $[\alpha]_D^{20}$−14.6 (*c* 0.50, MeOH), −7.2 (*c* 0.50, CHCl₃); UV (CH₃OH) λ_{max} (log *ε*) 257 (3.24), 288

TABLE 1 | ^{1}H and ^{13}C NMR spectroscopic data for compounds **1** and **2** in DMSO-d_6.

No	1		2	
	δ_C	δ_H (*J* in Hz)	δ_C	δ_H (*J* in Hz)
1	64.1 C		64.2 C	
2	196.0 C		196.0 C	
3	112.5 C		112.5 C	
4	41.1 CH	3.15 t (2.8)	41.1 CH	3.12 t (2.6)
5	72.9 C		72.9 C	
6	209.6 C		209.6 C	
7	45.3 CH	3.11 dd (10.6, 5.8)	45.4 CH	3.05 dd (10.6, 5.8)
8 (a)	31.3 CH₂	2.90 ddd (13.2, 10.6, 2.8)	31.4 CH₂	2.88 ddd (13.4, 10.6, 2.8)
(b)		1.70 ddd (13.2, 5.8, 2.8)		1.68 ddd (13.4, 5.8, 2.8)
9	178.7 C		178.6 C	
10 (a)	31.5 CH₂	2.67 dt (14.0, 7.5)	31.5 CH₂	2.65 dt (14.0, 7.0)
(b)		2.48 dt (14.0, 6.7)		2.45 dt (14.0, 6.6)
11	28.9 CH₂	2.32 m	28.9 CH₂	2.33 m
12	129.6 CH	5.49 m (overlap)	129.6 CH	5.47 m (overlap)
13	125.9 CH	5.49 m (overlap)	125.9 CH	5.49 m (overlap)
14	17.7 CH₃	1.56 d (4.7)	17.7 CH₃	1.57 d (4.7)
15	134.3 C		132.8 C	
16	111.6 CH	6.53 d (1.5)	112.1 CH	6.49 d (1.8)
17	148.3 C		147.2 C	
18	147.8 C		145.5 C	
19	111.6 CH	6.83 d (8.2)	115.2 CH	6.63 d (8.1)
20	120.2 CH	6.51 dd (8.2, 1.5)	120.6 CH	6.37 dd (8.1, 1.8)
21	10.7 CH₃	0.71 s	10.7 CH₃	0.70 s
22	23.6 CH₃	1.13 s	23.6 CH₃	1.14 s
17-OMe	55.1 CH₃	3.64 s	55.3 CH₃	3.65 s
18-OMe	55.4 CH₃	3.70 s		
5-OH		5.98 s		5.96 s
9-OH		14.68 br s		14.69 br s
18-OH				8.92 s

(3.61) nm; ECD (MeOH) λ_{max} ($\Delta\varepsilon$) 201 (−4.63), 231 (+0.68), 297 (−3.29), 337 (+1.77) nm; ^{1}H and ^{13}C NMR data, see **Table 1**; HRESIMS *m/z* 437.1951 [M+Na]⁺ (calcd for $C_{24}H_{30}O_6Na$, 437.1940), 413.1958 [M−H]⁻ (calcd for $C_{24}H_{29}O_6$, 413.1964).
Sorbicatechol D (2): yellow oil; $[\alpha]20$ D −19.1 (*c* 0.35, MeOH); UV (Me) λ_{max} (log *ε*) 268 (2.42), 286 (2.50) nm; ECD (MeOH) λ_{max} ($\Delta\varepsilon$) 230 (−0.87), 231 (+2.24), 296 (−12.30), 335 (+11.58) nm; ^{1}H and ^{13}C NMR data, see **Table 1**; HRESIMS *m/z* 399.1790 [M−H]⁻ (calcd for $C_{23}H_{27}O_6$, 399.1808).

ECD Calculation

As reported previously (Niu et al., 2020), conformational analyses were carried out *via* random searching in the Sybyl-X 2.0 using the MMFF94S force field with an energy cutoff of 2.0 kcal/mol. Subsequently, the lowest energy conformer was re-optimized using DFT at b3lyp/6-31+g(d,p) level in MeOH by the GAUSSIAN 09 program. The energies, oscillator strengths, and rotational strengths (velocity) of the first 30 electronic excitations were calculated using the TDDFT methodology at the cam-b3lyp/TZVP level using the polarizable continuum model in MeOH. The ECD spectrum were simulated by the overlapping Gaussian function (half the bandwidth at 1/e peak height, σ = 0.35, UV correction = 23 nm).

Antiproliferative Bioassay

Briefly, four cancer cell lines of breast cancer cells (MCF-7), colon cancer cells (HT-29), hepatoma cells (HuH-7), and prostate cancer cells (LNCap) were treated with different concentrations of compounds **1**–**5** for 48 h. The cell viability was evaluated using MTT assay.
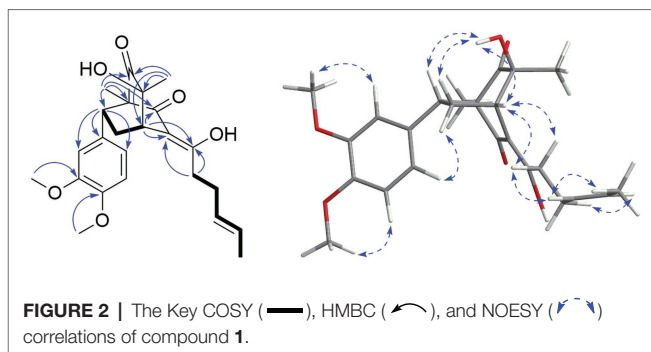
Cell Cycle Experiment

HT-29 cells were treated with tested compounds. After 48 h, they were collected by trypsin and dehydrated with 70% EtOH overnight at 4°C. After alcohol was removed, cells were washed twice using PBS and were labeled by DAPI (1:10000 dilution in PBS, D8417 from Sigma-Aldrich, Saint Louis, MO, United States) for 10 min. Finally, fluorescence was measured by flow cytometry using PB450-A (CytoFLEX, Beckman Coulter, Kraemer Boulevard Brea, CA, United States).

Western Blotting

Cell lysates were boiled in sodium dodecyl sulfate (SDS) sample loading buffer, resolved by 10% SDS-polyacrylamide gel electrophoresis (SDS-PAGE) and transferred to nitrocellulose. The membranes were blocked in 5% milk in Tris-buffered saline and Tween 20 [TBST; 10 mM Tris-HCl (pH 8.0), 150 mM NaCl, and 0.05% Tween 20] for 1 h at room temperature. After washing twice with TBST, the membranes were incubated with appropriate primary antibodies in TBST for 1 h and then washed twice, probed with horseradish peroxide-linked anti-immunoglobulin (1:5000 dilution) for 1 h at room temperature. After three washes with TBST, immunoreactive products were visualized using enhanced chemiluminescence reagents and autoradiography.

RESULTS AND DISCUSSION

Compound **1** was isolated as a yellow oil. The sodiated molecular ion peak at m/z 495.1951 [M + Na]$^+$ in the HRESIMS indicated its molecular formula as $C_{24}H_{30}O_6$, requiring 10 degrees of unsaturation. The ^{1}H NMR spectrum showed two methyl singlets [δ_H 0.71 (3H, s, Me-21), 1.13 (3H, s, Me-22)], one methyl doublet [δ_H 1.56 (3H, d, J = 4.7 Hz, Me-14)], three typical ABX aromatic protons [δ_H 6.51 (1H, dd, J = 8.2, 1.5 Hz, H-20), 6.53 (1H, d, J = 1.5 Hz, H-16), 6.83 (1H, d, J = 8.2 Hz, H-19)], and two methoxyls [δ_H 3.64 (3H, s, 17-OMe), 3.70 (3H, s, 18-OMe)]. The ^{13}C NMR spectrum indicated 24 carbon resonances including three methyls (δ_C 10.7, 17.7, and 23.6), three methylenes, seven methines (two olefinic and three aromatic), nine quaternary carbons (two ketones at δ_C 196.0 and 209.6, two olefinic at δ_C 112.5 and 178.7, and three aromatic at δ_C 134.3, 147.8, and 148.3), and two methoxyls. Since the ABX aromatic moiety, two ketones, and the other four olefinic carbons accounted for eight unsaturations, compound **1** was deduced to be a bicyclic molecule. In the ^{1}H–^{1}H COSY spectrum, two segments could easily be deduced on the basis of correlations of H$_2$-8 to H-4/H-7 and Me-14 *via* H-12/H-13 to H$_2$-11/Hab-10 (**Figure 2**). These two segments along with the ABX aromatic moiety could

FIGURE 2 | The Key COSY (━━), HMBC (⌒), and NOESY (⤺⤻) correlations of compound **1**.

be connected by the HMBC correlations of Me-21 to C-1 (δ_C 64.1 s)/C-2 (δ_C 196.0 s)/C-6 (δ_C 209.6 s)/C-7 (δ_C 45.3 d), Me-22 to C-4 (δ_C 41.1 d)/C-5 (δ_C 72.9 s)/C-6, H-4 (δ_H 3.15, t, J = 2.8 Hz) to C-2/C-3 (δ_C 112.5 s)/C-9 (δ_C 178.7 s), H-7 (δ_H 3.11, dd, J = 10.6, 5.8 Hz) to C-15 (δ_C 134.3 s)/C-16 (δ_C 111.6 d)/C-20 (δ_C 120.2 d), Hab-10 (δ_H 2.67, dt, J = 14.0, 7.5 Hz; 2.48, dt, J = 14.0, 6.7 Hz) to C-3/C-9, 17-OMe to C-17 (δ_C 148.3 s), and 18-OMe to C-18 (δ_C 147.8 s). Accordingly, the planar structure of compound **1** was established as a sorbicillinoid derivate, structurally related to sorbicatechol A. In the NOESY spectrum, 5-OH (δ_H 5.98 s) was correlated to H-7 (δ_H 3.11, dd, J = 10.6, 5.8 Hz)/Ha-8 (δ_H 2.90, ddd, J = 13.2, 10.6, 2.8 Hz), while Hb-8 (δ_H 1.70, ddd, J = 13.2, 5.8, 2.8 Hz) was correlated to H-16/H-20. This suggested co-plane of H-7 and 5-OH. Furthermore, correlations of Hab-10 (δ_H 2.67, dt, J = 14.0, 7.5 Hz, Ha-10; 2.48, dt, J = 14.0, 6.7 Hz, Hb-10) to H-4/H-12(H-13) deduced the *Z*-orientation of the olefinic bonds of C-3/C-9. Since the chemical shifts of H-12 and H-13 were overlapped, it was impossible to assign the configuration by their coupling constants. However, the NOESY correlations of Me-14 to H-12(H-13) but not H$_2$-11 could suggest the *E*-orientation of C-12/C-13. On the basis of the above evidences, the relative configuration of compound **1** was, therefore, determined undoubtedly.

To further assign its absolute stereochemistry, the theoretical calculation of the electronic circular dichroism (ECD) was conducted. As shown in **Figure 3**, the experimental ECD spectrum of compound **1** showed the same Cotton effects as those of 1*R*,4*S*,5*S*,7*R*-**1** (**1a**). Therefore, the absolute stereochemistry of compound **1** was assigned as 10,11-dihydrosorbicatechol A, and named sorbicatechol C.

Compound **2** was also isolated as a yellow oil. The molecular formula was assigned as $C_{23}H_{28}O_6$ on the basis of the HRESIMS at m/z 399.1790 [M−H]$^-$ (calcd for $C_{23}H_{27}O_6$, 399.1808). The ^{1}H and ^{13}C NMR spectroscopic data (**Table 1**) indicated 23 carbon resonances including two methyl singlets, one methyl doublet, three methylenes, seven methines (two olefinic and three aromatic), nine quaternary carbons (two ketones at δ_C 196.0 and 209.6, two olefinics at δ_C 112.5 and 178.6, and three aromatics at δ_C 132.8, 145.5, and 147.2), and one methoxyl. These signals were very similar to those of compound **1**, except that the methoxyl group at the C-18 position in compound **1** was changed to a hydroxy moiety in compound **2**. This was evidenced by an additional hydroxy unit and the absence of a methoxyl group in compound **2**. Further confirmation could
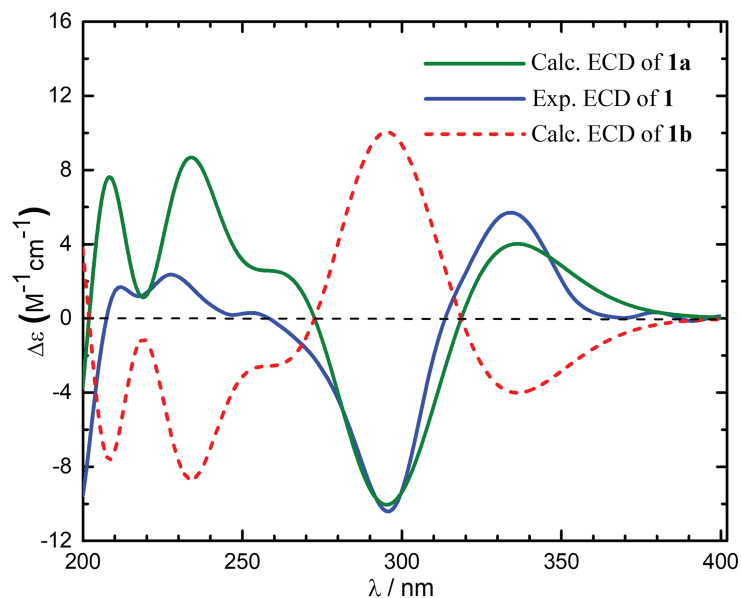
FIGURE 3 | Experimental and calculated electronic circular dichroism (ECD) spectra of compound **1** in MeOH.
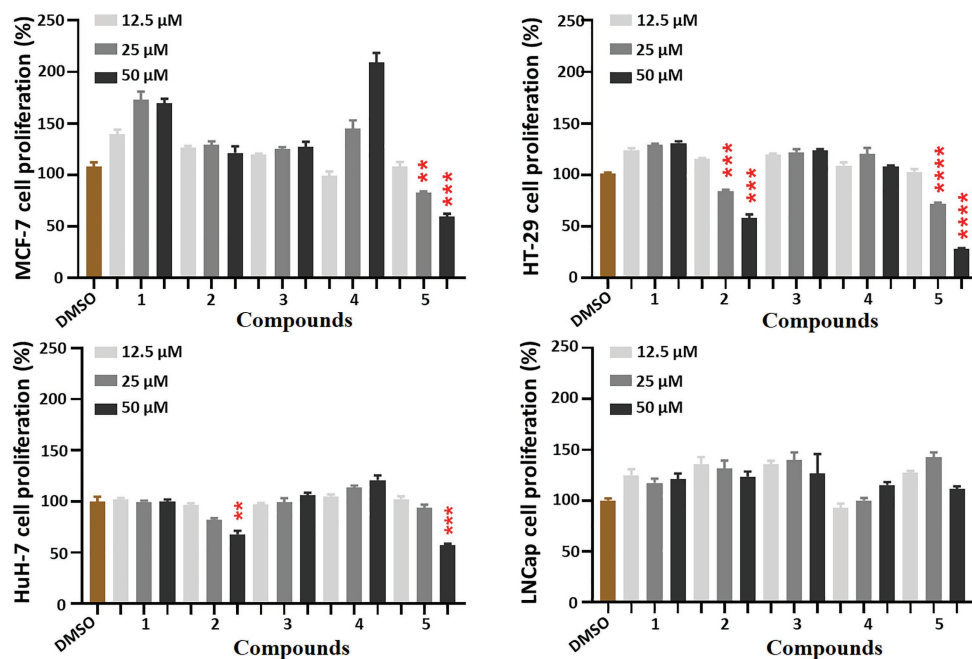
FIGURE 4 | Antiproliferative effects of compounds **1–5** against four cancer cells. Cells were treated with five compounds in a dose-course (12.5, 25, and 50 μM) for 48 h, which were analyzed by MTT assays to compare the cell proliferation levels. All the bar graphs represent mean ± SEM of three independent experiments. **$p < 0.01$, ***$p < 0.001$, ****$p < 0.0001$ vs. the DMSO group.

be found by the HMBC correlations of the hydroxy at δ_H 8.92 s to C-19 (δ_C 115.2 d). By detailed analysis of its heteronuclear single quantum correlations (HSQC), correlation spectroscopy (COSY), heteronuclear multiple-bond correlation (HMBC), and nuclear overhauser effect (NOESY) spectroscopic data

(**Supplementary Table S1** of the Supporting Information), the structure and relative configuration of the compound **2** were determined. The absolute configuration of compound **2** was assigned to be identical to that of compound **1** based on their similar specific rotations and ECD data. Compound **2** was
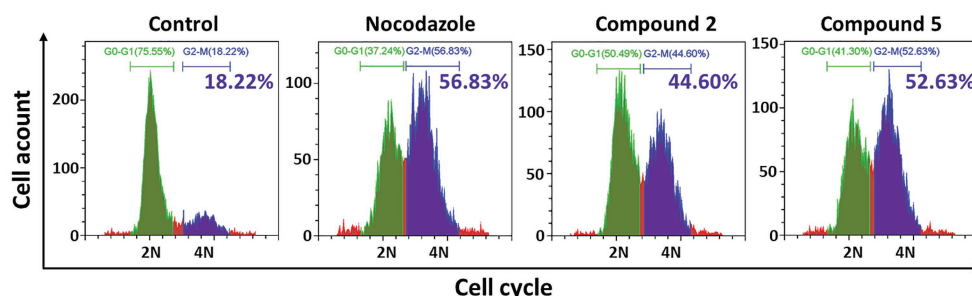
FIGURE 5 | Effects of compounds **2** and **5** on cell cycle by flow cytometry. HT-29 cells were treated with compound **2** (50 µM, 48 h) or **5** (30 µM, 48 h), which were stained with DAPI for the following cell cycle FCM assay. The blue part indicated the cells in G0-G1 phase, the green part showed the G2-M phase cells, and the green numbers showed the G2-M phase proportion.
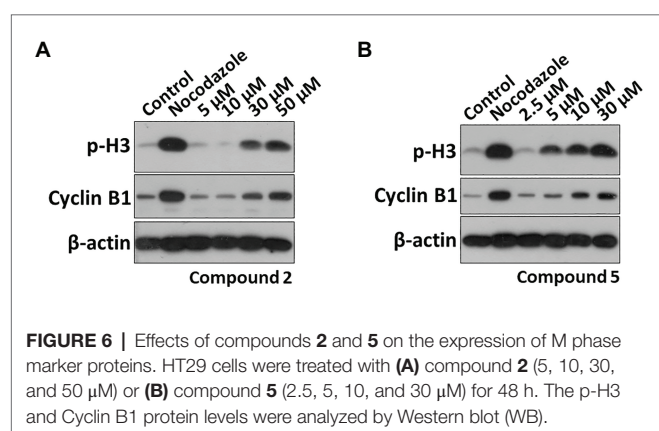
FIGURE 6 | Effects of compounds **2** and **5** on the expression of M phase marker proteins. HT29 cells were treated with **(A)** compound **2** (5, 10, 30, and 50 µM) or **(B)** compound **5** (2.5, 5, 10, and 30 µM) for 48 h. The p-H3 and Cyclin B1 protein levels were analyzed by Western blot (WB).

then established as 18-*O*-demethyl derivate of sorbiallisatol A, and named sorbicatechol D.

Hybrid sorbicillinoids are derived from either a Diels-Alder or a Michael reaction of a monomeric sorbicillinoid diene and a second non-sorbicillinoid dienophile (Meng et al., 2016). Noteworthily, compounds **1** and **2** are two novel hybrid sorbicillinoids derived from dihydrosorbicillinols which were very rarely in nature. Their biogenetic origin might be involved ferulic acid and 2',3'-dihydrosorbicillinol *via* an intermolecular Diels-Alder condensation followed by a decarboxylation (Peng et al., 2014).

By comparison of NMR spectroscopic data with those published in the literatures, three known compounds were determined to be sohirnone A (**3**), 2',3'-dihydrosorbicillin (**4**; Maskey et al., 2005), and sorbicillin (**5**; Trifonov et al., 1983).

All five isolates were subjected to the preliminary screening tests for antiproliferative activity against MCF-7, HT-29, HuH-7, and LNCap tumor cells. Compounds **2** and **5** could inhibit the proliferation of HT-29 cells in a dose-dependent manner (**Figure 4**).

Interestingly, after treatment by compounds **2** and **5**, many HT-29 cells became more rounded and less adherent under the microscope, which suggested cell cycle was disrupted and resulted in M-phase arresting. Therefore, further investigation of the cell cycle was conducted by flow cytometry. As expected, they significantly blocked 40.96 and 41.69% tumor cells in G2-M phase, respectively (**Figure 5**). Therefore, compounds **2** and **5** could blocked HT-29 cells in G2-M phase.

Phosphorylation of histone H3 (p-H3) is one of the methods of histone modification. It occurs at specific periods and chromosomal sites during mitosis and meiosis. Cyclin B1 also plays an important role in cell cycle regulation. The overexpression of cyclinB1 can promote G2/M phase conversion and even lead to uncontrolled cell proliferation and malignant transformation (Hartwell and Kastan, 1994; Hwang et al., 1995). Therefore, the expression of M phase markers p-H3 and cyclin B1 was further detected. As shown in **Figure 6**, they could significantly increase the protein levels of p-H3 and cyclin B1 in a dose-dependent effect, confirming compounds **2** and **5** indeed induced M phase arresting. The effective concentrations of compounds **2** and **5** were 30 and 5 µM, respectively.

CONCLUSION

From the deep-sea-derived *Penicillium allii-sativi* MCCC 3A00580, five sorbicillinoids (**1–5**) were obtained. Compounds **1** and **2** are two novel hybrid dihyrosorbicillinoids. While compounds **3–5** are three known monomeric sorbicillinoids. Although several examples were found for monomeric, dimeric, and trimeric sorbicillinoids in which C-2'/C-3' double bonds were reduced, compounds **1** and **2** are the first two examples for hybrid sorbicillinoids. Therefore, the discovery of compounds **1** and **2** has expanded the diversity and complexity of sorbicillinoids. Compounds **2** and **5** could inhibit HT-29 tumor cells in a good dose-dependent manner. They significantly induced cell cycle G2-M phase arresting by increasing the protein levels of p-H3 and cyclin B1.

DATA AVAILABILITY STATEMENT

The raw data supporting the conclusions of this article will be made available by the authors, without undue reservation.

AUTHOR CONTRIBUTIONS

C-LX performed chemical investigations. DZ conducted biological experiments. TL, Z-HH, and Q-XY assisted C-LX's chemical

experiments. QC assisted DZ's bioactive experiments. X-KZ, X-WY, and H-FC initiated and oversaw all research. All authors contributed to the article and approved the submitted version.

(DY135-B2-08), and the Xiamen Southern Oceanographic Center (17GYY002NF02).

SUPPLEMENTARY MATERIAL

The Supplementary Material for this article can be found online at: https://www.frontiersin.org/articles/10.3389/fmicb.2020.636948/full#supplementary-material

REFERENCES

Abe, N., Sugimoto, O., Tanji, K. -I., and Hirota, A. (2000). Identification of the quinol metabolite "sorbicillinol", a key intermediate postulated in bisorbicillinoid biosynthesis. *J. Am. Chem. Soc.* 122, 12606–12607. doi: 10.1021/ja003013l

Abe, N., Yamamoto, K., Arakawa, T., and Hirota, A. (2001). The biosynthesis of bisorbicillinoids: evidence for a biosynthetic route from bisorbicillinol to bisorbibutenolide and bisorbicillinolide. *Chem. Commun.* 2001, 23–24. doi: 10.1039/B007181L

Fahad, A. A., Abood, A., Fisch, K. M., Osipow, A., Davison, J., Avramović, M., et al. (2013). Oxidative dearomatisation: the key step of sorbicillinoid biosynthesis. *Chem. Sci.* 5, 523–527. doi: 10.1039/c3sc52911h

Harned, A. M., and Volp, K. A. (2011). The sorbicillinoid family of natural products: isolation, biosynthesis, and synthetic studies. *Nat. Prod. Rep.* 28, 1790–1810. doi: 10.1039/c1np00039j

Hartwell, L. H., and Kastan, M. B. (1994). Cell cycle control and cancer. *Science* 266, 1821–1828. doi: 10.1126/science.7997877

Hwang, A., Maity, A., McKenna, W. G., and Muschel, R. J. (1995). Cell cycle-dependent regulation of the cyclin B1 promoter. *J. Biol. Chem.* 270, 28419–28424. doi: 10.1074/jbc.270.47.28419

Kahlert, L., Bassiony, E. F., Cox, R. J., and Skellam, E. J. (2020). Diels-Alder reactions during the biosynthesis of sorbicillinoids. *Angew. Chem. Int. Ed. Eng.* 59, 5816–5822. doi: 10.1002/anie.201915486

Maskey, R. P., Grun-Wollny, I., and Laatsch, H. (2005). Sorbicillin analogues and related dimeric compounds from *Penicillium notatum*. *J. Nat. Prod.* 68, 865–870. doi: 10.1021/np040137t

Meng, J., Gu, G., Dang, P., Zhang, X., Wang, W., Dai, J., et al. (2019). Sorbicillinoids from the fungus *Ustilaginoidea virens* and their phytotoxic, cytotoxic, and antimicrobial activities. *Front. Chem.* 7:435. doi: 10.3389/fchem.2019.00435

Meng, J., Wang, X., Xu, D., Fu, X., Zhang, X., Lai, D., et al. (2016). Sorbicillinoids from fungi and their bioactivities. *Molecules* 21, 715–733. doi: 10.3390/molecules21060715

Niu, S., Fan, Z. W., Xie, C. L., Liu, Q., Luo, Z. H., Liu, G., et al. (2017). Spirograterpene A, a tetracyclic spiro-diterpene with a fused 5/5/5/5 ring system from the deep-sea-derived fungus *Penicillium granulatum* MCCC 3A00475. *J. Nat. Prod.* 80, 2174–2177. doi: 10.1021/acs.jnatprod.7b00475

Niu, S., Xie, C. L., Xia, J. M., Liu, Q. M., Peng, G., Liu, G. M., et al. (2020). Botryotins A–H, tetracyclic diterpenoids representing three carbon skeletons from a deep-sea-derived *Botryotinia fuckeliana*. *Org. Lett.* 22, 580–583. doi: 10.1021/acs.orglett.9b04332

Peng, J., Zhang, X., Du, L., Wang, W., Zhu, T., Gu, Q., et al. (2014). Sorbicatechols A and B, antiviral sorbicillinoids from the marine-derived fungus *Penicillium chrysogenum* PJX-17. *J. Nat. Prod.* 77, 424–428. doi: 10.1021/np400977e

Trifonov, L. S., Bieri, J. H., Prewo, R., Dreiding, A. S., Hoesch, L., and Rast, D. M. (1983). Isolation and structure elucidation of three metabolites from *Verticillium intertextum*: sorbicillin, dihydrosorbicillin and bisvertinoquinol. *Tetrahedron* 39, 4243–4256. doi: 10.1016/S0040-4020(01)88647-6

Xie, C. L., Chen, R., Yang, S., Xia, J. M., Zhang, G. Y., Chen, C. H., et al. (2019a). Nesteretal A, a novel class of cage-like polyketide from marine-derived actinomycete *Nesterenkonia halobia*. *Org. Lett.* 21, 8174–8177. doi: 10.1021/acs.orglett.9b02634

Xie, C. L., Xia, J. M., Lin, T., Lin, Y. J., Lin, Y. K., Xia, M. L., et al. (2019b). Andrastone A from the deep-sea-derived fungus *Penicillium allii-sativi* acts as an inducer of caspase and RXRa-dependent apoptosis. *Front. Chem.* 7:692. doi: 10.3389/fchem.2019.00692

Yang, X. W., Peng, K., Liu, Z., Zhang, G. Y., Li, J., Wang, N., et al. (2013). Strepsesquitriol, a rearranged zizaane-type sesquiterpenoid from the deep-sea-derived actinomycete *Streptomyces* sp. SCSIO 10355. *J. Nat. Prod.* 76, 2360–2363. doi: 10.1021/np400923c

Endogenous 2µ Plasmid Editing for Pathway Engineering in *Saccharomyces cerevisiae*

Bo-Xuan Zeng[1,2], Ming-Dong Yao[1,2], Wen-Hai Xiao[1,2], Yun-Zi Luo[1,3], Ying Wang[1,2]* and Ying-Jin Yuan[1,2]

[1] Frontier Science Center for Synthetic Biology and Key Laboratory of Systems Bioengineering (Ministry of Education), School of Chemical Engineering and Technology, Tianjin University, Tianjin, China, [2] Collaborative Innovation Center of Chemical Science and Engineering (Tianjin), Tianjin University, Tianjin, China, [3] Department of Gastroenterology, State Key Laboratory of Biotherapy, West China Hospital, Sichuan University, Chengdu, China

In *Saccharomyces cerevisiae,* conventional 2µ-plasmid based plasmid (pC2µ, such as pRS425) have been widely adopted in pathway engineering for multi-copy overexpression of key genes. However, the loss of partition and copy number control elements of yeast endogenous 2µ plasmid (pE2µ) brings the issues concerning plasmid stability and copy number of pC2µ, especially in long-term fermentation. In this study, we developed a method based on CRISPR/Cas9 to edit pE2µ and built the pE2µ multi-copy system by insertion of the target DNA element and elimination of the original pE2µ plasmid. The resulting plasmid pE2µRAF1 and pE2µREP2 demonstrated higher copy number and slower loss rate than a pC2µ control plasmid pRS425RK, when carrying the same target gene. Then, moving the essential gene *TPI1* (encoding triose phosphate isomerase) from chromosome to pE2µRAF1 could increase the plasmid viability to nearly 100% and further increase the plasmid copy number by 73.95%. The expression using pE2µ multi-copy system demonstrated much smaller cell-to-cell variation comparing with pC2µ multi-copy system. With auxotrophic complementation of *TPI1*, the resulting plasmid pE2µRT could undergo cultivation of 90 generations under non-selective conditions without loss. Applying pE2µ multi-copy system for dihydroartemisinic acid (DHAA) biosynthesis, the production of DHAA was increased to 620.9 mg/L at shake-flask level in non-selective rich medium. This titer was 4.73-fold of the strain constructed based on pC2µ due to the more stable pE2µ plasmid system and with higher plasmid copy number. This study provides an improved expression system in yeast, and set a promising platform to construct biosynthesis pathway for valuable products.

Keywords: 2µ plasmid, CRISPR, plasmid copy number, dihydroartemisinic acid, *Saccharomyces cerevisiae*

INTRODUCTION

For the high transformation efficiency and easy manipulation, plasmids have been developed as important tools and were widely applied in many kinds of organisms (Mignon et al., 2015; Lian et al., 2016). The multi-copy plasmids are always used to overexpress genes of interest (Kang et al., 2018). In *Saccharomyces cerevisiae*, conventional 2µ-based plasmid (pC2µ) such as pYES2,

pRS426, and pESC were widely used multi-copy plasmids for production of recombinant proteins as well as construction of metabolic pathway. For example, overexpression of Syn_ALD (aldehyde dehydrogenase of *Synechocystis sp.* PCC6803) and CCD2 (carotenoid cleavage dioxygenase of *Crocus*) by pRS426 increased crocetin production by about 1-fold (Chai et al., 2017). However, like all kinds of multi-copy plasmids, the plasmid viability in cells always depends on the selectivity pressure generated by the medium (with antibiotics or auxotroph medium) (Karim et al., 2013; Lian et al., 2016). In condition without selective pressure, pC2μ hardly keeps its high copy number and are difficult to be maintained in the host cell (**Figure 1A**). The loss frequency could reach to about 5% per generation (Gnügge and Rudolf, 2017), and nearly 50–60% of the cells lose their plasmid after about 24 h cultivation in non-selective medium (Christianson et al., 1992). For strain harboring pC2μ with auxotroph marker, the rich medium such as YPD is not suitable for long-term fermentation because of the loss of the plasmid, although the strain grows faster in these kinds of media; And for that with antibiotic marker, the addition of expensive drugs

is inevitable and it is not economic for fermentation of industrial scale.

Plasmid pC2μ was derived from the yeast endogenous 2μ plasmid (pE2μ) which presents in most wild-type and laboratory *S. cerevisiae* strain (Gnügge and Rudolf, 2017). The pE2μ is a selfish episomal circular DNA element in *S. cerevisiae* (Rizvi et al., 2017a). It contains a special replication origin (2μ ori), two FRT sites (*FLP1* recognized target site), and sequences encoding four known genes: *REP1*, *REP2*, *RAF1*, and *FLP1* (Gnügge and Rudolf, 2017; McQuaid et al., 2017; Rizvi et al., 2017a; see **Supplementary Figure 1**). *FLP1* and both FRT sites are essential for the amplification of pE2μ. This amplification system is based on the *FLP1*-mediated recombination and follows the special Futcher's model (Futcher, 1986; Rizvi et al., 2017a), thus each plasmid could reproduce more than one copy in one cell cycle to restore the steady-state for plasmid copy number (PCN) under missegregation and consequent perturbations (Rizvi et al., 2017a). Whereas, pC2μ plasmid contains only one FRT site. So that pC2μ cannot be amplified as Futcher's model itself, and the amplification of pC2μ is not efficient as pE2μ. Therefore, the PCN of pC2μ cannot compete with native pE2μ, even though

FIGURE 1 | Design and construction of pE2μ multi-copy system. **(A)** The comparison of the copy number of the inserted target gene using pC2μ (conventional 2μ-based plasmid) derivate plasmid and pE2μ (endogenous 2μ plasmid) derivate plasmid. **(B)** The process of pC2μ multi-copy system and pE2μ multi-copy system. The 2μ ori (original of replication of wild type endogenous plasmid) is shown in blue, other parts of endogenous plasmid are shown in purple, the Target gene of interest is shown in red. The scissors represent the CRISPR/Cas9 tool to edit the plasmid. **(C)** The construction and optimization of the pE2μ derivate plasmid.

weaken the expression of the selective marker by truncated or weaker promoter could increase the average plasmid copy number of pC2μ by eliminating the cells with less plasmid (Karim et al., 2013).

REP1 and *REP2* are essential for the partition system of pE2μ. *REP1* and *REP2* form the *REP1-REP2* complex which binds to the *cis*-acting locus (STB locus) (see **Supplementary Figure 1**) located within the 2μ ori to ensure equal segregation of plasmids from mother to daughter cells (Gnügge and Rudolf, 2017; Rizvi et al., 2017a); *RAF1* is responsible for the regulation of partition and amplification system to keep the plasmid copy number of pE2μ and minimize the cell-to-cell variations (McQuaid et al., 2017; Rizvi et al., 2017b). Based on the tightly controlled partition system and amplification system described above, pE2μ could be segregated equally and the copy number could be restored in some missegregation events, leading to very low loss frequency (<0.01%) (Gnügge and Rudolf, 2017). The pC2μ only contains 2μ ori and does not contain *REP1* and *REP2*, so the maintenance of pC2μ has to depend on pE2μ (**Figure 1B**). Rising from segregation instability, the loss frequency of pC2μ is about 50% per generation in strains without pE2μ (Gnügge and Rudolf, 2017). Therefore, to achieve stable and high-level expression of the targeted genes, we intended to employ pE2μ rather than pC2μ as an expression vector. Yukie Misumi once constructed the plasmid YHp (Misumi et al., 2019) based on the structure of pE2μ and applied in the *S. cerevisiae* strain without endogenous 2μ plasmid. However, because of the similar structure, YHp is not compatible with wild type pE2μ and was not suitable for application in commonly used laboratory *S. cerevisiae* strain which harboring wild type pE2μ.

In our work, we developed a novel multi-copy plasmid system which based on editing pE2μ by CRISPR/Cas9 genome engineering tools (**Figures 1B,C**). The laboratory strain CEN.PK2-1C was chosen as the host. It contains the natural wild type pE2μ plasmid. By using this pE2μ multi-copy plasmid system, the target gene could be overexpressed more stable and at higher level than using the commonly used pC2μ multi-copy plasmid system (**Figure 1A**). Although the edited pE2μ was still lost during long-term cultivation in non-selective medium, the plasmid viability was much higher than that of pC2μ. To further reduce the loss frequency of pE2μ, auxotrophy complementation strategy was applied by introducing the essential gene *TPI1* (encoding triose phosphate isomerase) into pE2μ by CRISPR/Cas9 system as well as knocking out the *TPI1* in the chromosome (**Figure 1C**). As a result, pE2μ plasmid (pE2μRT) could be maintained in cells for long-term cultivation. And its PCN was also increased. Although p425RT (pC2μ derived plasmid carrying *TPI1*) in strain without chromosome *TPI1* could also be maintained in cell after long-term cultivation in YPD, the average level and stability of p425RT could not compared with that of pE2μRT. At last, we applied the method for optimization of the metabolic pathway of dihydroartemisinic acid (DHAA) production in non-selective medium. The production was successfully increased to 620.9 mg/L which was 4.73-fold higher than the strain using pC2μ to overexpress the gene of the same biosynthetic pathway.

MATERIALS AND METHODS

Strains and Medium

Escherichia coli DH5α was used for construction of all the plasmids and was cultured at 37°C in Luria-Bertani (LB) medium (1% tryptone, 0.5% yeast extract, and 1% NaCl) with 100 μg/ml ampicillin or 34 μg/ml chloramphenicol if necessary. All engineered yeast strains were derived from *S. cerevisiae* CEN.PK2-1C (Entian and Kötter, 2007) obtained from EUROSCARF (Frankfurt, Germany). The yeast strains were cultured at 30°C in YPD medium (2% peptone, 1% yeast extract, and 2% glucose) or in synthetic complete (SC) drop-out medium. G418 was added to medium in final concentration of 200 μg/ml if necessary. The strains for DHAA production was derivative from Sc027 (Zeng et al., 2020). All *S. cerevisiae* strains used in this study were listed in **Table 1**.

Construction of pE2μ Derivate Plasmid

All the plasmids constructed in this study were listed in **Table 2**. The primer used in this study were listed in **Supplementary Table 1**.

Three CRISPR/Cas9 plasmid pCasRAF1, pCasREP2, and pCasE2μ were constructed based on pRS416 (**Supplementary Figure 2**). Took the construction of pCasRAF1 for example: P_{SNR52}(RAF1) was amplified from pNA0304 by PCR using primer 18Q3-pSNR52-F and 18Q0b-pSNR52-R; Cassette gRNA.2μ.RAF1-T_{SUP4}-T_{CYC1} was amplified from pNA0304

TABLE 1 | Yeast strains used in this study.

Yeast Strains	Description	Source
CEN.PK2-1C	*MAT a; ura3-52, trp1-289, leu2-3,112, his3Δ1, MAL2-8C, SUC2*	Invitrogen
Sc382	*CEN.PK2-1C derivative; Δ2μ:: pE2μRAF1*	This study
Sc534	*CEN.PK2-1C derivative; pRS425RK*	This study
Sc438	*CEN.PK2-1C derivative; Δ2μ::pE2μREP2*	This study
Sc591	*Sc382 derivative; ΔE2μRAF1::pE2μRT*	This study
Sc594	*Sc591 derivative; ΔTPI1(chromosome)::leu2*	This study
Sc530	*CEN.PK2-1C derivative; p425RT; ΔTPI1(chromosome)::his3*	This study
Sc027	CEN.PK2-1C derivative; *leu2-3,112::KanMX6_P_{GAL7}-CYB5_T_{ERG19}(RC)-ERG19(RC)-P_{GAL1}(RC)_P_{GAL10}-ERG8-T_{ERG8}; his3Δ1::HIS3_P_{GAL7}-ALDH1-T_{TDH1}_T_{ERG12}(RC)-ERG12(RC)-P_{GAL1}(RC)_P_{GAL10}-ERG10-T_{ERG10}; ade1Δ::T_{HMG1}(RC)-tHMG1(RC)-P_{GAL1}(RC)_P_{GAL10}-IDI1-T_{IDI1}_ADE1; ura3-52::T_{HMG1}(RC)-tHMG1(RC)-P_{GAL1}(RC)_P_{GAL10}-ERG13-T_{ERG13}; trp1-289::T_{HMG1}(RC)-tHMG1(RC)-P_{GAL1}(RC)_P_{GAL10}-ERG20-T_{ERG20}_TRP1; gal1/10/7Δ::natA_P_{GAL3}-CPR1-T_{CYC1};*	Zeng et al., 2020
Sc341	*Sc027 derivative; Δgal80::P_{CYC1}-GAL4-T_{GAL4}_P_{GAL7}-ADH1-T_{TDH1}; ΔKanMX6::P_{TDH1}-HEM1-T_{HEM1}_P_{PGK1}-CTT1-T_{CTT1}_hphA*	This study
Sc366	*Sc341 derivative; p425DCA*	This study
Sc343	*Sc341 derivative; Δ2μ::pE2μDCA*	This study
Sc582	*Sc343 derivative; ΔpE2μDCA::pE2μDCAT*	This study
Sc584	*Sc582 derivative; ΔTPI1::leu2*	This study

TABLE 2 | Plasmids used in this study.

Plasmid	Description	Source
pNA0306	$pRS415\_P_{TEF1}-Cas9-T_{CYC1}$	Xie et al., 2018
pNA0304	$pRS426-P_{SNR52}-gRNA-T_{SUP4}$	Xie et al., 2018
pCasRAF1	$pRS416\_P_{TEF1}-Cas9-T_{CYC1}\_P_{SNR52}-gRNA.2μ.RAF1-T_{SUP4}-T_{CYC1}$	This study
pCasREP2	$pRS416\_P_{TEF1}-Cas9-T_{CYC1}\_P_{SNR52}-gRNA.2μ.REP2-T_{SUP4}-T_{CYC1}$	This study
pCasE2μ	$pRS416\_P_{TEF1}-Cas9-T_{CYC1}\_P_{SNR52}-gRNA.E2μ-T_{SUP4}-T_{CYC1}$	This study
pDonorRAF1	$pSB1C3\_P_{TDH3}-RFP-T_{ADH1}\_KanMX6(RC)\_T_{PGI1}(RC)\_homoRAF1(RC)\_T_{RAF1}$ (RC)	This study
pDonorREP2	$pSB1C3\_P_{TDH3}-RFP-T_{ADH1}\_KanMX6(RC)\_T_{CPS1}$ (RC)_homoREP2(RC)_T_{REP2} (RC)	This study
pE2μRAF1	$pSB1C3_P_{TDH3}-RFP-T_{ADH1}_KanMX6(RC)_T_{PGI1}(RC)-RAF1(RC)-$$P_{RAF1}(RC)\_rep1\_FRT(RC)\_flp1(RC)\_rep2\_2μ$ ori	This study
pE2μREP2	$pSB1C3\_P_{TDH3}-RFP-T_{ADH1}\_KanMX6(RC)\_T_{PGI1}(RC)-RAF1(RC)-$$P_{RAF1}(RC)_rep1_FRT(RC)_flp1(RC)_rep2_2μ$ ori	This study
pRS425RK	$pRS425\_P_{TDH3}-RFP-T_{ADH1}(RC)\_KanMX6(RC)$	This study
pE2μRT	$pSB1C3_P_{TPI1}(RC)-TPI1(RC)-T_{TPI1}(RC)_P_{TDH3}-RFP-$$T_{ADH1}\_G418R(RC)\_T_{PGI1}(RC)-RAF1(RC)-$$P_{RAF1}(RC)_rep1_FRT(RC)_flp(RC)_rep2_2μ$ ori	This study
p425RT	$pRS425\_P_{TPI1}(RC)-TPI1(RC)-T_{TPI1}(RC)\_P_{TDH3}-RFP-T_{ADH1}$	This study
p425DCA	$pRS425_T_{CYC1}(RC)-DBR2(RC)-P_{GAL10}(RC)-_P_{GAL1}-ADS-T_{PGK1}_P_{GAL7}-$$CYP71AV1^*-T_{ADH1}$	This study
pDonorDCA	$pSB1C3\_T_{CYC1}(RC)-DBR2(RC)-P_{GAL10}(RC)-\_P_{GAL1}-ADS-T_{PGK1}\_P_{GAL7}-$$CYP71AV1^*-T_{ADH1}_KanMX6(RC)_T_{PGI1}(RC)_homoRAF1(RC)_Pmel_T_{RAF1}$ (RC)	This study
pE2μDCA	$pSB1C3_T_{CYC1}(RC)-DBR2(RC)-P_{GAL10}(RC)-_P_{GAL1}-ADS-T_{PGK1}_P_{GAL7}-$$CYP71AV1^*-T_{ADH1}\_KanMX6(RC)\_T_{PGI1}(RC)\_$$RAF1(RC)-P_{RAF1}(RC)_rep1_FRT(RC)_flp1(RC)_rep2_2μ$ ori	This study
pE2μDCAT	$pSB1C3_P_{TPI1}-TPI1(RC)-T_{TPI1}(RC)_T_{CYC1}(RC)-DBR2(RC)-P_{GAL10}(RC)-$$\_P_{GAL1}-ADS-T_{PGK1}\_P_{GAL7}-CYP71AV1^*-T_{ADH1}\_KanMX6(RC)\_T_{PGI1}(RC)\_$$RAF1(RC)-P_{RAF1}(RC)_rep1_FRT(RC)_flp1(RC)_rep2_2μ$ ori	This study
stALG2	$pRS425\_ALG9(partial)\_ P_{TDH3}-RFP-T_{ADH1}\_KanMX6(RC)$	This study
pSB1C3	Backbone for plasmid construction, CmR	Zeng et al., 2020
pRS416	Backbone for plasmid construction. Amp, Ura3	GenBank: U03450.1

The DNA fragment followed by "(RC)" represented the orientation of the DNA fragment was reversed.
CYP71AV1*: all CYP71AV1 used in this study was optimized by replacing the N-terminal membrane anchoring sequence (15-residue peptide) with the more hydrophilic 8-residue peptide from bovine (8RP) (Chen et al., 2017).

by PCR using primer 18Q0b-gRNA-F and 18Q3-cyc1t-R; Two DNA fragment were assembled together to constructed cassette P_{SNR52}-gRNA.2μ.RAF1-T_{SUP4}-T_{CYC1} by OE-PCR (overlap extension PCR) using primer 18Q3-cyc1t-R and 18Q3-pSNR52-F. Cassette P_{TEF1}-cas9-T_{CYC1} was amplified by PCR from pNA0306 using primer 18Q3-cas9-F and 18Q3-cas9-R. Cassette P_{SNR52}-gRNA.2μ.RAF1-T_{SUP4}-T_{CYC1} was digested by SphI and NotI; Cassette P_{TEF1}-Cas9-T_{CYC1} was digested by KpnI and SphI; pRS416 was digested by KpnI and NotI. Three digested DNA fragments were ligated together by T4 ligase to construct pCasRAF1. pCasREP2 and pCasE2μ were constructed in similar way.

Plasmids pDonorRAF1, pDonorREP2, pDonorDCA were donor plasmid. Took the construction of pDonorRAF1 for example: T_{GPI1}, homoRAF1, T_{RAF1} were amplified by PCR from the genome of CEN.PK2-1C using primers 18Q2a-pgi1t-R/18Q2a-pgi1t-F, 18Q2a-homodown-F/18Q2a-homodown-R, 18Q2a-homoup-F/18Q2a-homoup-R. The DNA fragment were assembled to construct T_{PGI1}_homoRAF1_PmeI_T_{RAF1} by OE-PCR and amplified using primer 18Q2a-pgi1t-F/18Q2a-homoup-R. Cassette P_{TDH3}-RFP-T_{ADH1} was amplified by

PCR using primer 18Q4-pTDH3-F/ 18Q4-adh1t-R. Cassette KanMX6 was amplified by PCR using primer 18Q4a-kanMX6-F/18Q4a-kanMX6-R. Cassette T_{PGI1}_homoRAF1_PmeI_T_{RAF1} was digested by PstI and XbaI; P_{TDH3}-RFP-T_{ADH1} was digested by EcoRI and XhoI; KanMX6 was digested by XhoI and XbaI; plasmid pSB1C3 was digested by PstI and EcoRI. All 4 digested fragment were ligated together by T4 ligase to construct pDonorRAF1. Donor plasmid pDonorREP2 and pDonorDCA was constructed in similar way.

For construction of the S. cerevisiae strain Sc382, donor plasmid pDonorRAF1 was linearized by PmeI and was co-transformed to CEN.PK2-1C with CRISPR/Cas9 plasmid pCasRAF1 to insert the whole donor DNA into endogenous 2μ plasmid. The SC-Ura plate with 200 mg/L G418 was used for selection of the correct transformants. After keeping the plate at 30°C for about 72 h, all the transformants were visible. The single colonies were picked up and transferred to SC-Ura plate with 200 mg/L G418 and incubated at 30°C for 24 h. Then, the colonies were identified by colony PCR. For strain Sc382, the primer pairs 2μori-test-F/BioBrick-R and 18Q-test-5/18Q-test-15 were used for verification of the insertion of the donor DNA.

The primer pair 2μori-test-F/18Q-test-5 was used for verification of the elimination of all wild type endogenous 2μ plasmid. The result was used for characterization of the efficiency of the method of editing endogenous 2μ plasmid by CRISPR/Cas9 system. After verification, the correct colonies were steaked on 5-FOA (5-Fluoroorotic acid) plate with 200 mg/L G418 to lose the pCasRAF1 plasmid.

The process of construction of strain Sc438 and Sc343 were similar to that of strain Sc382. Donor plasmid pDonorREP2 and pCasREP2 were used for co-transformation into CEN.PK2-1C to construct strain Sc438 (harboring plasmid pE2μREP2); Donor plasmid pDonorDCA and pCasRAF1 were used for co-transformation into CEN.PK2-1C to construct strain Sc343 (harboring plasmid pE2μDCA).

To introduce *TPI1* to pE2μ, DNA fragment tpi1-1 was amplified from genome of CEN.PK2-1C by PCR using primer 20QRcT-R4/20QRcT-F4, tpi1-2 was amplified from tpi1-1 by PCR using primer 20QRcT-R5/20QRcT-F5, tpi1-3 was amplified from tpi1-2 by PCR using primer 20QRcT-R6/20QRcT-F6. The DNA fragment tpi1-3 was co-transformed to strain Sc382 (containing pE2μRAF1) and Sc343 (containing pE2μDCA) with CRISRP/Cas9 plasmid pCasE2μ to insert *TPI1* into pE2μRAF1 or pE2μDCA to construct strain Sc591 and Sc582.

To delete the *TPI1* of chromosome, leu2-1 was amplified from pRS425 by PCR using primer dTPI1-leu2-F1/dTPI1-leu2-R1; Then, leu2-2 was amplified from leu2-1 by PCR using primer dTPI1-leu2-F2/dTPI1-leu2-R2; and leu2-3 was amplified from leu2-2 by PCR using primer dTPI1-leu2-F3/dTPI1-leu2-R3. DNA fragment leu2-3 was introduced to Sc591 and Sc582 for deletion of TPI1 to construct strain Sc594 and Sc584. For construction of strain Sc530, p425RT was introduced into CEN.PK2-1C and then chromosome *TPI1* was deleted by *his3*.

Plasmid Stability Assay

To characterize the property of plasmid pE2μ and pC2μ, strain Sc382, Sc438, Sc534, Sc530, and Sc594 were tested in non-selective YPD medium. The single colony from selective YPD+G418 medium plate was inoculated to 3 ml YPD+G418 medium (for Sc530, the medium was SC-Leu). The saturated culture was re-inoculated to 3 ml YPD+G418 medium (for Sc530, the medium was SC-Leu) at an optical density (OD$_{600}$) 0.05 and grown for 10 h at 30°C. The culture was at 0 generation and was prepared for characterization. Then the culture was re-inoculated to non-selective YPD medium at OD$_{600}$ = 0.05 and grown for 10 h at 30°C again to obtain the culture at 5 generation. Then serial sub-cultures were conducted every 5 generation until the 30th generation. The cultures at 5, 10, 20, and 30 generation were prepared for characterization.

For measurement of the fluorescence of RFP (Red fluorescence protein), plate reader (SpectraMAX M2, Molecular Devices) was used with a 587 nm excitation filter and a 610 nm emission filter. The fluorescence of RFP at single cell level was measured by flow cytometer (NovoCyte D2040R). The culture of each generation was diluted and plated on YPD medium and YPD+G418 medium (for Sc530, the selective medium was SC-Leu) to calculate the viability of the plasmid by counting the colony number of each plate.

Determination of Plasmid Copy Number (PCN)

The plasmid copy number (PCN) was measured by quantitative PCR using the total DNA extracted from the strain. The process of total DNA extraction: the cells was harvest at mid-log phase, and were treated with lysis buffer (20 mM phosphate buffer at pH = 7.2, 1.2 M sorbitol, 15 U zymolyase) at 37°C for 20 min; The total DNA was extracted by boiling the sample for 15 min, −80°C for 15 min and then boiling again for 15 min (Lian et al., 2016). The suspension was diluted 10-fold before qPCR analyze. The absolute quantitative method referred to Lee et al. (2006). The plasmid stALG2 (contain ALG9, RFP, KanMX6) and p425DCA (containing ADS) was used for construction of the standard curve. TransStart® Top Green qPCR SuperMix (purchased from TransGen Biotech Co., Ltd) were used for qPCR analyze on Real time fluorescent quantitative PCR (Molarray MA-6000). The primers used for qPCR were listed in **Supplementary Table 1**.

Fermentation and Measurement of the DHAA

The medium used for fermentation was YPD medium and FM medium (as our previous work (Zeng et al., 2020)). The FM medium was composed of 8 g/L KH$_2$PO$_4$, 15 g/L (NH4)$_2$SO$_4$, 6.2 g/L MgSO$_4$·7H$_2$O, 40 g/L glucose, 12 ml/L vitamin solution, and 10 ml/L trace metal solution and 10 ml/L Amino acid solution. Vitamin solution included 0.05 g/L biotin, 1 g/L calcium pantothenate, 1 g/L nicotinic acid, 25 g/L myo-inositol, 1 g/L thiamine HCl, 1 g/L pyridoxal HCl, 0.2 g/L p-aminobenzoic acid, and 2 g/L adenine sulfate. Trace metal solution is composed of 5.75 g/L ZnSO$_4$·7H$_2$O, 0.32 g/L MnCl$_2$·4H$_2$O, 0.32 g/L Anhydrous CuSO$_4$, 0.47 g/L CoCl$_2$·6H$_2$O, 0.48 g/L Na$_2$MoO$_4$·2H$_2$O, 2.9 g/L CaCl$_2$·2H$_2$O, 2.8 g/L FeSO$_4$·7H$_2$O, and 80 ml/L EDTA solution (containing 0.5 mol/L Na$_2$EDTA pH = 8.0). Amino acid solution is composed of 2 g/L methionine, 6 g/L tryptophan, 8 g/L isoleucine, 5 g/L phenylalanine, 10 g/L sodium glutamate, 20 g/L threonine, 10 g/L aspartate, 15 g/L valine, 40 g/L serine, and 2 g/L arginine. The selective medium for Sc366 was FM medium adding 50 mg/L uracil, the selective medium for Sc343 and Sc584 was FM medium adding 200 mg/L leucine, and 50 mg/L uracil and 200 mg/L G418. The non-selective medium for all strains were YPD medium. To test the productivity of the strains, the single colony from plate was inoculated to selective medium and cultured for 18–24 h at 30°C. The seeds were re-inoculated to 3 ml selective medium at OD$_{600}$ = 0.05 and cultured for another 18–24 h at 30°C. The seed culture of each strain was transferred 250 ml flask containing 25 ml selective medium and flask containing 25 ml non-selective medium at initial OD$_{600}$ of 0.2. The cell was grown at 30°C with shaking at 200 rpm. After 24 h, 5 ml dodecane and 20 g/L ethanol was added to each flask. The whole fermentation process continued for 120 h until harvest.

After harvest, the fermentation broth was centrifuged at 12,000 × *g* for 2 min and the dodecane phase was collected. And then 50 μL organic phase was mixed with 950 μL methanol. After filtrated with 0.22 μm Nylon 66 filter, the sample was ready for HPLC analysis. The method for HPLC analysis and

the measurement of DHAA and other intermediates had been reported in previous work (Zeng et al., 2020).

Measurement of Relative mRNA Level

During the fermentation of Sc366 and Sc343, 1 ml samples was collected at 40 h. Total RNA was extracted from the cell using Yeast RNA kit (Omega bio-tek). The Reverse transcription procedure was used TransScript® First-Strand cDNA Synthesis SuperMix (purchased from TransGen Biotech Co., Ltd). The relative cDNA level of *ADS*, *CYP71AV1*, *DBR2* were measured by qPCR. *ALG9* was the reference gene, and the result was relative to that of Sc366. The primers used for qPCR were listed in **Supplementary Table 1**.

RESULTS AND DISCUSSION

The Construction of pE2μ Multi-Copy System

In order to construct the multi-copy system, we intended to insert the target DNA into the wild type pE2μ plasmid of CEN.PK2-1C. The pDonor plasmid which harboring homologous arms of wild type pE2μ was designed to carry target DNA. After linearization, pDonor could be transformed into CEN.PK2-1C and inserted into wild type pE2μ by homologous recombination to form the recombinant plasmid. Since the incompatibility between the recombinant plasmid and the original wild type pE2μ plasmid, the CRISPR/Cas9 plasmid was designed to and enhance the recombination of pDonor with pE2μ and eliminate all the original wild type pE2μ without insertion of pDonor. The resulting strain only contained the recombinant plasmid with multi-copies (**Figure 1C**).

To insert the target DNA into pE2μ, the site for recombination and the editing target of CRISPR/Cas9 plasmid had to be determined. Beside the four known genes, there are several uncharacterized transcripts transcribed from wild type pE2μ plasmid (Rizvi et al., 2017a). All the elements described above covered almost the whole plasmid. To avoid the disruption of the plasmid function, only two sites can be chosen as the targets for insertion of foreign DNA fragment: One is at the downstream of the *RAF1* (**Supplementary Figure 1A**), another is at the end of ORF of *REP2* (**Supplementary Figure 1B**). The CRISPR/Cas9 plasmid pCasRAF1 and pCasREP2 were constructed for each target described above. Each of two plasmids encoded both the RNA-guided endonuclease Cas9 and the guide RNA (gRNA) of corresponding (see **Supplementary Figure 2**). The centromeric plasmid pRS416 was used as the backbone to construct the CRISPR/Cas9 plasmid. Although using multi-copy plasmid such as pRS426 might increase the efficiency of genome or plasmid editing and had been successfully applied for multi-genes disruption (Jakounas et al., 2015; Lian et al., 2018), the recombination between pRS426 and endogenous 2μ plasmid through FRT sites by FLP1 was not desired during the plasmid editing process.

In order to facilitate the introduction of foreign DNA and characterize the modified 2μ plasmid, we designed two donor plasmids pDonorRAF1 and pDonorREP2. The vector composed

of backbone of pSB1C3, *KanMX6* for selection, RFP (Red fluorescent protein) cassette as reporter, homologous arms and a terminator (**Figure 1**). Different from common genome editing by CRISPR/Cas9 system, *KanMX6* is necessary selective marker for editing the wild type 2μ plasmid, because there is no essential gene on it. The terminator would help to finish the transcription of *RAF1* or *REP2* which might be influenced by inserted DNA. RFP cassette was used for characterization of the modified 2μ plasmid and two *Bsa*I restriction endonuclease sites flanked by RFP were designed for substitute RFP cassette by other gene of interest. After linearized by *Pme*I, the donor plasmid pDonorRAF1 or pDonorREP2 was co-transformed with their corresponding CRISPR/Cas9 system plasmid (pCasRAF1 or pCasREP2) into host CEN.PK2-1C. After plasmid editing and recombination, the strain Sc382 (harboring recombinant plasmid pE2μRAF1) and Sc438 (harboring recombinant plasmid pE2μREP2) were constructed (see **Figure 1C**).

Take the construction of Sc382 for example, we randomly picked 36 single colonies for verification by colony PCR. Among them, 22 colonies (about 61.1%) were successfully transformed by linearized DNA. And no wild type endogenous 2μ plasmid remained in these colonies. The yeast plasmids extracted from strain Sc438 and Sc382 could be successfully transformed to *E. coli* and obtain the plasmid pE2μRAF1 and pE2μREP2. The sequencing result of the 2μ related part of pE2μRAF1 and pE2μREP2 were consistent with reported endogenous 2μ plasmid of CEN.PK113-7D (GenBank: CP025735.1) (Piroon et al., 2018), and the editing process was further proved to be successful.

Although CRISPR/Cas9 system has been successfully applied in genome editing, it was the first attempt to edit the multi-copy plasmid. Comparing with the efficiency of genome editing which was almost 100% (Jakounas et al., 2015; Generoso et al., 2016), the efficiency of multi-plasmid editing was not as high as that. Multi-copy target sequences and the special amplification system of endogenous 2μ plasmid (Gnügge and Rudolf, 2017) made the work of CRISPR/Cas9 system not easy. Some strategies for optimization CRISPR/Cas9 system increasing might be helpful for increasing the efficiency of 2μ plasmid editing, such as increasing activity of cleavage by using Cas9 variants (Bao et al., 2014), changing the promoter for optimization of gRNA expression (Gao and Zhao, 2013), and facilitating gRNA-transient expression system (Easmin et al., 2019). Anyway, the method for plasmid editing applied in this work had been proved to be viable and successful to insert the target DNA element into the pE2μ to form a new recombinant multi-copy plasmid and eliminate the original pE2μ plasmid.

Characterization of the Plasmids From pE2μ Multi-Copy System

To characterize the property of pE2μ, we chose pC2μ plasmid pRS425RK as a control. pRS425RK was constructed based on conventional 2μ plasmid pRS425. RFP cassette and KanMX6 of pRS425RK were used for characterization. The strain Sc534 which harboring pRS425RK was constructed. We evaluated the stability of Sc382 and Sc438 compared with control strain

Sc534 by plasmid stability assay. The strains were culture in YPD media without selective pressure and were transferred to fresh media every 5 generation. The fluorescence at single cell level was measured at 5, 10, 20, and 30 generation (**Figure 2**). Under condition with selective pressure (at 0 generation), the cells of the strains with pE2μ (Sc382 and Sc438) showed less cell-to-cell variation (smaller CV %) than that with pRS425RK (Sc534) (**Figure 2A**). The average fluorescence of strains Sc438 and Sc382 was also 3.42 to 3.67-fold higher than that with pRS425RK (**Supplementary Figure 3**). The cell growth of Sc382 and Sc438 higher than that of Sc534 after 48 h fermentation in condition with selective pressure (**Figure 2C**). The PCN of Sc382 (pE2μRAF1) achieved 10.4 and was about 1.67-fold higher than that of Sc534, while the average PCN of Sc438 (pE2μREP2) was 10.8 copies and also higher than that of Sc534 (**Figure 2D**).

After culturing in the condition without selective pressure, all the strains began to lose the plasmid. Nearly 94% cells of the Sc534 (pRS425RK) lost their plasmid after culture of 10 generation and hardly to find cells with plasmid after 20 generation. The frequency of plasmid lost is lower at strain Sc382 and Sc438. Only about 20–23% of the cells lost their plasmid before 10 generation, but 88–89% of the cells had lost their plasmid until 30 generation (**Figure 2B**). There was no significant difference in PCN and plasmid stability between pE2μRAF1 and pE2μREP2. Although the stability of the strain with pE2μ is higher than the strain with conventional 2μ plasmid, it is much lower than the wild type endogenous 2μ plasmid.

The PCN control system of 2μ plasmid based on *RAF1* and *REP1-REP2* complex could tightly control its copy number (McQuaid et al., 2017; Rizvi et al., 2017a). *REP1-REP2* complex is responsible for stability of plasmid and repression of FLP to control the PCN; *RAF1* could repress the formation of *REP1-REP2* to derepress the expression of *FLP1* to increase the PCN (Rizvi et al., 2017b). The pC2μ is out of this copy number control
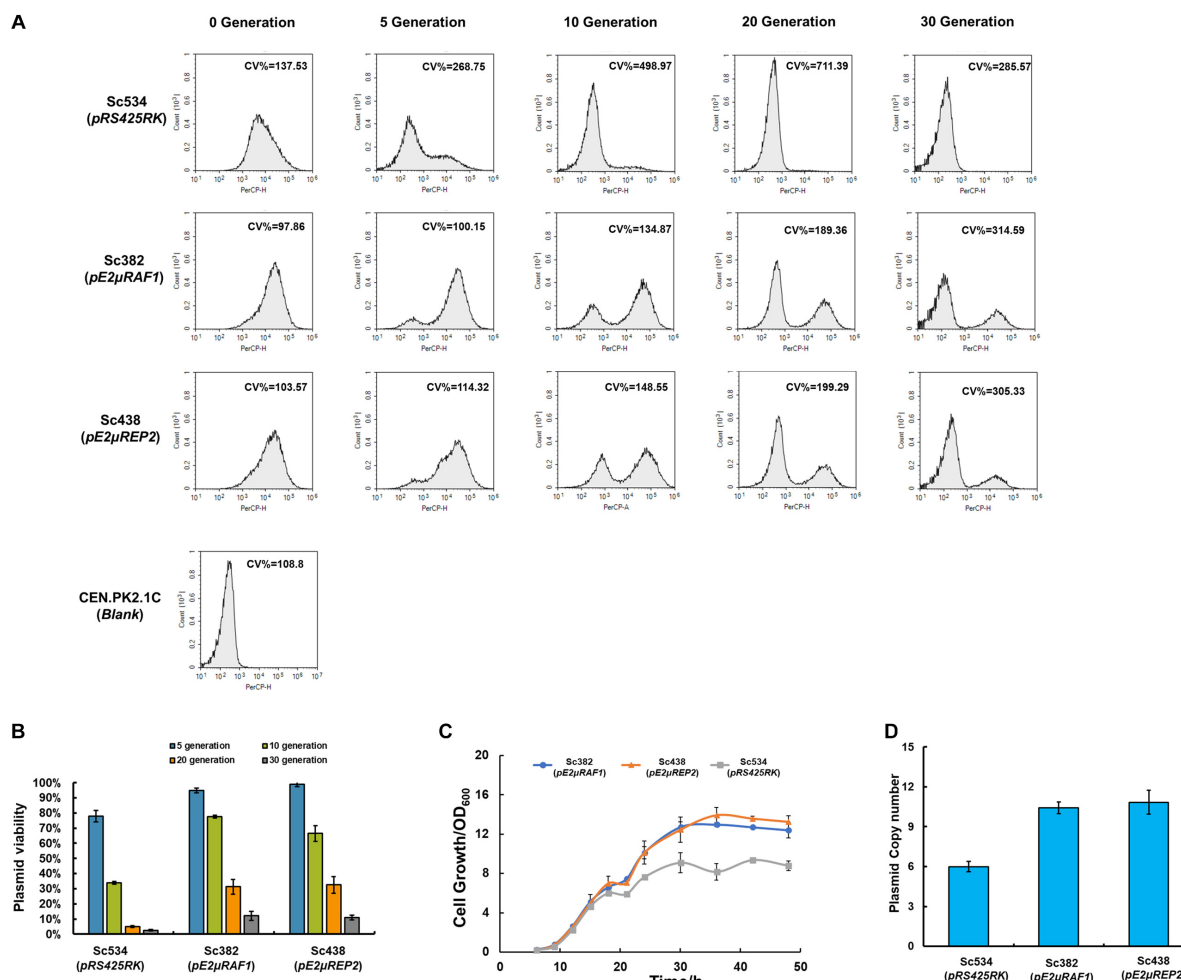
FIGURE 2 | Comparing the strains harboring pC2μ derivate plasmid (pRS425RK) and stains harboring pE2μ derivate plasmid (pE2μRAF1 or pE2μREP2) when carrying RFP expression cassettes. **(A)** Fluorescence at the single-cell analyzed by flow cytometry during cultivation of 30 generations in non-selective YPD medium. Strain CEN.PK2-1C which didn't express RFP was set as the blank. Different plasmids harbored by strain were shown in the bracket. CV %, coefficient of variance. **(B)** Comparison of PCN of different strains in selective YPD+G418 medium (at 0 generation). **(C)** The cell growth of Sc534, Sc438, and Sc382 in selective YPD+G418 medium **(D)** Comparison of plasmid stability assay for strains Sc534, Sc382, and Sc438 in non-selective YPD medium.

system, and difficult to keep the stability and equality even in condition with selective pressure. While, the pE2μ could facilitate the PCN control system to keep its equality of PCN, and is more stable. The insertion of foreign DNA didn't disrupt any known genes on the 2μ plasmid, but it might influence the expression level of these genes or other unknown function transcripts to reduce the stability of 2μ plasmid. In spite of that, pE2μ is might be a better choice than pC2μ plasmid to overexpress the genes of interest by increasing its copy number. Strain Sc382 was chosen as the host for further optimization.

Optimization of pE2μ Multi-Copy System by Auxotrophy Complementation of Essential Gene *TPI1*

The maintenance of the plasmid in the cell is very important for long-term fermentation. To eliminate the plasmid loss of pE2μ in non-selective condition, an auxotroph marker based on essential gene *TPI1* was constructed. Gene *TPI1* encodes triose phosphate isomerase which is required for growth on glucose and makes up about 2% of the soluble cellular protein (Scott and Baker, 1993). The strategy of using essential gene to substitute the one on the chromosome to construct the selective pressure-free system and optimize the plasmid system had been used in *E. coli* (Chen, 2012; Kang et al., 2018). However, fewer studies focused on the optimization of plasmid in *S. cerevisiae*. CRISPR/Cas9 plasmid pCasE2μ was constructed for insertion of *TPI1* into plasmid pE2μRAF1 of strain Sc382. The editing target of pCasE2μ was on the pSB1C3 backbone of pE2μRAF1. After insertion of *TPI1* into pE2μRAF1 (the resulting plasmid was pE2μRT) and deletion of native *TPI1* in chromosome by *his3*, the strain Sc594 was constructed (see **Figure 1C**). For comparison, strain Sc530 which harboring plasmid p425RT (based on pRS425 and containing *TPI1*) and the deletion of the native *TPI1* was constructed. Compared with wild type CEN.PK2-1C, both Sc594 and Sc530 showed similar cell growth for 48 h fermentation in non-selective YPD medium (see **Figure 3B**). The plasmid viability of both strains was evaluated by a very long-term cultivation (90 generation) without any selective pressure in YPD medium. For both strains, the viability was nearly 100% (see **Figure 3D**), and no plasmid-free cell was found at 90 generation, all cells plated on YPD plate were expressing RFP (see **Supplementary Figure 4A**). *TPI1* was the key enzyme for both glycolysis and gluconeogenesis process, cells without *TPI1* are inviable (Giaever et al., 2002). For strain Sc594, after moving the TPI1 from chromosome to plasmid, TPI1 became an auxotrophy selective marker of the plasmid. Since TPI1 is an essential gene, this auxotrophy selective marker have no requirement of the condition, and the plasmid-free cells was inviable. On the contrary, for strain Sc382 or Sc438, the selective marker of their plasmid was KanMX6, the plasmid only could be kept in condition with G418, the cells would lose the plasmid in non-selective YPD medium. Therefore, the plasmid viability of Sc594 or Sc530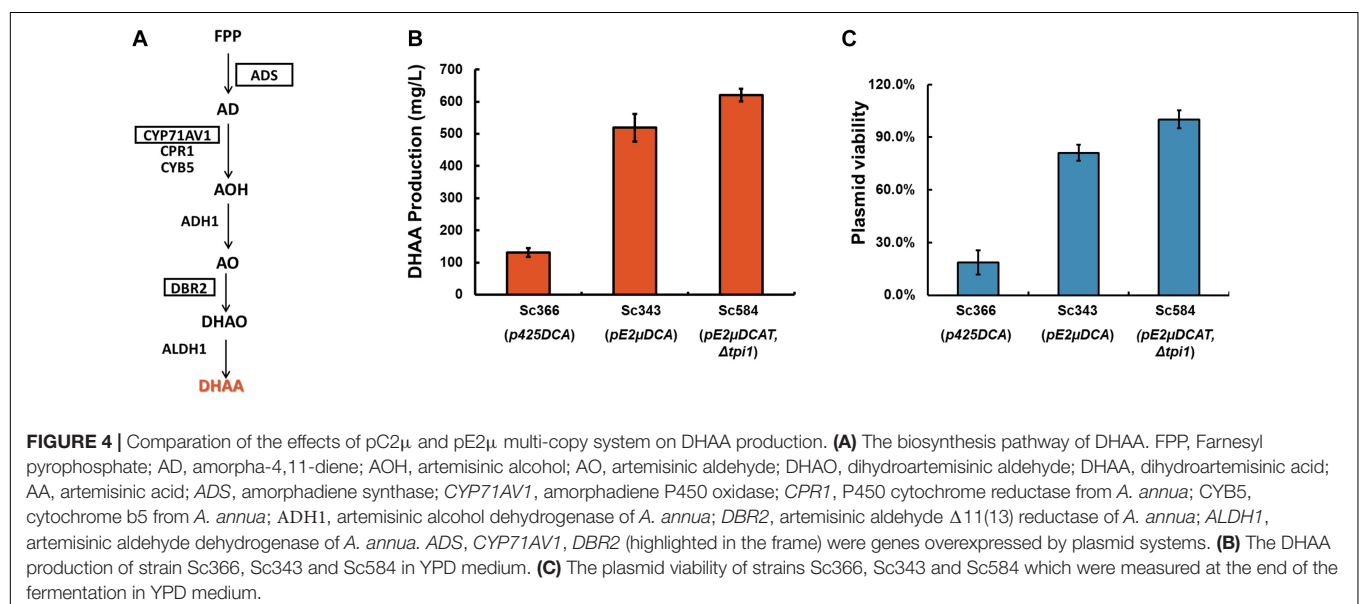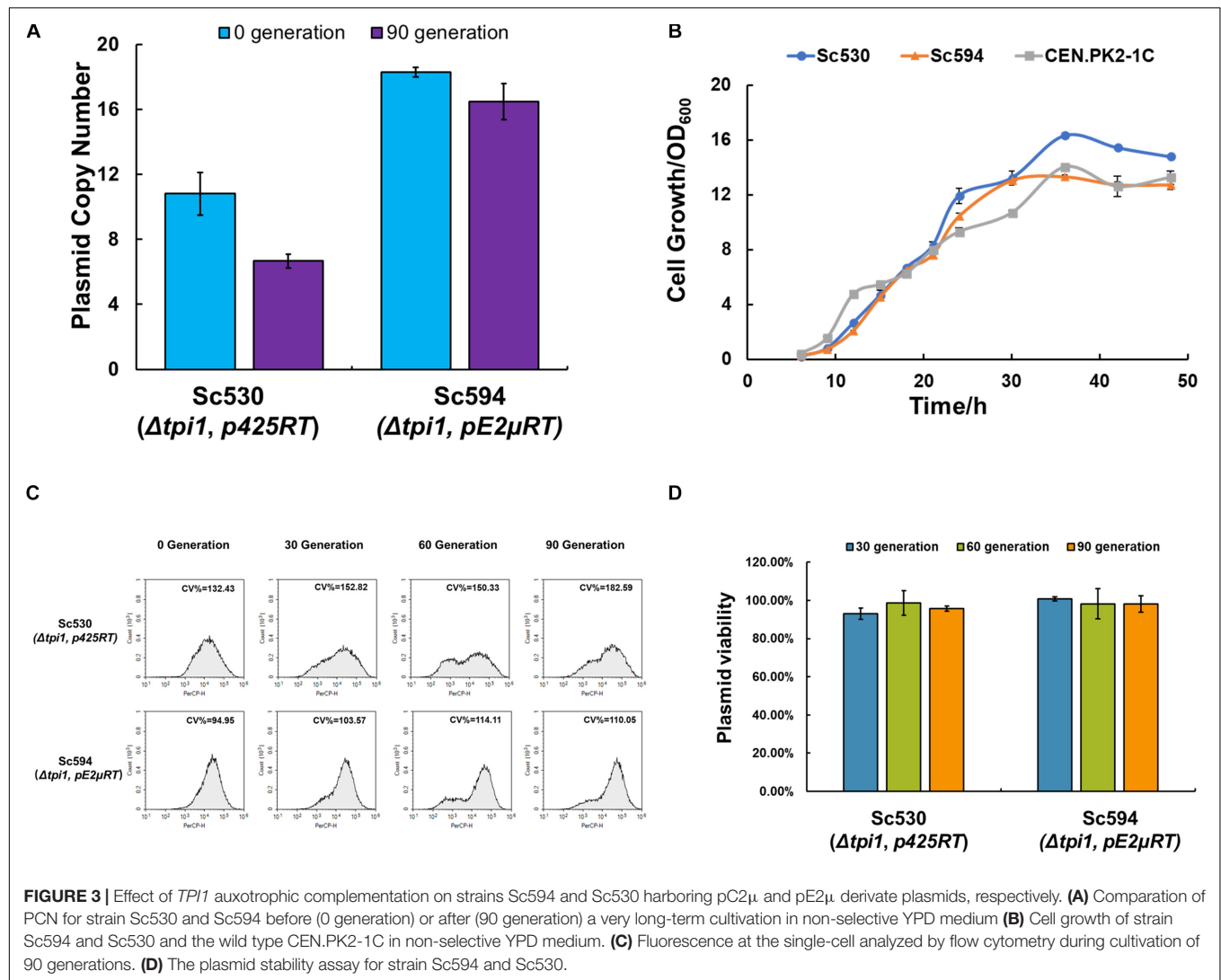 was shown higher than that of Sc382 or Sc438. Optimization of the plasmid by auxotrophy complementation of essential gene *TPI1* could also increase the PCN of both pC2μ and pE2μ derivate plasmid. The PCN of pE2μRT in

Sc594 achieved to about 18.3 and was 1.76-fold higher than that of pE2μRAF1 in Sc382 at 0 generation; while the PCN of p425RT in Sc530 was also increased to 10.8 and was 1.80-fold higher than that of pRS425RK in Sc534 (**Figure 3A**). During the long-term cultivation in non-selective medium, the pE2μ derivate plasmid showed higher stability in PCN and less cell-to-cell variation comparing with pC2μ derivate plasmid. The CV% of Sc530 was increased by 37% from 132.32 (0 generation) to 182.59 (90 generation) (**Figure 3C**) and the average PCN of p425RT decreased by 38.2% to 6.67 (**Figure 3A**); While CV % of Sc594 was only increased by 15.90% from 94.95 to 110.05 (90 generation) and lower than that of Sc530 in any generations (see **Figure 3B**). The average PCN of pE2μRT only decreased by 8.74% to 16.7 after cultivation of 90 generation in non-selective medium (see **Figure 3A**), the average expression level of the RFP in Sc594 was obviously higher than that of Sc530 (**Supplementary Figure 4B**). The stability of the expression for the target gene using optimized pE2μ multi-copy system was proved to undergo very long-term cultivation. The strategy of introduction of *TPI1* into plasmid to substitute the native *TPI1* was proved to optimize both pC2μ derivate plasmid and pE2μ derivate plasmid. And the resulting plasmid pE2μRT showed higher PCN and less cell-to-cell variations. Therefore, pE2μRT was thought to be better choice for overexpression of target genes in high copy.

Application pE2μ Multi-Copy System for DHAA Production

To demonstrate pE2μ could be applied for optimization of metabolic pathway, dihydroartemisinic acid (DHAA) biosynthesis was chosen as an example. DHAA is the precursor of the anti-malaria drug artemisinin (Paddon and Keasling, 2014). The biosynthesis pathways of DHAA (see **Figure 4A**) starts from farnesyl pyrophosphate. In this pathway, *ADS*, *CYP71AV1*, and *DBR2* are the key genes for biosynthesis of DHAA and are thought to be overexpressed in high level to increase the production of DHAA. Several studies about the biosynthesis of DHAA in *S. cerevisiae* had been reported (Yansheng et al., 2008; Chen et al., 2017; Zeng et al., 2020). All of these works facilitated pC2μ based plasmids such as pESC-LEU, pRS425, pYES260 to overexpress the key genes of the biosynthesis pathway. Therefore, pE2μ multi-copy system was thought to be helpful for further enhancing the biosynthesis of DHAA by optimization of the plasmid.

In this work, Sc366 was used as the control strain. Sc366 harbored plasmid p425DCA which was constructed based on pRS425 and contained three key genes *ADS*, *CYP71AV1*, and *DBR2*. Strain Sc343 harbored pE2μ plasmid pE2μDCA which contained *ADS*, *CYP71AV1*, and *DBR2*. And Sc584 was modified from Sc343 by introducing the *TPI1* to pE2μDCA (resulting plasmid was plasmid pE2μDCAT) to substitute the native chromosome *TPI1*. In non-selective rich medium (YPD medium), nearly 82% cells of Sc366 lost their plasmid during the fermentation (see **Figure 4C**), the production of DHAA was only 131.0 mg/L (**Figure 4B**); For strain Sc343 which harbored plasmid pE2μDCA, only 29.8% of cells lost their plasmid, and

FIGURE 3 | Effect of *TPI1* auxotrophic complementation on strains Sc594 and Sc530 harboring pC2μ and pE2μ derivate plasmids, respectively. **(A)** Comparison of PCN for strain Sc530 and Sc594 before (0 generation) or after (90 generation) a very long-term cultivation in non-selective YPD medium **(B)** Cell growth of strain Sc594 and Sc530 and the wild type CEN.PK2-1C in non-selective YPD medium. **(C)** Fluorescence at the single-cell analyzed by flow cytometry during cultivation of 90 generations. **(D)** The plasmid stability assay for strain Sc594 and Sc530.

FIGURE 4 | Comparison of the effects of pC2μ and pE2μ multi-copy system on DHAA production. **(A)** The biosynthesis pathway of DHAA. FPP, Farnesyl pyrophosphate; AD, amorpha-4,11-diene; AOH, artemisinic alcohol; AO, artemisinic aldehyde; DHAO, dihydroartemisinic aldehyde; DHAA, dihydroartemisinic acid; AA, artemisinic acid; *ADS*, amorphadiene synthase; *CYP71AV1*, amorphadiene P450 oxidase; *CPR1*, P450 cytochrome reductase from *A. annua*; CYB5, cytochrome b5 from *A. annua*; ADH1, artemisinic alcohol dehydrogenase of *A. annua*; *DBR2*, artemisinic aldehyde Δ11(13) reductase of *A. annua*; *ALDH1*, artemisinic aldehyde dehydrogenase of *A. annua*. ADS, CYP71AV1, DBR2 (highlighted in the frame) were genes overexpressed by plasmid systems. **(B)** The DHAA production of strain Sc366, Sc343 and Sc584 in YPD medium. **(C)** The plasmid viability of strains Sc366, Sc343 and Sc584 which were measured at the end of the fermentation in YPD medium.

the production achieved to 519.2 mg/L and was 3.96-fold higher than that of strain harboring pC2µ plasmid (**Figures 4B,C**); After optimization with substitution the location of essential *TPI1*, the resulting strain Sc584 didn't lose the plasmid, and got higher production to 620.9 mg/L. The average copy number of Sc366, Sc343, and Sc584 was 3.33, 6.57, and 9.32, respectively (**Supplementary Figure 5**). The relationship of mRNA levels of the key genes for different strain was consist with the result of average copy number (**Supplementary Figure 6**). Comparing with Sc594, the PCN of Sc584 was decreased by about 44.5%. The plasmid stability might be influenced by the overexpression of CYP71AV1 and CPR1, or the rapid accumulation of AA (artemisinic acid) and DHAA. It was consistent with the result of the work of Amyris (Paddon et al., 2013) which found the effect on the plasmid by overexpression of CYP71AV1 or accumulation of product.

The medium with selective pressure for yeast was auxotrophic synthetic medium or the rich medium. However, the non-selective pressure rich medium such as YPD or YPG would help strain to produce more production even the plasmid was not stable (Ro et al., 2008) during the large scale and long-time fermentation (Wang et al., 2017). In rich medium, approximately half of the proteome mass saved by amino acid could be redirected to protein engaged in translation (Bjrkeroth et al., 2020). It could promote cell growth and might increase the expression of the target gene. Therefore, the optimized pE2µ multi-copy system platform was suitable for *S. cerevisiae* to overexpress target gene in non-selective rich medium with higher PCN and has the patent for optimization of biosynthetic pathway and maximize the biochemical production.

In this work, we developed the toolbox for editing the 2µ plasmid to maintain and increase the copy number of the target gene for all *S. cerevisiae* with or without wild type pE2µ (see **Supplementary Figure 7**). For strain without pE2µ, the plasmid pE2µRAF1 or pE2µREP2 could be used as the backbone directly. The target DNA elements could be inserted into these plasmids *in vitro* or *in vivo*. For strains with wild type pE2µ, the CRISPR/Cas9 plasmid could be used for editing the wild type pE2µ plasmid. And the donor plasmid pDonorRAF1 or pDonorREP2 could be used as the backbone to harbor the target DNA. The example of DHAA production in our work proved that this method could successfully increase the copy number of the target gene. The strain Sc594 was constructed as a convenient chassis for overexpression of the target gene efficiently (**Supplementary Figure 7**). The pE2µRT could also undergo a serial of editing steps to insert the DNA element of interest. During these steps, extra selective marker is not necessary to insert into the plasmid, and the whole editing process of pE2µ is same to the process for editing the genome of chromosome which had been widely used for optimization of *S. cerevisiae*. And higher copy number of the inserted genes could be easily obtained.

Considering the very low loss frequency of wild type pE2µ, the performance of the loss frequency for pE2µRAF1 and pE2µREP2 was unexpected. Although introduction of essential gene *TPI1* to substitute the original *TPI1* on chromosome could eliminate the plasmid-free cells during the long-term cultivation, the reason for the increasing loss of the plasmid leaded by insertion of foreign DNA into wild type pE2µ plasmid was still needed to be studied. The future study might focus on the regulation of the gene or unknown transcript units of pE2µ plasmid and the stability and the copy number of the pE2µ might be further increased.

CONCLUSION

In this work, the endogenous 2µ plasmid had been successfully and perfectly edited by CRISPR/Cas9 system and the donor plasmid. The foreign gene could be inserted to 2µ plasmid in higher copy number for overexpression. The resulting plasmid pE2µ had higher PCN and higher stability than the conventional 2µ based plasmid. In single cell level, the distribution of pE2µ in each cell was more balanced than pC2µ plasmid. Taking these advantages, pE2µ was applied for the heterologous biosynthesis of DHAA, and increased the production titer by 4.73-fold higher than that of control. This study showed the potential of pE2µ for optimization of metabolic pathway by stable and efficiently overexpressing a serial of genes.

DATA AVAILABILITY STATEMENT

The original contributions presented in the study are included in the article/**Supplementary Material**, further inquiries can be directed to the corresponding author.

AUTHOR CONTRIBUTIONS

B-XZ and YW conceived the study as well as participated in strain construction and carried out the molecular genetic studies. B-XZ and W-HX participated in fermentation. Y-JY, M-DY, Y-ZL, and W-HX participated in design and coordination of the study as well as helped to draft the manuscript. YW supervised the whole research and revised the manuscript. All the authors read and approved the final manuscript.

FUNDING

ACKNOWLEDGMENTS

SUPPLEMENTARY MATERIAL

The Supplementary Material for this article can be found online at: https://www.frontiersin.org/articles/10.3389/fmicb.2021.631462/full#supplementary-material

REFERENCES

Bao, Z., Xiao, H., Liang, J., Zhang, L., Xiong, X., Sun, N., et al. (2014). A Homology Integrated CRISPR-Cas (HI-CRISPR) system for one-step multi-gene disruptions in *Saccharomyces cerevisia*. *Acs Synthetic Biol.* 4, 585–594. doi: 10.1021/sb500255k

Bjrkeroth, J., Campbell, K., Malina, C., Yu, R., and Nielsen, J. (2020). Proteome reallocation from amino acid biosynthesis to ribosomes enables yeast to grow faster in rich media. *Proc. Natl. Acad. Sci. U.S.A.* 117, 21804–21812. doi: 10.1073/pnas.1921890117

Chai, F., Wang, Y., Mei, X., Yao, M., Chen, Y., Liu, H., et al. (2017). Heterologous biosynthesis and manipulation of crocetin in *Saccharomyces cerevisiae*. *Microb. Cell Fact.* 16:54.

Chen, R. (2012). Bacterial expression systems for recombinant protein production: E. coli and beyond. *Biotechnol. Adv.* 30, 1102–1107. doi: 10.1016/j.biotechadv.2011.09.013

Chen, X., Zhang, C., and Too, H. P. (2017). Multienzyme biosynthesis of dihydroartemisinic acid. *Molecules* 22:1422. doi: 10.3390/molecules22091422

Christianson, T. W., Sikorski, R. S., Dante, M., Shero, J. H., and Hieter, P. (1992). Multifunctional yeast high-copy-number shuttle vectors. *Gene* 110, 119–122. doi: 10.1016/0378-1119(92)90454-w

Easmin, F., Hassan, N., Sasano, Y., Ekino, K., Taguchi, H., and Harashima, S. (2019). gRNA-transient expression system for simplified gRNA delivery in CRISPR/Cas9 genome editing. *J. Biosci. Bioeng.* 128, 373–378. doi: 10.1016/j.jbiosc.2019.02.009

Entian, K. D., and Ktter, P. (2007). 25 yeast genetic strain and plasmid collections. *Methods Microbiol.* 36, 629–666. doi: 10.1016/s0580-9517(06)36025-4

Futcher, A. B. (1986). Copy number amplification of the 2 micron circle plasmid of *Saccharomyces cerevisiae*. *J. Theor. Biol.* 119, 197–204. doi: 10.1016/s0022-5193(86)80074-1

Gao, Y., and Zhao, Y. (2013). Self- processing of ribozyme- flanked RNAs into guide RNAs in vitro and in vivo for CRISPR- mediated genome editing. *J. Integr. Plant Biol.* 56, 343–349. doi: 10.1111/jipb.12152

Generoso, W. C., Gottardi, M., Oreb, M., and Boles, E. (2016). Simplified CRISPR-Cas genome editing for *Saccharomyces cerevisiae*. *J. Microbiol. Methods* 127, 203–205. doi: 10.1016/j.mimet.2016.06.020

Giaever, G., Chu, A. M., Ni, L., Connelly, C., Riles, L., Véronneau, S., et al. (2002). Functional profiling of the *Saccharomyces cerevisiae* genome. *Nature* 418, 387–391. doi: 10.1038/nature00935

Gnügge, R., and Rudolf, F. (2017). *Saccharomyces cerevisiae* Shuttle vectors. *Yeast* 34, 205–221.

Jakounas, T., Sonde, I., Herrgard, M., Harrison, S. J., and Keasling, J. D. (2015). Multiplex metabolic pathway engineering using CRISPR/Cas9 in *Saccharomyces cerevisiae*. *Metab. Eng.* 28, 213–222. doi: 10.1016/j.ymben.2015.01.008

Kang, C. W., Gyu, L. H., Yang, J., Hyun, N. M., Woo, S. S., and Yeol, J. G. (2018). Synthetic auxotrophs for stable and tunable maintenance of plasmid copy number. *Metab. Eng.* 48, 121–128. doi: 10.1016/j.ymben.2018.05.020

Karim, A. S., Curran, K. A., and Alper, H. S. (2013). Characterization of plasmid burden and copy number in *Saccharomyces cerevisiae* for optimization of metabolic engineering applications. *Fems Yeast Res.* 13, 107–116. doi: 10.1111/1567-1364.12016

Lee, C., Kim, J., Shin, S. G., and Hwang, S. (2006). Absolute and relative QPCR quantification of plasmid copy number in *Escherichia coli*. *J. Biotechnol.* 123, 273–280. doi: 10.1016/j.jbiotec.2005.11.014

Lian, J., Bao, Z., Hu, S., and Zhao, H. (2018). Engineered CRISPR/Cas9 system for multiplex genome engineering of polyploid industrial yeast strains. *Biotechnol. Bioeng.* 115, 1630–1635. doi: 10.1002/bit.26569

Lian, J., Jin, R., and Zhao, H. (2016). Construction of plasmids with tunable copy numbers in *Saccharomyces cerevisiae* and their applications in pathway optimization and multiplex genome integration. *Biotechnol. Bioeng.* 113, 2462–2473. doi: 10.1002/bit.26004

McQuaid, M. E., Pinder, J. B., Arumuggam, N., Lacoste, J. S. C., Chew, J. S. K., and Dobso, M. J. (2017). The yeast 2-μm plasmid Raf protein contributes to plasmid inheritance by stabilizing the Rep1 and Rep2 partitioning proteins. *Nucleic Acids Res.* 45, 10518–10533. doi: 10.1093/nar/gkx703

Mignon, C., Sodoyer, R., and Werle, B. (2015). Antibiotic-free selection in biotherapeutics: now and forever. *Pathogens* 4:157. doi: 10.3390/pathogens4020157

Misumi, Y., Nishioka, S., Fukuda, A., Uemura, T., Nakamura, M., Hoshida, H., et al. (2019). YHp as a highly stable, hyper-copy, hyper-expression plasmid constructed using a full 2−μm circle sequence in cir0 strains of *Saccharomyces cerevisiae*. *Yeast* 36, 249–257. doi: 10.1002/yea.3371

Paddon, C. J., and Keasling, J. D. (2014). Semi-synthetic artemisinin: a model for the use of synthetic biology in pharmaceutical development. *Nat. Rev. Microbiol.* 12:355. doi: 10.1038/nrmicro3240

Paddon, C. J., Westfall, P. J., Pitera, D. J., Benjamin, K., Fisher, K., McPhee, D., et al. (2013). High-level semi-synthetic production of the potent antimalarial artemisinin. *Nature* 496, 528–532. doi: 10.1038/nature12051

Piroon, J., Thidathip, W., Rui, P., Preecha, P., Ussery, D. W., Jens, N., et al. (2018). Complete genomic and transcriptional landscape analysis using third-generation sequencing: a case study of *Saccharomyces cerevisiae* CEN.PK113-7D. *Nucleic Acids Res.* 46:e38. doi: 10.1093/nar/gky014

Rizvi, S. M. A., Prajapati, H. K., and Ghosh, S. K. (2017a). The 2 micron plasmid: a selfish genetic element with an optimized survival strategy within *Saccharmyces cerevisiae*. *Curr. Genet.* 64, 25–42. doi: 10.1007/s00294-017-0719-2

Rizvi, S. M. A., Prajapati, H. K., Nag, P., and Ghosh, S. K. (2017b). The 2-μm plasmid encoded protein Raf1 regulates both stability and copy number of the plasmid by blocking the formation of the Rep1–Rep2 repressor complex. *Nucleic Acids Res.* 45, 7167–7179. doi: 10.1093/nar/gkx316

Ro, D.-K., Ouellet, M., Paradise, E. M., Burd, H., Eng, D., Paddon, C. J., et al. (2008). Induction of multiple pleiotropic drug resistance genes in yeast engineered to produce an increased level of anti-malarial drug precursor, artemisinic acid. *BMC Biotechnol.* 8:83. doi: 10.1186/1472-6750-8-83

Scott, E. W., and Baker, H. V. (1993). Concerted action of the transcriptional activators REB1, RAP1, and GCR1 in the high-level expression of the glycolytic gene TPI. *Mol. Cell Biol.* 13, 543–550. doi: 10.1128/mcb.13.1.543

Wang, R., Gu, X., Yao, M., Pan, C., Liu, H., Xiao, W., et al. (2017). Engineering of beta-carotene hydroxylase and ketolase for astaxanthin overproduction in *Saccharomyces cerevisiae*. *Front. Chem. Sci. Eng.* 11:89–99. doi: 10.1007/s11705-017-1628-0

Xie, Z. X., Mitchell, L. A., Liu, H. M., Li, B. Z., Liu, D., Agmon, N., et al. (2018). Rapid and Efficient CRISPR/Cas9-based mating-type switching of *Saccharomyces cerevisiae*. *G3 (Bethesda)* 8, 173–183. doi: 10.1534/g3.117.300347

Yansheng, Z., Teoh, K. H., Reed, D. W., Lies, M., Alain, G., Olson, D. J. H., et al. (2008). The molecular cloning of artemisinic aldehyde Delta11(13) reductase and its role in glandular trichome-dependent biosynthesis of artemisinin in Artemisia annua. *J. Biol. Chem.* 283:21501. doi: 10.1074/jbc.m803090200

Zeng, B.-X., Yao, M.-D., Wang, Y., Xiao, W.-H., and Yuan, Y.-J. (2020). Metabolic engineering of *Saccharomyces cerevisiae* for enhanced dihydroartemisinic acid production. *Front. Bioeng. Biotechnol.* 8:152. doi: 10.3389/fbioe.2020.00152

p-Terphenyls From *Aspergillus* sp. GZWMJZ-055: Identification, Derivation, Antioxidant and α-Glycosidase Inhibitory Activities

Yanchao Xu[1,2,3†], Yong Wang[1,2,3†], Dan Wu[1,3], Wenwen He[1,3], Liping Wang[1,2,3*] and Weiming Zhu[1,4*]

[1] State Key Laboratory of Functions and Applications of Medicinal Plants, Guizhou Medical University, Guiyang, China, [2] School of Pharmaceutical Sciences, Guizhou Medical University, Guiyang, China, [3] Key Laboratory of Chemistry for Natural Products of Guizhou Province, Chinese Academy of Sciences, Guiyang, China, [4] Laboratory for Marine Drugs and Bioproducts, Pilot National Laboratory for Marine Science and Technology, School of Medicine and Pharmacy, Ocean University of China, Qingdao, China

One new (**1**) and fifteen known (**2–16**) *p*-terphenyls were isolated from a solid culture of the endophytic fungus *Aspergillus* sp. GZWMJZ-055 by adding the leaves of its host *Eucommia ulmoides*. Furthermore, nine *p*-terphenyls (**17–25**) were synthesized from the main compounds (**5–7**), among which derivatives **18**, **19**, **21**, **22**, and **25** are new *p*-terphenyls. Compounds **15** and **16** were also, respectively, synthesized from compounds **6** and **7** by oxidative cyclization of air in the presence of silica gel. These *p*-terphenyls especially those with 4,2′,4″-trihydroxy (**4–7**, **20**, **21**) or 4, 4″-dihydroxy-1,2,1′,2′-furan (**15**, **16**) substituted nucleus, exhibited significant antioxidant and α-glucosidase inhibitory activities and lower cytotoxicity to caco-2 cells. The results indicated their potential use as lead compounds or dietary supplements for treating or preventing the diabetes.

Keywords: endophytic fungus, *Aspergillus* sp., antioxidant activity, α-glucosidase inhibition, *Eucommia ulmoides*

INTRODUCTION

Diabetes is a chronic metabolic disease characterized by high blood sugar (HBS). Long-term HBS causes the damage to blood vessels and endangers various organs such as the heart, brain, kidneys, peripheral nerves, and eyes, and thus seriously affects the life quality of patients. Studies show that oxidative stress may be one of the important causes for diabetes and its complications. Too much reactive oxygen species in the body will increase the maturation disorder and apoptosis of pancreatic β-cells, leading to decrease insulin synthesis and secretion. Hyperglycemia and hyperlipidemia in diabetic patients can promote the production of active oxides, causing oxidative stress, then oxidative stress and hyperglycemia promote each other, leading to a vicious circle (Karunakaran and Park, 2013). At present, the treatment of type 2 diabetes is based on oral drugs, mainly containing metformin, α-glucosidase inhibitors, dipeptidyl peptidase IV inhibitors, and

sodium-glucose cotransporter 2 inhibitors. Among them, α-glucosidase inhibitors can inhibit the degradation of polysaccharides to glucose and delay the absorption of glucose in the small intestine to reduce blood sugar. Such drugs can effectively reduce postprandial hyperglycemia without causing symptoms of hypoglycemia and are highly beneficial to patients who use carbohydrates as their main source of calories.

The α-glucosidase inhibitors, such as acarbose, miglitol, and voglibose currently used clinically are all microbial metabolites or their derivatives. Therefore, discovery of the new α-glucosidase inhibitors from microbial natural products (NPs) has unique advantages. *p*-Terphenyls, as an important kind of fungal NPs, its chemical investigation could be dated back to 1877 (Liu, 2006). At present, over 230 *p*-terphenyls have been isolated from fungi and lichens (Li et al., 2018). In addition, some *p*-terphenyl derivatives were also total synthesized (Yonezawa et al., 1998; Takahashi et al., 2017; Zhang et al., 2018). As reported, *p*-terphenyls had a broad spectrum of biological properties, such as cytotoxic (Wang et al., 2019, 2020), antimicrobial (Intaraudom et al., 2017), and phosphodiesterase inhibitory (El-Elimat et al., 2013) activities, but the most interesting bioactivities were antioxidative (Kuhnert et al., 2015) and α-glucosidase inhibitory activities (Ma et al., 2014). Furthermore, *p*-terphenyls can also be isolated from edible mushroom (Liu et al., 2004; Ma et al., 2014; Wang et al., 2014), indicating that this kind of compounds have low toxicity in the human body and are very suitable for the research of anti-diabetic drugs.

During our research for new compounds with α-glucosidase inhibitory activity from the plant endophytes, we isolated and identified a *p*-terphenyls-producing strain, *Aspergillus* sp. GZWMJZ-055 endophytic with the famous Chinese medical plant *Eucommia ulmoides*. The fermentation potency (5.3–9.5 g/kg) and the α-glucosidase inhibitory activity (IC_{50} 15.0 to 2.0 μg/mL) of the ethyl acetate (EtOAc) extracts of the fermentation significantly increased after adding the leaves of *Eucommia ulmoides* to the culture medium (**Figure 1**). Chemical investigation led to the isolation of sixteen *p*-terphenyls, including the new 3-*O*-methyl-4″-deoxyterprenin (**1**) as well as the known 4-deoxyterphenyllin (**2**) (Lin et al., 2019), 4″-deoxy-2′-methoxyterphenyllin (**3**) (Shan et al., 2019), 5′-methoxy-[1,1′:4′,1″-terphenyl]-2′,3′,4,4″-tetraol (**4**) (Zhang et al., 2018), terphenyllin (**5**) (Kamigauchi et al., 1998), 3-hydroxyterphyllin (**6**) (Liu et al., 2012), 3,3″-dihydroxyterphyllin (**7**) (Liu et al., 2012), 4″-deoxyterphenyllin (**8**) (Shan et al., 2019), 4″-deoxy-3-hydroxyterphenyllin (**9**) (Wang et al., 2020), 3′-*O*-methylterphenyllin (**10**) (Yan et al., 2017), 4″-deoxyprenylterphenyllin (**11**) (Wei et al., 2007), prenylterphenyllin A (**12**) (Cai et al., 2011), 3-methoxyterprenin (**13**) (Kamigauchi et al., 1998), 4″-deoxycandidusin A (**14**) (Guo et al., 2012), candidusin A (**15**) (Wang et al., 2020), and candidusin B (**16**) (Liu et al., 2012; **Figure 2**). Compounds **15** and **16** were also, respectively, prepared from compounds **6** and **7** by an intramolecular oxidative cyclization of air catalyzed by silica gel (**Scheme 1**). In addition, nine *p*-terphenyls (**17–25**) were synthesized from the main NPs (**5–7**) (**Scheme 1**), among which derivatives **18**, **19**, **21**, **22**, and **25** are new *p*-terphenyls. These

p-terphenyls showed antioxidant and α-glycosidase inhibitory activities (**Table 1**).

MATERIALS AND METHODS

General Experimental Procedures

UV spectra were measured on a Waters 2487 dual λ absorbance detector. IR spectra were recorded on a Nicolet Nexus 470 spectrophotometer as KBr disks. ^{1}H, ^{13}C NMR and 2D NMR spectra were recorded on Bruker-600 MHz using TMS as an internal standard. ESIMS and HR-ESIMS analysis were carried out on Waters Xevo TQS and Agilent Technologies 6530 Accurate-Mass Q-TOF LC/MS, respectively. Column chromatography was performed on silica gel (200–300 mesh; Qingdao Puke Parting Materials Co., Ltd., China), Sephadex LH-20 (Amersham Biosciences, Uppsala, Sweden), silica gel H, and plates precoated with silica gel GF254 (Qingdao Puke Parting Materials Co., Ltd., China), respectively. HPLC separation was performed on HITACHI Primaide with an ODS column (YMC-pack ODS-A, 10 mm × 250 mm, 5 μm, 4 mL/min). Synthetic compounds were also purified using a SepaBean machine equipped with SepaFlash columns (Santai Technologies Inc., China).

Fungal Material

The fungus *Aspergillus* sp. GZWMJZ-055 was isolated from the leaves of *Eucommia ulmoides* collected from Guiyang Medicinal Botanical Garden and was determined as *Aspergillus* sp. by the phylogenetic tree (**Supplementary Figure 1**) of the ITS sequence (GenBank No. KY038594). The strain was deposited in Guiyang laboratory in 20% glycerol at −80°C.

Cultural Media

The working strain was prepared on PDA agar medium, containing 20% potato, 2.0% glucose, 2.0% agar, and 1 L tap water. The seed medium contained 2.0% maltose, 2.0% mannitol, 1.0% glucose, 1.0% sodium glutamate, 0.3% yeast extract, 0.1% corn extract, 0.1% KH_2PO_4, 0.05% $MgSO_4 \cdot 7H_2O$, 1 L tap water. The solid fermentation medium was prepared from 100 g rice, 1 g dry leaves of *Eucommia ulmoides* and 120 mL distilled water in a 1000-mL Erlenmeyer flask.

Fermentation, Extraction and Isolation

The fungal strain GZWMJZ-055 was cultured on PDA at 28°C for 3 days to prepare the seed culture. Spores were incubated at 28°C for 2 days, a rotary shaker with shaking at 120 rpm in a 500 mL cylindrical flask containing 150 mL seed medium. The seed medium (5 mL) was added to the above rice fermentation medium in a 1000-mL Erlenmeyer flask. Totally, 100 Erlenmeyer flasks were incubated at room temperature (rt) under static conditions for 30 days. The cultures were then extracted by ethyl acetate (EtOAc) (500 mL for each) three times and the combined EtOAc extracts were dried *in vacuo* until constant weigh to yield 423.5 g of EtOAc extract.

The EtOAc extract (423.5 g, adsorbed in 500 g 100–200 mesh silica gel) was chromatographed on a silica gel (2 kg, 200–300
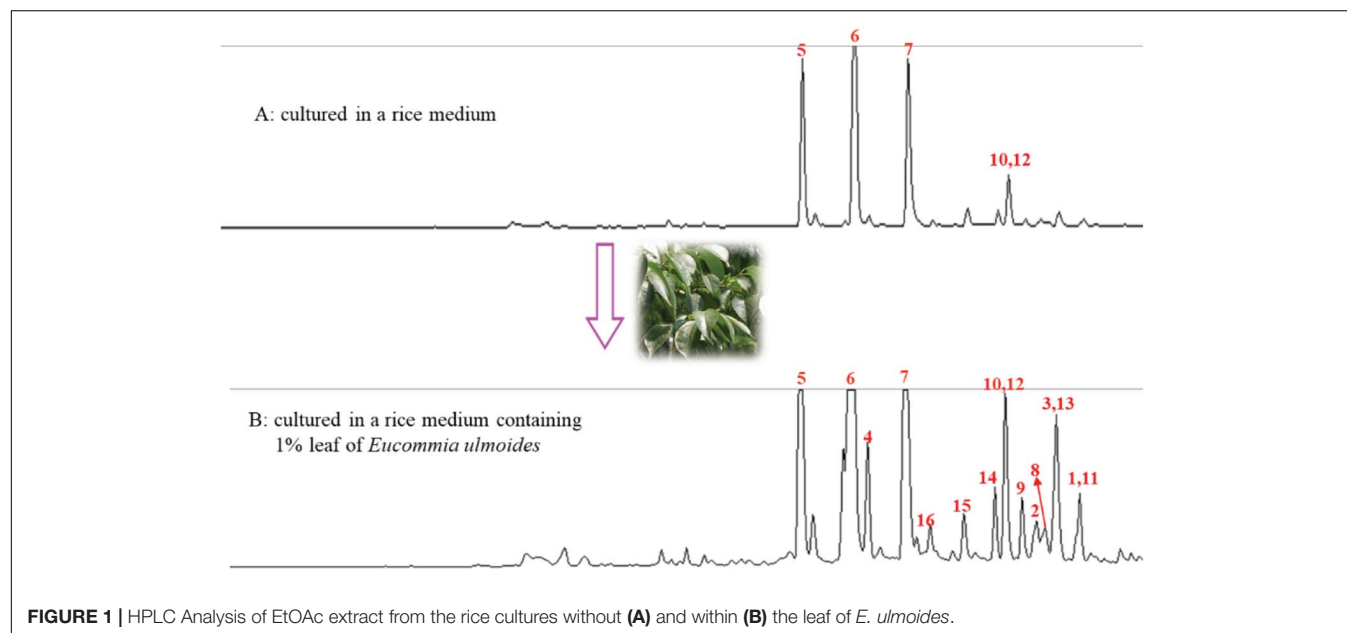
FIGURE 1 | HPLC Analysis of EtOAc extract from the rice cultures without **(A)** and within **(B)** the leaf of *E. ulmoides*.

1: R= H, **13**: R= OH

14: $R_1=R_2=$ H
15: $R_1=$ H, $R_2=$ OH
16: $R_1=R_2=$ OH

2: $R_1=R_2=R_3=R_5=$ H, $R_4=$ Me, $R_6=$ OH
3: $R_1=R_5=R_6=$ H, $R_2=$ OH, $R_3=R_4=$ Me
4: $R_1=R_3=R_4=R_5=$ H, $R_2=R_6=$ OH
5: $R_1=R_3=R_5=$ H, $R_2=R_6=$ OH, $R_4=$ Me
6: $R_1=R_2=R_6=$ OH, $R_3=R_5=$ H, $R_4=$ Me
7: $R_1=R_2=R_5=R_6=$ OH, $R_3=$ H, $R_4=$ Me
8: $R_1=R_3=R_5=R_6=$ H, $R_2=R_4=$ Me
9: $R_1=R_2=$ OH, $R_3=R_5=R_6=$ H, $R_4=$ Me
10: $R_1=R_5=$ H, $R_2=R_6=$ OH, $R_3=R_4=$ Me
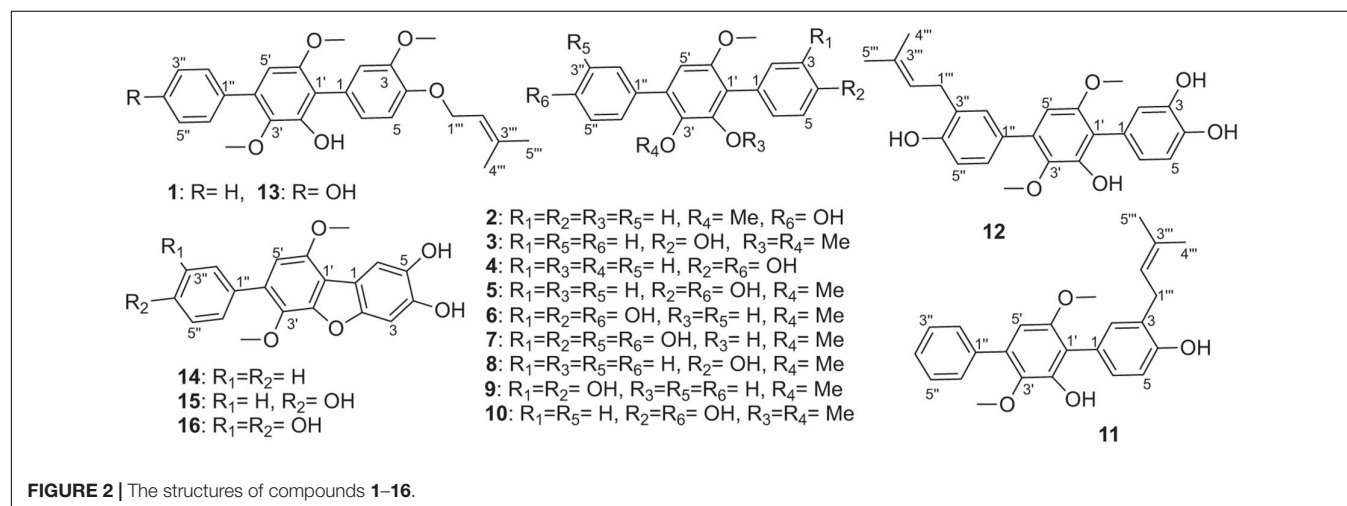
FIGURE 2 | The structures of compounds **1–16**.

mesh) column (10 cm × 100 cm) using step gradient elution of CH_2Cl_2–MeOH (v/v100:0, 100:1, 50:1, 25:1, 10:1, 5:1, 1:1, 1:2, 1:5, and 1:10, each 8 L) to yield fifteen fractions (Fr.1–Fr.15). Fraction 2 (18.7 g, adsorbed in 50 g 100–200 mesh silica gel) was then subjected to a silica gel (400 g, 200–300 mesh) column (6 cm × 61 cm), eluting with CH_2Cl_2–MeOH (100:1, v/v) to afford sixteen subfractions (Fr.2-1∼Fr.2-16). Subfraction Fr.2–3 (1.2 g) was separated with silica gel chromatography eluted by CH_2Cl_2 to yield five fractions (Fr.2-3-1∼Fr.2-3-5). Subfraction Fr.2-3-4 (100.6 mg) was purified by semi-preparative HPLC [80% MeOH/H_2O with 0.15% trifluoroacetic acid (TFA)] to yield compound **1** (17.2 mg, t_R 14.0 min). Fraction 2-7 (2.8 g) was further separated into six subfractions by Sephadex LH-20 eluting with MeOH-CH_2Cl_2 (1:1, v/v). Subfraction 2-7-4 (455.0 mg) was separated with silica gel chromatography eluted by CH_2Cl_2 to yield three fractions (Fr.2-7-4-1∼Fr.2-7-4-3). Subfraction 2-7-5 (58.8 mg) was purified by semi-preparative

HPLC (80% MeOH/H_2O) to yield compound **11** (9.7 mg, t_R13.6 min). Fraction 2-9 (185 mg) was further separated into five subfractions (Fr.2-9-1∼Fr.2-9-5) by Sephadex LH-20 eluting with MeOH-CH_2Cl_2 (1:1, v/v). Subfraction 2-9-3 separated with silica gel chromatography eluted by CH_2Cl_2 to yield five fractions (Fr.2-9-3-1∼Fr.2-9-3-5). Fr.2-9-3-5 was further purified by semi-preparative HPLC (80% MeOH/H_2O) to yield compound **14** (5.6 mg, t_R 7.0 min). Subfraction 2-9-5 was purified by semi-preparative HPLC (70% MeOH/H_2O) to yield compound **12** (6.0 mg, t_R 7.2 min). Fraction 2-13 (240.2 mg) was further separated into fourteen subfractions by Sephadex LH-20 eluting with MeOH-CH_2Cl_2 (1:1, v/v). Subfraction 2-13-10 was further separated into four subfractions separated with silica gel chromatography eluted by MeOH-CH_2Cl_2 (1:80, v/v). Fr.2-13-10-2 was purified by semi-preparative HPLC (75% MeOH/H_2O) to yield compound **3** (12.5 mg, t_R 10.0 min). Subfraction 2-13-13 was purified by semi-preparative HPLC (70% MeOH/H_2O) to
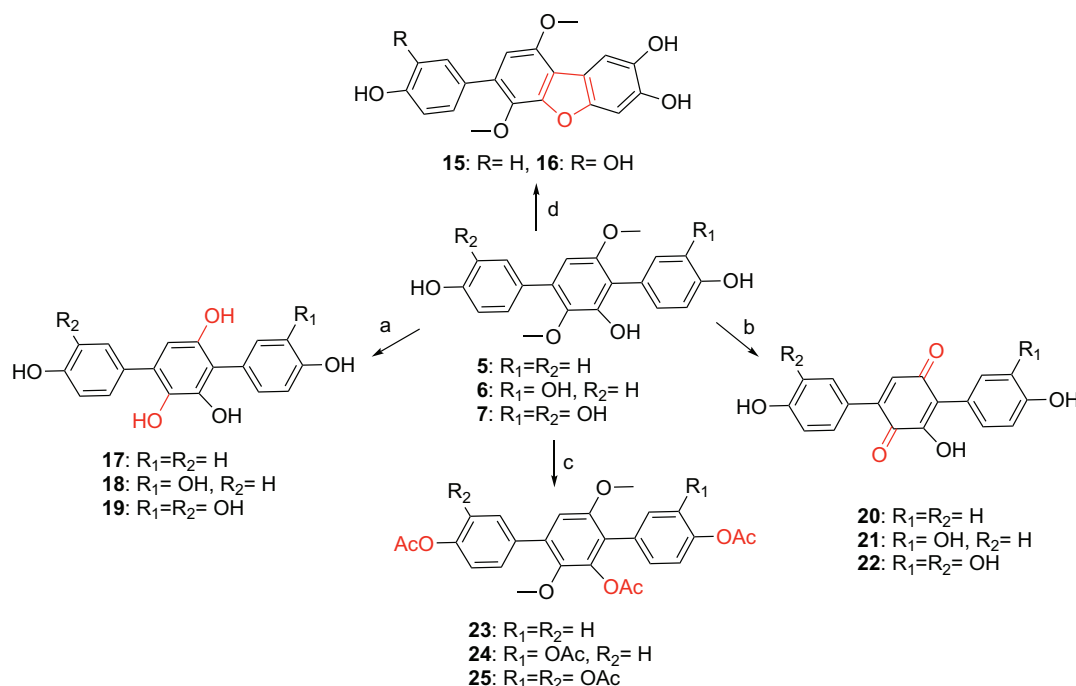
SCHEME 1 | Synthesis of compounds **15–25** from **5** to **7** (a. BBr$_3$/CH$_2$Cl$_2$, −20°C to rt; b. BBr$_3$/CH$_2$Cl$_2$, −20°C to rt, then O$_2$/silica gel/MeOH; c. Ac$_2$O, DMAP, CH$_2$Cl$_2$, 40°C; d. O$_2$/silica gel/MeOH, rt).

yield compound **2** (7.1 mg, t$_R$ 8.7 min). Fraction 2-14 (452.3 mg) was further separated into six subfractions separated with silica gel chromatography eluted by CH$_2$Cl$_2$. Fr.2-14-5 (20.6 mg) was purified by semi-preparative HPLC (80% MeOH/H$_2$O) to yield compound **13** (6.1 mg, t$_R$ 16.0 min). Fraction 9 (3.5 g) was subjected to a silica gel column, elution with step gradient elution of CH$_2$Cl$_2$–MeOH (0–100%, v/v) to afford three subfractions (Fr.9-1∼Fr.9-3). Fraction 9-2 (1.2 g) was further separated into nine subfractions by Sephadex LH-20 eluting with MeOH. Fraction 9-2-3 (418.2 mg) was further separated into seven subfractions separated with silica gel chromatography eluted by MeOH-CH$_2$Cl$_2$ (1:20, v/v). Fraction 9-2-3-2 (20.0 mg) was purified by HPLC on an ODS column (75% MeOH/H$_2$O) to give compound **8** (4.0 mg, t$_R$ 8.0 min). Fraction 9-2-3-5 (26.1 mg) was purified by HPLC on an ODS column (75% MeOH/H$_2$O) to give compound **9** (6.4 mg, t$_R$ 4.5 min). Fraction 9-2-9 (29.7 mg) was purified by HPLC on an ODS column (65% MeOH/H$_2$O) to give compound **15** (6.1 mg, t$_R$ 5.0 min). Fraction 9-3 (1.3 g) was further separated into thirteen subfractions by Sephadex LH-20 eluting with MeOH. Fraction 9-3-7 (317.1 mg) was further separated into nine subfractions separated with silica gel chromatography eluted by MeOH-CH$_2$Cl$_2$ (1:10, v/v). Fraction 9-3-7-4 (10.7 mg) was purified by HPLC on an ODS column (55% MeOH/H$_2$O) to give compound **10** (2.8 mg, t$_R$ 18.2 min). Fraction 9-3-8 was further separated with silica gel chromatography eluted by MeOH-CH$_2$Cl$_2$ (1:15, v/v) to get compound **5** (900 mg). Fraction 9-3-12 (52.7 mg) was purified by HPLC on an ODS column (60% MeOH/H$_2$O) to give compounds **4** (6.6 mg, t$_R$ 10.4 min) and **16** (6.0 mg, t$_R$ 18.0 min). Fraction

10 (2.8 g) was chromatographed on a silica gel column using step gradient elution of CH$_2$Cl$_2$–MeOH (5–100%, v/v) to yield compounds **6** (700 mg) and **7** (1.2 g).

Compound **1**: white powder; UV (MeOH) λ$_{max}$ (log ε) 230 (4.03), 276 (3.96) nm; IR (KBr) ν$_{max}$ 3486, 2934, 1517, 1482, 1461, 1399, 1238, 1117, 1075, 1009, 770, and 703 cm^{-1}; HR ESIMS *m/z* 443.1837 [M+Na]$^+$ (calcd. for C$_{26}$H$_{28}$O$_5$Na, 443.1829) (**Supplementary Figure 2**); ^{1}H and ^{13}C NMR data, see **Table 2** and **Supplementary Figures 3–7**.

Chemical Synthesis Procedures
Synthesis of Compounds 15 and 16
Compound **6** (30 mg, 85 μmol) was dissolved in MeOH (10 mL), and 200–300 mesh silica gel (4 g) was then added to the solution. After the reaction was stirred overnight at rt, the solvent was evaporated. The residue was purified by flash column chromatography (FCC) eluting with EtOAc-CH$_2$Cl$_2$ (v/v 1:5) to give compound **15** (26 mg, 74 μmol, 87% yield) as a light-yellow solid (*R$_f$* 0.4). By the same procedure, compound **16** (24 mg, 65 μmol, 80% yield) was prepared from the reaction of compound **7** (30 mg, 81 μmol) and purified as a light-yellow solid (*R$_f$* 0.4) by FCC eluting with EtOAc-CH$_2$Cl$_2$ (v/v 1:3).

Compound **15**: ^{1}H NMR (600 MHz, DMSO-*d$_6$*) and ^{13}C NMR (150 MHz, DMSO-*d$_6$*) data, see **Supplementary Table 5** and **Supplementary Figures 8, 9**. ESIMS *m/z* 351.0 [M−H]$^-$.

Compound **16**: ^{1}H NMR (600 MHz, DMSO-*d$_6$*) and ^{13}C NMR (150 MHz, DMSO-*d$_6$*) data, see **Supplementary Table 5** and **Supplementary Figures 10, 11**. ESIMS *m/z* 367.1 [M−H]$^-$.

TABLE 1 | Antioxidant and α-glycosidase activities of compounds **1–25**.

Compound	DPPH (IC$_{50}$, μM)	ORAC (μmole TE/μmole)	α-glucosidase (IC$_{50}$, μM)	α-glucosidase in caco-2 (IC$_{50}$, μM)
1	>100	1.0 ± 0.04	>500	–
2	>100	1.2 ± 0.09	239.1 ± 5.9	–
3	>100	2.1 ± 0.5	>500	–
4	1.7 ± 0.02	6.8 ± 0.05	5.9 ± 0.6	–
5	10.9 ± 0.3	6.0 ± 0.09	2.8 ± 0.2	0.38 ± 0.01
6	1.4 ± 0.01	5.7 ± 0.3	10.9 ± 1.3	0.29 ± 0.02
7	1.1 ± 0.03	4.5 ± 0.4	18.3 ± 0.9	0.36 ± 0.01
8	57.8 ± 0.8	0.5 ± 0.01	129.8 ± 3.5	–
9	1.9 ± 0.04	0.5 ± 0.06	464.5 ± 23.6	–
10	>100	0.5 ± 0.03	>500	–
11	1.6 ± 0.01	1.2 ± 0.5	34.4 ± 1.1	–
12	1.6 ± 0.02	1.4 ± 0.01	64.4 ± 1.2	–
13	>100	0.4 ± 0.07	152.5 ± 9.6	–
14	4.0 ± 0.2	0.4 ± 0.06	128.3 ± 2.3	–
15	3.6 ± 0.06	2.1 ± 0.06	13.1 ± 0.2	0.11 ± 0.02
16	3.2 ± 0.1	2.0 ± 0.06	7.9 ± 0.3	0.36 ± 0.01
17	5.3 ± 0.06	4.8 ± 0.3	25.1 ± 0.7	–
18	3.7 ± 0.07	3.7 ± 0.1	25.0 ± 0.8	–
19	1.8 ± 0.04	2.6 ± 0.1	19.4 ± 0.1	–
20	5.9 ± 0.08	6.1 ± 0.2	8.9 ± 0.4	0.11 ± 0.01
21	1.6 ± 0.04	3.9 ± 0.1	4.0 ± 0.08	0.12 ± 0.01
22	1.7 ± 0.02	2.8 ± 0.3	10.1 ± 0.1	–
23	>100	0.1 ± 0.01	>500	–
24	37.8 ± 0.1	0.8 ± 0.07	>500	–
25	11.0 ± 0.1	1.7 ± 0.07	>500	–
VC	2.8 ± 0.03			
Acarbose			265.4 ± 10.2	157.7 ± 14.0

– not tested.

Synthesis of Compounds 17–19

Compound **5** (30 mg, 89 μmol) was dissolved in CH$_2$Cl$_2$ (5 mL), and BBr$_3$ (0.8 mL, 0.54 mmol, 17% in CH$_2$Cl$_2$) was then added at −20°C under the protection of argon. The reaction mixture was warmed up to rt and stirred overnight. The reaction was quenched by adding H$_2$O (20 mL) at 0°C, and EtOAc (200 mL) was then added. The EtOAc phase was washed with H$_2$O (20 mL × 4), dried over anhydrous Na$_2$SO$_4$, and concentrated in vacuo. The residue was purified by semipreparative HPLC eluting with 40% MeOH/H$_2$O containing 0.15% TFA to provide compound **17** (26 mg, 84 μmol, 94% yield, t_R 7.5 min) as an orange solid. By the same procedures, compound **18** (25 mg, 77 μmol, 91% yield, t_R 8 min) was prepared from the reaction of compound **6** (30 mg, 85 μmol) and BBr$_3$ (0.76 mL, 0.51 mmol) in CH$_2$Cl$_2$ and purified from HPLC by 30% MeOH/H$_2$O containing 0.15% TFA, while compound **19** (25 mg, 73 μmol, 90% yield, t_R 7 min) was prepared from the reaction of **7** (30 mg, 81 μmol) and BBr$_3$ (0.72 mL, 0.48 mmol) in CH$_2$Cl$_2$ and purified from HPLC by 25% MeOH/H$_2$O containing 0.15% TFA.

Compound **17**: ^{1}H NMR (600 MHz, DMSO-d_6) and ^{13}C NMR (150 MHz, DMSO-d_6) data, see **Supplementary Table 6** and **Supplementary Figures 12, 13**. ESIMS m/z 309.2 [M−H]$^−$.

Compound **18**: IR (KBr) v_{max} 3122, 2355, 2337, 1714, 1653, 1504, 1392, 1236, 1109, 1030, 827, 671 cm^{-1}. HR

ESIMS m/z 325.0716 [M−H]$^−$ (calcd. for C$_{18}$H$_{13}$O$_6$, 325.0707) (**Supplementary Figure 14**). ^{1}H NMR (600 MHz, DMSO-d_6) and ^{13}C NMR (150 MHz, DMSO-d_6) data, see **Table 2** and **Supplementary Figures 15, 16**.

Compound **19**: IR (KBr) v_{max} 3134, 2357, 2339, 1682, 1653, 1556, 1508, 1456, 1279, 1184, 1107, 1032, 872, 667 cm^{-1}. HRESIMS m/z 343.0808 [M+H]$^+$ (calcd. for C$_{18}$H$_{15}$O$_7$, 343.0812) (**Supplementary Figure 17**). ^{1}H NMR (600 MHz, DMSO-d_6) and ^{13}C NMR (150 MHz, DMSO-d_6) data, see **Table 2** and **Supplementary Figures 18, 19**.

Synthesis of Compounds 20–22

Compound **5** (1 g, 3.0 mmol) was dissolved in CH$_2$Cl$_2$ (100 mL), and BBr$_3$ (27 mL, 18 mmol, 17% in CH$_2$Cl$_2$) was added at −20°C under the argon atmosphere. After stirring overnight at rt, H$_2$O (40 mL) was added to quench the reaction at 0°C. The CH$_2$Cl$_2$ was evaporated and then EtOAc (200 mL) was added. The EtOAc phase was washed with H$_2$O (20 mL × 4) and concentrated in vacuo. The residue was dissolved in MeOH (50 mL), and silica gel (200–300 mesh, 20 g) was added to the solution. The reaction mixture was stirred overnight at rt and then the solvent was evaporated in vacuo. The residue was purified by FCC eluting with EtOAc-CH$_2$Cl$_2$ (v/v 1:1) to provide compound **20** (550 mg, 1.78 mmol, 59% yield) as a dark red

TABLE 2 | ^{1}H (600 MHz) and ^{13}C (150 MHz) NMR data of compounds **1**, **18**, and **19** in DMSO-d_6.

Position	1		18		19	
	δ$_C$	δ$_H$ (J in Hz)^a	δ$_C$	δ$_H$ (J in Hz)	δ$_C$	δ$_H$ (J in Hz)
1	126.5, C		125.7, C		125.7, C	
2	115.0, CH	6.88, d (1.8)	118.6, CH	6.75, d (2.0)	118.6, CH	6.74, d (2.0)
3	148.2, C		143.8, C		143.7, C	
4	146.7, C		144.3, C		144.2, C	
5	112.5, CH	6.96, d (8.3)	114.8, CH	6.71, d (8.0)	114.8, CH	6.71, d (8.0)
6	123.1, CH	6.82, dd (8.3, 1.8)	122.0, CH	6.60, dd (8.0, 2.0)	122.0, CH	6.59, dd (8.0, 1.9)
1′	117.7, C		116.0, C		115.8, C	
2′	148.3, C		145.0, C		144.9, C	
3′	139.5, C		134.4, C		134.4, C	
4′	132.7, C		129.6, C		130.1, C	
5′	103.2, CH	6.46, s	106.5, CH	6.26, s	106.5, CH	6.24, s
6′	153.2, C		148.2, C		148.1, C	
1″	138.2, C		128.2, C		128.2, C	
2″	128.7, CH	7.61, d (7.5)	130.0, CH	7.35, d (8.5)	116.6, CH	6.97, d (2.0)
3″	128.4, CH	7.47, t (7.5)	114.9, CH	6.79, d (8.5)	144.7, C	
4″	127.3, CH	7.37, t (7.5)	156.2, C		144.2, C	
5″	128.4, CH	7.47, t (7.5)	114.9, CH	6.79, d (8.5)	115.3, CH	6.75, d (8.0)
6″	128.7, CH	7.61, d (7.5)	130.0, CH	7.35, d (8.5)	119.9, CH	6.79, dd (8.0, 2.0)
1‴	64.8, CH$_2$	4.53, d (6.7)				
2‴	120.4, CH	5.47, t (6.7)				
3‴	136.9, C					
4‴	18.0, CH$_3$	1.72, s				
5‴	25.5, CH$_3$	1.76, s				
3-OMe	55.5, CH$_3$	3.73, s				
3′-OMe	60.4, CH$_3$	3.30, s				
6′-OMe	55.7, CH$_3$	3.67, s				
2′-OH		8.68, s				

^{a}d, dd, s, t respectively means doublet, a doublet of doublets, singlet and triplet.

solid (R_f 0.2). By the same procedures, compound **21** (389 mg, 1.2 mmol, 86% yield, R_f 0.2) was prepared from the reaction of compound **6** (500 mg, 1.4 mmol) with BBr$_3$ (12.7 mL, 8.4 mmol) in CH$_2$Cl$_2$ and then 200–300 mesh silica gel (12 g) in MeOH, and purified by FCC eluting with EtOAc-CH$_2$Cl$_2$ (v/v 2:1), while compound **22** (58 mg, 0.17 mmol, 63% yield, R_f 0.3) was prepared from the reaction of compound **7** (100 mg, 0.27 mmol) with BBr$_3$ (2.4 mL, 1.62 mmol) in CH$_2$Cl$_2$ and then 200–300 mesh silica gel (6 g) in MeOH, and purified by FCC eluting with EtOAc-CH$_2$Cl$_2$ (v/v 4:1).

Compound **20**: ^{1}H NMR (600 MHz, DMSO-d_6) and ^{13}C NMR (150 MHz, DMSO-d_6) data, see **Supplementary Table 6** and **Supplementary Figures 20, 21**. ESIMS m/z 307.1 [M−H]$^-$.

Compound **21**: IR (KBr) v_{max} 3122, 2359, 2339, 1653, 1602, 1510, 1404, 1335, 1281, 1228, 1176, 1101, 841, 667, 538 cm^{-1}. HR ESIMS m/z 325.0704 [M+H]$^+$ (calcd. for C$_{18}$H$_{13}$O$_6$, 325.0707) (**Supplementary Figure 22**). ^{1}H NMR (600 MHz, DMSO-d_6) and ^{13}C NMR (150 MHz, DMSO-d_6) data, see **Table 3** and **Supplementary Figures 23, 24**.

Compound **22**: IR (KBr) v_{max} 3417, 3130, 2357, 2333, 1655, 1618, 1552, 1506, 1281, 1201, 1099, 933, 876, 820, 779, 667 cm^{-1}. HR ESIMS m/z 341.0649 [M + H]$^+$ (calcd. for C$_{18}$H$_{13}$O$_7$, 341.0656) (**Supplementary Figure 25**). ^{1}H NMR (600 MHz, DMSO-d_6) and ^{13}C NMR (150 MHz, DMSO-d_6) data, see **Table 3** and **Supplementary Figures 26, 27**.

Synthesis of Compounds 23–25

Compound **5** (30 mg, 89 μmol) was dissolved in CH$_2$Cl$_2$ (3 mL), then DMAP (102 mg, 0.8 mmol) and acetic anhydride (0.08 mL, 0.8 mmol) were added sequentially. After stirring for 2 h at 40°C, the CH$_2$Cl$_2$ was evaporated and EtOAc (20 mL) was added. The obtained organic phase was washed with H$_2$O (20 mL × 4), dried over anhydrous Na$_2$SO$_4$, and concentrated *in vacuo*. The residue was purified by SepaBean machine eluting with 5–70% MeOH/H$_2$O to provide **23** (36 mg, 78 μmol, 88% yield) as a white solid. By the same procedures, compounds **24** (35 mg, 67 μmol, 79% yield) and **25** (38 mg, 66 μmol, 81% yield) were, respectively, prepared from the reaction of compound **6** (30 mg, 85 μmol) with DMAP (124 mg, 1.02 mmol) and acetic anhydride (0.1 mL, 1.02 mmol) in CH$_2$Cl$_2$ (3 mL), and compound **7** (30 mg, 81 μmol) with DMAP (148 mg, 1.21 mmol) and acetic anhydride (0.12 mL, 1.21 mmol) in CH$_2$Cl$_2$ (3 mL). Both compounds **24** and **25** were purified by SepaBean machine eluting with 5–65% MeOH/H$_2$O.

TABLE 3 | [1]H (600 MHz) and ^{13}C (150 MHz) NMR data of compounds **21**, **22**, and **25** in DMSO-d_6.

Position	21		22		25[a]	
	δ_C	δ_H (*J* in Hz)[b]	δ_C	δ_H (*J* in Hz)	δ_C	δ_H (*J* in Hz)
1	122.4, C		122.4, C		130.8, C	
2	119.0, CH	6.81, d (2.0)	118.9, CH	6.81, d (2.0)	124.9, CH	7.10, s
3	144.2, C		144.2, C		141.5, C	
4	145.1, C		145.0, C		141.3, C	
5	114.7, CH	6.74, d (8.2)	114.7, CH	6.73, d (8.2)	123.2, CH	7.32, d (8.5)
6	121.6, CH	6.66, dd (8.2, 2.0)	121.6, CH	6.66, dd (8.2, 2.0)	128.4, CH	7.17, d (8.5)
1′	118.4, C		118.3, C		122.7, C	
2′	152.2, C		152.2, C		142.4, C	
3′	183.4, C		183.3, C		143.0, C	
4′	141.6, C		141.6, C		132.9, C	
5′	131.2, CH	6.72, s	131.2, CH	6.65, s	110.5, CH	7.04, s
6′	187.0, C		186.9, C		152.6, C	
1″	123.1, C		123.5, C		135.4, C	
2″	130.8, CH	7.46, d (8.5)	116.6, CH	7.04, d (2.2)	124.0, CH	7.54, s
3″	115.3, CH	6.85, d (8.5)	147.5, C		141.9, C	
4″	159.1, C		145.1, C		141.6, C	
5″	115.3, CH	6.85, d (8.5)	115.5, CH	6.80, d (8.0)	123.7, CH	7.39, d (8.5)
6″	130.8, CH	7.46, d (8.5)	120.9, CH	6.94, dd (8.0, 2.0)	127.1, CH	7.58, d (8.5)
3′-OMe					60.8, CH$_3$	3.42, s
6′-OMe					56.2, CH$_3$	3.79, s

[a]The ^{1}H and ^{13}C NMR Data for five acetoxy were δ_H 2.06 (s, 3H), 2.29 (s, 3H), 2.31 (s, 9H), and δ_C 168.3 × 2 (C), 168.4 × 2 (C), 168.7 (C), 20.0 (CH$_3$), 20.4 × 4 (CH$_3$), respectively. [b]d, dd, s respectively means doublet, a doublet of doublets, and singlet.

Compound 23: IR (KBr) ν_{max} 3132, 2356, 2333, 1761, 1653, 1562, 1522, 1479, 1396, 1228, 1201, 1667, 1107, 1082, 1009, 920, 841, 671 cm^{-1}. HR ESIMS *m/z* 465.1537 [M+H]$^+$ (calcd. for C$_{26}$H$_{25}$O$_8$, 465.1544) (**Supplementary Figure 28**). ^{1}H NMR (600 MHz, DMSO-d_6) and ^{13}C NMR (150 MHz, DMSO-d_6) data, see **Supplementary Table 6** and **Supplementary Figures 29, 30**.

Compound 24: ^{1}H NMR (600 MHz, DMSO-d_6) and ^{13}C NMR (150 MHz, DMSO-d_6) data, see **Supplementary Table 6** and **Supplementary Figures 31, 32**. ESIMS *m/z* 545.0 [M+Na]$^+$.

Compound 25: IR (KBr) ν_{max} 3128, 2359, 2337, 1768, 1655, 1558, 1522, 1475, 1400, 1203, 1115, 1093, 899, 671 cm^{-1}. HR ESIMS *m/z* 603.1470 [M+Na]$^+$ (calcd. for C$_{30}$H$_{28}$O$_{12}$Na, 603.1473) (**Supplementary Figure 33**). ^{1}H NMR (600 MHz, DMSO-d_6) and ^{13}C NMR (150 MHz, DMSO-d_6) data, see **Table 3** and **Supplementary Figures 34, 35**.

Oxygen Radical Absorbance Capacity (ORAC) Assay

The anti-oxidative activity of compounds was evaluated by ORAC assay (Huang et al., 2002) that was carried out mainly by using 2,2′-azobis(2-amidinopropane) dihydrochloride (AAPH, 153.0 μM), fluorescein (FL, 81.6 nM), testing compounds, and trolox as a positive control, all of which were dissolved in phosphate buffer solution (PBS, 75 mM, pH 7.4). The concentrations were 6.25 μM for compounds **4–7** and trolox, 12.5 μM for compounds **1–3**, **8–16** and trolox, and 25.0 μM for compounds **17–25** and trolox, respectively (**Supplementary Figure 36**). In short, each 25 μL of testing compounds, blank (PBS), negative (PBS) and trolox, and 150 μL of FL were added

in each well and incubated at 37°C for 10 min. Each 25 μL of AAPH was then added to the testing compounds, blank and trolox groups, and 25 μL of PBS was added to the negative group. Fluorescence intensity of each well was measured one time every 1 min for 90 cycles using a Fluoroskan Ascent FL plate-reader (Thermo Scientific Varioskan LUX) at excitation of λ 485 nm and emission of λ 530 nm. The relative fluorescence intensity *f* was equaled to the ratio of the absolute fluorescence reading to the initial fluorescence reading, and the net area under curve (AUC) was obtained by subtracting the AUC of the blank from that of the compound. The AUC was calculated as $0.5 + f_1 + \dots f_i + \dots + f_{89} + 0.5 \times f_{90}$, in which f_i means the ratio of fluorescence reading at time *i* to the initial fluorescence reading. The final ORAC values were calculated as micromole of trolox equivalents per micromole of the compound (μmole TE/μmole) by using a regression equation between the trolox concentration and the net area under the FL decay curve. That is, the relative ORAC value = (AUC$_{compound}$ − AUC$_{blank}$)/(AUC$_{trolox}$ − AUC$_{blank}$).

DPPH Radical-Scavenging Assay

The anti-oxidative activity of compounds was also evaluated by 2,2-diphenyl-1-picrylhydrazyl (DPPH) radical-scavenging assay (Wang et al., 2007). The experiment was divided into the following five groups, blank (methanol, MeOH), sample (mix compound and DPPH solution), background (pure compound solution), negative (pure DPPH solution), and positive [mix vitamin C (VC) and DPPH solution] controls. DPPH (0.15 mM), compounds (1–100 μM), and VC (1–100 μM) that was regarded as a compound sample in the following procedures all were

dissolved in MeOH. Each 160 μL of MeOH was placed in negative control and blank groups, while each 160 μL of testing compounds or VC was placed in sample and background groups. Then, MeOH (each 40 μL) was, respectively, added to blank and background groups, while 40 μL of DPPH was, respectively, added to negative, positive, and sample controls. After 30-min incubation in the dark at rt, the decrease in DPPH radical concentration was monitored by measuring the absorbance at λ 517 nm with a microplate reader (Multiskan Spectrum, Thermo Scientific Varioskan LUX). The DPPH radical-scavenging rate was calculated as:

$$\text{Scavenging rate (\%)} = [(A_{negative} - A_{blank})$$
$$- (A_{sample} - A_{background})]/$$
$$(A_{negative} - A_{blank}) \times 100\%.$$

The IC$_{50}$ (half maximal inhibitory concentration) values of compounds and VC were calculated by SPSS (Statistical Package for the Social Sciences) software from the radical-scavenging rates at the final concentrations of 100, 50, 10, 5, and 1 μ M.

α-Glucosidase Inhibitory Assays

α-Glucosidase Inhibitions in *Saccharomyces cerevisiae*

The inhibitions of the compounds against α-glucosidase from *Saccharomyces cerevisiae* were assayed by reported method (Xu et al., 2018). The testing compounds were dissolved in dimethyl sulfoxide (DMSO) to obtain stock solution (10 mM) and then diluted into the concentrations by PBS (pH 6.8), while α-glucosidase (2.0 U/mL, Sigma), 4-nitrophenyl-α-D-glucopyranoside (PNPG, 2.5 mM, Macklin), Na$_2$CO$_3$ (0.2 M), and acarbose (2.5 mg/mL, Sigma) were directly dissolved in PBS. 20 μL of the compound solution and acarbose were, respectively, mixed in a 96-well microplate with 20 μL of α-glucosidase and 60 μL of PBS as the drug and positive groups, while the pure PBS solution was used as the blank group. After incubation for 15 min at 37°C, 20 μL of PNPG solution was added to each well of testing groups and further incubated at 37°C for 30 min. Finally, 80 μL of Na$_2$CO$_3$ solution was added to each well to stop the reaction and the absorbance was measured by a microplate reader (Multiskan Spectrum, Thermo Scientific Varioskan LUX) at λ 405 nm. The inhibitory rate (%) was calculated as $[1 - (A_{drug}/A_{blank})] \times 100\%$. The IC$_{50}$ values were calculated by SPSS software from the drug inhibitory rates at the final concentrations of 500, 250, 50, 25, 5, and 1 μM (**Table 3**).

α-Glucosidase Inhibitions in Caco-2 Cell Line

The α-glucosidase inhibition assay was also carried out in caco-2 cell line (Hansawasdi and Kawabata, 2006). Caco-2 cells at logarithmic growth stage were inoculated in a 6-well plate with an inoculation density of 4000/cm^2 and cultured in an incubator with 5% CO$_2$ at 37°C in a Dulbecco's Modified Eagle Medium (DMEM) supplemented with 10% fetal bovine serum, 1% non-essential amino acid, 1% penicillin/streptomycin, 1% L-glutamine, and 0.25 mg plasmocin. The DMEM medium was changed one time every 2 days for 24 days. Then, the culture medium was removed, and the cell surface was washed three times by a PBS solution (pH 7.4) at 37°C. 1.0 mL of sucrose/maltose (both 28 mM) PBS solution was added to the control well, 1 mL of PBS was added to the blank well, 0.2 mL of compounds or acarbose (positive control) with different concentration and 0.8 mL of above sucrose/maltose solution were added to the drug well. The final concentration gradients of compounds and acarbose were 1.0, 0.3, 0.1, 0.03, 0.01 μM and 10000, 3000, 1000, 300, 100 μg/mL, respectively. The obtained solutions for the enzymatic hydrolysis reactions of sucrose and maltose were incubated at 37°C for 60 min. After terminating the reactions in an ice bath for 10 min, 10 μL of the reaction mixture was added into 1 mL of the glucose kit (Nanjing Jiancheng Bioengineering Institute Co., Ltd.) and maintain 10 min at 37°C. The α-glucosidase inhibitory activity of the compounds was then determined by measuring the glucose content in the reaction solution (pipette 100 μL reaction solution into 96-well plate) via the absorbance at λ 505 nm with a microplate reader (BioTek Synergy H1, BioTek, VT, United States). The α-glucosidase inhibitory rate (%) was calculated as $[1 - (A_{drug} - A_{blank})/(A_{control} - A_{blank})] \times 100\%$. The IC$_{50}$ values were calculated as showed in **Table 3** by SPSS software.

The cytotoxic effects on the coca-2 cells were evaluated by the CTG assay (Elisia and Kitts, 2008; Wang et al., 2019). Briefly, coca-2 cells were seeded in 96-well plates at a density of 2×10^3 cells/well and treated with the final concentration of 1.0 μM of the compounds. After 72 h incubation, 100 μL of CTG solution (Promega) was added into each well. The luminescence value was tested by using a microplate reader (BioTek Synergy H1) after staying at rt for 10 min.

RESULTS AND DISCUSSION

Metabolic Regulation of the Fungus

After adding the leaves of *Eucommia ulmoides* in the rice medium, both the production and the α-glucosidase inhibitory activity of the EtOAc extracts of the solid-state fermentation increased significantly from 5.3 to 9.5 g/kg and from the IC$_{50}$ value of 15.0 to 2.0 μg/mL, respectively. The original *p*-terphenyl products **5–7**, **10**, and **12** in the rice medium also largely increased by adding the leaves of *E. ulmoides*. In addition, the number of the *p*-terphenyl-type chromophores also increased significantly. For example, *p*-terphenyls **1–4**, **8**, **9**, **11**, and **13–16** were newly produced after adding the leaves of *E. ulmoides* (**Figure 1**). The results indicated that the content and diversity of the microbial natural products could increase highly by adding the host materials to the culture media of the microorganisms via the chemical microbe-host interaction.

The Identification of the New *p*-Terphenyl (1)

Compound **1** was obtained as a white powder. Its molecular formula was determined as C$_{26}$H$_{28}$O$_5$ according to its HR-ESIMS peak at *m/z* 443.1837 [M+Na]$^+$ (**Supplementary Figure 2**).

FIGURE 3 | Key HMBC (red arrows) and COSY (blue bold lines) of compound **1**.
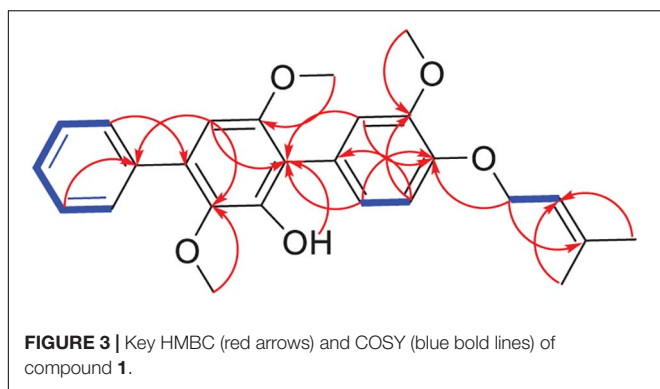
The NMR spectra displayed nine sp^2- non-hydrogenated carbons, ten sp^2-methines, one sp^3-methylene, three methoxyls, and two methyls (**Supplementary Figures 3–5**). Except for the lack of 4″-hydroxyl, these data (**Table 2**) were very similar to those reported 3-methoxyterprenin (**13**), indicating compound **1** as a highly oxygenated *p*-terphenyl. The signals of five mono-substituted phenyl protons at δ_H 7.61 (d, *J* = 7.5 Hz, H-2″/H-6″), 7.47 (t, *J* = 7.5 Hz, H-3″/H-5″), and 7.37 (t, *J* = 7.5 Hz, H-4″) which showed ^{1}H-^{1}H COSY correlations (**Figure 3** and **Supplementary Figure 6**) of H-2″/H-3″/H-4″ confirmed replacement of 4″-OH in **13** by a hydrogen atom in **1**. Furthermore, the ^{1}H-^{1}H COSY between H-5 (δ_H 6.96) and H-6 (δ_H 6.82), H-1‴ (δ_H 4.53) and H-2‴ (δ_H 5.47), along with the key HMBC connections (**Figure 3** and **Supplementary Figure 7**) from H-1‴ to C-3‴ (δ_C 136.9) and C-4 (δ_C 146.7), H-4‴ (δ_H 1.72) to C-2‴ (δ_C 128.7) and C-5‴ (δ_C 25.5), and H-2″/H-6″ to C-4′ (δ_C 132.7) supported the structure. Thus, compound **1** was identified as 3-*O*-methyl-4″-deoxyterprenin.

Synthesis of *p*-Terphenyls 17–25

As shown in **Scheme 1**, compounds **17–19** were synthesized from compounds **5–7** by demethylation reaction using BBr$_3$, which were further transformed to compounds **20–22** by oxidation of air in the system of silica gel and MeOH. The acetylation of compounds **5–7** provided compounds **23–25** by Ac$_2$O/DMAP. It is interesting that compounds **15** and **16** could be synthesized from compounds **6** and **7** by an oxidative dehydrocyclization of air in the system of silica gel and MeOH. But compound **5** cannot undergo the same reaction to form the corresponding 2,2′-oxygen bridged *p*-terphenyl derivative, indicating that the oxidative cyclization might be carried out by a radical process. That is, compounds **6** and **7** formed a radical intermediate **a** which underwent an intramolecular cyclization to generate the keto intermediate **b** in the presence of SiO$_2$ and O$_2$. Compounds **15** and **16** were then yielded by a keto-enol tautomerization of the intermediate **b** in the SiO$_2$ and MeOH (**Scheme 2**). To confirm the effect of silica gel and O$_2$, the reaction of compound **6** was carried out in the four conditions, i.e., O$_2$, silica gel/argon, silica gel/air, and silica gel/O$_2$. The results showed that compound **6** could not be converted to compound **15** without silica gel. Both the reaction and conversion rates increased in the order of O$_2$, silica gel/argon, silica gel/air, and silica gel/O$_2$ (**Supplementary Figure 37**). And the silica gel acted as a catalyst to accelerate the tautomerization between keto and enol. The fact that a little compound **15** was also formed in the silica gel/argon system could be explained from the air adsorbed in the silica gel.

The Bioactivities of *p*-Terphenyls

All of the obtained *p*-terphenyls (**1–25**) were tested for the anti-oxidative activity against DPPH radicals and ORAC as well as the α-glucosidase inhibitions. The results (**Table 3**) showed that compounds **4–7**, **17**, and **20** have a significant antioxidant capacity with the ORAC values of 6.8, 6.0, 5.7, 4.5, 4.8, and 6.1 µmole TE/µmole, respectively, indicating that 4-, 2′-, and 4″-hydroxys are active sites of *p*-terphenyls. When these hydroxyls were changed to hydrogens or etherified in part or wholly, the antioxidant capacity was greatly reduced. Compounds **4**, **6**, **7**, **9**, **11**, **12**, **19**, **21**, and **22** showed more potent DPPH radical-scavenging activity than VC with the IC$_{50}$ value of 1.7, 1.4, 1.1, 1.6, 1.6, 1.8, 1.6, 1.7, and 2.8 (VC) µM, respectively, indicating
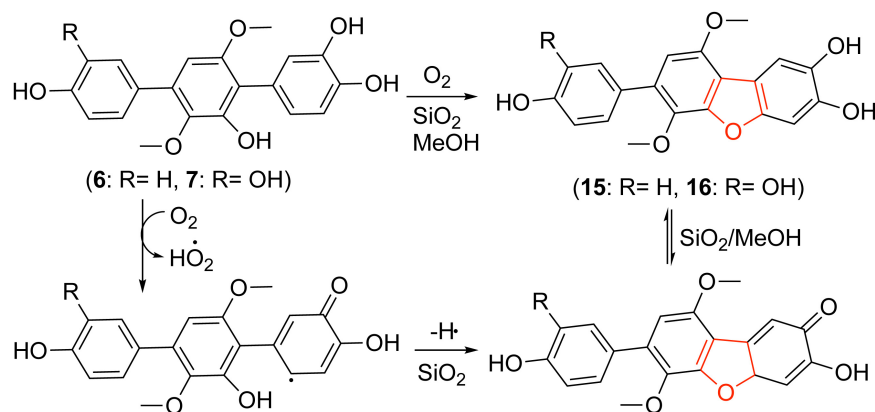
SCHEME 2 | A possible mechanism forming **15** and **16** by an oxidative cyclization of **6** and **7**.

that 4- and 2′-hydroxys are very important active sites of the *p*-terphenyls. As the disappearance of the two hydroxys, changing to hydrogens, methoxyls or acetoxyls, for example, the DPPH radical-scavenging activity of *p*-terphenyls was greatly reduced. However, the activity is still maintained when the 2′-hydroxy formed a furan ring with C-6.

The most obvious inhibition against α-glucosidase from *Saccharomyces cerevisiae* was observed for compounds **4**, **5**, **16**, **20**, and **21** whose IC_{50} values were 5.9, 2.8, 7.9, 8.9, and 4.0 μM, respectively. The results indicated that 4-, 2′,- and 4″-hydroxys are the most important active-sites for α-glucosidase inhibition of *p*-terphenyls, two or three of which were replaced by hydrogens, methoxyls or acetoxyls resulted in the loss or decrease of α-glucosidase inhibitory activity. Seven compounds (**5–7**, **15**, **16**, **20**, and **21**) with significant antioxidant and α-glucosidase inhibitory activities could be prepared on a large scale, were further tested for the α-glucosidase inhibitions in caco-2 cell line. As expected, these seven compounds exhibited the announced activity with the IC_{50} values of 0.38, 0.29, 0.36, 0.11, 0.36, 0.11, and 0.12 μM, respectively. It is interesting that these seven compounds were not toxic to the caco-2 cells at the concentration of 1 μM, whose inhibitory rate was 0.4%, 0.2%, 0.5%, 20.5%, 2.7%, 0.4%, and 1.2%, respectively.

CONCLUSION

There is a mutually beneficial relationship between endophytes and their host plants. Adding the host plants to the culture medium of endophytes could enhanced the metabolic potential of the endophytic strains and thus enriched the chemodiversity of the microbial natural products. *p*-Terphenyls, especially those 4,2′,4″-trihydroxy or 4,4″-dihydroxy-1,2,1′,2′-furan substituted ones, have a stronger antioxidant activity, α-glucosidase inhibitory activity and lower cytotoxicity, implying their

potential use in the fight against diabetes as the drug leads or dietary supplements.

DATA AVAILABILITY STATEMENT

Publicly available datasets were analyzed in this study. This data can be found here: GenBank No. KY038594.

AUTHOR CONTRIBUTIONS

YX isolated the fungus and compounds, performed the structure elucidation, and assayed part of the bioactivity. YW synthesized the compounds. DW assayed part of the bioactivity. WH did fermentation and extraction. LW directed the implementation of the study and prepared the manuscript. WZ designed the study and revised the manuscript. All authors contributed to the article and approved the submitted version.

SUPPLEMENTARY MATERIAL

The Supplementary Material for this article can be found online at: https://www.frontiersin.org/articles/10.3389/fmicb.2021.654963/full#supplementary-material

REFERENCES

Cai, S., Sun, S., Zhou, H., Kong, X., Zhu, T., Li, D., et al. (2011). Prenylated polyhydroxy-p-terphenyls from *Aspergillus taichungensis* ZHN-7-07. *J. Nat. Prod.* 74, 1106–1110. doi: 10.1021/np2000478

El-Elimat, T., Figueroa, M., Raja, H. A., Graf, T. N., Adcock, A. F., Kroll, D. J., et al. (2013). Benzoquinones and terphenyl compounds as phosphodiesterase-4B inhibitors from a fungus of the order Chaetothyriales (MSX 47445). *J. Nat. Prod.* 76, 382–387. doi: 10.1021/np300749w

Elisia, I., and Kitts, D. D. (2008). Anthocyanins inhibit peroxyl radical-induced apoptosis in Caco-2 cells. *Mol. Cell. Biochem.* 312, 139–145. doi: 10.1007/s11010-008-9719-1

Guo, Z. K., Yan, T., Guo, Y., Song, Y. C., Jiao, R. H., Tan, R. X., et al. (2012). p-Terphenyl and diterpenoid metabolites from endophytic *Aspergillus* sp. YXf3. *J. Nat. Prod.* 75, 15–21. doi: 10.1021/np200321s

Hansawasdi, C., and Kawabata, J. (2006). α-Glucosidase inhibitory effect of mulberry (*Morus alba*) leaves on caco-2. *Fitoterapia* 77, 568–573. doi: 10.1016/j.fitote.2006.09.003

Huang, D., Ou, B., Hampsch-Woodill, M., Flanagan, J. A., and Prior, R. L. (2002). High-throughput assay of oxygen radical absorbance capacity (ORAC) using a multichannel liquid handling system coupled with a microplate fluorescence reader in 96-well format. *J. Agric. Food Chem.* 50, 4437–4444. doi: 10.1021/jf0201529

Intaraudom, C., Bunbamrung, N., Dramae, A., Boonyuen, N., Kongsaeree, P., Srichomthong, K., et al. (2017). Terphenyl derivatives and drimane-phthalide/isoindolinones from *Hypoxylon fendleri* BCC32408. *Phytochemistry* 139, 8–17. doi: 10.1016/j.phytochem.2017.03.008

Kamigauchi, T., Sakazaki, R., Nagashima, K., Kawamura, Y., Yasuda, Y., Matsushima, K., et al. (1998). Terprenins, novel immunosuppressants produced by *Aspergillus candidus*. *J. Antibiot.* 51, 445–450. doi: 10.7164/antibiotics.51.445

Karunakaran, U., and Park, K.-G. (2013). A systematic review of oxidative stress and safety of antioxidants in diabetes: focus on islets and their defense. *Diabetes Metab. J.* 37, 106–112. doi: 10.4093/dmj.2013.37.2.106

Kuhnert, E., Surup, F., Herrmann, J., Huch, V., Müller, R., and Stadler, M. (2015). Rickenyls A-E, antioxidative terphenyls from the fungus *Hypoxylon rickii* (Xylariaceae, Ascomycota). *Phytochemistry* 118, 68–73. doi: 10.1016/j.phytochem.2015.08.004

Li, W., Li, X. B., and Lou, H. X. (2018). Structural and biological diersity of natural pterphenyls. *J. Asian. Nat. Prod. Res.* 20, 1–13. doi: 10.1080/10286020.2017.1381089

Lin, Y.-K., Xie, C.-L., Xing, C.-P., Wang, B.-Q., Tian, X.-X., Xia, J.-M., et al. (2019). Cytotoxic *p*-terphenyls from the deep-sea-derived *Aspergillus candidus*. *Nat. Prod. Res.* doi: 10.1080/14786419.2019.1633651 [Epub ahead of print].

Liu, J. K. (2006). Natural terphenyls: developments since 1877. *Chem. Rev.* 106, 2209–2223. doi: 10.1002/chin.200639247

Liu, J. K., Hu, L., Dong, Z. J., and Hu, Q. (2004). DPPH radical scavenging activity of ten natural *p*-terphenyl derivatives obtained from three edible mushrooms indigenous to China. *Chem. Biodivers.* 1, 601–605. doi: 10.1002/cbdv.200490050

Liu, S. S., Zhao, B. B., Lu, C. H., Huang, J. J., and Shen, Y. M. (2012). Two new *p*-terphenyl derivatives from the marine fungal strain *Aspergillus sp.* AF119. *Nat. Prod. Commun.* 7, 1057–1062.

Ma, K., Han, J., Bao, L., Wei, T., and Liu, H. (2014). Two sarcoviolins with antioxidative and α-glucosidase inhibitory activity from the edible mushroom *Sarcodon leucopus* collected in Tibet. *J. Nat. Prod.* 77, 942–947. doi: 10.1021/np401026b

Shan, T., Sun, J., Mao, Z., Mao, Z., Wang, S., Wang, Y., et al. (2019). Rapid separation and preparation method of symbiotic fungus *Aspergillus* sp. Bdf-2 monomer compounds and application thereof. *Faming Zhuanli Shenqing* 2019:110283053A.

Takahashi, S., Suda, Y., Nakamura, T., Matsuoka, K., and Koshino, H. (2017). Total synthesis of kehokorins A-E, cytotoxic pterphenyls. *J. Org. Chem.* 82, 3159–3166. doi: 10.1021/ acs.joc.7b0 0147

Wang, D., Qu, P., Zhou, J., Wang, Y., Wang, L., and Zhu, W. (2020). *p*-Terphenyl alcohols from a marine sponge-derived fungus, *Aspergillus candidus* OUCMDZ-1051. *Mar. Life Sci. Technol.* 2, 262–267. doi: 10.1007/s42995-020-00039-x

Wang, D., Wang, Y., Ouyang, Y., Fu, P., and Zhu, W. (2019). Cytotoxic *p*-terphenyls from a marine-derived *Nocardiopsis* species. *J. Nat. Prod.* 82, 3504–3508. doi: 10.1021/acs.jnatprod.9b00963

Wang, S. M., Han, J. J., Ma, K., Jin, T., Bao, L., Pei, Y. F., et al. (2014). New α-glucosidase inhibitors with *p*-terphenyl skeleton from the mushroom *Hydnellum concrescens*. *Fitoterapia* 98, 149–155. doi: 10.1016/j.fitote.2014.07.019

Wang, W.-L., Zhu, T.-J., Tao, H.-W., Lu, Z.-Y., Fang, Y.-C., Gu, Q.-Q., et al. (2007). Three novel, structurally unique spirocyclic alkaloids from the halotolerant B-17 fungal strain of *Aspergillus variecolor*. *Chem. Biodivers* 4, 2913–2919. doi: 10.1002/cbdv.200790240

Wei, H., Inada, H., Hayashi, A., Higashimoto, K., Pruksakorn, P., Kamada, S., et al. (2007). Prenylterphenyllin and its dehydroxyl analogs, new cytotoxic substances from a marine-derived fungus *Aspergillus candidus* IF10. *J. Antibiot.* 60, 586–590. doi: 10.1038/ja.2007.75

Xu, Y., Wang, C., Liu, H., Zhu, G., Fu, P., Wang, L., et al. (2018). Meroterpenoids and isocoumarinoids from a *Myrothecium* fungus associated with *Apocynum venetum*. *Mar. Drugs* 16:363. doi: 10.3390/md16100363

Yan, W., Li, S. J., Guo, Z. K., Zhang, W. J., and Wei, W. (2017). New *p*-terphenyls from the endophytic fungus *Aspergillus* sp. YXf3. *Bioorg. Med. Chem. Lett.* 27, 51–54. doi: 10.1016/j.bmcl.2016.11.033

Yonezawa, S., Komurasaki, T., Kawada, K., Tsuri, T., Fuji, M., Kugimiya, A., et al. (1998). Total synthesis of terprenin, a novel immunosuppressive *p*-terphenyl derivative. *J. Org. Chem.* 63, 5831–5837. doi: 10.1021/jo98 0349t

Zhang, X. Q., Mou, X. F., Mao, N., Hao, J. J., Liu, M., Zheng, J. Y., et al. (2018). Design, semisynthesis, α-glucosidase inhibitory, cytotoxic, and antibacterial activities of *p*-terphenyl derivatives. *Eur. J. Med. Chem.* 146, 232–244. doi: 10.1016/j.ejmech.2018.01.057

Check for updates

One-Step Biosynthesis of Vitamin C in *Saccharomyces cerevisiae*

Mengyu Zhou[1,2], Yanhui Bi[1,2], Mingzhu Ding[1,2]* and Yingjin Yuan[1,2]

[1] *Key Laboratory of Systems Bioengineering (Ministry of Education), Frontier Science Center for Synthetic Biology, School of Chemical Engineering and Technology, Tianjin University, Tianjin, China,* [2] *Collaborative Innovation Center of Chemical Science and Engineering (Tianjin), Tianjin University, Tianjin, China*

Vitamin C (VC) is comprehensively applied in foods, cosmetics, pharmaceuticals, and especially clinical medicine. Nowadays, the industrial production of VC mainly relies on the classic two-step fermentation route, and researchers have explored the way for one-step fermentation of VC in recent years. In this study, a VC biosynthesis pathway that directly produced VC from glucose was reconstructed in *Saccharomyces cerevisiae*, and the protein engineering and metabolic engineering strategies were adopted to improve it. First, five exogenous modules from *Arabidopsis* were introduced into the chassis cells by synthetic biology approaches to obtain the strain YLAA harboring VC biosynthesis. In addition, L-galactose dehydrogenase (L-GalDH) and L-galactono-1,4-lactone dehydrogenase (L-GLDH) were fused and expressed in *S. cerevisiae* cells for the first time, which increased the intracellular VC accumulation by 2.78-fold, reaching 9.97 ± 0.09 mg/L. Through copy number engineering, it was further confirmed that the last step catalyzed by L-GLDH is the rate-limiting step. GDP-L-galactose phosphorylase (GPP) encoded by vtc2 is another rate-limiting enzyme confirmed by GAL1p overexpression results. Finally, by balancing gene expression and cell growth, the highest production strain with overexpressing vtc2 by multicopy plasmids was constructed. The VC accumulation reached 24.94 ± 1.16 mg/L, which was currently the highest production from glucose in *S. cerevisiae*. The production of the recombinant strain reached nearly 44 mg/L with the exogenous addition of L-galactose or glutathione. The results further emphasized the importance of the step catalyzed by GPP. The investigation provided experience for the efficient biosynthesis of VC and the determination of rate-limiting steps.

Keywords: vitamin C, *Saccharomyces cerevisiae*, protein engineering, copy number engineering, synthetic biology

INTRODUCTION

Vitamin C (VC) is a water-soluble vitamin, which is closely related to human beings. For more than 80 years since the discovery of VC, its physiological activities and biological functions have been continuously developed (King and Waugh, 1932; Naidu, 2003; Grosso et al., 2013; Camarena and Wang, 2016). As a result of the strong reducing ability of ascorbic acid, it is an important antioxidant, free radical scavenger, and one of the nutrients for preventing sepsis (Padh, 1990; Timoshnikov et al., 2020). By the 1950s, VC was considered to have an anti-cancer effect

by participating in the redox reaction to affect the growth of cancer cells and even kill them (McCormick, 1954; Yun et al., 2015; De Francesco et al., 2017). Recently, researchers discovered VC advanced plasma cell difference to enhance antibody production, and high injecting doses enhanced the effectiveness of antibodies and slowed down or even prevented the growth of cancer (Magrì et al., 2020; Qi et al., 2020). What is more, VC could also be used in the treatment of leukemia by regulating the number and function of blood-forming blood stem cells and reducing the patients' pain as a cofactor for the synthesis of substances that had analgesic effects (Prigge et al., 2000; Yeom et al., 2007; Harrison and May, 2009; Agathocleous et al., 2017; Carr and McCall, 2017; Cimmino et al., 2017).

Nowadays, the industrial production of VC mainly relies on the classic two-step fermentation method (CTFR) to convert D-sorbitol to 2-keto-L-gulonic acid (2-KLG, the precursor for VC) (Reichstein and Grüssner, 1934; Pan et al., 2017). Afterward, researchers improved the fermentation process to optimize CTFR by the improvement of the fermentation process and the reconstruction of microorganisms, such as the exogenous addition of cofactors or specific complex nutrients (Gao and Yuan, 2011; Zou et al., 2012; Huang et al., 2013), the reconstruction of the helper microorganisms (Zhou et al., 2011; Du et al., 2012; Zhu et al., 2012a,b), the optimization of the metabolic pathway in the production microorganisms (Cai et al., 2012; Du et al., 2013; Pan et al., 2017), and a new design of bacterial consortia (Mandlaa et al., 2013; Jia et al., 2016).

In addition, researchers have been working on the production of VC in one-step fermentation over the years. It seemed to be the most direct method for one-step fermentation producing 2-KLG that CFTR-related dehydrogenases were introduced into a certain microorganism (Gao et al., 2014; Zeng et al., 2020). Furthermore, the direct biosynthesis of VC from D-glucose or D-sorbitol was a practical approach. Although most microalgae had a complete path to synthesize VC, its cultivation cost was much higher than that of microorganisms, which greatly limited its application (Running et al., 2002). Yeast could synthesize D-erythorbic acid (D-EAA), a structural and functional analog of VC (Huh et al., 1998). Compared with the transformation process of VC synthesis in plants, the molecular configuration changes in the last two steps were very similar (Kim et al., 1998). With the continuous exploration, researchers gradually discovered the enzymes lacking in yeast to synthesize VC. Rosa et al. (2013) transferred the VC synthesis pathway of plants to *Kluyveromyces lactis*, but the maturity of its genetic manipulation and the breadth of its application were not as good as *Saccharomyces cerevisiae*. Martani et al. (2013) introduced this pathway into *S. cerevisiae*, giving it the ability to synthesize VC with the production of 0.2 mg/L (Branduardi et al., 2007).

In this study, *S. cerevisiae* cells were selected as the chassis cells to construct the strains capable of biosynthesizing VC. Furthermore, the rate-limiting steps of the VC synthesis pathway in *S. cerevisiae* were investigated. The effect of the fusion protein expression, the promoter optimization, copy number engineering or the addition of intermediate products, and GSH on VC accumulation was revealed. Finally, based on the above research, a *S. cerevisiae* strain with the highest production of VC from

glucose by one-step fermentation was obtained. The research process can provide an effective reference for designing a one-step fermentation route to efficiently produce VC or other chemicals in *S. cerevisiae* strains.

MATERIALS AND METHODS

Gene Amplification and Plasmid Construction

Plasmids used in this study are all listed in **Table 1**. Genes synthesized in this study are all listed in **Supplementary Table S3**. All syngeneic genes for the reconstruction of the VC synthesis pathway in yeasts were optimized with yeast codons and obtained by Kingsley Corporation. The fragments of constitutive promoters and terminators were amplified from *S. cerevisiae* genome. The fragments used for strain constructions and the primers used for fragments for this study are listed in **Supplementary Table S1**. All fragments were amplified using Phanta® Super-Fidelity DNA Polymerase (Vazyme Biotech.) and were gel purified using a kit (TIANGEN) before cloning. Fragment assembly was performed using the Gibson method (Gibson, 2011) or yeast assembly (Gibson et al., 2008).

As shown in **Supplementary Figure S1**, five exogenous modules were subcloned into pRS416 (ura3 auxotrophic marker) digested by *Kpn*I and *Not*I, resulting in the p2-4-6-1 vector. The exogenous modules expressing gldh was subcloned into pRS415 (leu2 auxotrophic marker) digested by *Not*I and *Sac*I, resulting in the pGLDH-1 vector.

In order to improve the recombination efficiency, 300 bp homologous fragments were used to construct the plasmids with overexpressing exogenous modules and fused proteins. As shown in **Supplementary Figure S2**, all exogenous optimized modules were subcloned into pRS426 (ura3 auxotrophic marker) digested by *Kpn*I and *Not*I, resulting in the vectors p2-4-6-1-2, pGME-VTC2, pVTC2-VTC4, and pGalDH-GLDH.

The fragments vtc2-gldh, alo1-vtc2, alo1-gldh, and TDH3p-alo1-ENO2t were obtained according to the designed order by overlap extension PCR (OE-PCR). The first three fragments were, respectively subcloned into pRS425 (leu2 auxotrophic marker) digested by *Xho*I and *Hin*dIII, resulting in the multi-copy plasmids pVTC2-GLDH, pALO1-VTC2, and pALO1-GLDH. The last fragment was subcloned into pRS423 (his3 auxotrophic marker) digested by *Xho*I and *Sal*I, resulting in the multi-copy plasmid overexpressing alo1 (**Supplementary Figure S3A**).

GAL1p-PGI1t was obtained after OE-PCR, digested by *Hin*dIII and *Not*I and eventually subcloned with linearized pRS413 (his3 auxotrophic marker), resulting in the GAL1p expression cassette. Each exogenous module was, respectively, subcloned into this cassette digested by *Bsa*I, resulting in five vectors pGME-Gal, pVTC2-Gal, pVTC4-Gal, pGalDH-Gal, and pGLDH-Gal (**Supplementary Figure S3B**). The fragment TEF2p-gldh-ENO2t was subcloned into pRS413 (HIS auxotrophic marker) digested by *Not*I and *Sac*I resulting in the vector pGLDH-2. All fragments of exogenous genes were amplified and then digested by *Not*I and *Sac*I. Each exogenous module was eventually subcloned with linearized

TABLE 1 | List of plasmids used in this study.

Plasmid	Description	Source
p2-4-6-1	pRS416-P$_{PGK1p}$-gme-HXT7t-P$_{GPM1p}$-vtc2-CYC1t-P$_{TDH3p}$-vtc4-GPM1t-P$_{TPI1p}$-galdh-PGK1t	This study
pGLDH-1	pRS415-P$_{TEF2p}$-gldh-ENO2t	This study
p2-4-6-1-2	pRS426-P$_{PGK1p}$-gme-HXT7t-P$_{GPM1p}$-vtc2-CYC1t-P$_{TDH3p}$-vtc4-GPM1t-P$_{TEF2p}$-gldh-ENO2t-P$_{TPI1p}$-galdh-PGK1t	This study
pGME-VTC2	pRS426-P$_{GPM1p}$-vtc2-gme-CYC1t-P$_{TDH3p}$-vtc4-GPM1t-P$_{TEF2p}$-gldh-ENO2t-P$_{TPI1p}$-galdh-PGK1t	This study
pVTC2-VTC4	pRS426-P$_{PGK1p}$-gme-HXT7t-P$_{GPM1p}$-vtc2-vtc4-GPM1t-gldh-ENO2t-P$_{TPI1p}$-galdh-PGK1t	This study
pGalDH-GLDH	pRS426-P$_{PGK1p}$-gme-HXT7t-P$_{GPM1p}$-vtc2-CYC1t-P$_{TDH3p}$-vtc4-GPM1t-P$_{TPI1p}$-galdh-gldh-ENO2t	This study
pVTC2-GLDH	pRS425-P$_{TEF1p}$-vtc2-CYC1t-P$_{TDH3p}$-gldh-ENO2t	This study
pALO1-VTC2	pRS425-P$_{GPM1p}$-alo1-HXT7t-P$_{TEF1p}$-vtc2-CYC1t	This study
pALO1-GLDH	pRS425-P$_{GPM1p}$-alo1-HXT7t-P$_{TDH3p}$-gldh-ENO2t	This study
pALO1	pPRS423-P$_{TDH3p}$-alo1-HXT7t	This study
pHE-Gal	pRS413-P$_{GAL1p}$-PGI1t	This study
pGME-Gal	pRS413-P$_{GAL1p}$-gme-PGI1t	This study
pVTC2-Gal	RS413-P$_{GAL1p}$-vtc2-PGI1t	This study
pVTC4-Gal	pRS413-P$_{GAL1p}$-vtc4-PGI1t	This study
pGalDH-Gal	pRS413-P$_{GAL1p}$-galdh-PGI1t	This study
pGLDH-Gal	pRS413-P$_{GAL1p}$-gldh-PGI1t	This study
pGLDH-2	pRS413-P$_{TEF2p}$-gldh-ENO2t	This study
pGME-425	pRS425-P$_{PGK1p}$-gme-HXT7t	This study
pVTC2-425	pRS425-P$_{GPM1p}$-vtc2-CYC1t	This study
pVTC4-425	pRS425- P$_{TDH3p}$-vtc4-GPM1t	This study
pGalDH-425	pRS425- P$_{TPI1p}$-galdh-PGK1t	This study
pGLDH-425	pRS425-P$_{TEF2p}$-gldh-ENO2t	This study

pRS425, resulting in five multicopy vectors pGME-425, pVTC2-425, pVTC4-425, pGalDH-425, and pGLDH-425 (**Supplementary Figure S3C**).

All the restriction enzymes and modification enzymes used in this study were from New England Biolabs.

Strains, Medium, and Culture Conditions

Yeast strains used in this study are listed in **Table 2**. Plasmid cloning work and circuit construction characterization were all performed in *Escherichia coli* Trans-T1 strains. They were grown in *Luria–Bertani broth* (LB) media (10 g/L of peptone, 5 g/L of NaCl, and 5 g/L of yeast extract) at 37℃ and 220 rpm. *S. cerevisiae* strain BY4741 (MATa his3Δ1 leu2Δ0 met15Δ0 ura3Δ0) was used as the parental strain in this study. All yeast transformations were performed using the LiAc/PEG/ss-DNA protocol. The parental yeast strain was treated under heat shock at 42°C for 15 min, recovered in 5 mM calcium chloride for 5 min after incubation, and eventually plated on a suitable selection medium (Martani et al., 2013). Engineered yeast strains were grown in synthetic complete (SC) medium (20 g/L of glucose, 6.7 g/L of yeast nitrogen base without amino acids, and appropriate amino acids) under auxotroph-screening conditions (Uracil 0.02 g/L, histidine 0.02 g/L, tryptophan 0.02 g/L, and leucine 0.1 g/L) or yeast extract–peptone–dextrose (YPD) medium (20 g/L of glucose, 10 g/L of yeast extract, and 20 g/L of peptone). They were grown in shake tubes at 30℃ and 220 rpm.

Yeast cells for intracellular VC determination were inoculated in 5 mL of SC medium with appropriate selectivity. After transferring, the culture was inoculated in the fermentation medium with an initial OD$_{600}$ = 0.1 for shake flask fermentation. The fermentation medium was YPD medium with diploid sugar (40 g/L of glucose). All strains were grown in shake flasks at 30°C and 150 rpm, and the ratio of flask volume:medium was 5:1. When GAL1p yeast strains completely consumed glucose for growth (24 h), galactose, with a final concentration of 20 g/L, was added to the medium to introduce gene overexpression.

The Extraction of Vitamin C

Yeast cells of 5 mL fermentation were harvested in a 10-mL ice-cold centrifugal tube by centrifugation at 4°C and 5,000 rpm for 10 min, washed once with ice-cold distilled water in a new ice-cold 2 mL centrifugal tube, and then resuspended in 400 μL ice-cold 2.5% metaphosphate and 100 μL 1 M DTT. The same cell volume of silicon dioxide was added, and the cells were vortexed vigorously for 5 min. Then they were immediately kept in ice for 5 min. After six cycles, the supernatant was then cleared from cell debris by centrifugation at 4°C and 12,000 rpm for 15 min and transferred to a new ice-cold 2-mL centrifugal tube with 15 μL of aqueous ammonia to adjust the pH. The supernatant passed through a 0.22-μm filter prior to high-performance liquid chromatography (HPLC) analyses.

Vitamin C, Glucose, and Ethanol Quantification

The identity of VC was confirmed by HPLC (Waters e2695–2489) with a Hypersil GOLD^{TM} HILIC column (5 μm inner diameter, 250 μm by 4.6 μm, Thermo Scientific, catalog no. 26505–254630) with 85% acetonitrile, 14.985% H$_2$O, and 0.015%

TABLE 2 | List of yeast strains and plasmids used in this study.

Strain	Genotype	Description	Source
BY4741	MATa; his3Δ 1; leu2Δ 0; met15Δ 0; ura3Δ 0	/	Our laboratory
YLAA	MATa; his3Δ 1; leu2Δ 0; met15Δ 0; ura3Δ 0	BY4741 (p2-4-6-1, pGLDH-1)	This study
YLAA-2	MATa; his3Δ 1; leu2Δ 0; met15Δ 0; ura3Δ 0	BY4741 (p2-4-6-1-2)	This study
YLAAF-1	MATa; his3Δ 1; leu2Δ 0; met15Δ 0; ura3Δ 0	BY4741 (pGME-VTC2)	This study
YLAAF-2	MATa; his3Δ 1; leu2Δ 0; met15Δ 0; ura3Δ 0	BY4741 (pVTC2-VTC4)	This study
YLAAF-3	MATa; his3Δ 1; leu2Δ 0; met15Δ 0; ura3Δ 0	BY4741 (pGalDH-GLDH)	This study
YLAA*	MATa; his3Δ 1; leu2Δ 0; met15Δ 0; ura3Δ 0	BY4741 (p2-4-6-1, pGLDH-2)	This study
YLAAK-1	MATa; his3Δ 1; leu2Δ 0; met15Δ 0; ura3Δ 0	YLAA* (pVTC2-GLDH)	This study
YLAAK-2	MATa; his3Δ 1; leu2Δ 0; met15Δ 0; ura3Δ 0	YLAA* (pALO1-VTC2)	This study
YLAAK-3	MATa; his3Δ 1; leu2Δ 0; met15Δ 0; ura3Δ 0	YLAA* (pALO1-GLDH)	This study
YLAAK-4	MATa; his3Δ 1; leu2Δ 0; met15Δ 0; ura3Δ 0	BY4741 (p2-4-6-1, pALO1, pVTC2-GLDH)	This study
GME-Gal	MATa; his3Δ 1; leu2Δ 0; met15Δ 0; ura3Δ 0	YLAA (pGME-Gal)	This study
VTC2-Gal	MATa; his3Δ 1; leu2Δ 0; met15Δ 0; ura3Δ 0	YLAA (pVTC2-Gal)	This study
VTC4-Gal	MATa; his3Δ 1; leu2Δ 0; met15Δ 0; ura3Δ 0	YLAA (pVTC4-Gal)	This study
GalDH-Gal	MATa; his3Δ 1; leu2Δ 0; met15Δ 0; ura3Δ 0	YLAA (pGalDH-Gal)	This study
GLDH-Gal	MATa; his3Δ 1; leu2Δ 0; met15Δ 0; ura3Δ 0	YLAA (pGLDH-Gal)	This study
GME-M	MATa; his3Δ 1; leu2Δ 0; met15Δ 0; ura3Δ 0	YLAA* (pGME-425)	This study
VTC2-M	MATa; his3Δ 1; leu2Δ 0; met15Δ 0; ura3Δ 0	YLAA* (pVTC2-425)	This study
VTC4-M	MATa; his3Δ 1; leu2Δ 0; met15Δ 0; ura3Δ 0	YLAA* (pVTC4-425)	This study
GalDH-M	MATa; his3Δ 1; leu2Δ 0; met15Δ 0; ura3Δ 0	YLAA* (pGalDH-425)	This study
GLDH-M	MATa; his3Δ 1; leu2Δ 0; met15Δ 0; ura3Δ 0	YLAA* (pGLDH-425)	This study

phosphoric acid, a flow rate of 1 mL/min, and UV detection set at 245 nm, with pure VC as the standard (as shown in **Supplementary Figure S3**).

The identity of glucose and ethanol was confirmed by HPLC with an Aminex® HPX-87H Ion Exclusion column (9-μm inner diameter, 300 μm by 7.8 μm, Bio-Rad, catalog no. 125–0140) with 5 mM H_2SO_4, a flow rate of 0.6 mL/min, at 65°C with glucose·$2H_2O$ and absolute ethanol as the standard.

Transcriptional Analysis

RNA was extracted using the Column Fungal RNAout (TIANDZ, catalog no. 80804-50). Nearly 1 μg of total RNA was used for cDNA synthesis with the SPARKscript II RT Kit (SparkJade), following the manufacturer's instructions. cDNA samples were diluted with ddH$_2$O and were used for fluorescence quantitative PCR (qPCR). qPCR analysis was performed on q225–0265 qPCR system (Kubo tech Ltd.) using Unique Aptamer^{TM} qPCR SYBR® Green Master Mix (Novogene). The primers used for qPCR to quantify relevant genes are listed in **Supplementary Table S2**. The internal standard is Gene TDH3.
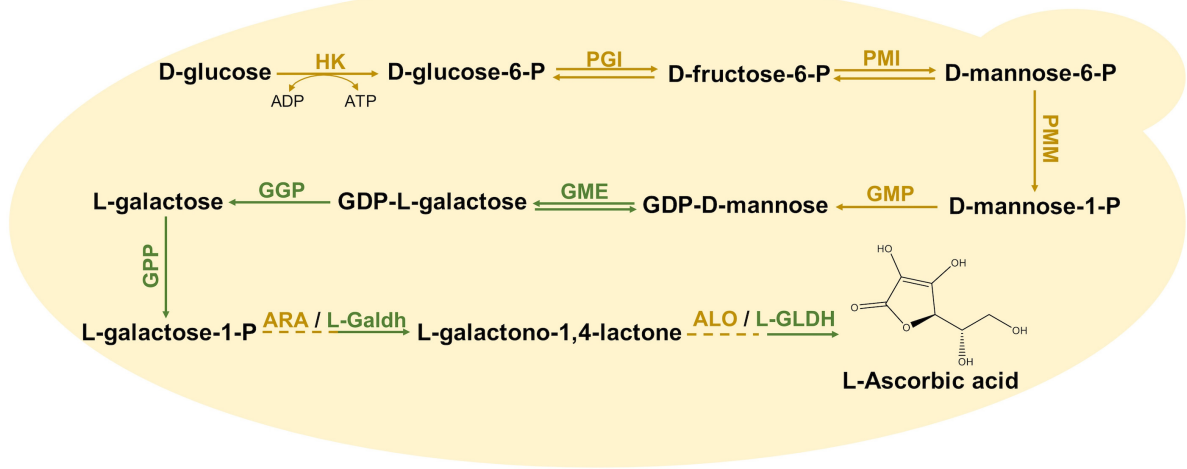
RESULTS

The Construction and Fermentation of Vitamin C Biosynthesis Strain

The VC synthesis pathway of plants starts with glucose, and it is finally produced after 10 steps of reactions (**Figure 1**; Wheeler et al., 1998). Three bio-reactive enzymes of this pathway, GME, GGP, and GPP, did not exist in *S. cerevisiae*, and the research of Branduardi et al. (2007) proved that

these genes from *Arabidopsis* could express exogenously. Since codon optimization would improve the efficiency of the enzyme (Wang et al., 2017), we optimized the codons of the genes related to this pathway from *Arabidopsis*. Each gene was collocated with a different constitutive promoter and terminator to construct an exogenous module, and all the modules were introduced to *S. cerevisiae* BY4741, but VC could not be detected. After that, two modules, respectively, expressing L-GalDH, L-GLDH were together transformed into BY4741 resulting in the recombinant stain YLAA. This construction enabled it to synthesize VC from glucose, and it accumulated 3.58 ± 0.40 mg/L of intracellular VC at 72 h (**Figure 2A**).

In order to investigate whether the introduction of exogenous modules related to VC synthesis would affect the normal cell growth, the curves of the growth, the glucose consumption, and the ethanol and VC production of strain BY4741 and YLAA are indicated in **Figure 2A**. The growth of YLAA was basically similar to BY4741, and 40 g/L of glucose was simultaneously consumed at the end of the logarithm. Following this, ethanol was consumed for the secondary growth of the strain with the final OD$_{600}$ of about 25 in the stationary phase. The results indicate that the introduction of the VC synthetic pathway did not bring additional growth burden and glucose requirement to *S. cerevisiae*. In addition, intracellular VC began to accumulate at 24 h and reached a maximum at 72 h. The reason for the decrease at 96 h might be due to its oxidation. It could be seen that VC synthesis was not synchronized with the growth in *S. cerevisiae*. It indicated that GDP-D-mannose was first used to synthesize cytoderm to achieve high cell concentration, and then the excess was converted to VC (Jiang et al., 2008).

FIGURE 1 | The Vitamin C biosynthesis pathway reconstructed in *S. cerevisiae*. The following enzymes are involved: HK, hexokinase; GPI, glucose-6-phosphate isomerase; MPI, mannose-6-phosphate isomerase; PMM, phosphomannomutase; GMP, GDP-mannose pyrophosphorylase; GME, GDP-mannose-3,5-epimerase; GGP, GDP-L-galactose phosphorylase; GPP, L-Galactose 1-phosphate phosphatase; ARA, D-Arabinose dehydrogenase; ALO, D-Arabinono-1,4-Lactone Oxidase; L-GalDH, L-galactose dehydrogenase; L-GLDH, L-galactono-1,4-lactone dehydrogenase. The introduced genes from *Arabidopsis* are marked in green.
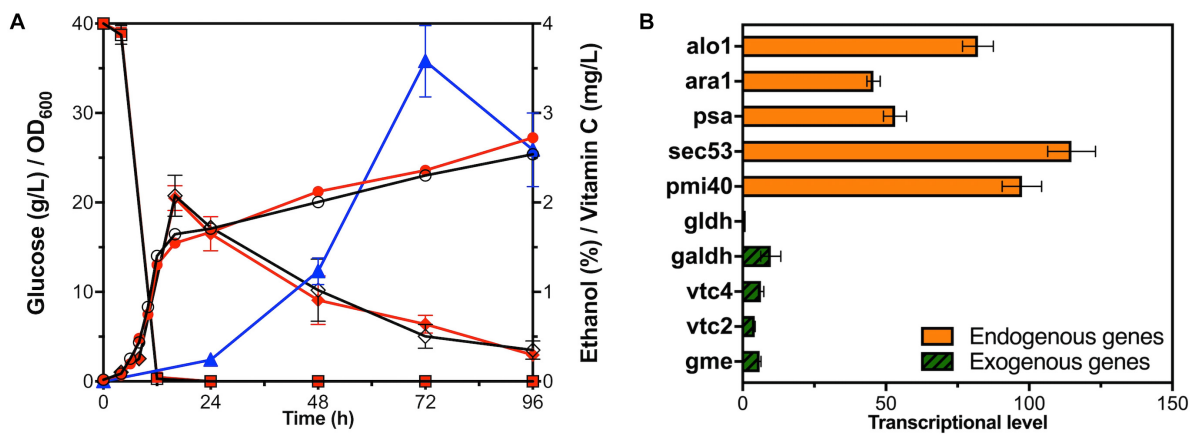

FIGURE 2 | Fermentation and transcriptional level analysis of YLAA. **(A)** Time courses showing changes in cell concentration (circles), glucose consumption (squares), ethanol production (rhombuses), and VC production (triangles) of YLAA (red solid) and BY4741 (black hollow) during fermentation. **(B)** The transcriptional level of genes involved in the VC biosynthetic pathway in strain YLAA. The control gene is Gene gldh. Error bars represent ± standard error of mean (SEM, *n* = 3).

In order to investigate the rate-limiting steps of the pathway, the transcriptional levels of five endogenous genes and five exogenous genes in YLAA were simultaneously detected (**Figure 2B**). It could be apparently seen that the transcriptional levels of the five endogenous genes were much higher than those of the exogenous genes. Among the transcriptional levels of endogenous genes, the highest one was sec53, and the lowest two

were psa1 and ara1. What was more critical was the comparison of the transcriptional level of exogenous genes. The gene with the highest transcriptional level was galdh, and the lowest two were vtc2 and gldh. The transcriptional level of galdh was about 10-fold that of gldh. The transcriptional level of ara1 was about 46-fold that of gldh. In summary, one of the sticking points to improve the production of VC was how to increase the

transcriptional level and expression intensity of exogenous genes, especially vtc2 and gldh.

Metabolic Pathway Optimization by Engineering Multiple Exogenous Modules

The Whole-Exogenous-Module Overexpression

Improving the transcription levels of exogenous genes was urgently needed, so five exogenous modules involved in the VC pathway were overexpressed by multicopy plasmid to obtain strain YLAA-2. After the shake flask fermentation of YLAA-2, the production of VC was detected at 72 h. Its production was increased by 61.5% compared with the initial strain YLAA, reaching 5.78 ± 0.04 mg/L (**Figure 3A**).
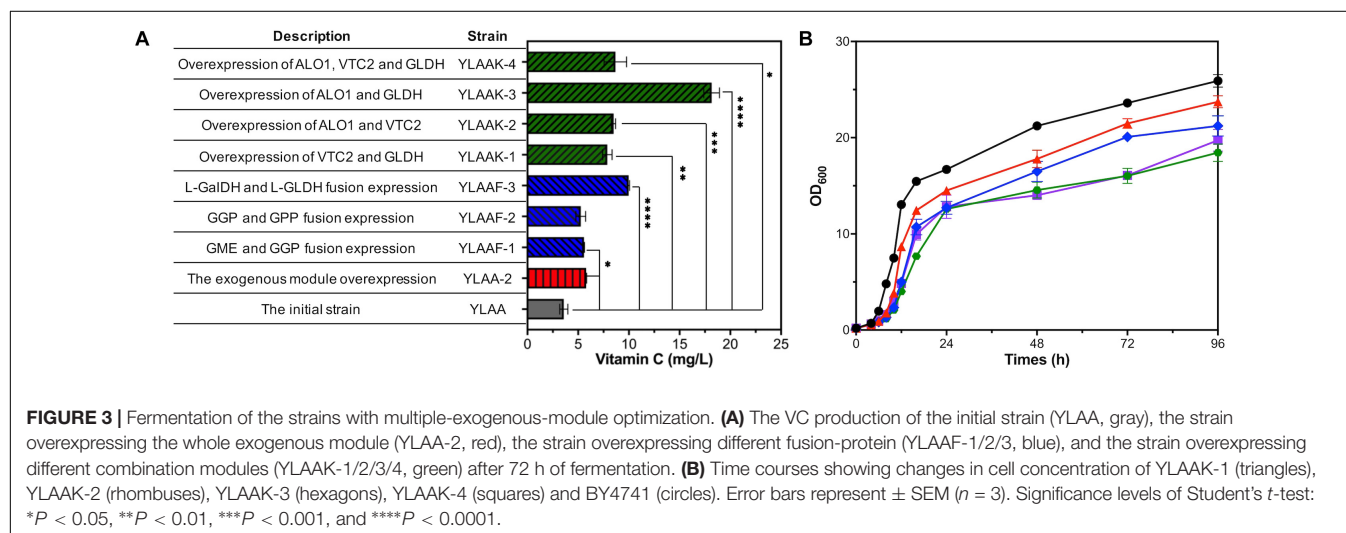
Protein Fusion Engineering

According to the above qPCR results, the rate-limiting enzymes of the VC synthesis pathway in *S. cerevisiae* were probably GPP and L-GLDH. The fusion protein had the complete coding sequence of each enzyme molecule, so it owned the respective catalytic functions of the enzyme molecules that composed it. Therefore, a protein engineering strategy using $(GGGGS)_3$ flexible linker for fusion overexpression of GPP or L-GLDH and its adjacent-step protein was adopted, resulting in constructing three recombinant strains (Huston et al., 1988). After fermentation for 72 h, only the fusion overexpression of L-Galdh and L-GLDH significantly increased the intracellular VC accumulation, reaching 9.97 ± 0.09 mg/L, which has been raised 1.78 times as against that of YLAA (**Figure 3A**). The production increase of the other two strains was not obvious, and it might be caused by the changes in enzyme structure or the inappropriate linker. The main reasons for the increase of strain YLAAF-3 might be the following: Proximity effects were exhibited by the fusion of enzymes in adjacent catalytic reactions, and transient time of reactions was decreased (Ljungcrantz et al., 1989,

1990). In addition, fusion-protein expression could reduce the degradation of intermediate metabolites by the intracellular proteases (Albertsen et al., 2011; Dai et al., 2012; Ignea et al., 2014).

Copy Number Engineering of the Possible Rate-Limiting Genes for Its Expression Optimization

It was inferred from qPCR results that it was urgent to increase the expression intensity of vtc2 and gldh. Some studies demonstrated that D-arabinono-1,4-lactone oxidase (ALO) was likely to be an isoenzyme of L-GLDH (Huh et al., 1994; Lee et al., 1999; Sauer et al., 2004). Sauer et al. (2004) found that overexpression of Gene alo1 and gldh enhanced yeast cells to accumulate VC, which indicated the significance of the last step. Three genes are divided into four combination modules: vtc2 and gldh; alo1 and vtc2; alo1 and gldh; and alo1, vtc2, and gldh. Aiming to improve the strength of expression initiation, each gene was equipped with a strong constitutive promoter, e.g., TEF1p, TDH3p, or GPM1p (Partow et al., 2010; Sun et al., 2012; Wang et al., 2015). Thus, four recombinant strains overexpressing the above gene modules were constructed. As shown in **Figure 3A**, YLAAK-3 had the highest production (16.97 ± 0.65 mg/L), which was consistent with the conclusion that the last step of the VC synthesis pathway was the rate-limiting step (Sauer et al., 2004). The others were similarly about twice that of YLAA.

From the growth curve of strains, the growth of four recombinant strains was obviously weaker than that of BY4741 and YLAA (**Figure 3B**). Its specific manifestations were long lag phase, lagging logarithmic phase, and low cell concentration. In addition, it was included that the overexpression of alo1 had a significant negative impact on the cell growth. The weakest strains were YLAAK-3 and YLAA-4, and the same genes they overexpressed were alo1 and gldh. In summary, overexpression of excessive gene modules indeed caused the growth and metabolism disorders in *S. cerevisiae*, especially the modules related to the important last step.

FIGURE 3 | Fermentation of the strains with multiple-exogenous-module optimization. **(A)** The VC production of the initial strain (YLAA, gray), the strain overexpressing the whole exogenous module (YLAA-2, red), the strain overexpressing different fusion-protein (YLAAF-1/2/3, blue), and the strain overexpressing different combination modules (YLAAK-1/2/3/4, green) after 72 h of fermentation. **(B)** Time courses showing changes in cell concentration of YLAAK-1 (triangles), YLAAK-2 (rhombuses), YLAAK-3 (hexagons), YLAAK-4 (squares) and BY4741 (circles). Error bars represent ± SEM ($n = 3$). Significance levels of Student's *t*-test: $*P < 0.05$, $**P < 0.01$, $***P < 0.001$, and $****P < 0.0001$.

Engineering the Pathway of Vitamin C by Improving Single Exogenous Module Expression

Due to the negative effects of overexpression of excessive gene modules, we attempted to overexpress one exogenous module. In this study, two overexpression methods were chosen: Fusions of an open reading frame to GAL1p inducible promoter; Using plasmid with multiple copies (Rine, 1991).

Improving an Exogenous Module Expression by Gal1p

The first step of gene expression is DNA transcription. The promoter is a sequence that RNA polymerase recognizes, binds, and begins to transcribe. Therefore, transcription with a suitable promoter was of considerable significance for metabolic engineering (Nevoigt et al., 2006). The GAL1 promotor initiated induction with galactose as the sole carbon source in the medium and had a strong transcriptional initiation strength (Stagoj and Komel, 2008). According to the above conclusions, VC was beginning to accumulate in *S. cerevisiae* cells when glucose was lacking. Therefore, GAL1p was used to induce the overexpression of target genes by exogenous addition of galactose after glucose has been completely consumed.
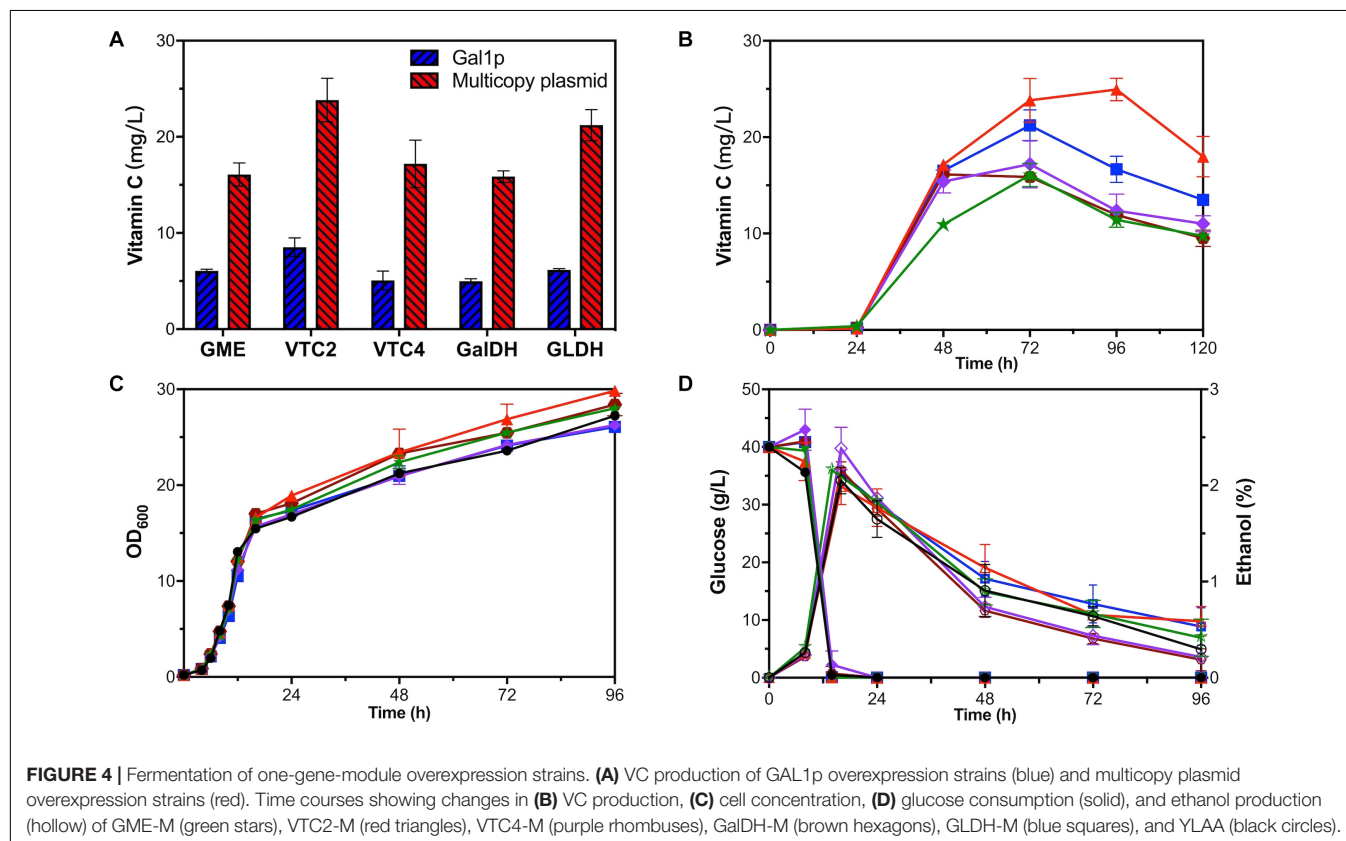
Each exogenous module, respectively, overexpressing gme, vtc2, vtc4, galdh, and gldh by GAL1p was introduced into strain YLAA to obtain five overexpression strains. Through HPLC results, we found that the use of GAL1p to overexpress any exogenous module indeed increased the intracellular accumulation of VC to varying degrees. Among them, strain VTC2-Gal had the greatest impact on the production (8.53 ± 0.95 mg/L), which indicated that vtc2 is one of the rate-limiting genes in this pathway (**Figure 4A**). However, the production was not as high as that of the previous strains, and the external addition of galactose caused a supernumerary increase in cost.

Balancing Gene Expression and Cell Growth by Copy Number Engineering

In addition to protein engineering, using multicopy plasmid was often used to increase the strength of gene expression in *S. cerevisiae* (Rine, 1991). What is more, increasing the copy numbers of too many gene modules caused disturbances in cell growth and metabolism. Therefore, the copy numbers of only one gene module were increased to improve its cell growth and metabolism.

Five recombinant strains were constructed to investigate the effect of a single gene overexpression by multicopy plasmid on the VC production in *S. cerevisiae*. As shown in **Figure 4A**, it could be clearly seen that the positive effect of using multicopy for overexpression on the production was better than using GAL1p. The production range was 15.86 ± 0.60– 23.83 ± 2.25 mg/L at 72 h. The production of strain VTC2-M was the highest, which has been raised nearly 5.66-fold compared with that in YLAA. As shown in **Figure 4B**, it could be clearly seen that all strains accumulated VC after 24 h, and

FIGURE 4 | Fermentation of one-gene-module overexpression strains. **(A)** VC production of GAL1p overexpression strains (blue) and multicopy plasmid overexpression strains (red). Time courses showing changes in **(B)** VC production, **(C)** cell concentration, **(D)** glucose consumption (solid), and ethanol production (hollow) of GME-M (green stars), VTC2-M (red triangles), VTC4-M (purple rhombuses), GalDH-M (brown hexagons), GLDH-M (blue squares), and YLAA (black circles).

the VC accumulation rate was fast from 24 to 48 h. It was worth paying attention that the difference from other strains was that VTC2-M reached the highest value of VC production of 24.94 ± 1.16 mg/L at 96 h (**Figure 4B**). The results once more indicated the importance of vtc2 in this pathway. From other aspects, overexpression of a single gene module promoted its cell concentration. Interestingly, the ethanol content of the two strains with the highest production was a little higher among five strains (**Figures 4C,D**). When secondary growth is caused by the consumption of ethanol and other metabolites in the stationary phase, their final OD_{600} was higher than YLAA. In particular, the cell growth of VTC2-M was better than others. The reason could be that higher VC bio-synthesis led to more reduction of reactive oxygen species (ROS) through redox reaction. By comparing the results of **Figures 3B**, **4C**, it was found that their cell concentration was higher than that of strains overexpressing combination modules, which might be due to the reduction of metabolic burden that allowed cells to perform normal physiological activities.

In order to quantify the increment of gene copy number, the transcriptional level of the corresponding gene in YLAA and five overexpression strains was analyzed (**Figure 5A**). Obviously, the overexpression by multicopy plasmid increased the transcription level by increasing its copy number. The copy number of vtc4 in VTC4-M increased the most, up by eightfold, followed by GME-M and GalDH-M. Both the copy number for gme and galdh almost increased by sixfold. The remaining VTC2-M or GLDH-M only increased by three or twofold, respectively. By combining with the VC production, there was a conclusion: For those genes whose transcriptional level were already relatively high, such as vtc4, gme, and galdh, the increased copy number was not as effective as the overexpression of genes with low transcription level, such as vtc2 and gldh. Furthermore, the strains with a low copy number increase had higher VC accumulation, which might be related to a more appropriate ratio of gene copy numbers. Through the analysis of the transcriptional level of all exogenous genes in VTC2-M, GLDH-M, and YLAA (**Figure 5B**), it was found

that overexpression of vtc2 or gldh not only increased its own transcriptional level but also increased the transcription level of others. It might be related to the accent and decline of the intermediate metabolite level.

The Effect of Adding Exogenous Substances on Vitamin C Production

In order to investigate which intermediate metabolites were still lacking in the process of the VC synthesis, 250 mg/L of L-galactose or L-galactono-1,4-lactone was exogenously added to the shake flask. What is more, the addition of glutathione (GSH) promoted thiamin/thiamin pyrophosphate (TPP) and GSH transport, increased the metabolism of tricarboxylic acid cycle and pentose phosphate pathway, and upregulated ROS detoxification proteins (Ma et al., 2012). At the same time, it was also an antioxidant, so 200 mg/L of GSH was exogenously added in the hope that it might reduce the loss of VC.

For VTC2-M, all three kinds of exogenous substances had a positive effect on the VC biosynthesis in late fermentation period (**Figure 6**). VTC2-M with the addition of GSH and L-galactose accumulated nearly 44 mg/L of VC intracellularly on the fifth day, and there seemed to be an upward trend. With the addition of L-galactono-1,4-lactone, the accumulation of VC reached the highest value (42.56 ± 0.65 mg/L) on the fourth day and then declined. Since L-galactose was the upstream intermediate metabolite of L-galactono-1,4-lactone, and the effect of adding this substance was consistent with that of vtc2 overexpression, we inferred that it was critical to reconstruct and even look for more efficient enzymes than GPP encoded by vtc2 from *Arabidopsis*. As for the reason for the positive effect of the addition of GSH, it could be further proved by transcription analysis in the future.

DISCUSSION

The two-step fermentation method, used in industrial production of VC, included two chemical reaction steps and two biological fermentation steps. Nowadays, people are focusing on achieving
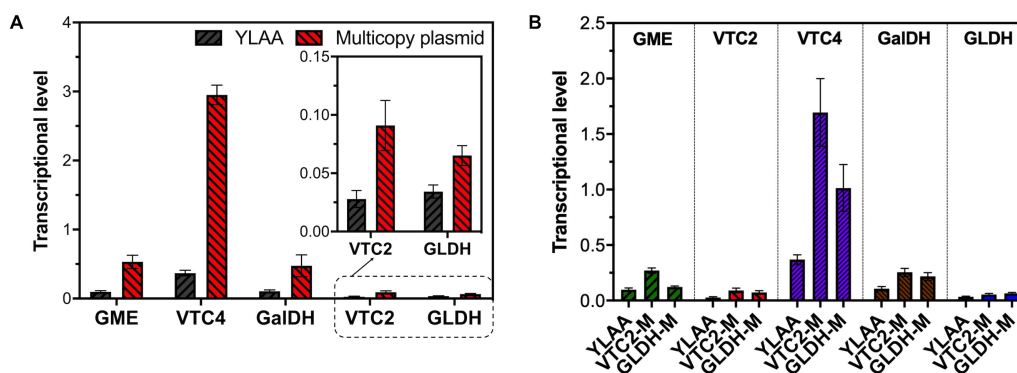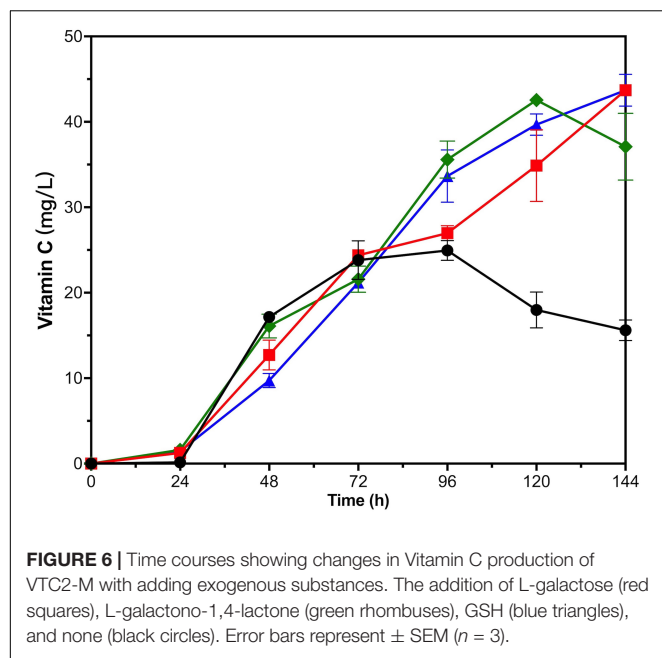

FIGURE 5 | The transcription level of multicopy plasmid overexpression stains. **(A)** The transcription level of corresponding exogenous genes in multicopy plasmid overexpression strains (red) and YLAA (gray). **(B)** The transcription level of exogenous genes, gme (green), vtc2 (red), vtc4 (purple), galdh (brown), and gldh (blue). The first bar of every group is the transcription level of gene in YLAA. The second one is that in VTC2-M. The third one is that in GLDH-M. Error bars represent ± SEM (*n* = 3).

FIGURE 6 | Time courses showing changes in Vitamin C production of VTC2-M with adding exogenous substances. The addition of L-galactose (red squares), L-galactono-1,4-lactone (green rhombuses), GSH (blue triangles), and none (black circles). Error bars represent ± SEM (*n* = 3).

one-step fermentation. Branduardi et al. (2007) first designed the metabolic pathway of synthesizing 0.2 mg/L of VC from glucose in *S. cerevisiae*. *S. cerevisiae* cells, as a model organism, were widely used to express exogenous genes for large-scale industrial production due to the well investigation of its genetic and growth characteristics (Lian et al., 2018). However, researchers were currently exploring the stress resistance of VC biosynthesis yeasts (Branduardi et al., 2007; Fossati et al., 2010; Martani et al., 2013). This research focused on exploring the rate-limiting steps and optimizing the VC biosynthesis in *S. cerevisiae*.

Overexpressing alo1 and gldh in several module combinations has the best effect to improve VC production, which emphasized the importance of the last step (**Figure 3**). Sauer et al. (2004) enhanced the ability of yeast cells to generate VC from L-galactose by overexpressing alo1 and gldh, which proved that the last step was the rate-limiting step. In addition, the results of overexpressing a single gene module proved that that the step catalyzed by GPP encoded by vtc2 was also one of crucial rate-limiting steps (**Figures 4A,B**).

Protein fusion could implement the balance and optimization of the synthesis pathway by increasing the concentration of enzymes and intermediate metabolites at the specific location. Özaydin et al. (2013) enhanced the biosynthesis of bisabolene through the fusion protein expression. Combining the fusion protein of t3CrGES/Erg20^{WW} and Erg20^{WW} increased the production of geraniol by 2.73 times (Jiang et al., 2017). The intensity of gene expression also played an important role for product synthesis. Kim et al. (2016) regulated gene expression by promoter engineering to achieve low ethanol production and high 2,3-butanediol production. Chen et al. (2012) improved the expression of exogenous proteins by multi-copy plasmids and enhanced patchoulol production. In

this study, the metabolic engineering methods were improved and applied to the optimization of one-step biosynthesis of VC in *S. cerevisiae*. First, the fusion expression of L-GalDH and L-GLDH was applied and increased intracellular VC production by 2.78-fold in *S. cerevisiae* (**Figure 3A**). In order to balance cell production and concentration, a single-module-overexpression strategy was adopted. The best recombinant strain overexpressing vtc2 could accumulate 24.94 ± 1.16 mg/L of intracellular VC at 96 h, and it could reach nearly 44 mg/L in 144 h with the exogenous addition of 250 mg/L of L-galactose or 200 mg/L GSH (**Figures 4, 6**). Our research provided the experience in engineering *S. cerevisiae* strains for one-step fermentation of VC or any other valuable chemical production.

One-step biosynthesis of VC by *S. cerevisiae* has been long sought for, but there is still a long way to go. What is more, a yeast capable of synthesizing VC improved its antioxidant and the tolerance to low pH, weak organic acids, and the positive effect of VC on the treatment of cancer was related to its influence on ROS (Branduardi et al., 2007; Yun et al., 2015). The recombinant yeast constructed in this study could also represent a cellular model to investigate the occurrence/protection of ROS in eukaryote.

DATA AVAILABILITY STATEMENT

The original contributions presented in the study are included in the article/**Supplementary Material**, further inquiries can be directed to the corresponding author/s.

AUTHOR CONTRIBUTIONS

MZ and YB performed the experiment together, analyzed the data, and wrote the first draft. MD is corresponding joint authors, was responsible for the manuscript writing, designed and guided this study, provided project funding, and revised the manuscript. YY participated in the design of the study and put forward constructive suggestions for solving problems. All authors contributed to the article and approved the final manuscript.

FUNDING

SUPPLEMENTARY MATERIAL

The Supplementary Material for this article can be found online at: https://www.frontiersin.org/articles/10.3389/fmicb.2021.643472/full#supplementary-material

REFERENCES

Agathocleous, M., Meacham, C. E., Burgess, R. J., Piskounova, E., Zhao, Z. Y., Crane, G. M., et al. (2017). Ascorbate regulates haematopoietic stem cell function and leukaemogenesis. *Nature* 549:476. doi: 10.1038/nature 23876

Albertsen, L., Chen, Y., Bach, L. S., Rattleff, S., Maury, J., Brix, S., et al. (2011). Diversion of flux toward sesquiterpene production in *Saccharomyces cerevisiae* by fusion of host and heterologous enzymes. *Appl. Environ. Microbiol.* 77, 1033–1040. doi: 10.1128/aem.01361-10

Branduardi, P., Fossati, T., Sauer, M., Pagani, R., Mattanovich, D., and Porro, D. (2007). Biosynthesis of vitamin C by yeast leads to increased stress resistance. *PLoS One* 2:e1092. doi: 10.1371/journal.pone.000 1092

Cai, L., Yuan, M. Q., Li, Z. J., Chen, J. C., and Chen, G. Q. (2012). Genetic engineering of Ketogulonigenium vulgare for enhanced production of 2-keto-L-gulonic acid. *J. Biotechnol.* 157, 320–325. doi: 10.1016/j.jbiotec.2011. 12.004

Camarena, V., and Wang, G. (2016). The epigenetic role of vitamin C in health and disease. *Cell. Mol. Life Sci.* 73, 1645–1658. doi: 10.1007/s00018-016-2145-x

Carr, A. C., and McCall, C. (2017). The role of vitamin C in the treatment of pain: new insights. *J. Trans. Med.* 15:14. doi: 10.1186/s12967-017-1179-7

Chen, Y., Partow, S., Scalcinati, G., Siewers, V., and Nielsen, J. (2012). Enhancing the copy number of episomal plasmids in *Saccharomyces cerevisiae* for improved protein production. *FEMS Yeast Res.* 12, 598–607. doi: 10.1111/j. 1567-1364.2012.00809.x

Cimmino, L., Dolgalev, I., Wang, Y. B., Yoshimi, A., Martin, G. H., Wang, J. J., et al. (2017). Restoration of TET2 function blocks aberrant self-renewal and leukemia progression. *Cell* 170, 1079–1095. doi: 10.1016/j.cell.2017. 07.032

Dai, Z. B., Liu, Y., Huang, L. Q., and Zhang, X. L. (2012). Production of miltiradiene by metabolically engineered *Saccharomyces cerevisiae*. *Biotechnol. Bioeng.* 109, 2845–2853. doi: 10.1002/bit.24547

De Francesco, E. M., Bonuccelli, G., Maggiolini, M., Sotgia, F., and Lisanti, M. P. (2017). Vitamin C and doxycycline: a synthetic lethal combination therapy targeting metabolic flexibility in cancer stem cells (CSCs). *Oncotarget* 8, 67269–67286. doi: 10.18632/oncotarget. 18428

Du, J., Bai, W., Song, H., and Yuan, Y. J. (2013). Combinational expression of sorbose/sorbosone dehydrogenases and cofactor pyrroloquinoline quinone increases 2-keto-L-gulonic acid production in Ketogulonigenium vulgare-Bacillus cereus consortium. *Metab. Eng.* 19, 50–56. doi: 10.1016/j.ymben.2013. 05.006

Du, J., Zhou, J., Xue, J., Song, H., and Yuan, Y. J. (2012). Metabolomic profiling elucidates community dynamics of the Ketogulonicigenium vulgare-Bacillus megaterium consortium. *Metabolomics* 8, 960–973. doi: 10.1007/s11306-011-0392-2

Fossati, T., Passolunghi, S., Branduardi, P., and Porro, D. (2010). Acid stress response and tolerance in vitamin C producing yeasts. *J. Biotechnol.* 150, S406–S407. doi: 10.1016/j.jbiotec.2010.09.541

Gao, L., Hu, Y., Liu, J., Du, G., Zhou, J., and Chen, J. (2014). Stepwise metabolic engineering of Gluconobacter oxydans WSH-003 for the direct production of 2-keto-L-gulonic acid from D-sorbitol. *Metab. Eng.* 24, 30–37. doi: 10.1016/j. ymben.2014.04.003

Gao, Y., and Yuan, Y. J. (2011). Comprehensive quality evaluation of corn steep liquor in 2-Keto-L-gulonic Acid Fermentation. *J. Agric. Food Chem.* 59, 9845–9853. doi: 10.1021/jf201792u

Gibson, D. G. (2011). Enzymatic assembly of overlapping DNA fragments. Methods Enzymol. 498, 349–361. doi: 10.1016/B978-0-12-385120-8.00015-2

Gibson, D. G., Benders, G. A., Axelrod, K. C., Zaveri, J., Algire, M. A., Moodie, M., et al. (2008). One-step assembly in yeast of 25 overlapping DNA fragments to form a complete synthetic *Mycoplasma genitalium* genome. *Proc. Natl. Acad. Sci. U S A.* 105, 20404–20409. doi: 10.1073/pnas.081101 1106

Grosso, G., Bei, R., Mistretta, A., Marventano, S., Calabrese, G., Masuelli, L., et al. (2013). Effects of Vitamin C on health: a review

of evidence. *Front. Bioscience-Landmark* 18:1017–1029. doi: 10.2741/4160

Harrison, F. E., and May, J. M. (2009). Vitamin C function in the brain: vital role of the ascorbate transporter SVCT2. *Free Radical Biol. Med.* 46, 719–730. doi: 10.1016/j.freeradbiomed.2008.12.018

Huang, Z., Zou, W., Liu, J., and Liu, L. (2013). Glutathione enhances 2-keto-L-gulonic acid production based on *Ketogulonicigenium vulgare* model iWZ663. *J. Biotechnol.* 164, 454–460. doi: 10.1016/j.jbiotec.2013.01.007

Huh, W. K., Lee, B. H., Kim, S. T., Kim, Y. R., Rhie, G. E., Baek, Y. W., et al. (1998). D-Erythroascorbic acid is an important antioxidant molecule in Saccharomyces cerevisiae. *Mol. Microbiol.* 30, 895–903. doi: 10.1046/j.1365-2958.1998. 01133.x

Huh, W. K., Kim, S. T., Yang, K. S., Seok, Y. J., Hah, Y. C., and Kang, S. O. (1994). Characterisation of D-arabinono-1,4-lactone oxidase from *Candida albicans* ATCC 10231. *Eur. J. Chem.* 225, 1073–1079. doi: 10.1111/j.1432-1033.1994. 1073b.x

Huston, J. S., Levinson, D., Mudgett-Hunter, M., Tai, M. S., Novotny, J., Margolies, M. N., et al. (1988). Protein engineering of antibody binding sites: recovery of specific activity in an anti-digoxin single-chain Fv analogue produced in *Escherichia coli. Proc. Natl. Acad. Sci. U.S.A.* 85, 5879–5883. doi: 10.1073/pnas. 85.16.5879

Ignea, C., Pontini, M., Maffei, M. E., Makris, A. M., and Kampranis, S. C. (2014). Engineering monoterpene production in yeast using a synthetic dominant negative geranyl diphosphate synthase. *ACS Synth. Biol.* 3, 298–306. doi: 10. 1021/sb400115e

Jia, N., Ding, M. Z., Gao, F., and Yuan, Y. J. (2016). Comparative genomics analysis of the companion mechanisms of *Bacillus thuringiensis* Bc601 and Bacillus endophyticus Hbe603 in bacterial consortium. *Sci. Rep.* 6:28794. doi: 10.1038/srep28794

Jiang, H., Ouyang, H., Zhou, H., and Jin, C. (2008). GDP-mannose pyrophosphorylase is essential for cell wall integrity, morphogenesis and viability of *Aspergillus fumigatus*. *Microbiology-Sgm* 154, 2730–2739. doi: 10.1099/mic.0.2008/019240-0

Jiang, G. Z., Yao, M. D., Wang Y., Zhou, L., Song, T. Q., Liu, H., et al. (2017). Manipulation of GES and ERG20 for geraniol overproduction in Saccharomyces cerevisiae. *Metab. Eng.* 41, 57–66. doi: 10.1016/j.ymben.2017. 03.005

Kim, J. W., Kim, J., Seo, S. O., Kim, K. H., Jin, Y. S., and Seo, J. H. (2016). Enhanced production of 2,3-butanediol by engineered Saccharomyces cerevisiae through fine-tuning of pyruvate decarboxylase and NADH oxidase activities. *Biotechnol. Biofuels* 9265. doi: 10.1186/s13068-016-0677-9

Kim, S. T., Huh, W. K., Lee, B. H., and Kang, S. O. (1998). D-arabinose dehydrogenase and its gene from *Saccharomyces cerevisiae. Biochimica Et Biophysica Acta-Protein Structure Mol. Enzymol.* 1429, 29–39. doi: 10.1016/ s0167-4838(98)00217-9

King, C. G., and Waugh, W. A. (1932). The chemical nature of vitamin C. *Science (New York, N.Y.)* 75, 357–358. doi: 10.1126/science.75.1944. 357-a

Lee, B. H., Huh, W. K., Kim, S. T., Lee, J. S., and Kang, S. O. (1999). Bacterial production of D-erythroascorbic acid and L-ascorbic acid through functional expression of *Saccharomyces cerevisiae* D-arabinono-1,4-lactone oxidase in *Escherichia coli*. Appl. Environ. Microbiol. 65, 4685–4687. doi: 10.1128/AEM. 65.10.4685-4687.1999

Lian, J., Mishra, S., and Zhao, H. (2018). Recent advances in metabolic engineering of Saccharomyces cerevisiae: new tools and their applications. *Metab. Eng.* 50, 85–108. doi: 10.1016/j.ymben.2018.04.011

Ljungcrantz, P., Bulow, L., and Mosbach, K. (1990). Construction and characterization of a recombinant tripartite enzyme, galactose dehydrogenase/beta-galactosidase/galactokinase. *FEBS Lett.* 275, 91–94. doi: 10.1016/0014-5793(90)81446-u

Ljungcrantz, P., Carlsson, H., Mansson, M. O., Buckel, P., Mosbac, K., and Bulow, L. (1989). Construction of an artificial bifunctional enzyme, beta-galactosidase/galactose dehydrogenase, exhibiting efficient galactose channeling. *Biochemistry* 28, 8786–8792. doi: 10.1021/bi00448a016

Magrì, A., Germano, G., Lorenzato, A., Lamba, S., Chila, R., Montone, M., et al. (2020). High-dose vitamin C enhances cancer immunotherapy. *Sci. Trans. Med.* 12:eaay8707. doi: 10.1126/scitranslmed.aay8707

Mandlaa, Yang, W., Han, L., Wang, Z., and Xu, H. (2013). Two-helper-strain co-culture system: a novel method for enhancement of 2-keto-l-gulonic acid production. *Biotechnol. Lett.* 35, 1853–1857. doi: 10.1007/s10529-013-1292-5

Ma, Q., Zhang, W. W., Zhang, L., Qiao, B., Pan, C. S., Yi, H., et al. (2012). Proteomic analysis of *Ketogulonicigenium vulgare* under glutathione reveals high demand for thiamin transport and antioxidant protection. *PLoS One* 7:e32156. doi: 10.1371/journal.pone.0032156

Martani, F., Fossati, T., Posteri, R., Signori, L., Porro, D., and Branduardi, P. (2013). Different response to acetic acid stress in *Saccharomyces cerevisiae* wild-type and l-ascorbic acid-producing strains. *Yeast* 30, 365–378. doi: 10.1002/yea.2969

McCormick, W. J. (1954). Cancer: the preconditioning factor in pathogenesis; a new etiologic approach. *Arch. Pediatrics* 71, 313–322.

Naidu, K. A. (2003). Vitamin C in human health and disease is still a mystery? an overview. *Nutrit. J.* 2:10. doi: 10.1186/1475-2891-2-7

Nevoigt, E., Kohnke, J., Fischer, C. R., Alper, H., Stahl, U., and Stephanopoulos, G. (2006). Engineering of promoter replacement cassettes for fine-tuning of gene expression in *Saccharomyces cerevisiae*. *Appl. Environ. Microbiol.* 72, 5266–5273. doi: 10.1128/aem.00530-06

Özaydin, B., Burd, H., Lee, T. S., and Keasling, J. D. (2013). Carotenoid-based phenotypic screen of the yeast deletion collection reveals new genes with roles in isoprenoid production. *Metab. Eng.* 15, 174–183. doi: 10.1016/j.ymben.2012.07.010

Padh, H. (1990). Cellular functions of ascorbic acid. *Biochem. Cell Biol.* 68, 1166–1173. doi: 10.1139/o90-173

Pan, C. H., Wang, E. X., Jia, N., Dong, X. T., Liu, Y., Ding, M. Z., et al. (2017). Reconstruction of amino acid biosynthetic pathways increases the productivity of 2-keto-l-gulonic acid in *Ketogulonicigenium vulgare-Bacillus endophyticus* consortium via genes screening. *J. Ind. Microbiol. Biotechnol.* 44, 1031–1040. doi: 10.1007/s10295-017-1928-x

Partow, S., Siewers, V., Bjorn, S., Nielsen, J., and Maury, J. (2010). Characterization of different promoters for designing a new expression vector in *Saccharomyces cerevisiae*. *Yeast* 27, 955–964. doi: 10.1002/yea.1806

Prigge, S. T., Mains, R. E., Eipper, B. A., and Amzel, L. M. (2000). New insights into copper monooxygenases and peptide amidation: structure, mechanism and function. *Cell. Mol. Life Sci.* 57, 1236–1259. doi: 10.1007/pl00000763

Qi, T., Sun, M., Zhang, C., Chen, P., Xiao, C., and Chang, X. (2020). Ascorbic acid promotes plasma cell differentiation through enhancing TET2/3-Mediated DNA demethylation. *Cell Rep.* 33:108452. doi: 10.1016/j.celrep.2020.108452

Rine, J. (1991). Gene overexpression in studies of Saccharomyces cerevisiae. *Methods Enzymol.* 194, 239–251. doi: 10.1016/0076-6879(91)94019-9

Reichstein, T., and Grüssner, A. (1934). Eine ergiebige Synthese der l-Ascorbinsäure (C-Vitamin). *Helvetica Chimica Acta* 17, 311–328.

Rosa, J. C. C., Colombo, L. T., Alvim, M., Avonce, N., Van Dijck, P., Passos, F. M., et al. (2013). Metabolic engineering of *Kluyveromyces lactis* for L-ascorbic acid (vitamin C) biosynthesis. *Microbial Cell Factories* 12:59. doi: 10.1186/1475-2859-12-59

Running, J. A., Severson, D. K., and Schneider, K. J. (2002). Extracellular production of L-ascorbic acid by *Chlorella protothecoides*, *Prototheca species*, and mutants of P-moriformis during aerobic culturing at low pH. *J. Ind. Microbiol. Biotechnol.* 29, 93–98. doi: 10.1038/sj.jim.7000275

Sauer, M., Branduardi, P., Valli, M., and Porro, D. (2004). Production of L-Ascorbic acid by metabolically engineered *Saccharomyces cerevisiae* and *Zygosaccharomyces bailii*. *Physiol. Biotechnol.* 70, 6086–6091. doi: 10.1128/aem.70.10.6086-6091.2004

Stagoj, M. N., and Komel, R. (2008). The GAL induction response in yeasts with impaired galactokinase Gal1p activity. *World J. Microbiol. Biotechnol.* 24, 2159–2166. doi: 10.1007/s11274-008-9724-4

Sun, J., Shao, Z., Zhao, H., Nair, N., Wen, F., Xu, J. H., et al. (2012). Cloning and characterization of a panel of constitutive promoters for applications in pathway engineering in *Saccharomyces cerevisiae*. *Biotechnol. Bioeng.* 109, 2082–2092. doi: 10.1002/bit.24481

Timoshnikov, V. A., Kobzeva, T. V., Polyakov, N. E., and Kontoghiorghes, G. J. (2020). Redox interactions of Vitamin C and iron: inhibition of the pro-oxidant activity by deferiprone. *Int. J. Mol. Sci.* 21:3967. doi: 10.3390/ijms21113967

Wang, D., Wang, L., Hou, L., Deng, X., Gao, Q., and Gao, N. (2015). Metabolic engineering of Saccharomyces cerevisiae for accumulating pyruvic acid. *Ann. Microbiol.* 65, 2323–2331. doi: 10.1007/s13213-015-1074-5

Wang, F. Q., Zhang, F., He, S., Li, W. J., Luo, H., and Wang, J. (2017). Cell surface Display and Enzymatic Property of Codon-optimized α-L-rhamnosidase Expressed in *Saccharomyces Cerevisiae*. ence of Sericulture.

Wheeler, G. L., Jones, M. A., and Smirnoff, N. (1998). The biosynthetic pathway of vitamin C in higher plants. *Nature* 393, 365–369. doi: 10.1038/30728

Yeom, C. H., Jung, G. C., and Song, K. J. (2007). Changes of terminal cancer patients' health-related quality of life after high dose vitamin C administration. *J. Korean Med. Sci.* 22, 7–11. doi: 10.3346/jkms.2007.22.1.7

Yun, J., Mullarky, E., Lu, C. Y., Bosch, K. N., Kavalier, A., Rivera, K., et al. (2015). Vitamin C selectively kills KRAS and BRAF mutant colorectal cancer cells by targeting GAPDH. *Science* 350, 1391–1396. doi: 10.1126/science.aaa5004

Zeng, W., Wang, P., Li, N., Li, J., Chen, J., and Zhou, J. (2020). Production of 2-keto-L-gulonic acid by metabolically engineered *Escherichia coli*. *Bioresource Technol.* 318, 124069–124069. doi: 10.1016/j.biortech.2020.124069

Zhou, J., Ma, Q., Yi, H., Wang, L., Song, H., and Yuan, Y. J. (2011). Metabolome profiling reveals metabolic cooperation between bacillus megaterium and ketogulonicigenium vulgare during induced swarm motility. *Appl. Environ. Microbiol.* 77, 7023–7030. doi: 10.1128/aem.05123-11

Zhu, Y., Liu, J., Du, G., Zhou, J., and Chen, J. (2012a). Sporulation and spore stability of Bacillus megaterium enhance *Ketogulonigenium vulgare* propagation and 2-keto-L-gulonic acid biosynthesis. *Bioresour. Technol.* 107, 399–404. doi: 10.1016/j.biortech.2011.12.080

Zhu, Y., Liu, J., Liu, J., Du, G., Zhou, J., and Chen, J. (2012b). A high throughput method to screen companion bacterium for 2-keto-L-gulonic acid biosynthesis by co-culturing *Ketogulonigenium vulgare*. *Process Biochem.* 47, 1428–1432. doi: 10.1016/j.procbio.2012.05.010

Zou, W., Liu, L. M., Zhang, J., Yang, H. R., Zhou, M. D., Hua, Q., et al. (2012). Reconstruction and analysis of a genome-scale metabolic model of the vitamin C producing industrial strain *Ketogulonicigenium vulgare* WSH-001. *J. Biotechnol.* 161, 42–48. doi: 10.1016/j.jbiotec.2012.05.015

Conflict of Interest: The authors declare that the research was conducted in the absence of any commercial or financial relationships that could be construed as a potential conflict of interest.

Coculture, An Efficient Biotechnology for Mining the Biosynthesis Potential of Macrofungi via Interspecies Interactions

Guihong Yu[1], Yuman Sun[1], Heyang Han[2], Xiu Yan[1], Yu Wang[1], Xiaoxuan Ge[1], Bin Qiao[3] and Lingling Tan[1]*

[1] Shandong Province Key Laboratory of Applied Mycology, and Qingdao International Center on Microbes Utilizing Biogas, School of Life Sciences, Qingdao Agricultural University, Qingdao, China, [2] College of Pharmacy, The Ohio State University, Columbus, OH, United States, [3] Key Laboratory of Systems Bioengineering, Ministry of Education, School of Chemical Engineering and Technology, Tianjin University, Tianjin, China

Macrofungi, which are also known as mushrooms, can produce various bioactive constituents and have become promising resources as lead drugs and foods rich in nutritional value. However, the production of these bioactive constituents under standard laboratory conditions is inefficiency due to the silent expression of their relevant genes. Coculture, as an important activation strategy that simulates the natural living conditions of macrofungi, can activate silent genes or clusters through interspecific interactions. Coculturing not only can trigger the biosynthesis of diverse secondary metabolites and enzymes of macrofungi, but is also useful for uncovering the mechanisms of fungal interspecific interactions and novel gene functions. In this paper, coculturing among macrofungi or between macrofungi and other microorganisms, the triggering and upregulation of secondary metabolites and enzymes, the potential medicinal applications, and the fungal–fungal interaction mechanisms are reviewed. Finally, future challenges and perspectives in further advancing coculture systems are discussed.

Keywords: macrofungus, coculture, interspecific interaction, biosynthesis potential, metabolite

INTRODUCTION

Macrofungi, most of which belong to basidiomycetes, with the minority belonging to ascomycetes, are fungi that produce spore-bearing structures visible to the naked-eye and are known for their nutritional properties, medical value, and/or degradation capacity. It is estimated that approximately 140,000 macrofungi exist in nature and now, approximately 20,000 species have been found (Zhang, 2002; Niskanen et al., 2018). Macrofungi live as haploid mycelia and grow vegetatively in soil, woods, or solid media to develop into fruiting body. The mycelium of macrofungi can also be cultivated under submerged fermentation in shaking flasks. Both the fruiting body and liquid-cultivated mycelium have been reported to produce a number of useful constituents, including bioactive lead compounds (such as alkaloids, polyketides, terpenoids, and steroids) and degradation-related oxidative enzymes (such as laccase, lignin peroxidase, and manganese peroxidase) (Qu et al., 2019; Shen et al., 2019; Zhang et al., 2019; Lira-Pérez et al., 2020), which make macrofungi an important resource for agriculture, industry, and medicine.

Currently, the genomes of more than 90 macrofungi have been sequenced, which provides great genetic knowledge for profound research (Li et al., 2018). However, the silent expression of genes or gene clusters has often been reported in macrofungi, suggesting that their potential capacities urgently need to be developed. For example, the whole-genome sequence of the widely known medicinal macrofungus *Ganoderma lucidum* indicated 16,113 annotated or predicted genes in its 43.3-Mb genome, suggesting that many gene clusters related to its metabolite or enzyme synthesis were present (Chen et al., 2012), but so far, only about 400 metabolites have been found. This meant that many genes remained cryptic or had low expression.

To explore the silent gene clusters of diverse fungi, including macrofungi, many strategies have often been used, such as the OSMAC (one strain many compounds) strategy, genetic engineering, and coculture (Scherlach and Hertweck, 2009). The OSMAC strategy, which is usually performed by altering the culture media and cultural conditions or adding the chemical inducers, is an important mean to explore the metabolic potential of fungi because of its simplicity and effectiveness, but it is difficult to produce certain types of targeted compounds in this way (Bode et al., 2002). Recently, the rapid development of biotechnology, such as the emergence of third-generation of genome sequencing and CRISPR-Cas9 (clustered regularly interspaced short palindromic repeat-Cas9) technology, has made fungal genetic manipulation for mining secondary metabolite potential (e.g., high expression of transcription factors, knockout of HDAC genes) relatively easier (Noedvig et al., 2015; Weber et al., 2015). However, the genetic system of macrofungi, especially many basidiomycetes, is much more complex than those of other fungi and is still challenging to efficiently manipulate. Only a few macrofungi, including *G. lucidum*, *Ganoderma lingzhi*, *Cordyceps militaris*, *Agaricus bisporus*, *Schizophyllum commune,* and *Coprinopsis cinerea*, have been reported to be edited by the CRISPR-Cas9 system or to achieve an overexpression system using traditional plasmids (Zhou et al., 2012; Qin et al., 2017; Sugano et al., 2017; Chen et al., 2018; Jan Vonk et al., 2019; Shen et al., 2019, 2020). By comparison, the coculture strategy can simulate the symbiotic relationship of microorganisms in nature and easily activate silenced gene clusters through the interaction between strains (Moody, 2014; Xu et al., 2018; Shen et al., 2019). Recently, coculturing has been widely used in mining unknown biosynthetic potential, such as discovering novel secondary metabolites and enzymes that might be applied in the fields of medicine, agriculture, and industry in the future (**Figure 1**). Further study of the interaction mechanisms in coculture systems is useful for understanding the relationship of fungal–fungal interactions in a certain ecological niche. The coculture of bacteria and filamentous fungi has been well-reviewed, but the coculture of macrofungi has not yet been reviewed in detail. In this paper, coculture among macrofungi or between macrofungi and other microorganisms, the triggering and upregulation of secondary metabolites and enzymes, the potential medicinal applications as well as the fungal–fungal interaction mechanisms are reviewed. Finally, future challenges and perspectives in further advancing coculture systems are also discussed.

INTERACTIONS OF MACROFUNGI IN NATURE

In nature, microorganisms always coexist in the same niche, and they inevitably interact with neighbors when competing for nutrients and space. These interactions can affect fungal morphologies, adaptation modes, and development patterns and trigger their ability to synthesize novel metabolites and release extracellular enzymes (Sandland et al., 2007; Bertrand et al., 2014). For macrofungi, the interactions mainly manifest as one of the relationships of antagonism, mutualism and parasitism, and sometimes, the relationships can switch from one type to another. These interactions have been used for mining the metabolic potential of fungi or for studying the relevant metabolic mechanisms.

Antagonism is the most common relationship between macrofungi living in nature, which combat via cell–cell contact or form a confrontation zone due to the production of antimicrobial substances or chemical signals, such as in relationships between *Cordyceps cicadae* and many of its endophytic bacteria (Qu et al., 2019). The appearance of confrontation zones usually indicates the induction of bioactive substances and their release to inhibit competitors. Mutualism and parasitism are also important relationships of macrofungi. For instance, the sclerotial formation of *Grifola umbellate* relies on the existence of its companion fungus *Grifola* sp., and the continuous growth and development of *G. umbellate* sclerotium requires *Armillariella mellea* as the nutrient source (Guo and Xu, 1992; Guo et al., 2001, 2002; Xing and Guo, 2003).

ADVANCES IN THE STUDY OF MACROFUNGAL COCULTURES FOR EXPLORING THE BIOSYNTHESIS POTENTIAL OF SECONDARY METABOLITES

To mimic the relationships of fungi in nature, different coculture systems, including macrofungi-macrofungi, macrofungi-microalgae, macrofungi-cyanobacteria, macrofungi-filamentous fungi, macrofungi-bacteria, and macrofungi-actinomycetes, have been established. These cocultures have shown various bioactivities, such as antimicrobial activity, antitumor activity, and antioxidant activity (Zheng et al., 2011; Shen et al., 2019).

Cocultures Among Macrofungi or of Macrofungi With Microalgae/Cyanobacteria

Currently, the cocultures of macrofungi-macrofungi or macrofungi with microalgae/cyanobacteria are mainly performed under submerged conditions with liquid media in view of sufficient exposure and competition. Given that the growth rates of macrofungi are similar, it is proper, convenient, and common to inoculate them simultaneously. Secondary metabolites of various structural types such as phenols, terpenoids, and exopolysaccharides (EPSs) have been reported

FIGURE 1 | Flow chart of the coculture strategy to explore the fungal biosynthesis potential.
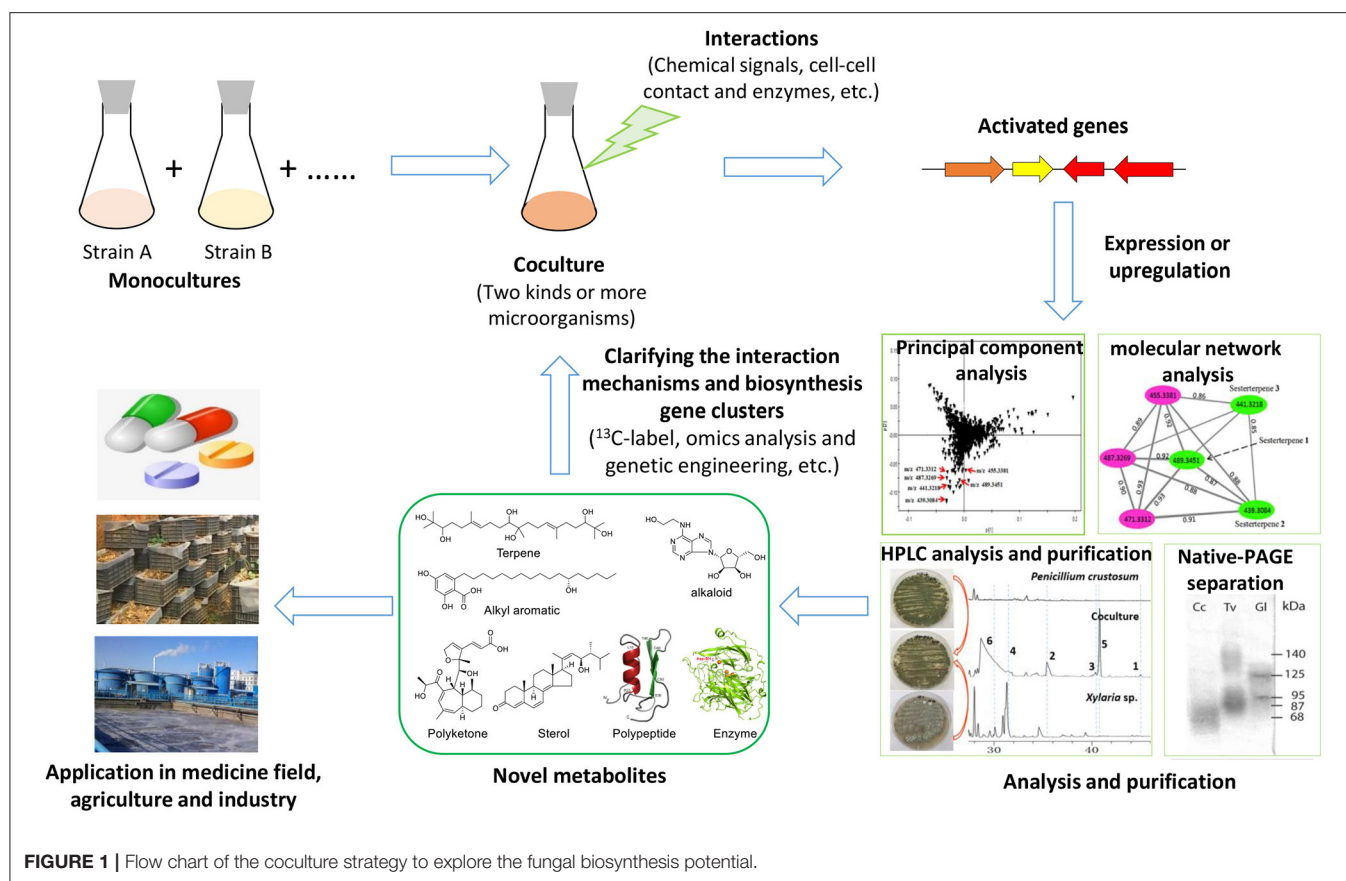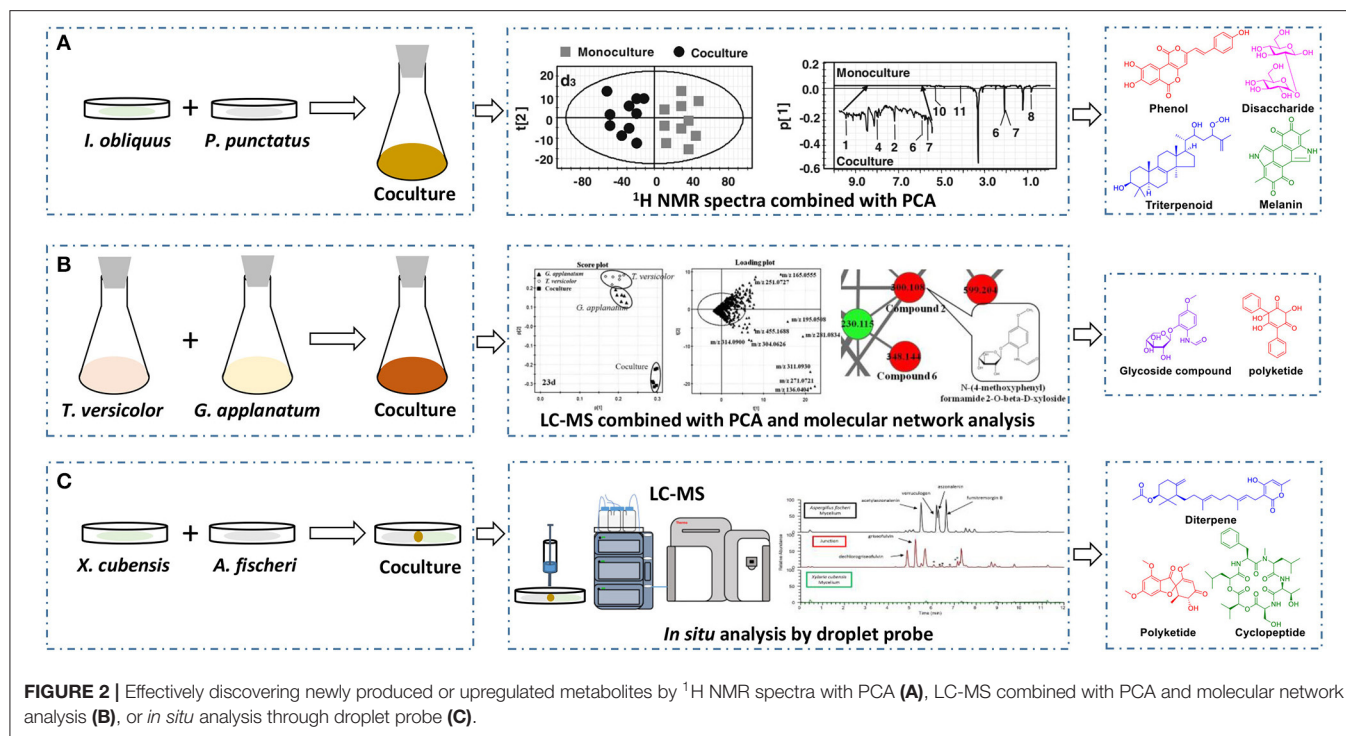
to be triggered or upregulated in these coculture systems (Zheng et al., 2011; Angelis et al., 2012).

The basidiomycete macrofungus *Inonotus obliquus* has been reported to generate diverse bioactive substances in natural habitats, but few have been reported in submerged liquid cultures. To increase its biosynthetic potential, Zheng et al. established a submerged coculture system of *I. obliquus* with another basidiomycete macrofungus *Phellinus punctatus*, resulting in the upregulation of many metabolites (Zheng et al., 2011). *I. obliquus* and *P. punctatus* were inoculated simultaneously at a ratio of 5:1 (w/w) in liquid medium, and mycelial extracts of both monocultures and coculture were analyzed by ^{1}H NMR with principal component analysis (PCA) (**Figure 2A**). The results indicated that the upregulation of phenols [such as phelligridin C (**1**), methyl inoscavin A (**2**), and davallialactone (**3**)], triterpenoids [such as foscoparianol D (**4**) and 21,24-cyclopentalanosta-3β,21,25-triol-8-ene (**5**)], disaccharides [for instance, the new compound inotodisaccharide (**6**)], and melanins [for instance, melanin (**7**)] during the cocultivation (**Table 1**). Moreover, these metabolites were shown to increase the antioxidant activity and inhibitory activity against HeLa 229 cells.

To observe the interactions among macrofungi, Yao et al. established 136 symbiotic systems using 17 basidiomycetes (Yao et al., 2016). The coculture of *Trametes versicolor* and *Ganoderma applanatum* showed the strongest antagonistic effect, with an

obvious confrontation zone on agar plate. Furthermore, they analyzed the crude extracts by LC-MS with PCA and found that 62 features were newly produced or upregulated during the coculture of *T. versicolor* and *G. applanatum* in liquid media (**Figure 2B**). Molecular network analysis was used to identify a new compound named *N*-(4-methoxyphenyl)formamide 2-*O*-β-D-xyloside (**8**) (**Table 1**), which could improve the cell viability of the human Beas-2B cell line at 1–5 μM. In addition, they found that the production of carboxylic acids such as 3-phenyllactic acid, gluconic acid, and orsellinic acid, was increased and that several glycosides were newly synthesized, including the known *N*-(4-methoxyphenyl)formamide 2-*O*-β-D-xylobioside and other undetermined glycosides. Based on these findings, they revealed a potential gene (GI: 636605689) encoding xylosyltransferases, which is responsible for glycoside production in *T. versicolor*. Moreover, the same research group found 28 additional features using optimized chromatography with PCA, leading to the production of a novel phenyl polyketide, 2,5,6-trihydroxy-4,6-diphenylcyclohex-4-ene-1,3-dione (**9**) (**Table 1**) with an over 15-fold increased titer in the coculture of *T. versicolor* and *G. applanatum* than monoculture of *T. versicolor* (Xu et al., 2018). Biological activity screening showed that this compound has potential cytotoxicity to the leukemic cell line U937 with a half maximal inhibitory concentration (IC$_{50}$) of 276 ± 5 μM. Moreover, it also showed moderate antioxidant activity (82.65 ± 1.25%) at a concentration of 200 μg/ml.

FIGURE 2 | Effectively discovering newly produced or upregulated metabolites by ^{1}H NMR spectra with PCA **(A)**, LC-MS combined with PCA and molecular network analysis **(B)**, or *in situ* analysis through droplet probe **(C)**.

With the increasing drug resistance of pathogenic fungi, human-pathogenic infections have become a major threat to human safety, especially infection with *Candida albicans* and *Cryptococcus neoformans*, which show high morbidity and mortality among immunodeficient individuals. To screen out novel leading compounds with efficient antifungal activity, Shen et al. conducted 110 pairs of cocultivations of basidiomycetes. The fermentation broth from the coculture of *Trametes robiniophila* Murr. and *Pleurotus ostreatus* showed the strongest inhibitory activity against the human-pathogenic fungi *C. albicans* and *C. neoformans* (Shen et al., 2019). The combination of metabolomics analysis and activity-guided isolation led to the discovery of three unusual linear sesterterpenes, postredienes A–C (**10–12**) (**Table 1**), with 80% minimum inhibitory concentrations (MIC$_{80}$) of 1 to 32 μg/ml against *C. albicans* and *C. neoformans*. In addition, dynamic ^{13}C-labeling analysis suggested that these sesterterpenes were produced by *P. ostreatus* under the induction of *T. robiniophila* Murr. (**Figure 3A**). Furthermore, the results of transcriptomic analysis and RT-qPCR helped determine a putative gene cluster for biosynthesizing these novel sesterterpenes and predict potential synthetic pathways (**Figure 3B**). Unlike the classic biosynthesis of the C25 precursor geranylfarnesyl diphosphate (GFPP), farnesyl-diphosphate farnesyltransferase (KDQ25270) was proposed to catalyze geranyl pyrophosphate (GPP) and farnesyl pyrophosphate (FPP) to form an unusual C25 precursor. Oxidase (KDQ25268) was suggested to further modify the C25 precursor through the epoxidation reactions at positions C-2, C-3, C-10, and C-11 to generate the final sesterterpenes of postrediene A to postrediene C. This impressive study indicates a great
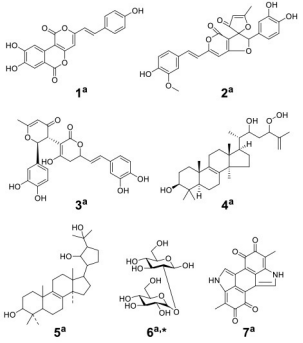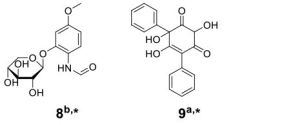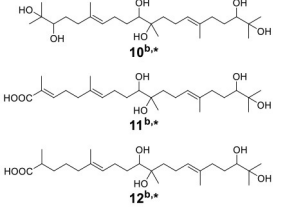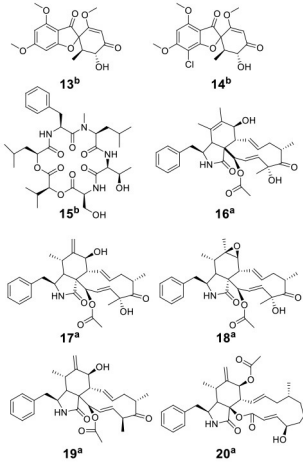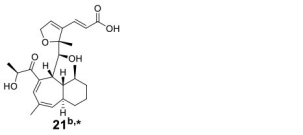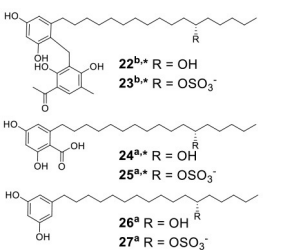
opportunity to discover unusual second metabolites and their relevant gene clusters by the coculture strategy.

Many EPSs produced by microalgae and macrofungi can enhance immunity to resist diseases such as cancer and hepatitis. Additionally, EPS generated by lignocellulolitic fungi is also of great importance in wood decay. Angelis et al. investigated the production of EPS in coculture of the basidiomycete *T. versicolor* and *Agaricus blazei*, as well as the cocultures of *T. versicolor* or *A. blazei* with microalgae and cyanobacteria in liquid fermentation (Angelis et al., 2012). The hydrosoluble EPS synthesized by monocultures and cocultures were compared using ^{13}C-NMR and GC-MS. The results indicated that the cocultures could not only obviously enhance the production of EPSs and reduce the fermentation time, but could also trigger the production of new polysaccharides. Although structural characterization of the polysaccharides requires further interpretation, this study provides a new strategy to improve the total production of EPSs and to activate new EPSs synthesis for medical and/or industrial applications.

Cocultures of Macrofungi and Filamentous Fungi
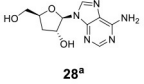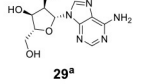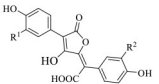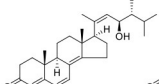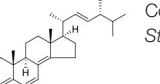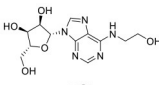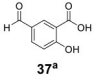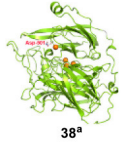
To explore the biosynthetic potential of secondary metabolites by coculturing of macrofungi and filamentous fungi, most studies have been carried out by cultivating the mycelium on solid media. Currently, a number of secondary metabolites, such as mycotoxins, alkyl aromatics, and nucleosides, have been reported to be synthesized through activation in these coculture systems (Zhou and Jiang, 2008; Yu et al., 2019; Knowles et al., 2020).

TABLE 1 | Typical macrofungi coculture groups and accordingly producing metabolites.

Coculture strains	Coculture types	Upregulated or newly produced metabolites	Bioactivities of the metabolites	References
Inonotus obliquus and *Phellinus punctatus*	Submerged culture in liquid medium		Showed the potential antioxidant activity or the inhibitory activity against HeLa 229 cells	Zheng et al., 2011
Trametes versicolor and *Ganoderma applanatum*	Submerged culture in liquid medium		Compound **9** has potential cytotoxicity to leukemic cell line U937 and moderate antioxidant activity	Yao et al., 2016; Xu et al., 2018
Trametes robiniophila Murr. and *Pleurotus ostreatus*	Submerged culture in liquid medium		Showed potent inhibitory activities against *Candida albicans* and *Cryptococcus neoformans*	Shen et al., 2019
Xylaria cubensis and *Aspergillus fischeri*	Unsubmerged culture in solid medium		Showed fungistatic properties or cytotoxicity	Knowles et al., 2019
Xylaria flabelliformis and *Aspergillus fischeri*	Submerged culture in liquid medium		Displayed cytotoxic activity against breast, ovarian, and melanoma cancer cell lines	Knowles et al., 2020
Xylaria sp. with *Penicillium crustosum*	Unsubmerged culture in solid medium		Compounds **23**, **24**, **26**, and **27** had obvious antibacterial activities	Yu et al., 2019

(Continued)

TABLE 1 | Continued

Coculture strains	Coculture types	Upregulated or newly produced metabolites	Bioactivities of the metabolites	References
Cordyceps militaris and *Monascus rubber*	Unsubmerged culture in solid medium	28[a] 29[a]	Showed the various potential activity, such as anti-tumor, anti-virus, and antimicrobial activities	Zhou and Jiang, 2008
Serpula lacrymans with different kinds of bacteria	Unsubmerged culture in solid medium	30[a] R¹=R²=H 31[a] R¹=OH, R²=H 32[a] R¹=H, R²=OH 33[a] R¹=R²=OH	–	Tauber et al., 2016, 2018
Pleosporales sp. and *Bacillus wiedmannii*	Submerged culture in liquid medium	34[b,*] 35[b]	Compound **34** can inhibit *Staphylococcus aureus*	Wang et al., 2019
Cordyceps cicadae and its endophytic bacteria	Submerged culture in liquid medium	36[a,*]	Have the potential bioactivity of enhancing immune regulation and renal function	Qu et al., 2019
Heterobasidion abietinum and *Streptomyces*	Submerged culture in liquid medium	37[a]	–	Keilhofer et al., 2018
Triple coculture of *Trichoderma viride*, *Aspergillus terreus,* and *Leptosphaerulina* sp.	Submerged culture in liquid medium	38[a]	Increased the removal rate of Reactive Black 5 dye	Copete-Pertuz et al., 2019

The metabolites with "ᵃ" represent the upregulated compounds, the metabolites with "ᵇ" represent the newly produced compounds, the metabolites with "" represent new compounds. "–" means no activities was reported.*

Knowles et al. cocultured *Xylaria cubensis* with *Aspergillus fischeri*, which can produce griseofulvin and a suite of mycotoxins, respectively (Knowles et al., 2019). The authors investigated the spatial distribution of the fungal secondary metabolites on solid medium in monocultures and coculture using a droplet-liquid microjunction-surface sampling probe (droplet probe; **Figure 2C**). For example, they found that the two compounds griseofulvin and dechlorogriseofulvin were only detected at the contact zone of the coculture but existed throughout the mycelia in monoculture of *X. cubensis* and showed more accumulation at the colony edge. Further large-scale fermentation revealed that the coculture of *X. cubensis* and *A. fischeri* not only triggered the production of 5′-hydroxygriseofulvin (**13**), dechloro-5′-hydroxygriseofulvin, (**14**), and hirsutatin A (**15**) but also increased the titers of cytochalasin C (**16**), cytochalasin D (**17**), cytochalasin Q (**18**), zygosporin E (**19**), and 7-*O*-acetylcytochalasin B (**20**)

(Knowles et al., 2019; **Table 1**). Moreover, they found a new compound, wheldone (**21**) (**Table 1**), which displayed cytotoxic activity against breast, ovarian, and melanoma cancer cell lines (Knowles et al., 2020). To explore the roles of secondary metabolites in interspecific interactions, they further established another cocultured system—*X. cubensis* with a mutant strain of *A. fischeri* that lacked the master regulator *lae*A in secondary metabolism. The mutant *A. fischeri* was found to be displaced by *X. cubensis* because it was unable to regulate secondary metabolite biosynthesis in the competition of the coculture (Knowles et al., 2019). Similarly, Yu et al. researched another *Xylaria* species by coculturing (Yu et al., 2019). In this experiment, four novel alkyl aromatics, penixylarins A-D (**22**–**25**) and two known compounds, 1,3-dihydroxy-5-(12-hydroxyheptadecyl)benzene (**26**) and 1,3-dihydroxy-5-(12-sulfoxyheptadecyl)benzene (**27**), were isolated when *Xylaria* sp. HDN13-249 was cocultured with *Penicillium crustosum*
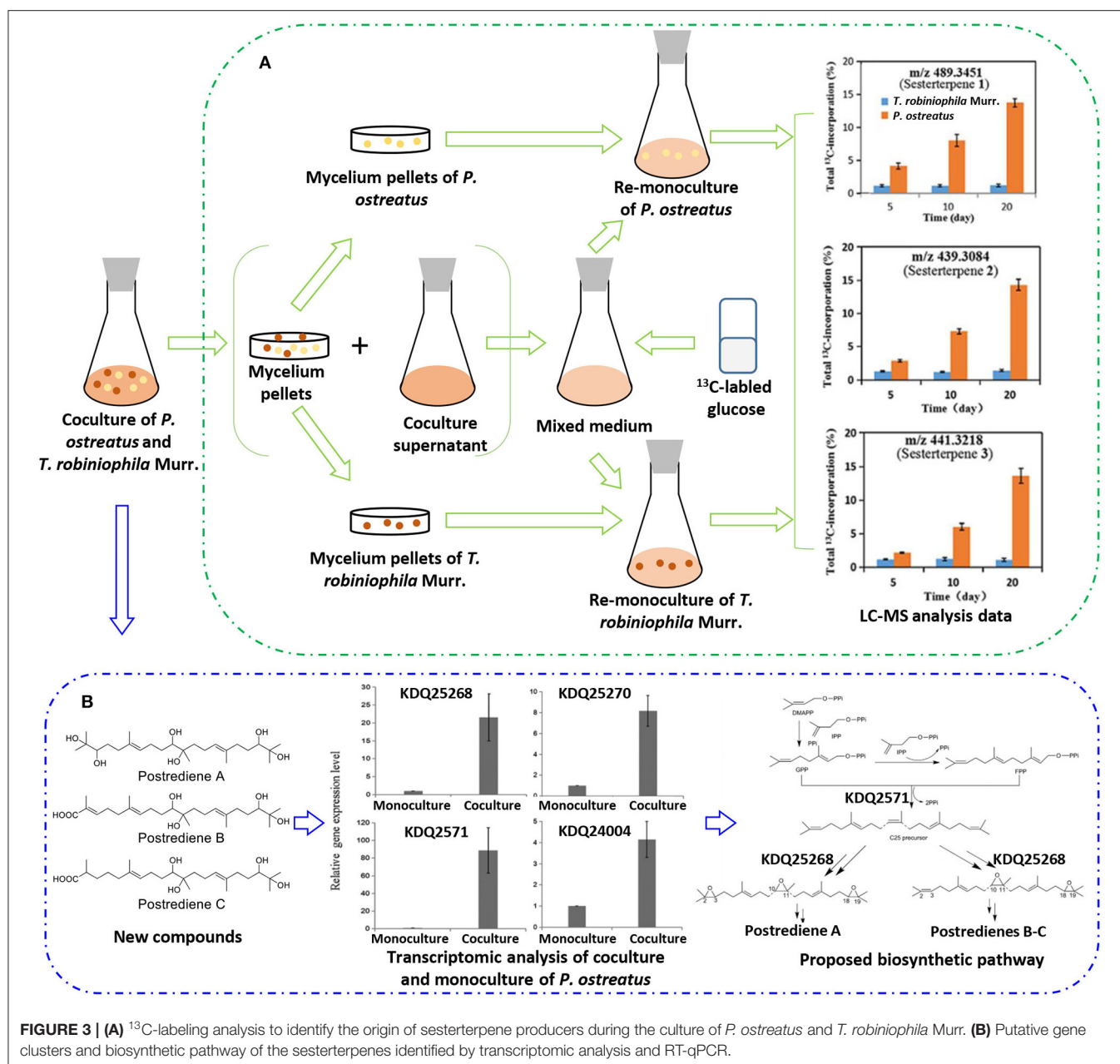
FIGURE 3 | **(A)** ^{13}C-labeling analysis to identify the origin of sesterterpene producers during the culture of *P. ostreatus* and *T. robiniophila* Murr. **(B)** Putative gene clusters and biosynthetic pathway of the sesterterpenes identified by transcriptomic analysis and RT-qPCR.

PRB-2 on solid medium (**Table 1**). Further analysis of the LC-MS results and the structural characteristics indicated that novel compounds **22** and **23** were formed in the coculture by a non-enzymatic Michael addition reaction between two fragments from *P. crustosum* PRB-2 and *Xylaria* sp. HDN13-249, respectively, while compounds **24–27** could be synthesized in monoculture of *Xylaria* sp. HDN13-249, but their titers were obviously enhanced in the coculture. These findings suggested that different mechanisms appeared to produce new compounds in the coculture system. Evaluation of the activities showed that compounds **23**, **24**, **26**, and **27** could inhibit bacterial growth, among which compound **24** displayed the best activity against

Mycobacterium phlei, with an MIC of 6.25 μM. This result suggested that compound **24** could be designed as a potential antituberculosis leading drug.

The macroascomycete *C. militaris* is a traditional Chinese medicine that produces a variety of bioactive components, such as adenosine and cordycepin. However, these active components usually have an issue of low production titers and high production costs. Researchers are attempting to solve this challenge through a coculture strategy. Zhou and Jiang cocultivated *C. militaris* CM9-26 and *Monascus rubber* MT305 on an optimized solid medium in an orthogonal test, resulting in the significant enhancement of many bioactive components

(Zhou and Jiang, 2008). The titers of cordycepin (**28**) and adenosine (**29**) were 2.5- and 5.1-fold higher than those in the monoculture of *C. militaris* CM9-26, respectively (**Table 1**). The pigments produced by *M. rubber* MT305 were 3-fold higher than those produced by its monoculture. Similarly, *C. militaris* was cocultured with *M. rubber* in an optimized solid medium, temperature and humidity. The titer of cordycepin (**28**) was increased by up to 1.4-fold of that in the monoculture of *C. militaris*, and its fruit-body production was increased as well (Liu, 2015; **Table 1**).

Cocultures of Macrofungi and Bacteria or Macrofungi and Actinomycetes

The cocultures of macrofungi and bacteria have been studied more extensively compared with other cultivated pairs. Both submerged liquid cultivations and solid cultivations have been investigated by adjusting the inoculation quantity and inoculation times, which induce various constituents such as antimicrobial peptides, pigments, and ergosterol (Essig et al., 2014; Tauber et al., 2016; Wang et al., 2019).

The basidiomycete macrofungus *C. cinerea* grows on the dung of herbivores, which provides a high humidity habitat with diverse microbes. To mimic this habitat and identify new antibiotics and fungicides, Essig et al. studied the interaction of *C. cinerea* with different bacteria in an artificial coculture system. *C. cinerea* was first grown on glass beads submerged in liquid medium, and after 60 h, this medium was replaced by a culture solution of bacteria including *Bacillus subtilis* 168, *Pseudomonas aeruginosa* 01, or *Escherichia coli* BL21 (Essig et al., 2014). *C. cinerea* was found to secrete some constituents to inhibit the growth of *B. subtilis* 168. Further study led to the identification of a novel antimicrobial peptide, copsin. Copsin showed broad inhibitory activity against diverse gram-positive bacteria, including human-pathogenic *Enterococcus faecium* and *Listeria monocytogenes*, through the mechanism of binding specifically with peptidoglycan precursor lipid II to interfere with the biosynthesis of the bacterial cell wall.

Atromentin has been proven to play a role in redox cycling, but there are still no clues about the function of this pigment in the interaction of natural systems. To solve this mystery, Tauber et al. established cocultured systems of the model basidiomycete *Serpula lacrymans* with many terrestrial bacteria, including *Bacillus subtilis* 3610, *Pseudomonas putida,* and *Streptomyces iranensis*, on solid medium. During cocultivation, *B. subtilis* 3610 and *P. putida* were precultured overnight, while *S. iranensis* was precultured for 4 days before spotting onto the fungal mycelial bed precultured for 13–14 days (Tauber et al., 2016). As a result, the gene cluster related to atromentin biosynthesis, including atromentin synthetase and aminotransferase was upregulated, and the corresponding atromentin-derived pigments, i.e., atromentic, xerocomic, isoxerocomic, and variegatic acids (**30–33**) (**Table 1**), were increased. Further bioinformatics suggested that highly conserved motifs of atromentin synthesis genes might be regulated by similar transcription factors through the same regulatory mechanisms. In addition, although these pigments had no antimicrobial activity, they might play a role in the

nutritional perspective and be related to the redox cycling of lignocellulose degradation. Thus, they could be induced by a nutritional response or coregulated along with other cellular processes, such as stress and secondary metabolism. In 2018, the same research group further investigated this phenomenon in depth, and they demonstrated that coculturing of *S. lacrymans* with 10 other bacteria (such as *Lysinibacillus fusiformis* M5, *Arthrobacter* spp., and *Micrococcus luteus*) could also improve the production of atromentin-derived pigments (Tauber et al., 2018). The exogenous addition of protease inhibitors and the use of heat-killed bacteria in coculture suggested that enzymatic hyphal damage and/or accordingly released peptides could trigger the synthesis of atromentin-derived pigments.

To diversify the synthesis of secondary metabolites of the endophytic macroascomycete *Pleosporales* sp. F46 isolated from *Mahonia fortunei*, Wang et al. treated *Pleosporales* sp. F46 with *Bacillus wiedmannii* Com1, which was an endophytic bacterium isolated from the same plant (Wang et al., 2019). In this coculture system, the bacterium *B. wiedmannii* Com1 was precultured for 3 days and then added to the coculture medium (solid rice medium). After 6 days, *Pleosporales* sp. F46 cells precultured for 7 days were added to the same coculture medium. By cocultivation, two new HPLC peaks were observed in the crude extracts, which were not detected in the individual monocultures. Further chemical structural analysis led to the identification of a new ergosterol derivative, 23*R*-hydroxy-(20*Z*,24*R*)-ergosta-4,6,8(14),20(22)-tetraen-3-one (**34**), and a known related compound, (22*E*,24*R*)-ergosta-4,6,8(14),22-tetraen-3-one (**35**) (**Table 1**). Compound **34**, with the MIC of 100 μg/ml against *Staphylococcus aureus*, was the first reported ergosterol derivative containing a side chain with a $\Delta^{20(22)}$-double bond.

Cordyceps cicadae as an ascomycete fungus is parasitic in the larvae of *Cicada flammata* and can produce diverse compounds such as *N*6-(2-hydroxyethyl)-adenosine (HEA) (**36**) (**Table 1**), adenosine, ergosterol, and cordycepin to improve immune regulation and renal function. Fifty-four endophytic bacteria were isolated along with *C. cicadae*, and four of them were chosen to be cocultured with *C. cicadae* according to metabolite analysis and their inhibitory phenomena (Qu et al., 2019). Coculture was performed with *C. cicadae* precultured for 5 days before inoculating bacteria (including *Enterobacter aerogenes* T4-4, *Serratia marcescens* T4-16, *Cedecea neteri* T4-8, and T4-11). Further metabolite profiling indicated that the titer of HEA was increased to at least 13-fold compared to that in the monoculture. Meanwhile, three nucleosides (i.e., adenosine, uridine, and guanosine), as the structural analogs of HEA, were found to be decreased significantly during the coculture.

There is little research on the cocultures of macrofungi and actinomycetes. One example is the coculture of *Heterobasidion abietinum* and *Streptomyces. Heterobasidion* spp. can cause root rot in *Norway spruce*, and its infection is further intensified by rhizospheric streptomycetes. To clarify their interaction mechanism, Keilhofer et al. studied the coculture system of *H. abietinum* 331 and *Streptomyces* AcH 505, including the mode of action on *Norway spruce* (Keilhofer et al., 2018). *Streptomyces* AcH 505 and *H. abietinum* 331 began to be cocultured in

liquid medium after the monocultivation for 2 and 7 days. HPLC analysis showed that 5-formylsalicylic acid (5-FSA) (**37**) produced by *H. abietinum* 331 was upregulated under the stimulation of *Streptomyces* AcH 505 (**Table 1**). *H. abietum* 331 cocultured with many other *Streptomycetes* isolated from soil had similar results. *Norway spruce* seedlings treated with 5-FSA indicated that ergosterol in infected roots was obviously increased, and the infection degree was comparable to that of the seedlings treated by *H. abietinum* 331 and *Streptomyces* AcH 505. Further research demonstrated that 5-FSA can interfere with the emission of defensive signals in *Arabidopsis thaliana* in a manner similar to salicylic acid.

ADVANCES IN THE STUDY OF MACROFUNGAL COCULTURES FOR EXPLORING THE BIOSYNTHESIS POTENTIAL OF FUNCTIONAL ENZYME

With continuous agricultural and industrial development, the environmental pollution caused by crop straw burning, petroleum hydrocarbon (PHC) overexploitation, and dye and pesticide abuse is emerging as a serious problem. Many macrofungi can produce various oxidative and degradative enzymes, such as laccase (**38**) (**Table 1**), lignin peroxidase, and manganese peroxidase. These enzymes not only have great potential in the treatment of agricultural and industrial wastes enriched with lignocellulose, but can also be used in industrial production, such as pulp delignification and bleaching, dye decolorization, sewage disposal, and food processing. Researchers have found that the coculture strategy can dramatically enhance the production of oxidative and degradative enzymes compared to the monoculture, including coculturing among macrofungi (such as *P. ostreatus* with *T. versicolor* and *Marasmius pallescens* with *Marasmiellus troyanus*), coculturing of macrofungi and filamentous fungi (such as *T. versicolor* with *Trichoderma harzianum*/*Candida* sp./*Aspergillus niger*, *Lentinula edodes* with *Trichoderma* sp., *P. ostreatus* with *Trichoderma longibrachiatum*, and *C. cinerea* with *Gongronella* sp.), and coculturing macrofungi and bacteria (such as *Fomitopsis pinicola* with *B. subtilis*) (Freitag and Morrel, 1992; Savoie et al., 1998; Baldrian, 2004; Velázquez-Cedeño et al., 2004; Ferreira Gregorio et al., 2006; Zhang et al., 2006; Chi et al., 2007; Stoilova and Krastanov, 2008; Flores et al., 2009; Wang et al., 2009; Hiscox et al., 2010; Wei et al., 2010; Chen et al., 2011; Kuhar et al., 2015; Ma and Ruan, 2015; Mewada et al., 2017; Huo et al., 2019; Kumar et al., 2019; Wiberth et al., 2019; Lira-Pérez et al., 2020). For example, the production of laccase in the coculture of *T. versicolor* and *T. harzianum* was more than 40-fold higher than that in the monoculture (Baldrian, 2004).

Cocultures Among Macrofungi

To enhance the production of functional enzymes, researchers have tried to set up cocultures among macrofungi in either liquid media or solid media, both of which have obtained good results with the increment of oxidative and degradative enzymes, such as P450 monooxygenases, dioxygenases, and laccases (Yanto and Tachibana, 2014).

Petroleum hydrocarbons (PHCs) and related products released into the environment during the exploitation, processing, and utilization of petroleum are carcinogenic and mutagenic pollutants that are seriously harmful to the health of humans and animals. An increasing number of studies have reported that microbial coculture can biodegrade PHCs more efficiently. Yanto and Tachibana studied how to efficiently degrade PHCs through the cocultures of different basidiomycetes, including *Trametes versicolor* U97, *Pleurotus ostreatus* PL1, *Cerena* sp. F0607, and *Polyporus* sp. S133 with ascomycetes *Pestalotiopsis* sp. NG007 (Yanto and Tachibana, 2014). The influence of different inoculation proportions was investigated for four pairs of these strains. The results showed that a 50/50 inoculation proportion of *Polyporus* sp. S133 and *Pestalotiopsis* sp. NG007 had higher biodegradation rates of PHCs. For example, the degradation rate of the main aromatic ingredients in PHCs increased from 53.06% (the monoculture of *Pestalotiopsis* sp. NG007 for 15 days) and 37.40% (the monoculture of *Polyporus* sp. S133 for 15 days) to 89.35% in this coculture for 15 days. *In vitro* crude enzymatic assays and inhibition experiments suggested that the increased production of degradative enzymes, such as P450 monooxygenases, dioxygenases, and laccases, led to the high biodegradation of PHCs.

Indigo carmine is a traditional dye that widely used in dyeing plastic and textiles. The methods of removing indigo carmine from polluted water include absorption, photocatalysis, and biodegradation. Among those methods, the absorption method is low cost and easy to operate. For instance, sesame straw, which is an abundant agricultural waste, can be used as an absorbent. Because the absorbance efficiency of sesame straw is limited (21.90 mg/g), Li et al. improved it by coculturing *Tremella fuciformis* and *Morchella* sp. with sesame straw (Li et al., 2019). The absorption efficiency of sesame straw fermented by the cocultured strains was increased nearly 2-fold compared with untreated or *Morchella* sp.-treated sesame straw and was up to 1.4-fold compared with *T. fuciformis*-treated sesame straw. Moreover, with the addition of inductors including acetic acid, Cu^{2+}, and alkaline lignin during fermentation by the coculture, the absorption of fermented sesame straw was further increased to 74.25 mg/g.

Malachite green (MG) is a triphenylmethane dye and antifungal agent that also shows high toxicity toward the health of mammals. In 2015, Kuhar et al. found that culturing *G. lucidum* and *T. versicolor* simultaneously in a sawdust-based medium resulted in increased laccase production by 3.5- and 9.2-fold than *G. lucidum* and *T. versicolor* in the monoculture. This finding inspired them to investigate the MG degradation ability of the coculture system. The results showed that the time required to completely decolorize MG in the coculture system was obviously decreased, and the half-life of decolorizing MG was approximately 1/3 that of the monocultures of *G. lucidum* and *T. versicolor* (Kuhar et al., 2015).

Similarly, cibracron brilliant red 3B-A dye is also widely used in textile industries and is harmful to the environment and

challenging to address. In 2018, Bankole et al. investigated the dye-degrading abilities of two ascomycete white-rot macrofungi, *Daldinia concentrica* and *Xylaria polymorpha* under the monoculture and coculture (Bankole et al., 2018). They found that coculturing *D. concentrica* and *X. polymorpha* by solid state fermentation could remove dye more efficiently than the monocultures of either strains. When cibracron brilliant red 3B-A dye was treated with the monoculture of *X. polymorpha,* the absorbance peak was deceased more efficiently than when treated with *D. concentrica*, but only less than half of the dye was degraded. In contrast, when treated with *D. concentrica* and *X. polymorpha* coculture, almost 100% of dye was degraded. In addition, phytotoxicity evaluation indicated that the degradation products of the cibracron brilliant red 3B-A dye produced by the coculture of *D. concentrica* and *X. polymorpha* became less toxic.

Cocultures of Macrofungi and Filamentous Fungi or Macrofungi and Bacteria

Lignocellulosic resources, such as agricultural residues, waste woods, and paper, are promising low-cost feedstocks for producing renewable energy. For example, to improve corn stover bioconversion, Ma and Ruan established an effective lignocellulose-biodegrading system by coculturing of *Coprinus comatus* and *Trichoderma reesei* in liquid medium (Ma and Ruan, 2015). Their research showed that the production of lignocellulolytic enzymes such as carboxymethyl cellulase, xylanase, and laccase in the coculture was much higher than that in the monocultures, and the lignocellulose delignification times were becoming shorter. To further improve the production of lignocellulolytic enzymes in the coculture system, they also investigated the influences of chemical inducers, metal ions, inoculation ratios, and inoculation intervals. The results suggested that those factors all have obviously influences, among which, with an inoculation ratio of *C. comatus* and *T. reesei* of 5:2 and an inoculation interval of 12 h, the production of laccase was increased 2.6-fold and the maximal production was obtained 3 days earlier, compared to the monoculture of *C. comatus*. In addition, the influences of the temperature, pH, and solid/liquid ratio on the delignification and saccharification of corn stover were also tested. The results suggested that the temperature of 50°C, the pH of 5.0, and the solid/liquid ratio of 1:20 were the optimal conditions, and a maximum delignification rate of 66.5% and the conversion rate of original polysaccharides to fermentable sugars of 82.2% were obtained at 50°C. This study provided a useful strategy for transforming corn stover into sugar by simultaneous biodelignification and saccharification.

Benzo[a]pyrene (BaP), which is a carcinogenic and mutagenic polycyclic aromatic hydrocarbon that exists in coal tar from the smoke of car exhaust, tobacco, and wood burning, etc., has been classified as a pollutant prior to treatment (Bhattacharya et al., 2017). Bhattacharya et al. focused on the treatment of BaP by cocultures of *P. ostreatus* PO-3 with bacteria or non-basidiomycete fungi. *P. ostreatus* PO-3 was precultured in liquid medium for 15 days and then cocultured with either the filamentous fungi *A. niger*, *Penicillium chrysogenum,* and *T. reesei* or the bacteria *P. aeruginosa* and *Bacillus cereus*. Among

these cocultures, cocultures of *P. ostreatus* PO-3 with *Penicillium chrysogenum* MTCC 787 or with *Pseudomonas aeruginosa* MTCC 1688 showed degradation rates at 86.1 and 75.1%, respectively, which were higher than that of the monoculture of *P. ostreatus* PO-3 (64.3%). Researchers proposed that the improvement of BaP degradation in fungal cocultures was related to the increased production of both lignolytic and non-lignolytic enzymes such as laccase, cytochrome P-450 monooxygenase, and epoxide hydrolases. The enhanced BaP degradation in the basidiomycete and bacterial cocultures was probably associated with bacterial surfactants and/or other bacterial enzymes such as salicylate hydroxylase, 2-caroxybenzaldehyde dehydrogenase, and catechol 1, 2-dioxygenase. In this study, BaP was degraded into polar and hydrosoluble products which could be further mineralized by other indigenous microorganisms.

In 2019, Copete-Pertuz et al. observed the production of ligninolytic enzymes with decolor ability in the ascomycete white-rot fungus of *Leptosphaerulina* sp. by coculturing with other microorganisms, including the species *Aspergillus*, *Trichoderma*, *Fusarium,* and *Penicillium* (Copete-Pertuz et al., 2019). Among these, *Trichoderma viride* and *Aspergillus terreus* showed the best inducing effect in solid media assays. Then, a triple-coculture system was established by response surface methodology, which was performed by inoculating *T. viride* (1,000 µl) and *A. terreus* (1,000 µl) into 7-day precultured *Leptosphaerulina* sp. in liquid medium. The amounts of laccase, versatile peroxidase, and manganese peroxidase were found to be increased by 8-, 36-, and 88-fold, respectively. The removal rate of Reactive Black 5 dye was increased by 1.2-fold compared with the monoculture of *Leptosphaerulina* sp.

These studies indicated the efficiency of macrofungal coculture in the eco-friendly restoration of polluted environments, providing an important direction for further research on treating organic pollution.

APPLICATION OF MACROFUNGI COCULTURES FOR GENERATING THE FRUITING BODY

With the increasing demand for edible and medicinal macrofungi, artificial cultivation is becoming increasingly common. However, researchers found that the fruiting bodies of some macrofungi were difficult to cultivate under the standard laboratory conditions, partly because of the lack of symbiotic microorganisms. Thus, the coculture strategy mimicking the natural environment was developed for fruiting body formation of these edible and medicinal macrofungi on solid media (Guo et al., 2001; Liu, 2015).

Grifola umbellate, which is a medicinal macrofungus whose sclerotium has the effect of diuresis and detumescence, is hard to artificially cultivate before researchers identified the symbiotic relationship with *Grifola* sp. (companion fungus of *G. umbellate*) and *A. mellea*. As mentioned earlier in this paper, Guo et al. conducted a systematic study on the cocultures of *G. umbellate*, *Grifola* sp., and *A. mellea* (Guo and Xu, 1992; Guo et al., 2001, 2002; Xing and Guo, 2003). The results showed that *G. umbellate*

could produce a mass of mycelium bundles on the surface of its colony when cocultured with its companion fungus *Grifola* sp. This was a phenomenon in the early stage of sclerotial formation, while almost no mycelium bundles was formed in the monoculture. *A. mellea* was found to infect *G. umbellate* after the sclerotium formation, and the following nutrient exchange could promote the sclerotium growth.

In addition to the example mentioned above, the coculture strategy can also improve the quality of the fruit body. For instance, Liu et al. found that the active constituent of cordycepin in the fruit body of *C. militaris* was enhanced by coculturing with *M. rubber* (Liu, 2015).

INTERACTION MECHANISMS IN MACROFUNGI COCULTURES

Elucidation of the potential interaction mechanisms is important for improving the application of coculture strategy. Generally, microorganisms are considered to communicate with each other through either chemical signals or cell–cell contact to change the production of related metabolites. In recent years, an increasing number of experiments have been carried out to demonstrate the interaction mechanisms, such as exogenous addition experiments, ^{13}C-labeling analysis, proteomic analysis, and genetic engineering.

Chemical Signals Mediating the Interactions in Cocultures

To compete for limited nutrition and living space, the microorganisms in the coculture system often produce diverse chemical signals to communicate with each other. These chemical signals can affect both cell growth and secondary metabolite production.

Ferreira-Gregorio et al. reported the rapid induction and release of laccase and manganese peroxidase into the culture supernatant when coculturing *M. pallescens* and *M. troyanus* in liquid medium. Neither enzyme was produced in the monocultures (Ferreira Gregorio et al., 2006). Further research showed that laccase could be induced to different degrees when adding the filter-sterilized or autoclaved supernatant of *M. pallescens* into *M. troyanus* culture, but no effect occurred in the opposite experiment. Both *M. troyanus* and *M. pallescens* (in a small quantity) were able to produce laccase when using the inducer 2,5-dimethylalanine. These results suggested that *M. pallescens* could secrete thermostable and thermolabile chemical signals to induce the laccase produced by *M. troyanus*. Huo et al. discovered that *C. cinerea* grew slowly and produced little laccase in a monoculture with sucrose as the carbon source, but the production of laccase was significantly increased in the coculture with *Gongronella* sp. w5 (Huo et al., 2019). Further study showed that strain w5 could hydrolyze sucrose to glucose and fructose during coculture, and fructose was an efficient carbon source for *C. cinerea* growth and laccase production. In addition, isolating strain w5 with *C. cinerea* by dialysis tubes still led to laccase activity similar to that of the coculture treatment, suggesting that certain extracellular metabolites, as chemical signals, were

also responsible for the increased production of laccase. Indeed, they found that the ethyl acetate extract of strain w5 could also increase the production of laccase in the monoculture of *C. cinerea*. *p*-Hydroxybenzoic acid was isolated from this extract, which could improve laccase production to a level similar to that of the coculture by using fructose as the carbon source.

As mentioned previously, Shen et al. discovered three novel sesterterpenes by coculturing of *P. ostreatus* and *T. robiniophila* Murr. They further applied dynamic ^{13}C-labeling analysis to find that ^{13}C-labeled sesterterpenes could only be produced when *P. ostreatus* was stimulated by *T. robiniophila* Murr. (**Figure 3A**). By further analyzing the ^{13}C-labeling patterns in the monoculture of *P. ostreatus* with the addition of the supernatant of the coculture, they speculated that the biosynthesis of sesterterpenes was triggered by some chemical signals released into the culture medium.

In addition, Knowles discovered that *X. cubensis* could produce more fungistatic compounds when cocultured with *A. fischeri*. Meanwhile, *A. fischeri* increased the titer of the mycotoxins. Furthermore, they explored the functions of secondary metabolites during the interaction by constructing a mutant *A. fischeri* lacking the master regulator *laeA* of secondary metabolism and coculturing it with *X. cubensis* (Knowles et al., 2019). The mutant *A. fischeri* was found to be displaced by *X. cubensis* because it lost the ability to regulate secondary metabolite biosynthesis in this competition system.

Cell–Cell Contact, Enzymes, or Related Proteins Mediating the Interactions in Cocultures

In addition to chemical signals, the enzymes or related proteins produced by cocultured microorganisms can also affect the metabolic pathways. Kumar et al. studied the interaction mechanism between *Trametes ljubarskyi* and *Rhodotorula mucilaginosa*, which was a coculture system that can efficiently produce laccase (Kumar et al., 2019). Investigation by electron microscopy indicated that the yeast *R. mucilaginosa* adhered to the mycelia of *T. ljubarskyi*, and the strong interactions resulted in morphologic changes in the yeast and mycelial surface damage of *T. ljubarskyi*. Further proteomic analysis indicated that the differential synthesis of a series of oxidoreductases, antioxidants, membrane-related proteins, and transporter proteins would be beneficial for the cosurvival of these two fungi.

As mentioned earlier in this paper, Tauber et al. found that the coculture of *S. lacrymans* with different bacteria increased the production of atromentin-derived pigments (Tauber et al., 2018). Further exogenous addition experiments showed that the addition of cell-wall-damaging enzymes (i.e., lytic enzymes and proteases) into *S. lacrymans* can also increase the production of those pigments, but other lysozymes or mechanical damage did not obtain the same effect. In addition, pigment production was obviously reduced when *S. lacrymans* was treated with heat-killed bacteria or by protease inhibitors and *B. subtilis* simultaneously. These results suggested that enzymatic hyphal damage and/or released peptides could promote the titers of atromentin-derived pigments.

Carbon Source Succession Mediating the Interactions of Cocultures

In the coculture systems, microorganisms compete with limited nutritions, such as carbon and nitrogen sources for survival, among which researchers demonstrate that carbon source succession is an important factor in the regulation of metabolic pathways. In 2009, Wang et al. found that laccase activity was increased to $10,500 \pm 160$ U/L by coculturing *T. versicolor* and *Candida* sp. HSD07A, 11.8-fold higher than that of the monoculture of *T. versicolor* (Wang et al., 2009). Enzymatic analysis of *Candida* sp. HSD07A suggested that it could not produce laccase but could excrete amylase and cellulase which can hydrolyze the cell walls of *T. versicolor*. Similar results have also indicated that amylase and cellulase could induce the production of pigments in *Monascus* by hydrolyzing its cell walls (Shin et al., 1998). Thus, Wang et al. speculated that the upregulation of laccase would be related to the effect of amylase and cellulase on the cell walls of *T. versicolor*. However, they noticed that the hydrolysis of cell walls or the addition of enzyme solutions could not result in the upregulation of laccase, suggesting that the hydrolysis of cell walls was not the key reason. Furthermore, researchers explored whether glucose starvation could lead to the upregulation of laccase in *T. versicolor* due to the high ability of *Candida* sp. HSD07A in assimilating glucose. This hypothesis was preliminarily supported by analyzing the relationship between the sugar amount and laccase activity.

Similarly, the mechanism of upregulating laccase by coculturing *G. lucidum* and *Candida* sp. HSD07A was studied by Li et al. (2010). This study revealed that the nitrogen source, sulfur source, hydrolytic enzymes, and inducers did not have obvious effects on laccase production, and glucose deprivation could only result in the upregulation of laccase to some extent. NMR and GC data indicated that *Candida* sp. HSD07A could transform glucose into glycerol and ethanol, among which glycerol was an effective carbon source for *G. lucidum*. Further glycerol addition experiments suggested that the production of glycerol was indeed another key reason for the upregulation of laccase in addition to glucose starvation. This was likely because glycerol could prolong the production time of laccase under the glucose starvation state. These studies demonstrate that the glucose starvation and glycerol succession that result from yeast *Candida* sp. HSD07A are new approach to improve laccase production in basidiomycete fungi.

CONCLUSION AND PERSPECTIVES

Compared with the complicated living conditions in nature, many genes or clusters of microorganisms are silent in standard culture under the laboratory conditions. To activate these silent genes or clusters, the coculture strategy is considered as an efficient approach, because it can mimic the symbiotic relationships of microorganisms in their intrinsic habitats (Moody, 2014; Xu et al., 2018; Shen et al., 2019). Secondary metabolites induced by cocultures, such as small molecular metabolites, polysaccharides, and polypeptides, usually display diverse bioactivities, including antimicrobial activity, antitumor activity, and antioxidant activity, and represent a potential and powerful resource to discover the leading compounds for medicinal development. Moreover, the cocultures of macrofungi can improve the production of oxidative and degradative enzymes, such as laccase, lignin peroxidase, and manganese peroxidase, which is very useful in agricultural and industrial wastes biodegradation, pulp delignification and bleaching, dye decolorization, sewage disposal, and food processing.

Notably, with in-depth coculture research, the detailed interaction mechanism is becoming a hot field for exploration but is still a mystery for researchers. Macrofungi cultivated in a given coculture system can communicate with each other by producing signal metabolites to reach an equilibrium relationship. This interaction process during communication is complicated and is often associated with more than one factor. A number of strategies, including exogenous addition experiments, dynamic ^{13}C-labeling analysis, proteomics, and genetic engineering, have been used, but the interaction mechanisms of most coculture systems have not been clarified. To further elucidate the mechanism, more approaches should be developed, for example, multi-omics technology and CRISPR-Cas9-based genetic editing, which will be helpful to confirm the functions of chemical signals, to identify genes and clusters for secondary metabolite biosynthesis and to determine the regulatory mechanisms. This understanding will in turn help simplify the culture conditions, such as by the addition of certain inducers, to achieve a similar or even better effect of that in the coculture. Overall, with the progress of macrofungal genetic manipulating tools, multi-omics technology and a deeper understanding of the interaction mechanisms, the macrofungal coculture systems will present broad applications.

AUTHOR CONTRIBUTIONS

GY and LT conceived and designed the review and wrote the main manuscript text, GY, YS, HH, XY, YW, XG, BQ, and LT searched the literatures and critically revised the manuscript. All authors contributed to the article and approved the submitted version.

FUNDING

REFERENCES

Angelis, S., Novak, A. C., Sydney, E. B., Soccol, V. T., Carvalho, J. C., Pandey, A., et al. (2012). Co-culture of microalgae, cyanobacteria, and macromycetes for exopolysaccharides production: process preliminary optimization and partial characterization. *Appl. Biochem. Biotechnol.* 167, 1092–1106. doi: 10.1007/s12010-012-9642-7

Baldrian, P. (2004). Increase of laccase activity during interspecific interactions of white-rot fungi. *FEMS Microbiol. Ecol.* 50, 245–253.

Bankole, P. O., Adekunle, A. A., and Govindwar, S. P. (2018). Biodegradation of a monochlorotriazine dye, cibacron brilliant red 3B-A in solid state fermentation by wood-rot fungal consortium, *Daldinia concentrica* and *Xylaria polymorpha*. *Int. J. Biol. Macromol.* 120, 19–27. doi: 10.1016/j.ijbiomac.2018.08.068

Bertrand, S., Bohni, N., Schnee, S., Schumpp, O., Gindro, K., and Wolfender, J.-L. (2014). Metabolite induction via microorganism co-culture: a potential way to enhance chemical diversity for drug discovery. *Biotechnol. Adv.* 32, 1180–1204. doi: 10.1016/j.biotechadv.2014.03.001

Bhattacharya, S., Das, A., Palaniswamy, M., and Angayarkanni, J. (2017). Degradation of benzo[a]pyrene by *Pleurotus ostreatus* PO-3 in the presence of defined fungal and bacterial co-cultures. *J. Basic Microbiol.* 57, 95–103. doi: 10.1002/jobm.201600479

Bode, H. B., Bethe, B., Hofs, R., and Zeeck, A. (2002). Big effects from small changes: possible ways to explore nature's chemical diversity. *ChemBioChem* 3, 619–627. doi: 10.1002/1439-7633(20020703)3:7<619::AID-CBIC619>3.0.CO;2-9

Chen, B., Wei, T., Ye, Z., Tang, H., Guo, L., Lin, J., et al. (2018). Efficient CRISPR-Cas9 gene disruption system in edible-medicinal mushroom *Cordyceps militaris*. *Front. Microbiol.* 9:1157. doi: 10.3389/fmicb.2018.01157

Chen, Q.-H., Krüegener, S., Hirth, T., Rupp, S., and Zibek, S. (2011). Co-cultured production of lignin-modifying enzymes with white-rot fungi. *Appl. Biochem. Biotechnol.* 165, 700–718. doi: 10.1007/s12010-011-9289-9

Chen, S., Xu, J., Liu, C., Zhu, Y., Nelson, D. R., Zhou, S., et al. (2012). Genome sequence of the model medicinal mushroom *Ganoderma lucidum*. *Nat. Commun.* 3:913. doi: 10.1038/ncomms1923

Chi, Y., Hatakka, A., and Maijala, P. (2007). Can co-culturing of two white-rot fungi increase lignin degradation and the production of lignin-degrading enzymes? *Int. Biodeterior. Biodegrad.* 59, 32–39. doi: 10.1016/j.ibiod.2006.06.025

Copete-Pertuz, L. S., Alandete-Novoa, F., Plácido, J., Correa-Londoño, G. A., and Mora-Martínez, A. L. (2019). Enhancement of ligninolytic enzymes production and decolourising activity in *Leptosphaerulina* sp. by co-cultivation with Trichoderma viride and Aspergillus terreus. *Sci. Total Environ.* 646, 1536–1545. doi: 10.1016/j.scitotenv.2018.07.387

Essig, A., Hofmann, D., Münch, D., Gayathri, S., Künzler, M., Kallio, P. T., et al. (2014). Copsin, a novel peptide-based fungal antibiotic interfering with the peptidoglycan synthesis. *J. Biol. Chem.* 289, 34953–34964. doi: 10.1074/jbc.M114.599878

Ferreira Gregorio, A. P., Da Silva, I. R., Sedarati, M. R., and Hedger, J. N. (2006). Changes in production of lignin degrading enzymes during interactions between mycelia of the tropical decomposer basidiomycetes *Marasmiellus troyanus* and *Marasmius pallescens*. *Mycol. Res.* 110, 161–168. doi: 10.1016/j.mycres.2005.10.002

Flores, C., Vidal, C., Trejo-Hernández, M. R., Galindo, E., and Serrano-Carreón, L. (2009). Selection of *Trichoderma* strains capable of increasing laccase production by *Pleurotus ostreatus* and *Agaricus bisporus* in dual cultures. *J. Appl. Microbiol.* 106, 249–257. doi: 10.1111/j.1365-2672.2008.03998.x

Freitag, M., and Morrel, J. J. (1992). Changes in selected enzyme activities during growth of pure and mixed cultures of the white-rot decay fungus *Trametes versicolor* and the potential biocontrol fungus *Trichoderma harzianum*. *Can. J. Microbiol.* 38, 317–323. doi: 10.1139/m92-053

Guo, S., Wang, Q., Zhang, J., and Xia, H. (2001). Studies on the cultivation method of sclerotium forming from hyphae of *Grifola umbellata*. *Chin. Pharmacol. J.* 36, 658–660.

Guo, S., Wang, Q., Zhuang, W., Zhang, J., and Xing, X. (2002). Discovery and application of the companion fungus related to sclerotial formation from hyphae of *Grifola umbellata*. *Acta Bot. Sin.* 44, 1151–1154.

Guo, S., and Xu, J. (1992). Nutrient source of sclerotia of *Grifola umbellata* and its relationship to *Armillaria mellea*. *Acta Bot. Sin.* 34, 576–580.

Hiscox, J., Baldrian, P., Rogers, H. J., and Boddy, L. (2010). Changes in oxidative enzyme activity during interspecific mycelial interactions involving the white-rot fungus *Trametes versicolor*. *Fungal Genet. Biol.* 47, 562–571. doi: 10.1016/j.fgb.2010.03.007

Huo, X., Li, H., Li, Z., Yan, C., Mathavan, S., Liu, J., et al. (2019). Transcriptomic analyses of oncogenic hepatocytes reveal common and different molecular pathways of hepatocarcinogenesis in different developmental stages and genders in kras(G12V) transgenic zebrafish. *Biochem. Biophys. Res. Commun.* 510, 558–564. doi: 10.1016/j.bbrc.2019.02.008

Jan Vonk, P., Escobar, N., Wösten, H. A. B., Lugones, L. G., and Ohm, R. A. (2019). High-throughput targeted gene deletion in the model mushroom *Schizophyllum commune* using pre-assembled Cas9 ribonucleoproteins. *Sci. Rep.* 9:7632. doi: 10.1038/s41598-019-44133-2

Keilhofer, N., Nachtigall, J., and Kulik, A. (2018). *Streptomyces AcH* 505 triggers production of a salicylic acid analogue in the fungal pathogen *Heterobasidion abietinum* that enhances infection of *Norway spruce* seedlings. *Antonie van Leeuwenhoek* 111, 691–704. doi: 10.1007/s10482-018-1017-9

Knowles, S. L., Raja, H. A., Isawi, I. H., Flores-Bocanegra, L., Reggio, P. H., Pearce, C. J., et al. (2020). Wheldone: characterization of a unique scaffold from the coculture of *Aspergillus fischeri* and *Xylaria flabelliformis*. *Org. Lett.* 22, 1878–1882. doi: 10.1021/acs.orglett.0c00219

Knowles, S. L., Raja, H. A., Wright, A. J., Lee, A. M. L., Caesar, L. K., Cech, N. B., et al. (2019). Mapping the fungal battlefield: using *in situ* chemistry and deletion mutants to monitor interspecific chemical interactions between fungi. *Front. Microbiol.* 10:285. doi: 10.3389/fmicb.2019.00285

Kuhar, F., Castiglia, V., and Levin, L. (2015). Enhancement of laccase production and malachite green decolorization by co-culturing *Ganoderma lucidum* and *Trametes versicolor* in solid-state fermentation. *Int. Biodeterior. Biodegrad.* 104, 238–243. doi: 10.1016/j.ibiod.2015.06.017

Kumar, A., Arora, J., Jain, K. K., and Sharma, K. K. (2019). Metabolic coupling in the co-cultured fungal-yeast suite of *Trametes ljubarskyi* and *Rhodotorula mucilaginosa* leads to hypersecretion of laccase isozymes. *Fungal Biol.* 123, 913–926. doi: 10.1016/j.funbio.2019.09.013

Li, H., Liu, S., Cui, Q., Xu, B., Xiao, L., and Zang, J. (2019). *Method for Removing Indigo Carmine by Sesame Straw Co-Fermented with Tremella fuciformis and Morchella sp. CN 109806846A*. China National Intellectural Property Administration.

Li, H., Wu, S., Ma, X., Chen, W., Zhang, J., Duan, S., et al. (2018). The genome sequences of 90 mushrooms. *Sci. Rep.* 8:9982. doi: 10.1038/s41598-018-28303-2

Li, P., Wang, H., Liu, G., Li, X., and Yao, J. (2010). The effect of carbon source succession on laccase activity in the co-culture process of *Ganoderma lucidum* and a yeast. *Enzyme Microb. Technol.* 48, 1–6. doi: 10.1016/j.enzmictec.2010.07.005

Lira-Pérez, J., Rodríguez-Vázquez, R., and Chan-Cupul, W. (2020). Effect of fungal co-cultures on ligninolytic enzyme activities, H_2O_2 production, and orange G discoloration. *Prep. Biochem. Biotechnol.* 50, 607–618. doi: 10.1080/10826068.2020.1721534

Liu, X. (2015). *Method for Increasing Content of Cordycepin in Cordyceps militaris Fruiting Bodies using Monascus species. CN 104756763A*. China National Intellectual Property Administration.

Ma, K., and Ruan, Z. (2015). Production of a lignocellulolytic enzyme system for simultaneous bio-delignification and saccharification of corn stover employing co-culture of fungi. *Bioresour. Technol.* 175, 586–593. doi: 10.1016/j.biortech.2014.10.161

Mewada, M., Albert, S., and Pandya, B. (2017). Enhancement of ligninolytic and xylanolytic enzyme activities in *Trichoderma reesei* co-cultured with two white rot fungi. *Int. J. Biochem. Biotechnol.* 13, 429–439.

Moody, S. C. (2014). Microbial co-culture: harnessing intermicrobial signaling for the production of novel antimicrobials. *Future Microbiol.* 9, 575–578. doi: 10.2217/fmb.14.25

Niskanen, T., Douglas, B., Kirk, P., Crous, P., Lücking, R., Matheny, P., et al. (2018). "State of the World's Fungi State of the World's Fungi 2018, Chapter 3. New discoveries: species of fungi described in 2017," in *State of the World's Fungi*, ed E.Willis (Kew: Royal Botanic Gardens), 18–23.

Noedvig, C. S., Nielsen, J. B., Kogle, M. E., and Mortensen, U. H. (2015). A CRISPR-Cas9 system for genetic engineering of filamentous fungi. *PLoS ONE* 10:e0133085. doi: 10.1371/journal.pone.0133085

Qin, H., Xiao, H., Zou, G., Zhou, Z., and Zhong, J.-J. (2017). CRISPR-Cas9 assisted gene disruption in the higher fungus *Ganoderma* species. *Process Biochem.* 56, 57–61. doi: 10.1016/j.procbio.2017.02.012

Qu, Q. S., Yang, F., Zhao, C. Y., and Shi, X. Y. (2019). Analysis of the bacteria community in wild *Cordyceps cicadae* and its influence on the production of HEA and nucleosides in *Cordyceps cicadae*. *J. Appl. Microbiol.* 127, 1759–1767. doi: 10.1111/jam.14432

Sandland, G. J., Rodgers, J. K., and Minchella, D. J. (2007). Interspecific antagonism and virulence in hosts exposed to two parasite species. *J. Invertebr. Pathol.* 96, 43–47. doi: 10.1016/j.jip.2007.02.005

Savoie, J. M., Mata, G., and Billette, C. (1998). Extracellular laccase production during hyphal interactions between *Trichoderma* sp. and Shiitake, Lentinula edodes. *Appl. Microbiol. Biotechnol.* 49, 589–593. doi: 10.1007/s002530051218

Scherlach, K., and Hertweck, C. (2009). Triggering cryptic natural product biosynthesis in microorganisms. *Org. Biomol. Chem*. 7, 1753–1760. doi: 10.1039/b821578b

Shen, X., Lv, Y., Wang, P., Han, S., Zeng, G., Zhou, C., et al. (2020). *Method for CRISPR/Cas9-Mediated Gene Editing of Agaricus bisporus and Application. CN 111349649A.* China National Intellectural Property Administration.

Shen, X., Mo, X., Zhu, L., Tan, L., Du, F., Wang, Q., et al. (2019). Unusual and highly bioactive sesterterpenes synthesized by *Pleurotus ostreatus* during coculture with *Trametes robiniophila* Murr. *Appl. Environ. Microbiol.* 85:e00293-19. doi: 10.1128/AEM.00293-19

Shin, C. S., Kim, H. J., Kim, M. J., and Ju, J. Y. (1998). Morphological change and enhanced pigment production of *Monascus* when cocultured with *Saccharomyces cerevisiae* or *Aspergillus oryzae*. *Biotechnol. Bioeng.* 59, 576–581.

Stoilova, I., and Krastanov, A. (2008). Overproduction of laccase and pectinase by microbial associations in solid substrate fermentation. *Appl. Biochem. Biotechnol.* 149, 45–51. doi: 10.1007/s12010-007-8013-2

Sugano, S. S., Suzuki, H., Shimokita, E., Chiba, H., Noji, S., Osakabe, Y., et al. (2017). Genome editing in the mushroom-forming basidiomycete *Coprinopsis cinerea*, optimized by a high-throughput transformation system. *Sci. Rep.* 7:1260. doi: 10.1038/s41598-017-00883-5

Tauber, J. P., Gallegos-Monterrosa, R., Kovács, Á., T., Shelest, E., and Hoffmeister, D. (2018). Dissimilar pigment regulation in *Serpula lacrymans* and *Paxillus involutus* during inter-kingdom interactions. *Microbiology* 164, 65–77. doi: 10.1099/mic.0.000582

Tauber, J. P., Schroeckh, V., Shelest, E., Brakhage, A. A., and Hoffmeister, D. (2016). Bacteria induce pigment formation in the basidiomycete *Serpula lacrymans*. *Environ. Microbiol.* 18, 5218–5227. doi: 10.1111/1462-2920.13558

Velázquez-Cedeño, M. A., Farnet, A. M., Ferré, E., and Savoie, J. M. (2004). Variations of lignocellulosic activities in dual cultures of *Pleurotus ostreatus* and *Trichoderma longibrachiatum* on unsterilized wheat straw. *Mycologia* 96, 712–719. doi: 10.1080/15572536.2005.11832919

Wang, H., Yu, G., Li, P., Gu, Y., Li, J., Liu, G., et al. (2009). Overproduction of *Trametes versicolor* laccase by making glucose starvation using yeast. *Enzyme Microb. Technol.* 45, 146–149. doi: 10.1016/j.enzmictec.2009.04.003

Wang, Z., Li, G., Ji, L. X., Wang, H., Gao, H., Peng, X., et al. (2019). Induced production of steroids by co-cultivation of two endophytes from *Mahonia fortunei*. *Steroids* 145, 1–4. doi: 10.1016/j.steroids.2019.02.005

Weber, T., Blin, K., Duddela, S., Krug, D., Kim, H. U., Bruccoleri, R., et al. (2015). antiSMASH 3.0-a comprehensive resource for the genome mining of biosynthetic gene clusters. *Nucleic Acids Res.* 43, W237–W243. doi: 10.1093/nar/gkv437

Wei, F., Hong, Y., Liu, J., Yuan, J., Fang, W., Peng, H., et al. (2010). *Gongronella* sp. induces overproduction of laccase in *Panus rudis*. *J. Basic Microbiol.* 50, 98–103. doi: 10.1002/jobm.200900155

Wiberth, C.-C., Casandra, A.-Z. C., Zhiliang, F., and Gabriela, H. (2019). Oxidative enzymes activity and hydrogen peroxide production in white-rot fungi and soil-borne micromycetes co-cultures. *Ann. Microbiol.* 69, 171–181. doi: 10.1007/s13213-018-1413-4

Xing, X. K., and Guo, S. X. (2003). Morphological studies on dual and triple culture of *Grifola umbellata*, an unnamed companion fungus and *Grmillariella mellea*. *Mycosystema* 22, 653–660. doi: 10.13346/j.mycosystema.2003.04.025

Xu, X., Shen, X., Yuan, X., Zhou, Y., Fan, H., Zhu, L., et al. (2018). Metabolomics investigation of an association of induced features and corresponding fungus during the co-culture of *Trametes versicolor* and *Ganoderma applanatum*. *Front. Microbiol.* 8:2647. doi: 10.3389/fmicb.2017.02647

Yanto, D. H. Y., and Tachibana, S. (2014). Potential of fungal co-culturing for accelerated biodegradation of petroleum hydrocarbons in soil. *J. Hazard. Mater.* 278, 454–463. doi: 10.1016/j.jhazmat.2014.06.039

Yao, L., Zhu, L. P., Xu, X. Y., Tan, L. L., Sadilek, M., Fan, H., et al. (2016). Discovery of novel xylosides in co-culture of basidiomycetes *Trametes versicolor* and *Ganoderma applanatum* by integrated metabolomics and bioinformatics. *Sci. Rep.* 6:33237. doi: 10.1038/srep33237

Yu, G., Sun, Z., Peng, J., Zhu, M., Che, Q., Zhang, G., et al. (2019). Secondary metabolites produced by combined culture of *Penicillium crustosum* and a *Xylaria* sp. *J. Nat. Prod.* 82, 2013–2017. doi: 10.1021/acs.jnatprod.9b00345

Zhang, B., Guan, Y., Hu, P., Chen, L., Xu, G., Liu, L., et al. (2019). Production of bioactive metabolites by submerged fermentation of the medicinal mushroom *Antrodia cinnamomea*: recent advances and future development. *Crit. Rev. Biotechnol.* 39, 541–554. doi: 10.1080/07388551.2019.1577798

Zhang, H., Hong, Y., Xiao, Y., Yuan, J., Tu, X., and Zhang, X. (2006). Efficient production of laccases by *Trametes* sp. AH28-2 in cocultivation with a *Trichoderma* strain. *Appl. Microbiol. Biotechnol.* 73, 89–94. doi: 10.1007/s00253-006-0430-6

Zhang, S. (2002). The numbers of mushnoom species. *Edible Fungi China* 21, 3–4.

Zheng, W., Zhao, Y., Zheng, X., Liu, Y., Pan, S., Dai, Y., et al. (2011). Production of antioxidant and antitumor metabolites by submerged cultures of *Inonotus obliquus* cocultured with *Phellinus punctatus*. *Appl. Microbiol. Biotechnol.* 89, 157–167. doi: 10.1007/s00253-010-2846-2

Zhou, L., and Jiang, C. (2008). Priminary research on the cofermentation of *Monascus ruber* and *Cordyceps militaris*. *Edible Fungi China* 174, 40–42.

Zhou, X. W., Su, K. Q., and Zhang, Y. M. (2012). Applied modern biotechnology for cultivation of *Ganoderma* and development of their products. *Appl. Biochem. Biotechnol.* 93, 941–963. doi: 10.1007/s00253-011-3780-7

Check for
updates

New Thio-Compounds and Monoterpenes With Anti-inflammatory Activities From the Fungus *Aspergillus* sp. CYH26

Guojun Pan[1], Yanling Li[1], Xinyu Che[2], Dan Tian[2], Wenjie Han[1], Zimin Wang[1], Yanfen Zhao[1], Shuang Ren[1], Yiru Xu[1], Gangping Hao[1], Mengfei Guo[3], Na Xiao[2,4]* and Fandong Kong[3]*

[1] College of Life Sciences, Shandong First Medical University, Shandong Academy of Medical Sciences, Tai'an, China,
[2] State Key Laboratory of Crop Biology, College of Agronomy, Shandong Agriculture University, Tai'an, China,
[3] Key Laboratory of Chemistry and Engineering of Forest Products, State Ethnic Affairs Commission, Guangxi Key Laboratory of Chemistry and Engineering of Forest Products, Guangxi Collaborative Innovation Center for Chemistry and Engineering of Forest Products, School of Chemistry and Chemical Engineering, Guangxi University for Nationalities, Nanning, China, [4] State Key Laboratory of Natural Medicines, China Pharmaceutical University, Nanjing, China

Two new thio-compounds named aspergerthinol A and B (**1** and **2**) and two new monoterpenes named aspergerthinacids A and B (**3** and **4**) were isolated from the fungus *Aspergillus* sp. CYH26 from the rhizosphere soil of *Cynanchum bungei* Decne. The structures of compounds were elucidated by spectroscopic data and quantum NMR and ECD calculations. Compounds **1** and **2** represented a new family of sulfur containing natural products with a 3-methyl-4*H*-cyclopenta[b]thiophen-4-one skeleton. Compounds **1–4** showed inhibitory activities against nitric oxide (NO) with IC_{50} values of 38.0, 19.8, 46.3, and 56.6 μM, respectively.

Keywords: *Aspergillus* sp. CYH26, thio-compounds, monoterpenes, anti-inflammatory activity, fungus

INTRODUCTION

Early inflammatory response is generally to eliminate the harmful stimulation condition (Cameron and Landreth, 2010). However, low-grade, chronic inflammation response plays a critical role in the pathological process of many diseases, such as arthritis, cancer, type 2 diabetes, and autoimmune diseases (Chen et al., 2017). Nitric oxide (NO) as a pro-inflammatory mediator is critical in the secretion of proinflammatory cytokines such as IL-6, TNF-α (Sharma et al., 2007). Thus, suppressing the production of NO could be a potential therapeutic method in the prevention of various diseases induced by excessive inflammation. Microorganism, including bacteria, actinomycetes, and fungi, have been proven to be a prolific source of structurally new and biologically active natural products (Qadri et al., 2013). The secondary metabolites obtained from fungi have gained considerable attention, as they contribute most of the new natural products from microorganism and many compounds from fungi possess unique structure with potent biological activity (Keller, 2019). In our ongoing search for new bioactive metabolites from fungi (Kong et al., 2017, 2019), the secondary metabolites produced by the soil fungus *Aspergillus* sp. CYH26 isolated from the rhizosphere soil of *Cynanchum bungei* Decne. from Mount Tai, China, were investigated, which resulted in the isolation and identification of two new thio compounds named aspergerthinol A and B (**1** and **2**) and two new monoterpenes named aspergerthinacids

A and B (**3** and **4**) (**Figure 1**). All of the compounds could suppress the over-production of NO without affecting the cell viability. Herein, we describe the isolation, structural elucidation, and bioactivities of compounds **1**–**4**.

MATERIALS AND METHODS

General Experimental Procedures

Optical rotations were measured on a JASCO P-1020 digital polarimeter, and UV spectra were measured on a Beckman DU 640 spectrophotometer. ECD data were collected using a JASCO J-715 spectropolarimeter. NMR spectra were recorded on a Bruckmercury Plus-400 or a JNM-ECZR-500 spectrometers with TMS as an internal standard. HRESIMS spectra were recorded with a Micromass Autospec -Uitima- TOF, API QSTAR Pulsar 1, or Waters Autospec Premier spectrometer. Semi-preparative HPLC was carried out using an ODS column (YMC-pack ODS-A, 10 × 250 mm, 5 μm, 4 mL/min). Thin layer chromatography (TLC) and column chromatography (CC) were performed on plates precoated with silica gel GF$_{254}$ (10–40 μm, Yantai Jiangyou Silicone Development Co., Ltd.).

Fungal Material and Fermentation

The fungus *Aspergillus* sp. CYH26 was isolated from the rhizosphere soil of *C. bungei* Decne., from Mount Tai, China in December 2018. After grinding, the sample (1.0 g) was diluted to 10^{-2} g/mL with sterile H$_2$O, 100 μL of which was deposited on PDA (potato 200 g, glucose 20 g, agar 20 g per liter of tap water) plate and Bengal red medium (maltose 20 g, monosodium glutamate 10 g, glucose 10 g, yeast extract 3 g, corn pulp 1 g, mannitol 20 g, sodium chloride 0.3 g, potassium dihydrogen phosphate 0.5 g, agar 20 g per liter of tap water) plate containing chloramphenicol (200 μg/mL) as a bacterial inhibitor. A single colony was transferred onto another PDA plate and was identified according to its morphological characteristics and ITS gene sequences (GenBank accession No. MW578366, **Supplementary Material**). A reference culture of *Aspergillus* sp. CYH26 maintained at −80°C is deposited in our laboratory. The isolate was cultured on plates of PDA medium at 28°C for 4 days. Plugs of agar supporting mycelium growth were cut and transferred aseptically to 5 × 250 mL Erlenmeyer flasks each containing 100 mL of liquid medium (potato 200 g, glucose 20 g per liter of tap water) and cultured at 28°C at 150 RPM for 3 days. The seed liquid was inoculated aseptically into 50 × 1,000 mL Erlenmeyer flasks each containing rice medium (80 g rice, 100 mL tap water) at 1% inoculation amount and incubated at room temperature under static conditions for 35 days.

FIGURE 1 | The chemical structures of compounds **1**–**4**.
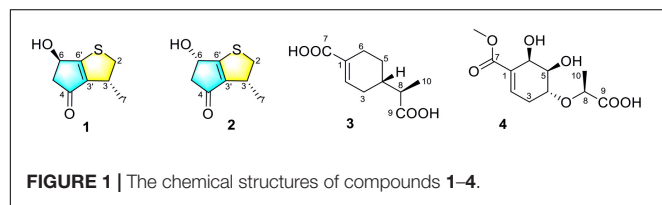
Extraction and Isolation

The cultures (4 kg) were then extracted in to EtOAc (20 L) by soaking overnight. The extraction was repeated for three times. The combined EtOAc extracts were dried under vacuum to produce 22.6 g of extract. The EtOAc extract was subjected to a silica gel VLC column, eluting with a stepwise gradient of 0, 9, 11, 15, 20, 30, 50, and 100% EtOAc in petroleum ether (v/v), to give eight fractions (Fr. 1–8). Fraction 4 (3.4 g) was applied to ODS silica gel with gradient elution of MeOH-H$_2$O (1:5, 2:3, 3:2, 4:1, and 1:0) to yield five subfractions (Fr. 4-1–Fr. 4-5). Fr. 4-2 (90 mg) was purified using semi-prep HPLC (isocratic system 50% MeOH/H$_2$O, v/v) to give compounds **4** (t_R 6.0 min; 7.7 mg) and **3** (t_R 9.5 min; 11 mg). Fraction 5 (1.3 g) was applied to ODS silica gel with gradient elution of MeOH-H$_2$O (1:5, 2:3, 3:2, 4:1, and 1:0) to yield four subfractions (Fr. 5-1–Fr. 5-5). Fr. 5-2 (71 mg) was further purified using semi-prep HPLC (isocratic system 40% MeOH/H$_2$O, v/v) to give compounds **1** (t_R 5.3 min; 5.3 mg) and **2** (t_R 5.6 min; 4.1 mg).

Aspergerthinol A (1): brown oils; $[\alpha]25$ D −10 (*c* 0.1, MeOH); UV (MeOH) λ_{max} (log ε): 304 (2.85) nm; ECD (1.18 mM, MeOH) λ_{max} 207 (−5.31), 298 (−4.71), 325 (+3.68) nm. ^{1}H and ^{13}C NMR data, **Table 1**; HRESIMS *m/z* 169.0318 [M-H]$^-$ (calcd for C$_8$H$_9$O$_2$S, 169.0329).

Aspergerthinol B (2): brown oils; $[\alpha]25$ D −7 (*c* 0.1, MeOH); UV (MeOH) λ_{max} (log ε): 304 (2.84) nm; ECD (0.35 mM, MeOH) λ_{max} 217 (+ 5.63), 296 (+ 3.27), 323 (−3.31) nm. ^{1}H and ^{13}C NMR data, **Table 1**; HRESIMS *m/z* 169.0323 [M-H]$^-$ (calcd for C$_8$H$_9$O$_2$S, 169.0329).

Aspergerthinacid A (3): yellow powder; $[\alpha]25$ D −46 (*c* 0.1, MeOH); UV (MeOH) λ_{max} (log ε): 218 (2.80) nm; ECD (1.2 mM, MeOH) λ_{max} 214 (−1.54) nm. ^{1}H and ^{13}C NMR data, **Table 2**; HRESIMS *m/z* 197.0811 [M-H]$^-$ (calcd for C$_{10}$H$_{13}$O$_4$, 197.0819).

Aspergerthinacid B (4): yellow powder; $[\alpha]25$ D −168 (*c* 0.1, MeOH); UV (MeOH) λ_{max} (log ε): 213 (2.83) nm; ECD (3.7 mM, MeOH) λ_{max} 213 (−2.58) nm. ^{1}H and ^{13}C NMR data, **Table 2**; HRESIMS *m/z* 259.0824 [M-H]$^-$ (calcd for C$_{11}$H$_{15}$O$_7$, 259.0823).

TABLE 1 | The ^{1}H (400 MHz) and ^{13}C NMR (100 MHz) Data of Compounds **1** and **2** in CD$_3$OD.

Position	1		2	
	δ$_C$	δ$_H$ (*J* in Hz)	δ$_C$	δ$_H$ (*J* in Hz)
2	49.0, CH$_2$	3.39, dd (11.5, 6.1)	49.0, CH$_2$	3.39, dd (11.5, 5.1)
		4.02, dd (11.5, 9.2)		4.03, dd (11.5, 9.1)
3	36.5, CH	3.26, m	36.4, CH	3.27, m
3'	147.7, C		147.8, C	
4	197.6, C		197.5, C	
5	51.7, CH$_2$	2.56, dd (18.0, 1.8)	51.7, CH$_2$	2.55, dd (18.0, 1.9)
		3.05, dd (18.0, 6.2)		3.08, dd (18.0, 6.2)
6	67.0, CH	4.89, m	67.2, CH	4.91, m
6'	187.7, C		187.8, C	
7	18.1, CH$_3$	1.25, d (6.8)	17.7, CH$_3$	1.19, d (6.8)

TABLE 2 | The ^{1}H (400 MHz) and ^{13}C NMR (100 MHz) Data of Compounds **3** and **4** in CD$_3$OD.

Position	3		4	
	δ_C	δ_H (*J* in Hz)	δ_C	δ_H (*J* in Hz)
1	131.4, C		129.8, C	
2	140.1, CH	6.95, m	139.4, CH	6.78, m
3	31.1, CH$_2$	2.03, m	28.6, CH$_2$	2.66, dddd (18.1, 4.7, 2.0, 2.0)
		2.25, m		2.29, dddd (18.1, 4.7, 1.6, 1.6)
4	37.1, CH	1.80, m	77.0, CH	3.79, ddd (7.1, 4.7, 4.7)
5	26.2, CH$_2$	1.31, m	71.0, CH	3.86, dd (7.1, 4.5)
		1.92, m		
6	25.3, CH$_2$	2.42, m	67.1, CH	4.40, m
		2.17, m		
7	170.7, C		168.6, C	
8	45.2, CH	2.32, overlap	74.8, CH	4.26, q (7.0)
9	179.8, C		176.0, C	
10	14.7, CH$_3$	1.18, d (7.0)	19.5, CH$_3$	1.34, d (6.9)

FIGURE 2 | Selected HMBC and COSY correlations of **1–4**.
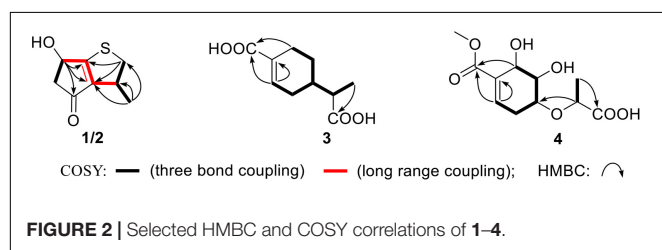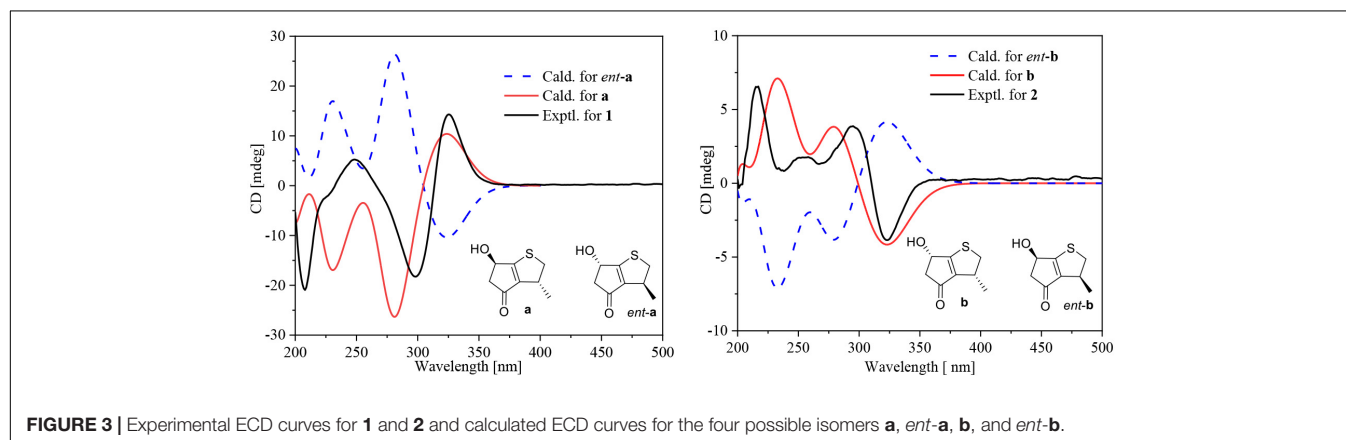
Bioactivity Assay

Cell viability of the isolated compounds was detected using MTT assay. Mouse macrophages (RAW264.7 cells) obtained from the Type Culture Collection of the Chinese Academy of Sciences (Shanghai, China), were cultured in DMEM (Gibco, United States) with 10% FBS at 37°C in a 5% CO$_2$ atmosphere. After that, cells were seeded in a 96-well plate (2 × 10^4 cells/well) and pre-treated with different doses of compounds for 24 h at 37°C. After that, 10 μL of MTT was added to each well and incubated for another 4 h. The media and MTT were removed and 150 μL of dimethylsulfoxide (DMSO) was added.

Following incubation for 0.5 h, the absorbance value was determined at 570 nm. For Determination of NO content, cells were seeded in a 96-well plate and pre-treated with different dose of compounds, and then stimulated with or without LPS (5 μg/mL) for another 24 h. The supernatants were analyzed for NO by commercial kit (Jiancheng, Nanjing, China). All tests were performed in triplicate. The NO inhibitory rate (%) was calculated as $[1 - (A_{drug} - A_{blank})/(A_{control} - A_{blank})] \times 100\%$. The IC$_{50}$ values were calculated using prism software (GraphPad). The NO inhibitory rate (%) was calculated as $[1 - (A_{drug} - A_{blank})/(A_{control} - A_{blank})] \times 100\%$. The IC$_{50}$ values were calculated using prism software (GraphPad).

RESULTS AND DISCUSSION

Structure Elucidation of Compounds

Compounds **1** and **2** were assigned the molecular formula C$_{10}$H$_8$O$_2$S by HRESIMS. The double-bond equivalents of **1** and **2** were calculated to be four. The ^{13}C and HSQC NMR spectra (**Table 1**) of **1** revealed a total of eight carbons including one ketone carbonyl, two olefinic non-protonated carbons, two sp^3 methylenes with one heteroatom-bonded, two sp^3 methines with one oxygenated, and one methyl. Detailed analysis of the COSY data (**Figure 2**) of **1** revealed the presence of two partial structures CH$_3$-7/CH-3/CH$_2$-2 and CH$_2$-4/CH(OH)-6. The presence of the α,β-unsaturated ketone moiety constructed by the remaining three non-protonated sp^2 carbons C-4 (δ_C 197.6), C-3′ (δ_C 147.7), and C-6′ (δ_C 187.7) was deduced by their characteristic chemical shifts and HMBC correlations (**Figure 2**) from both H$_2$-5 and H-6 to C-4, C-3′, and C-6′. The connection between C-3 and C-3′ was revealed by the HMBC correlation from H$_3$-7 to C-3′. The connections of C-6′/C-6 and C-3′/C-4 to construct a five-membered carbon ring were deduced by the long-range coupling (**Figure 2**) between H-3 and H-6 as well as the HMBC correlations from H$_2$-5 to C-3′. The above data accounted for three out of four double-bond equivalent, indicating the presence of another ring in the molecule. According to the molecular formula, a sulfur atom was present in the structure of **1**. Considering the above, a linkage between C-2 and C-6′ through a sulfur atom was proposed, as also suggested by the chemical
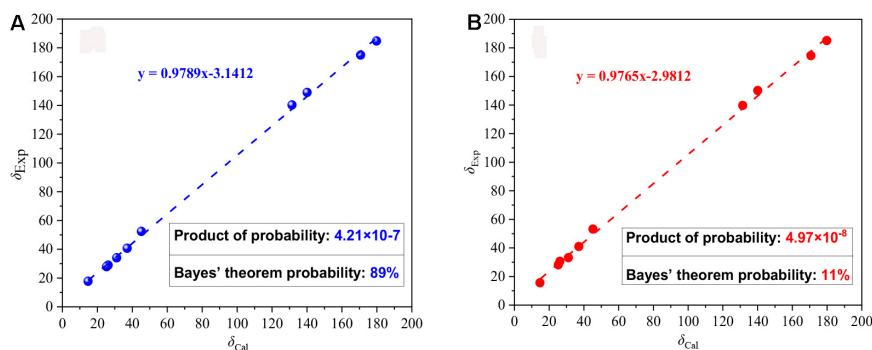

FIGURE 3 | Experimental ECD curves for **1** and **2** and calculated ECD curves for the four possible isomers **a**, *ent*-**a**, **b**, and *ent*-**b**.

FIGURE 4 | Linear correlations and DP4 probabilities between the experimental and calculated ^{13}C NMR chemical shifts for **3 (A)** and 4-*epi*-**3 (B)**.
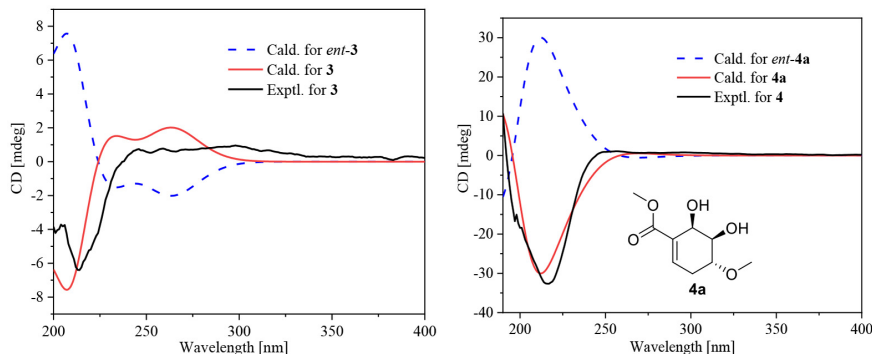

FIGURE 5 | Experimental ECD curve for **3** and **4** and calculated ECD curves for **3**, *ent*-**3**, **4a**, and *ent*-**4a**.
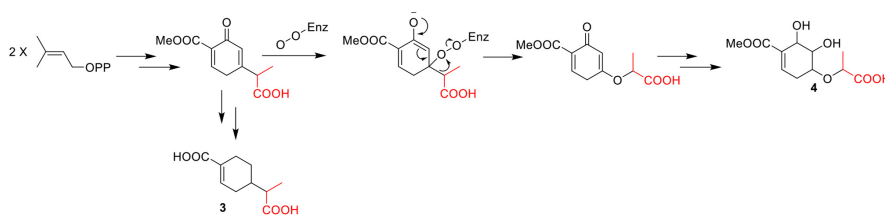

FIGURE 6 | Hypothetical biogenetic pathway of compound **3** and **4**.

shifts of CH$_2$-2 ($\delta_{C/H}$ 49.0/4.02, 3.39) and C-6′ (δ_C 187.7). The planar structure of **2** was assigned the same as **1** by their same 2D NMR data (**Figure 2**). Because there are only two stereogenic centers in the structure, **2** was thus assigned to be the C-3 or C-6 epimer of **1**. The determination of the relative configurations of **1** and **2** using NOESY spectra was failed for the far spatial distance between the two stereogenic centers, and the ^{13}C NMR calculation method would not work either due to the nearly identical ^{13}C NMR data between **1** and **2**. In order to determine the absolute configurations of **1** and **2**, quantum ECD calculations (Kong et al., 2019) of the four possible stereoisomers **a**, *ent*-**a**, **b**, and *ent*-**b** were thus performed (**Figure 3** and **Supplementary Figure 1**), and the calculated UV and ECD curves were compared with the experimental ones of **1** and **2**. The results showed that the experimental UV curves of **1** and **2** were in good agreement

with those of the calculated (**Supplementary Figure 2**), which further confirmed the planar structure of **1** and **2**. Furthermore, the ECD curves of **1** and **2** matched well with the calculated ECD curves of **a** and **b** (**Figure 3**), respectively, thus assigning the absolute configurations of **1** and **2** as (3*R*,6*R*)- and (3*R*,6*S*)-, respectively. Molecular orbital (MO) analysis (**Supplementary Figure 3**) revealed that the strong Cotton effects (CEs) around 300 and 325 nm in **1** and **2** were resulted from π → π* (MO45 → MO46) and n → π* (MO44 → MO46) transitions in the α,β-unsaturated ketone, respectively. It has been reported (Gawronski et al., 1996) that the signs of the CEs related to the π → π* and n → π* transitions of the α,β-unsaturated ketone in a five-membered ring correlated with the configuration of the chiral carbon at the γ position, i.e., C-6 in **1** and **2**. Thus, the nearly reverse CEs around 300 and 325 nm between **1** and **2**

also confirmed their different configurations at C-6. Structurally, compounds **1** and **2** represented a new family of sulfur containing natural products with a 3-methyl-4*H*-cyclopenta[b]thiophen-4-one skeleton.

Compound **3** was obtained as a yellow powder, and its molecular formula was determined as $C_{10}H_{14}O_4$ according to the HRESIMS data, with four degrees of unsaturation. The ^{13}C NMR and DEPT spectra displayed signals for two carboxylic carbonyls, one tri-substituted double bond, three sp^3 methylenes, two sp^3 methines, and one methyl. In the COSY spectrum (**Figure 2**), correlations of H_3-10/H-8/H-4/H_2-5/H_2-6 and H-8/H_2-3/H-2 were observed. In the HMBC spectrum (**Figure 2**), H_3-10 correlated with the C-9 carboxylic carbonyl, and H_2-6 and H-2 correlated with both C-1 and C-9 carboxylic carbonyl. The above data led to the determination of the planar structure of **3**. In order to determine the relative configuration of **3**, the ^{13}C NMR calculations (Kong et al., 2019) of **3** and 4-*epi*-**3** at the B3LYP/6-311 + + G(2d,p) level were performed (**Figure 4** and **Supplementary Figures 4, 5**). As shown in **Figure 4**, the calculated NMR chemical shifts of **3** (**Figure 4A**) coincided better with the experimental data compared to those of 4-*epi*-**3** (**Figure 4B**). The DP4 probability analysis (Lv et al., 2019) also showed that **3** had 89% probability while only 11% for 4-*epi*-**3** (**Figure 4** and **Supplementary Table 1**). These data led to the assignment of the relative configuration of **3**. Based on the above assignment, the ECD curves of **3** and *ent*-**3** were calculated (**Figure 5**). The calculated ECD curve for **3** matched well with the experimental one, thus assigning the absolute configuration as (4*S*,8*R*)-.

The molecular formula of compound **4** was established as $C_{11}H_{16}O_7$ by HRESIMS. The double-bond equivalent of **4** was calculated to be four. The HSQC spectrum indicated the presence of four oxymethines, one sp3 methylene, and two methyl with one methoxy, one carboxylic acid and a α,β-unsaturated carboxylic acid or ester group. The presence of two carbonyls and one tri-substituted double bond (**Supplementary Table 1**) indicated that **4** has a ring in its structure. Analysis of the COSY data (**Figure 2**) suggested the presence of the substructures CH-2/CH_2-3/CH-4/CH-5/CH-6 and CH_3-10/CH-8. HMBC correlations from H-2 and H-6 to C-1 and C-7 carbonyl led to the construction of the skeleton of **4**. HMBC correlations from CH_3-10 to the carboxylic carbonyl C-9 and from H-8 to the oxymethine C-4 led to the assignment of the full structure of **4**. The large *J* value (7.1 Hz) (**Table 2**) between H-4 and H-5 indicated their *trans* relationship, while the small *J* value (4.7 Hz) between H-5 and H-6 suggested their *cis* orientation. In order to assign absolute configuration of **4**, the ECD curves of the simplified structure **4a** of **4** was calculated and the resulted ECD curve showed good agreement with the experimental ECD spectrum (**Figure 5**), thus assigning the absolute configurations of C-4, C-5, and C-6 as *R*, *R*, and *R*, respectively. The skeletons of **3** and **4** are very similar with the only difference being the presence of an oxygen atom between C-4 and C-8 in **4**, which suggested that the biosynthetic pathways of **3** and **4** are closely related. A biosynthetic pathway including a Baeyer-Villiger like oxidation key step to afford **4** was thus proposed (**Figure 6**). Based on the biosynthetic consideration, the absolute configuration of C-8 of
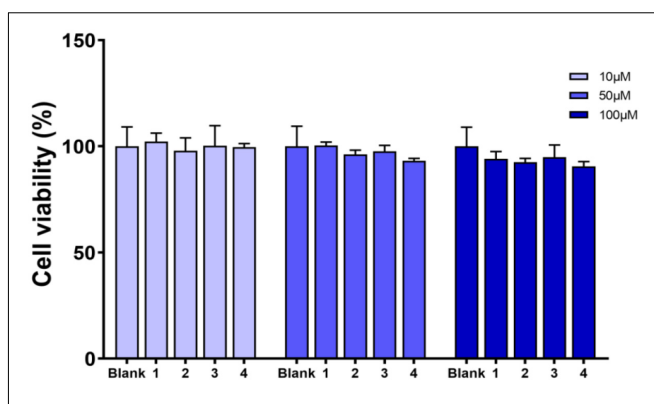

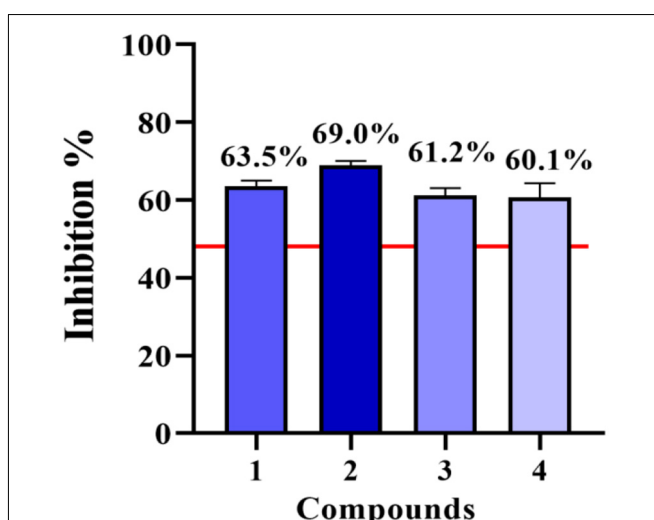**FIGURE 7** | Viability effects of compounds **1–4** against RAW264.7 cells.

FIGURE 8 | NO inhibitory activities of compounds **1–4** at 80 μM.

4 was tentatively assigned to be *S* according to the assigned C-8 configuration of **3**.

Bioactivity Assay

Compounds **1–4** were evaluated for cell viability using MTT assay. As shown in **Figure 7**, all the compounds have no obvious effect on the cell viability of RAW264.7 cells at three different concentrations (10, 50, and 100 μM) (**Figure 7**). Based on this, the suppressive effects of compounds **1–4** on the over-production of NO in cells were tested (Cao et al., 2021) at the concentration of 80 μM. The result showed that all the tested compounds were active (**Figure 8**). The IC$_{50}$ values of compounds **1–4** against the over-production of NO in cells were finally determined to be 38.0, 19.8, 46.3, and 56.6 μM, respectively (positive control dexamethasone, IC$_{50}$: 7.5 μM). Besides, the antibacterial activity of **1–4** against *Staphylococcus aureus* were also evaluated (Pierce et al., 2008), and all of the compounds were inactive.

CONCLUSION

In summary, from the fungus *Aspergillus* sp. CYH26, two new thio compounds (**1** and **2**) and two new monoterpenes (**3** and **4**) were isolated and identified. Compounds **1** and **2** are identified as rare sulfur containing natural products with a 3-methyl-4*H*-cyclopenta[b]thiophen-4-one skeleton, which are first encountered in nature. Compounds **1**–**4** could suppress the over-production of NO without affecting the cell viability. These results further demonstrated that fungi is an abundant source of new bioactive products with medicinal use.

DATA AVAILABILITY STATEMENT

The datasets presented in this study can be found in online repositories. The names of the repository/repositories and accession number(s) can be found in the article/**Supplementary Material**.

AUTHOR CONTRIBUTIONS

GP conceived and designed the experiments, and was involved in isolation of compounds. YL, XC, DT, WH, ZW, and YZ contributed to isolation of compounds. SR, GH, and YX performed genetic manipulation, strain fermentation, and extraction. MG contributed to the collection of the physicochemical data of compounds. NX contributed to bioactivity assay and revised the manuscript. FK supervised the work and prepared the manuscript. All authors contributed to the article and approved the submitted version.

SUPPLEMENTARY MATERIAL

The Supplementary Material for this article can be found online at: https://www.frontiersin.org/articles/10.3389/fmicb.2021.668938/full#supplementary-material

REFERENCES

Cameron, B., and Landreth, G. E. (2010). Inflammation, microglia, and Alzheimer's disease. *Neurobiol. Dis*. 37, 503–509. doi: 10.1016/j.nbd.2009.10.006

Cao, J., Li, Q., Shen, X., Yao, Y., Li, L., and Ma, H. (2021). Dehydroepiandrosterone attenuates LPS-induced inflammatory responses via activation of Nrf2 in RAW264.7 macrophages. *Mol. Immunol.* 131, 97–111. doi: 10.1016/j.molimm.2020.12.023

Chen, L., Deng, H., Cui, H., Fang, J., Zuo, Z., Deng, J., et al. (2017). Inflammatory responses and inflammation-associated diseases in organs. *Oncotarget* 9, 7204–7218. doi: 10.18632/oncotarget.23208

Gawronski, J. K., Oeveren, A., Deen, H., Leung, C. W., and Feringa, B. L. (1996). Simple circular dichroic method for the determination of absolute configuration of 5-substituted 2(5*H*)-furanones. *J. Org. Chem.* 61, 1513–1515. doi: 10.1021/jo951400l

Keller, N. P. (2019). Fungal secondary metabolism: regulation, function and drug discovery. *Nat. Rev. Microbiol.* 17, 167–180. doi: 10.1038/s41579-018-0121-1

Kong, F. D., Fan, P., Zhou, L. M., Ma, Q. Y., Xie, Q. Y., Zheng, H. Z., et al. (2019). Penerpenes A-D, Four indole terpenoids with potent protein tyrosine phosphatase inhibitory activity from the marine-derived fungus *Penicillium* sp. KFD28. *Org. Lett.* 21, 4864–4867. doi: 10.1021/acs.orglett.9b01751

Kong, F. D., Ma, Q. Y., Huang, S. Z., Wang, P., Wang, J. F., Zhou, L. M., et al. (2017). Chrodrimanins K-N and related meroterpenoids from the fungus *Penicillium* sp. SCS-KFD09 isolated from a marine worm, *Sipunculus nudus*. *J. Nat. Prod.* 80, 1039–1047. doi: 10.1021/acs.jnatprod.6b01061

Lv, Q. Q., Fan, Y. Q., Tao, G., Fu, P., Zhai, J., Ye, B. P., et al. (2019). Sekgranaticin, a SEK34b-granaticin hybrid p from *Streptomyces* sp. 166. *J. Org. Chem.* 84, 9087–9092. doi: 10.1021/acs.joc.9b01022

Pierce, C., Uppuluri, P., Tristan, A., Wormley, F., Mowat, E., Ramage, G., et al. (2008). A simple and reproducible 96-well plate-based method for the formation of fungal biofilms and its application to antifungal susceptibility testing. *Nat. Protoc.* 3, 1494–1500. doi: 10.1038/nport.2008.141

Qadri, M., Johri, S., Shah, B. A., Khajuria, A., Sidiq, T., Lattoo, S. K., et al. (2013). Identification and bioactive potential of endophytic fungi isolated from selected plants of the Western Himalayas. *SpringerPlus* 2:8. doi: 10.1186/2193-1801-2-8

Sharma, J. N., Al-Omran, A., and Parvathy, S. S. (2007). Role of nitric oxide in inflammatory diseases. *Inflammopharmacology* 15, 252–259. doi: 10.1007/s10787-007-0013-x

Introducing a Thermo-Alkali-Stable, Metallic Ion-Tolerant Laccase Purified From White Rot Fungus *Trametes hirsuta*

Jing Si*, Hongfei Ma, Yongjia Cao, Baokai Cui* and Yucheng Dai*

Institute of Microbiology, School of Ecology and Nature Conservation, Beijing Forestry University, Beijing, China

This study introduces a valuable laccase, designated ThLacc-S, purified from white rot fungus *Trametes hirsuta*. ThLacc-S is a monomeric protein in nature with a molecular weight of 57.0 kDa and can efficiently metabolize endocrine disrupting chemicals. The enzyme was successfully purified to homogeneity via three consecutive steps consisting of salt precipitation and column chromatography, resulting in a 20.76-fold increase in purity and 46.79% yield, with specific activity of 22.111 U/mg protein. ThLacc-S was deciphered as a novel member of the laccase family and is a rare metalloenzyme that contains cysteine, serine, histidine, and tyrosine residues in its catalytic site, and follows Michaelis-Menten kinetic behavior with a K_m and a k_{cat}/K_m of 87.466 μM and 1.479 $s^{-1}\mu M^{-1}$, respectively. ThLacc-S exerted excellent thermo-alkali stability, since it was markedly active after a 2-h incubation at temperatures ranging from 20 to 70°C and retained more than 50% of its activity after incubation for 72 h in a broad pH range of 5.0–10.0. Enzymatic activities of ThLacc-S were enhanced and preserved when exposed to metallic ions, surfactants, and organic solvents, rendering this novel enzyme of interest as a green catalyst for versatile biotechnological and industrial applications that require these singularities of laccases, particularly biodegradation and bioremediation of environmental pollutants.

Keywords: laccase (Lac), white rot fungi (WRF), enzymatic performance, endocrine disrupting chemicals (EDC), bioremediation

INTRODUCTION

Enzymes are currently receiving considerable interest from the public due to their impressive catalytic functionality, relatively broad abundance, and environmentally friendly nature (Buchholz and Bornscheuer, 2017; Wiltschi et al., 2020). Laccase (*p*-diphenol: dioxygen oxidoreductase, EC1.10.3.2) is a well-studied enzyme belonging to a family of polyphenol oxidases that have a copper-containing catalytic core, are widely distributed in fungi, bacteria, insects, and plants, and are classified based on molecular complexity and biological distribution (Thurston, 1994; Claus, 2004; Baldrian, 2006; Mate and Alcalde, 2015). Laccases of white rot fungi origin are ubiquitously superior to other enzymes in terms of lignin degradation. Thus, a series of laccases obtained from white rot fungi have attracted significant interest (Baldrian, 2006; Rivera-Hoyos et al., 2013; Chen et al., 2019). Laccases are involved in the metabolism of a multifarious range

of aromatic compounds, organic pollutants, and inorganic substrates, with a concomitant four-electron reduction process that only generates water as a by-product. Consequently, these enzymes have huge potential as green catalysts in the fields of pulping and papermaking, biosynthesis, food processing, biosensor manufacturing, and bioconversion and refinement of agricultural and forestry wastes, in particular biodegradation and bioremediation of environmental contaminants (Giardina et al., 2010; Pezzella et al., 2015; Senthivelan et al., 2016; Bilal et al., 2019). To keep pace with rapidly increasing industrial demands, it is imperative to capture laccases capable of tolerating high temperature, alkali pH, the existence of metallic ions and chemical reagents, or other harsh environments from high-producing and easily available white rot fungal repositories (Si et al., 2013; Zheng et al., 2017; Liu et al., 2020).

Endocrine disrupting chemicals (EDCs), which are widespread in eco-environments and used in large amounts globally, are a category of emerging, highly toxic pollutants that include naturally produced compounds such as estrogens, androgens, and phytoestrogens, as well as various industrial chemicals and household products such as synthetic hormones, polycyclic aromatic hydrocarbons (PAHs), and pharmaceuticals (Darbre, 2019; Kasonga et al., 2021). These compounds can interfere with hormonal systems and adversely impact sexual development, reproduction, the nervous system, and immunity of both wildlife and humans, even at concentrations as low as parts per million (ppm) and parts per billion (ppb) (Su et al., 2020; Viguié et al., 2020). For example, 17β-estradiol (E2) is a representative estrogen that causes serious environmental and global issues owing to its induction of reproductive disorders, immune deficiencies, and even carcinogenic risks (Ye et al., 2017; Du et al., 2020).

This study aimed to purify an extracellular laccase ThLacc-S from white rot fungus *Trametes hirsuta* and obtain data on its enzymatic performance to scrutinize its functional involvement in bioremediation of EDCs and potential use as a green catalyst in industrial and biotechnological applications.

MATERIALS AND METHODS

Chemicals

All chemicals used in this study were of analytical reagent grade. E2 was prepared by filtration through a 0.22-μm membrane to remove bacteria. Cetyl trimethyl ammonium bromide (CTAB) rapid plant genome extraction kits-DN14 were purchased from Aidlab Biotechnologies Co., Ltd, Beijing, China. Agar, 2,2'-azino-bis(3-ethylbenzothiazoline-6-sulfonic acid) (ABTS), bovine serum albumin (BSA), diethylaminoethyl (DEAE)-Cellulose ionic exchange column packing, Sephadex G-100 column packing, β-mercaptoethanol, guaiacol, trypsin, iodoacetic acid (IAA), tosyl-L-lysine chloroethyl ketone (TLCK), phenylmethylsulfonyl fluoride (PMSF), diethylpyrocarbonate (DEP), *N*-acetylimidazole (NAI), and ethylenediaminetetraacetic acid (EDTA) were all Sigma-Aldrich (St. Louis, MO, United States) reagents.

Fungal Strain and Culture Conditions

A strain of *T. hirsuta* was isolated from a harvested fruiting body and cultivated on malt yeast agar (MYA) slants (g/L ultrapure water: malt extract 5, glucose 20, agar 20, KH$_2$PO$_4$ 1, MgSO$_4$·7H$_2$O 0.5, ZnSO$_4$·7H$_2$O 0.1, CuSO$_4$·5H$_2$O 0.1, and vitamin B1 0.01) for 7 days at 28°C. When mycelia covered the MYA slants, cultures were stored at 4°C and were sub-cultured once every 2 months.

Ribosomal DNA (rDNA) Sequencing Analysis

Identification of the *T. hirsuta* isolate was carried out by sequencing analysis of the internal transcribed spacer (ITS) rDNA. Mycelia from overgrown MYA plates covered with cellophane membrane were harvested for total genomic DNA extraction using the improved CTAB protocol (Cui et al., 2019) with some modifications. Regions of ITS-rDNA (ITS-1, 5.8S, and ITS-2) were amplified by PCR using the universal primers ITS5 (5′-GGAAGTAAAAGTCGTAACAAGG-3′) and ITS4 (5′-TCCTCCGCTTATTGATATGC-3′). The PCR program comprised 95°C for 3 min, followed by 34 cycles of denaturation (94°C, 40 s), primer annealing (54°C, 45 s), and extension (72°C, 1 min), then a final 10-min extension at 72°C followed by cooling to 4°C. Amplification products were sequenced and compared with those in the GenBank database using the National Center for Biotechnology Information (NCBI)-BLAST tool.

Inoculum Preparation and Flask Fermentation Cultivation

To prepare seed inoculum, the maintained strain was initially activated on MYA in a Petri dish for 6 days. Five 1-cm^2 areas of the agar culture were chipped off with a sterilized perforator and transferred into a 250-mL Erlenmeyer flask containing 100 mL liquid malt yeast medium (MY, identical to MYA without agar). After cultivation for 6 days at 28°C on a rotary shaker at 150 rpm, the culture broth was mildly homogenized with a blender at 5,000 rpm for 1 min then used as seed inoculum.

Flask fermentation experiments were performed in 250-mL Erlenmeyer flasks containing 100 mL MY medium inoculated with 10 mL seed inoculum and cultivated at 28°C on a rotary shaker at 150 rpm for 6 days. Subsequently, mycelia and cell debris in the fermentation broth were removed by centrifugation (12,000 rpm, 20 min) and the resulting cell-free supernatant was deemed an extracellular enzyme source for further purification and was designated ThLacc.

ThLacc Activity Assay and Protein Quantification

A ThLacc activity assay was implemented quantitatively as described by Si et al. (2013), based on colorimetric measurement at 420 nm by monitoring the change in absorbance due to oxidation of the substrate ABTS. One unit of laccase activity is the amount of enzyme required to cause one absorption increase per minute per milliliter of reaction mixture under assay conditions. A Bradford assay was used to evaluate protein concentration at 280 nm using BSA as a standard (Bradford, 1976).

ThLacc Purification Procedure

Initially, the cell-free supernatant containing laccase ThLacc, seized through flask fermentation cultivation, was saturated up to 75% with solid $(NH_4)_2SO_4$ under constant stirring at 4 ℃ then under stationary conditions overnight. The precipitate recovered after centrifugation at 12,000 rpm for 20 min at 4℃ was suspended in 0.1 M citrate-phosphate buffer (pH 5.0) and dialyzed overnight against repeated changes of ultrapure water.

The isolated retentate was chromatographed onto a DEAE-Cellulose ionic exchange column (27 × 350 mm) pre-equilibrated with 0.1 M citrate-phosphate buffer (pH 5.0). The column was extensively washed-out with the citrate-phosphate buffer at a flow rate of 3.0 mL/min to remove unbound proteins until the absorbance at 280 nm was < 0.05. A linear gradient concentration of NaCl from 0.0 to 1.0 M at a flow rate of 1.0 mL/min was used for stepwise elution of the bound fractions, collecting 5.0 mL eluate/tube. Fractions were then examined for enzymatic activity and protein content. All fractions exhibiting laccase activity were pooled in their respective peak, dialyzed, and concentrated by ultrafiltration with a 50-kDa cut-off.

The fraction with highest laccase activity was subsequently gel-filtered on a Sephadex G-100 column (27 × 600 mm) pre-balanced with the citrate-phosphate buffer. Elution from the column was achieved with the same buffer at a flow rate of 1.0 mL/min. Fractions were collected (5.0 mL/tube) and the absorbance was detected at wavelengths of 420 and 280 nm; fractions with laccase activity were pooled, dialyzed, and concentrated for further study.

Electrophoresis, Mass Spectrometry, and Amino Acid Sequencing

Uniformity and subunit molecular weight (Mw) of ThLacc-S was authenticated using denaturing sodium dodecyl sulfate-polyacrylamide gel electrophoresis (SDS-PAGE), composed of a 12% (w/V) separating gel (pH 8.8) and a 5% (w/V) stacking gel (pH 6.8), as portrayed by Laemmli (1970). A pre-stained protein marker mixture with apparent Mws from 10 to 100 kDa was applied for calibration, and protein bands formed in gels were visualized by staining with Coomassie Brilliant Blue R250.

To reflect the presence of laccase, native PAGE was deployed in a similar manner as SDS-PAGE without the addition of SDS and reducing reagent (β-mercaptoethanol) and without boiling the protein sample. After electrophoresis, the gel was washed with ultrapure water and subjected to a staining solution of 1.0 mM ABTS or guaiacol until colorized bands appeared.

Native Mw was unearthed by comparing the elution volume of ThLacc-S with reference proteins passed to a Sephadex G-100 gel filtration column and eluted with 0.1 M citrate-phosphate buffer (pH 5.0) at a flow rate of 1.0 mL/min. Reference protein markers used for calibration were aldolase (158.0 kDa), conalbumin (75.0 kDa), BSA (67.0 kDa), ovalbumin (43.0 kDa), carbonic anhydrase (29.0 kDa), ribonuclease A (13.7 kDa), and aprotinin (6.5 kDa).

For *N*-terminal amino acid sequencing, purified ThLacc-S was run on native PAGE then transferred to trypsin digestion. After staining with ABTS, the blotted protein band was excised, destained, and sent for sequencing to identify the protein of interest. The Mw of ThLacc-S was also determined by matrix-assisted laser desorption/ionization time-of-flight mass spectrometry (MALDI-TOF MS; AB SCIEX, United States) with a MALDI matrix composed of α-cyano-4-hydroxycinnamic acid. Mass spectra were processed through the MASCOT search engine (Matrix Science, United Kingdom) and laccase sequences were retrieved using the NCBI-BLAST database to search for fungal laccases with a high level of sequence similarity. Homologous sequences were aligned by using the ClustalX1.83 algorithm and DNAMAN6.0 software.

Determination of Enzymatic Performance

The optimum pH where ThLacc-S exerted greatest activity was explored via an enzymatic assay at 25℃ using ABTS as the substrate and adjusting the pH from 1.0 to 13.0 in increments of 1.0 pH unit with various buffers. These buffer systems included glycine-HCl buffer (pH 1.0–3.0), citrate-phosphate buffer (pH 3.0–5.0), 2-(*N*-morpholino)ethanesulfonic acid buffer (pH 5.0–6.0), phosphate buffer (pH 6.0–8.0), Tris-HCl buffer (pH 8.0–9.0), glycine-NaOH buffer (pH 9.0–11.0), Na_2HPO_4-NaOH buffer (pH 11.0–12.0), and KCl-NaOH buffer (pH 12.0–13.0). The pH stability of ThLacc-S was estimated from pH 1.0 to 13.0 by pre-incubating the purified enzyme at 25°C for 72 h. ThLacc-S activity in response to temperature was assessed between 10 and 90°C, in increments of 5°C, by incubating the enzyme at optimum pH with ABTS as the substrate. Thermostability of ThLacc-S was determined by pre-incubating the enzyme for 2 h at the aforenoted temperature ranges and conditions. Aliquots of samples were taken for measurement of remaining laccase activity toward ABTS and were expressed as percentage to highest activity.

ThLacc-S activity in the presence of various metallic ions (Li^+, Na^+, Mg^{2+}, Al^{3+}, K^+, Ca^{2+}, Mn^{2+}, Fe^{2+}, Fe^{3+}, Ni^{2+}, Cu^{2+}, Zn^{2+}, Pb^{2+}, Ag^+, Cd^{2+}, Ba^{2+}, or Hg^{2+}) at final concentrations of 25.0 mM was investigated. Specific inhibitors of enzymatic activity such as IAA (cysteine protease inhibitor), TLCK (lysine protease inhibitor), PMSF (serine protease inhibitor), DEP

TABLE 1 | Summary of purification steps of laccase ThLacc-S from *Trametes hirsuta*.

Purification step	Total activity (U/mL)	Total protein (mg/mL)	Specific activity (U/mg)	Purification fold	Yield (%)
Crude extract	1.276	1.198	1.065	1	100
Salt precipitation	1.072	0.759	1.412	1.33	84.01
DEAE-Cellulose ionic exchange chromatography	0.759	0.265	2.864	2.69	59.48
Sephadex G-100 gel filtration chromatography	0.597	0.027	22.111	20.76	46.79

(histidine protease inhibitor), NAI (tyrosine protease inhibitor), pepstatin A (aspartate protease inhibitor), and EDTA (chelator), surfactants such as SDS (ionic surfactant) and Triton X-100 (non-ionic surfactant), and organic solvents such as methanol, ethanol, propanol, hexane, acetone, toluene, and chloroform, were assayed at different concentrations for their influences on ThLacc-S activity. Assays were conducted by pre-incubating ThLacc-S with the respective additive at pre-selected concentrations at 50℃ for 20 min, followed by evaluation of residual activity using the standard method with ABTS as the substrate. A control using ultrapure water instead of additives was accepted as 100% relative activity.

The Michaelis-Menten constant (K_m) and catalytic constant (k_{cat}) of ThLacc-S were determined, by using ABTS as a substrate at various concentrations ranging from 0.1 to 1.0 mM in 0.1 M citrate-phosphate buffer (pH 5.0) at optimum pH and temperature conditions. A Lineweaver-Burk plot was applied for calculation of kinetic parameters by linear regression.

Detection of EDC-Bioremediating Capacity

Bioremediation of EDCs by ThLacc-S was achieved in a 10.0-mL mixture of 1.0 M citrate-phosphate buffer (pH 5.0) containing 5.0 U/mL purified enzyme solution and 0.01 mM E2. The mixture was treated dynamically at 55°C for 72 h in darkness under a shaking speed of 150 rpm. Control groups with inactivated ThLacc-S or EDC-free reactions were set at the same conditions. At desired time intervals, reactions were stopped by adding 10.0 mL methanol and centrifuging at 12,000 rpm for 20 min. The resulting supernatants were concentrated by rotary vacuum evaporator and used for gas chromatography-mass spectrometry (GC-MS) analysis to identify partial by-products of E2 metabolized by ThLacc-S. Aliquots (0.1 mL) of supernatant were injected into a Shimadzu QP2010-SE GC-MS Spectrometer (Shimadzu, Japan) equipped with an ionization detector using a Resteck column (0.25 × 30 nm, XTI-5). The mobile gas was ultrapure helium gas at a flow rate of 0.7 mL/min in a linear 30-min run time. The initial column temperature was held at 70°C for 2 min, then subjected to an increase of 10°C/min up to 280°C, and finally held at 280°C for 9 min. Chemical formulas of the possible metabolic by-products were clarified based on mass spectra and retention times on their gas chromatographs.

Statistical Analysis

This study was conducted with completely randomized experimental designs. All determinations were performed in triplicate. Data comparison was statistically computed by analysis of variance (ANOVA) followed by Waller-Duncan test using SPSS 20.0 software.

RESULTS AND DISCUSSION

Purification of ThLacc

Sequencing analysis was used for identification of the fungal isolate based on amplification of the ITS5 and ITS4 regions.

A BLAST search of the ITS-rDNA sequence of the isolate compared with those in the GenBank database suggested 99% similarity with *T. hirsuta*, thereby verifying that the isolate was white rot fungus *T. hirsuta* (GenBank accession number: MW881532).

Extracellular laccase ThLacc from *T. hirsuta* was purified to homogeneity via three consecutive procedures consisting of $(NH_4)_2SO_4$ saturation (5–100%) followed by ionic exchange and
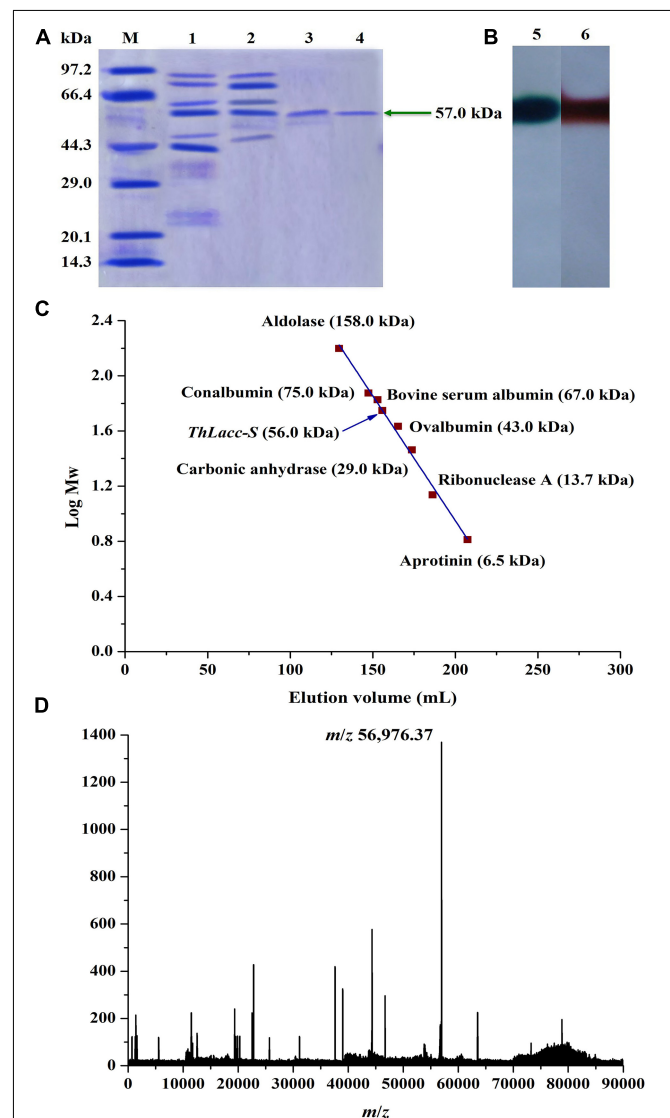
FIGURE 1 | Molecular weight authentication of laccase ThLacc-S from *Trametes hirsuta*. **(A)** SDS-PAGE consisting of a 12% (w/v) separating gel (pH 8.8) and a 5% (w/v) stacking gel (pH 6.8) visualized with Coomassie Brilliant Blue R250 staining. Lane M, protein marker; lane 1, crude extract ThLacc; lane 2, laccase ThLacc purified by salt precipitation; lane 3, laccase ThLacc purified by DEAE-Cellulose ionic exchange chromatography; lane 4, laccase ThLacc purified by Sephadex G-100 gel filtration chromatography. **(B)** Native PAGE. Lane 5, ABTS staining; lane 6, guaiacol staining. **(C)** Gel filtration chromatography on a Sephadex G-100 column. **(D)** Mass spectrum acquired by MALDI-TOF MS.
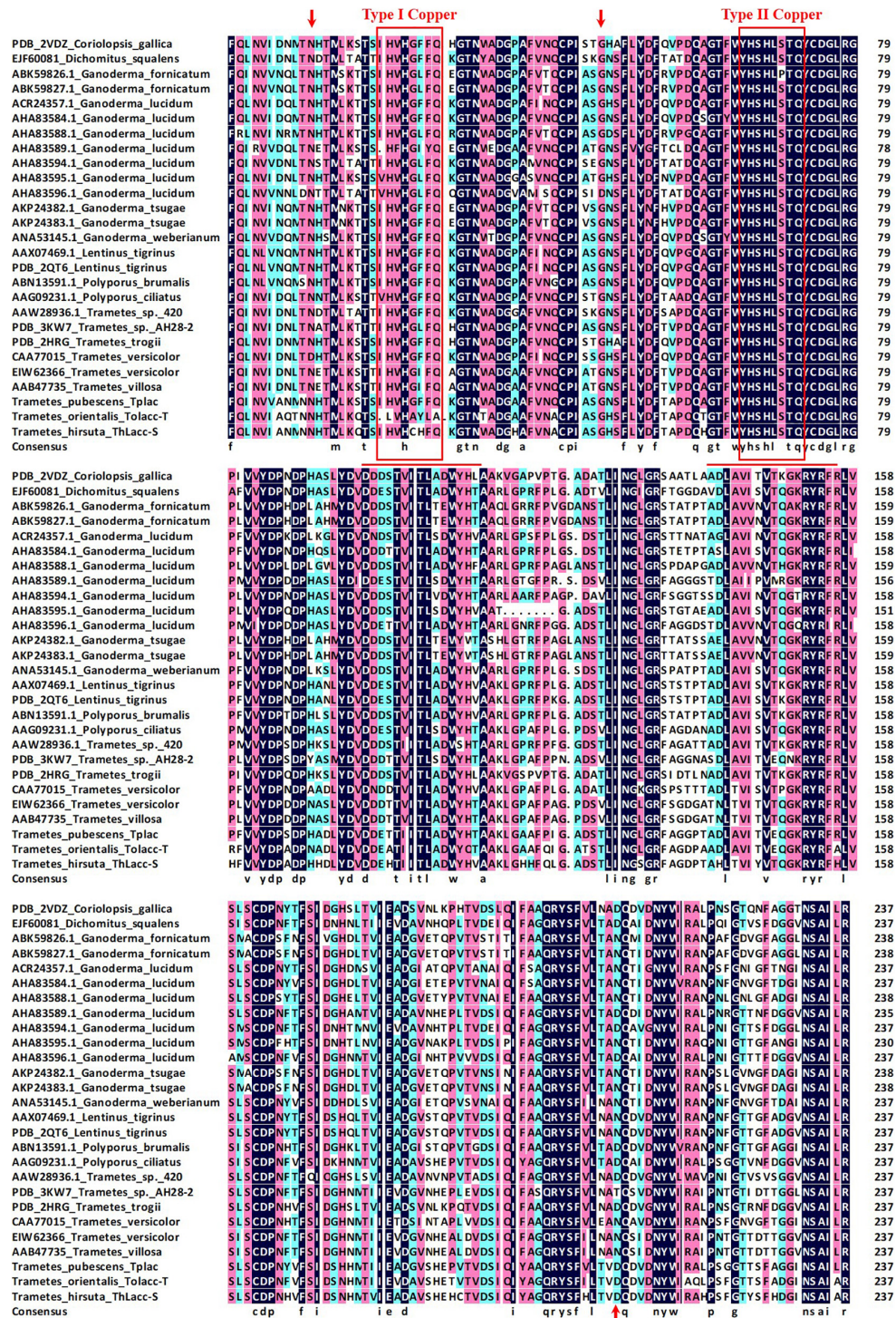
FIGURE 2 | Multiple alignment of the amino acid sequence of laccase ThLacc-S from *Trametes hirsuta* with those of other fungal laccases including *Coriolopsis gallica* (PDB: 2VDZ), *Dichomitus squalens* (EJF60081), *Ganoderma fornicatum* (ABK59826.1 and ABK59827.1), *G. lucidum* (ACR24357.1, AHA83584.1, AHA83588.1, AHA83589.1, AHA83594.1, AHA83595.1, and AHA83596.1), *G. tsugae* (AKP24382.1 and AKP24383.1), *G. weberianum* (ANA53145.1), *Lentinus tigrinus* (AAX07469.1 and PDB: 2QT6), *Polyporus brumalis* (ABN13591.1), *P. ciliatus* (AAG09231.1), *Trametes* sp. 420 (AAW28936.1), *Trametes* sp. AH28-2 (PDB: 3KW7), *T. trogii* (PDB: 2HRG), *T. versicolor* (CAA77015 and EIW62366), *T. villosa* (AAB47735), *T. pubescens* Tplac, and *T. orientalis* Tolacc-T. Numbers on the right are the positions of the final amino acids in each line. Residues assumed to be involved in binding to copper are boxed in red and residues identical in all 27 sequences are highlighted with a black background. Potential glycosylation sites are indicated with red arrows. Underlined residues indicate the sequences generated through MALDI-TOF MS.

gel filtration chromatography. A summary of all purification data is tabulated in **Table 1**. Culture supernatant containing laccase (1.065 U/mg protein) was firstly precipitated with 5–100% $(NH_4)_2SO_4$. After dialysis, the retentate saturated with 75% $(NH_4)_2SO_4$ (1.412 U/mg protein) was loaded onto a DEAE-Cellulose ionic exchange column to seize five fractions ThLacc-Fis, ThLacc-S, ThLacc-T, ThLacc-Fo, and ThLacc-Fif; the second fraction, ThLacc-S, eluted with 0.3 M NaCl had the highest specific activity of 2.864 U/mg protein, with a 2.69-fold increase in purity and 59.48% yield. ThLacc-S was therefore re-chromatographed on a Sephadex G-100 gel filtration column and this generated: a 20.76-fold increase in purity and 46.79% yield, with specific activity of 22.111 U/mg protein.

Uniformity and Molecular Weight of ThLacc-S

Uniformity and subunit Mw of ThLacc-S were estimated by gel electrophoresis under denaturing and non-denaturing conditions. ThLacc-S emerged as a single band corresponding to an Mw of 57.0 kDa on the SDS-PAGE gel (**Figure 1A**). In the native PAGE spectrum stained with ABTS or guaiacol, a clear band that was responsible for laccase activity and migrated at the same Mw as in the SDS-PAGE was visualized (**Figure 1B**). This authenticated the monomeric nature of this enzyme and constituted a subunit Mw. Gel filtration chromatography on a Sephadex G-100 column with reference proteins supported that the native Mw of ThLacc-S was 56.0 kDa (**Figure 1C**). Furthermore, mass spectra from MALDI-TOF MS confirmed that ThLacc-S possessed an apparent Mw of 56976.37 Da (**Figure 1D**). Laccases originating from fungi exhibit single-subunit type protein structures, termed monomeric proteins, in SDS-PAGE and native PAGE gels and abundantly variable Mws that might possibly be ascribed to genetic discrepancies among different species (Claus, 2004; Baldrian, 2006; Rivera-Hoyos et al., 2013; Si et al., 2013; Mate and Alcalde, 2015; Zheng et al., 2017; Sadeghian-Abadi et al., 2019). These observations implied that ThLacc-S was a monomeric protein with an Mw of 57.0 kDa.

Identification of ThLacc-S

The *N*-terminal amino acid sequence of ThLacc-S (UniProt Knowledgebase accession number: C0HLV6) was acquired through trypsin digestion, ABTS staining, sequencing, and MALDI-TOF MS. Multiple alignment of the amino acid sequence of ThLacc-S with other fungal laccases (**Figure 2**) indicated that ThLacc-S contained representative conserved I and II copper-binding domains and shared three potential glycosylation sites (Thurston, 1994; Claus, 2004). The alignment also revealed that the *N*-terminal amino acid sequence of ThLacc-S shared sequence identity with laccases from other species of the genus *Trametes*, attaining 83.61 and 82.85% sequence similarity with Tplac from *Trametes pubescens* and Tolacc-T from *Trametes orientalis*, respectively. Moreover, the sequence of ThLacc-S harbored similarities with other laccases, including 75.63% sequence similarity with *Lentinus tigrinus* AAX07469.1 and *Polyporus ciliatus* AAG09231.1, 75.21% with *L. tigrinus* PDB: 2QT6, 74.79% with *Polyporus brumalis* ABN13591.1, 73.11% with *Trametes versicolor* CAA77015, 72.69% with *Ganoderma lucidum* AHA83584.1, 71.85% with *Trametes trogii* PDB: 2HRG and *Dichomitus squalens* EJF60081, 71.43% with *Coriolopsis gallica* PDB: 2VDZ, 70.59% with *T. versicolor* EIW62366, *Ganoderma weberianum* ANA53145.1, *G. lucidum* AHA83595.1 and ACR24357.1, and *Trametes villosa* AAB47735, 70.17% with *Trametes* sp. 420 AAW28936.1, 69.33% with *Trametes* sp. AH28-2 PDB: 3KW7, 68.49% with *G. lucidum* AHA83594.1, 68.20% with *G. lucidum* AHA83588.1, 68.07% with *G. lucidum* AHA83589.1, 67.65% with *G. lucidum* AHA83596.1, 65.69% with *Ganoderma fornicatum* ABK59827.1, 64.85% with *Ganoderma tsugae* AKP24383.1 and AKP24382.1, and 64.44% with *G. fornicatum* ABK59826.1, respectively. This indicated that ThLacc-S from *T. hirsuta* was a novel member of the laccase family.

Effect of pH and Temperature on ThLacc-S Activity and Stability

ThLacc-S was $\geq$ 60% active over a wide pH range from 4.0 to 10.0, with maximum activity (0.612 U/mL) at pH 6.0 (**Figure 3A**);
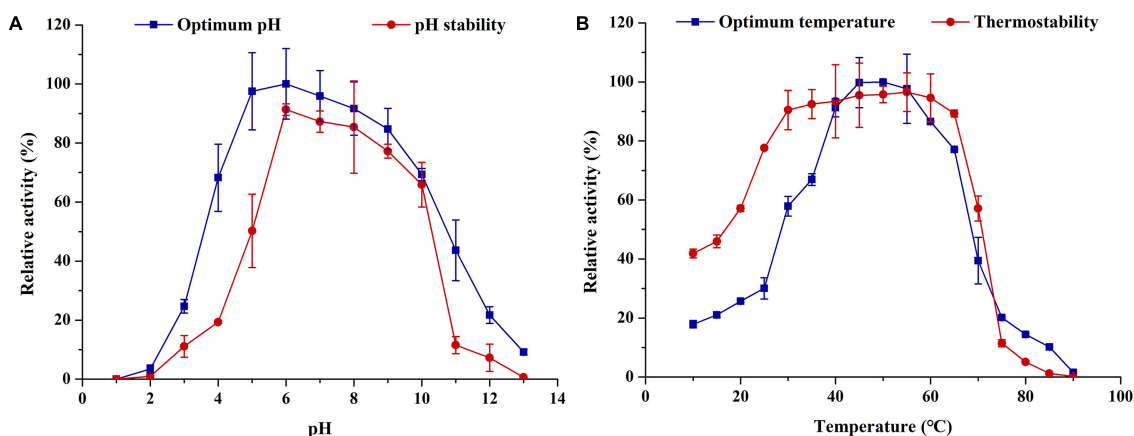

FIGURE 3 | (A) Optimum pH and **(B)** thermostability of laccase ThLacc-S from *Trametes hirsuta*.

the enzyme was more active in neutral and alkaline pH. There was a sharp decline in laccase activity at pH < 4.0 or > 10.0, presumably attributed to enzyme denaturation or inactivation. Congruent with the activity data, ThLacc-S stability was higher within the pH range of 5.0–10.0 compared with pH outside this range, as evidenced by preservation of enzyme activity above 50% after incubation at pH 5.0–10.0 for 72 h. The wide pH tolerance of this enzyme could be explained by increases in charges of amino acid residues within the active site (Claus, 2004; Pezzella et al., 2015).

Of the tested temperatures (10–90°C) depicted in **Figure 3B**, the range 30–65°C was beneficial for ThLacc-S as the enzyme maintained more than 57% of its activity at these temperatures. The optimum temperature for ThLacc-S activity was 50°C, equivalent to specific activity of 2.037 U/mL. Incubation at < 25°C or > 70°C dramatically reduced activity and stability of ThLacc-S. However, comparable marked improvements in ThLacc-S activity were observed after incubation for 2 h at 10–40 and 60–70°C. The activity and stability of this enzyme, as well as the reduced sensitivity to extreme temperatures, are superior to those of other previously described laccases (Rivera-Hoyos et al., 2013; Sadeghian-Abadi et al., 2019).

Hence, one important feature of ThLacc-S that is applicable to numerous industrial and biotechnological areas operating under severe conditions, is the thermo-alkali stability across considerably abundant pH and temperature ranges for a prolonged duration.

Effect of Metallic Ions, Specific Inhibitors, Surfactants, and Organic Solvents on ThLacc-S Activity

The impact of metallic ions, specific inhibitors, surfactants, and organic solvents on ThLacc-S activity are outlined in **Table 2**.

Laccase activity relative to the control was 261.97, 252.56, 244.13, 220.42, 217.71, 177.96, 173.39, 159.66, 144.02, or 126.98%, following separate addition of 25.0 mM Cu^{2+}, Mg^{2+}, K^+, Cd^{2+}, Zn^{2+}, Ni^{2+}, Na^+, Fe^{2+}, Pb^{2+}, or Mn^{2+}, respectively. This indicated that ThLacc-S requires these metallic ions to retain the conformation of its active site. The greatest effect of Cu^{2+} on laccase activity might be owing to this ion being involved in the catalytic process, since typical laccases are known to contain three types of copper sites and a core center with a cluster of four copper atoms (Thurston, 1994; Claus, 2004). Other metallic ions like Li^+, Al^{3+}, Ca^{2+}, Ba^{2+}, or Fe^{3+} inhibited ThLacc-S activity possibly due to binding near the T1 site, which blocks access of substrates to the site and thus the ions act as competitive inhibitors for electron donors (Thurston, 1994; Si et al., 2013). Obviously, Hg^{2+} strongly inhibited ThLacc-S activity and is presumed to be a key inactivator of ThLacc-S as this metallic ion can react with sulfhydryl groups present on histidine residues of the catalytic site and displace other active metallic ions from their binding positions; such competitive binding results in enzymatic deactivation (Claus, 2004; Yahiaoui et al., 2019).

TABLE 2 | Effect of metallic ions, specific inhibitors, surfactants, and organic solvents on activity of laccase ThLacc-S from *Trametes hirsuta*.

Additive		Concentration	Relative activity (%)
Control	—	—	100 ± 0.30
Metallic ion	Li^+	25.0 mM	89.95 ± 4.08 jklm
	Na^+	25.0 mM	173.39 ± 4.24 de
	Mg^{2+}	25.0 mM	252.56 ± 5.74 ab
	Al^{3+}	25.0 mM	69.63 ± 4.60 op
	K^+	25.0 mM	244.13 ± 12.60 b
	Ca^{2+}	25.0 mM	51.06 ± 1.30 qr
	Mn^{2+}	25.0 mM	126.98 ± 12.22 gh
	Fe^{2+}	25.0 mM	159.66 ± 8.12 ef
	Fe^{3+}	25.0 mM	11.96 ± 1.53 tuv
	Ni^{2+}	25.0 mM	177.96 ± 9.86 d
	Cu^{2+}	25.0 mM	261.97 ± 11.43 a
	Zn^{2+}	25.0 mM	217.71 ± 5.89 c
	Pb^{2+}	25.0 mM	144.02 ± 10.07 fg
	Ag^+	25.0 mM	101.49 ± 7.60 ijk
	Cd^{2+}	25.0 mM	220.42 ± 7.64 c
	Ba^{2+}	25.0 mM	24.68 ± 1.77 stu
	Hg^{2+}	25.0 mM	2.83 ± 1.61 v
Specific inhibitor	IAA (cysteine protease inhibitor)	2.0 mM	Not detected
		5.0 mM	Not detected
		10.0 mM	Not detected
	TLCK (lysine protease inhibitor)	2.0 mM	100 ± 2.94 jk
		5.0 mM	100 ± 3.01 jk
		10.0 mM	99.17 ± 8.55 jk
	PMSF (serine protease inhibitor)	2.0 mM	Not detected
		5.0 mM	Not detected
		10.0 mM	Not detected
	DEP (histidine protease inhibitor)	2.0 mM	Not detected
		5.0 mM	Not detected
		10.0 mM	Not detected
	NAI (tyrosine protease inhibitor)	2.0 mM	Not detected
		5.0 mM	Not detected
		10.0 mM	Not detected
	Pepstatin A (aspartate protease inhibitor)	2.0 mM	100 ± 5.83 jk
		5.0 mM	100 ± 10.24 jk
		10.0 mM	99.84 ± 8.64 jk
	EDTA (cheating agent)	2.0 mM	45.67 ± 2.05 qr
		5.0 mM	26.54 ± 2.49 st
		10.0 mM	7.76 ± 0.31 uv
Surfactant	SDS (ionic surfactant)	2.0 mM	75.50 ± 7.62 mnop
		5.0 mM	62.46 ± 4.99 pq
		10.0 mM	36.21 ± 3.10 rs
	Triton X-100 (non-ionic surfactant)	10% (V/V)	103.42 ± 8.58 ij
		30% (V/V)	117.79 ± 3.41 hi
Organic solvent	Methanol	10% (V/V)	95.32 ± 7.12 jkl
		30% (V/V)	81.43 ± 7.95 lmno
	Ethanol	10% (V/V)	90.54 ± 6.67 jklm
		30% (V/V)	84.32 ± 0.27 klmno
	Propanol	10% (V/V)	87.47 ± 2.45 jklmn
		30% (V/V)	79.56 ± 8.17 lmnop
	Hexane	10% (V/V)	92.78 ± 4.99 jklm
		30% (V/V)	76.26 ± 5.01 mnop
	Acetone	10% (V/V)	62.18 ± 3.24 pq
		30% (V/V)	50.06 ± 4.69 qr
	Toluene	10% (V/V)	135.05 ± 8.68 gh
		30% (V/V)	167.98 ± 12.67 de
	Chloroform	10% (V/V)	85.37 ± 5.69 klmno
		30% (V/V)	70.51 ± 7.68 nop

Data are mean ± standard deviation. Different lowercase letters represent significant differences at P < 0.05 level by Waller-Duncan test.

Protease inhibitors are efficient tools for delimiting categories of enzymes (Powers et al., 2002). IAA (cysteine protease inhibitor), PMSF (serine protease inhibitor), DEP (histidine protease inhibitor), and NAI (tyrosine protease inhibitor) abolished ThLacc-S activity at 2.0, 5.0, and 10.0 mM, respectively. This indicated that cysteine, serine, histidine, and tyrosine residues were present in the functional site of this enzyme. Complete inhibition by IAA also supported that sulfhydryl groups are required to retain the structural conformation of ThLacc-S, as evidenced by Hg^{2+} being a key inactivator of this enzyme. There were negligible changes in ThLacc-S activity after incubation with TLCK (lysine protease inhibitor) or pepstatin A (aspartate protease inhibitor), indicating that ThLacc-S was not a lysine or aspartate protease. The chelator EDTA at 2.0, 5.0, and 10.0 mM resulted in gradual decreases in ThLacc-S activity to 45.67, 26.54, and 7.76%, respectively, expounding that metallic ions are involved in enzymatic catalysis by ThLacc-S, and therefore ThLacc-S is a rare metalloenzyme.

Surfactants, including ionic and non-ionic types, are reported to influence enzymatic conformation by interacting with charges on the surface of the enzyme (Shao et al., 1993). SDS, a recognized ionic surfactant, interfered with ThLacc-S activity at all assayed concentrations (2.0, 5.0, and 10.0 mM), with diminished activities of 75.50, 62.46, and 36.21%, respectively. A slight promotion of ThLacc-S activity was observed in the presence of 10 or 30% (V/V) non-ionic surfactant Triton X-100. This is attributed to Triton X-100

preventing formation of self-aggregates of ThLacc-S and stabilizing folding of the enzyme.

In the presence of organic solvents, ThLacc-S was strongly activated by toluene, attaining approximately 1.68-fold laccase activity compared with the control. Over 70% of ThLacc-S activity was preserved by separate supplements of ethanol, methanol, propanol, hexane, and chloroform, respectively, whereas acetone reduced laccase activity by almost 50% compared with the control. These findings endorsed that when encountering organic solvents, enzymatic activity is affected by the distribution of water molecules and characteristics of organic solvents like hydrophobicity and polarity, in addition to the conformation of the enzyme itself (Wan et al., 2010).

The observed enhancement and maintenance of ThLacc-S activity demonstrate the extraordinary tolerance of this novel enzyme toward metallic ions, surfactants, and organic solvents, and render it a promising catalyst to suffice industrial demands.
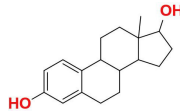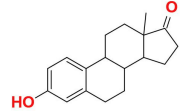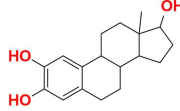
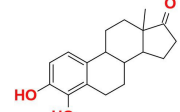## Kinetic Parameters of ThLacc-S
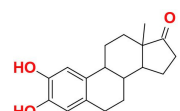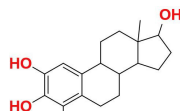
A Lineweaver-Burk plot relating reaction velocity of ThLacc-S to ABTS concentrations can be seen in **Supplementary Figure 1**. Kinetic parameters K_m and k_{cat}/K_m of ThLacc-S against the substrate ABTS were calculated to be 87.466 µM and 1.479 $s^{-1}µM^{-1}$, respectively. Comparisons of the kinetic parameters of ThLacc-S with those of other reported laccases are shown in **Table 3**. The lower K_m and higher k_{cat}/K_m values compared with the values for the other laccases affirmed the

TABLE 3 | Comparisons of the kinetic parameters of laccase ThLacc-S from *Trametes hirsuta* with those of other reported laccases.

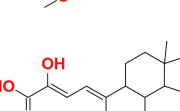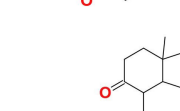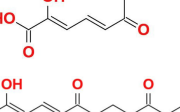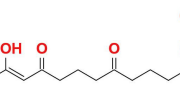| Laccase producing source	Name	K_m (µM)	k_{cat} (s^{-1})	k_{cat}/K_m ($s^{-1}µM^{-1}$)	References
Trametes hirsuta	ThLacc-S	87.466	129.367	1.479	This study
Agaricus bisporus CU13	Lacc1	0.394	-	-	Othman et al., 2018
	Lacc2	0.158	-	-	
Cerrena unicolor GSM-01	CUL	302.7	286.5	0.946	Wang et al., 2017
Ganoderma lucidum	-	47	54	1.149	Manavalan et al., 2013
Lentinus strigosus 1566	Laccase I	11.0	460.97	41.906	Kolomytseva et al., 2019
	Laccase II	17.0	141.02	8.295	
	Laccase III	263.2	522.38	1.985	
Marasmius sp.	Laccase-related enzyme I	3.9	120	30.769	Schückel et al., 2011
Oudemansiella canarii EF72	-	46.18	-	-	Iark et al., 2019
Pleurotus ostreatus HAUCC 162	rLACC6	459	81.35	0.177	Zhuo et al., 2018
	rLACC9	413	20.10	0.049	
	rLACC10	43	15.50	0.360	
Pycnoporus coccineus BRFM 938	BRFM 938 laccase	26	218.1	8.388	Uzan et al., 2010
Pycnoporus sanguineus BRFM 902	BRFM 902 laccase	32	236.9	7.403	
Py. sanguineus BRFM 66	BRFM 66 laccase	33	214.3	6.494	
Thielavia sp.	TaLac1	23.70	4.14	0.175	Mtibaà et al., 2018
Trametes orientalis	Tolacc-T	333.3	21.81	0.065	Zheng et al., 2017
Trametes pubescens Cui 7571	Tplac	105.0	876	8.343	Si et al., 2013
Trametes trogii BAFC 463	LCC3	250	399	1.596	Campos et al., 2016
Tr. trogii S0301	Lac 37 II	16.1	2977	184.907	Yang et al., 2020
Trametes versicolor	LC	4.05	-	-	Kelbert et al., 2021
Trametes sp. LAC-01	LAC-01	30.28	-	-	Ling et al., 2015
Trametes sp. F1635	TsL	18.58	-	-	Wang et al., 2018

All data were obtained by using ABTS as substrates.

TABLE 4 | Partial metabolic by-products of 17β-estradiol (E2) identified through GC-MS in the reaction process mediated by laccase ThLacc-S from *Trametes hirsuta*.

Compound	*m/z*	Chemical formula	Deduced chemical structure
E2	272.97	$C_{18}H_{24}O_2$	
Estrone (E1)	271.06	$C_{18}H_{22}O_2$	
2-OH-E2	288.31	$C_{18}H_{24}O_3$	
4-OH-E1	286.36	$C_{18}H_{22}O_3$	
2-OH-E1	286.74	$C_{18}H_{22}O_3$	
2-OH-E2-OCH$_3$	317.95	$C_{19}H_{26}O_4$	
E2-BP1	318.31	$C_{18}H_{22}O_5$	
E2-BP2	335.12	$C_{18}H_{22}O_6$	
E2-BP3	351.05	$C_{18}H_{22}O_7$	
E2-BP4	369.94	$C_{17}H_{22}O_9$	

strong affinity and reaction velocity of this enzyme toward the substrate (Rivera-Hoyos et al., 2013; Yang et al., 2020). This kinetic behavior may be dependent on genetic diversity of the different laccase producing sources as well as the nature and structure of the enzyme (Rivera-Hoyos et al., 2013; Kelbert et al., 2021).

EDC-Bioremediating Capacity of ThLacc-S

Partial metabolic by-products of E2 in the ThLacc-S-mediated reaction process were identified through GC-MS analysis and comprised estrone (E1), 2-OH-E2, 4-OH-E1, 2-OH-E1, 2-OH-E2-OCH$_3$, E2-BP1, E2-BP2, E2-BP3, and E2-BP4 (**Table 4** and **Supplementary Table 1**). This finding was in accordance with a previous study reporting similar E2 metabolites mediated by the *T. versicolor* laccase (Liu et al., 2021). These data substantiated that ThLacc-S could efficiently catalyze the transformation of dominant, highly toxic, natural estrogen such as E2 in the absence of redox mediators, with formation of corresponding phenoxy radical intermediates, accompanied by four-electron reduction of molecular oxygen to water. In view of the detected by-products and pertinent literatures (Ye et al., 2017; Li et al., 2020; Wang et al., 2020), different metabolic pattern of E2 form products with additional hydroxyl and methoxyl groups to E2 and E1, and the degradation routes by ThLacc-S were deduced to be accomplished by oxidation, hydroxylation, carboxylation, dehydrogenation, dehydroxylation, demethylation, and methoxylation. Particularly noticeable are studies showing that E2 metabolized by methoxylation can hinder formation of its quinone form that are major carcinogenic metabolites (Cavalieri and Rogan, 2011). These results marked that this type of metabolism was also admitted to be a detoxification behavior and suggested that ThLacc-S would be an effective, safe, and green catalyst for various industrial applications, especially those involving bioremediation and biodegradation. Further investigations are necessary to elucidate the detailed mechanism of E2 metabolism by laccase, to explore estrogenic activities of the intermediates, and to determine the laccase functionality at more environmentally relevant concentrations of EDCs.

CONCLUSION

This study identified an efficient laccase, ThLacc-S, from white rot fungus *T. hirsuta* that could be competent with multifarious hardness because it can tolerate wide ranges of thermo-alkali conditions and is active in the presence of diverse metallic ions, surfactants, and organic solvents. Furthermore, this enzyme proved to be a robust, eco-friendly, bioremediating agent for E2 removal. The findings of this study not only enrich those of existing laccases as emerging, environmentally safe candidates for industrial applications such as bioremediation, but also provide new insights into the functional involvement of laccases in the metabolism of EDCs.

DATA AVAILABILITY STATEMENT

The datasets presented in this study can be found in online repositories. The names of the repository/repositories and accession number(s) can be found below: UniProt Knowledgebase, accession no: C0HLV6; NCBI, accession no: MW881532.

AUTHOR CONTRIBUTIONS

JS and BC conceived and designed experiments. JS, HM, and YC performed experiments. JS, BC, and YD wrote the manuscript. All authors reviewed the manuscript before submission.

FUNDING

ACKNOWLEDGMENTS

SUPPLEMENTARY MATERIAL

The Supplementary Material for this article can be found online at: https://www.frontiersin.org/articles/10.3389/fmicb.2021.670163/full#supplementary-material

REFERENCES

Baldrian, P. (2006). Fungal laccases - occurrence and properties. *FEMS Microbiol. Rev.* 30, 215–242. doi: 10.1111/j.1574-4976.2005.00010.x

Bilal, M., Rasheed, T., Nabeel, F., Iqbal, H. M. N., and Zhao, Y. P. (2019). Hazardous contaminants in the environment and their laccase-assisted degradation - a review. *J. Environ. Manage.* 234, 253–264. doi: 10.1016/j.jenvman.2019.01.001

Bradford, M. M. (1976). A rapid and sensitive method for the quantitation of microgram quantities of protein utilizing the principle of protein-dye binding. *Anal. Biochem.* 72, 248–254. doi: 10.1016/0003-2697(76)90527-3

Buchholz, K., and Bornscheuer, U. T. (2017). "Enzyme technology: history and current trends," in *Applied Bioengineering: Innovations and Future Directions*, 1st Edn, ed. T. Yoshida, (Weinheim: Wiley-VCH Verlag GmbH & Co), 13–46.

Campos, P. A., Levin, L. N., and Wirth, S. A. (2016). Heterologous production, characterization and dye decolorization ability of a novel thermostable laccase isoenzyme from *Trametes trogii* BAFC 463. *Process Biochem.* 51, 895–903. doi: 10.1016/j.procbio.2016.03.015

Cavalieri, E. L., and Rogan, E. G. (2011). Unbalanced metabolism of endogenous estrogens in the etiology and prevention of human cancer. *J. Steroid Biochem. Mol. Biol.* 125, 169–180. doi: 10.1016/j.jsbmb.2011.03.008

Chen, M. Y., Waigi, M. G., Li, S. Y., Sun, K., and Si, Y. B. (2019). Fungal laccase-mediated humification of estrogens in aquatic ecosystems. *Water Res.* 166, 115040. doi: 10.1016/j.watres.2019.115040

Claus, H. (2004). Laccases: structure, reactions, distribution. *Micron* 35, 93–96. doi: 10.1016/j.micron.2003.10.029

Cui, B. K., Li, H. J., Ji, X., Zhou, J. L., Song, J., Si, J., et al. (2019). Species diversity, taxonomy and phylogeny of Polyporaceae (Basidiomycota) in China. *Fungal Divers.* 97, 137–392. doi: 10.1007/s13225-019-00427-4

Darbre, P. D. (2019). The history of endocrine-disrupting chemicals. *Curr. Opin. Endocr. Metab. Res.* 7, 26–33. doi: 10.1016/j.coemr.2019.06.007

Du, B. H., Fan, G. D., Yu, W. W., Yang, S., Zhou, J. J., and Luo, J. (2020). Occurrence and risk assessment of steroid estrogens in environmental water samples: a five-year worldwide perspective. *Environ. Pollut.* 267:115405. doi: 10.1016/j.envpol.2020.115405

Giardina, P., Faraco, V., Pezzella, C., Piscitelli, A., Vanhulle, S., and Sannia, G. (2010). Laccases: a never-ending story. *Cell. Mol. Life Sci.* 67, 369–385. doi: 10.1007/s00018-009-0169-1

Iark, D., Buzzo, A. J. R., Garcia, J. A. A., Côrrea, V. G., Helm, C. V., Corrêa, R. C. G., et al. (2019). Enzymatic degradation and detoxification of azo dye Congo red by a new laccase from *Oudemansiella canarii*. *Bioresour. Technol.* 289:121655. doi: 10.1016/j.biortech.2019.121655

Kasonga, T. K., Coetzee, M. A. A., Kamika, I., Ngole-Jeme, V. M., and Momba, M. N. B. (2021). Endocrine-disruptive chemicals as contaminants of emerging concern in wastewater and surface water: a review. *J. Environ. Manage.* 277:111485. doi: 10.1016/j.jenvman.2020.111485

Kelbert, M., Pereira, C. S., Daronch, N. A., Cesca, K., Michels, C., de Oliveira, D., et al. (2021). Laccase as an efficacious approach to remove anticancer drugs: a study of doxorubicin degradation, kinetic parameters, and toxicity assessment. *J. Hazard. Mater.* 409:124520. doi: 10.1016/j.jhazmat.2020.124520

Kolomytseva, M. P., Myasoedova, N. M., Chernykh, A. M., Gaidina, A. S., Shebanova, A. D., Baskunov, B. P., et al. (2019). Laccase isoform diversity in basidiomycete *Lentinus strigosus* 1566: potential for phenylpropanoid polymerization. *Int. J. Biol. Macromol.* 137, 1199–1210. doi: 10.1016/j.ijbiomac.2019.07.056

Laemmli, U. K. (1970). Cleavage of structural proteins during the assembly of the head of bacteriophage T4. *Nature* 227, 680–685. doi: 10.1038/227680a0

Li, S. Y., Liu, J., Williams, M. A., Ling, W. T., Sun, K., Lu, C., et al. (2020). Metabolism of 17β-estradiol by *Novosphingobium* sp. ES2-1 as probed via HRMS combined with ^{13}C3-labeling. *J. Hazard. Mater.* 389:121875. doi: 10.1016/j.jhazmat.2019.121875

Ling, Z. R., Wang, S. S., Zhu, M. J., Ning, Y. J., Wang, S. N., Li, B., et al. (2015). An extracellular laccase with potent dye decolorizing ability from white rot fungus *Trametes* sp. LAC-01. *Int. J. Biol. Macromol.* 81, 785–793. doi: 10.1016/j.ijbiomac.2015.09.011

Liu, Q. Z., Liu, J., Hong, D., Sun, K., Li, S. Y., Latif, A., et al. (2021). Fungal laccase-triggered 17β-estradiol humification kinetics and mechanisms in the presence of humic precursors. *J. Hazard. Mater.* 412, 125197. doi: 10.1016/j.jhazmat.2021.125197

Liu, Y., Luo, G., Ngo, H. H., Guo, W. S., and Zhang, S. C. (2020). Advances in thermostable laccase and its current application in lignin-first biorefinery: a review. *Bioresour. Technol.* 298:122511. doi: 10.1016/j.biortech.2019.122511

Manavalan, T., Manavalan, A., Thangavelu, K. P., and Heese, K. (2013). Characterization of optimized production, purification and application of laccase from *Ganoderma lucidum*. *Biochem. Eng. J.* 70, 106–114. doi: 10.1016/j.bej.2012.10.007

Mate, D. M., and Alcalde, M. (2015). Laccase engineering: from rational design to directed evolution. *Biotechnol. Adv.* 33, 25–40. doi: 10.1016/j.biotechadv.2014.12.007

Mtibàa, R., Barriuso, J., de Eugenio, L., Aranda, E., Belbahri, L., Nasri, M., et al. (2018). Purification and characterization of a fungal laccase from the ascomycete *Thielavia* sp. and its role in the decolorization of a recalcitrant dye. *Int. J. Biol. Macromol.* 120, 1744–1751. doi: 10.1016/j.ijbiomac.2018.09.175

Othman, A. M., Elsayed, M. A., Elshafei, A. M., and Hassan, M. M. (2018). Purification and biochemical characterization of two isolated laccase isoforms from *Agaricus bisporus* CU13 and their potency in dye decolorization. *Int. J. Biol. Macromol.* 113, 1142–1148. doi: 10.1016/j.ijbiomac.2018.03.043

Pezzella, C., Guarino, L., and Piscitelli, A. (2015). How to enjoy laccases. *Cell. Mol. Life Sci.* 72, 923–940. doi: 10.1007/s00018-014-1823-9

Powers, J. C., Asgian, J. L., Ekici, Ö. D., and James, K. E. (2002). Irreversible inhibitors of serine, cysteine, and threonine proteases. *Chem. Rev.* 102, 4639–4750. doi: 10.1021/cr010182v

Rivera-Hoyos, C. M., Morales-Alvarez, E. D., Poutou-Piñales, R. A., Pedroza-Rodríguez, A. M., Rodríguez-Vazquez, R., and Delgado-Boada, J. M. (2013). Fungal laccases. *Fungal Biol. Rev.* 27, 67–82. doi: 10.1016/j.fbr.2013.07.001

Sadeghian-Abadi, S., Rezaei, S., Yousefi-Mokri, M., and Faramarzi, M. A. (2019). Enhanced production, one-step affinity purification, and characterization of laccase from solid-state culture of *Lentinus tigrinus* and delignification of pistachio shell by free and immobilized enzyme. *J. Environ. Manage.* 244, 235–246. doi: 10.1016/j.jenvman.2019.05.058

Schückel, J., Matura, A., and van Pée, K. H. (2011). One-copper laccase-related enzyme from *Marasmius* sp.: purification, characterization and bleaching of textile dyes. *Enzyme Microb. Technol.* 48, 278–284. doi: 10.1016/j.enzmictec.2010.12.002

Senthivelan, T., Kanagaraj, J., and Panda, R. C. (2016). Recent trends in fungal laccase for various industrial applications: an eco-friendly approach - A review. *Biotechnol. Bioproc. Eng.* 21, 19–38. doi: 10.1007/s12257-015-0278-7

Shao, Z. Z., Li, Y. P., Krishnamoorthy, R., Chermak, T., and Mitra, A. K. (1993). Differential effects of anionic, cationic, nonionic, and physiologic surfactants on the dissociation, α-chymotryptic degradation, and enteral absorption of insulin hexamers. *Pharm. Res.* 10, 243–251.

Si, J., Peng, F., and Cui, B. K. (2013). Purification, biochemical characterization and dye decolorization capacity of an alkali-resistant and metal-tolerant laccase from *Trametes pubescens*. *Bioresour. Technol.* 128, 49–57. doi: 10.1016/j.biortech.2012.10.085

Su, C., Cui, Y., Liu, D., Zhang, H., and Baninla, Y. (2020). Endocrine disrupting compounds, pharmaceuticals and personal care products in the aquatic environment of China: Which chemicals are the prioritized ones? *Sci. Total Environ.* 720:137652. doi: 10.1016/j.scitotenv.2020.137652

Thurston, C. F. (1994). The structure and function of fungal laccases. *Microbiology* 140, 19–26. doi: 10.1099/13500872-140-1-19

Uzan, E., Nousiainen, P., Balland, V., Sipila, J., Piumi, F., Navarro, D., et al. (2010). High redox potential laccases from the ligninolytic fungi *Pycnoporus coccineus* and *Pycnoporus sanguineus* suitable for white biotechnology: from gene cloning to enzyme characterization and applications. *J. Appl. Microbiol.* 108, 2199–2213. doi: 10.1111/j.1365-2672.2009.04623.x

Viguié, C., Chaillou, E., Gayrard, V., Picard-Hagen, N., and Fowler, P. A. (2020). Toward a better understanding of the effects of endocrine disrupting compounds on health: Human-relevant case studies from sheep models. *Mol. Cell. Endocrinol.* 505, 110711. doi: 10.1016/j.mce.2020.110711

Wan, Y. Y., Lu, R., Xiao, L., Du, Y. M., Miyakoshi, T., Chen, C. L., et al. (2010). Effects of organic solvents on the activity of free and immobilised laccase from *Rhus vernicifera*. *Int. J. Biol. Macromol.* 47, 488–495. doi: 10.1016/j.ijbiomac.2010.07.003

Wang, R., Li, F., Ruan, W. F., Tai, Y. P., Cai, H. B., and Yang, Y. (2020). Removal and degradation pathway analysis of 17β-estradiol from raw domestic wastewater using immobilised functional microalgae under repeated loading. *Biochem. Eng. J.* 161:107700. doi: 10.1016/j.bej.2020.107700

Wang, S. N., Chen, Q. J., Zhu, M. J., Xue, F. Y., Li, W. C., Zhao, T. J., et al. (2018). An extracellular yellow laccase from white rot fungus *Trametes* sp. F1635 and its mediator systems for dye decolorization. *Biochimie* 148, 46–54. doi: 10.1016/j.biochi.2018.02.015

Wang, S. S., Ning, Y. J., Wang, S. N., Zhang, J., Zhang, G. Q., and Chen, Q. J. (2017). Purification, characterization, and cloning of an extracellular laccase with potent dye decolorizing ability from white rot fungus *Cerrena unicolor* GSM-01. *Int. J. Biol. Macromol.* 95, 920–927. doi: 10.1016/j.ijbiomac.2016.10.079

Wiltschi, B., Cernava, T., Dennig, A., Casas, M. G., Geier, M., Gruber, S., et al. (2020). Enzymes revolutionize the bioproduction of value-added compounds: from enzyme discovery to special applications. *Biotechnol. Adv.* 40:107520. doi: 10.1016/j.biotechadv.2020.107520

Yahiaoui, M., Laribi-Habchi, H., Bouacem, K., Asmani, K. L., Mechri, S., Harir, M., et al. (2019). Purification and biochemical characterization of a new organic solvent-tolerant chitinase from *Paenibacillus timonensis* strain LK-DZ15 isolated from the Djurdjura Mountains in Kabylia, Algeria. *Carbohydr. Res.* 483:107747. doi: 10.1016/j.carres.2019.107747

Yang, X. L., Wu, Y. Y., Zhang, Y., Yang, E., Qu, Y., Xu, H. N., et al. (2020). A thermo-active laccase isoenzyme from *Trametes trogii* and its potential for dye decolorization at high temperature. *Front. Microbiol.* 11:241. doi: 10.3389/fmicb.2020.00241

Ye, X. Y., Wang, H., Kan, J., Li, J., Huang, T. W., Xiong, G. M., et al. (2017). A novel 17β-hydroxysteroid dehydrogenase in *Rhodococcus* sp. P14 for transforming 17β-estradiol to estrone. *Chem. Biol. Interact.* 276, 105–112. doi: 10.1016/j.cbi.2017.06.010

Zheng, F., An, Q., Meng, G., Wu, X. J., Dai, Y. C., Si, J., et al. (2017). A novel laccase from white rot fungus *Trametes orientalis*: purification, characterization, and application. *Int. J. Biol. Macromol.* 102, 758–770. doi: 10.1016/j.ijbiomac.2017.04.089

Zhuo, R., Yu, H. B., Yuan, P., Fan, J. H., Chen, L. J., Li, Y., et al. (2018). Heterologous expression and characterization of three laccases obtained from *Pleurotus ostreatus* HAUCC 162 for removal of environmental pollutants. *J. Hazard. Mater.* 344, 499–510. doi: 10.1016/j.jhazmat.2017.10.055

Compartmentalized Reconstitution of Post-squalene Pathway for 7-Dehydrocholesterol Overproduction in *Saccharomyces cerevisiae*

Xiao-Jing Guo[1,2], Ming-Dong Yao[1,2], Wen-Hai Xiao[1,2], Ying Wang[1,2]*, Guang-Rong Zhao[1,2] and Ying-Jin Yuan[1,2]

[1] Frontier Science Center for Synthetic Biology and Key Laboratory of Systems Bioengineering (Ministry of Education), School of Chemical Engineering and Technology, Tianjin University, Tianjin, China, [2] Collaborative Innovation Center of Chemical Science and Engineering (Tianjin), Tianjin University, Tianjin, China

7-Dehydrocholesterol (7-DHC) is the direct precursor to manufacture vitamin D_3. Our previous study has achieved 7-DHC synthesis in *Saccharomyces cerevisiae* based on the endogenous post-squalene pathway. However, the distribution of post-squalene enzymes between the endoplasmic reticulum (ER) and lipid bodies (LD) might raise difficulties for ERG proteins to catalyze and deliver sterol intermediates, resulting in unbalanced metabolic flow and low product yield. Herein, we intended to rearrange the subcellular location of post-squalene enzymes to alleviate metabolic bottleneck and boost 7-DHC production. After identifying the location of DHCR24 (C-24 reductase, the only heterologous protein for 7-DHC biosynthesis) on ER, all the ER-located enzymes were grouped into four modules: ERG1/11/24, ERG25/26/27, ERG2/3, and DHCR24. These modules attempted to be overexpressed either on ER or on LDs. As a result, expression of LD-targeted DHCR24 and ER-located ERG1/11/24 could promote the conversion efficiency among the sterol intermediates to 7-DHC, while locating module ERG2/3 into LDs improved the whole metabolic flux of the post-squalene pathway. Coexpressing LD-targeted ERG2/3 and DHCR24 (generating strain SyBE_Sc01250035) improved 7-DHC production from 187.7 to 308.2 mg/L at shake-flask level. Further expressing ER-targeted module ERG1/11/24 in strain SyBE_Sc01250035 dramatically reduced squalene accumulation from 620.2 mg/L to the lowest level (by 93.8%) as well as improved 7-DHC production to the highest level (to 342.2 mg/L). Then targeting module ERG25/26/27 to LDs further increased 7-DHC titer to 360.6 mg/L, which is the highest shake-flask level production for 7-DHC ever reported. Our study not only proposes and further proves the concept of pathway compartmentalized reconstitution to regulate metabolic flux but also provides a promising chassis to produce other steroidal compounds through the post-squalene pathway.

Keywords: compartmentation, endoplasmic reticulum, lipid bodies, post-squalene pathway, 7-dehydrocholesterol, *Saccharomyces cerevisiae*
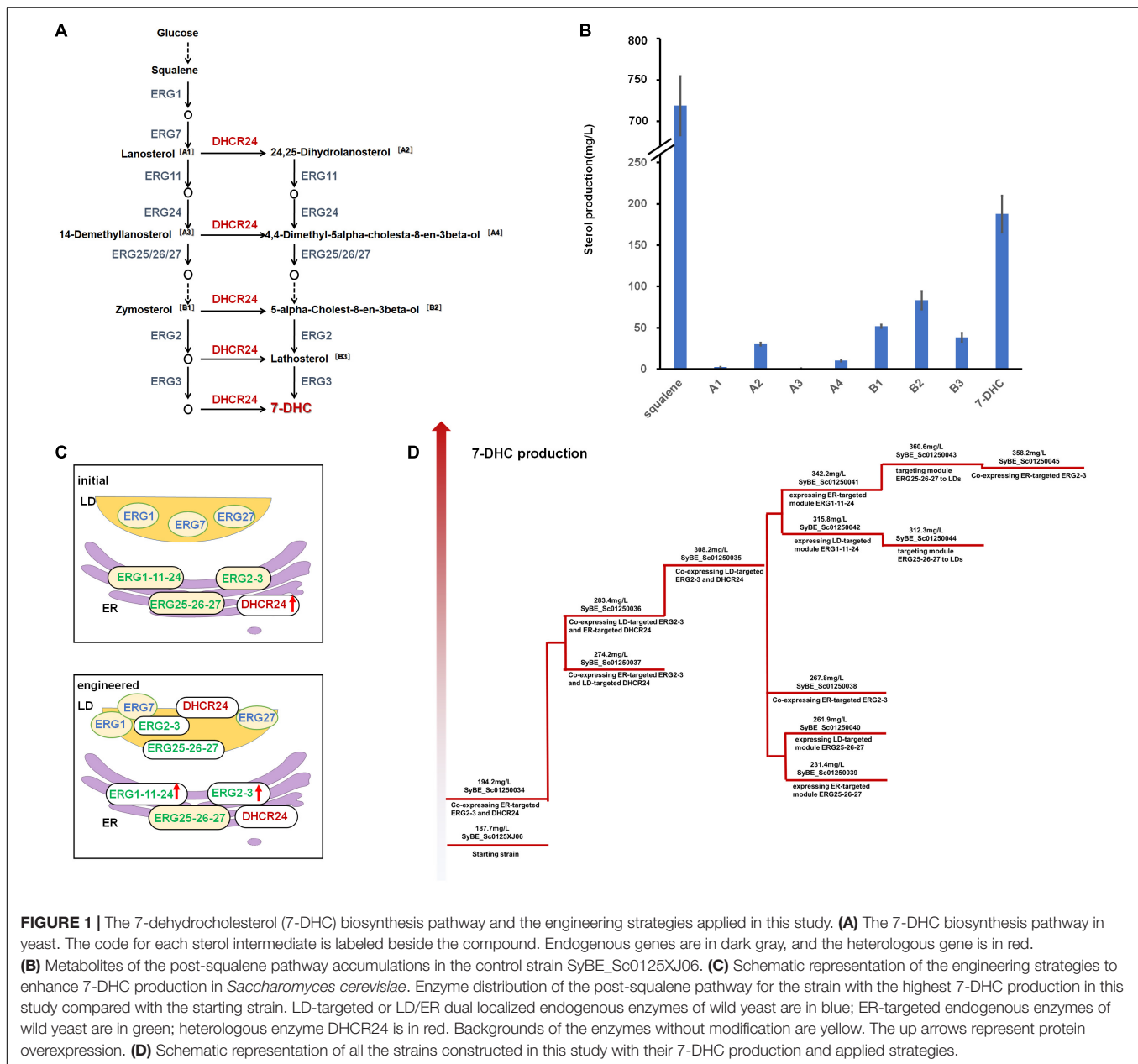
BACKGROUND

7-Dehydrocholesterol (7-DHC) is a high-valued sterol, which could be converted into vitamin D_3 (VD_3) when exposed to UV (Bendik et al., 2014). Besides being an essential nutriment, VD_3 and its derivatives [such as 25-OH-VD_3 and 1,25-(OH)$_2$-VD_3] are also medicines for many diseases (Bendik et al., 2014; de Sousa Almeida-Filho et al., 2017; Lu et al., 2017; Ali, 2020; D'Avolio et al., 2020; Kanstrup et al., 2020; Maghbooli et al., 2020). So far, *de novo* biosynthesis of 7-DHC has been realized in *Saccharomyces cerevisiae* by introducing heterologous Δ^{24}-dehydrocholesterol reductase (DHCR24) based on endogenous ergosterol synthesis pathway (Lang and Veen, 2011; Hohmann et al., 2012; Su et al., 2015; Guo et al., 2018), in which squalene is a key node separating the pre-squalene pathway and post-squalene pathway. The engineering approaches applied on pre-squalene pathway hardly affect the metabolic flux through the post-squalene pathway. As there is only one heterologous enzyme involved in 7-DHC synthesis (**Figure 1A**), therefore, the production of 7-DHC largely depends on the behavior of the post-squalene pathway. Although 7-DHC production has been greatly boosted by many metabolic engineering strategies, such as blocking the competitive ergosterol accumulation (Hohmann et al., 2012; Su et al., 2015), improving precursor supply (Lang and Veen, 2011; Su et al., 2015; Guo et al., 2018), screening the key enzyme sources (Hohmann et al., 2012; Guo et al., 2018), alleviating redox imbalance (Su et al., 2015), as well as regulating lipid metabolism (Guo et al., 2018), a large amount of post-squalene intermediates [e.g., squalene, zymosterol (B1), and 5alpha-Cholest-8-en-3beta-ol (B2)] still accumulated within the producing strains, such as our previously constructed strain SyBE_Sc0125XJ06 (Guo et al., 2018; **Figure 1B**). In this strain, all the mevalonate (MVA) pathway genes (*ERG10*, *ERG13*, *tHMG1*, *ERG12*, *ERG8*, *ERG19*, *IDI1*, and *ERG20*) were overexpressed for enhancing precursor supply; *ERG5* and *ERG6* were knocked out to block the branch pathway. Two copies of heterologous gene *DHCR24* were introduced and overexpressed under GAL1 promoter. Notably, squalene accumulation is the biggest obstacle at the current stage. There was 187.7 mg/L of 7-DHC obtained along with 718.9 mg/L of squalene produced at shake-flask level (**Figure 1B**). These metabolic bottlenecks within the post-squalene pathway seriously obstruct the conversion from upstream metabolites to 7-DHC.

Balancing the expression level of the modules besides the metabolic node is a promising strategy to reduce the bottleneck of our desired pathway. There are nine ERG proteins catalyzing 16 steps of reactions within the post-squalene pathway (**Figure 1A**). Our previous study once tempted to tune the expression level of DHCR24 (Guo et al., 2018) and every post-squalene proteins (Zhang et al., 2016). However, the effect of these modification on the metabolic flow of the post-squalene pathway is very limited, which pushed us to seek other solutions for this issue. Fortunately, the subcellular distribution of these ERG proteins gives us a hint of the potential solution to those metabolic bottlenecks. As shown in **Figure 1C**, post-squalene enzymes are not organized in one single organelle in the *S. cerevisiae* cytoplasm, but distribute between the endoplasmic reticulum (ER) and lipid bodies (LDs). To be specific, ERG1 and ERG27

are found on both organelles, while ERG7 is the only enzyme that located only in LDs (Milla et al., 2002). The rest of the ERG proteins locate in the ER (Ott et al., 2005). This distribution pattern might raise difficulties for ERG proteins to catalyze and deliver sterol intermediates, resulting in unbalanced metabolic flow and even low product yield of the desired product. Meanwhile, excess sterols generated in yeast cells are always stored in LDs in their ester forms (Zweytick et al., 2000; Jacquier and Schneiter, 2012). Ott et al. (2005) once reported the existence of sterol metabolites (e.g., B1) accumulated in LDs at significant levels in the strain with the same $\Delta ERG6$ background as our strain SyBE_Sc0125XJ06 (**Figure 1C**). These parts of sterols are hard to be catalyzed by ER-located proteins like ERG2 for its direct substrate B1. Moreover, organelles can provide different intracellular environments for enzyme catalysis, such as different pH environments or redox states. Therefore, a certain organelle may be more conducive to the catalysis of a specific protein. It was reported that mitochondria provided a preferable environment for amorphadiene synthase (ADS) activity, which caused enhanced amorphadiene production when ADS was overexpressed in yeast mitochondria compared with in the cytosol (Yuan and Ching, 2016). Thus, the subcellular distribution of post-squalene enzymes might be the limiting factor for the metabolic flux of this pathway. In addition, compartmentalized reconstitution, which used to be an effective way to improve outputs of many natural products (Lin et al., 2017; Sadre et al., 2019; Yang et al., 2019; Yee et al., 2019; Jia et al., 2020; Liu et al., 2020), also would be a promising solution to boost 7-DHC titer when applied in the post-squalene pathway.

In this study, after identifying the location of the only heterologous enzyme DHCR24 (C-24 reductase) on ER like most of the other ERG enzymes, all the ER-located proteins within the post-squalene pathway were chosen to prove the concept of pathway compartmentalized reconstitution on regulation of metabolic flux. Strain SyBE_Sc0125XJ06 with double deletion of *ERG5/ERG6* and two copies of gallus DHCR24 was employed as the starting strain. The whole post-squalene pathway was divided into two parts by B1, and all the ER-located enzymes were grouped into four modules: ERG1/11/24, ERG25/26/27, ERG2/3, and DHCR24. These modules were individually overexpressed on ER or in LDs (**Figure 1D**). Also, their effects on the production of 7-DHC as well as the accumulation of sterol intermediates were investigated, revealing an effective effort of pathway compartmentalization to pull down the metabolic flux through the post-squalene pathway. Eventually, targeting modules ERG25/26/27, ERG2/3, and DHCR24 into LDs along with supplementing another copy of ER-located ERG1/11/24 promoted 7-DHC production from the initial 187.7–360.6 mg/L at shake-flask level in strain SyBE_SC01250043, while the squalene accumulation was dramatically reduced by 95.5% to 32.4 mg/L. Although adding another copy of ER-located ERG2/3 into strain SyBE_SC01250043 did not further improve the 7-DHC titer, it increased the 7-DHC ratio to 39% of the total sterols, which is 2.29-fold of the initial ratio. This study achieves the highest shake-flask level titer of 7-DHC as known, which demonstrates a promising strategy to regulate metabolic flux by pathway compartmentalized reconstitution. In

FIGURE 1 | The 7-dehydrocholesterol (7-DHC) biosynthesis pathway and the engineering strategies applied in this study. **(A)** The 7-DHC biosynthesis pathway in yeast. The code for each sterol intermediate is labeled beside the compound. Endogenous genes are in dark gray, and the heterologous gene is in red. **(B)** Metabolites of the post-squalene pathway accumulations in the control strain SyBE_Sc0125XJ06. **(C)** Schematic representation of the engineering strategies to enhance 7-DHC production in *Saccharomyces cerevisiae*. Enzyme distribution of the post-squalene pathway for the strain with the highest 7-DHC production in this study compared with the starting strain. LD-targeted or LD/ER dual localized endogenous enzymes of wild yeast are in blue; ER-targeted endogenous enzymes of wild yeast are in green; heterologous enzyme DHCR24 is in red. Backgrounds of the enzymes without modification are yellow. The up arrows represent protein overexpression. **(D)** Schematic representation of all the strains constructed in this study with their 7-DHC production and applied strategies.

addition, sterol intermediates within the post-squalene pathway are also precursors to manufacture other valuable steroidal compounds; therefore, this study also provides an efficient chassis for microbial steroidogenesis.

RESULTS AND DISCUSSION

Identifying the Subcellular Location of the Desired Protein in *Saccharomyces cerevisiae*

A 7-DHC-producing strain SyBE_Sc0125XJ06, which was constructed in our previous study (7-DHC titer of 187.7 mg/L),

was chosen as the starting strain for pathway compartmentation. In this strain, MVA pathway genes were all overexpressed under GAL promoters (Westfall et al., 2012) to enhance precursor supply (Guo et al., 2018). GAL promoters were functioned as inducible promoters during cultivation (Westfall et al., 2012) to separate the 7-DHC production stage from the cell growth stage. In strain SyBE_Sc0125XJ06, the genes *ERG5/ERG6* were knocked out to block branch metabolic flow to ergosterol, while one copy of gallus DHCR24, which was controlled by GAL1 promoter, was integrated into the *GAL1,7,10* locus (Johnston, 1987; Peng et al., 2017). As mentioned above, we have already known all the subcellular locations of the whole post-squalene proteins in *S. cerevisiae*, but not for DHCR24. DHCR24 is the only heterologous enzyme catalyzing one of the rate-limiting

FIGURE 2 | Identifying the subcellular localization of gallus DHCR24 and verifying the reported LD localization sequence in *S. cerevisiae*. **(A)** Analysis of subcellular localization of gallus DHCR24 in *S. cerevisiae*. Sec61 is the specific marker of yeast ER. **(B)** Analysis of subcellular localization of two LD tags including oleosin (Ole) and AAM-B. ERG7 is the specific marker of yeast LDs. **(C)** Measurement of the expression levels of ER-/LD-located protein. Their expression levels were determined by the relative fluorescence units (RFU) of RFP fused with the enzymes. Significance levels of *t*-test: *$P < 0.05$, **$P < 0.01$.

steps in the 7-DHC synthetic pathway. However, there is little research on gallus DHCR24 so far. According to Wu et al. (2004), research on human DHCR24, endogenous DHCR24, was located on the ER under basal conditions in human cells. The N-terminus of the human DHCR24 is identified as a potential transmembrane domain. This part of the sequences is predicted to partially embed in the membrane as a stem or "peduncle" rather than to traverse the membrane bilayer, which firmly anchors the protein to the membrane (Lu et al., 2012; Zerenturk et al., 2013). With a similar structure, when gallus DHCR24 (Caldwell et al., 2005) was introduced into *S. cerevisiae*, it would locate at a specific membrane structure with a high probability. However, yeasts have large and diverse membranes, making the issue on enzyme original location loss a possibility. Thus, we need to explore whether the relocating site of gallus DHCR24 in *S. cerevisiae* is still on the ER. Correspondingly, red fluorescent protein (RFP) was fused to the C-terminal of DHCR24 and coexpressed with green fluorescent protein (GFP)-linked Sec61, which was recognized as the specific marker for ER (Wilkinson et al., 1996; Kim et al., 2019). Confocal laser scanning microscopy demonstrated overlapped fluorescence signal patterns between DHCR24-RFP and Sec61-GFP (**Figure 2A**) proving that gallus DHCR24 is indeed located on the ER in yeast, which is consisted to DHCR24 in human cells.

As we illustrated above, the ERG protein distribution in yeast cells may cause an unbalanced metabolic flow. Since most of these proteins are mainly localized on the ER, we intended to express another copy on LDs to accelerate the delivering of intermediate metabolites. As reported, the protein oleosin from *Zea mays*

(van Rooijen and Moloney, 1995; Mullner et al., 2004; Lin et al., 2017) and the N-terminal of a putative methyltransferase AAM-B (Zehmer et al., 2008) are commonly used peptides to direct the desired enzymes to yeast LDs. These two LD-targeting sequences are usually attached to the N-terminal of the target enzymes. We chose the yeast native enzymes ERG2/ERG3 and foreign enzyme DHCR24 to verify the function of these peptides especially on proteins with original transmembrane regions responding to ER location. As demonstrated in **Figure 2B**, oleosin was fused to ERG3, while AAM-B tag was fused to ERG2 and DHCR24, respectively. In order to verify whether these oleosin or AAM-B tag linked proteins were expressed in LDs, RFP was fused to their C-terminals. In the meanwhile, ERG7, which is the unique sterol synthesis enzyme that only localized on LDs, was selected as the LD-specific marker and expressed along with GFP fused to its C-terminal. Both the RFP and GFP fused proteins were co-expressed in the same cell. As a result, all the images of the red fluorescence signals were mainly coincident with the corresponding green ones (**Figure 2B**), suggesting that oleosin and AAM-B tags could target the ER proteins onto yeast LDs.

To test if relocation of enzymes could affect the protein expression levels, all the relocated enzymes and the original ER-located enzymes were fused with RFP, and their expression levels were determined by measuring the relative fluorescence units (RFU) of these enzymes. As shown in **Figure 2C**, fusing with the LD-relocating sequences did not improve protein expression of these relocated proteins, indicating that further increasing 7-DHC production by relocating post-squalene proteins to LDs were likely caused by other reasons.
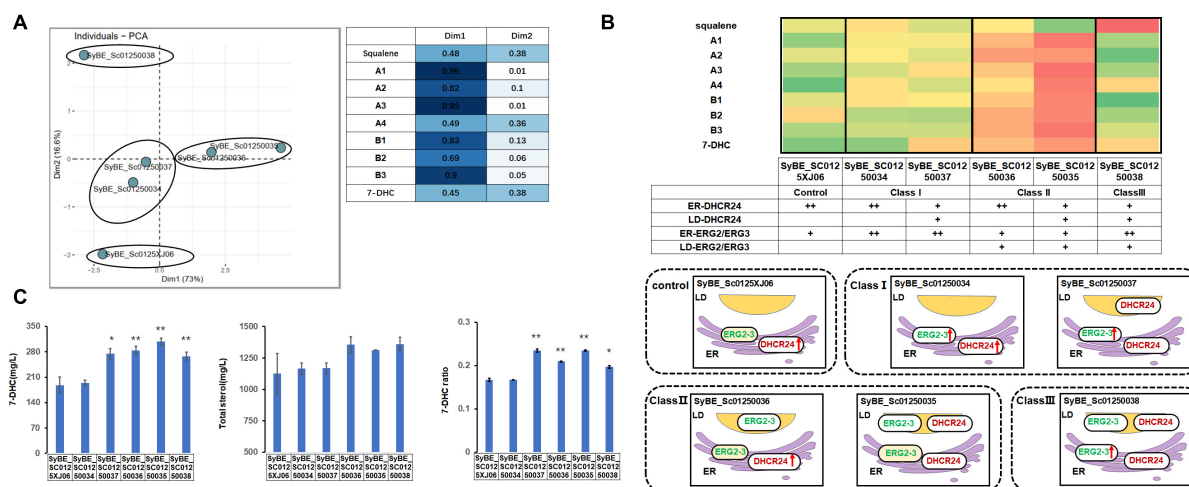
FIGURE 3 | Compartmentalized reconstitution of downstream post-squalene enzymes. **(A)** Principal component analysis (PCA) of sterol intermediates of the strains under compartmentalized reconstitution of downstream ERG enzymes (after B1). Different classes of strains are circled by ellipses. The table shows the composition of the two principal components in the PCA experiment (Dim1 and Dim2). **(B)** The post-squalene pathway metabolic flux heat map. The accumulation levels of post-squalene intermediates were normalized according to $Y = (X - \mu)/\sigma$, where Y represents the normalized value, X represents the original value, μ represents the mean value, and σ represents the standard deviation. The larger Y is presented by a color that is close to red, while the smaller one is close to green. The locations of engineered ERG proteins in the constructed strains are presented below the heat map. Backgrounds of the enzymes without modification are yellow. The up arrows represent protein overexpression. **(C)** 7-DHC productions, total sterols, and 7-DHC ratios of the constructed stains. All data were from at least triplicate experiments. *T*-test was conducted between the corresponding strain and the control strain SyBE_Sc0125XJ06. Significance levels of *t*-test: *$P < 0.05$, **$P < 0.01$.

Compartmentalized Reconstitution of Downstream Post-squalene Pathway After Zymosterol

Post-squalene pathway synthesizes subsequent sterols of squalene. Our former experiments showed that the main sterol intermediates accumulated in the post-squalene pathway are always distributed downstream of B1 (**Figure 1B**). These accumulated compounds also include B2 and lathosterol (B3). Sterols in the upstream pathway before B1 had little accumulation except squalene (**Figure 1B**). Therefore, the whole post-squalene pathway was divided into two parts: the pathway before B1 and the pathway after B1, and the pathway downstream of B1 (including B1) was optimized first. All the enzymes from this part were divided into two modules: ERG2/3 and DHCR24. Those modules were overexpressed either on ER or in LDs. To be specific, the control strain SyBE_0125XJ06 has one copy of the original ERG2/3 and two copies of DHCR24s expressed on ER. As shown in **Figure 1D**, we overexpressed ERG2/ERG3 by supplementing another ER- or LD-targeted copy in strain SyBE_0125XJ06, producing strain SyBE_01250034 or SyBE_01250036. Then one copy of the ER-targeted DHCR24 in strain SyBE_01250034 or SyBE_01250036 was replaced by the LD-targeted DHCR24, generating strain SyBE_01250037 or SyBE_01250035. One copy of ER-targeted ERG2/3 was further introduced into strain SyBE_Sc01250035, obtaining strain SyBE_Sc01250038. The production of 7-DHC and the accumulation of other metabolic intermediates from the post-squalene pathway in all these ERG2/3- or DHCR24-relocalized strains were evaluated by GC/MS after a 100-h shake-flask fermentation.

In order to better explore the impact of the modification of strains on the 7-DHC metabolic pathways, we conducted the principal component analysis (PCA) on the data presented in **Supplementary Table 1**. Through PCA experiments, we calculated out two principal components, Dim1 and Dim2. Lanosterol (A1), 24,25-dihydrolanosterol (A2), 14-demethyllanosterol (A3), B1, B2, and B3 contributed mainly to Dim1, while squalene, 7-DHC, and 4,4-dimethyl-5alpha-cholesta-8-en-3beta-ol (A4) contributed both to Dim1 and Dim2 (**Figure 3A**). According to the PCA results (**Figure 3A**), all the tested strains were divided into three categories, i.e., Class I for SyBE_Sc01250034 and SyBE_Sc01250037, Class II for SyBE_Sc01250036 and SyBE_Sc01250035, and Class III for SyBE_Sc01250038. The differences among the strains belonging to these three classes depended on the location of ERG2/3, which might be the main cause of the changes in the metabolic flow of the three classes of strains, suggesting that the location of ERG2/3 was the key point in the modification of downstream proteins for improving 7-DHC production.

To be specific, in Class I, the strains have overexpressed ERG2/3, which were only located in the ER (**Figure 3B**). In the strains of this class, metabolites upstream of B1 were increased compared with the control strain in general, while the intermediate B2 was significantly reduced (**Figure 3B**). The decrease in B2 might be due to the enhanced catalytic efficiency of ER-located ERG2, and we also speculated that the increased accumulation of B3 might be brought by insufficient catalytic ability of ERG3. Compared with the control strain SyBE_Sc0125XJ06, the amounts of total sterols had no significant change, while only strain SyBE_Sc01250037, which harbors one copy of the LD-expressed DHCR24, achieved
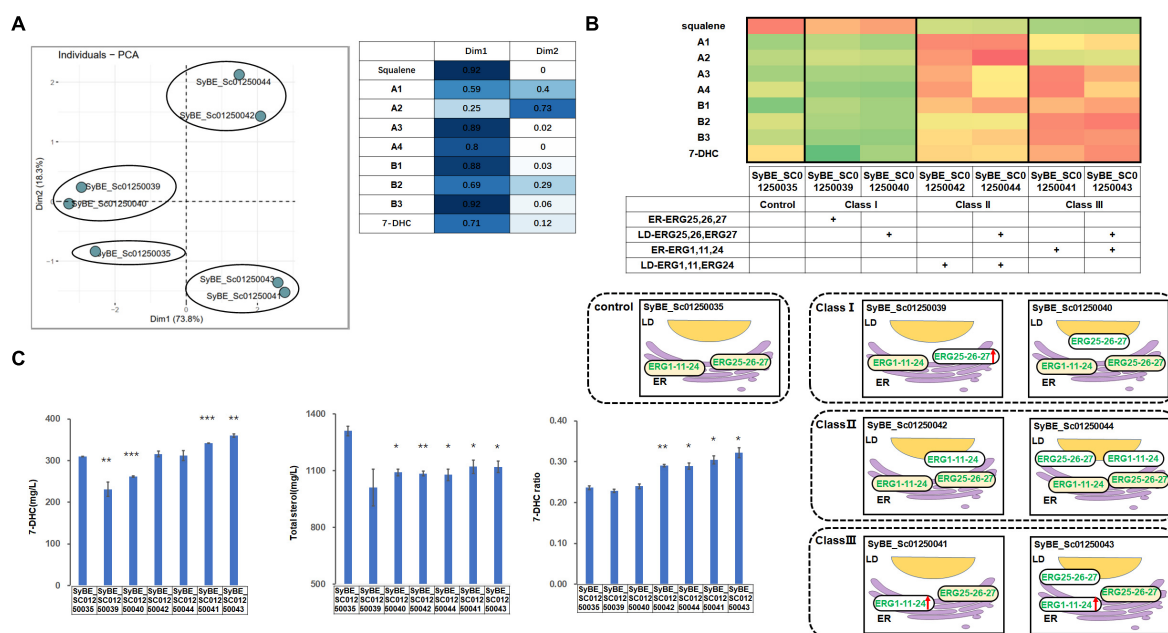
FIGURE 4 | Compartmentalized reconstitution of upstream post-squalene enzymes. **(A)** PCA analysis of sterol intermediates of the strains under compartmentalized reconstitution of upstream ERG enzymes (before B1). Different classes of strains are circled by ellipses. The table shows the composition of the two principal components in the PCA experiment (Dim1 and Dim2). **(B)** The post-squalene pathway metabolic flux heat map. The accumulation levels of post-squalene intermediates were normalized according to $Y = (X - \mu)/\sigma$, where Y represents the normalized value, X represents the original value, μ represents the mean value, and σ represents the standard deviation. The larger Y is presented by the color which is close to red, while the smaller one is close to green. The locations of engineered ERG proteins in the constructed strains are presented below the heat map. Backgrounds of the enzymes without modification are yellow. The up arrows represent protein overexpression. **(C)** 7-DHC productions, total sterols, and 7-DHC ratios of the constructed strains. All data were from at least triplicate experiments. T-test was conducted between the corresponding strain and the control strain SyBE_Sc0125XJ06. Significance levels of t-test: *P < 0.05, **P < 0.01, ***P < 0.001.

significant improvement on both 7-DHC production (by 46.1% to 274.2 mg/L) as well as 7-DHC ratio (increased by 40.7%) (**Figure 3C**). The increase in 7-DHC output came from the promoted conversion of sterol intermediates by targeting DHCR24 into LDs. That function of LD-targeted DHCR24 has also been proved by strains and SyBE_Sc01250035 from Class II.

In Class II the strains harbor another copy of LD-expressed ERG2/3 (**Figure 3B**). Most metabolites in the post-squalene pathway had been enhanced except squalene in strain SyBE_Sc01250035 (**Figure 3B**). The 7-DHC production of these two strains were both increased by 51.0% (to 283.4 mg/L) and 64.2% (to 308.2 mg/L), respectively (**Figure 3C**). In the meanwhile, their 7-DHC ratios were improved by 25.1 and 40.7%, respectively (**Figure 3C**). These data revealed that targeting ERG2/3 into LDs would not only improve the whole metabolic flux of the post-squalene pathway but also would be a benefit for the transformation of sterol intermediates into 7-DHC. The latter effect could be further enhanced by LD-targeted DHCR24.

Though 7-DHC production of strain SyBE_Sc01250035 increased most in the first part of our study, the intermediates like B2 and B3 also accumulated on a large scale. Thus, we introduced ER-located ERG2 and ERG3 to reduce B2 and B3. Thus, in Class III, the strain has overexpressed ER-located ERG2/3 as well as one copy of LD-targeted ERG2/3 (**Figure 3B**). Fermentation results showed that B2 and B3 of strain SyBE_Sc01250038 decreased sharply compared with strain SyBE_Sc01250035 as were our expectations. Among those post-squalene metabolites, only

squalene and A4 were significantly accumulated and higher than those in the control strain. The accumulation of squalene was raised out of our expectation (**Figure 3B**), which was detrimental to 7-DHC production. Compared with the control strain, even though the 7-DHC ratio as well as the 7-DHC production were enhanced by 18.0%, and 42.7% (to 267.8 mg/L), respectively, the 7-DHC output was lower than strain SyBE_Sc01250035 without another copy of the ER-targeted ERG2/3 (**Figure 3C**). In addition, the Class III strain also took no advantage over strain SyBE_Sc01250035 on both total sterol accumulation and 7-DHC ratio, suggesting that further overexpressing ER-targeted ERG2/3 brought no benefit to 7-DHC synthesis. Therefore, strain SyBE_Sc01250035 was selected as the target for the next round of optimization.

Compartmentalized Reconstitution of Upstream Post-squalene Pathway Before Zymosterol

A similar strategy was conducted on the pathway upstream of B1. ER-located post-squalene enzymes upstream of B1 were divided into two parts according to their catalytic order in the pathway, i.e., module ERG1/11/24 and module ERG25/26/27. Those modules were overexpressed either in the ER or in LDs (**Figure 1D**). To be specific, introducing one copy of ER- or LD-targeted ERG25/26/27 into strain SyBE_Sc01250035 generated strains SyBE01250039 and SyBE01250040,
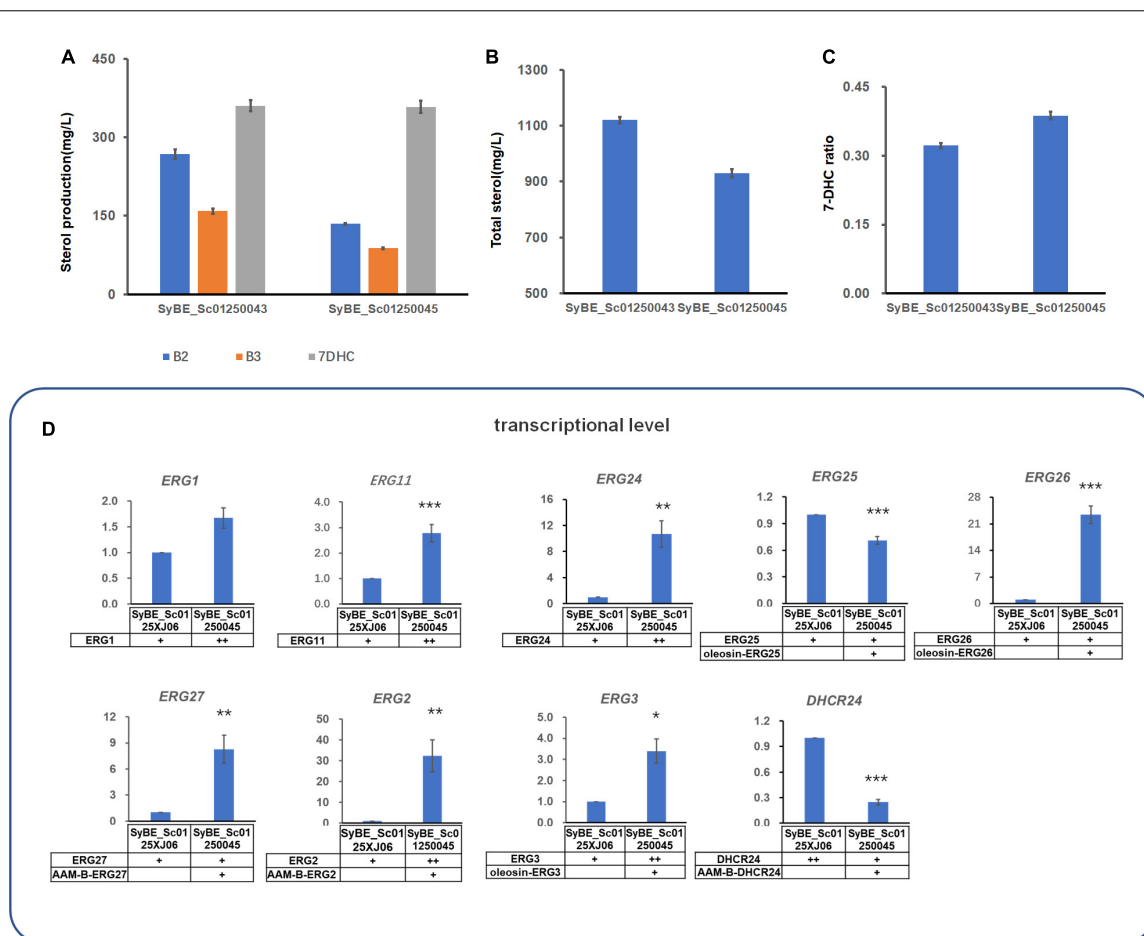
FIGURE 5 | 7-DHC production and metabolic flux changes caused by adding ER-targeted ERG2 and ERG3 to strain SyBE_Sc01250043. **(A)** B2, B3, and 7-DHC amounts change between SyBE_Sc01250043 and SyBE_Sc01250045. **(B)** Total sterols of the two strains. **(C)** 7-DHC ratios of the two strains. **(D)** The modified post-squalene pathway gene transcriptional levels in strain SyBE_Sc01250045 compared with the control strain SyBE_Sc0125XJ06. All data were from at least triplicate experiments. *T*-test was conducted between the corresponding strain and the control strain SyBE_Sc0125XJ06. Significance levels of *t*-test: $*P < 0.05$, $**P < 0.01$, $***P < 0.001$.

respectively, while introducing one copy of ER- or LD-targeted ERG1/11/24 into strain SyBE_Sc01250035 produced strains SyBE01250041 and SyBE01250042, respectively. Then a supplement of another copy of LD-expressed ERG25/26/27 into strains SyBE01250041 and SyBE01250042 obtained strains SyBE01250043 and SyBE01250044, respectively. These constructed strains were also cultivated for 100 h to measure their products by GC/MS.

PCA experiments was also conducted on the data presented in **Supplementary Table 2**. Through PCA experiments, we calculated out two principal components, Dim1 and Dim2. Except A1, A2, and B2 contributing both to Dim1 and Dim2, other sterols like squalene, B3, A3, A4, etc., contributed most to Dim1. According to the results of PCA experiments (**Figure 4A**), all the tested strains were divided into three categories, i.e., Class I for SyBE_Sc01250039 and SyBE_Sc01250040, Class III for SyBE_Sc01250042, and SyBE_Sc01250044, as well as Class II for SyBE_Sc01250041 and SyBE_Sc01250043. The differences among the strains belonging to these three classes depended

on whether ERG1/11/24 was overexpressed and where it was overexpressed, suggesting that the expression level as well as the location of ERG1/11/24 were the key points in the modification of upstream proteins for improving 7-DHC production.

In Class I, module ERG25/26/27 was overexpressed. As a result, no matter where ERG25/26/27 was located, there was still a dramatic accumulation of squalene (**Figure 4B**). Only A4 was sharply decreased (**Figure 4B**), due to overexpression of ERG25/26/27. Compared with the control strain SyBE_Sc01250035, the total sterol accumulation of SyBE_Sc01250040 as well as 7-DHC productions of strains SyBE_Sc01250039 and SyBE_Sc01250040 were both decreased, along with no improvement on the 7-DHC ratio.

In Class II, one copy of the LD-targeted ERG1/11/24 was introduced into the control strain SyBE_Sc01250035. Compared with the control strain, the accumulation of squalene declined dramatically by 78.9 and 81.1%, respectively, for strains SyBE_Sc01250042 and SyBE_Sc01250044. This part of squalene was mainly transformed into sterols upstream of B1 (**Figure 4B**).

With unchanged 7-DHC productions and decreased total sterol amounts, 7-DHC ratios were improved by 22.9%.

Different from Class II, in Class III, one copy of ER-expressed ERG1/11/24 was introduced into the control strain SyBE_Sc01250035. Compared with the Class II strains, the accumulation of squalene in Class III strains was further reduced along with decreased amounts of upstream sterols A1 and A2 as well as increased production of downstream sterols B2, B3, and 7-DHC (**Figure 4B**), suggesting that ER-expressed ERG1/11/24, but not LD-targeted ERG1/11/24, could pull the metabolic flow from upstream squalene to the downstream sterols. Since either ER-expressed or LD-targeted ERG1/11/24 could reduce squalene accumulation, we speculated that ERG1 might function well on both organelles, but ERG11/24 might be more suitable in the ER than in LDs. As a result, even though the amounts of total sterols were also lower than that of the control strain, 7-DHC production of strains SyBE_Sc01250041 and SyBE_Sc01250043 increased by 10.5% (to 342.2 mg/L) and 16.4% (to 360.6 mg/L), respectively (**Figure 4C**), along with enhanced 7-DHC ratios. The improved 7-DHC titer and ratio of strain SyBE_Sc01250043 than SyBE_Sc01250041 was due to another copy of LD-expressed ERG25/26/27. Although this modification brought no positive effect in Class I strains, it reduced the accumulation of the substrates A3 and A4, and increased the production of B1 in both Class II and Class III strains (**Figure 4B**). It was deduced that overexpressing ERG25/26/27 in LDs converted more their precursors into downstream intermediates, which could help increase 7-DHC production in some strains like SyBE_Sc01250043. Strain SyBE_Sc01250043 achieved the highest 7-DHC production at shake-flask level as was known.

Further Reducing the Metabolites of the Strain Modified by Compartmentalized Reconstitution

According to our conclusions from a former part of the study, ER-located ERG2/3 could lower some sterols downstream of B1. In order to further reduce the accumulation of sterol metabolites, one copy of ER-expressed ERG2/3 was introduced into strain SyBE_Sc01250043, generating SyBE_Sc01250045. In strain SyBE_Sc01250045, 7-DHC had no significant change to strain SyBE_Sc01250043 (**Figure 5A**). Amounts of B2 and B3, the direct precursor of ERG2 and ERG3, both decreased dramatically (**Figure 5A**), and other sterols' amounts had little change with strain SyBE_Sc01250043 (**Supplementary Table 2**). Therefore, the total sterol amounts of strain SyBE_Sc01250045 decreased (**Figure 5B**), and 7-DHC ratio increased, compared with those of strain SyBE_Sc01250043 (**Figure 5C**). The growth curves of all strains in this study were identical (**Supplementary Figure 1**). Also, the real-time quantitative PCR (QPCR) test results showed that transcription levels of most of the modified genes in strain SyBE_Sc01250045 (except *ERG1*, *ERG25*, and *DHCR24*) were increased compared with SyBE_Sc0125XJ06 (**Figure 5D**), which is one of the reasons for enhanced 7-DHC production. We speculated that the increased transcription levels of these genes may be due to the raised copy number of these genes.

TABLE 1 | *Saccharomyces cerevisiae* strains used in this study.

Strain	Description	Source
CEN.PK2-1D	*MATα, URA3-52, TRP1-289, LEU2-3,112, HIS3Δ1, MAL2-8C, SUC2*	EUROSCARF
SyBE_Sc0125 × 001	CEN.PK2-1D, *LEU2:BieR-ERG19*-P$_{GAL1,10}$-*ERG8*, *ADE1:tHMG1*-P$_{GAL1,10}$-*IDI1_ADE1*, *HIS3:HIS3-ERG12*- P$_{GAL1,10}$-*ERG10*, *URA3:tHMG1*- P$_{GAL1,10}$-*ERG13-URA3*, *TRP1:tHMG1*- P$_{GAL1,10}$-*ERG20-TPR1*, *GAL1,7, 10:HphR ΔERG5 GAL7,10,1*:P$_{GAL1}$-*Gg_DHCR24*-T$_{CYC1}$	Previous study
SyBE_Sc0125XJ06	SyBE_Sc0125 × 001, *ΔERG6*:P$_{GAL1}$-*DHCR24*-T$_{CYC1}$- *LEU2*-	Previous study
SyBE_Sc01250034	SyBE_Sc0125XJ06, *HO*:URA3-P$_{GAL1}$-*ERG3*-T$_{FBA1t}$-P$_{GAL7}$-*ERG2*-T$_{PGK1t}$	This study
SyBE_Sc01250035	SyBE_Sc0125 × 001, *ΔERG6*:P$_{GAL1}$-*AAMB-DHCR24*-T$_{CYC1}$-*LEU2 HO*:URA3-P$_{GAL1}$-*Oleosin-ERG3*-T$_{FBA1t}$-P$_{GAL7}$-*AAMB-ERG2*-T$_{PGK1t}$	This study
SyBE_Sc01250036	SyBE_Sc0125XJ06, *HO*:URA3-P$_{GAL1}$-*Oleosin-ERG3*-T$_{FBA1t}$-P$_{GAL7}$-*AAMB-ERG2*-T$_{PGK1t}$	This study
SyBE_Sc01250037	SyBE_Sc0125 × 001, *ΔERG6*:P$_{GAL1}$-*AAMB-DHCR24*-T$_{CYC1}$-*LEU2 HO*:URA3-P$_{GAL1}$-*ERG3*-T$_{FBA1t}$-P$_{GAL7}$-*ERG2*-T$_{PGK1t}$	This study
SyBE_Sc01250038	SyBE_Sc01250035, *Delta15*: P$_{GAL1}$-*ERG3*-T$_{FBA1t}$-P$_{GAL7}$-*ERG2*-T$_{PGK1t}$	This study
SyBE_Sc01250039	SyBE_Sc01250035, *Delta22*: P$_{GAL1}$-*ERG25-GGGGS-ERG26*-T$_{FBA1t}$-P$_{GAL7}$-*ERG27*-T$_{PGK1t}$	This study
SyBE_Sc01250040	SyBE_Sc01250035, *Delta22*:P$_{GAL1}$-*ERG25-Oleosin-ERG26*-T$_{FBA1t}$-P$_{GAL7}$-*AAMB-ERG27*-T$_{PGK1t}$	This study
SyBE_Sc01250041	SyBE_Sc01250035, *Delta22*:P$_{GAL1}$-*ERG1-GGGGS-ERG11*-T$_{FBA1t}$-P$_{GAL7}$-*ERG24*-T$_{PGK1t}$	This study
SyBE_Sc01250042	SyBE_Sc01250035, *Delta22*:P$_{GAL1}$-*ERG1-Oleosin-ERG11*-T$_{FBA1t}$-P$_{GAL7}$-*AAMB-ERG24*-T$_{PGK1t}$	This study
SyBE_Sc01250043	SyBE_Sc01250040, *Delta15*:P$_{GAL1}$-*ERG1-GGGGS-ERG11*-T$_{FBA1t}$-P$_{GAL7}$-*ERG24*-T$_{PGK1t}$	This study
SyBE_Sc01250044	SyBE_Sc01250040, *Delta15*:P$_{GAL1}$-*ERG1-Oleosin-ERG11*-T$_{FBA1t}$-P$_{GAL7}$-*AAMB-ERG24*-T$_{PGK1t}$	This study
SyBE_Sc01250045	SyBE_Sc01250043, *Tau3*:KANMX-P$_{GAL1}$-*ERG3*-T$_{FBA1t}$-P$_{GAL7}$-*ERG2*-T$_{PGK1t}$	This study
SyBE_Sc0125P001	CEN.PK2-1D, PRS425K-P$_{GAL1}$-*Gg_DHCR24-RFP*-T$_{FBA1}$, PRS416- P$_{GAL1}$*SEC61-GFP*-T$_{FBA1}$	This study
SyBE_Sc0125P002	CEN.PK2-1D, PRS425K-P$_{GAL1}$-*AAMB-DHCR24-RFP*-T$_{FBA1}$, PRS416- P$_{GAL1}$*ERG7-GFP*-T$_{FBA1}$	This study
SyBE_Sc0125P003	CEN.PK2-1D, PRS425K-P$_{GAL1}$-*AAMB-ERG2-RFP*-T$_{FBA1}$, PRS416- P$_{GAL1}$*ERG7-GFP*-T$_{FBA1}$	This study
SyBE_Sc0125P004	CEN.PK2-1D, PRS425K-P$_{GAL1}$-*Oleosin-ERG3-RFP*-T$_{FBA1}$, PRS416- P$_{GAL1}$*ERG7-GFP*-T$_{FBA1}$	This study

Besides, another reason for raised transcription levels may be enzymes relocated to the LDs. To be noticed, in the former study, when SyBE_Sc01250035 was introduced the same module (ER-located ERG2/3), the overall metabolic flux reduced, while only squalene increased in strain SyBE_Sc01250038. The reason why introducing the same ER-expressed ERG2/3 in different strains had a so different impact on metabolic flux still needs to be explained. In the meanwhile, since we presumed that ER-located ERG3 might have insufficient catalytic ability due to the increased accumulation of B3 in strains SyBE_Sc01250034 and SyBE_Sc01250037, other heterologous ERG3s should be screened and introduced into the 7-DHC-producing strain. In addition, a more delicate compartmentation test on those key modules like ERG2/3 and ERG1/11/24 should be also conducted by targeting a single ERG protein to one organelle at one time. Besides, we can further rearrange the LD-located enzymes like ERG7 to ER in the strains constructed in this study and investigate their effects on the accumulation of 7-DHC and other sterol intermediates.

CONCLUSION

In this study, subcellular locations of post-squalene pathway enzymes were rearranged in order to improve the unbalanced metabolic flow and low product yield caused by the dual organelle locations. All the ER-located enzymes of the post-squalene pathway were grouped into four modules: ERG1/11/24, ERG25/26/27, ERG2/3, and DHCR24. These modules were overexpressed on ER or on LDs. We subsequently rearranged the locations of enzymes downstream and upstream of B1. We conducted PCA experiments to classify the strains and analyzed the metabolic flux of strains in each class. We also obtain some strains in which 7-DHC production and 7-DHC ratio both dramatically increased through rearranging the post-squalene pathway enzymes. Eventually, targeting modules ERG25/26/27 and ERG2/3 into LDs along with supplementing another copy of ER-located ERG1/11/24 promoted 7-DHC production from the initial 187.7–360.6 mg/L at shake-flask level in strain SyBE_SC01250043, while the squalene accumulation was dramatically reduced by 95.5% to 32.4 mg/L. Although adding another copy of ER-located ERG2/3 into strain SyBE_SC01250043 did not improve the 7-DHC titer, the 7-DHC ratio further increased to 39% of the total sterols, which is 2.32-fold of the initial ratio. This study achieves the highest shake-flask level titer of 7-DHC as was known, which demonstrated that compartmentalized reconstitution of the post-squalene pathway was an efficient way to optimize metabolic flux in the 7-DHC pathway and promote 7-DHC production and ratio.

MATERIALS AND METHODS

Strains, Media, and Cultivation

All E. coil and S. cerevisiae strains used in this work are summarized in **Table 1**. All modified yeast strains were derived from CEN.PK2-1D. E. coli DH5α was used for molecular cloning. E. coli was grown in Luria broth (LB) medium containing 50 μg ml^{-1} of ampicillin or 50 μg ml^{-1} of kanamycin for construction

of plasmids and strains. Solid synthetic complete (SC) medium (0.67% yeast nitrogen base, amino acid supplements, and 2% glucose) lacking the appropriate nutrient component were used to select recombinational yeast strains. Shake-flask fermentation was performed in modified YPD medium [2% peptone, 1% yeast extract, 4% glucose, and 1% D-(+)-galactose] at 30°C.

For shake-flask fermentation, constructed strains were cultured and purified on an SC plate. A single colony was cultivated in 5 ml of YPD medium overnight at 30°C, and the culture was transferred into 40 ml of modified YPD when cells entered the mid-exponential phase. The initial glucose concentration in YPD medium was 40 g/L and OD$_{600}$ was 0.2. D-galactose (10 g/L) was added into the media at the beginning of fermentation for inducing GAL promoters of recombinational strains. Shake-flask fermentation lasted for 100 h.

Construction of Plasmids and Strains

For constructing ERG2, ERG3, and DHCR24 relocalizing strains, ERG2 and ERG3 were fused with LD-targeting sequence AAM-B and oleosin to their 3'-terminuses individually by OE-PCR (**Supplementary Figure 2**). Modified genes AAM-B-ERG2 and oleosin-ERG3 were cloned into expression cassettes containing GAL7 or GAL1 promoter, which were built in our previous study. The original genes ERG2 and ERG3 were also cloned into the corresponding expression cassettes for control. Expression cassettes containing the desired genes "TDH2t-GAL1p-gene1-FBA1t" and "FBA1t-GAL7p-gene2-PGK1t" were then PCR amplified with 20-bp overlap to plasmid PRS425K and flanking specific restriction enzyme sites at one terminus, and the two expression cassettes also had a 20-bp overlap at their adjacent ends. The two resulting amplicons were assembled into linearized vector PRS425K with SE Seamless Cloning and Assembly Kit (Beijing Zoman Biotechnology). The recombinant modules containing two gene expression cassettes were released from plasmids by corresponding restriction enzymes cutting at the 5' and 3' terminus of the whole modules as genomic integration fragment (no. 1). Genomic sequences covering around 700 bp upstream of the desired integration site, selection marker, and terminator TDH2t (no selection marker if the integration was in the CRISPR method, when ERG2 and ERG3 were integrated in the YPRCΔ15 locus) were amplified from S. cerevisiae genome and joined by overlap PCR. The resulting amplicon was ligated into a PEAZY-blunt vector, and the recombinant plasmids were digested by restriction enzymes to yield the left arm fragment of the homologous recombination (no. 2). The right arm fragment (no. 3) was obtained in the same way as terminator PGK1t and 700-bp downstream of the desired integration locus. The three fragments above were transformed using the LiAc/SS carrier DNA/PEG method. For integration of ERG2/ERG3 in YPRCΔ15 locus, the CRISPR method was used. Two complementary primers from the target sequence YPRCΔ15 were annealed and ligated into CRISPR plasmid (carrying cas9 and incomplete gRNA), generating the complete guide RNA. The resulting CRISPR plasmid was transformed with the three recombination fragments above. The DHCR24 expression module and the left/right arm fragments of homologous recombination were obtained from our previous study and

integrated into genome *ERG6* locus in a similar way. For constructing ERG1, ERG11, ERG24, ERG25, ERG26, and ERG27 overexpressing or relocalizing strains, the similar molecular manipulation strategy was applied except two differences: (1) According to Lin et al. (2017), oleosin sequence could relocalize two proteins into the LDs simultaneously when proteins fused to its 5′-and 3′-terminus. *ERG1*, oleosin, and *ERG11* were amplified and combined by OE-PCR (**Supplementary Figure 1**), the resulting amplicons were recombined into the *GAL1p* expression cassette. In order to be consistent with the relocalization method, ERG1 and ERG11 used DNA linker GGGGS to became a fused protein for their overexpression experiment. ERG25 and ERG26 overexpressing or relocalizing strains were also constructed in the same way. (2) The right arm fragment of the homologous recombination for *ERG* genes integrating upstream of B1 was different. Expression cassette "*FBA1t-GAL7p-gene-PGK1t*" and about 700 bp of overlap of downstream, the desired genomic integration site was joined by OE-PCR as the right arm fragment to reduce the number of recombination fragments to three.

Extraction and Analysis of Sterols

Sterol extraction was performed as previously described (Guo et al., 2018). Yeast cells were harvested by centrifugation at 12,000 rpm for 2 min after fermentation process and boiled in 3 N HCl for 5 min to break the cell wall. Cells were pelleted and washed by distilled water to remove the remaining HCl. After neutralizing by NaOH, saponification reaction of cells was carried out in 3 M NaOH-methanol solution at 60°C for 4 h. n-Hexane and silica sand were added for sterol extraction with vortex. The n-hexane phase was collected and dried by a centrifugal vacuum evaporator. N-methyl-N-(trimethylsilyl) trifluoroacetamide (MSTFA) was used to derivatize the obtained sterols (30°C for h) and samples were ready for GC-MS analysis.

Sterols were separated and analyzed by GCMS-QP2020 (SHIMADZU, Japan) using a DB-5 fused-silica capillary column (30 m × 0.25 mm i.d., film thickness 0.25 μm, J&W Scientific, CA). Mass spectra ranged at 50–800 m/z, and helium was used as the carrier gas. Operating conditions were inlet temperature 260°C, initial temperature 70°C for 2 min then ramp 30°C/min to 250°C then ramp 10°C/min to 280°C and held for 15 min. Finally, the temperature increased to 290°C at 5°C/min and was held for 5 min. Sterol standards (squalene, A1, A2, B3, B1, 7-DHC, etc.) were purchased from Sigma-Aldrich (United States).

Principal Component Analysis

All visualizations of principal component analysis (Pearson, 2010) were performed in the R package FactoMineR (Lê et al., 2008).

Protein Expression Level Analysis

Strains were cultured in SC-leu medium with 20 g/L of galactose for 60 h. A plate reader (SpectraMAX M2, Molecular Devices)

used with a 587-nm excitation filter and a 610-nm emission filter was for measurement of the fluorescence of RFP.

Genes Transcriptional Analysis

The real-time quantitative PCR (QPCR) process was similar to our published article (Guo et al., 2018). Strains were cultured in a shake flask for 30 h (ethanol consumption phase) and then harvested. Total RNA extraction, reverse transcription, and QPCR were carried out by Apexbio Inc. (China). The gene *ALG9* was used for normalization.

DATA AVAILABILITY STATEMENT

The original contributions presented in the study are included in the article/**Supplementary Material**, further inquiries can be directed to the corresponding author/s.

AUTHOR CONTRIBUTIONS

X-JG and YW conceived the study as well as participated in the strain construction and carried out the molecular genetic studies. X-JG and W-HX conducted the fermentation. M-DY, G-RZ, and Y-JY participated in the design and coordination of the study as well as helped draft the manuscript. YW supervised the whole research and revised the manuscript. All authors read and approved the final manuscript.

FUNDING

ACKNOWLEDGMENTS

SUPPLEMENTARY MATERIAL

The Supplementary Material for this article can be found online at: https://www.frontiersin.org/articles/10.3389/fmicb.2021.663973/full#supplementary-material

REFERENCES

Ali, N. (2020). Role of vitamin D in preventing of COVID-19 infection, progression and severity. *J. Infect. Public Health* 13, 1373–1380. doi: 10.1016/j.jiph.2020.06.021

Bendik, I., Friedel, A., Roos, F. F., Weber, P., and Eggersdorfer, M. (2014). Vitamin D: a critical and essential micronutrient for human health. *Front. Physiol.* 5:248.

Caldwell, R. B., Kierzek, A. M., Arakawa, H., Bezzubov, Y., Zaim, J., Fiedler, P., et al. (2005). Full-length cDNAs from chicken bursal lymphocytes to facilitate gene function analysis. *Genome Biol.* 6:R6.

D'Avolio, A., Avataneo, V., Manca, A., Cusato, J., De Nicolo, A., Lucchini, R., et al. (2020). 25-hydroxyvitamin D concentrations are lower in patients with positive PCR for SARS-CoV-2. *Nutrients* 12:1359. doi: 10.3390/nu12051359

de Sousa Almeida-Filho, B., De Luca Vespoli, H., Pessoa, E. C., Machado, M., Nahas-Neto, J., and Nahas, E. A. P. (2017). Vitamin D deficiency is associated with poor breast cancer prognostic features in postmenopausal women. *J. Steroid Biochem. Mol. Biol.* 174, 284–289. doi: 10.1016/j.jsbmb.2017.10.009

Guo, X. J., Xiao, W. H., Wang, Y., Yao, M. D., Zeng, B. X., Liu, H., et al. (2018). Metabolic engineering of *Saccharomyces cerevisiae* for 7-dehydrocholesterol overproduction. *Biotechnol. Biofuels* 11:192.

Hohmann, H. P., Lehmann, M., and Merkamm, M. (2012). *Production of Non-Yeast Sterols by Yeast*. US Patent, 20120231495. Washington, DC: U.S. Patent and Trademark Office.

Jacquier, N., and Schneiter, R. (2012). Mechanisms of sterol uptake and transport in yeast. *J. Steroid Biochem. Mol. Biol.* 129, 70–78. doi: 10.1016/j.jsbmb.2010.11.014

Jia, H., Chen, T., Qu, J., Yao, M., Xiao, W., Wang, Y., et al. (2020). Collaborative subcellular compartmentalization to improve GPP utilization and boost sabinene accumulation in *Saccharomyces cerevisiae*. *Biochem. Eng. J.* 164:107768. doi: 10.1016/j.bej.2020.107768

Johnston, M. (1987). A model fungal gene regulatory mechanism-the GAL genes of *Saccharomyces cerevisiae*. *Microbiol. Rev.* 51, 458–476. doi: 10.1128/mmbr.51.4.458-476.1987

Kanstrup, C., Teilum, D., Rejnmark, L., Bigaard, J. V., Eiken, P., Kroman, N., et al. (2020). 25-hydroxyvitamin D at time of breast cancer diagnosis and breast cancer survival. *Breast Cancer Res. Treat* 179, 699–708. doi: 10.1007/s10549-019-05486-4

Kim, J. E., Jang, I. S., Son, S. H., Ko, Y. J., Cho, B. K., Kim, S. C., et al. (2019). Tailoring the *Saccharomyces cerevisiae* endoplasmic reticulum for functional assembly of terpene synthesis pathway. *Metab. Eng.* 56, 50–59. doi: 10.1016/j.ymben.2019.08.013

Lang, C., and Veen, M. (2011). *Preparation of 7-Dehydrocholesterol and/or the Biosynthetic Intermediates and/or Secondary Products Thereof in Transgenic Organisms*. US Patent 12607017. Washington, DC: U.S. Patent and Trademark Office.

Lê, S., Josse, J., and Husson, F. (2008). FactoMineR: anRpackage for multivariate analysis. *J. Stat. Softw.* 25, 1–18.

Lin, J. L., Zhu, J., and Wheeldon, I. (2017). Synthetic protein scaffolds for biosynthetic pathway colocalization on lipid droplet membranes. *ACS Synth. Biol.* 6, 1534–1544. doi: 10.1021/acssynbio.7b00041

Liu, G. S., Li, T., Zhou, W., Jiang, M., Tao, X. Y., Liu, M., et al. (2020). The yeast peroxisome: a dynamic storage depot and subcellular factory for squalene overproduction. *Metab. Eng.* 57, 151–161. doi: 10.1016/j.ymben.2019.11.001

Lu, G., Li, J., Chu, J., Jin, S., Fu, Z., Miao, D., et al. (2017). 1,25(OH)2D3 deficiency increases TM40D tumor growth in bone and accelerates tumor-induced bone destruction in a breast cancer bone metastasis model. *Biomed. Pharmacother.* 95, 1033–1039. doi: 10.1016/j.biopha.2017.09.018

Lu, X., Li, Y., Liu, J., Cao, X., Wang, X., Wang, D., et al. (2012). The membrane topological analysis of 3beta-hydroxysterol-Delta24 reductase (DHCR24) on endoplasmic reticulum. *J. Mol. Endocrinol.* 48, 1–9. doi: 10.1530/jme-11-0132

Maghbooli, Z., Sahraian, M. A., Ebrahimi, M., Pazoki, M., Kafan, S., Tabriz, H. M., et al. (2020). Vitamin D sufficiency, a serum 25-hydroxyvitamin D at least 30 ng/mL reduced risk for adverse clinical outcomes in patients with COVID-19 infection. *PLoS One* 15:e0239799. doi: 10.1371/journal.pone.0239799

Milla, P., Athenstaedt, K., Viola, F., Oliaro-Bosso, S., Kohlwein, S. D., Daum, G., et al. (2002). Yeast oxidosqualene cyclase (Erg7p) is a major component of lipid particles. *J. Biol. Chem.* 277, 2406–2412. doi: 10.1074/jbc.m104195200

van Rooijen, G. J., and Moloney, M. M. (1995). Structural requirements of oleosin domains for subcellular targeting to the oil body. *Plant Physiol.* 109, 1353–1361. doi: 10.1104/pp.109.4.1353

Mullner, H., Zweytick, D., Leber, R., Turnowsky, F., and Daum, G. (2004). Targeting of proteins involved in sterol biosynthesis to lipid particles of the yeast Saccharomyces cerevisiae. *Biochim. Biophys. Acta* 1663, 9–13. doi: 10.1016/j.bbamem.2004.03.001

Ott, R. G., Athenstaedt, K., Hrastnik, C., Leitner, E., Bergler, H., and Daum, G. (2005). Flux of sterol intermediates in a yeast strain deleted of the lanosterol C-14 demethylase Erg11p. *Biochim. Biophys. Acta* 1735, 111–118. doi: 10.1016/j.bbalip.2005.05.003

Pearson, K. (2010). LIII. On lines and planes of closest fit to systems of points in space. The London, Edinburgh, and Dublin. *Philos. Mag. J. Sci.* 2, 559–572. doi: 10.1080/14786440109462720

Peng, B., Plan, M. R., Carpenter, A., Nielsen, L. K., and Vickers, C. E. (2017). Coupling gene regulatory patterns to bioprocess conditions to optimize synthetic metabolic modules for improved sesquiterpene production in yeast. *Biotechnol. Biofuels* 10:43.

Sadre, R., Kuo, P., Chen, J., Yang, Y., Banerjee, A., Benning, C., et al. (2019). Cytosolic lipid droplets as engineered organelles for production and accumulation of terpenoid biomaterials in leaves. *Nat. Commun.* 10:853.

Su, W., Xiao, W. H., Wang, Y., Liu, D., Zhou, X., and Yuan, Y. J. (2015). Alleviating redox imbalance enhances 7-dehydrocholesterol production in engineered *Saccharomyces cerevisiae*. *PLoS One* 10:e0130840. doi: 10.1371/journal.pone.0130840

Westfall, P. J., Pitera, D. J., Lenihan, J. R., Eng, D., Woolard, F. X., Regentin, R., et al. (2012). Production of amorphadiene in yeast, and its conversion to dihydroartemisinic acid, precursor to the antimalarial agent artemisinin. *Proc. Natl. Acad. Sci. U.S.A.* 109, E111–E118.

Wilkinson, B. M., Critchley, A. J., and Stirling, C. J. (1996). Determination of the transmembrane topology of yeast Sec61p, an essential component of the endoplasmic reticulum translocation complex. *J. Biol. Chem.* 271, 25590–25597. doi: 10.1074/jbc.271.41.25590

Wu, C., Miloslavskaya, I., Demontis, S., Maestro, R., and Galaktionov, K. (2004). Regulation of cellular response to oncogenic and oxidative stress by Seladin-1. *Nature* 432:640. doi: 10.1038/nature03173

Yang, K., Qiao, Y., Li, F., Xu, Y., Yan, Y., Madzak, C., et al. (2019). Subcellular engineering of lipase dependent pathways directed towards lipid related organelles for highly effectively compartmentalized biosynthesis of triacylglycerol derived products in *Yarrowia lipolytica*. *Metab. Eng.* 55, 231–238. doi: 10.1016/j.ymben.2019.08.001

Yee, D. A., Denicola, A. B., Billingsley, J. M., Creso, J. G., Subrahmanyam, V., and Tang, Y. (2019). Engineered mitochondrial production of monoterpenes in *Saccharomyces cerevisiae*. *Metab. Eng.* 55, 76–84. doi: 10.1016/j.ymben.2019.06.004

Yuan, J., and Ching, C. B. (2016). Mitochondrial acetyl-CoA utilization pathway for terpenoid productions. *Metab. Eng.* 38, 303–309. doi: 10.1016/j.ymben.2016.07.008

Zehmer, J. K., Bartz, R., Liu, P., and Anderson, R. G. (2008). Identification of a novel N-terminal hydrophobic sequence that targets proteins to lipid droplets. *J. Cell Sci.* 121, 1852–1860. doi: 10.1242/jcs.012013

Zerenturk, E. J., Sharpe, L. J., Ikonen, E., and Brown, A. J. (2013). Desmosterol and DHCR24: unexpected new directions for a terminal step in cholesterol synthesis. *Prog. Lipid Res.* 52, 666–680. doi: 10.1016/j.plipres.2013.09.002

Zhang, W. Q., Xiao, Z., Xiao, W. H., and Wang, Y. (2016). Effect of post-squalene genes on the synthesis of 7-dehydrocholesterol in the artificial *Saccharomyces cerevisiae*. *China Biotechnol.* 36, 39–50.

Zweytick, D., Leitner, E., Kohlwein, S. D., Yu, C., Rothblatt, J., and Daum, G. (2000). Contribution of Are1p and Are2p to steryl ester synthesis in the yeast *Saccharomyces cerevisiae*. *Eur. J. Biochem.* 267, 1075–1082. doi: 10.1046/j.1432-1327.2000.01103.x

Check for
updates

Three New Quinazoline-Containing Indole Alkaloids From the Marine-Derived Fungus *Aspergillus* sp. HNMF114

Sha-Sha Liu¹ᵗ, Li Yang²ᵗ, Fan-Dong Kong³ᵗ, Jia-Hui Zhao⁴, Li Yao⁴, Zhi-Guang Yuchi⁴, Qing-Yun Ma², Qing-Yi Xie², Li-Man Zhou³, Meng-Fei Guo³, Hao-Fu Dai⁵, You-Xing Zhao²* and Du-Qiang Luo¹**

¹ College of Life Science, Key Laboratory of Medicinal Chemistry and Molecular Diagnosis of Ministry of Education, Hebei University, Baoding, China, ² Haikou Key Laboratory for Research and Utilization of Tropical Natural Products, Institute of Tropical Bioscience and Biotechnology, CATAS, Haikou, China, ³ Key Laboratory of Chemistry and Engineering of Forest Products, State Ethnic Affairs Commission, Guangxi Key Laboratory of Chemistry and Engineering of Forest Products, Guangxi Collaborative Innovation Center for Chemistry and Engineering of Forest Products, School of Chemistry and Chemical Engineering, Guangxi University for Nationalities, Nanning, China, ⁴ Tianjin Key Laboratory for Modern Drug Delivery & High-Efficiency, Collaborative Innovation Center of Chemical Science and Engineering, School of Pharmaceutical Science and Technology, Tianjin University, Tianjin, China, ⁵ Hainan Institute for Tropical Agricultural Resources, CATAS, Haikou, China

By feeding tryptophan to the marine-derived fungus *Aspergillus* sp. HNMF114 from the bivalve mollusk *Sanguinolaria chinensis*, 3 new quinazoline-containing indole alkaloids, named aspertoryadins H–J (**1**–**3**), along with 16 known ones (**4**–**19**), were obtained. The structures of the new compounds were elucidated by the analysis of spectroscopic data combined with quantum chemical calculations of nuclear magnetic resonance (NMR) chemical shifts and electron capture detector (ECD) spectra. Structurally, compound **3** represents the first example of this type of compound, bearing an amide group at C-3. Compounds **10** and **16** showed potent α-glucosidase inhibitory activity with IC$_{50}$ values of 7.18 and 5.29 μM, and compounds **13** and **14** showed a clear activation effect on the ryanodine receptor from *Spodoptera frugiperda* (sfRyR), which reduced the [Ca^{2+}]$_{ER}$ by 37.1 and 36.2%, respectively.

Keywords: marine-derived fungus, *Aspergillus* sp., indole alkaloids, α-glucosidase inhibitory activity, ryanodine receptor

INTRODUCTION

While plants and terrestrial microorganisms have been in the limelight of natural product research for several decades, the marine environment is one of the current hotspots for the bio-prospection of new bioactive molecules, and it is considered to be a new reservoir for drug discovery (Montaser and Luesch, 2011). Marine microorganisms are some of the most prolific sources of structurally novel and biologically active compounds (Bugni and Ireland, 2004; Shen et al., 2009; Arasu et al., 2013; Manimegalai et al., 2013; Xiong et al., 2013).

Among the marine-derived fungi, the genus *Aspergillus* is a prolific source of bioactive secondary metabolites (Blunt et al., 2017). In our search for marine active natural products, the fungus *Aspergillus* sp. HNMF114 was isolated and identified from a bivalve mollusk, *Sanguinolaria chinensis*, collected in Haikou Bay, China. Our previous research (Kong et al., 2019)

on the secondary metabolites of this fungus reported a series of quinazoline-containing indole alkaloids. Biogenetically, these compounds are all derived from tryptophan and anthranilic acid, along with other amino acids. It has been reported that feeding tryptophan is beneficial to the production of quinazoline-containing indole alkaloids (Guo et al., 2020). Thus, in order to tap the metabolic potential of this fungus, the continuous chemical investigation on the fermentation broth of the fungus *Aspergillus* sp. HNMF114 supplemented with L-tryptophan was carried out, which led to the isolation of 3 new quinazoline-containing indole alkaloids, aspertoryadins H–J (**1**–**3**), along with 16 known ones, tryptoquivaline H (**4**) (Buttachon et al., 2012), norquinadoline A (**5**) (Peng et al., 2013), *epi*-fiscalin D (**6**) (Qian et al., 2018), *epi*-fiscalin A (**7**) (Buttachon et al., 2012), deoxynortryptoquivaline (**8**) (Lin et al., 2013), scequinadolines D (**9**) (Huang et al., 2017), lapatin A (**10**) (Wu and Ma, 2013), fiscalin A (**11**) (Buttachon et al., 2012), oxoglyantrypine (**12**) (Peng et al., 2013), quinadoline B (**13**) (Koyama et al., 2008), tryptoquivalines L (**14**) (Buttachon et al., 2012), quinadoline A (**15**) (Koyama et al., 2008), scequinadolines E (**16**) (Huang et al., 2017), scequinadoline G (**17**) (Huang et al., 2017), glyantrypine (**18**) (Penn et al., 1992), and tryptoquivalines F (**19**) (Buttachon et al., 2012) (**Figure 1**). Interestingly, these compounds were all different from those of our previous report (Kong et al., 2019). Herein, the isolation, structure elucidation, and bioactivities of these compounds are reported.

MATERIALS AND METHODS

General Experimental Procedure

Nuclear magnetic resonance (NMR) spectra were obtained on a Bruker AV-600 spectrometer (Bruker, Bremen, Germany) with tetramethylsilane (TMS) as an internal standard. HRESIMS data were determined on a mass spectrometer API QSTAR Pulsar (Bruker, Bremen, Germany). Optical rotations were achieved on a JASCO P-1020 digital polarimeter and IR spectra were recorded on a Shimadzu UV2550 spectrophotometer. UV spectra were measured on a Beckman DU 640 spectrophotometer. Electron capture detector (ECD) data were collected using a JASCO J-715 spectropolarimeter. Silica gel (200–300 mesh, Qingdao Marine Chemical Inc., Qingdao, China) and Sephadex LH-20 (40–70 μm, Merck, Darmstadt, Germany) were used for column chromatography. Semipreparative high-performance liquid chromatography (HPLC) equipped with octadecyl silane column (YMC-pack ODS-A, 10 × 250 mm, 5 μm, 4 mL/min). Spots were visualized by heating silica gel plates sprayed with 10% H_2SO_4 in EtOH.

Fungal Material

The fungal information of *Aspergillus* sp. HNMF114 has been described in our previous report (Kong et al., 2019).

Fermentation, Extraction, and Isolation

The fungus was cultured was cultured for 30 days in 100 × 1,000 mL erlenmeyer flasks each containing 100 g of rice, 100 mL H_2O (33 g sea salt, and 2 g tryptophan per liter of tap water) were autoclaved at 121°C for 25 min. The fermented material was extracted three times with EtOAc (20 L for each time) to give 230 g of crude extract. The extract was extracted between petroleum ether and 90% methanol (1:1) to remove the oil. The methanolic extract (119 g) was subjected to a silica gel vacuum-liquid chromatographed (VLC) column, eluting with a stepwise gradient of petroleum ether/EtOAc (10:1, 8:1, 6:1, 4:1, 2:1, 1:1, 1:2, v/v) to afford 10 fractions (Fr.1–Fr.10). Fr.5 (3.0 g) was applied to octadecylsilane (ODS) silica gel with a gradient elution of MeOH-H_2O (1:4, 1:3, 2:3, 1:1, 3:2, 4:1, 9:1, and 1:0) to get eight subfractions (Fr.5-1-Fr.5-8). Fr. 5-3 (368 mg) was separated by ODS silica gel MeCN-H_2O (1:3, 2:3, 1:1, 3:2, 4:1, 9:1, and 1:0) to afford two subfractions. Subfraction Fr.5-3-1 was applied to semipreparative HPLC (60% MeOH-H_2O; 4 mL/min) to give compounds **3** (t_R = 5.8 min; 2.3 mg), **4** (t_R = 7.3 min; 3.3 mg), and **6** (t_R = 8.3 min; 6.1 mg). Fr.5-3-2 was applied to ODS silica gel with gradient elution of MeCN-H_2O (1:3 to 4:1) semipreparative HPLC (C 60% MeOH-H_2O; 4 mL/min) to obtain compounds **5** (t_R = 8.2 min; 5.0 mg), **9** (t_R = 10.4 min; 5.3 mg), and **10** (t_R = 10.7 min; 3.4 mg). Fr. 5-5 (56.0 mg) was further chromatographed by silica gel CC eluted with gradient Petroleum ether-EtOAc (10:1, 8:1, 6:1, 4:1, 2:1, 1:1, 1:2, v/v) to afford seven subfractions (Fr.5-5-1–Fr.5-5-7). Fr.5-5-3 were purified by semipreparative HPLC (55% MeOH-H_2O; 4 mL/min) to yield compounds **11** (t_R = 13.3 min; 1.8 mg), **12** (t_R = 13.8 min; 3.4 mg), **14** (t_R = 15.2 min; 4.7 mg), and **16** (t_R = 17.8 min; 2.7 mg). Fr.6 (2.7 g) was applied to an open ODS column chromatography eluted with stepwise gradient of MeOH-H_2O (1:5, 1:4, 1:3, 2:3, 1:1, 3:2, 4:1, 9:1, 1:0) to get nine subfractions (Fr.6-1 to Fr.6-9). Fr.6-4 (158 mg) was further separated by Sephadex LH-20 column chromatography, followed by semipreparative HPLC (50% MeCN-H_2O; containing 0.1% TFA; 4 mL/min) to afford compounds **2** (t_R = 10.3 min; 1.9 mg), **8** (t_R = 17.8 min; 3.8 mg), and **1** (t_R = 27.7 min; 3.4 mg). Fr. 6-5 was subjected to an ODS column chromatography by stepwise gradient elution of MeOH-H_2O (1:5, 1:4, 1:3, 2:3, 1:1, 3:2, 4:1, 9:1, and 1:0) to get nine subfraction (Fr.6-5-1 to Fr.6-5-9). The subfraction 6-5-4 (53.2 mg) was purified by semipreparative HPLC (45% MeCN-H_2O; 4 mL/min) to obtain compounds **7** (t_R 8.8 min; 2.3 mg), **13** (t_R 11.4 min; 37.7 mg), **15** (t_R 15.2 min; 4.3 mg), **19** (t_R 15.6 min; 2.8 mg). Compounds **17** (36.2 mg) and **18** (15.3 mg) were combined and crystallized from the Fr.6-5-5 and Fr.6-5-6, respectively.

*Aspertoryadin H (**1**)*: yellow powder solid; [α]25 D -131 (*c* 0.1, MeOH); UV (MeOH) λ_{max} (log ε): 200 (3.6), 229 (3.4), 279 (2.9, and 308 (2.6) nm; ECD (MeOH) λ_{max} (Δε): 197 (−5.78), 213 (14.45), 232 (−21.54), 330 (−0.17) nm; IR (KBr) υ_{max} (cm^{-1}): 3,345 (−OH), 2,961 (−CH), 2,925 (−CH), 1,684 (−C=O), 1,602 (−NH), 1,475(−C−N), and 1,031 (−C-C−); ^{1}H NMR and ^{13}C NMR data, see **Table 1**; HRESIMS *m/z* [M − H]$^-$ 500.2310 (calcd for $C_{28}H_{30}N_5O_4$, 500.2303).

*Aspertoryadin I (**2**)*: yellow powder solid; [α]25 D −144 (*c* 0.1, MeOH); UV (MeOH) λ_{max} (log ε): 205 (3.6), 226 (3.4), 279 (2.8), and 309 (2.5) nm; ECD (MeOH) λ_{max} (Δε): 200 (2.59), 210 (27.82), 231 (−22.02), 316 (−0.95) nm; IR (KBr) υ_{max} (cm^{-1}): 3,354 (−OH), 2,965 (−CH), 2,926 (−CH), 1,677(−C=O), 1,602
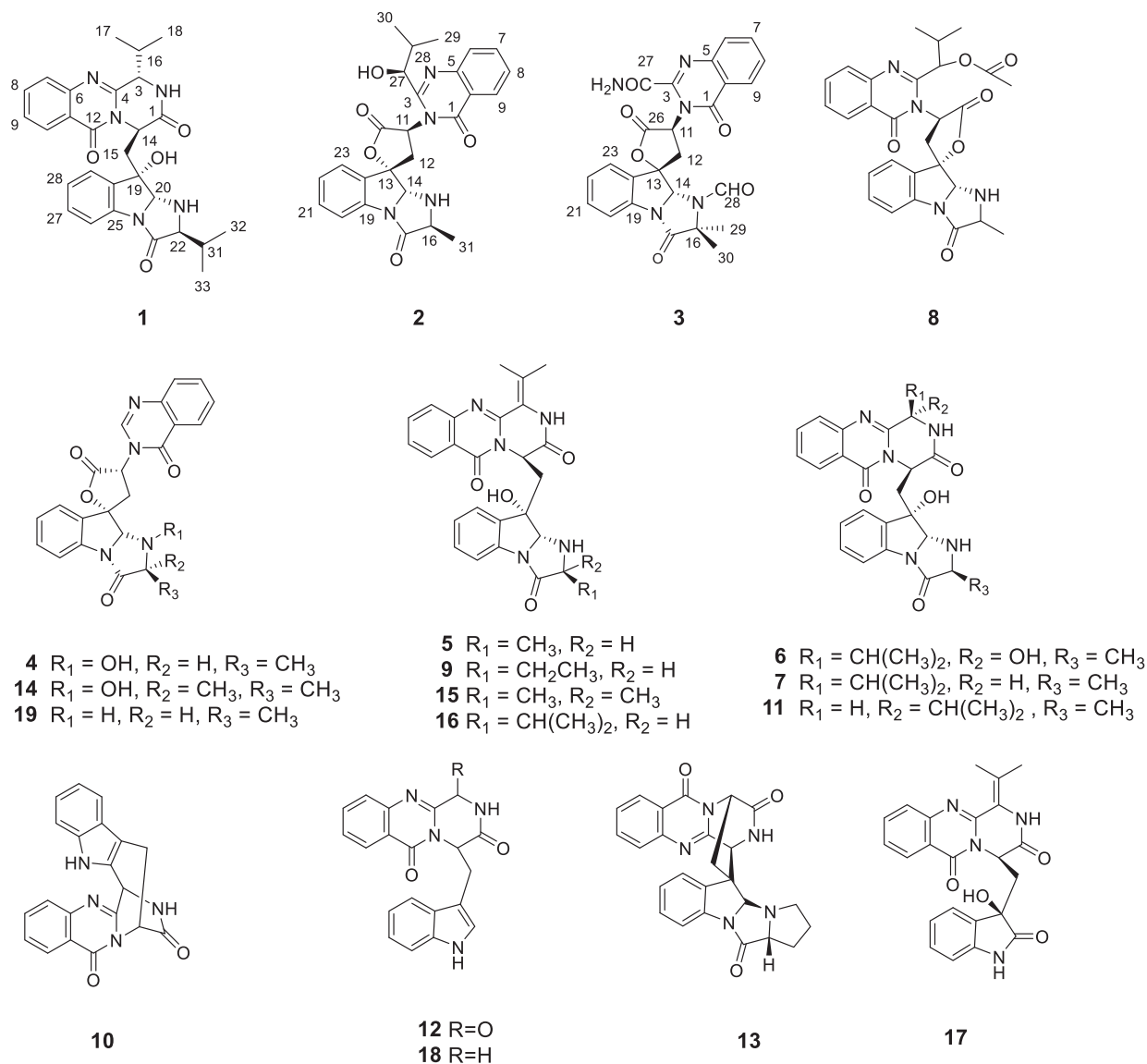
FIGURE 1 | The structures of compounds **1**–**19**.

(−NH), 1,475(-C-N), and 1,066 (−C-C-); ¹H NMR and ¹³C NMR data, see **Table 1**; HRESIMS *m/z* [M − H]⁻ 473.1833 (calcd for $C_{26}H_{25}N_4O_5$, 473.1830).

Aspertoryadin J (3): yellow powder solid; [α]25 D +32 (*c* 0.1, MeOH); UV (MeOH) λ_{max} (log ε): 206 (3.8), 228 (3.7), 276 (3.1), and 304 (3.9) nm; ECD (MeOH) λ_{max} (Δε): 219 (−5.83), 230 (−47.81), 300 (−4.07), 320 (−2.66), 360 (−0.14); IR (KBr) υ_{max} (cm⁻¹): 3,412 (−OH), 2,925 (−CH), 1,678 (−C=O), 1,474 (−C−N), and 1,027(-C-C-); ¹H NMR and ¹³C NMR data, see **Table 1**; HRESIMS *m/z* [M − H]⁻ 486.1421 (calcd for $C_{25}H_{20}N_5O_6$, 486.1419).

Computational Section

The initial conformational search was carried out in Confab (O'Boyle et al., 2011) using the MMFF94 molecular mechanics force field. Density functional theory calculations were performed using the Gaussian 16 package (Frisch et al., 2019). These conformers were optimized at B3LYP/6-31G (d) in the gas phase, and the conformers with a population over 1% were kept. Then, these conformers were further subjected to geometry optimizations at B3LYP/6-311G (d) in the gas phase, and frequency analysis of all optimized conformations was also performed at the same level of theory to exclude the imaginary frequencies. NMR shielding tensors were calculated with the gauge-independent atomic orbital (GIAO) method at mPW1PW91/6-311G (d,p) level with the IEFPCM solvent model in DMSO. The shielding constants obtained were converted into chemical shifts by referencing to TMS at 0 ppm (δcal = σTMS − σcal), where the σTMS was the shielding constant of

TABLE 1 | ^{1}H (600 MHz) and ^{13}C NMR (150 MHz) data of compounds **1–3**.

	1 (in DMSO-d_6)		2 (in DMSO-d_6)		3 (in DMSO-d_6)	
	δ_C	δ_H (*J* in Hz)	δ_C	δ_H (*J* in Hz)	δ_C	δ_H (*J* in Hz)
1	160.3		161.2		160.9	
3	57.7	4.79 (1H, d, 1.8)	156.6		150.2	
4	151.3					
5			146.2		146.4	
6	146.8		127.3	7.72 (1H, d, 7.8)	128.0	7.82 (1H, d, 9.0)
7	127.2	7.66 (1H, d, 8.4)	135.3	7.89 (1H, t, 7.8)	136.1	7.97 (1H, t, 9.0)
8	134.6	7.83 (1H, dd, 7.2, 8.4)	127.5	7.60 (1H, t, 7.8)	128.9	7.69 (1H, t, 9.0)
9	126.9	7.53 (1H, dd, 7.2, 8.4)	126.2	8.19 (1H, d, 7.8)	126.9	8.27 (1H, d, 9.0)
10	126.3	8.15 (1H, d, 8.4)	120.1		121.4	
11	120.1		54.8	6.07 (1H, t, 9.6)	56.8	5.73 (1H, dd, 10.2, 12.0)
12	160.4		30.8	2.75 (1H, dd, 9.6, 12.6)	27.0	3.31 (1H, dd, 10.2, 16.8)
				3.33 (1H, overlap)		3.40 (1H, dd, 13.2, 16.8)
13			86.1		84.4	
14	52.7	5.35 (1H, dd, 3.6, 7.8)	85.1	5.44 (1H, d, 7.2)	81.5	6.09 (1H, s)
15	37.6	2.80 (1H, dd, 3.6, 14.4)				
		2.67 (1H, dd, 7.8, 14.4)				
16	28.3	2.98 (1H, m)	59.5	3.61 (1H, m)	64.6	
17	19.0	1.16 (3H, d, 7.2)	177.2		172.9	
18	15.4	0.91 (3H, d, 7.2)				
19	74.9		140.9		138.8	
20	83.0	5.01 (1H, d, 7.2)	117.1	7.45 (1H, d, 7.8)	116.8	7.56 (1H, d, 9.0)
21			131.5	7.55 (1H, td, 1.2, 7.8)	132.2	7.61 (1H, t, 9.0)
22	69.9	3.47 (1H, dd, 4.2, 4.2)	126.0	7.38 (1H, td, 1.2, 7.8)	127.2	7.45 (1H, t, 9.0)
23	173.4		125.5	7.67 (1H, d, 7.8)	127.3	8.01 (1H, d, 9.0)
24			132.3		133.9	
25	137.7					
26	114.9	7.36 (1H, d, 7.8)	171.1		171.5	
27	129.6	7.33 (1H, t, 7.8)	80.2	4.35 (1H, dd, 4.8, 9.6)	163.5	
28	124.8	7.13 (1H, t, 7.8)	32.6	2.14 (1H, m)	162.5	8.64 (1H, s)
29	124.9	7.43 (1H, d, 7.8)	19.7	1.14 (3H, d, 6.0)	25.9	1.53 (3H, s)
30	138.3		19.2	0.83 (3H, d, 6.6)	27.0	1.70 (3H, s)
31	31.2	1.81 (1H, m)	17.6	1.36 (3H, d, 7.2)		
32	18.6	0.74 (3H, d, 6.6)				
33	17.5	0.76 (3H, d, 6.6)				
2-NH		8.45 (1H, br s)				
19-OH		5.66 (1H, s)				
15-NH				4.01 (1H, dd, 7.2, 7.2)		
21-NH		3.13 (1H, overlap)				
27-OH				6.56 (1H, d, 4.8)		
27-CONH$_2$						8.36 (1H, br s)
						8.66 (1H, br s)

TMS calculated at the same level. For each candidate, the parameters a and b of the linear regression δcal = *a*δexp + *b*; the correlation coefficient, R^2; the mean absolute error (MAE) defined as Σ*n* |δcal – δexp| /*n*; the corrected mean absolute error (CMAE), defined as Σ*n* |δcorr – δexp|/*n*, where δcorr = (δcal – *b*)/*a*, were calculated. DP4+ probability analysis was performed using the calculated NMR shielding tensors (Grimblat et al., 2015). The ECD spectra were calculated by the TDDFT methodology at the B3LYP/TZVP utilizing IEFPCM in methanol. ECD spectra

were simulated using SpecDis 1.71 (Bruhn et al., 2013) with σ = 0.30 eV.

α-Glucosidase Inhibition Assay

Yeast α-*glucosidase* (0.2 U/mL) in 0.1 M phosphate buffer (pH 6.8), was used as an enzyme source. The substrate solution of *p*-nitrophenyl-α-D-glucopyranoside (PNPG, 2.5 mM), was prepared in 0.1 M phosphate buffer (pH 6.8) solution. The tested compounds were prepared at different concentrations (250, 500, 1,000, 2,000, and 4,000 μg/mL) in DMSO. The tested

compound solution (10 μL) was pre-incubated with 100 μL α-glucosidase solution for 15 min. After pre-incubation, 45 μL of the substrate was added and further incubated for another 15 min at room temperature. The absorbance of each well was measured in Microplate Reader (Thermo Fisher Scientific, United States) reader at 405 nm. All experiments were carried out in triplicate (Dan et al., 2019).

Homology Modeling of α-Glucosidase

Since there is no structural information of α-glucosidase, we model the homology of it by modeler 9.20 (Webb and Sali, 2016). The amino acid sequence of α-glucosidase AL12 from Baker's yeast was retrieved from UniProt protein knowledgebase (accession number P53341). The crystal structure of isomaltase (PDBID:3A4A), with 75% sequence identity with the target sequence as the template for homology modeling, was selected after a search in the Protein Data Bank (PDB) at National Center or Biotechnology and Information (NCBI) using BLAST. The constructed model was validated by Procheck, ERRATE, and verify3D programs (Laskowski et al., 1993; Eisenberg et al., 1997).

Molecular Docking

The 3D structures of the active compounds **10** and **16** were constructed and minimized by MM2 force field using Chemoffice 14.0 software. All hydrogen atoms and gasteiger charges were added to modeled receptor by AutoDock Tools. Docking was performed centered at the active pocket of the α-glucosidase with Autodock vina software (Trott and Olson, 2010). The poses were ranked by their binding affinities and the lowest one was selected as the predicted protein–ligand complexes. The results were presented by Pymol[1].

Time-Lapse $[Ca^{2+}]_{ER}$ Measurements

The biological activity of compounds against the insect ryanodine receptor (RyR) was tested using HEK cells stably expressing RyR from *Spodoptera frugiperda* (sfRyR) or RyR1 from rabbit (rRyR1), and R-CEPIA1er, an engineered endoplasmic reticulum (ER)-targeting fluorescent protein used to measure ER luminal Ca^{2+} concentration ($[Ca^{2+}]_{ER}$) (Suzuki et al., 2014). Cells were cultured in Dulbecco's modified Eagle medium containing 10% fetal bovine serum, 15 mg/mL blasticidin, 100 mg/mL hygromycin, and 400 mg/mL G418 first in Petri dishes, and later seeded into 96-well plates at a density of 10^4 cells/well. After seeding for 24 h, 2 mg/mL doxycycline was added to induce the expression of RyR. After 48 h of induction, the medium was replaced by HEPES-buffered Krebs solution, and $[Ca^{2+}]_{ER}$ was measured using FlexStation 3 fluorometer (Molecular Devices) by monitoring the fluorescence signal changes. The R-CEPIAer signal, which is excited at 560 nm and emitted at 610 nm, was captured every 10s for 300s. The compounds for screening were
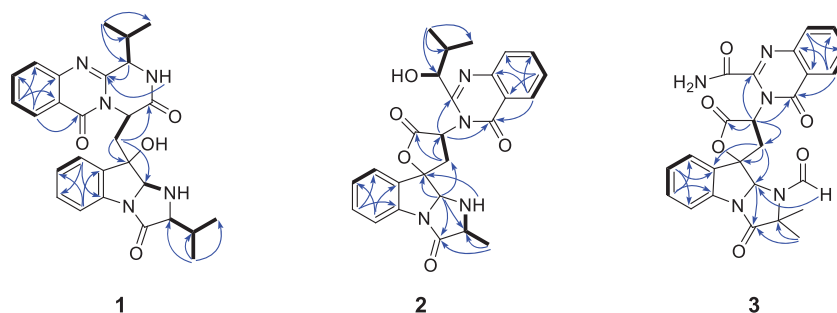
---

[1]https://pymol.org

FIGURE 2 | The key HMBC (arrows) and COSY (bold) correlations for compounds **1**–**3**.
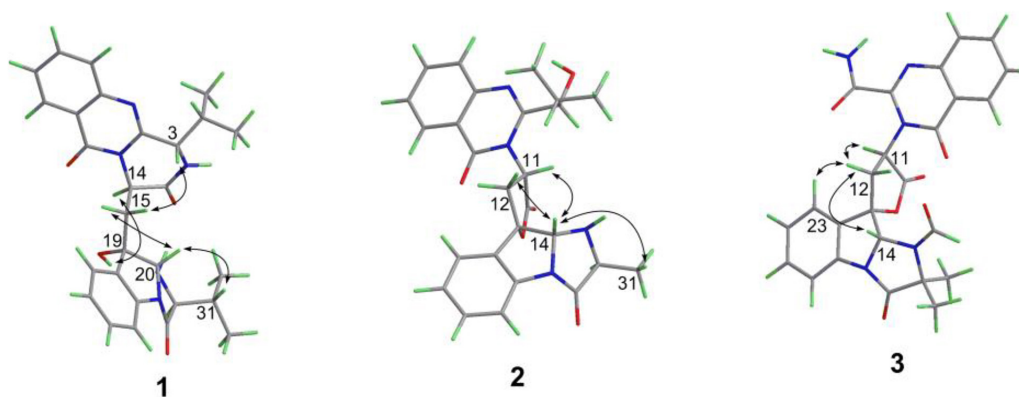
FIGURE 3 | Key ROESY correlations (double arrows) of compounds **1**–**3**.

FIGURE 4 | Experimental and calculated ECD curves for compound 1 (A); compound 2 (B); compound 3 (C).

FIGURE 5 | Docking analysis of 10 (green ball and stick) and 16 (cyan ball and stick) with α-glucosidase (A). 3D cartoon diagram of the interactions of 10 (B) and 16 (C) with α-glucosidase.
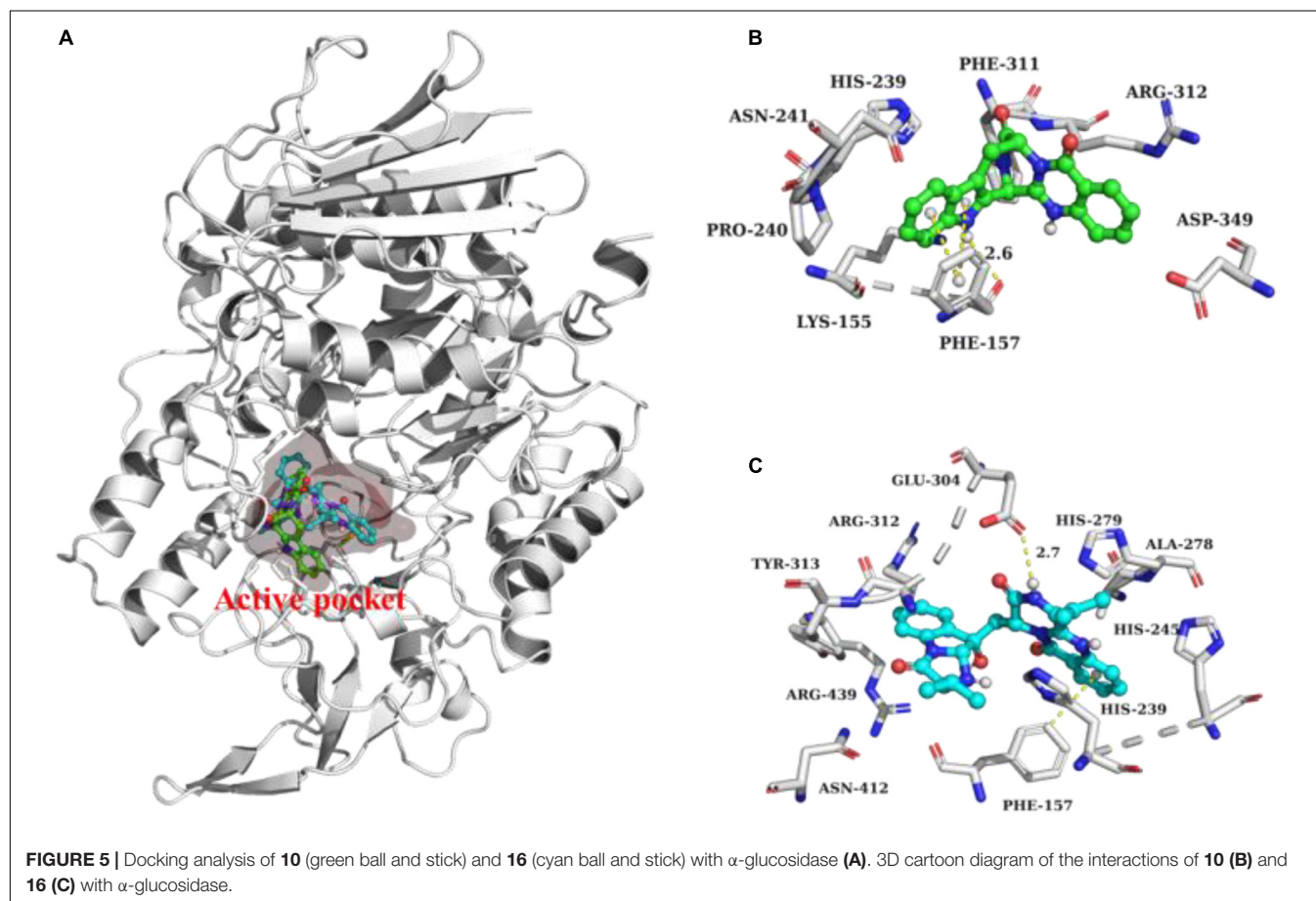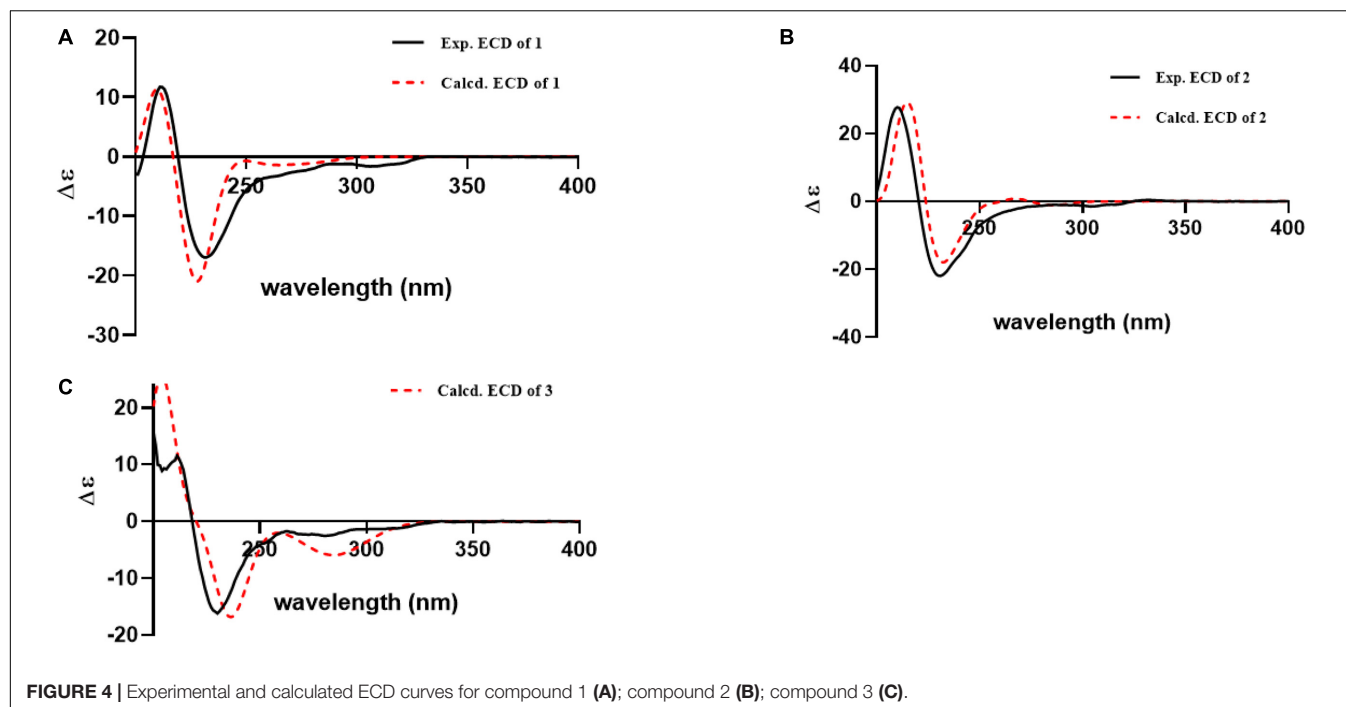
added 100s after the recording started. The ratio of the average fluorescence for the last 100s (F) and first 100s (F0), F/F0, was used to report the fluorescence change caused by the compounds. All experiments were carried out in triplicate and repeated twice.

RESULTS AND DISCUSSION

Structure Elucidation

Compound **1** was obtained as yellow powder solid, and its molecular formula was determined to be $C_{28}H_{31}N_5O_4$ on the basis of HRESIMS, indicating 16 degrees of unsaturation. The ^{1}H NMR spectrum (**Table 1**) showed the obvious resonances for eight aromatic protons attributed to two disubstituted benzene rings and four methyl protons. Its ^{13}C, DEPT, and HSQC NMR data (**Table 1**) revealed a total of 28 carbons, including four methyls, one methylene, 14 methines (six sp[3] and eight olefinic), and nine quaternary carbons (including three carbonyl groups and five olefinic). A detailed comparison of the NMR data of **1** with those of *epi*-fiscalin C (Buttachon et al., 2012) indicated that they shared the same skeleton with the only difference being the presence of an isopropyl at C-22 in **1** instead of two methyls in *epi*-fiscalin C. The key ^{1}H-^{1}H COSY cross-peaks of H-22/H-31/H-32 (H-33) and the HMBC correlations from H_3-32 and H_3-33 to C-31 and C-22 confirmed the assignment of the isopropyl at C-22. Thus, the planar structure of **1** was established as shown in **Figure 2**. The relative configuration of the

quinazoline and 5/5/6 tri-cyclic rings (**Figure 3**) were determined by the rotating frame overhauser effect spectroscopy (ROESY) spectrum, in which the correlations of H-20 with H-15a (δ_H 2.67) and H-31 revealed that H-20, H-31, and CH_2-15 were on the same face of the 5/5/6 tri-cyclic ring system. The ROESY correlation between H-3 and H-15b indicated that H-3 and C-15 should be placed on the same face of the quinazoline ring. Due to the flexibility of the single bonds C14-C15 and C15-C19, the relative configuration of **1** could not be clearly determined by ROESY spectrum. Therefore, a theoretical NMR calculation with DP4+ analysis was applied to clarify the relative configuration of **1**. The chemical shifts of two isomers (3*S*,14*R*,19*S*,20*R*,22*S*)-**1** and (3*R*,14*S*,19*S*,20*R*,22*S*)-**1**, were predicted using the GIAO method. DP4+ probability analysis showed that (3*S*,14*R*,19*S*,20*R*,22*S*)-**1** was the most likely candidate structure, with a 100% DP4+ (all data). As for the absolute configuration of **1**, the ECD spectrum of (3*S*,14*R*,19*S*,20*R*,22*S*)-**1** was calculated, the result of which matched well with an experimental curve (**Figure 4A**), establishing the absolute configuration of **1** as presented in **Figure 1**.

Compound **2** was isolated as yellow powder solid and had the molecular formula $C_{26}H_{26}N_4O_5$ as established by HRESIMS data with 16 degrees of unsaturation. Its ^{13}C (**Table 1**), DEPT, and HSQC NMR spectra revealed a total of 26 carbons including 13 aromatic carbons (eight protonated), one sp[3] methylene, three carbonyl carbons, five sp[3] methine, three methyls, and one oxygenated sp3 quaternary carbon. The above data were similar
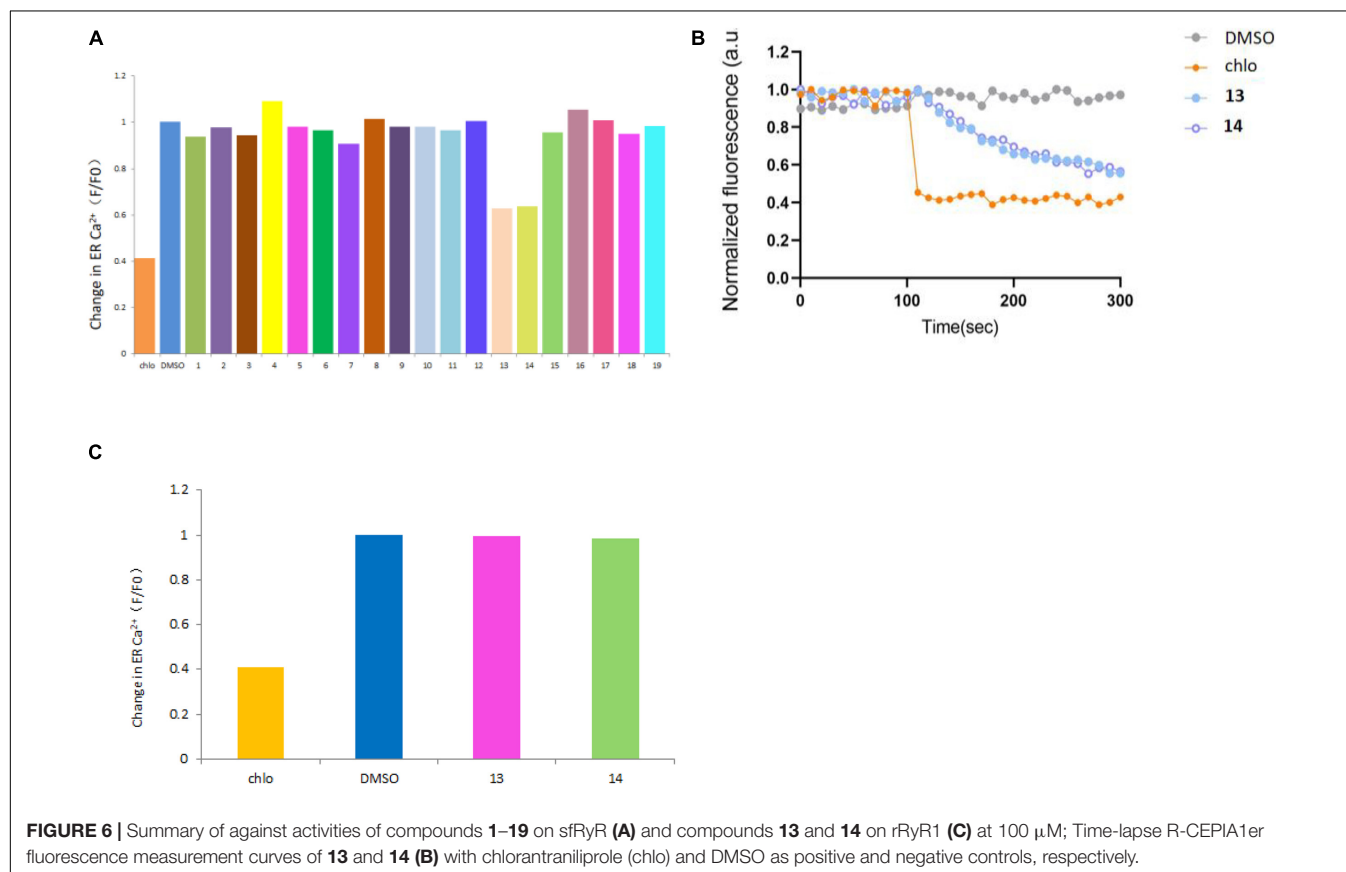

FIGURE 6 | Summary of against activities of compounds **1–19** on sfRyR **(A)** and compounds **13** and **14** on rRyR1 **(C)** at 100 μM; Time-lapse R-CEPIA1er fluorescence measurement curves of **13** and **14 (B)** with chlorantraniliprole (chlo) and DMSO as positive and negative controls, respectively.

to those of aspertoryadin A (Kong et al., 2019), indicating that they had a similar skeleton. The obvious structural difference between them is that a hydrogen on N-15 in **2** replaced the methyl sulfonyl group in aspertoryadin A. In addition, there are two methyls at C-16 in aspertoryadin A, but one methyl in **2**. The above deduction was supported by the contiguous COSY cross-peaks (**Figure 2**) of H-14/NH-15/H-16/H-31 and the key HMBC correlations (**Figure 2**) from H$_3$-31 and H-14 to C-16 and C-17. The relative configuration of **2** was established by ROESY spectrum. The ROESY cross-peaks (**Figure 3**) of H-11/H-14/H-12a and H-14/H$_3$-31 led to the assignment of the relative configurations for the stereocenters C-13, C-14, C-11, and C-16. The stereocenter C-27 was far away from other stereocenters and no ROE correlation was available for the assignment of its relative configuration. Thus, the chemical shifts of two isomers (11S,13S,14R,16S,27S)-**2** and (11S,13S,14R,16S,27R)-**2**, were calculated and the former showed 100% DP4+ (all data) probability, enable assignment of 27S^* configuration for **2**. The absolute configuration of **2** was confirmed as 11S,13S,14R,16S,27S by comparison of its experimental ECD spectrum with the calculated ECD curves of **2** (**Figure 4B**).

Compound **3**, a yellow powder solid, was assigned the molecular formula $C_{25}H_{21}N_5O_6$ by its HRESIMS, requiring 18 degrees of unsaturation. The ^{13}C NMR and DEPT spectra displayed five carbonyl carbons (including an aldehyde carbon and four amide or ester carbonyls), 13 aromatic carbons (eight protonated), one sp^3 methylene, two sp^3 methines, and two sp^3 quaternary carbons (one oxygenated). These data were also indicative of a quinazoline-containing indole alkaloid skeleton as that of **2**. A direct comparison of the NMR data of **3** with those of **2** revealed that the differences between them are the presence of an additional aldehyde group and one additional methyl group at the N-15 and C-16 in **3**, respectively, as well as the attachment of an amide moiety in **3** instead of an isobutyl unit at C-3 as in **2**. The additional groups were supported by the HMBC correlations (**Figure 2**) from H-28 (δ_H 8.64) to C-14 (δ_C 81.5) and from H$_3$-29 and H$_3$-30 to C-16, and C-17. The ROESY cross-peaks of H-12a/H-14/H-11 and H-23/H-12b indicated that **3** possessed the same relative configurations at C-11, C-13, and C-14 as aspertoryadin A (**Figure 3**). The absolute configuration was determined to be 11S, 13S, and 14R by ECD calculation (**Figure 4C**).

α-Glucosidase Inhibition Assay

All of the compounds isolated were evaluated for α-glucosidase inhibitory activity (Apostolidis et al., 2007). Compounds **10** and **16** exhibited potent α-glucosidase inhibitory activities with the IC$_{50}$ values of 7.18 and 5.29 μM, respectively (Acarbose as a positive control, IC$_{50}$: 213.0 μM).

Molecular Docking

The intermolecular interaction and potential binding sites between compounds **10**, **16**, and α-glucosidase were investigated via molecular docking simulations. The docking simulation results (**Figure 5**) demonstrated that compound **10** could interact with α-glucosidase by forming one hydrogen bond and π–π interactions with residues PHE 157 (**Figure 5B**). While

compound **16** could generate one hydrogen bond with residues GLU 340 and also form π–π interactions with residues PHE 157 in α-glucosidase (**Figure 5C**).

Biological Activity Against RyR

Ryanodine receptor, an intracellular calcium channel located on ER membrane, is a well-known insecticide target. The top-selling diamide insecticides, such as flubendiamide, chlorantraniliprole, and cyantraniliprole, all target insect RyRs. The insecticidal activities of all compounds were tested against RyRs from an agricultural pest, *S. frugiperda*, using time-lapse [Ca^{2+}]$_{ER}$ measurements. At 100 μM concentration, compounds **13** and **14**, showed a clear activation effect against sfRyR, which reduced the [Ca^{2+}]$_{ER}$ by 37.1 and 36.2%, respectively (**Figure 6A**). While their effect in intracellular Ca2 release is similar to that of the positive control chlo, the release rate is much slower (**Figure 6B**) suggesting different binding sites and different mechanisms of action on the sfRyR. Compounds **1**, **2**, and **3** also showed some weak activation effects on sfRyR (**Figure 6A**). The species selectivity of **13** and **14** was further characterized by comparing their activity against rabbit RyR1 (rRyR1). Interestingly, both compounds showed no clear activation activity on rRyR1, suggesting that they can selectively act on insect RyRs and have good potential to be developed into insecticidal molecules (**Figure 6C**).

CONCLUSION

In summary, 19 quinazoline-containing indole alkaloids (**1–19**), including 3 new ones, were isolated from the marine-derived fungus *Aspergillus* sp. HNMF114 by supplemented L-tryptophan to its fermentation broth. Among them, compounds **10** and **16** showed α-glucosidase inhibitory activity, that significant activity with potential for further development. Compounds **1**, **2**, and **3** showed weak activities against sfRyR, and **13** and **14** showed moderate activities against sfRyR. Compounds **13** and **14** also have no clear activation activity on rRyR1, which means **13** and **14** could selectively act on insect RyRs and have good potential for the development of insecticidal drugs.

DATA AVAILABILITY STATEMENT

The original contributions presented in the study are included in the article/**Supplementary Material**, further inquiries can be directed to the corresponding authors.

AUTHOR CONTRIBUTIONS

Y-XZ and D-QL contributed to the conception and design of the study. LYan and F-DK determined the plane structure and absolute configuration. S-SL wrote the first draft of the manuscript and performed all of the experimental work. Q-YM and Q-YX contributed to the isolation of compounds. J-HZ, LYao, and L-MZ contributed to the bioactivity assay. Z-GYC and H-FD improved

the manuscript. All authors contributed to manuscript revision as well as read and approved the submitted version.

SUPPLEMENTARY MATERIAL

The Supplementary Material for this article can be found online at: https://www.frontiersin.org/articles/10.3389/fmicb.2021.680879/full#supplementary-material

REFERENCES

Apostolidis, E., Kwon, Y. I., and Shetty, K. (2007). Inhibitory potential of herb, fruit, and fungal-enriched cheese against key enzymes linked to type 2 diabetes and hypertension. *Innov. Food Sci. Emerg.* 1, 46–54. doi: 10.1016/j.ifset.2006.06.001

Arasu, M. V., Duraipandiyan, V., and Ignacimuthu, S. (2013). Antibacterial and antifungal activities of polyketide metabolite from marine *Streptomyces* sp. AP-123 and its cytotoxic effect. *Chemosphere* 90, 479–487. doi: 10.1016/j.chemosphere.2012.08.006

Blunt, J. W., Copp, B. R., Keyzers, R. A., Munro, M. H., and Prinsep, M. R. (2017). Marine natural products. *Nat. Prod. Rep.* 34, 235–294. doi: 10.1039/C7NP00052A

Bruhn, T., Schaumloffel, A., Hemberger, Y., and Bringmann, G. (2013). SpecDis: quantifying the comparison of calculated and experimental electronic circular dichroism spectra. *Chirality* 25, 243–249. doi: 10.1002/chir.22138

Bugni, T. S., and Ireland, C. M. (2004). Marine-derived fungi: a chemically and biologically diverse group of microorganisms. *Nat. Prod. Rep.* 21, 143–163. doi: 10.1039/b301926h

Buttachon, S., Chandrapatya, A., Manoch, L., Silva, A., Gales, L., Bruyére, C., et al. (2012). Sartorymensin, a new indole alkaloid, and new analogues of tryptoquivaline and fiscalins produced by *Neosartorya siamensis* (KUFC 6349). *Tetrahedron* 68, 3253–3262. doi: 10.1016/j.tet.2012.02.024

Dan, W. J., Zhang, Q., Zhang, F., Wang, W. W., and Gao, J. M. (2019). Benzonate derivatives of acetophenone as potent α-glucosidase inhibitors: synthesis, structure-activity relationship and mechanism. *J. Enzyme Inhib. Med. Chem.* 34, 937–945. doi: 10.1080/14756366.2019.1604519

Eisenberg, D., Luthy, R., and Bowie, J. U. (1997). VERIFY3D: assessment of protein models with three-dimensional profiles. *Method. Enzymol.* 277, 396–404. doi: 10.1016/s0076-6879(97)77022-8

Frisch, M. J., Trucks, G. W., Schlegel, H. B., Scuseria, G. E., Robb, M. A., Cheeseman, J. R., et al. (2019). *Gaussian 16, Revision C.01*. Wallingford CT: Gaussian, Inc.

Grimblat, N., Zanardi, M. M., and Sarotti, A. M. (2015). Beyond DP4: an improved probability for the stereochemical assignment of isomeric compounds using quantum chemical calculations of NMR shifts. *J. Org. Chem.* 80, 12526–12534. doi: 10.1021/acs.joc.5b02396

Guo, Y. W., Liu, X. J., Yuan, J., Li, H. J., Mahmud, T., Hong, M. J., et al. (2020). L-tryptophan induces a marine-derived *Fusarium* sp. to produce indole alkaloids with activity against the Zika Virus. *J. Nat. Prod.* 11, 3372–3380. doi: 10.1021/acs.jnatprod.0c00717

Huang, L. H., Xu, M. Y., Li, H. J., Li, J. Q., Chen, Y. X., Ma, W. Z., et al. (2017). Amino acid-directed strategy for inducing the marine-derived fungus *Scedosporium apiospermum* F41-1 to maximize alkaloid diversity. *Org. Lett.* 19, 4888–4891. doi: 10.1021/acs.orglett.7b02238

Kong, F. D., Zhang, S. L., Zhou, S. Q., Ma, Q. Y., Xie, Q. Yi, Chen, J. P., et al. (2019). Quinazoline-containing indole alkaloids from the marine-derived fungus *Aspergillus* sp. HNMF114. *J. Nat. Prod.* 82, 3456–3463. doi: 10.1021/acs.jnatprod.9b00845

Koyama, N., Inoue, Y., Sekine, M., Hayakawa, Y., Homma, H., Omura, S., et al. (2008). Relative and absolute stereochemistry of quinadoline B, an inhibitor of lipid droplet synthesis in macrophages. *Org. Lett.* 22, 5273–5276. doi: 10.1021/ol802089p

Laskowski, R. A., Macarthur, M. W., Moss, D. S., and Thornton, J. M. (1993). PROCHECK: a program to check the stereochemical quality of protein structures. *J. Appl. Cryst.* 26, 283–291. doi: 10.1107/S0021889892009944

Lin, T., Tan, T., and Liu, T. X. (2013). A study on secondary metabolites PJX-41 mangrove-derived fungi and their antitumor activity. *J. Nanjing Agric. Univ.* 3, 117–123. doi: 10.7685/j.issn.1000-2030.2013.03.020

Manimegalai, K., Devi, N. K. A., and Padmavathy, S. (2013). Marine fungi as a source of secondary metabolites of antibiotics. *Int. J. Biotechnol. Bioeng. Res.* 4, 275–282.

Montaser, R., and Luesch, H. (2011). Marine natural products: a new wave of drugs. *Future Med. Chem.* 3, 1475–1489. doi: 10.4155/fmc.11.118

O'Boyle, N. M., Vandermeersch, T., Flynn, C. J., Maguire, A. R., and Hutchison, G. R. (2011). Confab–systematic generation of diverse low-energy conformers. *J. Cheminform.* 3:8. doi: 10.1186/1758-2946-3-8

Peng, J. X., Lin, T., Wang, W., Xin, Z. H., Zhu, T. J., Gu, Q. Q., et al. (2013). Antiviral alkaloids produced by the mangrove-derived fungus *Cladosporium* sp. PJX-41. *J. Nat. Prod.* 76, 1133–1140. doi: 10.1021/np400200k

Penn, J., Mantle, P. G., Bilton, J. N., and Sheppard, R. N. (1992). Glyantrypine, a novel anthranilic acid-containing metabolite of *Aspergillus clavatus*. *J. Chem. Soc. Pak.* 1, 1495–1496. doi: 10.1039/P19920001495

Qian, S. Y., Yang, C. L., Khan, A., Chen, R. X., Wu, M. S., Tuo, L., et al. (2018). New pyrazinoquinazoline alkaloids isolated from a culture of *Stenotrophomonas maltophilia* QB-77. *Nat. Prod. Res.* 9, 1387–1391. doi: 10.1080/14786419.2018.1475381

Shen, S., Li, W., Ouyang, M. A., Wu, Z. J., Lin, Q. Y., and Xie, L. H. (2009). Identification of two marine fungi and evaluation of their antivirus and antitumor activities. *Acta. Microbiol. Sin.* 49, 1240–1246. doi: 10.13343/j.cnki.wsxb.2009.09.008

Suzuki, J., Kanemaru, K., Ishii, K., Ohkura, M., Okubo, Y., Iino, M., et al. (2014). Imaging intraorganellar Ca2+ at subcellular resolution using CEPIA. *Nat. Commun.* 5, 4153–4165. doi: 10.1038/ncomms5153

Trott, O., and Olson, A. J. (2010). AutoDock vina: improving the speed and accuracy of docking with a new scoring function, efficient optimization, and multithreading. *J. Comput. Chem.* 31, 455–461. doi: 10.1002/jcc.21334

Webb, B., and Sali, A. (2016). Comparative protein structure modeling using MODELLER. *Curr. Protoc. Bioinformatics* 54, 5.6.1–5.6.37. doi: 10.1002/cpbi.3

Wu, M., and Ma, D. (2013). Total syntheses of (±)-spiroquinazoline, (-)-alantryphenone, (+)-lapatin A, and (-)-quinadoline B. *Angew. Chem. Int. Ed.* 52, 9759–9762. doi: 10.1002/anie.201303893

Xiong, Z. Q., Wang, J. F., Hao, Y. Y., and Wang, Y. (2013). Recent advances in the discovery and development of marine microbial natural products. *Mar. Drugs* 11, 700–717. doi: 10.3390/md11030700

Check for
updates

Evaluation of Laccase Activities by Three Newly Isolated Fungal Species in Submerged Fermentation With Single or Mixed Lignocellulosic Wastes

Mei-Ling Han[1,2,3], Jing Yang[1], Ze-Yang Liu[1], Chun-Rui Wang[1], Si-Yu Chen[1], Ning Han[1], Wen-Yao Hao[1], Qi An[1,2]* and Yu-Cheng Dai[4]*

[1] College of Life Sciences, Langfang Normal University, Langfang, China, [2] Technical Innovation Center for Utilization of Edible and Medicinal Fungi in Hebei Province, Langfang, China, [3] Edible and Medicinal Fungi Research and Development Center of Universities, Colleges in Hebei Province, Langfang, China, [4] Beijing Advanced Innovation Center for Tree Breeding By Molecular Design, Beijing Forestry University, Beijing, China

Three newly isolated fungal species, namely, *Cerrena unicolor* Han 849, *Lenzites betulina* Han 851, and *Schizophyllum commune* Han 881, isolated from their native habitats in Wulingshan National Nature Reserve of Hebei Province of northern China, were screened for laccase production with single or mixed lignocellulosic wastes. *C. unicolor* Han 849 was found to express the highest levels of laccase with single or mixed lignocellulosic wastes compared with *L. betulina* Han 851 and *S. commune* Han 881. The highest laccase activity from the mixed fungal culture of *C. unicolor* Han 849 and *S. commune* Han 881 or *L. betulina* Han 851 on *Firmiana platanifolia* was 1,373.12 ± 55.93 and 1,144.85 ± 34.97 U/L, respectively, higher than that from other tested conditions. *L. betulina* Han 851 or *S. commune* Han 881 mixed with other species was also helpful for accelerating laccase secretion due to reach maximum enzyme activity quickly. The treatment of mixing different species, including the mixture of two or three species, was obviously conducive to the improvement of laccase activity on *Firmiana platanifolia*. These results revealed that the fungal co-culture and the mixed lignocellulosic wastes contribute to the improvement of laccase activities and enhance laccase activities within a short period. These findings would be helpful for providing a new method for rapid production of low-cost laccase and for optimization of integrated industrial laccase production.

Keywords: laccase activity, co-culture, single lignocellulosic waste, mixed lignocellulosic wastes, submerged fermentation

INTRODUCTION

The rapid development of agriculture and forestry is conducive to economic development and environmental protection. Meanwhile, it also brings some environmental problems, and the most important is agricultural and forestry residues. Also, if agricultural and forestry waste is burned, it will cause even more serious air pollution. Agricultural and forestry waste is an important kind

of lignocellulosic biomass. Lignocellulosic biomass, versatile and most abundant natural renewable resources, have attracted more attention and considerable interest due to their abilities to convert into green second-generation energy fuels and valued industrial chemicals *via* the various bio-treatment process of lignocellulosic biomass (Haldar et al., 2016; Pinar et al., 2017; An et al., 2020b; Gaikwad and Meshram, 2020). Using various lignocellulosic wastes, such as corncob, cottonseed hull, bamboos, coffee shell, and tree leaves, to produce enzymes (especially laccase) had been widely investigated in recent years due to the low-cost and vast amounts of lignocellulosic wastes (Lizardi-Jimenez et al., 2019; Thamvithayakorn et al., 2019; Wang et al., 2019; Agrawal and Verma, 2020; Atilano-Camino et al., 2020; Pinheiro et al., 2020; Xu et al., 2020).

Laccase (EC 1.10.3.2, *p*-benzenediol: oxygen oxidoreductase) belongs to a family of copper oxidases and widely distributes in various higher plants, fungi, bacteria, and some insects (Zhang et al., 2020). Due to the ability of laccase to oxidize a wide range of phenolic and non-phenolic compounds, laccase can be used in the various biotechnological process, including materials science, bioremediation, biofuels, fiber modified, nanobiotechnology, biosensor, food chemistry, paper and pulp industry, and biodegradation (Yang et al., 2017; Becker and Wittmann, 2019; Bilal et al., 2019; Singh and Arya, 2019; Unuofin et al., 2019a; Wang et al., 2019; Zerva et al., 2019; An et al., 2020a). White-rot fungi, belonging to basidiomycetes, are well known for their essential role in degrading lignocellulose in their native habitats due to their ability to secrete various extracellular ligninolytic enzymes (Thamvithayakorn et al., 2019). Among ligninolytic enzymes, laccase is the oldest and important enzyme that could degrade lignin. Meanwhile, white-rot fungi are considered the famous laccase producer, and almost all species among them have the capacity for secreting laccase to some extent (Agrawal et al., 2018; An et al., 2019; Huang et al., 2019; Lira-Perez et al., 2020).

Due to its wide application in numerous fields of biotechnology, more and more researchers have shown great interest in all aspects of laccase (Ma and Ruan, 2015; Wang et al., 2015; An et al., 2016a, 2018; Rodriguez et al., 2019; Zhang et al., 2020). Meanwhile, large amounts of laccase with low cost were required for the widespread use of laccase in the various biotechnological process (Osma et al., 2011; An et al., 2018; Zerva et al., 2019; Zhang et al., 2020). To enhance the laccase production and reduce the cost of producing laccase, optimization of fermentation condition, fermentation method, and developing new productivity strains are very effective methods. Optimization of fermentation condition was mainly included the following categories: (1) category, concentration, and proportion of carbon and nitrogen sources (Kannaiyan et al., 2012; Birhanli and Yeşilada, 2013; Zhou et al., 2014; Han et al., 2017, 2020b; Palazzolo et al., 2019; Thamvithayakorn et al., 2019; Unuofin et al., 2019b); (2) metal ions, such as copper ion, ferrous ion, manganese ion, silver ion, zinc ion, and magnesium ion (Hu et al., 2014; Yang et al., 2016; Zhuo et al., 2017; Xu et al., 2018; An et al., 2020a); (3) temperature and pH (Hu et al., 2014; Kaira et al., 2015; Mazlan and Abu Hanifah, 2017; Saoudi et al., 2017; Bettin et al., 2019); and (4) secondary metabolites, e.g., ferulic acid and veratrol (Janusz et al., 2015; Yang et al., 2016). The fermentation

method was divided into solid-state fermentation, submerged fermentation, and unconventional solid-state fermentation combined with agitated submerged fermentation (An et al., 2016b). The advantage of solid-state fermentation is that it is closer to the natural environment of fungi and more energy-efficient, such as using less water. The advantage of submerged fermentation is that it is more manageable and durable, and industrial applications were more preferred to submerged fermentation. Different species or different strains belonging to the same species affected the laccase activity significantly (Janusz et al., 2015; An et al., 2020a). Thus, developing new strains with the capacity of producing laccase is very meaningful work.

Previous studies had indicated the capacity of secreting laccase by *Cerrena unicolor* (Mazur et al., 2015; Songulashvili et al., 2015; Wang et al., 2017; Zhang et al., 2018). However, the ability to secrete laccase from *Lenzites betulinus* and *Schizophyllum* sp. had not been reported. Co-culture of fungi has been studied in recent years and has a good effect on secreting laccase, whereas almost all studies investigated the white-rot fungi combined with mycete or yeasts to produce laccase (Rodriguez et al., 2019; Lira-Perez et al., 2020; Zhang et al., 2020). The effect of using two or three white-rot fungi combined with each other to produce laccase was rarely investigated (Kuhar et al., 2015; Vibha and Negi, 2018). Most studies had used only one lignocellulosic material to explore the effect on laccase secreted by fungi, and very few had considered using a mixture of two lignocellulosic materials to explore the effect on laccase secretion by fungi (Lallawmsanga, Leo et al., 2019; Thamvithayakorn et al., 2019; Unuofin et al., 2019b; Gaikwad and Meshram, 2020; Xu et al., 2020). However, evaluation of laccase activities from *C. unicolor*, *Lenzites betulinus*, and *Schizophyllum* sp. had not been investigated till now, not only the effects of co-culture of these species but also the effects of mixed lignocellulosic wastes on their enzyme production. Under the circumstances, the laccase production capacity of three newly isolated fungal species with single or mixed lignocellulosic wastes was analyzed in the present work. Also, the effect of co-culture of these species on laccase activity was investigated at the same time. The results were contributed to provide new methods to improve laccase production and obtain low-cost laccase.

MATERIALS AND METHODS

Culture of Microorganisms

Three fungal species, *C. unicolor* Han 849, *Lenzites betulina* Han 851, and *Schizophyllum* sp. Han 881, were newly isolated from their native habitats in Wulingshan National Nature Reserve of Hebei Province of northern China. These species were isolated and purified on complete yeast medium (CYM), and the pure cultures of these species were preserved on malt extract agar medium at 4°C in the College of Life Science, Langfang Normal University.

Collection of Lignocellulosic Wastes

Lignocellulosic wastes, *Pinus tabuliformis* and *Firmiana platanifolia*, were obtained from Chengde city (Hebei province,

China). All these lignocellulosic wastes were air-dried and milled to a particle size of between 20 and 60 mesh.

Microbial Culture and Inoculum Preparation

To activate the used three strains, all microorganisms were incubated on CYM for 7 days at 26°C. Then, five inoculants holed by a perforator with a diameter of 5 mm from corresponding Petri plates were placed in 250-ml flasks containing 100 ml of CYM without agar. All flasks were cultured in an oscillating culture shaker with a speed of 150 rpm at 26°C. After 7 days, the mycelium pellets in the Erlenmeyer flask were homogenized by modular homogenizer HFJ-10 (Tianjin HengAo Technology Co., Ltd.) at 5,000 rpm for 2 min. Also, the homogenized liquid was used as an inoculum.

Time Course of Laccase Activity

Erlenmeyer flasks (250 ml) containing 2-g single lignocellulosic waste or mixed with two kinds of lignocellulosic wastes were soaked with 100 ml of solution (1.5-g monopotassium phosphate dissolved into 1 L of deionized water) and autoclaved at 121°C for 30 min. All flasks were sterilized at 121°C for 30 min. After autoclaving, each Erlenmeyer flasks was added to the 3 ml of homogenized inoculum according to the list in **Table 1**. Then, all flasks were transferred to a rotary shaker (26°C, 150 rpm) for various fermentation times.

Preparation of Crude Enzyme

To obtain the crude enzyme solution, the liquid in the Erlenmeyer flask at different fermentation times was filtered through a filter paper. The obtained filtrate was centrifuged at 4°C with a speed of 12,000 rpm for 20 min, and the supernatant was used for the determination of laccase activity.

Assay of Laccase Activity

Laccase activity was assayed using 2,2′-azinobis-[3-ethyltiazoline-6-sulfonate] as substrate and monitored by an iMark^{TM} microplate absorbance reader (Bio-Rad, Hercules, CA, United States). The details of the reaction mixture involving the amount of each component and the process of determining laccase at 415 nm were referred to in the method of Han et al. (2020b). One unit of laccase activity was defined as the amount of enzyme required to oxidize 1 μmol of 2,2′-azinobis-[3-ethyltiazoline-6-sulfonate] per minute (ϵ_{415} = 3.16 × 10^4 M^{-1} cm^{-1}).

Data Analysis

Results in this study were the mean values of triplicate experiments. Two-way analysis of variance followed by the Tukey *post-hoc* test was applied to examine the effects of lignocellulosic wastes and species on laccase activities according to An et al. (2020a,b), and the analysis of statistical tests was performed by SPSS software version 22.0 (PROC GLM, IBM SPSS software version 22.0, Armonk, NY, United States). All colorful figures were generated by Origin 2016 software (OriginLab Corporation, Northampton, MA, United States).

TABLE 1 | Description of each component of the experimental group.

Species	Lignocellulosic wastes	Solution (ml)	Homogenized inoculum
Cerrena unicolor Han 849	*Pinus tabuliformis* 2 g	100	3 ml
	Firmiana platanifolia 2 g	100	3 ml
	Pinus tabuliformis 1 g and *Firmiana platanifolia* 1 g	100	3 ml
Lenzites betulina Han 851	*Pinus tabuliformis* 2 g	100	3 ml
	Firmiana platanifolia 2 g	100	3 ml
	Pinus tabuliformis 1 g and *Firmiana platanifolia* 1 g	100	3 ml
Schizophyllum sp. Han 881	*Pinus tabuliformis* 2 g	100	3 ml
	Firmiana platanifolia 2 g	100	3 ml
	Pinus tabuliformis 1 g and *Firmiana platanifolia* 1 g	100	3 ml
C. unicolor Han 849 and *L. betulina* Han 851	*Pinus tabuliformis* 2 g	100	1.5 ml of Han 849 and 1.5 ml of Han 851
	Firmiana platanifolia 2 g	100	1.5 ml of Han 849 and 1.5 ml of Han 851
	Pinus tabuliformis 1 g and *Firmiana platanifolia* 1 g	100	1.5 ml of Han 849 and 1.5 ml of Han 851
C. unicolor Han 849 and *Schizophyllum* sp. Han 881	*Pinus tabuliformis* 2 g	100	1.5 ml of Han 849 and 1.5 ml of Han 881
	Firmiana platanifolia 2 g	100	1.5 ml of Han 849 and 1.5 ml of Han 881
	Pinus tabuliformis 1 g and *Firmiana platanifolia* 1 g	100	1.5 ml of Han 849 and 1.5 ml of Han 881
L. betulina Han 851 and *Schizophyllum* sp. Han 881	*Pinus tabuliformis* 2 g	100	1.5 ml of Han 851 and 1.5 ml of Han 881
	Firmiana platanifolia 2 g	100	1.5 ml of Han 851 and 1.5 ml of Han 881
	Pinus tabuliformis 1 g and *Firmiana platanifolia* 1 g	100	1.5 ml of Han 851 and 1.5 ml of Han 881
C. unicolor Han 849, *L. betulina* Han 851 and *Schizophyllum* sp. Han 881	*Pinus tabuliformis* 2 g	100	1.0 ml of Han 849, 1.0 ml of Han 851 and 1.0 ml of Han 881
	Firmiana platanifolia 2 g	100	1.0 ml of Han 849, 1.0 ml of Han 851 and 1.0 ml of Han 881
	Pinus tabuliformis 1 g and *Firmiana platanifolia* 1 g	100	1.0 m of Han 849, 1.0 ml of Han 851 and 1.0 ml of Han 881

Identification of the Fungus *Schizophyllum* sp. Han 881

Mycelia of *Schizophyllum* sp. Han 881 used for DNA extraction was grown on CYM medium for 7 days. An appropriate amount of mycelium was scraped by a sterile surgical blade, transferred into the EP tube, and ground by a TGrinder OSE-Y30 Tissue Homogenizer (Tiangen Biotech Co., Ltd., Beijing, China). The genomic DNA of *Schizophyllum* sp. Han 881 was extracted by cetyltrimethylammonium bromide rapid plant genome extraction kit-DN14 (Aidlab Biotechnologies Co., Ltd., Beijing, China) according to the instructions with some modifications (Han et al., 2016, 2020a). The primer pairs and PCR reaction schedule for amplifying the internally transcribed spacer regions of ribosomal DNA of Han 881 were referred to the method of Han et al. (2021b). The PCR products were sequenced with the same primer pairs and measured at Beijing Genomics Institute (Beijing, China). The sequence was analyzed and submitted to GenBank. Phylogenetic analysis followed Han et al. (2016). Maximum parsimony analysis was performed in PAUP* version 4.0b10 (Swofford, 2002). All characters were equally weighted, and gaps were treated as missing data. Trees were inferred using the heuristic search option with TBR branch swapping and 1,000 random sequence additions. Max trees were set to 5,000, branches of zero length were collapsed, and all parsimonious trees were saved. Clade robustness was assessed using a bootstrap analysis with 1,000 replicates (Felsenstein, 1985). Branches that received bootstrap values for MP greater than or equal to 75% were considered as significantly supported. Phylogenetic trees were visualized using Treeview (Page, 1996).

RESULTS

Molecular Biological Results of Fungus *Schizophyllum* sp. Han 881

The GenBank number of its sequence for Han 881 was MW 767989. The fungus *Schizophyllum* sp. Han 881 was grouped with samples of *Schizophyllum commune* downloaded from GenBank in the internally transcribed spacer phylogenetic tree (**Figure 1**) and then was identified as *S. commune*.

Statistical Analysis Results

As shown in **Table 2**, the effect of species on laccase activity was significant ($P < 0.001$) during the whole process of submerged fermentation. Lignocellulosic wastes affected the laccase activity throughout the submerged fermentation phase ($P < 0.001$). Furthermore, the interaction of species and lignocellulosic wastes on laccase activity was significant in the whole fermentation stage ($P < 0.001$).
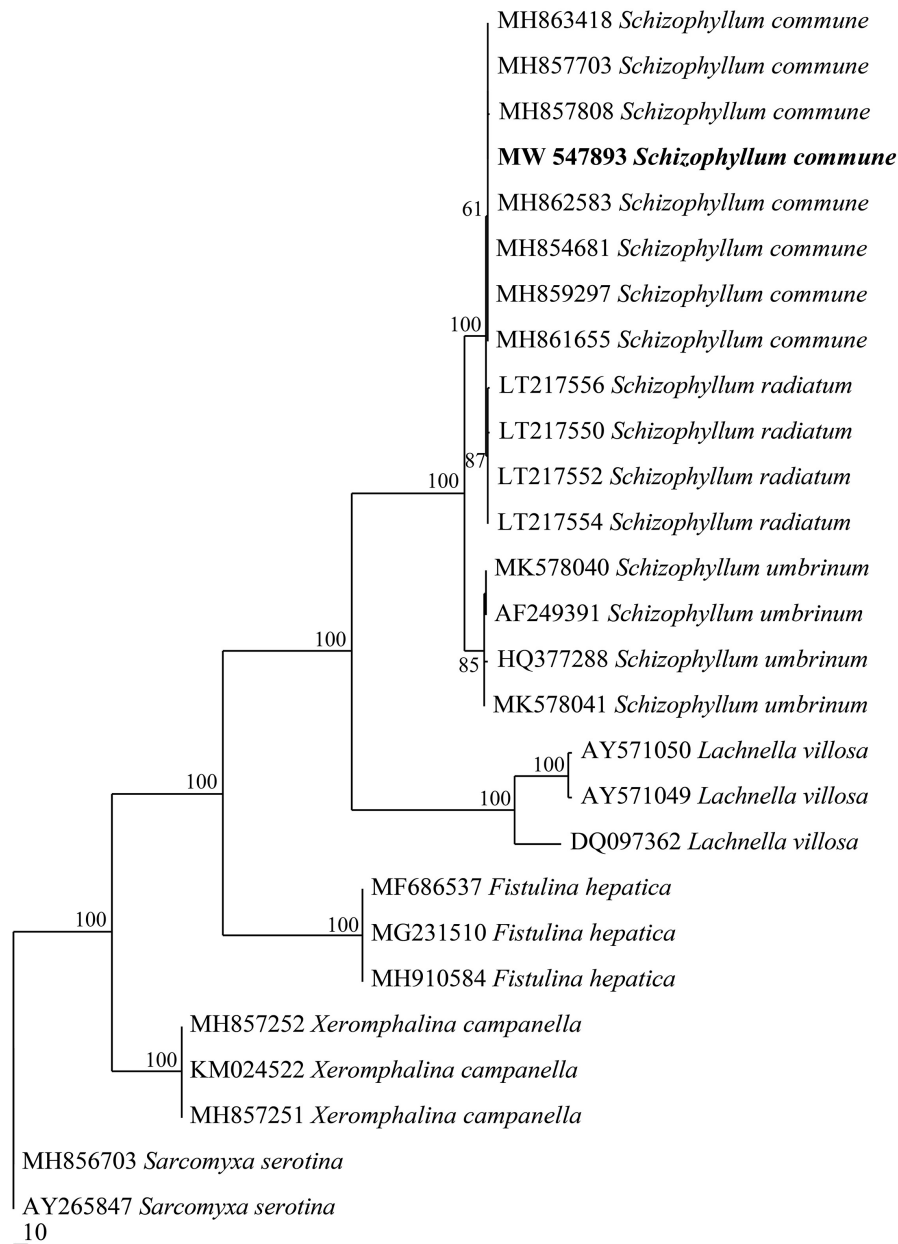
Evaluation of Laccase Activity From Single or Mixed Fungal Species on *Pinus tabuliformis*

In terms of the value of laccase activity on the first day, laccase activity values from *C. unicolor* Han 849, *L. betulina* Han 851, *S. commune* Han 881, a mixture of Han 849 and Han 881, a

mixture of Han 851 and Han 881, a mixture of Han 849 and Han 851, and a mixture of Han 849, Han 851, and Han 881 were 42.29 ± 3.83, 0, 0, 48.52 ± 3.78, 14.47 ± 1.31, 24.01 ± 0.46, and 9.54 ± 0.46 U/L, respectively (**Supplementary Tables 1–7**). Based on this, a mixture of Han 849 and Han 881 was helpful to enhance the laccase activity. Laccase activity from *C. unicolor* Han 849 was 223.53 ± 21.06 U/L on the 2nd day, higher than others (**Table 3**). The first appearance time of laccase activity from *L. betulina* Han 851 was on the fourth day, and a corresponding value of laccase activity was only 8.54 ± 0.70 U/L (**Supplementary Table 2**). The laccase activity from *S. commune* Han 881 was only detected on the third day, which was only 1.51 ± 0.00 U/L (**Supplementary Table 3**). Maximum laccase activity from *C. unicolor* Han 849 was 223.53 ± 21.06 U/L on day 2, which was higher than that from *L. betulina* Han 851 (36.57 ± 3.39 U/L, day 6), *S. commune* Han 881 (1.51 ± 0.00 U/L, day 3), a mixture of Han 849 and Han 881 (219.41 ± 11.63 U/L, day 7), a mixture of Han 851 and Han 881 (96.04 ± 3.93 U/L, day 4), a mixture of Han 849 and Han 851 (60.38 ± 2.93 U/L, day 4), and a mixture of Han 849, Han 851, and Han 881 (44.71 ± 1.36 U/L, day 2), nearly 6.11, 148. 03−, 1. 02−, 2. 33−, 3. 70−, and 5.00-fold, respectively (**Table 3**). The enzyme production trend of *C. unicolor* Han 849, *S. commune* Han 881, a mixture of Han 851 and Han 881, a mixture of Han 849 and Han 851 (60.38 ± 2.93 U/L, day 4), and a mixture of Han 849, Han 851, and Han 881 (44.71 ± 1.36 U/L, day 2) was similar, and the maximum laccase activity appeared in the early fermentation stage (day ≤ 4). However, the trend of producing laccase from *C. unicolor* Han 849 and a mixture of Han 849, Han 851, and Han 881 was similar, and corresponding maximum laccase activity appeared in the intermediate stage of fermentation (day ≥ 6) (**Figure 2**). Compared with the single *L. betulina* Han 851 or *S. commune* Han 881, *L. betulina* Han 851 or *S. commune* Han 881 mixed with other species, e.g., a mixture of Han 849 and Han 881, a mixture of Han 851 and Han 881, a mixture of Han 849 and Han 851, and a mixture of Han 849, Han 851, and Han 881, were helpful for improving laccase activity based on the value of maximum laccase activity (**Figure 2**). Also, the time of maximum laccase activity from *L. betulina* Han 851 or *S. commune* Han 881 mixed with other species was earlier than that from single *L. betulina* Han 851 or *S. commune* Han 881 (**Figure 2**). Meanwhile, *L. betulina* Han 851 or *S. commune* Han 881 mixed with other species was also helpful for accelerating laccase secretion due to the first time laccase was detected (**Figure 2**).

Evaluation of Laccase Activity From Single or Mixed Fungal Species on *Firmiana platanifolia*

Laccase activity values from *C. unicolor* Han 849, *L. betulina* Han 851, *S. commune* Han 881, a mixture of Han 849 and Han 881, a mixture of Han 851 and Han 881, a mixture of Han 849 and Han 851, and a mixture of Han 849, Han 851, and Han 881 were 20.90 ± 1.94, 2.01 ± 0.17, 0, 206.95 ± 12.14, 15.47 ± 0.97, 88.71 ± 6.19, and 9.34 ± 0.52 U/L, respectively, on the first day (**Supplementary Tables 1–7**). Obviously, laccase activity values

FIGURE 1 | Maximum parsimony strict consensus tree illustrating the phylogeny of *Schizophyllum commune* and related species based on internally transcribed spacer sequence data. Branches are labeled with parsimony bootstrap proportions high than 50%.

from a mixture of Han 849 and Han 881 were nearly 9. 90−, 102. 96−, 13. 38−, 2. 33−, and 22.16-fold higher than that from *C. unicolor* Han 849, *L. betulina* Han 851, a mixture of Han 851 and Han 881, a mixture of Han 849 and Han 851, and a mixture of Han 849, Han 851, and Han 881, respectively. Maximum laccase activity values from a mixture of Han 849 and Han 881 (1,373.12 ± 55.93 U/L, day 6), which was higher than that from *C. unicolor* Han 849 (552.34 ± 49.14 U/L, day 3), *L. betulina* 851 (309.72 ± 12.53 U/L, day 7), *S. commune* Han 881 (5.22 ± 0.35 U/L, day 7), a mixture of Han 851 and Han 881 (549.83 ± 12.42 U/L, day 5), a mixture of Han 849 and Han 851 (1144.85 ± 34.97

U/L, day 10), and a mixture of Han 849, Han 851, and Han 881 (774.96 ± 13.79 U/L, day 10), nearly 2. 49−, 4. 43−, 263. 05−, 2. 50−, 1. 20−, and 1.77−fold, respectively (**Table 3**). Based on this, it was obvious that the treatment of mixing different species, whether the mixture of two or three species, was conducive to the improvement of laccase activity. Meanwhile, the treatment of mixing different species was helpful for occurring the continuous, higher, and stable laccase activity throughout the fermentation stage (**Figure 3**). Another, the capacity of secreting laccase by *C. unicolor* Han 849 was superior to *L. betulina* Han 851 and *S. commune* Han 881.

TABLE 2 | Two-way ANOVA of variance to examine the effects of species, lignocellulosic wastes, and the interactions of species and lignocellulosic wastes on laccase activity.

Incubation Period (d)	Species	Lignocellulosic wastes	Species × lignocellulosic wastes
1	680.059***	606.774***	577.374***
2	1463.494***	2439.607***	733.093***
3	1677.145***	2447.436***	364.129***
4	2883.911***	4248.612***	734.370***
5	1339.770***	3504.977***	352.862***
6	1737.832***	3543.392***	387.125***
7	668.056***	2097.517***	181.140***
8	866.986***	3181.248***	299.093***
9	1010.451***	3565.245***	486.254***
10	1152.112***	4664.800***	740.748***

df = 6, 2, 12; ***P < 0.001.

Evaluation of Laccase Activity From Single or Mixed Fungal Species on a Mixture by *Pinus tabuliformis* and *Firmiana platanifolia*
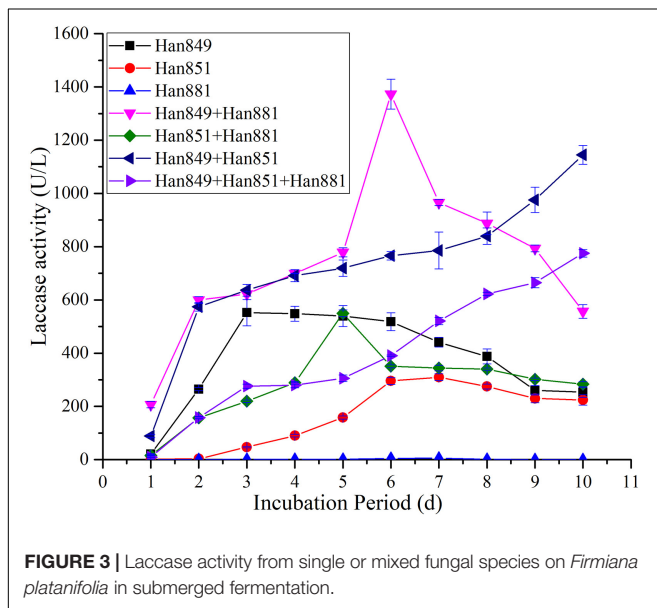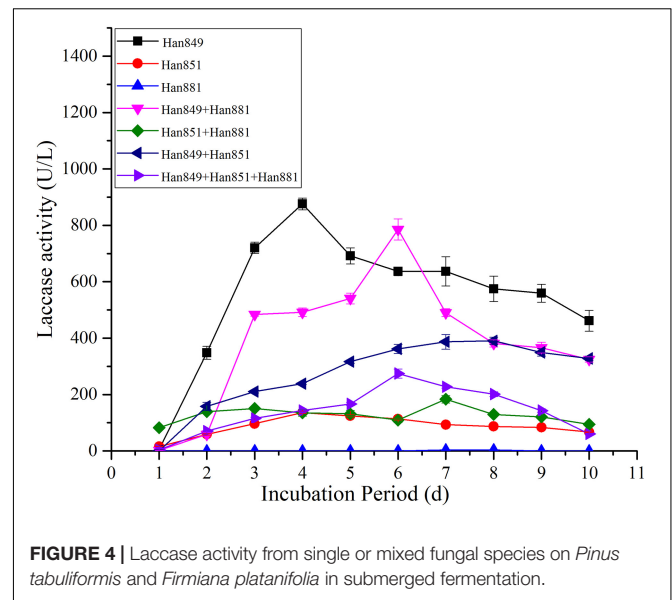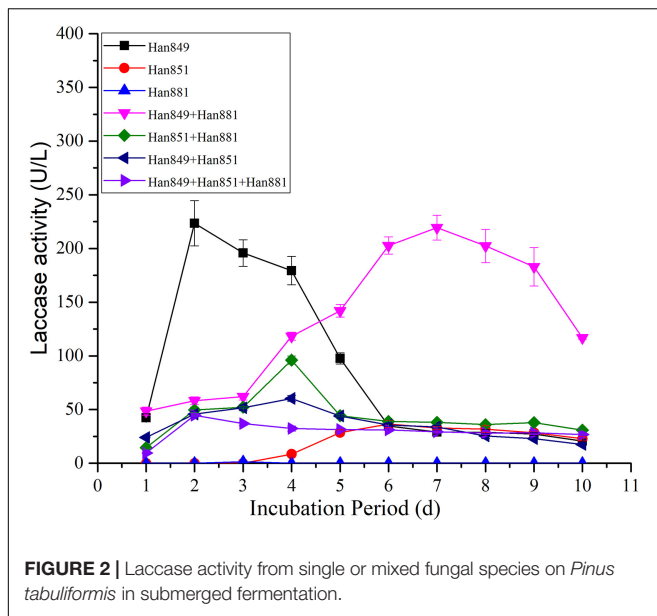
Laccase activity values from *C. unicolor* Han 849, *L. betulina* Han 851, *S. commune* Han 881, a mixture of Han 849 and Han 881, a mixture of Han 851 and Han 881, a mixture of Han 849 and Han 851, and a mixture of Han 849, Han 851, and Han 881 were 5.32 ± 0.17, 15.67 ± 0.52, 0.00, 1.51 ± 0.00, 82.38 ± 4.44, 0.00, and 3.72 ± 0.35 U/L on the first day (**Supplementary Tables 1–7**). Maximum laccase activity from *C. unicolor* Han 849 (876.23 ± 20.82 U/L, day 4), which was higher than that from *L. betulina* Han 851 (136.23 ± 3.67 U/L, day 4), *S. commune* Han 881 (3.32 ± 0.30 U/L, day 8), a mixture of Han 849 and Han 881 (785.61 ± 37.51 U/L, day 6), a mixture of Han 851 and Han 881 (183.34 ± 13.13 U/L, day 7), a mixture of Han 849 and Han 851 (390.30 ± 12.89 U/L, day 8), and a mixture of Han 849, Han 851, and Han 881 (274.46 ± 16.10 U/L, day 6), nearly 6. 43−, 263. 92−, 1. 12−, 4. 78−, 2. 25−, and 3.19-fold, respectively (**Table 3**). The enzyme production trend of *C. unicolor* Han 849 and *L. betulina* Han 851 was similar, and the maximum laccase activity appeared in the early fermentation stage (day ≤ 4). In contrast, the trend of producing laccase from *S. commune* Han 881, a mixture of Han 849 and Han 881, a mixture of Han 851 and Han 881, a mixture of Han 849 and Han 851, and a mixture of Han 849, Han 851, and Han 881 was similar, and corresponding maximum laccase activity appeared in the intermediate stage of fermentation (day ≥ 6) (**Figure 4**). Compared with the single *L. betulina* Han 851, *L. betulina* Han 851 mixed with other species, e.g., a mixture of Han 851 and Han 881, a mixture of Han 849 and Han 851, and a mixture of Han 849, Han 851, and Han 881, were helpful for improving laccase activity based on the value of maximum laccase activity (**Figure 4**). However, the time of maximum laccase activity from *L. betulina* Han 851 mixed with other species was later than that from the condition of single *L. betulina* Han 851 (**Figure 4**).

TABLE 3 | Maximum laccase production, Lignocellulosic wastes, and time of *Cerrena unicolor* Han 849, *Lenzites betulina* Han 851, and *Schizophyllum commune* Han 881.

Maximum laccase production (U/L)	Lignocellulosic wastes	Fungi species	Time (day)
223.53 ± 21.06	*Pinus tabuliformis*	Han 849	2
552.34 ± 49.14	*Firmiana platanifolia*	Han 849	3
876.23 ± 20.82	*Pinus tabuliformis* and *Firmiana platanifolia*	Han 849	4
36.57 ± 3.39	*Pinus tabuliformis*	Han 851	6
309.72 ± 12.53	*Firmiana platanifolia*	Han 851	7
136.23 ± 3.67	*Pinus tabuliformis* and *Firmiana platanifolia*	Han 851	4
1.51 ± 0.00	*Pinus tabuliformis*	Han 881	3
5.22 ± 0.35	*Firmiana platanifolia*	Han 881	7
3.32 ± 0.30	*Pinus tabuliformis* and *Firmiana platanifolia*	Han 881	8
219.41 ± 11.63	*Pinus tabuliformis*	Han 849 and Han 881	7
1, 373.12 ± 55.93	*Firmiana platanifolia*	Han 849 and Han 881	6
785.61 ± 37.51	*Pinus tabuliformis* and *Firmiana platanifolia*	Han 849 and Han 881	6
96.04 ± 3.93	*Pinus tabuliformis*	Han 851 and Han 881	4
549.83 ± 12.42	*Firmiana platanifolia*	Han 851 and Han 881	5
183.34 ± 13.13	*Pinus tabuliformis* and *Firmiana platanifolia*	Han 851 and Han 881	7
60.38 ± 2.93	*Pinus tabuliformis*	Han 849 and Han 851	4
1, 144.85 ± 34.97	*Firmiana platanifolia*	Han 849 and Han 851	10
390.30 ± 12.89	*Pinus tabuliformis* and *Firmiana platanifolia*	Han 849 and Han 851	8
44.71 ± 1.36	*Pinus tabuliformis*	Han 849, Han 851 and Han 881	2
774.96 ± 13.79	*Firmiana platanifolia*	Han 849, Han 851 and Han 881	10
274.46 ± 16.10	*Pinus tabuliformis* and *Firmiana platanifolia*	Han 849, Han 851 and Han 881	6

Data are presented as mean ± standard deviation for triplicates and are expressed as U/L.

FIGURE 2 | Laccase activity from single or mixed fungal species on *Pinus tabuliformis* in submerged fermentation.

FIGURE 4 | Laccase activity from single or mixed fungal species on *Pinus tabuliformis* and *Firmiana platanifolia* in submerged fermentation.

FIGURE 3 | Laccase activity from single or mixed fungal species on *Firmiana platanifolia* in submerged fermentation.

Comparative of Laccase Activity From Single or Mixed Fungal Species on Different Lignocellulosic Wastes

Maximum laccase activity values from *C. unicolor* Han 849 on *P. tabuliformis*, *F. platanifolia*, and a mixture of *P. tabuliformis* and *F. platanifolia* were 223.53 ± 21.06, 552.34 ± 49.14, and 876.23 ± 20.82 U/L, respectively (**Table 3**). Obviously, the presence of mixed lignocellulosic wastes was a benefit for promoting the secretion of laccase by *C. unicolor* Han 849. Furthermore, a continuous and stable laccase activity from *C. unicolor* Han 849 could be achieved on *F. platanifolia*, and a mixture of *P. tabuliformis* and *F. platanifolia* (**Figures 3**, **4**). Apart from *C. unicolor* Han 849, maximum laccase activity

from other conditions on *F. platanifolia* was higher than that from *P. tabuliformis* or a mixture of *P. tabuliformis* and *F. platanifolia*. Maximum laccase activity from *L. betulina* Han 851 on *F. platanifolia* was 309.72 ± 12.53 U/L, nearly 8.47— and 2.27-fold higher than that on *P. tabuliformis* and a mixture of *P. tabuliformis* and *F. platanifolia*, respectively (**Figures 2–4**). Maximum laccase activity from the mixed fungal culture of Han 849 and Han 881 on *F. platanifolia* was 1,373.12 ± 55.93 U/L, nearly 6.26— and 1.75-fold higher than that on *P. tabuliformis* and a mixture of *P. tabuliformis* and *F. platanifolia*, respectively. Maximum laccase activity from the mixed fungal culture of Han 851 and Han 881 on *F. platanifolia* was 549.83 ± 12.42 U/L, nearly 5.73— and 3.00—fold higher than that on *P. tabuliformis* and a mixture of *P. tabuliformis* and *F. platanifolia*, respectively (**Figures 2–4**). Maximum laccase activity from the mixed fungal culture of Han 849 and Han 851 on *F. platanifolia* was 1,144.85 ± 34.97 U/L, nearly 18.96— and 2.93-fold higher than that on *P. tabuliformis* and a mixture of *P. tabuliformis* and *F. platanifolia*, respectively. Maximum laccase activity from the mixed fungal culture of Han 849, Han 851, and Han 881 on *F. platanifolia* was 774.96 ± 13.79 U/L, nearly 17.33— and 2.82-fold higher than that on *P. tabuliformis* and a mixture of *P. tabuliformis* and *F. platanifolia*, respectively (**Figures 2–4**). So, the mixed fungal culture of Han 849 with Han 851 or Han 881 on *F. platanifolia* was conducted to improving laccase activity compared with other conditions. Meanwhile, the laccase activity of either single species or mixed species on *P. tabuliformis* was lower than that on *F. platanifolia* or a mixture by *P. tabuliformis* and *F. platanifolia*.

DISCUSSION

Recent works have shown the ability of lignocellulosic biomass stimulating laccase production by basidiomycetes (Birhanli and Yeşilada, 2013; Zhou et al., 2014; Han et al., 2017;

Palazzolo et al., 2019; Thamvithayakorn et al., 2019; Unuofin et al., 2019b; Han et al., 2020b, 2021a). Also, the selection of appropriate residues for fungus growth and target enzyme synthesis plays an important role in the development of efficient biotechnology (Elisashvili et al., 2008). Elisashvili et al. (2008) reported that laccase activity values from *Pleurotus ostreatus* IBB 8, *P. ostreatus* 2175, *Pleurotus tuberregium* IBB 624, *Lentinus edodes* IBB 123, *L. edodes* IBB 363, and *L. edodes* IBB 369 on tree leaves or wheat straw *via* solid-state fermentation were 7 ± 0.7 U/flask or 7 ± 0.8 U/flask, 15 ± 1.4 or 12 ± 1.2 U/flask, 20 ± 1.8 or 10 ± 1.0 U/flask, 57 ± 4.7 or 20 ± 1.5 U/flask, 52 ± 4.9 or 55 ± 5.1 U/flask, and 7 ± 0.7 or 38 ± 4.0 U/flask, respectively. The highest laccase activity values were 386 U/L for *Trametes trogii* incubated in a medium containing pulverized apricot seed shell and 1,216 U/L for *Trametes versicolor* grown in a medium containing pulverized bulrush in submerged fermentation (Birhanli and Yeşilada, 2013). The highest laccase from *Pseudolagarobasidium* sp. PP17-33 was 5.841 U/g using the oil palm decanter cake as materials for optimization of the production of enzymes through Plackett–Burman design (Thamvithayakorn et al., 2019). The optimal conditions for laccase production from *T. versicolor* were found at 35°C and 5 g/L of wheat bran as substrate, reaching approximately 200 U/ml on 11 days in submerged fermentation (Atilano-Camino et al., 2020). An et al. (2020b) reported that laccase production from *P. ostreatus* and *Flammulina velutipes* strains grown on cottonseed hull was better than that on corncob or poplar wood, and laccase production from *P. ostreatus* CCEF 89 grown on cottonseed hull, corncob, and poplar sawdust ranged from 61.38 ± 4.09 to 748.24 ± 9.53 U/L, 26.12 ± 2.28 to 699.12 ± 44.91 U/L, and 3.32 ± 0.30 to 509.75 ± 15.43 U/L, respectively. So, previous studies were mainly focused on the effect of single lignocellulosic biomass on laccase activity. Of course, some studies focused on the effect of different kinds of lignocellulosic biomass on laccase production secreted by fungi. However, no studies have been conducted on fermentation of laccase by using single coniferous trees, or broadleaf trees, or by mixing coniferous and broadleaf trees. Also, the effects of *P. tabuliformis* belonging to coniferous trees and *F. platanifolia* belonging to broadleaf trees on laccase activity secreted by three newly isolated species were investigated, and the effect of the mixture of *P. tabuliformis* and *F. platanifolia* on laccase activity was also studied. The results showed that the presence of a mixture by *P. tabuliformis* and *F. platanifolia* was a benefit for promoting the laccase activity by *C. unicolor* Han 849. Apart from *C. unicolor* Han 849, the effect of *F. platanifolia* was more contributed to tested fungi secreting laccase than the effect of *P. tabuliformis*.

Previous studies had indicated that different species or different strains belonging to the same species are an important factor affecting laccase activity (Lamia et al., 2017; Huang et al., 2019; An et al., 2020a,b; Han et al., 2020b). In other words, the biosynthetic potential of Basidiomycetes was highly dependent on the species of fungi (Han et al., 2021a). An et al. (2020b) reported that the capacity of secreting laccase of *P. ostreatus* strains was superior to *F. velutipes* strains due to the maximum laccase production on cottonseed hull, corncob, and poplar wood.

A previous study indicated that maximum laccase activity of *P. ostreatus* CY 568 and CCEF 99 on poplar sawdust appeared on the fifth day and the nineth day (Han et al., 2020b). In this study, the capacity of secreting laccase from *C. unicolor* Han 849 was stronger than *L. betulinus* Han 851 and *S. commune* Han 881.

For the higher yield of ligninolytic enzymes, the cocultivation of *Phanerochaete chrysosporium* and *P. ostreatus* was investigated (Verma and Madamwar, 2002). Maximum laccase activity from the mixed fungal culture of *Trametes hirsuta* and *Phanerochaete* sp. was found to be 78.25 U/g with wheat bran:pulse husk:mustard peel (WB:PH:MP) in 2:2:1 ratio as substrate at pH 5.0 temperature 30°C and incubation time of 7 days (Vibha and Negi, 2018). Kuhar et al. (2015) reported that cocultivation of *Ganoderma lucidum* and *T. versicolor* was performed and showed remarkable enhancement of laccase activity. Similarly, *L. betulina* Han 851 or *S. commune* Han 881 mixed with other species was also helpful for accelerating laccase secretion in this study. Furthermore, it was obvious that the treatment of mixing different species, whether the mixture of two or three species, was conducive to the improvement of laccase activity on *F. platanifolia*.

CONCLUSION

The effects of single or mixed lignocellulosic wastes and single or mixed fungal cultures were investigated in the present study. The presence of a mixture of *P. tabuliformis* and *F. platanifolia* was a benefit for promoting the laccase activity by *C. unicolor* Han 849. Apart from *C. unicolor* Han 849, the effect of *F. platanifolia* was more contributed to tested fungi secreting laccase than the effect of *P. tabuliformis*. The capacity of secreting laccase by *C. unicolor* Han 849 that was superior to *L. betulina* Han 851 and *S. commune* Han 881. *L. betulina* Han 851 or *S. commune* Han 881 mixed with other species was also helpful for accelerating laccase secretion. The treatment of mixing different species, including the mixture of two or three species, was obviously conducive to the improvement of laccase activity on *F. platanifolia*.

DATA AVAILABILITY STATEMENT

The datasets presented in this study can be found in online repositories. The names of the repository/repositories and accession number(s) can be found in the article/**Supplementary Material**.

AUTHOR CONTRIBUTIONS

M-LH, QA, and Y-CD: conceptualization. QA and M-LH: funding acquisition. M-LH, Z-YL, JY, C-RW, S-YC, NH, and W-YH: methodology. Z-YL, JY, C-RW, S-YC, NH, W-YH, and QA: data analysis. M-LH, W-YH, and QA: collect the materials. M-LH, JY, and C-RW: writing—original draft. QA and Y-CD:

writing—review and editing. All authors contributed to the article and approved the submitted version.

FUNDING

SUPPLEMENTARY MATERIAL

The Supplementary Material for this article can be found online at: https://www.frontiersin.org/articles/10.3389/fmicb.2021.682679/full#supplementary-material

Supplementary Table 1 | Laccase activity from *Cerrena unicolor* Han 849 grown on *Pinus tabuliformis*, *Firmiana platanifolia*, and a mixture by *Pinus tabuliformis* and *Firmiana platanifolia*.

Supplementary Table 2 | Laccase activity from *Lenzites betulina* Han 851 grown on *Pinus tabuliformis*, *Firmiana platanifolia*, and a mixture by *Pinus tabuliformis* and *Firmiana platanifolia*.

Supplementary Table 3 | Laccase activity from *Schizophyllum commune* Han 881 grown on *Pinus tabuliformis*, *Firmiana platanifolia*, and a mixture by *Pinus tabuliformis* and *Firmiana platanifolia*.

Supplementary Table 4 | Laccase activity from *Cerrena unicolor* Han 849 and *Schizophyllum commune* Han 881 grown on *Pinus tabuliformis*, *Firmiana platanifolia*, and a mixture by *Pinus tabuliformis* and *Firmiana platanifolia*.

Supplementary Table 5 | Laccase activity from *Lenzites betulina* Han 851 and *Schizophyllum commune* Han 881 grown on *Pinus tabuliformis*, *Firmiana platanifolia*, and a mixture by *Pinus tabuliformis* and *Firmiana platanifolia*.

Supplementary Table 6 | Laccase activity from *Cerrena unicolor* Han 849 and *Lenzites betulina* Han 851 grown on *Pinus tabuliformis*, *Firmiana platanifolia*, and a mixture by *Pinus tabuliformis* and *Firmiana platanifolia*.

Supplementary Table 7 | Laccase activity from *Cerrena unicolor* Han 849, *Lenzites betulina* Han 851 and *Schizophyllum commune* Han 881 grown on *Pinus tabuliformis*, *Firmiana platanifolia*, and a mixture by *Pinus tabuliformis* and *Firmiana platanifolia*.

REFERENCES

Agrawal, K., Chaturvedi, V., and Verma, P. (2018). Fungal laccase discovered but yet undiscovered. *Bioresour. Bioprocess.* 5:4. doi: 10.1186/s40643-018-0190-z

Agrawal, K., and Verma, P. (2020). Production optimization of yellow laccase from Stropharia sp. ITCC 8422 and enzyme-mediated depolymerization and hydrolysis of lignocellulosic biomass for biorefinery application. *Biomass Convers. Biorefin. Early Access* doi: 10.1007/s13399-020-00869-w

An, Q., Han, M. L., Bian, L. S., Han, Z. C., Han, N., Xiao, Y. F., et al. (2020a). Enhanced laccase activity of white rot fungi induced by different metal ions under submerged fermentation. *Bioresources* 15, 8369–8383. doi: 10.15376/biores.15.4.8369-8383

An, Q., Han, M. L., Wu, X. J., Si, J., Cui, B. K., Dai, Y. C., et al. (2016a). Laccase production among medicinal mushrooms from the Genus *Flammulina* (Agaricomycetes) under different treatments in submerged fermentation. *Int. J. Med. Mushrooms* 18, 1049–1059. doi: 10.1615/IntJMedMushrooms.v18.i11.90

An, Q., Ma, H. F., Han, M. L., Si, J., and Dai, Y. C. (2018). Effects of different induction media as inducers on laccase activities of *Pleurotus ostreatus* strains in submerged fermentation. *Bioresources* 13, 1143–1156. doi: 10.15376/biores.13.1.1143-1156

An, Q., Qiao, J., Bian, L. S., Han, M. L., Yan, X. Y., Liu, Z. Z., et al. (2020b). Comparative study on laccase activity of white rot fungi under submerged fermentation with different lignocellulosic wastes. *Bioresources* 15, 9166–9179. doi: 10.15376/biores.15.4.9166-9179

An, Q., Wu, X. J., and Dai, Y. C. (2019). Comparative genomics of 40 edible and medicinal mushrooms provide an insight into the evolution of lignocellulose decomposition mechanisms. *3 Biotech* 9:157. doi: 10.1007/s13205-019-1689-5

An, Q., Wu, X. J., Han, M. L., Cui, B. K., He, S. H., Dai, Y. C., et al. (2016b). Sequential solid-state and submerged cultivation of white rot fungus *Pleurotus ostreatus* on lignocellulosic biomass for the activity of lignocellulolytic enzymes. *Bioresources* 11, 8791–8805. doi: 10.15376/biores.11.4.8791-8805

Atilano-Camino, M. M., Alvarez-Valencia, L. H., Garcia-Gonzalez, A., and Garcia-Reyes, R. B. (2020). Improving laccase production from *Trametes versicolor* using lignocellulosic residues as cosubstrates and evaluation of enzymes for blue wastewater biodegradation. *J. Environ. Manage.* 275:111231. doi: 10.1016/j.jenvman.2020.111231

Becker, J., and Wittmann, C. (2019). A field of dreams: lignin valorization into chemicals, materials, fuels, and health-care products. *Biotechnol. Adv.* 37:107360. doi: 10.1016/j.biotechadv.2019.02.016

Bettin, F., Cousseau, F., Martins, K., Zaccaria, S., Girardi, V., da Silveira, M. M., et al. (2019). Effects of pH, temperature and agitation on the decolourisation of dyes by laccase-containing enzyme preparation from *Pleurotus sajor-caju*. *Braz. Arch. Biol. Technol.* 62:e19180338. doi: 10.1590/1678-4324-2019180338

Bilal, M., Rasheed, T., Nabeel, F., Iqbal, H. M. N., and Zhao, Y. P. (2019). Hazardous contaminants in the environment and their laccase-assisted degradation–a review. *J. Environ. Manage.* 234, 253–264. doi: 10.1016/j.jenvman.2019.01.001

Birhanli, E., and Yeşilada, Ö (2013). The utilization of lignocellulosic wastes for laccase production under semisolid-state and submerged fermentation conditions. *Turk. J. Biol.* 37, 450–456. doi: 10.3906/biy-1211-25

Elisashvili, V., Penninckx, M., Kachlishvili, E., Tsiklauri, N., Metreveli, E., Kharziani, T., et al. (2008). Lentinus edodes and *Pleurotus* species lignocellulolytic enzymes activity in submerged and solid-state fermentation of lignocellulosic wastes of different composition. *Bioresour. Technol.* 99, 457–462. doi: 10.1016/j.biortech.2007.01.011

Felsenstein, J. (1985). Confidence intervals on phylogenetics: an approach using bootstrap. *Evolution* 39, 783–791. doi: 10.2307/2408678

Gaikwad, A., and Meshram, A. (2020). Effect of particle size and mixing on the laccase-mediated pretreatment of lignocellulosic biomass for enhanced saccharification of cellulose. *Chem. Eng. Commun.* 207, 1696–1706. doi: 10.1080/00986445.2019.1680364

Haldar, H., Se, D., and Gayen, K. (2016). A review on the production of fermentable sugars from lignocellulosic biomass through conventional and enzymatic route—a comparison. *Int. J. Green Energy* 13, 1232–1253. doi: 10.1080/15435075.2016.1181075

Han, M. L., An, Q., Fu, W. X., Cheng, X., Bu, T., and Li, W. J. (2020a). Morphological characteristics and phylogenetic analyses reveal *Antrodia yunnanensis* sp. nov. (*Polyporales*, *Basidiomycota*) from China. *Phytotaxa* 460, 1–11. doi: 10.11646/phytotaxa.460.1.1

Han, M. L., An, Q., He, S. F., Zhang, X. L., Zhang, M. H., Gao, X. H., et al. (2020b). Solid-state fermentation on poplar sawdust and corncob wastes for lignocellulolytic enzymes by different *Pleurotus ostreatus* strains. *Bioresources* 15, 4982–4995. doi: 10.15376/biores.15.3.4982-4995

Han, M. L., An, Q., Ma, K. Y., An, W. N., Hao, W. Y., Liu, M. Y., et al. (2021a). A comparative study on the laccase activity of four basidiomycete fungi with different lignocellulosic residues via solid-state fermentation. *BioResources* 16, 3017–3031. doi: 10.15376/biores.16.2.3017-3031

Han, M. L., An, Q., Wu, X. J., Zheng, F., and Si, J. (2017). Effects of different lignocellulose as inducers on laccase activities of *Pleurotus ostreatus* in submerged fermentation. *Mycosystema* 36, 349–357. doi: 10.13346/j.mycosystema.160055

Han, M. L., Bian, L. S., Zhang, Y. X., Zhu, M. C., and An, Q. (2021b). *Pseudolagarobasidium baiyunshanense* sp. nov. from China inferred from

morphological and sequence analyses. *Phytotaxa* 483, 169–176. doi: 10.11646/phytotaxa.483.2.9

Han, M. L., Chen, Y. Y., Shen, L. L., Song, J., Vlasák, J., Dai, Y. C., et al. (2016). Taxonomy and phylogeny of the brown-rot fungi: *Fomitopsis* and its related genera. *Fungal Divers.* 80, 343–373. doi: 10.1007/s13225-016-0364-y

Hu, X., Wang, C. Y., Wang, L., Zhang, R. R., and Chen, H. (2014). Influence of temperature, pH and metal ions on guaiacol oxidation of purified laccase from *Leptographium qinlingensis*. *World J. Microb. Biot.* 30, 1285–1290. doi: 10.1007/s11274-013-1554-3

Huang, L., Sun, N., Ban, L., Wang, Y., and Yang, H. P. (2019). Ability of different edible fungi to degrade crop straw. *AMB Express* 9:4. doi: 10.1186/s13568-018-0731-z

Janusz, G., Czuryło, A., Frąc, M., Rola, B., Sulej, J., Pawlik, A., et al. (2015). Laccase production and metabolic diversity among *Flammulina velutipes* strains. *World J. Microb. Biot.* 31, 121–133. doi: 10.1007/s11274-014-1769-y

Kaira, G. S., Dhakar, K., and Pandey, A. (2015). A psychrotolerant strain of *Serratia marcescens* (MTCC 4822) produces laccase at wide temperature and pH range. *AMB Express* 5:92. doi: 10.1186/s13568-014-0092-1

Kannaiyan, R., Mahinpey, N., Mani, T., Martinuzzi, R. J., and Kostenko, V. (2012). Enhancement of *Dichomitus squalens* tolerance to copper and copper-associated laccase activity by carbon and nitrogen sources. *Biochem. Eng. J.* 67, 140–147. doi: 10.1016/j.bej.2012.06.007

Kuhar, F., Castiglia, V., and Levin, L. (2015). Enhancement of laccase production and malachite green decolorization by co-culturing *Ganoderma lucidum* and *Trametes versicolor* in solid-state fermentation. *Int. Biodeter. Biodegr.* 104, 238–243. doi: 10.1016/j.ibiod.2015.06.017

Lallawmsanga, Leo, V. V., Passari, A. K., Muniraj, I. K., Uthandi, S., Hashem, A., et al. (2019). Elevated levels of laccase synthesis by *Pleurotus pulmonarius* BPSM10 and its potential as a dye decolorizing agent. *Saudi J. Biol. Sci.* 26, 3464–3468. doi: 10.1016/j.sjbs.2018.10.006

Lamia, M. H., Farid, Z., Sonia, M. A., Sevastianos, R., Samia, A., Véronique, D., et al. (2017). Selective isolation and screening of actinobacteria strains producing lignocellulolytic enzymes using olive pomace as substrate. *Iran. J. Biotechnol.* 15, 74–77. doi: 10.15171/ijb.1278

Lira-Perez, J., Rodriguez-Vazquez, R., and Chan-Cupul, W. (2020). Effect of fungal co-cultures on ligninolytic enzyme activities, H2O2 production, and orange G discoloration. *Prep. Biochem. Biotech.* 50, 607–618. doi: 10.1080/10826068.2020.1721534

Lizardi-Jimenez, M. A., Ricardo-Diaz, J., Quinones-Munoz, T. A., Hernandez-Rosas, F., and Hernandez-Martinez, R. (2019). Fungal strain selection for protease production by solid-state fermentation using agro-industrial waste as substrates. *Chem. Pap.* 73, 2603–2610. doi: 10.1007/s11696-019-00814-w

Ma, K. D., and Ruan, Z. Y. (2015). Production of a lignocellulolytic enzyme system for simultaneous bio-delignification and saccharification of corn stover employing co-culture of fungi. *Bioresour. Technol.* 175, 586–593. doi: 10.1016/j.biortech.2014.10.161

Mazlan, S. Z., and Abu Hanifah, S. (2017). Effects of temperature and pH on immobilized laccase activity in conjugated methacrylate-acrylate microspheres. *Int. J. Polym. Sci.* 2017:5657271. doi: 10.1155/2017/5657271

Mazur, I., Rola, B., Stolarczyk, K., Nazaruk, E., Bilewicz, R., Rogalski, J., et al. (2015). The large scale production of *Cerrena unicolor* laccase on waste agricultural based media. *J. Fac. Agric. Kyushu Univ.* 60, 297–302.

Osma, J. F., Toca-Herrera, J. L., and Rodriguez-Couto, S. (2011). Cost analysis in laccase production. *J. Environ. Manage.* 92, 2907–2912. doi: 10.1016/j.jenvman.2011.06.052

Page, R. D. M. (1996). Treeview: application to display phylogenetic trees on personal computers. *Comput. Appl. Biosci.* 12, 357–358. doi: 10.1093/bioinformatics/12.4.357

Palazzolo, M. A., Postemsky, P. D., and Kurina-Sanz, M. (2019). From agro-waste to tool: Biotechnological characterization and application of *Ganoderma lucidum* E47 laccase in dye decolorization. *3 Biotech* 9:213. doi: 10.1007/s13205-019-1744-2

Pinar, O., Karaosmanoðlu, K., Sayar, N. A., Kula, C., Kazan, D., and Sayar, A. A. (2017). Assessment of hazelnut husk as a lignocellulosic feedstock for the production of fermentable sugars and lignocellulolytic enzymes. *3 Biotech* 7:367. doi: 10.1007/s13205-017-1002-4

Pinheiro, V. E., Michelin, M., Vici, A. C., de Almeida, P. Z., and Polizeli, M. D. T. D. (2020). Trametes versicolor laccase production using agricultural wastes: a comparative study in Erlenmeyer flasks, bioreactor and tray. *Bioproc. Biosyst. Eng.* 43, 507–514. doi: 10.1007/s00449-019-02245-z

Rodriguez, R. D., Heredia, G., Siles, J. A., Jurado, M., Saparrat, M. C. N., Garcia-Romera, I., et al. (2019). Enhancing laccase production by white-rot fungus *Funalia floccosa* LPSC 232 in co-culture with *Penicillium commune* GHAIE86. *Folia. Microbiol.* 64, 91–99. doi: 10.1007/s12223-018-0635-y

Saoudi, O., Ghaouar, N., and Othman, T. (2017). Conductivity measurements of laccase for various concentrations, pH and ionic liquid solutions. *Fluid Phase Equilibr.* 433, 184–192. doi: 10.1016/j.fluid.2016.10.032

Singh, G., and Arya, S. K. (2019). Utility of laccase in pulp and paper industry: a progressive step towards the green technology. *Int. J. Biol. Macromol.* 134, 1070–1084. doi: 10.1016/j.ijbiomac.2019.05.168

Songulashvili, G., Spindler, D., Jimenez-Tobon, G. A., Jaspers, C., Kerns, G., and Penninckx, M. J. (2015). Production of a high level of laccase by submerged fermentation at 120-L scale of *Cerrena unicolor* C-139 grown on wheat bran. *CR. Biol.* 338, 121–125. doi: 10.1016/j.crvi.2014.12.001

Swofford, D. L. (2002). *PAUP*: Phylogenetic Analysis Using Parsimony (*and other methods), version 4.0 Beta*. Sunderland, MA: Sinauer.

Thamvithayakorn, P., Phosri, C., Pisutpaisal, N., Krajangsang, S., Whalley, A. J. S., and Suwannasai, N. (2019). Utilization of oil palm decanter cake for valuable laccase and manganese peroxidase enzyme production from a novel white-rot fungus, *Pseudolagarobasidium* sp. PP17–33. *3 Biotech* 9:417. doi: 10.1007/s13205-019-1945-8

Unuofin, J. O., Okoh, A. I., and Nwodo, U. U. (2019a). Aptitude of oxidative enzymes for treatment of wastewater pollutants: a laccase perspective. *Molecules* 24:2064. doi: 10.3390/molecules24112064

Unuofin, J. O., Okoh, A. I., and Nwodo, U. U. (2019b). Utilization of agroindustrial wastes for the production of laccase by *Achromobacter xylosoxidans* HWN16 and *Bordetella bronchiseptica* HSO16. *J. Environ. Manage.* 231, 222–231. doi: 10.1016/j.jenvman.2018.10.016

Verma, P., and Madamwar, D. (2002). Production of ligninolytic enzymes for dye decolorization by cocultivation of white-rot fungi *Pleurotus ostreatus* and *Phanerochaete chrysosporium* under solid-state fermentation. *Appl. Biochem. Biotechnol.* 102, 109–118. doi: 10.1385/ABAB:102:1-6:109

Vibha, K., and Negi, S. (2018). Enhanced production of laccase and pectinase using co-culture of *Trametes hirsuta* and *Phanerochaete* sp through EVOP-factorial design technique. *3 Biotech* 8:490. doi: 10.1007/s13205-018-1516-4

Wang, F., Xu, L., Zhao, L. T., Ding, Z. Y., Ma, H. L., and Terry, N. (2019). Fungal laccase production from lignocellulosic agricultural wastes by solid-state fermentation: a review. *Microorganisms* 7:665. doi: 10.3390/microorganisms7120665

Wang, H., Peng, L., Ding, Z. Y., Wu, J. Y., and Shi, G. Y. (2015). Stimulated laccase production of *Pleurotus ferulae* JM301 fungus by *Rhodotorula mucilaginosa* yeast in co-culture. *Process. Biochem.* 50, 901–905. doi: 10.1016/j.procbio.2015.03.004

Wang, S. S., Ning, Y. J., Wang, S. N., Zhang, J., Zhang, G. Q., and Chen, Q. J. (2017). Purification, characterization, and cloning of an extracellular laccase with potent dye decolorizing ability from white rot fungus *Cerrena unicolor* GSM-01. *Int. J. Biol. Macromol.* 95, 920–927. doi: 10.1016/j.ijbiomac.2016.10.079

Xu, S., Wang, F., Fu, Y. P., Li, D., Sun, X. Z., Li, C. T., et al. (2020). Effects of mixed agro-residues (corn crop waste) on lignin-degrading enzyme activities, growth, and quality of *Lentinula edodes*. *RSC Adv.* 10, 9798–9807. doi: 10.1039/c9ra10405d

Xu, X. Q., Huang, X. H., Liu, D., Lin, J., Ye, X. Y., and Yang, J. (2018). Inhibition of metal ions on *Cerrena* sp laccase: kinetic, decolorization and fluorescence studies. *J. Taiwan Inst. Chem. Eng.* 84, 1–10. doi: 10.1016/j.jtice.2017.12.028

Yang, J., Li, W. J., Ng, T. B., Deng, X. Z., Lin, J., and Ye, X. Y. (2017). Laccases: production, expression regulation, and applications in pharmaceutical biodegradation. *Front. Microbiol.* 8:832. doi: 10.3389/fmicb.2017.00832

Yang, J., Wang, G. Z., Ng, T. B., Lin, J., and Ye, X. Y. (2016). Laccase production and differential transcription of laccase genes in *Cerrena* sp. in response to metal ions, aromatic compounds, and nutrients. *Front. Microbiol.* 6:1558. doi: 10.3389/fmicb.2015.01558

Zerva, A., Simic, S., Topakas, E., and Nikodinovic-Runic, J. (2019). Applications of microbial laccases: patent review of the past decade (2009-2019). *Catalysts* 9:12. doi: 10.3390/catal9121023

Zhang, J., Sung, L., Zhang, H., Wang, S. F., Zhang, X. Y., and Geng, A. L. (2018). A novel homodimer laccase from *Cerrena unicolor* BBP6: purification, characterization, and potential in dye decolorization and denim bleaching. *PLoS One* 13:e0202440. doi: 10.1371/journal.pone.0202440

Zhang, J. F., Ke, W., and Chen, H. (2020). Enhancing laccase production by white-rot fungus *Trametes hirsuta* SSM-3 in co-culture with yeast *Sporidiobolus pararoseus* SSM-8. *Prep. Biochem. Biotech.* 50, 10–17. doi: 10.1080/10826068.2019.1655764

Zhou, J., Yang, T., Mei, Y. Z., Kang, L., and Dai, C. C. (2014). Laccase production by *Phomopsis liquidambari* B3 cultured with food waste and wheat straw as the main nitrogen and carbon sources. *J. Air Waste Manage.* 64, 1154–1163. doi: 10.1080/10962247.2014.930077

Zhuo, R., Yuan, P., Yang, Y., Zhang, S., Ma, F. Y., and Zhang, X. Y. (2017). Induction of laccase by metal ions and aromatic compounds in *Pleurotus* *ostreatus* HAUCC 162 and decolorization of different synthetic dyes by the extracellular laccase. *Biochem. Eng. J.* 117, 62–72. doi: 10.1016/j.bej.2016.09.016

Harnessing the Endogenous 2μ Plasmid of *Saccharomyces cerevisiae* for Pathway Construction

Jing Yang[1†], Yujuan Tian[2†], Huayi Liu[2], Yeyi Kan[2], Yi Zhou[2], Ying Wang[1] and Yunzi Luo[1,2*]

[1] Frontier Science Center for Synthetic Biology and Key Laboratory of Systems Bioengineering (Ministry of Education), School of Chemical Engineering and Technology, Collaborative Innovation Center of Chemical Science and Engineering (Tianjin), Tianjin University, Tianjin, China, [2] Department of Gastroenterology, State Key Laboratory of Biotherapy, West China Hospital, Sichuan University, Chengdu, China

pRS episomal plasmids are widely used in *Saccharomyces cerevisiae*, owing to their easy genetic manipulations and high plasmid copy numbers (PCNs). Nevertheless, their broader application is hampered by the instability of the pRS plasmids. In this study, we designed an episomal plasmid based on the endogenous 2μ plasmid with both improved stability and increased PCN, naming it p2μM, a 2μ-modified plasmid. In the p2μM plasmid, an insertion site between the *REP1* promoter and *RAF1* promoter was identified, where the replication (ori) of *Escherichia coli* and a selection marker gene of *S. cerevisiae* were inserted. As a proof of concept, the tyrosol biosynthetic pathway was constructed in the p2μM plasmid and in a pRS plasmid (pRS423). As a result, the p2μM plasmid presented lower plasmid loss rate than that of pRS423. Furthermore, higher tyrosol titers were achieved in *S. cerevisiae* harboring p2μM plasmid carrying the tyrosol pathway-related genes. Our study provided an improved genetic manipulation tool in *S. cerevisiae* for metabolic engineering applications, which may be widely applied for valuable product biosynthesis in yeast.

Keywords: 2μ plasmid, plasmid stability, tyrosol, pRS423, *Saccharomyces cerevisiae*

INTRODUCTION

Yeast, especially *Saccharomyces cerevisiae* (*S. cerevisiae*), has been developed as a host organism for the heterologous production of high-value compounds (Luo et al., 2015; Suastegui and Shao, 2016; Gao et al., 2017; Cao M. et al., 2020; Cao X. et al., 2020; Liu H. et al., 2020; Liu Q. et al., 2020; Ren et al., 2020), free fatty acid (Zhang et al., 2019), soluble cytosolic proteins (Boulet et al., 2017; González et al., 2018; Huang et al., 2018; Zhang et al., 2019), and biofuels (Zhang et al., 2021). Many genetic manipulations of *S. cerevisiae* rely on the utilization of plasmids (Romanos et al., 1992). There are three commonly used plasmids: (1) yeast-integrating plasmid (YIp) lacks the yeast replication initiation site and can only be stabilized when integrated into the yeast chromosome (Jensen et al., 2014). However, YIp brings only one copy of target sequences to the chromosome. (2) Yeast centromere plasmid (YCp) contains an autonomously replicating sequence (ARS) and a yeast centromere (CEN) (Chlebowicz-Śledziewska and Śledziewski, 1985; Lee et al., 2016), which has high mitotic stability but low copy number. (3) Yeast episomal plasmid (YEp) harbors a 2μ plasmid replication origin and a partitioning locus (*STB* or *REP3*) (Murray and Cesareni, 1986),

which has high copy numbers but low stability (Hohnholz et al., 2017). In summary, plasmids with stable expression usually cannot provide high copy number, while plasmids with high copy number will be easily lost after long-term fermentation in the nutrient medium. Therefore, a stable plasmid system with high copy number is urgently needed.

Yeast endogenous 2μ plasmid is a cryptic nuclear plasmid (Stevens and Moustacchi, 1971; Petes and Williamson, 1975), which confers no phenotype beyond the ability to maintain itself a high copy number at 60–330 copies per cell with the help of FLP-mediated recombination (Gerbaud et al., 1979; Murray and Cesareni, 1986; Reider Apel et al., 2017). The 2μ plasmid is a circular DNA plasmid with a size of 6,318 bp and a circumference of about 2 μm (Hartley and Donelson, 1980).

In the 2μ plasmid, there is an ∼600-bp DNA sequence essential for the faithful partitioning of the 2μ plasmid along with the trans-acting ORFs REP1 and REP2 (Kikuchi, 1983), named STB (Murray and Cesareni, 1986). In the absence of STB, the 2μ-based plasmids are rapidly lost due to extreme mother bias during mitosis. In addition, the 2μ plasmid codes for four proteins (REP1, REP2, RAF1, and FLP) that are vital for its own survival. REP1 and REP2 are the primary factors responsible for the 2μ plasmid stability (Jayaram et al., 1983). RAF1 interacts with both REP1 and REP2 independently and blocks their interaction, thus reducing the cellular concentration of the REP1–REP2 complex that acts as a repressor of REP1, FLP, and RAF1 genes. This blockage resulted in reduced plasmid stability and increased plasmid copy number (PCN). Both the deletion and overexpression of RAF1 have a similar effect on the plasmid stability and copy number, resulting in an increased PCN and decreased plasmid stability (Rizvi et al., 2018). FLP is a conservative site-specific recombinase (Sadowski, 1995). The flip of one half of the 2μ plasmid with respect to the other is predominantly FLP dependent (Gerbaud et al., 1979; Broach and Hicks, 1980). The FLP-mediated recombination is also believed to be responsible for the interconversion of the plasmid replication between the theta and the rolling circle modes of replication.

Many researchers took advantage of the high PCN and stable inheritance of the 2μ plasmid to directly transform 2μ plasmid as an expression tool. Ludwig et al. selected the HPAI restriction site of STB as the insertion site (Ludwig and Bruschi, 1991), but the loss of STB led to a high loss rate of the plasmid (Murray and Szostak, 1983; McQuaid et al., 2019). Misumi et al. (2018) inserted the yeast promoter, terminator, and nutritional deficiency marker gene leu2 between RAF1 and STB and called this plasmid YHp. The application of YHp was restricted in [cir⁰] strains (Misumi et al., 2018). Zeng et al. (2021) chose two sites as the targets for insertion of heterogeneous DNA fragment: one is at the downstream of the RAF1, while the other is at the end of REP2. The derivative plasmids generated by inserting the same target gene at these two sites have lower plasmid loss rates and better expression level than the conventional 2μ-based plasmid pRS425 (Zeng et al., 2021). To our knowledge, no commonly used methods have been developed in laboratory strains with the wild-type (WT) 2μ plasmid (Supplementary Figure 1A).

Based on these previous studies described above (Hartley and Donelson, 1980; Jayaram et al., 1983; Rizvi et al., 2018; McQuaid et al., 2019), we identified a new insertion site between the REP1 promoter and RAF1 promoter (Supplementary Figure 1B). The pBR322ori, KanMX selection marker gene, and three endonuclease sites XhoI/PmeI/NotI were inserted in this site. The 2μ-modified plasmid was named p2μM. In plasmid stability measurement, the p2μM plasmid system was more stable than the pRS423 plasmid system. To test the application of p2μM in the biosynthesis of natural products, the tyrosol [a phenethyl alcohol derivative that has antioxidant and anti-inflammatory effects (Choe et al., 2012)] pathway-related genes were introduced into p2μM. The results confirmed that the stability and property of the p2μM were better than those of the pRS423M plasmid. Our study provided an improved genetic manipulation tool in S. cerevisiae for metabolic engineering applications, and it may be widely applied in valuable natural product biosynthesis in yeast.

DESIGN AND CONSTRUCTION OF ENDOGENOUS 2μ-BASED PLASMIDS IN VITRO

In order to construct a stable endogenous 2μ-based plasmid and apply it for DNA expression and pathway construction, the proper insertion site should be selected to insert essential elements and heterogeneous DNA fragments. Besides the known genes and sequences, there are still uncharacterized transcripts transcribed from the 2μ plasmid (Rizvi et al., 2017). It was found that the promoters of RAF1 and REP1 on the endogenous 2μ plasmid were adjacent and there was no other element between them by analyzing the elements related to stability. Thus, this site was selected as the insertion site (Supplementary Figure 1A). To edit the endogenous 2μ plasmid for a better genetic manipulation tool, the origin replication of Escherichia coli, combined with G418 resistance marker, was chosen to be inserted to construct p2μM (Supplementary Figure 1B).

To characterize the property of the p2μM plasmid, plasmid pRS423 with G418 resistance was chosen as a control to generate plasmid pRS423M (Supplementary Figure 1C). Plasmid pRS423 is also commonly used in yeast among the YEp pRS42 series plasmids due to its relatively high stability and copy number (Christianson et al., 1992).

Tyrosol is mainly extracted from olive oil, wine, and plant tissues. It has proven to be an effective cellular antioxidant and is widely used in food and medicine industries (Benedetto et al., 2007; Karković Marković et al., 2019). Taking into account the impact of the size of inserted fragment on the p2μM plasmid, we constructed three modules of different sizes using genes of the tyrosol biosynthetic pathway (Supplementary Figure 1D). The small module (mutation module, 3.8 kb) of $ARO4^{K229L}$ and $ARO7^{G141S}$ could efficiently relieve feedback inhibition and increase the production of tyrosol in S. cerevisiae (Liu H. et al., 2020), which was introduced to generate plasmid p2μM-$ARO4^{K229L}$-$ARO7^{G141S}$ (p2μM-small-module). The rewiring module containing pentose phosphate pathway genes TKL1 and RKI1 could tune the flux of the precursor

pathway (Walfridsson et al., 1996; Kondo et al., 2004; Bera et al., 2011). The adjustment module that contains *ARO2* and *ARO10* could adjust the shikimate pathway and L-tyrosine branch by catalyzing the conversion of chorismate from EPSP and the decarboxylation of 4-HPP to 4-HPPA (Liu H. et al., 2020), respectively. The medium module (9.8 kb) composed of the rewiring module and the adjustment module was overexpressed by p2μM plasmid, resulting in plasmid p2μM-*TKL1-RKI1-ARO10-ARO2* (p2μM-medium-module). Finally, the medium module was introduced into plasmid p2μ-small-module, resulting in plasmid p2μM-*TKL1-RKI1-ARO10-ARO2-ARO4^{K229L}-ARO7^{G141}S* (p2μM-large-module, the size of the large module was 13.6 kb). Then, these three modules were also inserted into the multiple cloning sites of plasmid pRS423M to generate pRS423M-small-module, pRS423M-medium-module, and pRS423M-large-module, collectively called pRS423M-based plasmids (**Supplementary Figure 1F**). The structures of the three modules are shown in **Supplementary Figure 2**.

DETERMINATION OF PLASMID STABILITY

Since the yeast endogenous 2μ plasmid showed high stability and copy number, we assumed that our p2μM plasmid could be more stable than the pRS423M plasmid. To test this hypothesis, the influences of the size of the inserted fragment on the stability of the p2μM plasmid were explored *via* measuring the plasmid loss rate. As shown in **Supplementary Tables 1**, **2**, the stabilities of the p2μM-based plasmids were significantly higher than those of the pRS423M-based plasmids. First, plasmid p2μM and pRS423M were transformed to *S. cerevisiae* strain CEN.PK2-1C, respectively. Then, the plasmid loss rates of the 10th, 20th, 40th, and 50th generation strains were tested in YPD without G418 and in YPD + G418 medium (**Figures 1A,B**). When the size of the inserted fragment was 0, the plasmid loss rates of plasmid p2μM in non-selective medium were 36.3 ± 6.0% for the 10th generation, 62.4 ± 3.3% for the 20th generation, 72.5 ± 7.9% for the 40th generation, and 85.7 ± 1.4% for the 50th generation, lower than those of the pRS423M plasmid (90.4 ± 2.9, 98.8 ± 0.9, 99.3 ± 0.2, and 99.9 ± 0.2%). Plasmid loss rates of p2μM in selective medium were 5.7 ± 1.3, 7.2 ± 0.7, 12.4 ± 0.8, and 27.1 ± 1.4% for each generation, which were much lower than those of pRS423M (17.8 ± 1.1, 31.4 ± 1.8, 74.8 ± 0.9, and 85.1 ± 2.2%).

Furthermore, three p2μM-based plasmids of the experimental group and three pRS423M-based plasmids of the control group mentioned above were transformed to strain CEN.PK2-1C, respectively. The results showed that the stabilities of p2μM-based plasmids were higher than those of pRS423M-based plasmids both in non-selective medium and selective medium (**Figures 1A,B**). For non-selective medium, when the sizes of the inserted fragments were 3,842 and 9,821 bp, the plasmid loss rates of p2μM-based plasmids were 54.3 ± 8.5 and 71.4 ± 5.6% (the 10th generation), 87.9 ± 2.4 and 95.8 ± 1.3% (the 20th generation), 91.9 ± 1.0 and 96.9 ± 0.8% (the 40th generation), and 96.4 ± 0.9 and 98.7 ± 0.3% (the 50th generation), while the
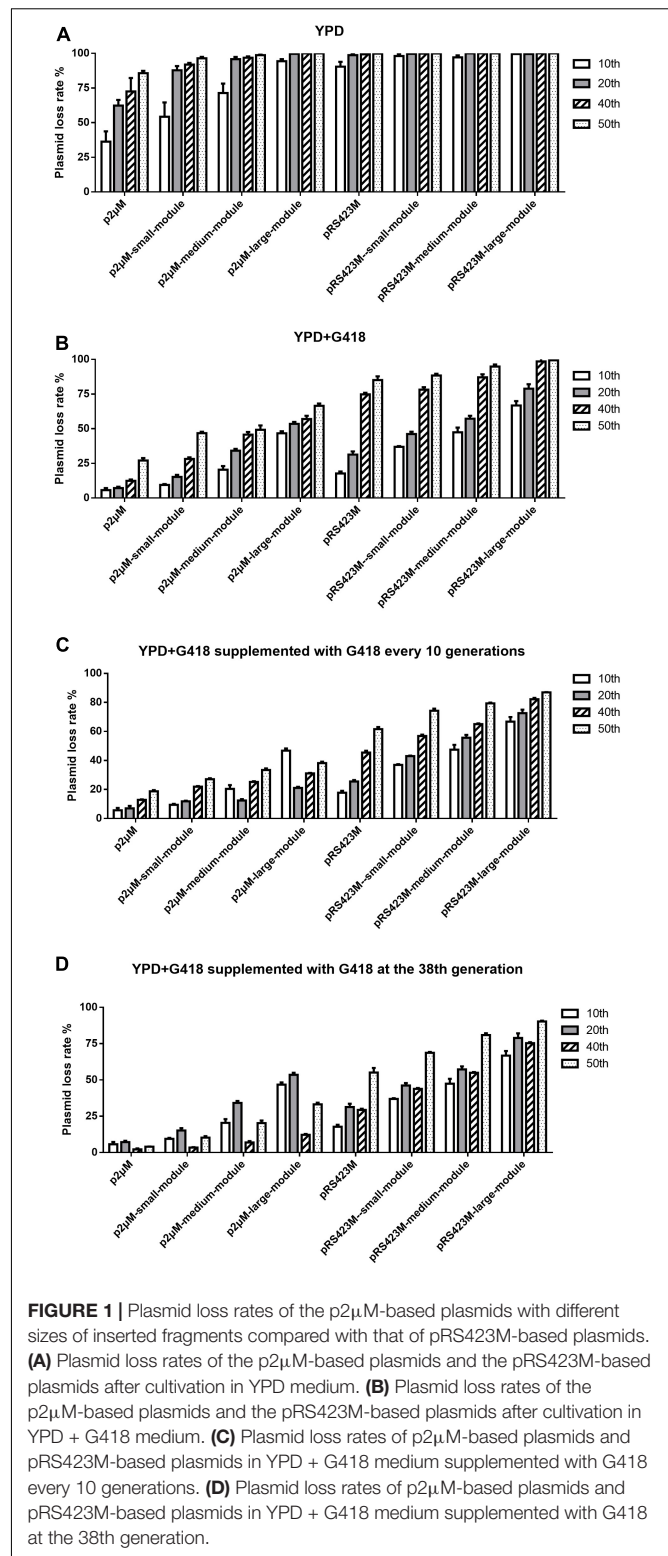

FIGURE 1 | Plasmid loss rates of the p2μM-based plasmids with different sizes of inserted fragments compared with that of pRS423M-based plasmids. **(A)** Plasmid loss rates of the p2μM-based plasmids and the pRS423M-based plasmids after cultivation in YPD medium. **(B)** Plasmid loss rates of the p2μM-based plasmids and the pRS423M-based plasmids after cultivation in YPD + G418 medium. **(C)** Plasmid loss rates of p2μM-based plasmids and pRS423M-based plasmids in YPD + G418 medium supplemented with G418 every 10 generations. **(D)** Plasmid loss rates of p2μM-based plasmids and pRS423M-based plasmids in YPD + G418 medium supplemented with G418 at the 38th generation.

plasmid loss rates of pRS423M-based plasmids were 98.1 ± 1.3 and 97.2 ± 1.1% for the 10th generation, and the plasmids were all lost at the 20th generation (99.7 ± 0.4 and 100.0%). Until the size of the inserted fragment increased to about 14 kb, the plasmid

loss rate of the experimental group was 94.3 ± 1.2% for the 10th generation, but plasmids of the control group were almost all lost. For cultures that were grown in selective medium, when the fragment of 9,821 bp was introduced, 49.3 ± 2.5% strains lost their plasmid p2μM-medium-module, but almost all strains lost the plasmid pRS423M-medium-module after fermentation for 50 generations (94.9 ± 1.3%). All strains lost the plasmid pRS423M-large-module at the 40th generation (98.6 ± 1.2%); however, the plasmid loss rate of the p2μM-large-module was merely 57.0 ± 1.9%. The amounts of plasmid loss in YPD + G418 medium were less than those in YPD medium without G418.

As shown in **Figure 1C**, supplementing antibiotics to YPD + G418 medium every 10 generations could maintain lower plasmid loss rates. Plasmid loss rates of the 40th generation were greatly decreased after G418 was supplemented at the 38th generation (**Figure 1D**). The plasmid loss rates of the 40th generation were lower than those of the 20th generation, and the plasmid loss rates of p2μ-derived plasmids were still much lower than those of pRS423-derived plasmids.

PLASMID p2μM APPLIED IN TYROSOL PRODUCTION

To demonstrate that p2μM could be applied for the optimization of natural product biosynthesis, the tyrosol biosynthetic pathway was chosen as an example. The WT strain CEN.PK2-1C was fermented in YPD medium. Engineered strains containing individual p2μM-based plasmids and pRS423M-based plasmids with different sizes of tyrosol biosynthesis-related modules were simultaneously fermented in both non-selective medium and selective medium.

As demonstrated in **Figure 2A**, after fermentation in YPD medium, tyrosol productions of the WT strain were 45.11 ± 0.85 mg/L at the 20th generation and 48.53 ± 0.98 mg/L at the 40th generation. In non-selective YPD medium, strain CEN.PK2-1C with p2μM produced 39.39 ± 0.97 mg/L tyrosol after 20 generations and 44.78 ± 0.64 mg/L tyrosol after 40 generations (**Figure 2B**), which were lower than those of the WT strain. When the plasmid p2μM-small-module was transformed into the strain CEN.PK2-1C, the tyrosol production was 47.79 ± 0.64 mg/L at the 20th generation and 54.46 ± 0.21 mg/L at the 40th generation, 12.2% greater than that of the WT strain and 9.7% greater than that of the strain with pRS423M-small-module. The strain CEN.PK2-1C carrying plasmid p2μM-medium-module accumulated 50.59 ± 1.12 mg/L tyrosol after 40 generations of fermentation. In the strain CEN.PK2-1C with p2μM-large-module, the tyrosol titer of 48.03 ± 0.45 mg/L was obtained, which was not as good as the WT strain but 7.3% higher than that of CEN.PK2-1C carrying p2μM. CEN.PK2-1C carrying plasmid pRS423M produced 35.99 ± 0.35 mg/L tyrosol at the 20th generation and 43.41 ± 0.94 mg/L tyrosol at the 40th generation, which were lower than those of the strain with p2μM and the WT strain. Tyrosol productions in strain CEN.PK2-1C with pRS423M-medium-module and pRS423M-large-module at each generation were all much lower than those of the strains carrying p2μM-based plasmids.

According to **Figure 2C**, after shake flask cultivation in YPD + G418 medium, the strain harboring p2μM generated tyrosol titer of 44.75 ± 0.83 mg/L at the 20th generation. At the 40th generation, tyrosol production was 49.05 ± 0.90 mg/L, which was higher than that of the WT strain and CEN.PK2-1C with p2μM fermented in non-selective medium; 71.11 ± 0.71 and 98.39 ± 0.41 mg/L tyrosol was produced in the strain containing p2μM-small-module after fermentation for 20 and 40 generations, respectively, which were much higher than that of CEN.PK2-1C with pRS423M-small-module (59.55 ± 0.16 mg/L). Tyrosol productions accumulated in the strain with p2μM-medium-module (47.71 ± 0.72 and 54.95 ± 0.50 mg/L) and p2μM-large-module (46.44 ± 0.65 and 50.20 ± 0.34 mg/L) after fermentation for 20 and 40 generations in selective medium were lower than those of the strain containing p2μM-small-module, but they were higher than those of CEN.PK2-1C with pRS423M-based plasmids. Strains carrying pRS423M produced 47.72 ± 0.18 mg/L tyrosol at the 40th generation, 2.8% lower than that of the strain with p2μM and 1.7% lower than that of the WT strain. The tyrosol yields of the strain containing plasmids pRS423M-small-module (59.55 ± 0.13 mg/L), pRS423M-medium-module (44.65 ± 1.46 mg/L), and pRS423M-large-module (25.64 ± 0.80 mg/L) at the 40th generation were all lower than those of the strains of p2μM-based plasmids with modules of the same size.

All results showed that the tyrosol yields of the strains with p2μM-based plasmids were higher than those of the strains with pRS423M-based plasmids both in non-selective medium and selective medium, which could be due to the instability of plasmid pRS423.

DISCUSSION

In this study, an endogenous 2μ-based expression vector with enhanced stability was developed in *S. cerevisiae*. The site between the *RAF1* promoter and *REP1* promoter on this plasmid was chosen as the insertion site for the gene of interest, which would not affect the functional elements and stability of the plasmid.

The plasmid loss rates were calculated on the strains harboring plasmids with inserted fragments of different sizes by culturing in non-selective YPD medium and YPD medium with selective pressure. After culturing without selective pressure for 40 generations, the loss rates of p2μM and pRS423M were about 73 and 100%, respectively. For plasmids containing modules of about 4 kb, the plasmid loss rates of p2μM-small-module and pRS423M-small-module in non-selective YPD medium were about 90 and 100%, respectively. All strains lost their plasmids by fermentation in YPD medium for 50 generations. Culturing in YPD + G418 medium for 50 generations, plasmid loss rate of p2μM was about 27% and that of pRS423M was about 85%. Plasmid pRS423M-large-module was all lost after 40 generations of cultivation, while merely 57% of the plasmid p2μM-large-module was lost. Continuous supplementation of G418 in YPD + G418 medium could help maintain the stability of plasmids, especially for p2μM-based plasmids. The plasmid loss rate of p2μM-large-module after 40 generations of cultivation
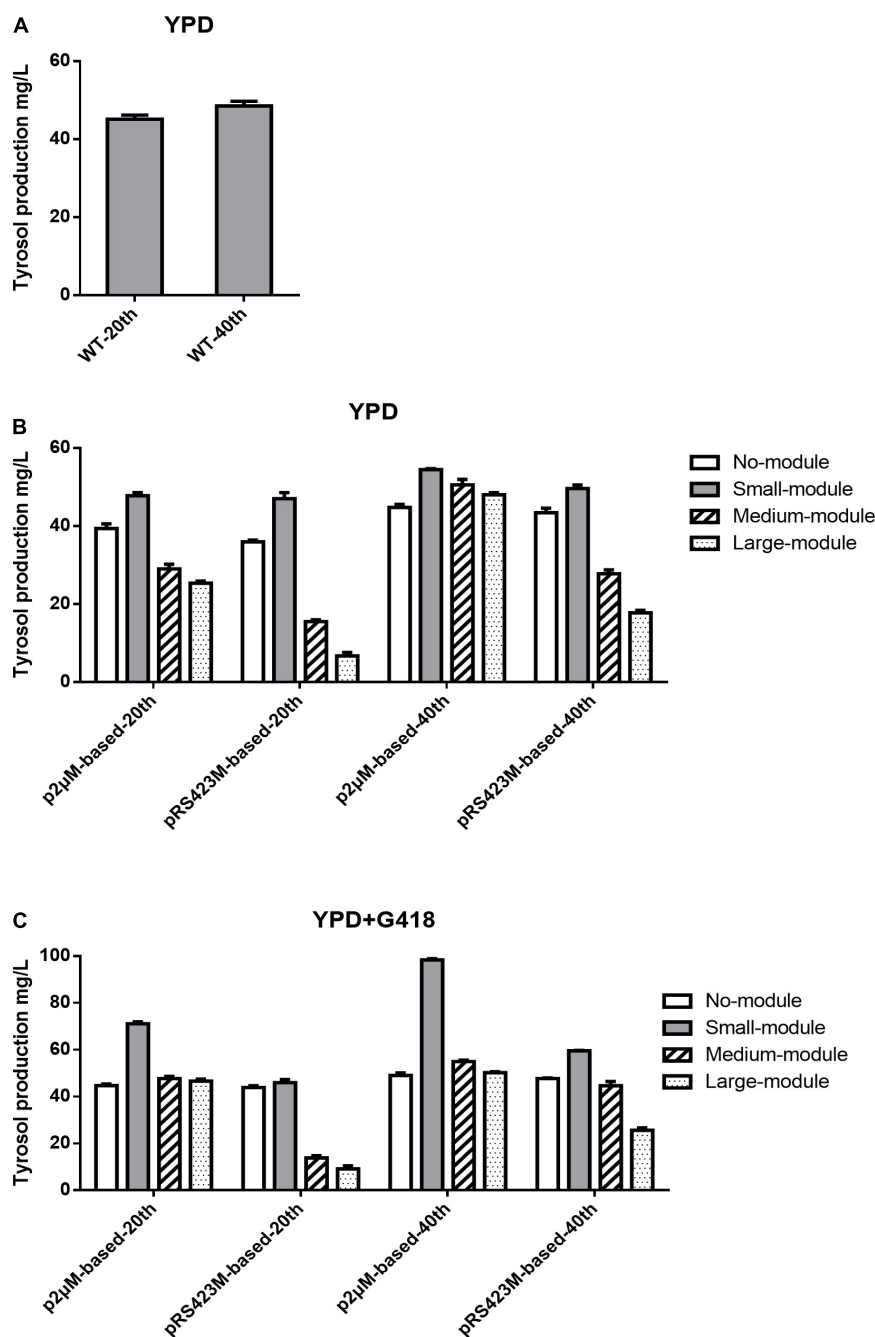
FIGURE 2 | Tyrosol production of strains containing a single plasmid with modules of different sizes after fermentation for 20 and 40 generations. **(A)** Tyrosol production of the WT strain CEN.PK2-1C. **(B)** Tyrosol production of strains CEN.PK2-1C with p2μM-based plasmids and CEN.PK2-1C with pRS423M-based plasmids after fermentation in YPD medium. **(C)** Tyrosol production of strains CEN.PK2-1C with p2μM-based plasmids and CEN.PK2-1C with pRS423M-based plasmids after fermentation in YPD medium with 200 μg/ml G418.

was about 31%, which was much lower than that of pRS423M-large-module (about 82%). Although the selection pressure was conducive to the stable existence and inheritance of plasmids, a large number of pRS423M-based plasmids were lost during long-time fermentation. The results showed that the stabilities of the p2μM-based plasmids were higher than those of the

pRS423M-based plasmids. It is estimated that an inserted fragment of 10 kb is acceptable for p2μM when there is no selection in the medium, and the inserted fragment of 14 kb is acceptable for p2μM under condition with selection. Zeng et al. (2021) moved the essential gene *TPI1* from chromosome to p2μ plasmid. With auxotrophic complementation of *TPI1*,

the resulting plasmid pE2μRT could undergo cultivation of 90 generations without loss under non-selective conditions.

Tyrosol biosynthetic pathway was introduced to demonstrate that the expression level of the p2μM-based plasmids was superior to that of the controls. After 40 generations of shake flask cultivation in YPD medium, the tyrosol yield of strain CEN.PK2-1C carrying plasmid p2μM-small-module was 54.46 ± 0.21 mg/L, about 9.7% higher than that of CEN.PK2-1C with pRS423M-small-module (49.64 ± 0.71 mg/L). The tyrosol titer of CEN.PK2-1C with p2μM-medium-module was 82.0% higher than that of strains carrying pRS423M-medium-module. The yield of tyrosol harvested from strains with p2μM-large-module was about threefold higher than that from strains with pRS423M-large-module. However, strains containing large module accumulated less tyrosol than strains containing small module and medium module, which was probably due to the instability of p2μM containing large module. Tyrosol production of the strain with p2μM-small-module at the 40th generation was 98.39 ± 0.41 mg/L with selective pressure, which was 80.7% greater than the strain with p2μM-small-module in non-selective medium and 65.2% higher than that of the strain with pRS423M-small-module in selective medium. The tyrosol yields of the strain containing plasmids pRS423M-medium-module and pRS423M-large-module at the 40th generation were all lower than those of the strains of p2μM-based plasmids with modules of the same size.

Taking these results into account, in order to improve the stability of endogenous 2μ-based expression vector in yeast, an essential gene could be introduced into the plasmid while knocking out the same essential gene in the genome to ensure the existence of engineered endogenous 2μ plasmid in yeast (Zeng et al., 2021). In the future, researchers could apply the CRISPR/Cas9 system to directly integrate metabolic pathways into the endogenous 2μ plasmid with an essential gene *in vivo* (Dean-Johnson and Henry, 1989; Zheng et al., 1993; Wang et al., 2020; Yang et al., 2021). In summary, our endogenous 2μ-based expression vector p2μM has improved stability than the commonly used YEp pRS423, so it could be applied in *S. cerevisiae* for genetic manipulations.

DATA AVAILABILITY STATEMENT

The original contributions presented in the study are included in the article/**Supplementary Material**, further inquiries can be directed to the corresponding author/s.

AUTHOR CONTRIBUTIONS

YT, JY, and YL conceived the study and carried out the molecular genetic studies as well as the strain construction. HL, YK, YZ, and YW participated in the design and coordination of the study. YT and JY performed the experiments and drafted the manuscript. YL supervised the whole research and revised the manuscript. All the authors read and approved the final manuscript.

FUNDING

SUPPLEMENTARY MATERIAL

The Supplementary Material for this article can be found online at: https://www.frontiersin.org/articles/10.3389/fmicb.2021.679665/full#supplementary-material

REFERENCES

Benedetto, R., Varì, R., Scazzocchio, B., Filesi, C., Santangelo, C., Giovannini, C., et al. (2007). Tyrosol, the major extra virgin olive oil compound, restored intracellular antioxidant defences in spite of its weak antioxidative effectiveness. *Nutr. Metab. Cardiovasc. Dis.* 17, 535–545. doi: 10.1016/j.numecd.2006.03.005

Bera, A. K., Ho, N. W., Khan, A., and Sedlak, M. (2011). A genetic overhaul of *Saccharomyces cerevisiae* 424A(LNH-ST) to improve xylose fermentation. *J. Ind. Microbiol. Biotechnol.* 38, 617–626. doi: 10.1007/s10295-010-0806-6

Boulet, A., Vest, K., Maynard, M., Gammon, M., Russell, A., Mathews, A., et al. (2017). The mammalian phosphate carrier SLC25A3 is a mitochondrial copper transporter required for cytochrome c oxidase biogenesis. *J. Biol. Chem.* 293:jbc.RA117.000265. doi: 10.1074/jbc.RA117.000265

Broach, J. R., and Hicks, J. B. (1980). Replication and recombination functions associated with the yeast plasmid, 2 mu circle. *Cell* 21, 501–508. doi: 10.1016/0092-8674(80)90487-0

Cao, M., Gao, M., Suastegui, M., Mei, Y., and Shao, Z. (2020). Building microbial factories for the production of aromatic amino acid pathway derivatives: from commodity chemicals to plant-sourced natural products. *Metab. Eng.* 58, 94–132. doi: 10.1016/j.ymben.2019.08.008

Cao, X., Yang, S., Cao, C., and Zhou, Y. J. (2020). Harnessing sub-organelle metabolism for biosynthesis of isoprenoids in yeast. *Synth. Syst. Biotechnol.* 5, 179–186. doi: 10.1016/j.synbio.2020.06.005

Chlebowicz-Śledziewska, E., and Śledziewski, A. Z. (1985). Construction of multicopy yeast plasmids with regulated centromere function. *Gene* 39, 25–31. doi: 10.1016/0378-1119(85)90103-9

Choe, K. I., Kwon, J. H., Park, K. H., Oh, M. H., Kim, M. H., Kim, H. H., et al. (2012). The antioxidant and anti-inflammatory effects of phenolic compounds isolated from the root of Rhodiola sachalinensis A. BOR. *Molecules* 17, 11484–11494. doi: 10.3390/molecules171011484

Christianson, T., Sikorski, R., Dante, M., Shero, J., and Hieter, P. (1992). Mulfunctional yeast high-copy-number shuttle vectors. *Gene* 110, 119–122. doi: 10.1016/0378-1119(92)90454-W

Dean-Johnson, M., and Henry, S. (1989). Biosynthesis of inositol in yeast. Primary structure of myo-inositol-1-phosphate synthase (EC 5.5.1.4) and functional analysis of its structural gene, the INO1 locus. *J. Biol. Chem.* 264, 1274–1283.

Gao, M., Cao, M., Suastegui, M., Walker, J., Rodriguez Quiroz, N., Wu, Y., et al. (2017). Innovating a Nonconventional Yeast Platform for Producing Shikimate as the Building Block of High-Value Aromatics. *ACS Synth. Biol.* 6, 29–38. doi: 10.1021/acssynbio.6b00132

Gerbaud, C., Fournier, P., Blanc, H., Aigle, M., Heslot, H., and Guerineau, M. (1979). High frequency of yeast transformation by plasmids carrying part or entire 2-micron yeast plasmid. *Gene* 5, 233–253. doi: 10.1016/0378-1119(79)90080-5

González, M., Brito, N., Hernández Bolaños, E., and Gonzalez, C. (2018). New tools for high-throughput expression of fungal secretory proteins in *Saccharomyces cerevisiae* and Pichia pastoris. *Microb. Biotechnol.* 12, 1139–1153. doi: 10.1111/1751-7915.13322

Hartley, J., and Donelson, J. (1980). Nucleotide sequence of the yeast plasmid. *Nature* 286, 860–865. doi: 10.1038/286860a0

Hohnholz, R., Pohlmann, K. J., and Achstetter, T. (2017). A set of isomeric episomal plasmids for systematic examination of mitotic stability in *Saccharomyces cerevisiae*. *Yeast* 34, 267–275. doi: 10.1002/yea.3231

Huang, M., Wang, G., Qin, J., Petranovic, D., and Nielsen, J. (2018). Engineering the protein secretory pathway of *Saccharomyces cerevisiae* enables improved protein production. *Proc. Natl. Acad. Sci. U. S. A.* 115, E11025–E11032. doi: 10.1073/pnas.1809921115

Jayaram, M., Li, Y. Y., and Broach, J. R. (1983). The yeast plasmid 2mu circle encodes components required for its high copy propagation. *Cell* 34, 95–104. doi: 10.1016/0092-8674(83)90139-3

Jensen, N. B., Strucko, T., Kildegaard, K. R., David, F., Maury, J., Mortensen, U. H., et al. (2014). EasyClone: method for iterative chromosomal integration of multiple genes in *Saccharomyces cerevisiae*. *FEMS Yeast Res.* 14, 238–248. doi: 10.1111/1567-1364.12118

Karković Marković, A., Torić, J., Barbarić, M., and Jakobusic Brala, C. (2019). Hydroxytyrosol, Tyrosol and Derivatives and Their Potential Effects on Human Health. *Molecules* 24:2001. doi: 10.3390/molecules24102001

Kikuchi, Y. (1983). Yeast plasmid requires a cis-acting locus and two plasmid proteins for its stable maintenance. *Cell* 35, 487–493. doi: 10.1016/0092-8674(83)90182-4

Kondo, H., Nakamura, Y., Dong, Y.-X., Nikawa, I., and Sueda, S. (2004). Pyridoxine biosynthesis in yeast: participation of ribose 5-phosphate ketol-isomerase. *Biochem. J.* 379, 65–70. doi: 10.1042/BJ20031268

Lee, D., Lloyd, N. D. R., Pretorius, I. S., and Borneman, A. R. (2016). Heterologous production of raspberry ketone in the wine yeast *Saccharomyces cerevisiae* via pathway engineering and synthetic enzyme fusion. *Microb. Cell Fact.* 15:49. doi: 10.1186/s12934-016-0446-2

Liu, H., Tian, Y., Zhou, Y., Kan, Y., Wu, T., Xiao, W., et al. (2020). Multi-modular engineering of *Saccharomyces cerevisiae* for high-titre production of tyrosol and salidroside. *Microb. Biotechnol.* doi: 10.1111/1751-7915.13667 [Epub Online ahead of print].

Liu, Q., Liu, Y., Chen, Y., and Nielsen, J. (2020). Current state of aromatics production using yeast: achievements and challenges. *Curr. Opin. Biotechnol.* 65, 65–74. doi: 10.1016/j.copbio.2020.01.008

Ludwig, D. L., and Bruschi, C. V. (1991). The 2-micron plasmid as a nonselectable, stable, high copy number yeast vector. *Plasmid* 25, 81–95. doi: 10.1016/0147-619x(91)90019-s

Luo, Y., Li, B. Z., Liu, D., Zhang, L., Chen, Y., Jia, B., et al. (2015). Engineered biosynthesis of natural products in heterologous hosts. *Chem. Soc. Rev.* 44, 5265–5290. doi: 10.1039/c5cs00025d

McQuaid, M. E., Polvi, E. J., and Dobson, M. J. (2019). DNA sequence elements required for partitioning competence of the *Saccharomyces cerevisiae* 2-micron plasmid STB locus. *Nucleic Acids Res.* 47, 716–728. doi: 10.1093/nar/gky1150

Misumi, Y., Nishioka, S., Fukuda, A., Uemura, T., Nakamura, M., Hoshida, H., et al. (2018). YHp as a highly stable, hyper-copy, hyper-expression plasmid constructed using a full 2-mum circle sequence in cir(0) strains of *Saccharomyces cerevisiae*. *Yeast* 36, 249–257. doi: 10.1002/yea.3371

Murray, A. W., and Szostak, J. W. (1983). Pedigree analysis of plasmid segregation in yeast. *Cell* 34, 961–970. doi: 10.1016/0092-8674(83)90553-6

Murray, J. A., and Cesareni, G. (1986). Functional analysis of the yeast plasmid partition locus STB. *EMBO J.* 5, 3391–3399. doi: 10.1002/j.1460-2075.1986.tb04655.x

Petes, T. D., and Williamson, D. H. (1975). Replicating circular DNA molecules in yeast. *Cell* 4, 249–253. doi: 10.1016/0092-8674(75)90172-5

Reider Apel, A., d'Espaux, L., Wehrs, M., Sachs, D., Li, R. A., Tong, G. J., et al. (2017). A Cas9-based toolkit to program gene expression in *Saccharomyces cerevisiae*. *Nucleic Acids Res.* 45, 496–508. doi: 10.1093/nar/gkw1023

Ren, Y., Liu, S., Jin, G., Yang, X., and Zhou, Y. J. (2020). Microbial production of limonene and its derivatives: achievements and perspectives. *Biotechnol. Adv.* 44:107628. doi: 10.1016/j.biotechadv.2020.107628

Rizvi, S. M. A., Prajapati, H. K., and Ghosh, S. K. (2018). The 2 micron plasmid: a selfish genetic element with an optimized survival strategy within *Saccharomyces cerevisiae*. *Curr. Genet.* 64, 25–42. doi: 10.1007/s00294-017-0719-2

Rizvi, S. M. A., Prajapati, H. K., Nag, P., and Ghosh, S. K. (2017). The 2-mum plasmid encoded protein Raf1 regulates both stability and copy number of the plasmid by blocking the formation of the Rep1-Rep2 repressor complex. *Nucleic Acids Res.* 45, 7167–7179. doi: 10.1093/nar/gkx316

Romanos, M. A., Scorer, C. A., and Clare, J. J. (1992). Foreign gene expression in yeast: a review. *Yeast* 8, 423–488. doi: 10.1002/yea.320080602

Sadowski, P. D. (1995). The Flp recombinase of the 2-microns plasmid of *Saccharomyces cerevisiae*. *Prog. Nucleic Acid Res. Mol. Biol.* 51, 53–91. doi: 10.1016/s0079-6603(08)60876-4

Stevens, B. J., and Moustacchi, E. (1971). Gamma satellite DNA and small twisted circular molecules in yeast *Saccharomyces cerevisiae*. *Exp. Cell Res.* 64, 259–266.

Suastegui, M., and Shao, Z. (2016). Yeast factories for the production of aromatic compounds: from building blocks to plant secondary metabolites. *J. Ind. Microb. Biotechnol.* 43, 1611–1624. doi: 10.1007/s10295-016-1824-9

Walfridsson, M., Hallborn, J., Penttilä, M., Keränen, S., and Hahn-Hägerdal, B. (1996). Xylose-metabolizing *Saccharomyces cerevisiae* strains overexpressing the TKL1 and TAL1 genes encoding the pentose phosphate pathway enzymes transketolase and transaldolase. *Appl. Enviro. Microbiol.* 61, 4184–4190. doi: 10.1128/AEM.61.12.4184-4190.1995

Wang, X., Chen, L., Liu, J., Sun, T., and Zhang, W. (2020). Light-Driven Biosynthesis of myo-Inositol Directly From CO2 in Synechocystis sp. PCC 6803. *Front. Microbiol.* 11:566117. doi: 10.3389/fmicb.2020.566117

Yang, Y., Hu, Y., Wu, L., Zhang, P., and Shang, J. (2021). dnm1 deletion blocks mitochondrial fragmentation in Deltafzo1 cells. *Yeast* 38, 197–205. doi: 10.1002/yea.3524

Zeng, B.-X., Yao, M.-D., Xiao, W.-H., Luo, Y.-Z., Wang, Y., and Yuan, Y.-J. (2021). Endogenous 2μ Plasmid Editing for Pathway Engineering in *Saccharomyces cerevisiae*. *Front. Microbiol.* 12:631462. doi: 10.3389/fmicb.2021.631462

Zhang, J., Chen, Y., Fu, L., Guo, E., Wang, B., Dai, L., et al. (2021). Accelerating strain engineering in biofuel research via build and test automation of synthetic biology. *Curr. Opin. Biotechnol.* 67, 88–98. doi: 10.1016/j.copbio.2021.01.010

Zhang, Y., Wang, J., Wang, Z., Zhang, Y., Shi, S., Nielsen, J., et al. (2019). A gRNA-tRNA array for CRISPR-Cas9 based rapid multiplexed genome editing in *Saccharomyces cerevisiae*. *Nat. Commun.* 10:1053. doi: 10.1038/s41467-019-09005-3

Zheng, P., Fay, D., Burton, J., Xiao, H., Pinkham, J., and Stern, D. (1993). SPK1 is an essential S-phase-specific gene of *Saccharomyces cerevisiae* that encodes a nuclear serine/threonine/tyrosine kinase. *Mol. Cell. Biol.* 13, 5829–5842. doi: 10.1128/MCB.13.9.5829

Check for
updates

Antifungal Secondary Metabolites Produced by the Fungal Endophytes: Chemical Diversity and Potential Use in the Development of Biopesticides

Kuo Xu†, Xiu-Qi Li†, Dong-Lin Zhao* and Peng Zhang*

Tobacco Research Institute of Chinese Academy of Agricultural Sciences, Qingdao, China

Plant diseases caused by phytopathogenic fungi can lead to huge losses in the agricultural fields and therefore remain a continuous threat to the global food security. Chemical-based fungicides contributed significantly in securing crop production. However, indiscriminate application of fungicides has led to increased chemical resistance and potential risks to human health and environment. Thus, there is an urgent need for searching for new bioactive natural products and developing them into new biopesticides. Fungal endophytes, microorganisms that reside in the fresh tissues of living plants, are regarded as untapped sources of novel natural products for exploitation in agriculture and/or medicine. Chemical examination of endophytic fungi has yielded enormous antifungal natural products with potential use in the development of biopesticides. This review summarizes a total of 132 antifungal metabolites isolated from fungal endophytes in the past two decades. The emphasis is on the unique chemical diversity of these metabolic products, together with their relevant antifungal properties. Moreover, some "star molecules," such as griseofulvin and trichothecene, as well as their synthetic derivatives that possess high potential as candidates of new natural fungicides, are also presented herein.

Keywords: fungal endophytes, secondary metabolites, chemical diversity, phytopathogenic fungi, antifungal activities, biopesticides

INTRODUCTION

Plant diseases caused by phytopathogenic fungi are continuing to be a huge threat in the agricultural fields. It is estimated that the global loss caused by plant diseases is more than 20% of the crop yield in the major food and cash crops worldwide (Kim et al., 2004). Fungal pathogens were responsible for the considerable postharvest losses of grain crops, fruits, and vegetables, which, in addition to causing decay, can produce mycotoxins that are harmful to humans and animals (Bai et al., 2013; Shi et al., 2017). Therefore, effective and sustained control of these fungal pathogens has become an urgent task. Chemical control has been widely adopted in crop production. During the past years, a great variety of chemical fungicides (agrochemicals), such as thiophanate-methyl, carbendazim, and imazalil, are designed and applied to control these diseases. It is indisputable that these chemicals have resulted in substantial increases in productivity and contributed significantly in agricultural industry. However, these most-applied chemical fungicides have been limited by many

serious problems. Indiscriminate use of these fungicides has led to the appearance of pathogens with multiple fungicide resistances, which further complicated the management of the diseases (Talibi et al., 2014). Furthermore, repeated and exclusive use of fungicides is increasingly restricted owing to their undesirable effects on non-target organisms (carcinogenicity, high and acute residual toxicity) and potential risks to environmental pollution (long degradation period) (Bai et al., 2013; Talibi et al., 2014). Thus, these synthetic chemical fungicides are subject to registration and permission for use, and are even no longer authorized in various countries.

Based on above questions, the challenge is to develop new and eco-friendly alternatives for the safe control of these pathogens, which pose low risk to human health and environment. Nowadays, many promising biological approaches were considered to be potential alternatives to synthetic fungicides, including (i) use of biocontrol microorganisms, (ii) application of naturally sourced metabolites, and (iii) induction of natural resistance (Talibi et al., 2014). Among them, naturally sourced secondary metabolites from microbes have attracted great attention. Microorganisms are well known for their ability to synthesize bioactive secondary metabolites, which have provided abundant chemical entities for pharmaceuticals and agrochemicals. Many natural antifungal fungicides, such as kasugamycin, polyoxins, validamycin, and blasticidin-S, have been obtained from microbial resources (Copping and Duke, 2007; Wang et al., 2016).

Fungal endophytes, microorganisms that asymptomatically reside in the internal tissues of plants, have been widely distributed in almost every plant and are rich in diversity (Jia et al., 2016). Endophytic fungi have a close and complex interaction with their hosts, which involve mutualism, antagonism and rarely parasitism (Gouda et al., 2016). These species are known to promote host growth and gain essential nutrition. They also provide tolerance to plants against various types of abiotic and/or biotic stresses. Most importantly, they possess the ability to produce plenty of structurally diverse and biologically active secondary metabolites to protect their hosts from pathogenic microorganisms and pests. In this sense, endophytic fungi are a treasure source of searching for novel secondary metabolites with immense potential agricultural applications. It has been reported that a large number of metabolites with different chemical skeletons have been deciphered from endophytic fungi, such as alkaloids, terpenoids, steroids, peptides, benzopyranones, quinones, and isocoumarins (Gouda et al., 2016). Chemically speaking, the discovery of these metabolites provided impressive chemical basis in the development of agrochemicals. Moreover, most of them exhibited promising bioactivities, such as antifungal, antibacterial, herbicidal, nematocidal, insecticidal, and other agricultural activities.

Therefore, the topical subject of antifungal secondary metabolites produced by fungal endophytes has been searched and analyzed. The literature search was conducted using the combined keywords "antifungal," "secondary metabolites," and "endophytic fungus" in the databases such as Web of Science, Google Scholar, and SciFinder Scholar, with a previously reported search method (Zhang et al., 2020). As a result, a total of 132 metabolites with anti-phytopathogenic activities from fungal endophytes in the past two decades (covering from 2000 to 2020) were included in this review. The present compounds possess diverse chemical structures, which were classified into alkaloids (including cytochalasins, indoles, diketopiperazines, and other nitrogen-containing compounds), terpenoids, polyketides (quinones, macrolides, benzopyrones and unsaturated lactones), and other miscellaneous compounds within a biogenetic context. Moreover, we also describe the sources, the producing strains, target plant pathogenic fungi, and their potential use as lead compounds in the development of biopesticides.

CONFUSED ISSUES NEED TO BE ADDRESSED

Prior to the beginning of this review, there are three issues that need to be addressed. (i) The level of antifungal potency should be standardized. As we can see from literatures, the literatures are replete with uncalibrated potency descriptors, including 'mild, moderate, strong, pronounced, significant, remarkable, and potent.' Apparently these descriptions confused the readers that which level means strong and which should be defined as weak. The unified standardization has not yet formed since the definition of the level of bioactivity just represents the individual judgment of the authors. However, in this review, the antifungal potency was distinguished as 'potent,' 'moderate,' and 'weak' based on the comparison with positive controls. We discretionarily define 'potent' as the antifungal activity higher than that of the positive controls, 'moderate' as the bioactivity equal to that of the positive controls, and 'weak' as that of lower than positive controls (or inactive) throughout this review. (ii) Quantitative comparisons of the results of the bioactivity tests between different studies are problematic. As the fungal pathogens used in bioassays may have different provenance and viability/sensitivity with different assay protocols, the comparisons should be qualified by consideration of positive/negative controls, and even then should be best limited within individual studies, rather than between different studies. (iii) The selection of different positive controls may lead to radically different results. Commercial fungicides were generally chosen as positive controls. However, since they belong to different chemical classes, they may present distinct potency and mechanisms of action.

CHEMICAL DIVERSITY OF ANTIFUNGAL SECONDARY METABOLITES FROM ENDOPHYTIC FUNGI

Cytochalasin Alkaloids

The cytochalasin alkaloids are a class of structurally related fungal metabolic products. To date, more than 300 cytochalasin analogs have been isolated from many genera of ascomycetes and

FIGURE 1 | Cytochalasin alkaloids characterized from endophytic fungi (1–14).
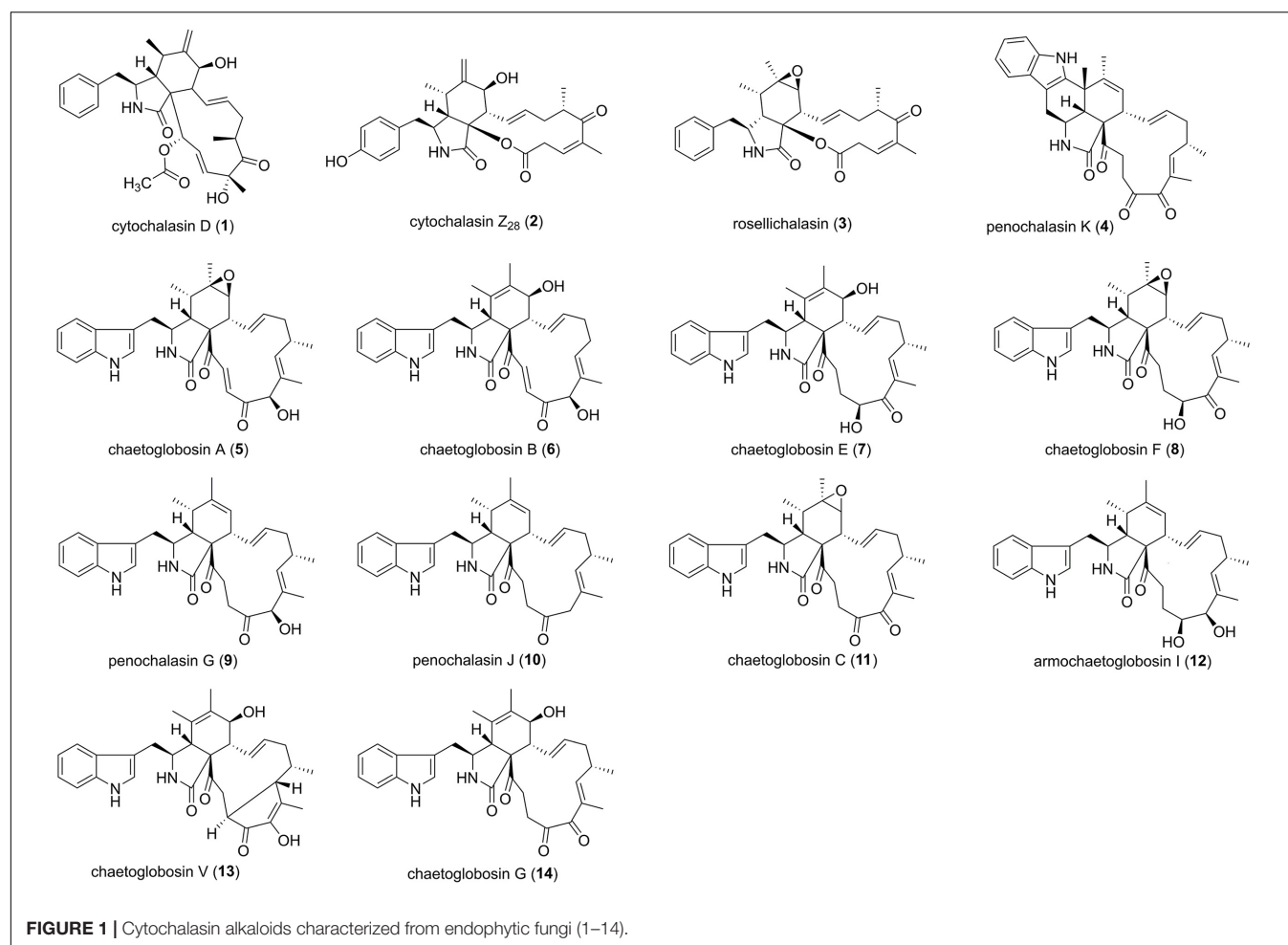
basidiomycetes, including *Aspergillus, Chaetomium, Penicillium, Phomopsis, Phoma, Spicaria, Xylaria,* and so on (Wei et al., 2017). Structurally, cytochalasins are characterized by a highly substituted perhydroisoindol-1-one moiety which is fused with a 9- to 15-membered macrocyclic ring. Many of cytochalasins exhibit a wide range of biological activities, such as cytotoxic, antimicrobial, and phytotoxic properties (Wei et al., 2017; Xu et al., 2017). 14 cytochalasins (**Figure 1**) isolated from fungal endophytes were reported to possess moderate to potent antifungal activity. Cytochalasin D (1) was produced by various endophytic fungi *Xylaria* sp., which were isolated from leaves of guarana plant (Elias et al., 2018). 1 showed fungistatic activity against the phytopathogen *Colletotrichum gloeosporioides*, which causes the anthracnose disease, with an MIC of 2.46 mM. Commercial fungicides captan and difenoconazole were applied as positive controls (MICs 16.63 and 0.02 mM, respectively) (Elias et al., 2018). Bioassay-guided separation of *Xylaria* sp. XC-16, an endophyte from *Toona sinensis* led to the discovery of five agriculturally active cytochalasin alkaloids, including a new compound cytochalasin Z_{28} (2) (Zhang Q. et al., 2014). Compound 2 showed potent fungicidal effect (MIC = 12.5 μM) against the phytopathogen *Gibberella saubinetti*, which was better than that of the positive control hymexazol (MIC = 25 μM)

(Zhang Q. et al., 2014). Chemical investigation of the biocontrol potential endophytic fungus *Aspergillus capensis* CanS-34A in *Brassica napus* has resulted in the isolation and identification the antifungal metabolite rosellichalasin (3) (Qin et al., 2019). 3 inhibited the plant pathogenic fungi *Botrytis cinerea, Monilinia fructicola, Sclerotinia sclerotiorum,* and *S. trifoliorum* with the EC_{50} values of 36.8, 87.1, 5.3, and 41.1 μM, respectively. Thus, *S. sclerotiorum* was the most sensitive target fungus (Qin et al., 2019). A new chaetoglobosin, penochalasin K (4) possessing a rare six-cyclic 6/5/6/5/6/13 fused ring system, was isolated from the solid culture of the mangrove endophytic fungus *Penicillium chrysogenum* V11 (Zhu et al., 2017b). Compound 4 displayed potent selective activities against *C. gloeosporioides* and *Rhizoctonia solani*, with MIC values of 6.13 and 12.26 μM, respectively, which were about ten-fold and two-fold better than that of the positive control carbendazim (Zhu et al., 2017b). Five metabolites, chaetoglobosins A (5), B (6), E (7), F (8), and penochalasin G (9), were obtained from endophytic *Chaetomium globosum*, isolating from the seeds of *Panax notoginseng* (Li et al., 2016). Some of them exhibited remarkable inhibition against phytopathogenic fungi causing root rot disease. For example, chaetoglobosin E (7) and penochalasin G (9) indicated potent inhibition against *Epicoccum nigrum* with the MICs < 2 μM
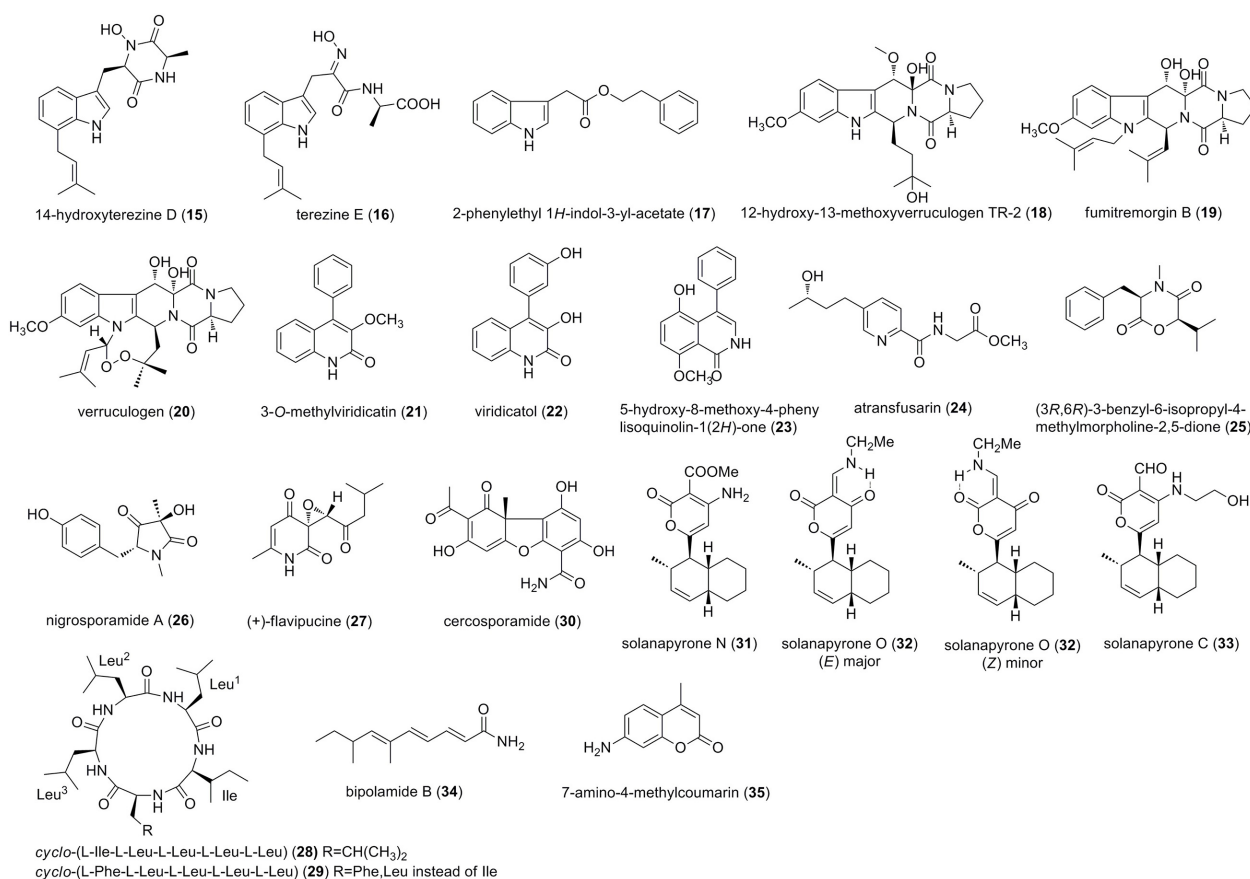
FIGURE 2 | Other alkaloids characterized from endophytic fungi (15–35).

(Li et al., 2016). A new chaetoglobosin named penochalasin J (10), as well as two known chaetoglobosins, chaetoglobosin C (11) and armochaetoglobosin I (12), were isolated from the mangrove endophytic fungus *P. chrysogenum* V11 (Huang et al., 2016). Compound 10 showed more potent antifungal activity against plant pathogen *C. gloeosporioides* with an MIC value of 25.08 μM, than the positive control carbendazim (MIC = 65.38 μM). Simultaneously, compounds 11 and 12 remarkably inhibited *R. solani*, with MIC values of 23.66 and 12.11 μM, respectively (Huang et al., 2016). Chaetoglobosins V (13) and G (14) were isolated from the culture of the endophytic fungus *C. globosum*, associated with the leaves of *Ginkgo biloba* tree (Xue et al., 2012). Compounds 13 and 14 exhibited potent antifungal activity against *Alternaria solani*, with MICs of 47.3 μM, while 14 also possessed potent activity against *A. alternate*, with an MIC of 47.3 μM (Xue et al., 2012). In total, the above results indicated that cytochalasin alkaloids could be used as fungicides or as leads of new fungicides to the related phytopathogenic fungi.

Alkaloids

Except for the cytochalasins, alkaloids also include indoles, diketopiperazines, cyclopeptides, amides, and other N-containing compounds (**Figure 2**). Two prenylated tryptophan

analogs, a previously reported 14-hydroxyterezine D (15) and a new terezine E (16), were isolated from an endophytic *Mucor* sp. from the medicinal plant *Centaurea stoebe* (Abdou et al., 2018). Both 15 and 16 exerted weak antifungal efficacy against *Aspergillus terreus*, with MICs of 127.8 and 111.2 μM, respectively (Abdou et al., 2018). Chemical investigation of the endophytic fungus *C. gloeosporioides* from the leaves of *Michelia champaca* resulted in the isolation of one new indole alkaloid, 2-phenylethyl 1*H*-indol-3-yl-acetate (17) (Chapla et al., 2014). 17 exhibited moderate activity against *Cladosporium cladosporioides* and *C. sphaerospermum* at 5 μg, which was comparable to that observed for the positive control nystatin (Chapla et al., 2014). Three prenylated indole diketopiperazine alkaloids, 12β-hydroxy-13α-methoxyverruculogen TR-2 (18), fumitremorgin B (19), and verruculogen (20), were isolated from *Aspergillus fumigatus* LN-4, an endophytic fungus isolated from the stem bark of *Melia azedarach* (Li et al., 2012). Compounds 18-20 showed broad-spectrum anti-phytopathogenic activities against eight fungi (*B. cinerea, A. solani, A. alternata, C. gloeosporioides, Fusarium solani, F. oxysporum* f. sp. *niveum, F. oxysporum* f. sp. *vasinfectum,* and *G. saubinettii*), with MIC values of 13.7-100 μM, which were comparable to the positive controls carbendazim and hymexazol (Li et al., 2012). Two quinolinones 3-O-methylviridicatin (21) and viridicatol (22), together with

FIGURE 3 | Terpenoids characterized from endophytic fungi (36–49).
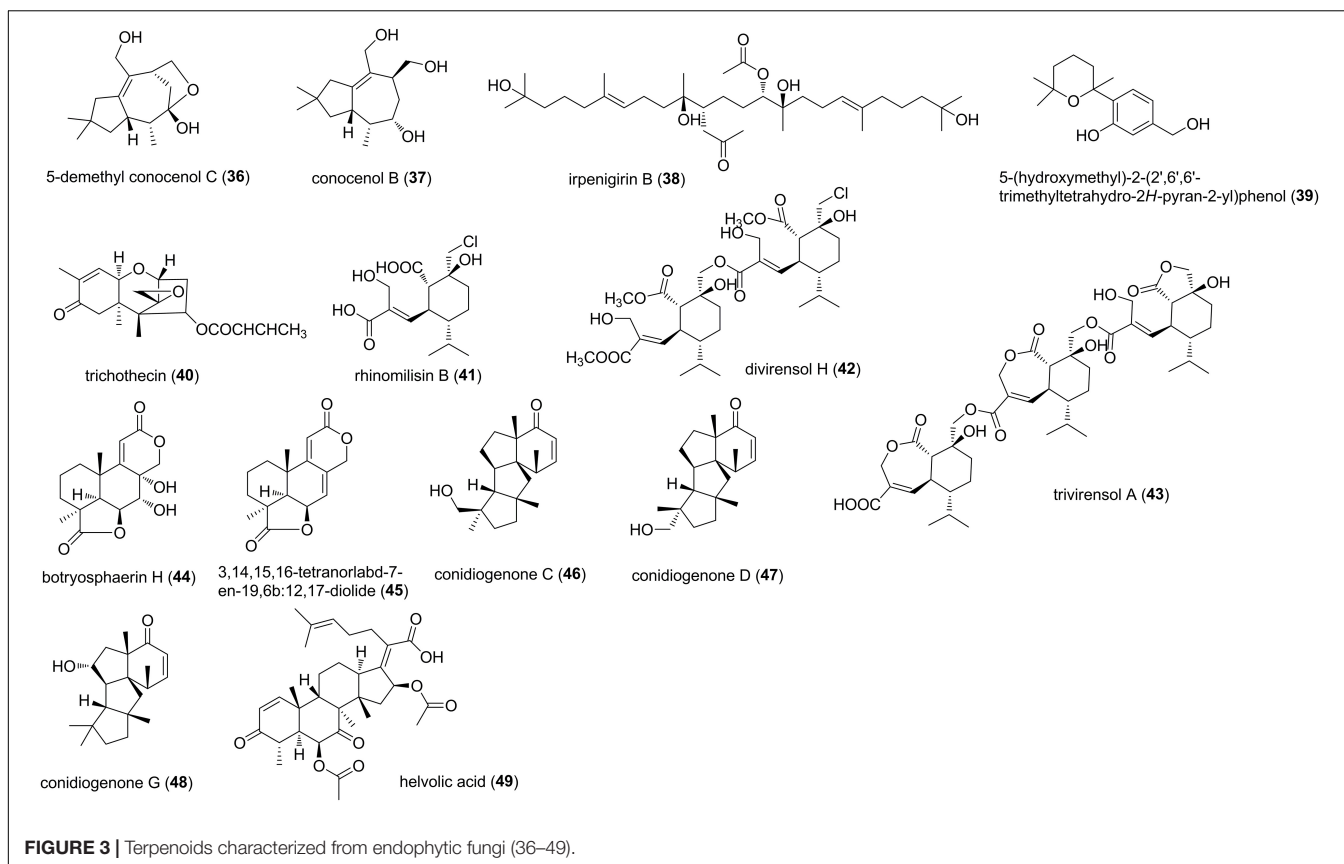
a new isoquinolone alkaloid named 5-hydroxy-8-methoxy-4-pheny lisoquinolin-1(2H)-one (23) were isolated from the fermentation of an endophytic fungus *Penicillium* sp. R22 in *Nerium indicum* (Ma et al., 2018). Compounds 21-23 exhibited weak to moderate antifungal activities against *Alternaria brassicae*, *A. alternate*, *B. cinerea*, and *Valsa mali* with MIC values of 124.3, 123.3, and 116.8 μM, respectively (Ma et al., 2018). A new fusaric acid derivative, atransfusarin (24), and (3R,6R)-3-benzyl-6-isopropyl-4-methylmorpholine-2,5-dione (25) were isolated from the culture of an endophyte *Alternaria atrans* MP-7, associated with the medicinal plant *Psidium guajava* (Yang Z. et al., 2019). Compound 25 exhibited potent antifungal activities against *A. solani*, *C. gloeosporioides,* and *Phyricularia grisea* with MICs of 6.25 μM, better than that of a broad-spectrum fungicide carbendazim. In contrast, 24 only exerted weak activities against *B. cinerea* and *A. solani* (MIC = 50 μM) (Yang Z. et al., 2019). A new pyrrolidinone derivative, named nigrosporamide A (26), was obtained from an endophytic fungus *Nigrospora sphaerica* ZMT05, which was isolated from *Oxya chinensis Thunberg* (Zhu et al., 2017a). 26 exhibited higher antifungal activity against *C. gloeosporioides* with an MIC value of 25.14 μM, than the positive control triadimefon (MIC = 272.39 μM) (Zhu et al., 2017a). It should be pointed out that the MIC of the positive control triadimefon (272.39 μM) seems to be outside the error measurements, probably because triadimefon is insensitive to *C. gloeosporioides*. As we discussed above, other appropriate positive controls should be rechose. From the culture extracts of

the endophytic fungus *Phoma* sp. isolated from the plant *Salsola oppositifolia*, a new pyridione epoxide derivative, (+)-flavipucine (27), was isolated and characterized (Loesgen et al., 2011). This metabolite showed strong antifungal inhibition down to 7.81 ppm (Inhibitory concentration, 90% of growth inhibition) against *Phytophthora infestans* and down to 31.3 ppm against *Septoria tritici* (Loesgen et al., 2011). Two cyclic pentapeptides 28 and 29 were isolated from *Cryptosporiopsis* sp., an endophytic fungus from *Zanthoxylum leprieurii* (Rutaceae) (Talontsi et al., 2012). Compounds 28 and 29 exhibited motility inhibitory and lytic activities against *Plasmopara viticola* zoospores, a grapevine downy mildew pathogen, at 17.7-44.3 μM. Moreover, both of them also displayed potent inhibitory effects against mycelial growth of *Pythium ultimum, Aphanomyces cochlioides,* and *R. solani* (Talontsi et al., 2012). A metabolite cercosporamide (30) was isolated from the endophytic fungus *Cadophora orchidicola* from *Kalimeris indica* (Wang et al., 2019). Antifungal assay revealed that 30 had potent growth inhibition against five plant pathogens, *Pestalotia diospyri, B. cinerea, Fusarium oxysporum, Sclerotium rolfsii,* and *Penicillum digitatum*, with EC$_{50}$ values of 16.0×10^{-3}, 1.8, 2.8, 2.89, and 20.2 μM, respectively (Wang et al., 2019). Two new solanapyrone analogs, solanapyrones N (31) and O (32), and the known solanapyrone C (33), were isolated from *Nigrospora* sp. YB-141, an endophytic fungus obtained from *Azadirachta indica* (Wu et al., 2009). Compound 32 was regarded as an inseparable mixture of (E)-32 and (Z)-32. Compound 31 showed moderate activity against *Penicillium islandicum* at
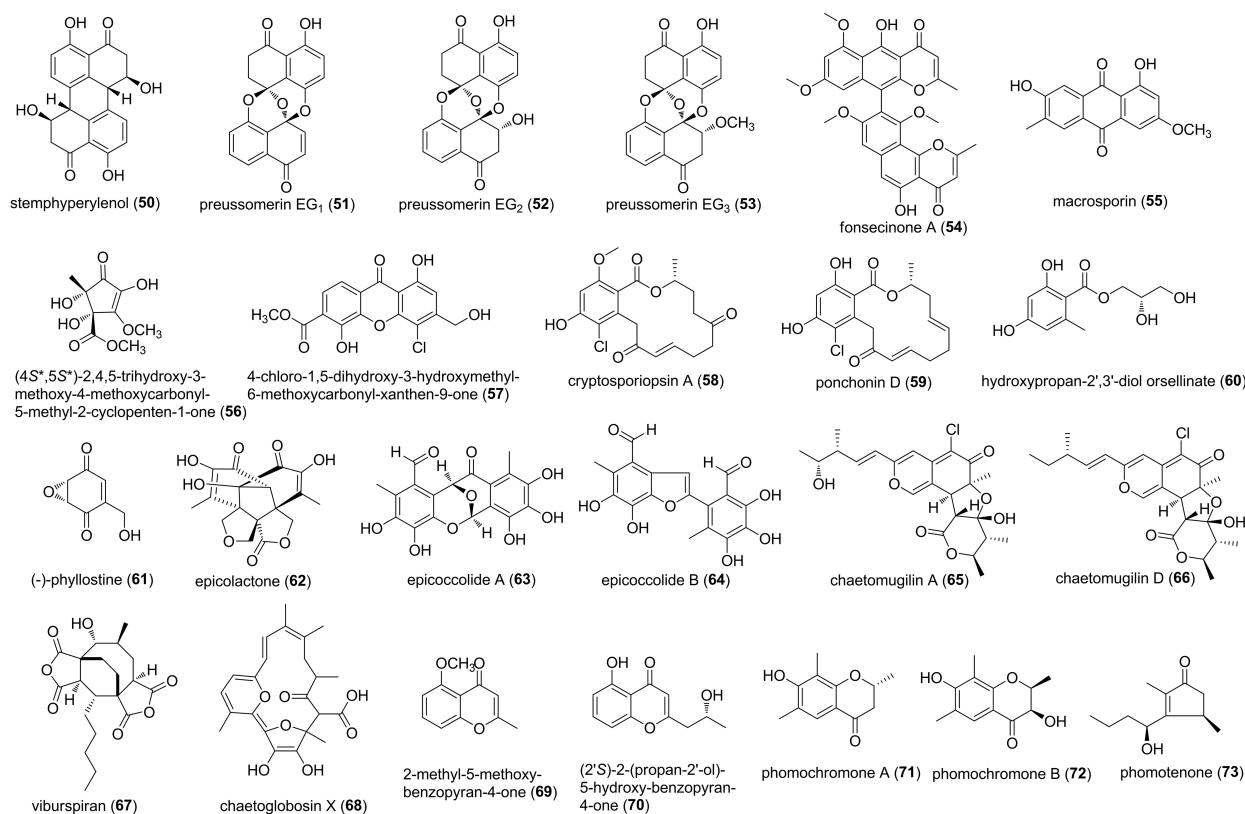
FIGURE 4 | Polyketides characterized from endophytic fungi (50–73).

equivalent concentration of 98.6 μM compared with the positive control nystatin (Wu et al., 2009). Bipolamide B (34), a new triene fatty acid amide, was discovered from the endophytic fungus *Bipolaris* sp. MU34 of Thai medicinal plants *Gynura hispida* (Siriwach et al., 2014). Compound 34 showed weak to meoderate broad-spectrum antifungal activities against *C. cladosporioides, C. cucumerinum, Saccharomyces cerevisiae, Aspergillus niger,* and *Rhizopus oryzae*, with MICs of 82.9, 165.8, 165.8, 331.6, and 331.6 μM, respectively (Siriwach et al., 2014). An endophytic *Xylaria* sp. with broad antimicrobial activity was isolated from *Ginkgo biloba* L. Bioactivity-guided fractionation led to the identification of 7-amino-4-methylcoumarin (35) (Liu et al., 2008). Antimicrobial assay showed that 35 inhibited the growth of the tested 13 pathogens including *Penicillium expansum* (MIC, 228.6 μM) and *A. niger* (142.8 μM) (Liu et al., 2008).

Terpenoids

Terpenoids produced by fungi are one of the most numerous and structurally diverse secondary metabolites with a wide array of pharmacological properties (**Figure 3**). The coculture of the phytopathogenic *Nigrospora oryzae* and endophytic *Irpex lacteus* from the same host *Dendrobium officinale* afforded a new tremulane sesquiterpene 5-demethyl conocenol C (36), conocenol B (37), and a new squalene irpenigirin B (38) (Wu et al., 2019). The new compounds 36 and 38 were active against *C. gloeosporioides*, with MICs of 31.7 and 13.4 μM, while 36

showed antifungal activity against *Didymella glomerata* with an MIC of 3.9 μM (Wu et al., 2019). It was also found that the mutually antagonistic relationship between the phytopathogens and endophytes can lead to the production of antibiotics, which inhibit the growth of phytopathogens and hinder certain phytotoxins (Wu et al., 2019). A new natural sesquiterpene 5-(hydroxymethyl)-2-(2′,6′,6′-trimethyltetrahydro-2H-pyran-2-yl)phenol (39) was characterized from endophytes belonging to the *Lophodermium* sp., which were isolated from the needles of superior *Pinus strobus* (eastern white pine) trees (Sumarah et al., 2011). 39 was antifungal against the rust *Microbotryum violaceum* with an MIC of 2 μM (Sumarah et al., 2011). *Trichothecium roseum* LZ93, an endophyte from medicinal plant *Maytenus hookeri*, was found to antagonize various phytopathogens *in vitro*. Chemical investigation of this fungal strain afforded a trichothecene, trichothecin (40), with weak to moderate inhibition on phytopathogenic fungi *Typhula incarnate* (MIC, 150.6 μM), *Gaeumannomyces graminis* (MIC, 90.4 μM), *Phytophthora infestans* (MIC, 90.4 μM), *A. solani* (MIC, 15.1 μM), and *Phyricularia oryzae* (MIC, 60.2 μM) (Zhang et al., 2010). A monosesquiterpene rhinomilisin B (41), a new dimeric sesquiterpene divirensol H (42), and an unprecedented trimeric sesquiterpene trivirensol A (43), were purified from *T. virens* FY06, an endophyte derived from *Litchi chinensis* Sonn (Hu et al., 2019). Compounds 41-43 exhibited moderate to potent activities on *Penicillium italicum,*
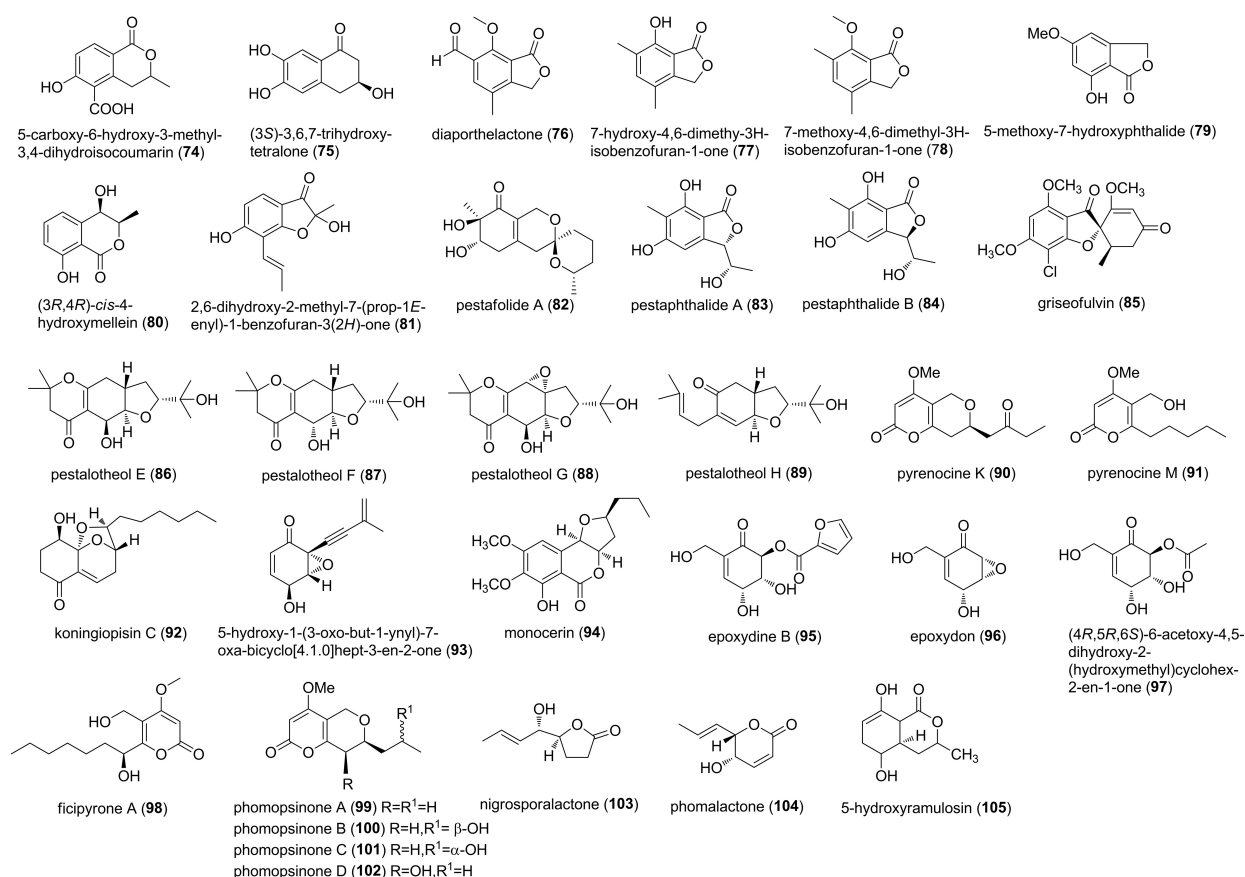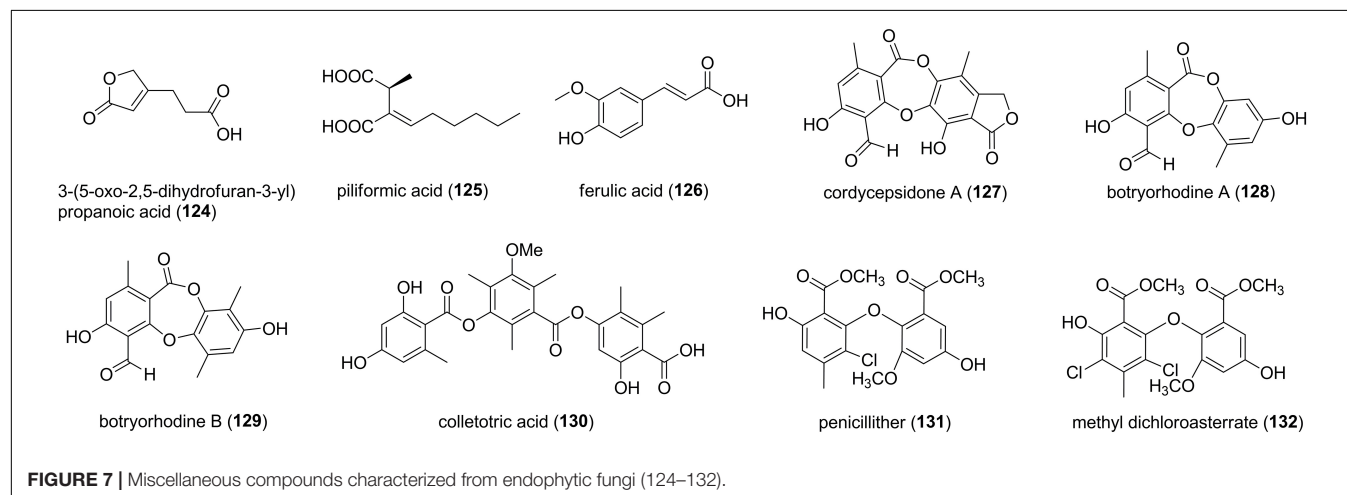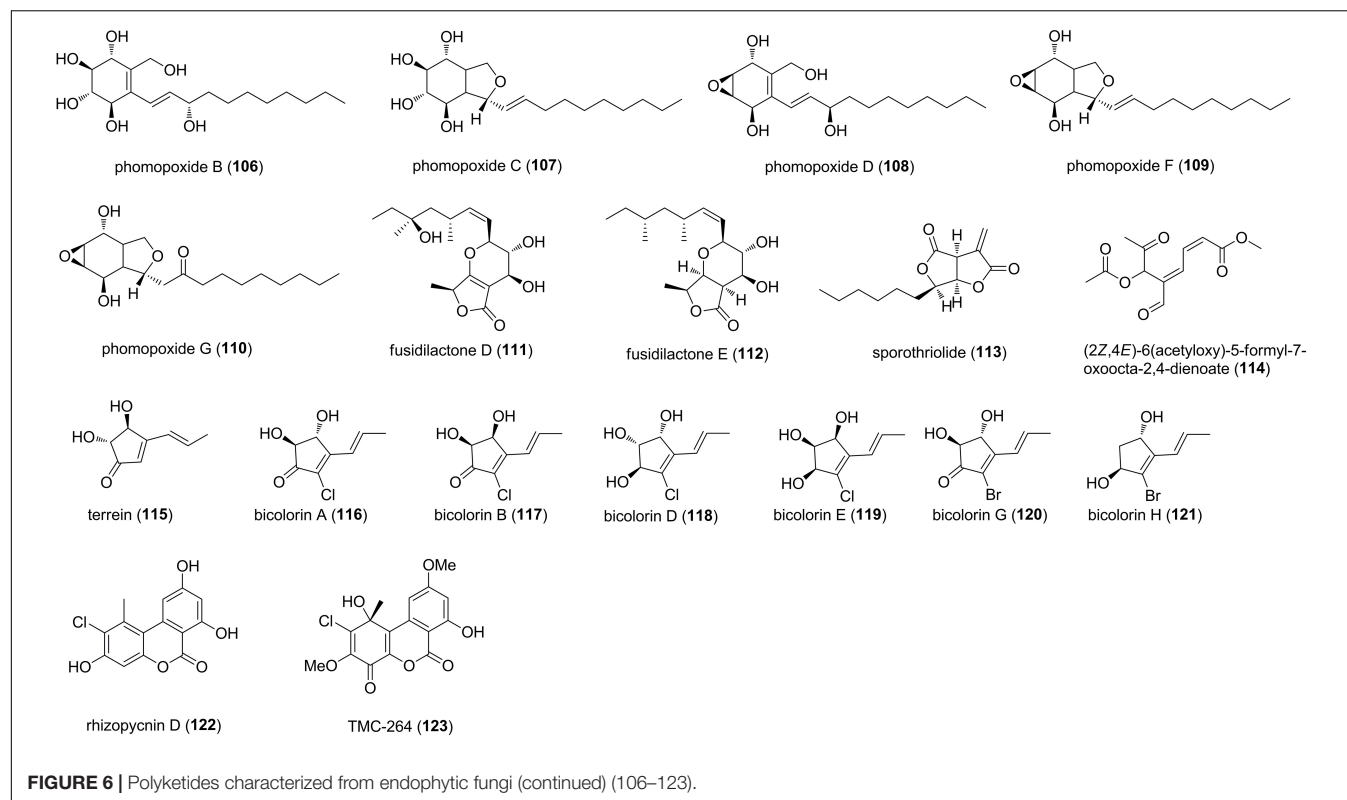
FIGURE 5 | Polyketides characterized from endophytic fungi (continued) (74–105).

F. oxysporum, F. graminearum, Colletotrichum musae, and *C. gloeosporioides.* 41 showed potent inhibitory activity against *C. musae,* with an MIC value of 37.4 μM, which was superior to that of the positive control triadimefon (273.0 μM). Moreover, 42 was more active toward *F. oxysporum, C. gloeosporioides, C. musae, P. italicm,* and *F. graminearum,* which were 8, 8, 3.2, 8, and 24 times as high as those of triadimefon (Hu et al., 2019). Interestingly, as metabolites of the endophytic fungus from *L. chinensis,* all the isolated sesquiterpenes presented potent antifungal activities against *C. gloeosporioides.* The phytopathogenic fungus *C. gloeosporioides* can cause anthracnose in *L. chinensis,* indicating that the metabolites produced by endophytes from its host may play a defensive role by inhibiting invasive phytopathogens. Two tetranorlabdane diterpenoids, botryosphaerin H (44) and 13,14,15,16-tetranorlabd-7-en-19,6β:12,17-diolide (45), were isolated from the endophytic fungus *Botryosphaeria* sp. P483 of the Chinese herbal medicine *Huperzia serrata* (Chen et al., 2015). Compounds 44 and 45 showed strong antifungal activities against *G. graminis, F. moniliforme, F. solani, F. oxysporum* and *Pyricularia oryzae* at 100 μg/disk (Chen et al., 2015). Three diterpenes, conidiogenones C (46), D (47), and G (48), were isolated from an endophytic fungus *Leptosphaeria* sp. XL026 derived from the leaves of *Panax notoginseng* (Chen et al., 2019). Compounds 46

and 48 showed moderate antifungal activity against *Rhizoctonia cerealis,* as well as 47 against *Verticillium dahlia,* with an MIC value of 41.4 μM (Chen et al., 2019). A nordammarane triterpenoid helvolic acid (49) was obtained from *Aspergillus fumigatus,* an endophytic fungus associated with *Melia azedarach* (Li et al., 2012). 49 exhibited broad-spectrum and potent antifungal activities against *B. cinerea, A. solani, A. alternata, C. gloeosporioides, F. solani, F. oxysporum, F. oxysporum,* and *G. saubinettii,* with MIC values of 11.0-88.1 μM (Li et al., 2012).

Polyketides

Polyketides are a large class of structurally diverse natural products that exhibit a wide range of bioactivities. These metabolites are generally biosynthesized by polyketide synthases, and simultaneously, some of them possess hybrid chemotypes derived from different biosynthetic pathways. In this review, chromones, quinines, macrolides, benzopyrones, unsaturated lactones, and phenols are all classified into polyketides (**Figures 4–6**). The culture of the fungus *Botryosphaeria dothidea* KJ-1, isolated from the stems of white cedar (*Melia azedarach* L.), yielded a perylenequinone derivative stemphyperylenol (50) (Xiao et al., 2014b). 50 displayed potent antifungal activity against *A. solani* with an MIC of 1.57 μM, compared to the commercially available fungicide carbendazim

FIGURE 6 | Polyketides characterized from endophytic fungi (continued) (106–123).

FIGURE 7 | Miscellaneous compounds characterized from endophytic fungi (124–132).

(Xiao et al., 2014b). Cultivation of the newly discovered fungal strain *Edenia gomezpompae*, an endophyte obtained from the leaves of *Callicarpa acuminata* (Verbenaceae), afforded three new naphthoquinone spiroketals, preussomerins EG$_1$ (51), EG$_2$ (52), and EG$_3$ (53) (Macías-Rubalcava et al., 2008). Spiroketals 51-53 displayed significant growth inhibition against four economically important phytopathogens (*Phythophtora capsici, P. parasitica, F. oxysporum,* and *A. solani*), with IC$_{50}$ values ranging from 57.5 to 447.4 µM (Macías-Rubalcava et al., 2008). Fonsecinone A (54), a dimeric naphtha-γ-pyrone, was characterized from the culture of *Aspergillus* sp. KJ-9, an endophytic fungus residing in the stem bark of *Melia azedarach*

(Xiao et al., 2014a). Compound 54 had marked inhibition of *G. saubinetti, Magnaporthe grisea, B. cinerea,* and *A. solani*, with MICs in the range of 6.25-50 µM, which were better than or similar to that of hymexazol (MIC 50 µM) (Xiao et al., 2014a). An anthraquinone, macrosporin (55), was isolated from the mangrove endophytic fungus *Phoma* sp. L28 (Huang et al., 2017). 55 possessed broad-spectrum antifungal activities against *F. oxysporum, F. graminearum, C. musae, P. italic, R. solani,* and *C. gloeosporioides,* with MIC values ranging from 13.2 to 252.1 µM. It should be pointed out that the inhibitory activity of 55 against *F. oxysporum* (MIC = 13.2 µM) was higher than that of the positive control carbendazim (MIC = 32.7 µM)

(Huang et al., 2017). Then, from the same host plant (semi-mangrove plant *Myoporum bontioides*), an endophytic fungus *Alternaria* sp. R6 was isolated. A racemic new cyclopentenone derivative, (±)-(4*S**,5*S**)-2,4,5-trihydroxy-3-methoxy-4-methoxycarbonyl-5-methyl-2-cyclopenten-1-one (56), and a new xanthone 4-chloro-1,5-dihydroxy-3-hydroxymethyl-6-methoxycarbonyl-xanthen-9-one (57), were characterized from this fungal strain (Wang et al., 2015). In comparison to the positive control triadimefon (MIC 510.64 µM), compounds 56 and 57 exhibited inhibitory activities against *F. graminearum* with MICs of 215.52 and 107.14 µM, respectively, while 57 also showed potent antifungal activity against *C. musae* with an MIC of 214.29 µM (Wang et al., 2015). *Cryptosporiopsis* sp., an endophytic fungus from the medicinal plant *Zanthoxylum leprieurii*, was the source of new polyketides, cryptosporiopsin A (58), ponchonin D (59), hydroxypropan-2′,3′-diol orsellinate (60), and (-)-phyllostine (61) (Talontsi et al., 2012). Compounds 59-61 exhibited motility inhibitory and zoosporicidal activities against *P. viticola* zoospores at 28.6-71.4 µM. Meanwhile, they also displayed mycelial growth of *P. ultimum, A. cochlioides*, and *R. solani* with MICs of 20-40 µg/disk (Talontsi et al., 2012). An endophytic fungus, *Epicoccum* sp. CAFTBO, obtained from the cocoa tree *Theobroma cacao* was found to produce three new unprecedented polyoxygenated polyketides, epicolactone (62), epiccolides A (63) and B (64) (Talontsi et al., 2013). Compounds 62-64 significantly inhibited the growth of three notorious crop-devastating phytopathogens *P. ultimum, A. cochlioides,* and *R. solani* with MICs of 20-80 µg/disk (Talontsi et al., 2013). Two chlorine-substituted azaphilones, chaetomugilins A (65) and D (66), were isolated from endophytic *C. globosum* of *Panax notoginseng* (Li et al., 2016). Compounds 65 and 66 had moderate activity against *E. nigrum* with the MIC values of 17.8 and 36.9 µM, respectively (Li et al., 2016). Viburspiran (67), a structurally novel maleic anhydride natural products with an additional ethylene bridge, was isolated the fungal endophyte *Cryptosporiopsis* sp. from *Viburnum tinus* (Saleem et al., 2011). 67 was active against *Microbotryum violaceum* and *B. cinerea*, with inhibition radius of 6 and 10 mm at 50 µg substance/filter disk (Saleem et al., 2011). A new macrocyclic metabolite, chaetoglobosin X (68), was isolated from an endophytic fungus *C. globosum* obtained from the medicinal plant *Curcuma wenyujin* (Wang Y. et al., 2012). 68 possessed reasonably potent fungistatic activities on *Exserohilum turcicum, F. oxysporum,* and *Curvularia lunata* with an MIC of 7.5 µM and showed moderate activity against *F. graminearum* and *F. moniliforme* with an MIC of 15.1 µM (Wang Y. et al., 2012). Two benzopyran derivatives, 2-methyl-5-methoxy-benzopyran-4-one (69) and (2′*S*)-2-(propan-2′-ol)-5-hydroxy-benzopyran-4-one (70), were isolated from the isolate of *Curvularia* sp., which was obtained from the leaves of a native plant *Ocotea corymbosa* (Teles et al., 2005). Compounds 69 and 70 exhibited moderate antifungal activity against *C. sphaerospermum* and *C. cladosporioides* with a detection limit of 10 µg (Teles et al., 2005). Two new chromones, phomochromones A and B (71 and 72), and one new natural cyclopentenone derivative, phomotenone (73), was obtained from *Phomopsis* sp., an endophyte isolated from

Cistus monspeliensis (Ahmed et al., 2011). Compounds 71-73 showed moderate antifungal properties toward *Microbotryum violaceum*, with the radius of the inhibition zone of 8, 5, and 8 mm, respectively, at concentration of 50 µL of 1 mg/mL (Ahmed et al., 2011).

5-carboxy-6-hydroxy-3-methyl-3,4-dihydroisocoumarin (74) was produced from the endophyte *Xylaria* sp., associated with leaves of *Casearia sylvestris* (Chapla et al., 2018). 74 exhibited potent antifungal activities against two phytopathogenic fungi *C. cladosporioides* and *C. sphaerospermum* at 10 µg (Chapla et al., 2018). Bioassay-guided fractionation of the endophytic fungus *Phoma* sp. ZJWCF006 in the Chinese medicinal plant *Arisaema erubescens* afforded a new α-tetralone derivative, (3*S*)-3,6,7-trihydroxy-α-tetralone (75) (Wang L. W. et al., 2012). 75 showed selective growth inhibition against *F. oxysporium* and *R. solani* with EC$_{50}$ values of 2.1 and 0.3 mM, respectively, whereas no obvious activity was observed against *C. gloeosporioides* and *Magnaporthe oryzae* (Wang L. W. et al., 2012). Three known isobenzofuranones including diaporthelactone (76), 7-hydroxy-4,6-dimethy-3*H*-isobenzofuran-1-one (77), and 7-methoxy-4,6-dimethyl-3*H*-isobenzofuran-1-one (78) were obtained from the mangrove endophytic fungus *Phomopsis* sp. A123 from the foliage of *Kandelia candel* (Zhang W. et al., 2014). Compounds 76 and 77 displayed antifungal activity against *A. niger* with MICs of 243 and 485 µM, respectively, while 78 inhibited the growth of *A. alternaria* with an MIC of 500 µM (Zhang W. et al., 2014). Chemical and biological study on an unidentified Ascomycete, an endophyte isolated from *Meliotus dentatus*, led to the isolation of 5-methoxy-7-hydroxyphthalide (79) and (3*R*,4*R*)-*cis*-4-hydroxymellein (80) (Hussain et al., 2009). Compounds 79 and 80 showed antifungal activity against *Microbotryum violaceum* with the radius of zone of inhibition of 7 and 8 mm at a concentration of 50 µL of 1 mg/mL (Hussain et al., 2009). An antifungal strain *Verticillium* sp. from the roots of *Rehmannia glutinosa* yielded 2,6-dihydroxy-2-methyl-7-(prop-1*E*-enyl)-1-benzofuran-3(2*H*)-one (81) (You et al., 2009). 81 clearly inhibited biomass accumulation at a low concentration of 4.4 µM on the pathogens *Septoria* sp. and *Fusarium* sp. The growth of the producing strain *Verticillium* sp. itself was also inhibited to some degree by 81 (You et al., 2009). Pestafolide A (82), a novel reduced spiro azaphilone derivative, and pestaphthalides A (83) and B (84), two new isobenzofuranones, were isolated from *Pestalotiopsis foedan*, an endophyte from an unidentified tree (Ding et al., 2008). 82 displayed antifungal activity against *A. fumigatus*, affording a zone inhibition of 10 mm at 100 µg/disk, whereas 83 and 84 showed activity against *C. albicans* and *G. candidum*, with the zone inhibition of 13 and 11 mm, respectively (Ding et al., 2008). Griseofulvin (85) was produced by *Nigrospora* sp. LLGLM003, an endophytic fungus of the medicinal plant *Moringa oleifera* Lam (Zhao et al., 2012). *In vitro* antifungal assay indicated that 85 displayed potent inhibition of the test eight plant pathogenic fungi; of particular note was the antifungal activity against *B. cinerea* and *Colletotrichum orbiculare* with the EC$_{50}$ of 0.6 and 1.4 µM, respectively (Zhao et al., 2012). Four new metabolites, pestalotheols E-H (86-89), containing a reduced tetrahydro-2*H*-furo[3,2-*g*]chromene unit, were isolated

from a fungal endophyte, an unidentified Ascomycete from the tree *Arbutus unedo* (Qin et al., 2011). Compounds 86-89 showed antifungal activity against *Microbotryum violaceum*, with the radius of the inhibition zone of 6, 8, 6, and 7 mm, respectively, at 50 μg of test substance/test filter disk (Qin et al., 2011). Phytochemical studies of the active constituents of the endophytic fungus *Phomopsis* sp. led to the isolation of two new pyrenocine derivatives pyrenocine K (90) and M (91) (Hussain et al., 2012a). Both compounds also showed antifungal activity against *M. violaceum* in an agar diffusion assay, with inhibition zone of 5 mm at a concentration of 0.05 mg (Hussain et al., 2012a). A new fungal polyketide, koningiopisin C (92), was characterized from the culture broth of the fungus *Trichoderma koningiopsis* YIM PH 30002 from the medicinal plant *Panax notoginseng* (Liu et al., 2016). 92 exhibited antifungal activity against *Plectosphaerella cucumerina* with an MIC of 57.1 μM (Liu et al., 2016). The endophyte *Drechslera* sp. strain 678 was isolated from the roots of an Australian native grass *Neurachne alopecuroidea*, which demonstrated efficacy against several plant pathogens (d'Errico et al., 2020). Metabolomic analysis revealed the presence of two major bioactive metabolites, an alkynyl substituted epoxycyclohexenone derivative (5-hydroxy-1-(3-oxo-but-1-ynyl)-7-oxa-bicyclo[4.1.0]hept-3-en-2-one) (93) and monocerin (94). 93 and 94 were active against *B. cinerea* and *S. sclerotiorum* at 10 and 100 μg (d'Errico et al., 2020). A new epoxydon derivate epoxydine B (95), along with two related metabolites, epoxydon (96) and (4R,5R,6S)-6-acetoxy-4,5-dihydroxy-2-(hydroxymethyl)cyclohex-2-en-1-one (97), were obtained from an endophytic fungus, *Phoma* sp., isolated from the plant *Salsola oppostifolia* (Qin et al., 2010). Compounds 95-97 were biologically active exhibiting antifungal activity against *M. violaceum* at a concentration of 0.05 mg (Qin et al., 2010). A new α-pyrone (2H-pyran-2-one), ficipyrone A (98), was isolated from solid cultures of the plant endophytic fungus *Pestalotiopsis fici* from the tea plant *Camellia sinensis* (Liu et al., 2013). 98 displayed weak antifungal activity against *Gibberella zeae*, with an IC$_{50}$ value of 15.9 μM, compared with the positive control ketoconazole (IC$_{50}$ 6.02 μM) (Liu et al., 2013). Structural elucidation of the metabolites produced by the endophytic *Phomopsis* sp. revealed four new α-pyrone derivatives, phomopsinones A-D (99-102) (Hussain et al., 2012b). 99 showed potent antifungal activity against *B. cinerea* (inhibition zone of 17 mm), *P. oryzae* (25 mm), and *Septoria tritici* (20 mm), while 102 was active against *B. cinerea* (10 mm) and *S. tritici* (10 mm) (Hussain et al., 2012b). The fermentation of the endophytic fungus *Nigrospora* sp. YB-141 isolated from *A. indica* yielded two lactones, nigrosporalactone (103) and phomalactone (104) (Wu et al., 2009). Compounds 103 and 104 were active against *B. cinerea* with MIC values of 200.3 and 405.8 μM (Wu et al., 2009). Preliminary screening for antimicrobial activity of the endophytic fungi from *Cinnamomum mollisimum* yielded a polyketide, 5-hydroxyramulosin (105), which was identified as the major constituent of the bioactive fungal extracts (Santiago et al., 2012). 105 inhibited the fungal pathogen *A. niger* with the IC$_{50}$ value of 7.9 μM (Santiago et al., 2012).

Five new polyoxygenated cyclohexenoids, phomopoxides B (106), C (107), D (108), F (109), and G (110), were isolated from an endophytic fungal strain *Phomopsis* sp. YE3250 from the medicinal plant *Paeonia delavayi* (Huang et al., 2018). Compounds 106-110 were active against five pathogenic fungi (*C. albicans, A. niger, P. oryzae, F. avenaceum,* and *Hormodendrum compactum*) with MICs of 46.5-372.1 μM (Huang et al., 2018). Investigatation of the metabolites produced by the endophytic *Fusidium* sp., isolated from the leaves of *Mentha arvensis*, found two new bicyclic fusidilactones D (111) and E (112) (Qin et al., 2009). Both compounds had only moderate activity toward *Microbotryum violaceum*, with the radius of the inhibition zone of 7 and 10 mm, respectively (Qin et al., 2009). Through screening antifungal activity of endophytic fungi and subsequent bioassay-guided fractionation, sporothriolide (113) was isolated from the selected endophyte *Nodulisporium* sp. A21 in *Ginkgo biloba* (Cao et al., 2016). 113 was validated to be potently antifungal against the mycelia growth of *R. solani, S. sclerotiorum* and inhibit conidium germination of *M. oryzae in vitro* and *in vivo* (Cao et al., 2016). The screening of fungal extracts of *Lophodermium* sp. isolated from *P. strobus* resulted in the discovery of a new aliphatic polyketide, (2Z,4E)-6(acetyloxy)-5-formyl-7-oxoocta-2,4-dienoate (114) (Sumarah et al., 2011). 114 was antifungal against *M. violaceum* with MIC of 2 μM (Sumarah et al., 2011). Terrein (115) was isolated from the endophytic fungus *Aspergillus terreus* JAS-2 associated with medicinal plant *Achyranthus aspera* (Goutam et al., 2017). In antifungal assay, 10 μg/μL concentration of 115 showed inhibition of *Bipolaris Sorokiniana* (57.14%), *A. flavus* (52.5%), and *A. alternata* (91.25%) as compared to control (Goutam et al., 2017). Six new halogenated cyclopentenones, including four chlorinated, bicolorins A (116), B (117), D (118), and E (119), and two brominated bicolorins G (120) and H (121), were isolated from the endophytic fungus *Saccharicola bicolor* of *Bergenia purpurascens* (Zhao et al., 2020). Compounds 116-121 possessed weak to moderate activity against five pathogenic fungi-*Uromyces viciae-fabae, Pythium dissimile, G. zeae, A. niger,* and *S. sclerotiorum*, with MICs of 26.8-380.9 μM. 117 and 118, in particular, exhibited moderate activity against *P. dissimile* with the MICs of 33.0 and 44.7 μM, respectively, compared with the positive control cycloheximide (MIC 30.6 μM). Additionally, 118 was proven to be potently antifungal against *S. sclerotiorum in vivo*, indicating its potential as a candidate of new natural fungicides (Zhao et al., 2020). A new dibenzo-α-pyrone rhizopycnin D (122) and a known congener TMC-264 (123) were isolated from the endophytic fungus *Rhizopycnis vagum* Nitaf22 obtained from *Nicotiana tabacum* (Lai et al., 2016). Both compounds inhibited the spore germination of *M. oryzae* with IC$_{50}$ values of 33.9 and 34.1 μM, respectively (Lai et al., 2016).

Miscellaneous Compounds

A new furan derivative named 3-(5-oxo-2,5-dihydrofuran-3-yl) propanoic acid (124) was isolated from an endophytic *Aspergillus tubingensis* of *Decaisnea insignis* (**Figure 7**; Yang X. F. et al., 2019). 124 exhibited potent antifungal activity against *F. graminearum* with MIC value of 102.6 μM (Yang X. F. et al., 2019). Piliformic acid (125), derived from octanoate that originates from a fatty acid synthase, was obtained from

endophytic fungi *Xylaria* sp., which were isolated from leaves of guarana plant (Elias et al., 2018). 125 had antifungal activity against *C. gloeosporioides* with an MIC of 2.92 µM (Elias et al., 2018). The endophytic fungus *Aspergillus* sp. from *Moringa oleifera* produced one phenolic acid, ferulic acid (126), which showed a weak antifungal activity at 500 µg/mL against *A. niger* with an inhibition zone diameter of 2 mm (Abonyi et al., 2018). Cordycepsidone A (127), a depsidone metabolite, was isolated from *Cordyceps dipterigena*, an endophytic fungus from *Desmotes incomparabilis* antagonistic to the phytopathogen *Gibberella fujikuroi* (Varughese et al., 2012). 127 showed a moderate to potent growth inhibitory activity against *G. fujikuroi* (MIC, 23.3 µM) and *Pythium ultimum* (MIC, 3.4 µM) (Varughese et al., 2012). An endophyte *Botryosphaeria rhodina* was isolated from the stems of the medicinal plant *Bidens pilosa* and was chosen for further chemical study due to its potent antifungal effects (Abdou et al., 2010). Bioactivity-guided fractionation of this strain yielded two new depsidones, botryorhodine A (128) and B (129), which were significantly active against *A. terreus* with MICs of 26.03 and 49.70 µM (Abdou et al., 2010). A new tridepside, colletotric acid (130), was characterized from *C. gloeosporioides*, an endophytic fungus colonized inside the stem of *Artemisia mongolica* (Zou et al., 2000). 130 inhibited the growth of the crop pathogenic fungus *Helminthosporium sativum* with an MIC of 95.4 µM (Zou et al., 2000). From an isolate of *Aspergillus* from a healthy plant of oilseed rape (*Brassica napus*), two chlorinated diphenyl ethers, penicillither (131) and methyl dichloroasterrate (132), were characterized (Qin et al., 2019). Both of them inhibited four plant pathogenic fungi (*B. cinerea, M. fructicola, S. sclerotiorum,* and *S. trifoliorum*) with the EC$_{50s}$ of 21.7-151.2 µM (Qin et al., 2019).

POTENTIAL USE IN THE DEVELOPMENT OF BIOPESTICIDES

As mentioned above, biologically active and structurally diverse fungal metabolites constitute a rich resource for drugs and pesticides discovery. These recently discovered metabolites 1-132, which possessed extensive chemical skeletons, exhibited moderate to potent anti-phytopathogenic activities. Therefore, some of them might have the potential use in the development of new biopesticides. Especially, based on these potential compounds, a series of novel derivatives with agricultural and pharmaceutical importance were designed and synthesized.

Griseofulvin

Griseofulvin (85), a secondary metabolite possessing spirocyclic benzofuran-3-one skeleton, was initially isolated from the fungus *Penicillium griseofulvum* in 1939 by Oxford et al. (Petersen et al., 2014). Then, this polyketide has also been found to be produced by several Ascomycetes including *Penicillium* sp., *Aspergillus* sp., and *Xylaria* sp. (Zhao et al., 2012). Griseofulvin has a rich chemical diversity, and until now, more than 400 griseofulvin analogs have been isolated and synthesized (**Figure 8**; Petersen et al., 2014). Griseofulvin was one of the first antifungal metabolic products in filamentous fungi, offered *in vitro* fungistatic effect against dermatomycoses. Recently, it has gained renewed

attention due to many reports of antifungal properties against plant pathogenic fungi. Zhao et al. reported that griseofulvin, produced by an endophyte *Nigrospora* sp., displayed clear growth inhibition of the test eight plant pathogenic fungi (*B. cinerea, Colletotrichum orbiculare, F. oxysporum f.sp. cucumerinum, F. oxysporum f.sp. melonis, Pestalotia diospyri, Pythium ultimum, R. solani,* and *S. sclerotiorum*) (Zhao et al., 2012). Among them, it exhibited potent activity against *B. cinerea* and *C. orbiculare* with the EC$_{50}$ values of 0.6 and 1.4 µM, respectively (Zhao et al., 2012). It should be pointed out that, its dechlorinated derivative, dechlorogriseofulvin, only showed weak activity, indicating that the chlorine played a decisive role in the antifungal activity. Tang et al. reported that griseofulvin isolated from *Penicillium brasilianum* displayed strong inhibitory effect on the growth of *A. solani* with an MIC of 3.13 µM (Tang et al., 2015). These impressive activities make this compound suitable candidate for biopesticide discovery and trigger the following synthesis studies, including semisynthesis from griseofulvin and *de novo* synthesis.

Bai et al. designed and synthesized 22 griseofulvin derivatives from commercially available griseofulvin (Bai et al., 2019). *In vitro* antifungal assay indicated that griseofulvin and its derivatives possessed remarkable activities against five phytopathogenic fungi (*Cytospora sp., C. gloeosporioides, B. cinerea, A. solani,* and *F. solani*) (Bai et al., 2019). Of significance was that, compounds numbered 6a-6f were found to have significant potential, which were superior to commercial fungicides hymexazol and thiophanate-methyl. The three-dimensional quantitative structure-activity relationship analysis revealed that the modification of the 4' position, for example, the suitable bulky and electronegative acyl-substituted groups at the 4' position, can significantly improve the antifungal activity, even up to 10-fold higher than inhibitory effect of the parent compound griseofulvin (Bai et al., 2019). Kartsev et al. carried out the synthetic studies of griseofulvin derivatives (Kartsev et al., 2019). As a result, a total of 42 new griseofulvin derivatives were designed and synthesized. These newly synthesized griseofulvin derivatives exhibited potent antifungal activity against *A. niger, A. ochraceus, A. fumigatus, A. versicolor, Penicillium funiculosum, P. ochrochloron, P. verucosum* var. *cyclopium, Trichoderma viride*. All compounds showed higher activity than the commercial antifungal drugs ketoconazole (7-42 times) and bifonazole (3-16 fold) (Kartsev et al., 2019). Interestingly, the synthesized compounds were more active than the parent compound griseofulvin (up to 4 times). Therefore, in conclusion, griseofulvin especially its derivatives can be further used for the development of new agricultural fungicides.

Trichothecene

Trichothecenes, a group of sesquiterpene-based fungal metabolites with a common tricyclic 12,13-epoxytrichothec-9-ene core, are found to be produced by various microorganisms such as Fusarium sp., Myrothecium sp., Spicellum sp., Stachybotrys sp., Cephalosporium sp., Trichoderma sp., and Trichothecium sp. Based on the substitution pattern, trichothecenes are classified into different families of nivalenols, neosolaniols, isotrichodermins, calonectrins, trichothecins, and trichobreols (**Figure 9**; Takahashi-Ando et al., 2020).
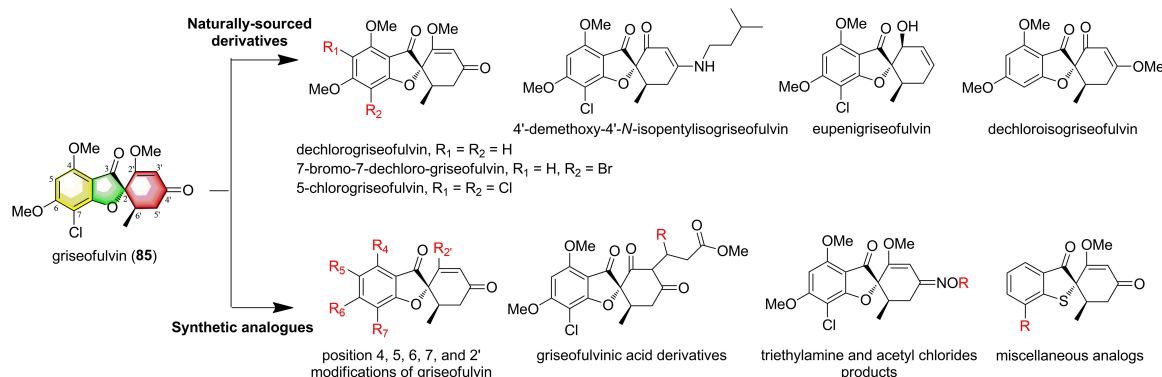
FIGURE 8 | Selected structures of naturally sourced griseofulvin derivatives and synthetic analogs.

FIGURE 9 | Representative antifungal trichothecene sesquiterpenes derivatives.

Trichothecenes are well-known as mycotoxins, causing significant negative effects on agriculture and human health. Initial study of trichothecenes was focused on the phytotoxicity and mammalian intoxications, and later emphasis was on exploring their complementary bioactivities. Some related compounds exhibited potent antitumor effect and have been used for clinical trials (Li et al., 2017). Meanwhile, trichothecenes showed varied role in the field of agriculture and may act as bio-control agents, strengthen the defense system of the plants against pathogens (Kumari et al., 2016). Previous structure–activity relationships study revealed that a slight modification of trichothecenes could dramatically decrease the toxicity but still retain its bioactivity (Li et al., 2017). In this case, there seems to be a special significance to search for new trichothecenes with agricultural applications.

Yamazaki et al. reported three new antifungal trichothecenes, trichobreols A-C, from the NaI-containing fermentation of the marine-derived Trichoderma cf. brevicompactum (Yamazaki et al., 2020a). Then, from the same fungus, another two new trichothecenes, trichobreols D and E, were obtained (Yamazaki et al., 2020b). Trichobreols showed good antifungal activity,

especially toward yeast-like pathogenic fungi. Moreover, five semisynthetic derivatives were prepared from trichobreol A to evaluate the structure–activity relationship of antifungal trichothecenes. The results indicated that the substituents at C-3 and C-4 positions were responsible for the potency of antifungal activity (Yamazaki et al., 2020b). Li et al. reported three new macrocyclic trichothecenes possessing rare 6'-ketal moieties, roridoxins A-C, from the insect-associated fungus Myrothecium roridum (Li et al., 2019). Roridoxins A and C were found to possess potent antifungal activity against Alternaria tenuissima, A. niger, Pyricularia grisea, and F. oxysporum (Li et al., 2019). These findings suggested that trichothecenes are also promising leads which are applicable for the development of new agrochemicals.

CONCLUSION AND FUTURE PERSPECTIVES

Fungal endophytes, which are ubiquitous in plants and symbiotic with their hosts, are well-known for producing a variety of

antimicrobial metabolites and enhancing plant resistance to pathogens and pests. These bioactive metabolites play a defensive role in protecting the host plants against pathogenic attacks. Therefore, antibiotic metabolites from the endophytes have the potential to be applied as agrochemicals to control pathogens. This review summarizes the structural/biogenetic types of 132 antifungal metabolites isolated from fungal endophytes in the past two decades. These present metabolites possess diverse chemical structures. Based on their putative biogenetic

origin, they were classified into alkaloids (including 1-14 for cytochalasins and 15-35 for other alkaloids), terpenoids (36-49), polyketides (50-123), and other miscellaneous compounds (124-132). It is worth mentioning that the structural classifications based on biogenetic categories are somewhat arbitrary, as many compounds are derived from mixed biosynthetic pathways. Taking compounds 86-89 as an example, they are new members of the chromenone-type of metabolites biogenetically derived from isoprenoids and a polyketide. As shown in **Figure 10**,
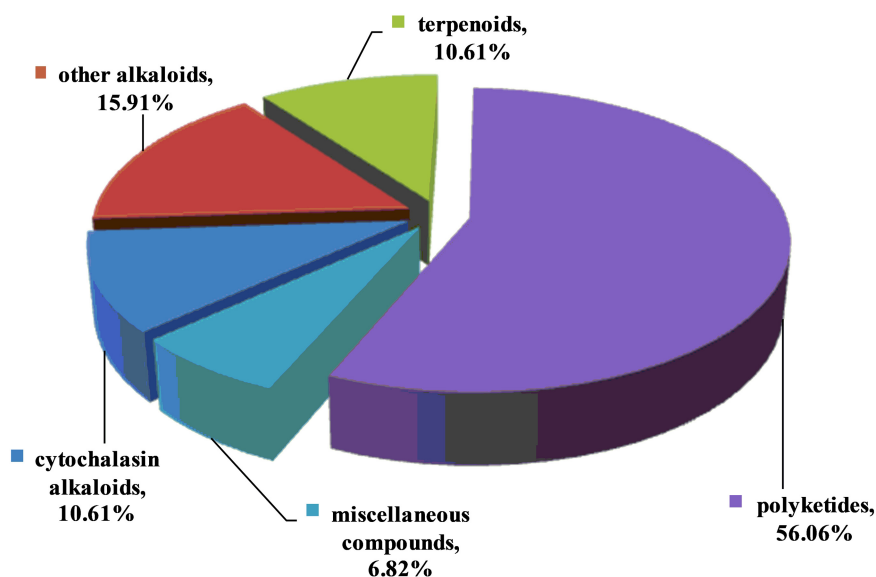

FIGURE 10 | Percentage distributions of antifungal metabolites based on their putative biogenetic origin.
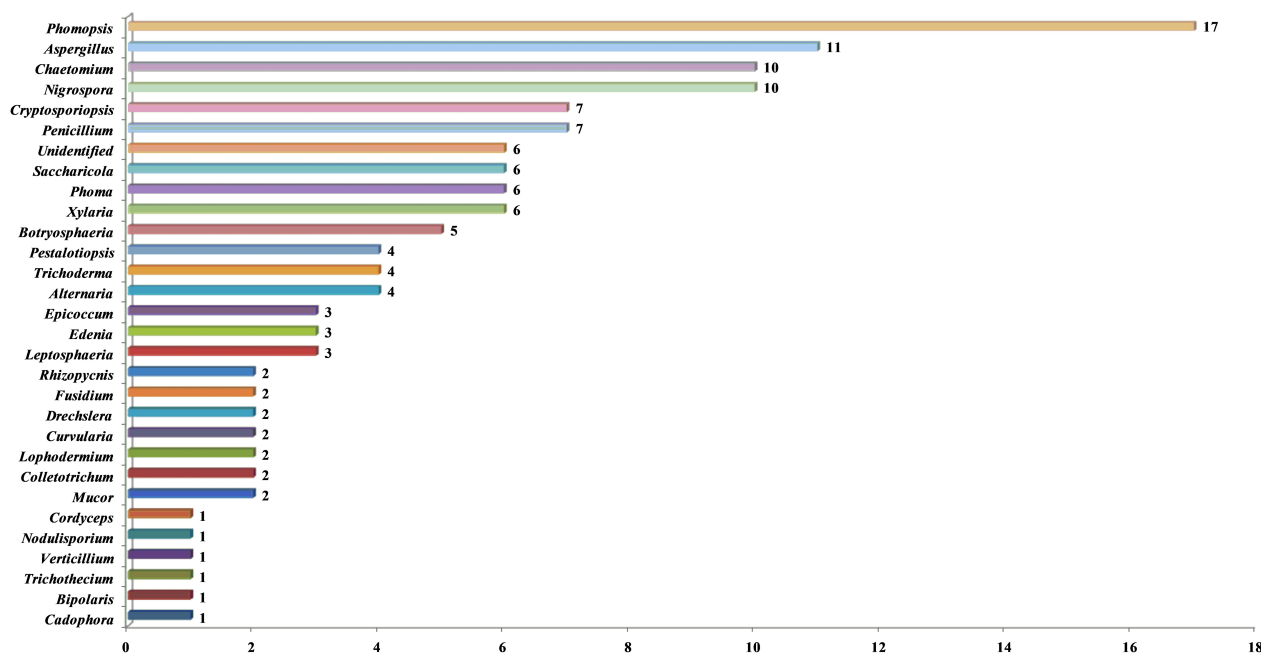

FIGURE 11 | Antifungal metabolites characterized from various producing strains.

among the 132 active metabolites, approximately 56% were polyketides. Molecules grouped as polyketides are significant in natural products research due to their biosynthetic complexity and high value in pharmaceutical and/or agrochemical industries. This finding revealed that polyketides are the most potential classes for the discovery of novel antifungal lead compounds. It should be pointed out that we divided cytochalasins into an individual group, since this kind of compounds constitutes 10.6% of the metabolites reported, nearly as many as terpenoids (10.6%) and other alkaloids (15.9%). Cytochalasins are a diverse group of fungal polyketide synthase-non-ribosomal peptide synthetase (PKS-NRPS) hybrid metabolites. This class of compounds are worthy of particular attention and may be applied in the field of bio-pesticides.

It is well-known that the endophytic fungi from terrestrial plants are a treasure house of bioactive secondary metabolites. Moreover, marine-derived endophytic fungi have also been considered as a non-negligible resource to search for antifungal lead compounds. In this review, compounds 4, 10-12, 55-57,

and 76-78 were isolated from marine mangrove-associated endophytic fungi. The marine environment is quite different from the terrestrial environment, which indicates that marine-derived endophytic fungi may possess unique metabolic pathways to produce interesting antifungal compounds with novel structures. As for the producing strains, the fungal genera *Phomopsis*, *Aspergillus*, *Chaetomium*, and *Nigrospora* are predominant genera as producers of these antifungal metabolites, with 17, 11, 10, and 10 compounds described, respectively (**Figure 11**). As shown in **Figure 11**, these metabolites are scattered across a variety of fungi belonging to 29 various genera, including some rare species. Among them, *C. globosum* is a creative species known for making a large number of exclusive and structurally significant bioactive chaetoglobosins. The antifungal activity of these metabolites against the phytopathogenic fungi indicated that the endophytes could protect their host plants by producing bioactive molecules, which may be toxic or even lethal to phytopathogens and highlighted the potential of endophytic fungi in producing
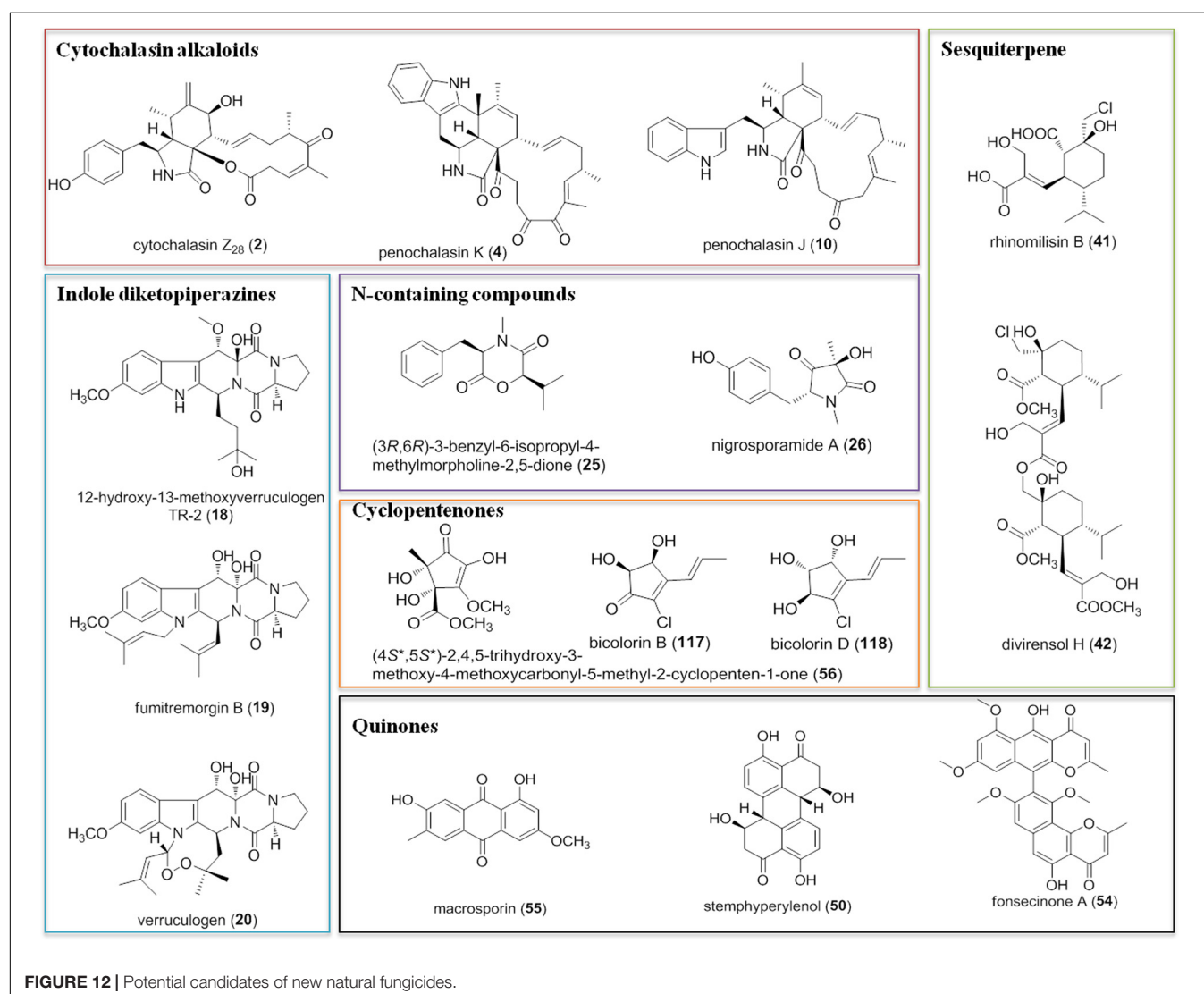

FIGURE 12 | Potential candidates of new natural fungicides.

valuable metabolites. Moreover, a chemical interaction between the endophytes and the host plants, which produces metabolites as chemical defense compounds, needs further investigation.

Most importantly, among the 132 antifungal metabolites presented in this review, some of them not only possessed intriguing chemical structures but also showed novel antifungal activities comparable to those of widely used chemical pesticides. These include cytochalasin alkaloids cytochalasin Z_{28} (2), penochalasin K (4), and penochalasin J (10), indole diketopiperazines 12β-hydroxy-13α-methoxyverruculogen TR-2 (18), fumitremorgin B (19), and verruculogen (20), N-containing compounds (3R,6R)-3-benzyl-6-isopropyl-4-methylmorpholine-2,5-dione (25) and nigrosporamide A (26), sesquiterpenes rhinomilisin B (41) and divirensol H (42), quinones stemphyperylenol (50), fonsecinone A (54), and macrosporin (55), cyclopentenones (4S*,5S*)-2,4,5-trihydroxy-3-methoxy-4-methoxycarbonyl-5-methyl-2-cyclopenten-1-one (56), bicolorin B (117), and D (118) (**Figure 12**). The above mentioned compounds showed potent (or significant) antifungal activities compared to those of positive controls (usually chemical pesticides such as difenoconazole, hymexazol, carbendazim, and triadimefon), which indicates that they could be used as potential alternatives to traditional pesticides.

Overall, endophytes are considered to be a treasure house of antifungal metabolites. This review summarizes 132 metabolites with moderate to potent antifungal activities isolated from fungal endophytes. We also list some "star molecules" such as griseofulvin and its derivatives that possess high potential

as candidates of new natural fungicides herein. It is believed that in the near future, research on antifungal metabolites of endophytic fungi will become more prolific and be beneficial for the development of new agrochemicals.

AUTHOR CONTRIBUTIONS

KX and X-QL performed the literature material's collection and reorganization. PZ and D-LZ wrote the manuscript. All authors reviewed the manuscript.

ACKNOWLEDGMENTS

SUPPLEMENTARY MATERIAL

The Supplementary Material for this article can be found online at: https://www.frontiersin.org/articles/10.3389/fmicb.2021.689527/full#supplementary-material

Supplementary Table 1 | The producing strain, environment source, and antifungal activities of compounds 1–132.

REFERENCES

Abdou, R., Scherlach, K., Dahse, H. M., Sattler, I., and Hertweck, C. (2010). Botryorhodines A-D, antifungal and cytotoxic depsidones from *Botryosphaeria rhodina*, an endophyte of the medicinal plant *Bidens pilosa*. *Phytochemistry* 71, 110–116. doi: 10.1016/j.phytochem.2009.09.024

Abdou, R., Shabana, S., and Rateb, M. E. (2018). Terezine E, bioactive prenylated tryptophan analogue from an endophyte of *Centaurea stoebe*. *Nat. Prod. Res.* 34, 503–510. doi: 10.1080/14786419.2018.1489393

Abonyi, D. O., Eze, P. M., Abba, C. C., Ujam, N. T., Proksch, P., Okoye, F. B. C., et al. (2018). Biologically active phenolic acids produced by *Aspergillus* sp., an endophyte of *Moringa oleifera*. *Eur. J. Biol. Res.* 8, 158–168. doi: 10.5281/zenodo.1404981

Ahmed, I., Hussain, H., Schulz, B., Draeger, S., Padula, D., Pescitelli, G., et al. (2011). Three new antimicrobial metabolites from the endophytic fungus *Phomopsis* sp. *Eur. J. Org. Chem.* 2011, 2867–2873.

Bai, Y. B., Gao, Y. Q., Nie, X. D., Tuong, T. M., Li, D., and Gao, J. M. (2019). Antifungal activity of griseofulvin derivatives against phytopathogenic fungi in vitro and in vivo and three-dimensional quantitative structure-activity relationship analysis. *J. Agric. Food Chem.* 67, 6125–6132. doi: 10.1021/acs.jafc.9b00606

Bai, Y. B., Zhang, A. L., Tang, J. J., and Gao, J. M. (2013). Synthesis and antifungal activity of 2-chloromethyl-1H-benzimidazole derivatives against phytopathogenic fungi in vitro. *J. Agric. Food Chem.* 61, 2789–2795. doi: 10.1021/jf3053934

Cao, L. L., Zhang, Y. Y., Liu, Y. J., Yang, T. T., Zhang, J. L., Zhang, Z. G., et al. (2016). Anti-phytopathogenic activity of sporothriolide, a metabolite from endophyte *Nodulisporium* sp. A21 in *Ginkgo biloba*. *Pestic. Biochem. Physiol.* 129, 7–13. doi: 10.1016/j.pestbp.2015.10.002

Chapla, V. M., Zeraik, M. L., Cafeu, M. C., Silva, G. H., Cavalheiro, A. J., Bolzani, V. S., et al. (2018). Griseofulvin, diketopiperazines and cytochalasins from

endophytic fungi colletotrichum crassipes and *Xylaria* sp., and their antifungal, antioxidant and anticholinesterase activities. *J. Braz Chem. Soc.* 29, 1707–1713. doi: 10.21577/0103-5053.20180045

Chapla, V. M., Zeraik, M. L., Leptokarydis, I. H., Silva, G. H., Bolzani, V. S., Young, M. C., et al. (2014). Antifungal compounds produced by *Colletotrichum gloeosporioides*, an endophytic fungus from *Michelia champaca*. *Molecules* 19, 19243–19252. doi: 10.3390/molecules191119243

Chen, H. Y., Liu, T. K., Shi, Q., and Yang, X. L. (2019). Sesquiterpenoids and diterpenes with antimicrobial activity from *Leptosphaeria* sp. XL026, an endophytic fungus in *Panax notoginseng*. *Fitoterapia* 137:104243. doi: 10.1016/j.fitote.2019.104243

Chen, Y. M., Yang, Y. H., Li, X. N., Zou, C., and Zhao, P. J. (2015). Diterpenoids from the endophytic fungus *Botryosphaeria* sp. P483 of the Chinese herbal medicine *Huperzia serrata*. *Molecules* 20, 16924–16932. doi: 10.3390/molecules200916924

Copping, L. G., and Duke, S. O. (2007). Natural products that have been used commercially as crop protection agents. *Pest. Manag. Sci.* 63, 524–554. doi: 10.1002/ps.1378

d'Errico, G., Aloj, V., Flematti, G. R., Sivasithamparam, K., Worth, C. M., Lombardi, N., et al. (2020). Metabolites of a *Drechslera* sp. endophyte with potential as biocontrol and bioremediation agent. *Nat. Prod. Res.* Online ahead of print. doi: 10.1080/14786419.2020.1737058

Ding, G., Liu, S., Guo, L., Zhou, Y., and Che, Y. (2008). Antifungal metabolites from the plant endophytic fungus *Pestalotiopsis foedan*. *J. Nat. Prod.* 71, 615–618. doi: 10.1021/np070590f

Elias, L. M., Fortkamp, D., Sartori, S. B., Ferreira, M. C., Gomes, L. H., Azevedo, J. L., et al. (2018). The potential of compounds isolated from *Xylaria* spp. as antifungal agents against anthracnose. *Braz J. Microbiol.* 49, 840–847. doi: 10.1016/j.bjm.2018.03.003

Gouda, S., Das, G., Sen, S. K., Shin, H. S., and Patra, J. K. (2016). Endophytes: a treasure house of bioactive compounds of medicinal importance. *Front. Microbiol.* 7:1538. doi: 10.3389/fmicb.2016.01538

Goutam, J., Sharma, G., Tiwari, V. K., Mishra, A., Kharwar, R. N., Ramaraj, V., et al. (2017). Isolation and characterization of "Terrein" an antimicrobial and antitumor compound from endophytic fungus *Aspergillus terreus* (JAS-2) associated from *Achyranthus aspera* Varanasi, India. *Front. Microbiol.* 8:1334. doi: 10.3389/fmicb.2017.01334

Hu, Z., Tao, Y., Tao, X., Su, Q., Cai, J., Qin, C., et al. (2019). Sesquiterpenes with phytopathogenic fungi inhibitory activities from fungus *Trichoderma virens* from *Litchi chinensis* Sonn. *J. Agric. Food Chem.* 67, 10646–10652. doi: 10.1021/acs.jafc.9b04053

Huang, R., Jiang, B. G., Li, X. N., Wang, Y. T., Liu, S. S., Zheng, K. X., et al. (2018). Polyoxygenated cyclohexenoids with promising α-glycosidase inhibitory activity produced by *Phomopsis* sp. YE3250, an endophytic fungus derived from *Paeonia delavayi*. *J. Agric. Food Chem.* 66, 1140–1146. doi: 10.1021/acs.jafc.7b04998

Huang, S., Chen, H., Li, W., Zhu, X., Ding, W., and Li, C. (2016). Bioactive chaetoglobosins from the mangrove endophytic fungus *Penicillium chrysogenum*. *Mar. Drugs* 14:172. doi: 10.3390/md14100172

Huang, S., Xu, J., Li, F., Zhou, D., Xu, L., and Li, C. (2017). Identification and antifungal activity of metabolites from the mangrove fungus *Phoma* sp. L28. *Chem. Nat. Compd.* 53, 237–240. doi: 10.1007/s10600-017-1961-z

Hussain, H., Ahmed, I., Schulz, B., Draeger, S., and Krohn, K. (2012a). Pyrenocines J-M: four new pyrenocines from the endophytic fungus, *Phomopsis* sp. *Fitoterapia* 83, 523–526. doi: 10.1016/j.fitote.2011.12.017

Hussain, H., Krohn, K., Ahmed, I., Draeger, S., Schulz, B., Di Pietro, S., et al. (2012b). Phomopsinones A-D: four new pyrenocines from endophytic fungus *Phomopsis* sp. *Eur. J. Org. Chem.* 2012, 1783–1789.

Hussain, H., Krohn, K., Draeger, S., Meier, K., and Schulz, B. (2009). Bioactive chemical constituents of a sterile endophytic fungus from *Meliotus dentatus*. *Rec. Nat. Prod.* 3, 114–117. doi: 10.1007/978-1-4020-8804-9_25

Jia, M., Chen, L., Xin, H. L., Zheng, C. J., Rahman, K., Han, T., et al. (2016). A friendly relationship between endophytic fungi and medicinal plants: a systematic review. *Front. Microbiol.* 7:906. doi: 10.3389/fmicb.2016.00906

Kartsev, V., Geronikaki, A., Petrou, A., Lichitsky, B., Kostic, M., Smiljkovic, M., et al. (2019). Griseofulvin derivatives: synthesis, molecular docking and biological evaluation. *Curr. Top. Med. Chem.* 19, 1145–1161. doi: 10.2174/1568026619666190523080136

Kim, Y. M., Lee, C. H., Kim, H. G., and Lee, H. S. (2004). Anthraquinones isolated from *Cassiatora* (*Leguminosae*) seed show an antifungal property against phytopathogenic fungi. *J. Agric. Food Chem.* 52, 6096–6100. doi: 10.1021/jf049379p

Kumari, I., Ahmed, M., and Akhter, Y. (2016). Multifaceted impact of trichothecene metabolites on plant-microbe interactions and human health. *Appl. Microbiol. Biotechnol.* 100, 5759–5771. doi: 10.1007/s00253-016-7599-0

Lai, D., Wang, A., Cao, Y., Zhou, K., Mao, Z., Dong, X., et al. (2016). Bioactive dibenzo-α-pyrone derivatives from the endophytic fungus *Rhizopycnis vagum* Nitaf22. *J. Nat. Prod.* 79, 2022–2031. doi: 10.1021/acs.jnatprod.6b00327

Li, T. X., Xiong, Y. M., Chen, X., Yang, Y. N., Wang, Y., Jia, X. W., et al. (2019). Antifungal macrocyclic trichothecenes from the insect-associated fungus *Myrothecium roridum*. *J. Agric. Food Chem.* 67, 13033–13039. doi: 10.1021/acs.jafc.9b04507

Li, W., Yang, X., Yang, Y., Duang, R., Chen, G., Li, X., et al. (2016). Anti-phytopathogen, multi-target acetylcholinesterase inhibitory and antioxidant activities of metabolites from endophytic *Chaetomium globosum*. *Nat. Prod. Res.* 30, 2616–2619. doi: 10.1080/14786419.2015.1129328

Li, X. J., Zhang, Q., Zhang, A. L., and Gao, J. M. (2012). Metabolites from *Aspergillus fumigatus*, an endophytic fungus associated with *Melia azedarach*, and their antifungal, antifeedant, and toxic activities. *J. Agric. Food Chem.* 60, 3424–3431. doi: 10.1021/jf300146n

Li, Y., Liu, D., Cheng, Z., Proksch, P., and Lin, W. (2017). Cytotoxic trichothecene-type sesquiterpenes from the sponge-derived fungus *Stachybotrys chartarum* with tyrosine kinase inhibition. *RSC Adv.* 7:7259. doi: 10.1039/C6RA26956G

Liu, K., Yang, Y., Miao, C. P., Zheng, Y. K., Chen, J. L., Chen, Y. W., et al. (2016). Koningiopisins A-H, polyketides with synergistic antifungal activities from the endophytic fungus *Trichoderma koningiopsis*. *Planta Med.* 82, 371–376. doi: 10.1055/s-0035-1558228

Liu, S., Liu, X., Guo, L., Che, Y., and Liu, L. (2013). 2H-Pyran-2-one and 2H-furan-2-one derivatives from the plant endophytic fungus *Pestalotiopsis fici*. *Chem. Biodivers.* 10, 2007–2013. doi: 10.1002/cbdv.201200361

Liu, X., Dong, M., Chen, X., Jiang, M., Lv, X., and Zhou, J. (2008). Antimicrobial activity of an endophytic *Xylaria* sp. YX-28 and identification of its antimicrobial compound 7-amino-4-methylcoumarin. *Appl. Microbiol. Biotechnol.* 78, 241–247. doi: 10.1007/s00253-007-1305-1

Loesgen, S., Bruhn, T., Meindl, K., Dix, I., Schulz, B., Zeeck, A., et al. (2011). (+)-Flavipucine, the missing member of the pyridione epoxide family of fungal antibiotics. *Eur. J. Org. Chem.* 2011, 5156–5162.

Ma, Y. M., Qiao, K., Kong, Y., Li, M. Y., Guo, L. X., Miao, Z., et al. (2018). A new isoquinolone alkaloid from an endophytic fungus R22 of *Nerium indicum*. *Nat. Prod. Res.* 32, 2375–2381. doi: 10.1080/14786419.2016.1258556

Macías-Rubalcava, M. L., Hernández-Bautista, B. E., Jiménez-Estrada, M., González, M. C., Glenn, A. E., Hanlin, R. T., et al. (2008). Naphthoquinone spiroketal with allelochemical activity from the newly discovered endophytic fungus *Edenia gomezpompae*. *Phytochemistry* 69, 1185–1196. doi: 10.1016/j.phytochem.2007.12.006

Petersen, A. B., Rønnest, M. H., Larsen, T. O., and Clausen, M. H. (2014). The chemistry of griseofulvin. *Chem. Rev.* 114, 12088–12107. doi: 10.1021/cr400368e

Qin, J., Lyu, A., Zhang, Q. H., Yang, L., Zhang, J., Wu, M. D., et al. (2019). Strain identification and metabolites isolation of *Aspergillus capensis* CanS-34A from *Brassica napus*. *Mol. Biol. Rep.* 46, 3451–3460. doi: 10.1007/s11033-019-04808-5

Qin, S., Hussain, H., Schulz, B., Draeger, S., and Krohn, K. (2010). Two new metabolites, epoxydine A and B, from *Phoma* sp. *Helv. Chim. Acta* 93, 169–174. doi: 10.1002/hlca.200900199

Qin, S., Krohn, K., Flörke, U., Schulz, B., Draeger, S., Pescitelli, G., et al. (2009). Two new fusidilactones from the fungal endophyte *Fusidium* sp. *Eur. J. Org. Chem.* 2009, 3279–3284.

Qin, S., Krohn, K., Hussain, H., Schulz, B., and Draeger, S. (2011). Pestalotheols E-H: antimicrobial metabolites from an endophytic fungus isolated from the tree Arbutus unedo. *Eur. J. Org. Chem.* 2011, 5163–5166.

Saleem, M., Hussain, H., Ahmed, I., Draeger, S., Schulz, B., Meier, K., et al. (2011). Viburspiran, an antifungal member of the octadride class of maleic anhydride natural products. *Eur. J. Org. Chem.* 2011, 808–812.

Santiago, C., Fitchett, C., Munro, M. H. G., Jalil, J., and Santhanam, J. (2012). Cytotoxic and antifungal activities of 5-hydroxyramulosin, a compound produced by an endophytic fungus isolated from *Cinnamomum mollisimum*. *Evid. Based Complement. Alternat. Med.* 2012:689310. doi: 10.1155/2012/689310

Shi, S., An, R., Zhang, W., Zhang, G., and Yu, Z. (2017). Stilbene derivatives from *Photorhabdus temperata* SN259 and their antifungal activities against phytopathogenic fungi. *J. Agric. Food Chem.* 65, 60–65. doi: 10.1021/acs.jafc.6b04303

Siriwach, R., Kinoshita, H., Kitani, S., Igarashi, Y., Pansuksan, K., Panbangred, W., et al. (2014). Bipolamides A and B, triene amides isolated from the endophytic fungus *Bipolaris* sp. MU34. *J. Antibiot.* 67, 167–170. doi: 10.1038/ja.2013.103

Sumarah, M. W., Kesting, J. R., Sørensen, D., and Miller, J. D. (2011). Antifungal metabolites from fungal endophytes of *Pinus strobus*. *Phytochemistry* 72, 1833–1837. doi: 10.1016/j.phytochem.2011.05.003

Takahashi-Ando, N., Matsui, K., Suzuki, T., Sadamatsu, K., Azuhata, H., Okada, A., et al. (2020). Trichothecene biosynthesis in different fungal genera: resistance mechanisms, pathway enzymes, and their product applications. *JSM Mycotoxins* 70, 67–74. doi: 10.2520/myco.70-2-3

Talibi, I., Boubaker, H., Boudyach, E. H., Ait Ben, and Aoumar, A. (2014). Alternative methods for the control of postharvest citrus diseases. *J. Appl. Microbiol.* 117, 1–17. doi: 10.1111/jam.12495

Talontsi, F. M., Dittrich, B., Schüffler, A., Sun, H., and Laatsch, H. (2013). Epicoccolides: antimicrobial and antifungal polyketides from an endophytic fungus *Epicoccum* sp. associated with *Theobroma cacao*. *Eur. J. Org. Chem.* 2013, 3174–3180. doi: 10.1002/ejoc.201300146

Talontsi, F. M., Facey, P., Tatong, M. D., Tofazzal Islam, M., Frauendorf, H., Draeger, S., et al. (2012). Zoosporicidal metabolites from an endophytic fungus *Cryptosporiopsis* sp. of *Zanthoxylum leprieurii*. *Phytochemistry* 83, 87–94. doi: 10.1016/j.phytochem.2012.06.006

Tang, H. Y., Zhang, Q., Li, H., and Gao, J. M. (2015). Antimicrobial and allelopathic metabolites produced by *Penicillium brasilianum*. *Nat. Prod. Res.* 29, 345–348. doi: 10.1080/14786419.2014.940347

Teles, H. L., Silva, G. H., Castro-Gamboa, I., Bolzani Vda, S., Pereira, J. O., Costa-Neto, C. M., et al. (2005). Benzopyrans from *Curvularia* sp., an endophytic fungus associated with *Ocotea corymbosa* (Lauraceae). *Phytochemistry* 66, 2363–2367. doi: 10.1016/j.phytochem.2005.04.043

Varughese, T., Riosa, N., Higginbotham, S., Arnold, A. E., Coley, P. D., Kursar, T. A., et al. (2012). Antifungal depsidone metabolites from *Cordyceps dipterigena*, an endophytic fungus antagonistic to the phytopathogen *Gibberella fujikuroi*. *Tetrahedron Lett.* 53, 1624–1626. doi: 10.1016/j.tetlet.2012.01.076

Wang, J., Ding, W., Wang, R., Du, Y., Liu, H., Kong, X., et al. (2015). Identification and bioactivity of compounds from the mangrove endophytic fungus *Alternaria* sp. *Mar. Drugs* 13, 4492–4504. doi: 10.3390/md13074492

Wang, J., He, W., Huang, X., Tian, X., Liao, S., Yang, B., et al. (2016). Antifungal new oxepine-containing alkaloids and xanthones from the deep-sea-derived fungus *Aspergillus versicolor* SCSIO 05879. *J. Agric. Food Chem.* 64, 2910–2916. doi: 10.1021/acs.jafc.6b00527

Wang, L. W., Xu, B. G., Wang, J. Y., Su, Z. Z., Lin, F. C., Zhang, C. L., et al. (2012). Bioactive metabolites from *Phoma* species, an endophytic fungus from the Chinese medicinal plant *Arisaema erubescens*. *Appl. Microbiol. Biotechnol.* 93, 1231–1239. doi: 10.1007/s00253-011-3472-3

Wang, L., Shen, J., Xu, L., Gao, J., Zhang, C., Wang, Y., et al. (2019). A metabolite of endophytic fungus *Cadophora orchidicola* from *Kalimeris indica* serves as a potential fungicide and TLR4 agonist. *J. Appl. Microbiol.* 126, 1383–1390. doi: 10.1111/jam.14239

Wang, Y., Xu, L., Ren, W., Zhao, D., Zhu, Y., and Wu, X. (2012). Bioactive metabolites from *Chaetomium globosum* L18, an endophytic fungus in the medicinal plant *Curcuma wenyujin*. *Phytomedicine* 19, 364–368. doi: 10.1016/j.phymed.2011.10.011

Wei, G., Tan, D., Chen, C., Tong, Q., Li, X. N., Huang, J., et al. (2017). Flavichalasines A–M, cytochalasan alkaloids from *Aspergillus flavipes*. *Sci. Rep.* 7:42434. doi: 10.1038/srep42434

Wu, S. H., Chen, Y. W., Shao, S. C., Wang, L. D., Yu, Y., Li, Z. Y., et al. (2009). Two new solanapyrone analogues from the endophytic fungus *Nigrospora* sp. YB-141 of *Azadirachta indica*. *Chem. Biodivers.* 6, 79–85. doi: 10.1002/cbdv.200700421

Wu, Y. M., Zhou, Q. Y., Yang, X. Q., Luo, Y. J., Qian, J. J., Liu, S. X., et al. (2019). Induction of antiphytopathogenic metabolite and squalene production and phytotoxin elimination by adjustment of the mode of fermentation in cocultures of phytopathogenic *Nigrospora oryzae* and *Irpex lacteus*. *J. Agric. Food Chem.* 67, 11877–11882. doi: 10.1021/acs.jafc.9b04209

Xiao, J., Zhang, Q., Gao, Y. Q., Shi, X. W., and Gao, J. M. (2014a). Antifungal and antibacterial metabolites from an endophytic *Aspergillus* sp. associated with *Melia azedarach*. *Nat. Prod. Res.* 28, 1388–1392. doi: 10.1080/14786419.2014.904308

Xiao, J., Zhang, Q., Gao, Y. Q., Tang, J. J., Zhang, A. L., and Gao, J. M. (2014b). Secondary metabolites from the endophytic *Botryosphaeria dothidea* of *Melia azedarach* and their antifungal, antibacterial, antioxidant, and cytotoxic activities. *J. Agric. Food Chem.* 62, 3584–3590. doi: 10.1021/jf500054f

Xu, D., Luo, M., Liu, F., Wang, D., Pang, X., Zhao, T., et al. (2017). Cytochalasan and tyrosine-derived alkaloids from the marine sediment-derived fungus *Westerdykella dispersa* and their bioactivities. *Sci. Rep.* 7:11956. doi: 10.1038/s41598-017-12327-1

Xue, M., Zhang, Q., Gao, J. M., Li, H., Tian, J. M., and Pescitelli, G. (2012). Chaetoglobosin Vb from endophytic *Chaetomium globosum*: absolute configuration of chaetoglobosins. *Chirality* 24, 668–674. doi: 10.1002/chir.22068

Yamazaki, H., Takahashi, O., Kirikoshi, R., Yagi, A., Ogasawara, T., Bunya, Y., et al. (2020a). Epipolythiodiketopiperazine and trichothecene derivatives from the NaI-containing fermentation of marine-derived *Trichoderma* cf. *brevicompactum*. *J. Antibiot.* 73, 559–567.

Yamazaki, H., Yagi, A., Takahashi, O., Yamaguchi, Y., Saito, A., Namikoshi, M., et al. (2020b). Antifungal trichothecene sesquiterpenes obtained from the culture broth of marine-derived *Trichoderma* cf. *brevicompactum* and their structure-activity relationship. *Bioorg. Med. Chem. Lett.* 30:127375. doi: 10.1016/j.bmcl.2020.127375

Yang, X. F., Wang, N. N., Kang, Y. F., and Ma, Y. M. (2019). A new furan derivative from an endophytic *Aspergillus tubingensis* of *Decaisnea insignis* (Griff.) Hook.f. & Thomson. *Nat. Prod. Res.* 33, 2777–2783. doi: 10.1080/14786419.2018.1501687

Yang, Z., Dan, W. J., Li, Y. X., Peng, G. R., Zhang, A. L., and Gao, J. M. (2019). Antifungal metabolites from *Alternaria atrans*: an endophytic fungus in *Psidium guajava*. *Nat. Prod. Commun.* 14:1934578X1984411. doi: 10.1177/1934578X19844116

You, F., Han, T., Wu, J. Z., Huang, B. K., and Qin, L. P. (2009). Antifungal secondary metabolites from endophytic *Verticillium* sp. *Biochem. Syst. Ecol.* 37, 162–165. doi: 10.1016/j.bse.2009.03.008

Zhang, P., Wei, Q., Yuan, X., and Xu, K. (2020). Newly reported alkaloids produced by marine-derived *Penicillium* species (covering 2014–2018). *Bioorg. Chem.* 99:103840. doi: 10.1016/j.bioorg.2020.103840

Zhang, Q., Xiao, J., Sun, Q. Q., Qin, J. C., Pescitelli, G., and Gao, J. M. (2014). Characterization of cytochalasins from the endophytic *Xylaria* sp. and their biological functions. *J. Agric. Food Chem.* 62, 10962–10969. doi: 10.1021/jf503846z

Zhang, W., Xu, L., Yang, L., Huang, Y., Li, S., and Shen, Y. (2014). Phomopsidone A, a novel depsidone metabolite from the mangrove endophytic fungus *Phomopsis* sp. A123. *Fitoterapia* 96, 146–151. doi: 10.1016/j.fitote.2014.05.001

Zhang, X., Li, G., Ma, J., Zeng, Y., Ma, W., and Zhao, P. (2010). Endophytic fungus *Trichothecium roseum* LZ93 antagonizing pathogenic fungi in vitro and its secondary metabolites. *J. Microbiol.* 48, 784–790. doi: 10.1007/s12275-010-0173-z

Zhao, J. H., Zhang, Y. L., Wang, W., Wang, J. Y., and Zhang, C. L. (2012). Bioactive secondary metabolites from *Nigrospora* sp. LLGLM003, an endophytic fungus of the medicinal plant *Moringa oleifera* Lam. *World J. Microbiol. Biotechnol.* 28, 2107–2112. doi: 10.1007/s11274-012-1015-4

Zhao, M., Guo, D. L., Liu, G. H., Fu, X., Gu, Y. C., Ding, L. S., et al. (2020). Antifungal halogenated cyclopentenones from the endophytic fungus *Saccharicola bicolor* of *Bergenia purpurascens* by the one strain-many compounds strategy. *J. Agric. Food Chem.* 68, 185–192. doi: 10.1021/acs.jafc.9b06594

Zhu, X., Chen, J., Zhu, S., He, Y., Ding, W., and Li, C. (2017a). Two new compounds from *Nigrospora sphaerica* ZMT05, a fungus derivated from *Oxya chinensis* Thunber. *Nat Prod Res.* 31, 951–958. doi: 10.1080/14786419.2017.1413566

Zhu, X., Zhou, D., Liang, F., Wu, Z., Shi, Z., and Li, C. (2017b). Penochalasin K, a new unusual chaetoglobosin from the mangrove endophytic fungus *Penicillium chrysogenum* V11 and its effective semisynthesis. *Fitoterapia* 123, 23–28. doi: 10.1016/j.fitote.2017.09.016

Zou, W. X., Meng, J. C., Lu, H., Chen, G. X., Shi, G. X., Zhang, T. Y., et al. (2000). Metabolites of *Colletotrichum gloeosporioides*, an endophytic fungus in *Artemisia mongolica*. *J. Nat. Prod.* 63, 1529–1530. doi: 10.1021/np000204t

A Novel Antifungal Actinomycete *Streptomyces* sp. Strain H3-2 Effectively Controls Banana Fusarium Wilt

Niexia Zou[1,2], Dengbo Zhou[2], Yinglong Chen[3], Ping Lin[1], Yufeng Chen[2], Wei Wang[2]*, Jianghui Xie[2]* and Mingyuan Wang[1]*

[1] *Institute of Horticultural Science and Engineering, Huaqiao University, Xiamen, China,* [2] *Key Laboratory of Biology and Genetic Resources of Tropical Crops, Ministry of Agriculture, Institute of Tropical Bioscience and Biotechnology, Chinese Academy of Tropical Agricultural Sciences, Haikou, China,* [3] *School of Agriculture and Environment, The UWA Institute of Agriculture, The University of Western Australia, Perth, WA, Australia*

Banana Fusarium wilt disease caused by *Fusarium oxyspoum* f. sp. *cubense* (Foc) seriously threatens the banana industry. Foc tropical race 4 (Foc TR4) can infect almost all banana cultivars. Compared with traditional physical and chemical practices, biocontrol strategy using beneficial microbes is considered as an environmentally sound option to manage fungal disease. In this study, a strain, H3-2, isolated from a non-infected banana orchard, exhibited high antifungal activity against Foc TR4. According to its morphological, physiological, and biochemical characteristics, the strain H3-2 was identified as *Streptomyces* sp. and convinced by the polymorphic phylogenic analysis of 16S *rRNA* sequences. Extracts of the strain H3-2 suppressed the growth and spore germination of Foc TR4 *in vitro* by destroying cell membrane integrity and mycelial ultrastructure. Notably, the strain and its extracts showed broad-spectrum antifungal activity against the selected seven fungal phytopathogens. Fourteen chemical compounds in the extracts were identified by gas chromatography–mass spectrometer (GC-MS), primarily phenolic compounds. Additional pot inoculation experiment demonstrated that the fermentation broth of the strain H3-2 promoted the growth of banana seedlings by efficiently inhibiting the spread of banana Fusarium wilt disease. This study demonstrated the potential application of the novel *Streptomyces* sp. H3-2 for the management of banana Fusarium wilt.

Keywords: *Streptomyces* sp., banana fusarium wilt, antifungal mechanism, pot experiment, GC-MS, biocontrol

INTRODUCTION

Banana (*Musa* spp.) is one of the most important fruit crops among the world's top 10 staple foods in terms of production and trade (Dita et al., 2018; Xu et al., 2020). However, Fusarium wilt disease, known as Panama disease, seriously causes a substantial loss in the banana industry (Dale et al., 2017). Banana Fusarium wilt is a soil-borne fungal pathogen, which is caused by *Fusarium oxysporum* f. sp. *cubense* (Foc). The Foc tropical race 4 (Foc TR4) strain can survive for more than 30 years in soil and infects over 80% of banana cultivars (Zhang et al., 2019).

Currently, physical and chemical methods are not effective in controlling the spread of banana Fusarium wilt disease. Additionally, chemical application can induce the development of resistant strains and cause environmental pollution (Kanini et al., 2013). Practical management, including the isolation of infested areas, remotion of infected plants, and disinfection of farm instruments, slows the spread of Foc to a certain extent (Dale et al., 2017). Biological control using functional microbes is considered to be an economically and environmentally friendly method to manage fungal phytopathogens (Abbas et al., 2020).

Actinobacteria belonging to Gram-positive bacteria have a great biosynthetic potential to produce large amounts of bioactive secondary metabolites (Jose et al., 2021). Some metabolites with novel structure and remarkable biological activity are widely used in agriculture, industry, and medicine (Uyeda et al., 2001; Kurniawati et al., 2016; Li et al., 2021a). Nearly 80% of antibiotics are produced by actinomycetes, such as *Streptomyces* (Yun et al., 2018). Many insecticides, bioherbicides, and antifungal agents are also made from *Streptomyces* (Barka et al., 2016). For example, ivermectin, a true success story in terms of anthelmintics killing a variety of parasites and insects, is a dehydro derivative of avermectin produced by *Streptomyces avermitilis* (Omura and Crump, 2014, 2017). Mildiomycin, a nucleoside fungicide isolated from the secondary metabolites of *Streptomyces rimofaciens*, has potent bioactivity against powdery mildews on cucumber or pumpkin (Feduchi et al., 1985; Huang et al., 2010; Zhao et al., 2016). Our previous study also showed that extracts of *Streptomyces* sp. H4 had strong inhibitory activity against *Colletotrichum fragariae* during strawberry fruit storage stage (Li et al., 2021a). *Streptomyces* sp. JBS5-6 also exhibits strong antifungal activity against Foc TR4 (Jing et al., 2020). However, these functional microbes for controlling plant diseases are limited by their different growth conditions or poor activity in a complex environment (Saravanan et al., 2003). The isolation and screening of broad-spectrum and highly efficient antagonistic agents are still necessary (Chen et al., 2018).

In this study, a novel strain H3-2 belonging to the genus *Streptomyces* was isolated from the rhizosphere of banana plantations, and its broad-spectrum antifungal activity was discovered. The morphological, physiological, and biochemical characteristics of *Streptomyces* sp. H3-2 were analyzed. The effects of its extracts on mycelial growth, morphology, and cell ultrastructure and the spore germination of Foc TR4 were also detected. In addition, the biocontrol ability of *Streptomyces* sp. H3-2 was further investigated in a pot experiment. The aim of this study was to excavate important actinobacterium resources to manage fungal phytopathogens. These findings will be helpful in searching novel natural compounds with high antifungal activities for the banana industry.

MATERIALS AND METHODS

Screening of Antifungal Actinomycetes

Actinomycetes were isolated from the rhizosphere of a banana orchard, where no disease symptoms of banana Fusarium wilt were recorded for more than 10 years in Lingao County, Hainan Province, China (19°47′1″N and 105°51′17″E). Isolated strains were preserved on ISP2 medium slants at 4°C in the Key Laboratory of Biology and Genetic Resources of Tropical Crops, Ministry of Agriculture, Institute of Tropical Bioscience and Biotechnology, Chinese Academy of Tropical Agricultural Sciences, Haikou, China. To screen the actinomycetes with antifungal activity against Foc TR4, a plate confrontation method on the potato dextrose agar (PDA) medium was performed *in vitro* according to the description of Li et al. (2021). The inhibition rates of fungal radial growth were calculated using the formula: Inhibition rates = $[(A-B)/(A-0.5)] \times 100$, where A and B are the mean colony diameters (cm) of phytopathogenic fungi in the control and treatment groups, respectively.

Identification of Strain H3-2

A H3-2 strain was identified by combining morphological, physiological, and biochemical characteristics (Qi et al., 2019). For molecular identification, the 16S *rRNA* gene sequence was amplified by polymerase chain reaction (PCR) using the prokaryotic universal primers (27F: 5′-AGTT TGATCMTGGCTCAG-3′ and 1492R: 5′-GGTTACCTTGTTACGACTT-3′) (Qi et al., 2019). The thermocycling condition for PCR included denaturation at 95°C for 3 min, followed by 32 cycles of denaturation at 94°C for 30 s, annealing at 55°C for 1 min, extension at 72°C for 2 min, and final extension at 72°C for 10 min in the Veriti thermal cycler (Applied Biosystems, Carlsbad, CA, United States). The amplified product was analyzed in 1.2% (w/v) of agarose gel electrophoresis and sequenced by Sangon Biotech Co., Ltd. (Shanghai, China). To perform a phylogenetic analysis, the 16S *rRNA* gene sequence was aligned against the NCBI GenBank entries using the BLAST algorithm[1] and the EzBioCloud database[2] to obtain the homology sequences. The phylogenetic tree was constructed using the neighbor-joining method of MEGA version 7.0.

Isolation of Stain H3-2 Crude Extracts

The H3-2 strain was cultured on ISP2 solid medium for 7 days at 28°C. A single colony was selected and inoculated into a 250-ml Erlenmeyer flask containing 100 ml of the ISP2 liquid medium at 200 rpm for 4 days at 28°C as a seed suspension. To obtain a mass culture fermentation broth, 20 ml of the seed culture broth was inoculated in 20 flasks (5 L) containing 1 L of sterilized soybean liquid culture medium (SLM, 15 g of soybean powder, 20 g of amylose, 5 g of yeast extracts, 2 g of bacterial peptone, 4 g of NaCl, 4 g of $CaCO_3$ per liter of distilled water, pH adjusted to 7.2 with 2 mol/L NaOH), respectively. The flasks were cultured at 200 rpm for 7 days at 28°C. The fermentation broth of the 7-day-old strain H3-2 was centrifuged at 8,000 × *g* for 15 min. The supernatant was concentrated under vacuum at 36°C using a rotary evaporator to obtain crude extracts (Jing et al., 2020).

---

[1] http://www.ncbi.nlm.nih.gov/BLAST
[2] https://www.ezbiocloud.net/identify

Zou et al.

Isolation and Identification of *Streptomyces* sp. H3-2

Purification of H3-2 Crude Extracts

After filtering with filter paper, crude extracts were eluted using a linear gradient (1 L each) of methanol: deionized water (50:50, 60:40, 70:30, 80:20, and 100:0) on a silica gel column (8.0 inner diameter, 60 cm length) and divided into five fractions. The five evaporated solutions were dissolved into 10% of dimethyl sulfoxide (DMSO) with a final concentration of 20.0 mg/ml, respectively. Then, inhibitory efficiency against Foc TR4 was carried out by a plate diffusion method according to previous reports (Jing et al., 2020; Li et al., 2021b): 20 mg/ml of five crude extract solutions were transferred to 60 ml of the autoclaved PDA medium at 50–55°C; 10% of DMSO was used as a control. A 5-mm-diameter fungal disc of Foc TR4 was inoculated in the center of plate. The inhibition rates of Foc TR4 were calculated at 28°C for 7 days as mentioned above. All experiments were repeated in triplicates.

Effect of Strain H3-2 Extracts on Mycelial Growth of Foc TR4

Growth inhibition of Foc TR4 was evaluated by mycelial growth rate. Strain H3-2 extracts isolated with 100% of methanol were added to the autoclaved PDA medium and diluted into different concentrations of 0.78, 1.56, 3.12, 6.25, 12.5, 25, 50, 100, and 200 μg/ml, respectively. The consistent concentration of DMSO was used as a negative control in each group. A 5-mm-diameter fungal disc of Foc TR4 was inoculated in the center of plate. The growth diameter of Foc TR4 was measured after 7 days at 28°C. Each treatment contained three replicates. A least square method was used to establish a linear regression equation, namely, a toxicity regression equation (Vanewijk and Hoekstra, 1993). A half maximal effective concentration (EC_{50}) value was calculated according to the toxicity regression equation.

Effect of Strain H3-2 Extracts on Mycelial Morphological Characteristics of Foc TR4

The morphological characteristics of Foc TR4 mycelia treated with H3-2 extracts were assessed by scanning electron microscopy (SEM; TM4000Plus, Hitachi, Japan). The methods of sample preparation and analysis were referred to the publication with a slight modification (Wei et al., 2020). A 5-mm-diameter disk of Foc TR4 was inoculated in the PDA plate containing $4 \times EC_{50}$ of strain H3-2 extracts. A transverse section (1 cm^2) was cut from the mycelial edges. The corresponding position was selected from the control plate containing an equal volume of DMSO. The hyphal samples were fixed with 2.5% (v/v) of glutaraldehyde at 4°C for 4 h and washed three times with 1.5 ml of phosphate-buffered saline (PBS, 0.1 mol/L) for 15 min. Samples were dehydrated through a gradient ethanol (30, 50, 70,80, 90, 95, and 100%) for 15 min. After replacing ethanol with isoamyl acetate, critical point drying was carried out with carbon dioxide. Finally, the dried samples coated with thin gold were observed under SEM.

Effect of Strain H3-2 Extracts on Mycelial Cell Ultrastructure of Foc TR4

The ultrastructure of Foc TR4 cells treated with H3-2 extracts was investigated by transmission electron microscopy (TEM, HT7700; Hitachi, Ibaraki, Japan). The methods for collection, fixation, and dehydration of samples were the same as described above. The samples were embedded in the Epon812 resin and then were aggregated at 35°C for 12 h, 45°C for 24 h, and 60°C for 48 h. Then, the embedded material was sliced into 70-nm slices by an ultramicrotome (EM UC6; Leica, Wetzlar, Germany) at room temperature. Subsequently, these sections were double-stained with uranyl acetate and lead citrate solution. After natural drying, the ultrastructure of mycelial cells was detected by TEM.

Effects of Strain H3-2 Extracts on Foc TR4 Spore Germination

The germination rate of Foc TR4 spores was assayed as reported previously with a minor modification (Li et al., 2021b). Briefly, 45 μl of spore suspension (1.0×10^6 CFU/ml) was completely mixed with an equal volume of strain H3-2 extracts with different concentrations of $1 \times EC_{50}$, $2 \times EC_{50}$, $4 \times EC_{50}$, $8 \times EC_{50}$, and $16 \times EC_{50}$, respectively. The mixture was added into concave slides and was incubated at 28°C for 12 h. The same concentration of DMSO or spore suspension was used as the negative control. All experiments were performed in triplicates. One hundred spores in each slide were observed by an optical inverted microscope (MMI Cellcut Plus; MMI, Glattbrugg, Switzerland). The inhibition efficiency was evaluated using the percentage of spore germination (Wei et al., 2020).

Assay of a Broad-Spectrum Antifungal Activity of Strain H3-2 and Its Extracts

To test the broad-spectrum antifungal activity of the stain H3-2 and its extracts, seven fungal phytopathogens, including Foc TR4 (ATCC 76255), *F. oxysporum f.* sp. *cucumerinum* (ATCC 204378), *Fusarium graminearum* (ATCCMYA-4620), *Colletotrichum gloeosporioides* (ATCCMYA-456), *Colletotrichum gloeosporioides* (ACCC 36351), *Pyricularia oryzae* (ATCC 52352), *Colletotrichum fragariae* (ATCC 58718), and *Curvularia lunata* (ATCC 12017), were selected from the Key Laboratory of Biology and Genetic Resources of Tropical Crops, Ministry of Agriculture, Institute of Tropical Bioscience and Biotechnology, Chinese Academy of Tropical Agricultural Sciences, Haikou, China. Strain H3-2 was inoculated at four symmetrical sites on the PDA plate. After 24 h at 28°C, a 5-mm-diameter disc of phytopathogenic fungi was added in the center of PDA plate. For further detection of antifungal activity of strain H3-2 extracts, each fungal phytopathogen was inoculated in the center of an autoclaved PDA medium with 200 μg/ml of final extract concentration. Antifungal activity was measured using the mycelial growth method. All experiments were repeated in triplicates.

Zou et al.

Isolation and Identification of *Streptomyces* sp. H3-2

Chemical Constituent Analysis of Strain H3-2 Extracts

The chemical constituent of H3-2 extracts was analyzed by a PerkinElmer 690 GC coupled to a PerkinElmer 8T Single Quadrupole MS. The Elite-5MS capillary column (30 m length, 0.25 mm inner diameter, 0.25 μm film thickness) and helium (1 ml min^{-1}) were used as stationary phase and mobile phase, respectively. The splitless mode was employed for injection with injection quantity of 1 μl and injector temperature control of 250°C. The column temperature program was set as follows: initial temperature kept at 60°C for 1 min, increased to 100°C at a rate of 5°C min^{-1} for 5 min, then increased to 250°C at a rate of 10°C min^{-1} for 35 min, programmed to 280°C at a rate of 10°C min^{-1}, and finally kept isothermally at 280°C for 25 min. The temperature of transfer line was 280°C, and the temperature of ion source was 240°C. The mass spectrometer was operated in electron ionization mode (70 eV) with a scan range of ions from 50 to 650 amu. Results of mass spectra were matched with the standard spectrum library of the National Institute of Standards and Technology (NIST).

Pot Inoculation Experiment of Banana Seedlings

The control efficiency of the strain H3-2 fermentation broth on banana Fusarium wilt disease was evaluated in a greenhouse with an average temperature of 28°C and relative humidity of 70% from March to April in 2021. Foc TR4 overexpressing a green fluorescent protein gene (GFP-Foc TR4) was provided by the Institute of Environment and Plant Protection, China Academy of Tropical Agricultural Sciences, Haikou, China. Banana ("Brazilian," *Musa acuminata* L. AAA genotype cv. Cavendish) tissue culture seedlings with three to four true leaves were transplanted from seedling bags (one seedling per bag) to a plastic basin (8 cm × 8 cm) containing 1 kg of sterilized soil (Xu et al., 2020). Three treatments were set up as follows: (1) H$_2$O (sterile deionized water, negative control); (2) Foc TR4 (positive control, inoculated with GFP-Foc TR4); (3) H3-2 + Foc TR4 (1.0 × 10^7 CFU ml^{-1} of strain H3-2 fermentation broth and 1.0 × 10^7 CFU ml^{-1} of GFP-Foc TR4). One hundred milliliters of mixture was added to the roots of banana seedlings as previously described (Wang et al., 2012). Banana seedlings were treated every 7 days. Each treatment contained 30 plants.

Assessment of Biocontrol Efficiency

After co-inoculation for 35 days, banana roots were collected and sliced using manual operation as thin as possible. The infection and colonization levels of GFP-Foc TR4 were detected immediately using a laser scanning confocal microscope (Olympus FV1000; Olympus, Tokyo, Japan). The excitation spectrum of GFP was set at 488 nm, and autofluorescence of root tissue was set 530 nm.

Plant height, chlorophyll contents of leaves, stem diameter, leaf area, and total dry weight were also measured. A total of 21 plants were selected form each treatment to assess the biocontrol efficiency. Disease symptoms were observed and recorded in each plant. The disease symptoms were classed into five from 0 to 4

as described by Mak et al. (2004). According to the disease class, the disease incidence (DI) was calculated as DI (%) = Σ(Value of class × Number of disease plants in that class)/(4 × Total number of assessed banana seedlings) × 100 according to the previous description (Xu et al., 2020). Biocontrol efficiency (BE) was measured according to the following formula: BE (%) = (DI in Foc TR4 group – DI in H3-2 + Foc TR4 group)/DI in Foc TR4 group × 100.

Data Analysis

Statistical analysis was performed using the SPSS 22 software (SPSS Inc., Chicago, IL, United States). The difference among treatments was determined using one-way analysis of variance (ANOVA). A Duncan's multiple range test was applied to determine a significant difference ($p < 0.05$).
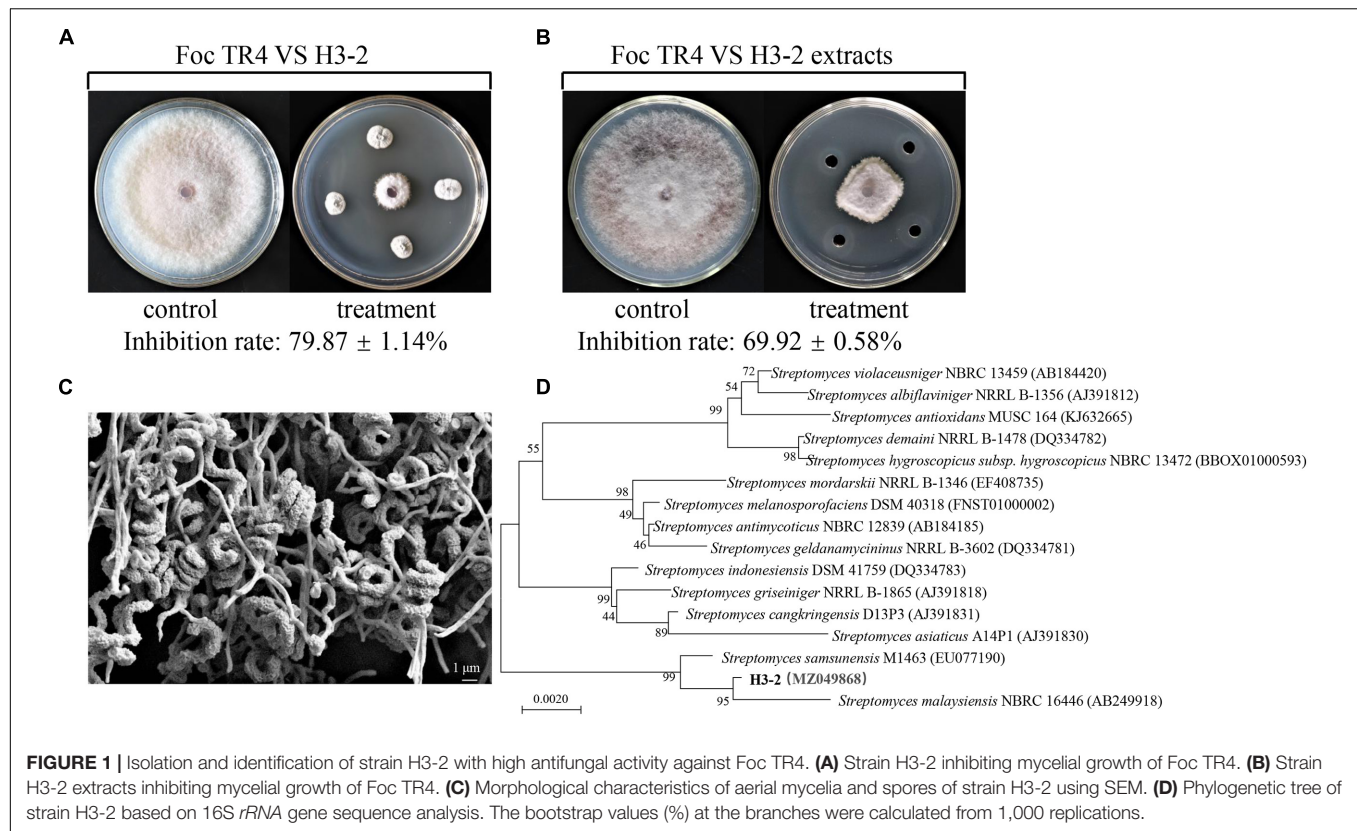
RESULTS

Isolation of Strain H3-2

A total of 44 strains of actinomycetes were isolated from the soil in the banana orchard. Among them, an actinomycete marked with H3-2 was of particular interest because of its potent antagonistic activity against Foc TR4. After dual culture with strain H3-2 for 7 days at 28°C, mycelial diameter of Foc TR4 was 20.0 mm ± 0.08 in comparison to 77.3 mm ± 0.33 in the control (**Figure 1A**). The inhibition percentage of mycelial growth was 79.9%. Further test on antifungal activity of strain H3-2 extracts showed that mycelial diameter was 29.7 mm ± 0.05 and mycelial inhibition percentage was 69.9% in the treatment group (**Figure 1B**). Therefore, strain H3-2 was selected for the following study.

Characteristics and Identification of Strain H3-2

Strain H3-2 grew well on seven different solid media at 28°C for 7 days. The pink soluble pigment was produced on ISP7 medium but was not produced on other media (**Supplementary Table 1**). The open spirals of spore-bearing mycelia with the revolutions of 3–4 were observed by SEM (**Figure 1C**). The physiological and biochemical characteristics showed that strain H3-2 exhibited an ability of gelatin liquefaction, can hydrolyze starch and cellulose, but cannot produce H$_2$S, urease and xylanase (**Supplementary Table 2**). It grew normally in the media with pH ranging from 6 to 8 and NaCl content less than 7%. Strain H3-2 could utilize all the tested carbon sources and most of nitrogen sources such as phenylalanine, ammonium sulfate, and potassium nitrate (**Supplementary Table 3**). These characteristics are typical morphological, physiological, and biochemical features of *Streptomycete*-like organisms. To further confirm phylogenetic relationship between H3-2 and *Streptomyces* spp., 16S *rRNA* sequence of H3-2 was amplified by PCR and sequenced. The sequence exhibited 99.7% similarity with *Streptomyces samsunensis* M1463(T)(EU077190) by alignment against EzBioCloud database and Blast X algorithm in GenBank. A phylogenetic tree constructed by

Zou et al.

Isolation and Identification of *Streptomyces* sp. H3-2

FIGURE 1 | Isolation and identification of strain H3-2 with high antifungal activity against Foc TR4. **(A)** Strain H3-2 inhibiting mycelial growth of Foc TR4. **(B)** Strain H3-2 extracts inhibiting mycelial growth of Foc TR4. **(C)** Morphological characteristics of aerial mycelia and spores of strain H3-2 using SEM. **(D)** Phylogenetic tree of strain H3-2 based on 16S *rRNA* gene sequence analysis. The bootstrap values (%) at the branches were calculated from 1,000 replications.

the neighbor-joining method showed that strain H3-2 and *S. samsunensis* M1463(T)(EU077190) clustered into the same group (**Figure 1D**). Thus, strain H3-2 was identified as *Streptomyces* spp. combining the morphological, physiological, and biochemical characteristics as well as the alignment result of 16S *rRNA* gene sequence.

Antagonistic Activity of Strain H3-2 Extracts Against Foc TR4

The crude extracts of strain H3-2 were further extracted with different concentrations of methanol (50–100%, v/v) for measurement of antagonistic activity against Foc TR4. The antagonistic activity of extracts increased significantly along with the increase of methanol concentrations (**Figure 2**). The inhibition rate of 80% methanol extracts to Foc TR4 was 84.7%. The antifungal activity of 100% methanol extracts was the strongest, and the inhibition rate was 93.4%. Hence, the effect of 100% methanol extracts of strain H3-2 on mycelial growth was selected for further investigations.

Strain H3-2 Extracts Inhibiting Mycelial Growth of Foc TR4

Strain H3-2 extracts observably inhibited mycelial growth of Foc TR4 after 7 days. The higher the concentration exhibited the more apparent the inhibition ability (**Figure 3A**). Compared with the growth diameter (8.27 cm $\pm$ 0.06) of Foc TR4 in the control plate, the mycelial growth diameter decreased markedly

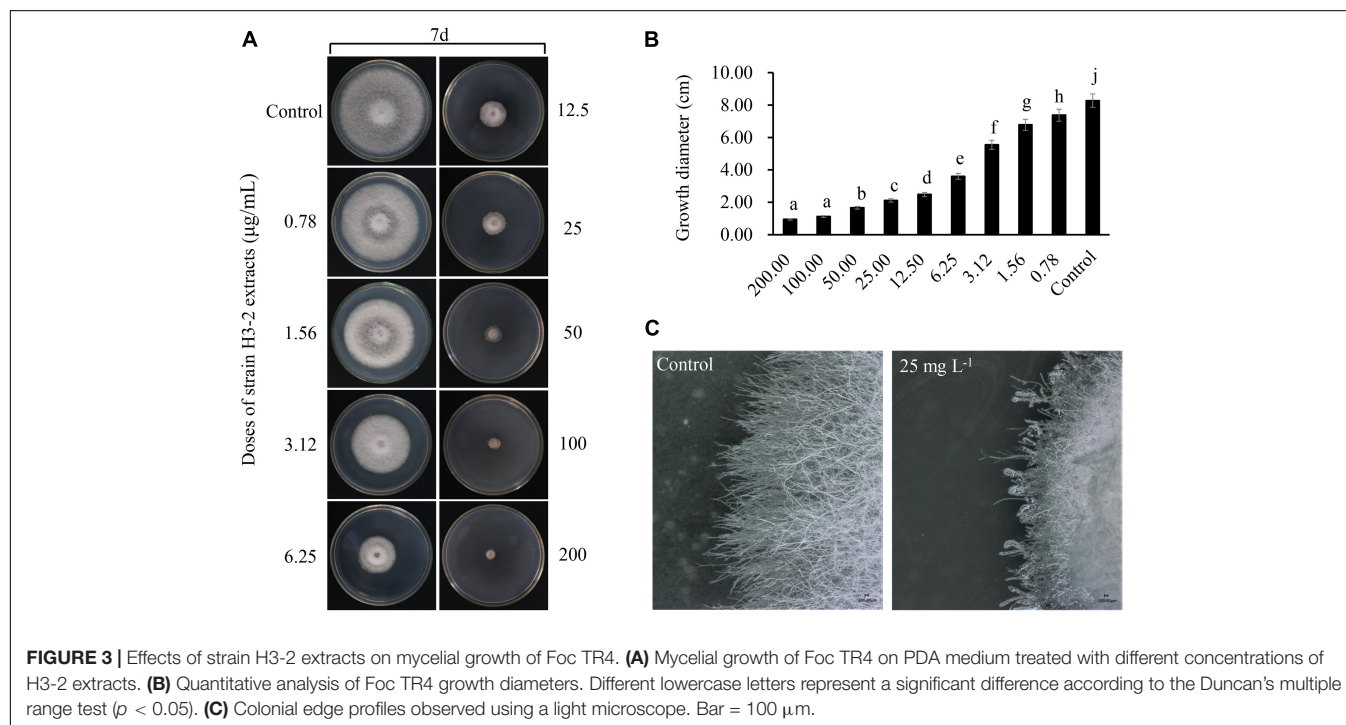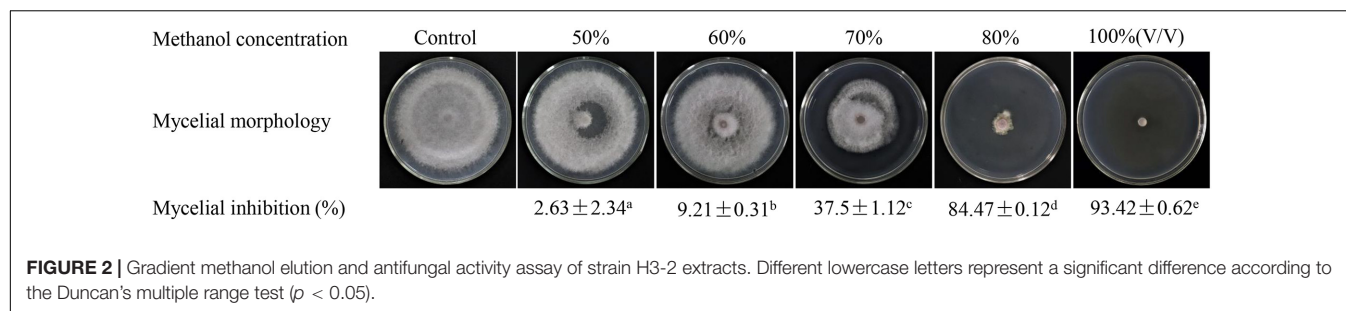to 2.48 cm $\pm$ 0.12 in the treatment group of 12.5-μg/ml extracts. When the concentration of strain H3-2 extracts reached 200 μg/ml, the colony growth was significantly inhibited and the inhibition rate reached 94.2% $\pm$ 0.64 (**Figure 3B**). In the presence of 25 mg/L extracts, the hyphae at the colony edges were short and thick and did not produce branches (**Figure 3C**). The toxic regression equation ($y = 1.1412x + 3.9204$, $R^2 = 0.9922$) was further established and the EC_{50} value of strain H3-2 extracts against Foc TR4 was 8.83 μg/ml, which was defined as $1 \times EC_{50}$ in a follow-up study.

Effects of Strain H3-2 Extracts on Mycelial Morphological Characteristics of Foc TR4

The Foc TR4 mycelia collected from the edge of the inhibition zone was different from that of the control by SEM. In the control group, the surface of normal mycelia was smooth and the tops were regular, mellow, and full (**Figure 4A**). Whereas, the mycelia treated with H3-2 extracts were rough, irregular swelling and cell wall collapsed. The mycelial tops had spherical, fusiform swelling and webbed-foot-shaped branches (**Figure 4B–D**).

Effects of H3-2 Extracts on Mycelial Cell Ultrastructure of Foc TR4

The mycelial cell ultrastructure of Foc TR4 was observed by TEM after treatment with 50 μg/ml of strain H3-2 extracts. In the control group, the cell wall and membrane were intact, and the cytoplasm was regular and uniform (**Figure 5A**). After treatment with strain H3-2 extracts, the cell wall and septum

FIGURE 2 | Gradient methanol elution and antifungal activity assay of strain H3-2 extracts. Different lowercase letters represent a significant difference according to the Duncan's multiple range test ($p < 0.05$).

FIGURE 3 | Effects of strain H3-2 extracts on mycelial growth of Foc TR4. **(A)** Mycelial growth of Foc TR4 on PDA medium treated with different concentrations of H3-2 extracts. **(B)** Quantitative analysis of Foc TR4 growth diameters. Different lowercase letters represent a significant difference according to the Duncan's multiple range test ($p < 0.05$). **(C)** Colonial edge profiles observed using a light microscope. Bar = 100 μm.

were thickened and the cell membrane was partly disrupted (**Figure 5B**). In addition, the increase of liposomes and electron transparent particles was also observed (**Figure 5C**). The cell nucleus swelled together with chromatin dissolving in the treatment group (**Figure 5D**).

Strain H3-2 Extracts Inhibiting Foc TR4 Spore Germination

Strain H3-2 extracts effectively inhibited the spore germination of Foc TR4. The inhibitory efficiency of spore germination was enhanced along with the concentration increase of extracts (**Figure 6**). Compared with the control group, the spore germination rates of Foc TR4 were 74.8, 42.3, and 16.5% after treatment with $1 \times EC_{50}$, $2 \times EC_{50}$, and $4 \times EC_{50}$ extracts for 12 h, respectively. The germination rate of $0.5 \times EC_{50}$ was not significantly different from that of the control group, but the length of the germ tube was shorter than that of the control group. The spore germination was completely inhibited, and the length of the germ tube significantly failed to develop at the treatment group of $8 \times EC_{50}$ extracts.

Assay of a Broad-Spectrum Antifungal Activity

The strain H3-2 and its extracts showed a broad-spectrum activity against the selected seven phytopathogenic fungi with inhibition rate in the range of 67.0–88.1% and 81.9–92.5%, respectively (**Figure 7**). The maximal and minimal inhibition activities of stain H3-2 were observed against *C. fragariae* and *F. graminearum*, respectively. For strain H3-2 extracts, the maximum inhibition activity of 92.5% was exhibited against *C. gloeosporioides*, and the lowest inhibition activity was 81.9% against *F. graminearum*.

Chemical Constituent Analysis of Strain H3-2 Extracts by GC-MS

Active chemical constituents of strain H3-2 extracts were analyzed by GC-MS. A total of 14 chemical constituents were identified by alignment of the NIST library based on retention time, molecular mass, match, and the molecular formula (**Table 1**). The predicted chemical constituents

Zou et al.

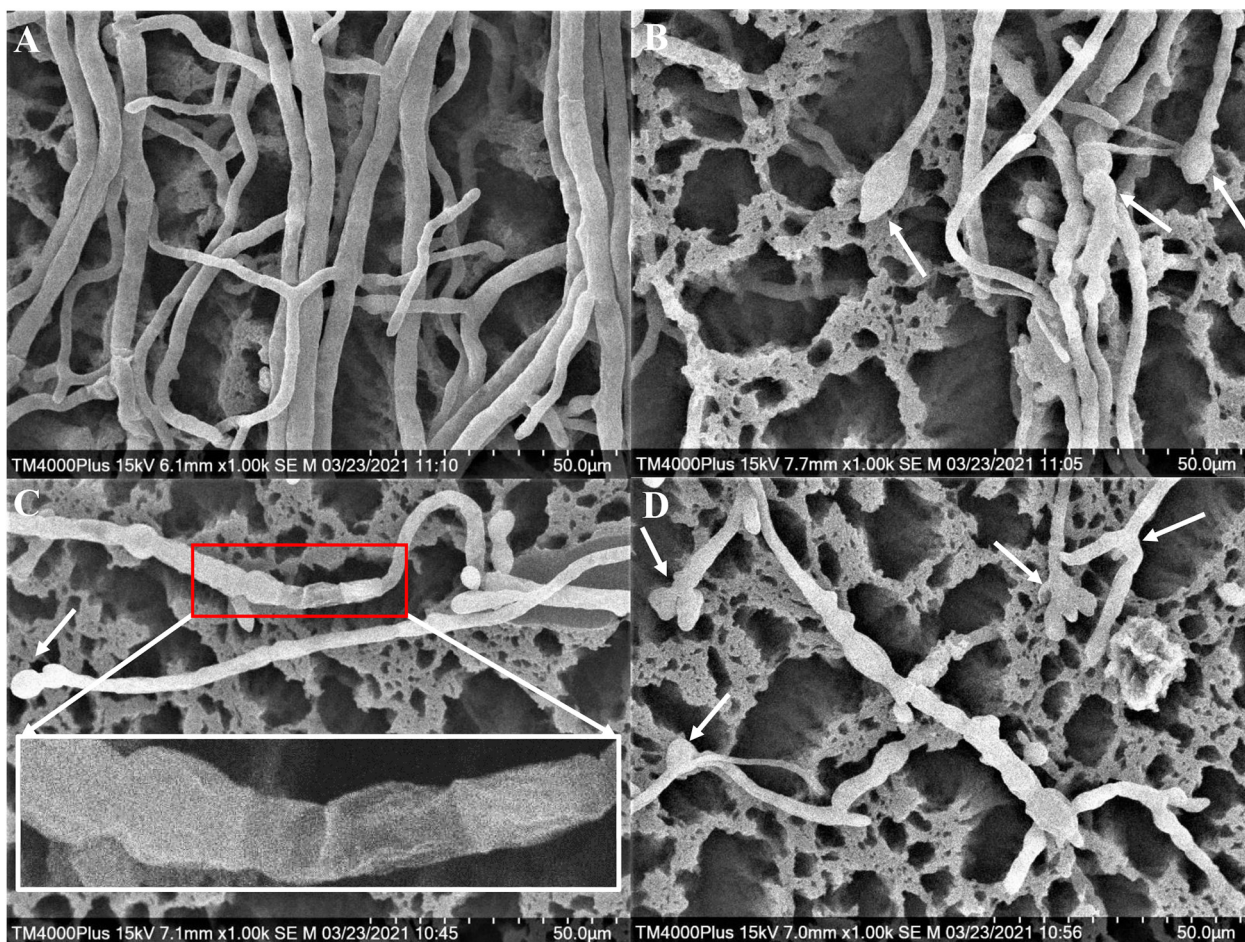Isolation and Identification of *Streptomyces* sp. H3-2

FIGURE 4 | Mycelial morphology of Foc TR4 observed under SEM. **(A)** Mycelial characteristics of Foc TR4 in the absence of stain H3-2 extracts. **(B–D)** Mycelial morphology of Foc TR4 treated with 25 µg/ml of strain H3-2 extracts. The arrows indicate damaged mycelia of Foc TR4 in the presence of strain H3-2 extracts.

were listed in **Supplementary Figure 1**, including (1) 4,6-dimethyldodecane, (2) Cyclohexane, octyl-, (3) Undecane, 3,7- dimethyl-, (4) Phenol, 2,4-bis(1,1-dimethylethyl)-, (5) Benzene, 1,2,3-trimethoxy-5-(2-propenyl)-, (6) Hexadecane, (7) Cyclohexane,(4-methylpentyl)-, (8) 9-Heptadecanone, (9) Benzeneprop anoic acid, 3,5-bis(1,1-dimethylethyl)-4- hydroxy-,octadecyl ester, (10) Nonadecane, 2- methyl-, (11) 2-methyloctaco sane, (12) Phenol, 2,2′-methylenebis[6-(1,1-dimethylethyl)-4- methyl-, (13) Hexadecanoic acid, 2-hydroxy-1-(hydroxymethyl) ethyl ester, and (14) Octadecanoi acid, 2-hydroxy-1-(hydroxymethyl)ethyl ester. The peak area represented a quantitative proportion of the predicted compound in the total of extracts.

Strain H3-2 Fermentation Broth on Biocontrol Efficiency of Banana Fusarium Wilt

After co-inoculation for 35 days, chlorosis and wilting symptoms appeared in old leaves in the Foc TR4 treatment group, while the banana seedlings had no disease symptoms after treatment with the strain H3-2 fermentation broth (**Figure 8A**). Compared with the H$_2$O and strain H3-2 groups, the growth of banana seedlings was significantly inhibited by Foc TR4. Furthermore, Foc TR4 spores extended from banana root vascular bundles to corms, causing corm rot in the control group. In the strain H3-2 treatment group, no obvious infection occurred in banana corms, and only a few spores of Foc TR4 invaded in the root epidermal cells (**Figure 8B**). Moreover, the disease index dropped below 1% and the biocontrol efficiency was 89.4% after treatment with H3-2 fermentation broth (**Figure 8C**).

Strain H3-2 Fermentation Broth Promoted the Growth of Banana Seedlings

The growth of banana seedlings was significantly promoted after treatment with the fermentation broth of strain H3-2. Compared with Foc TR4 and H3-2 + Foc TR4 groups, the stem diameter, plant height, leaf area, chlorophyll content and dry weight were increased by 27.6, 27.5, 59.6, 24.7, and 80.0%, respectively (**Figures 9A–E**). Therefore, the fermentation broth
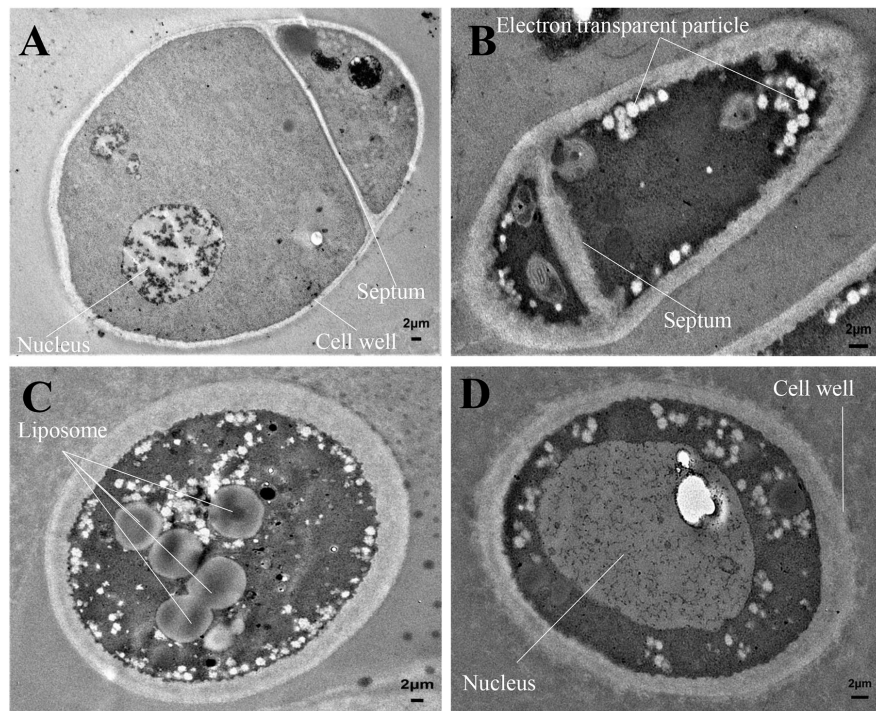
Zou et al.

Isolation and Identification of *Streptomyces* sp. H3-2

FIGURE 5 | Mycelial cell ultrastructure of Foc TR4 observed under TEM. **(A)** Ultrastructure characteristics of Foc TR4. **(B–D)** Ultrastructure characteristics of Foc TR4 treated with 50 μg/ml of strain H3-2 extracts. The arrows indicate Foc TR4 ultrastructure damaged by strain H3-2 extracts. Bar = 2 μm.
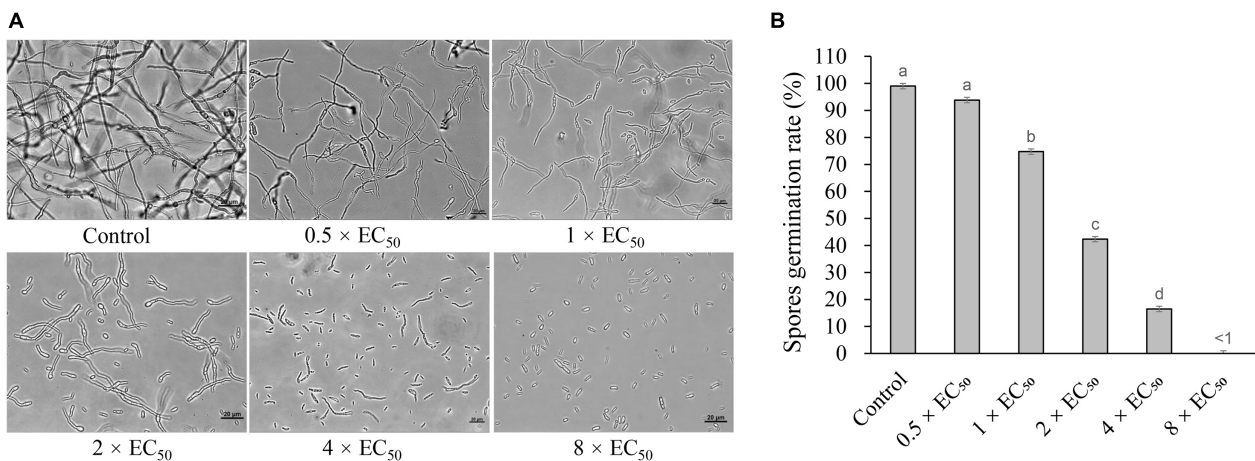

FIGURE 6 | Inhibition of strain H3-2 extracts on spore germination of Foc TR4. **(A)** Spore germination characteristics of Foc TR4 after treatment with 0.5×, 1×, 2×, 4× or 8× EC_{50} extracts. 10% of DMSO was used as a control. Bar = 20 μm. **(B)** The spore germination rate (%) of Foc TR4 after treatment with different dose extracts. Different lowercase letters indicate a significant difference according to the Duncan's multiple range test ($p < 0.05$).

of *Streptomyces* sp. H3-2 showed a growth-promoting role on banana seedlings.

DISCUSSION

Plant fungal diseases, especially Fusarium wilt, has seriously limited the sustainable development of the banana industry

(Li et al., 2021b). Biological control is considered to be high efficiency, broad spectrum, and environment friendly (Chen et al., 2018). Our previous study found that a banana orchard had no disease symptoms of Fusarium wilt for more than 10 years, in which rhizosphere soil was found to contain many functional microorganisms (Zhou et al., 2019). Especially, most of secondary metabolites of *Streptomyces* sp. had a broad-spectrum antifungal activity in controlling plant diseases
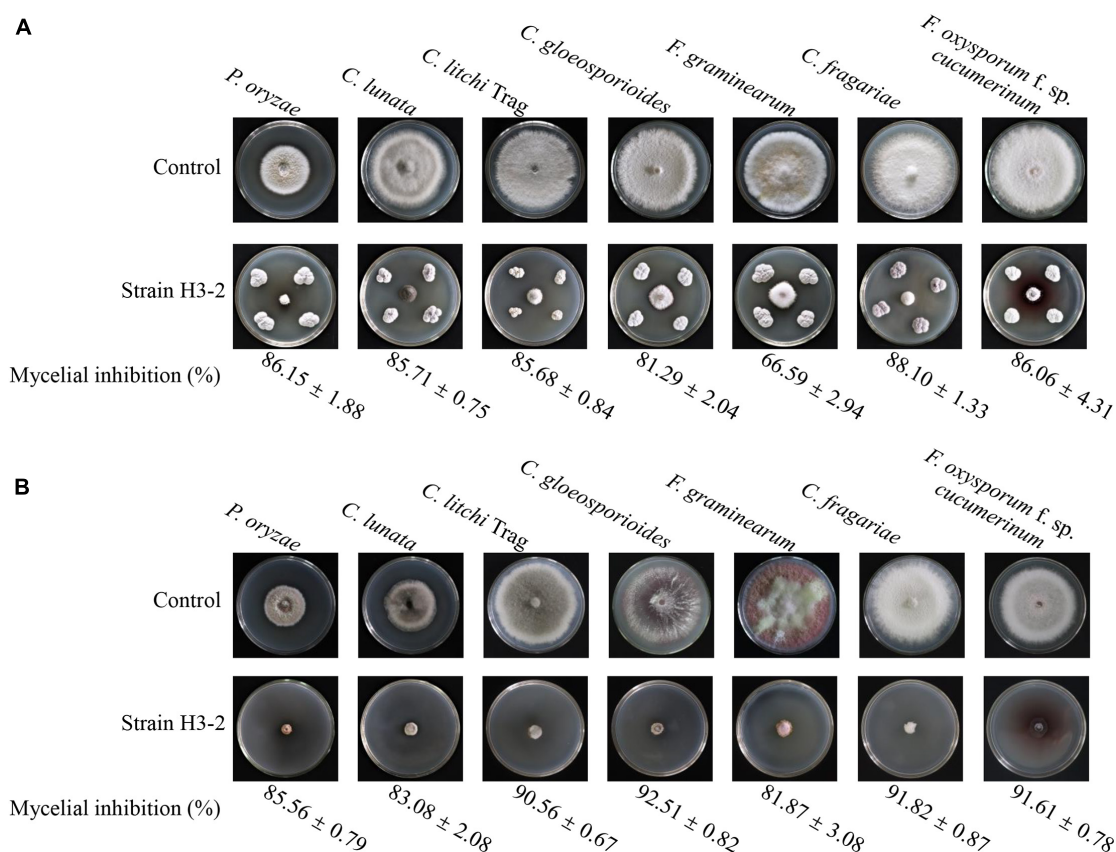
FIGURE 7 | A broad-spectrum antifungal activity of strain H3-2 **(A)** and its extracts **(B)** against the selected seven plant pathogenic fungi.

TABLE 1 | Chemical constituents in strain H3-2 extracts analyzed by GC-MS.

No.	Predicted compounds	Match	Probability (%)	RT (min)	Area (%)	Chemical formula	Activity	References
1	4,6-dimethyldodecane	774	6.5	16.020	1.93	$C_{14}H_{30}$	Antimicrobial, antioxidant	Geethalakshmi and Sarada, 2013
2	Cyclohexane, octyl-	879	47.5	19.873	1.63	$C_{14}H_{28}$	No activity reported	
3	Undecane, 3,7-dimethyl-	770	7.2	20.436	0.7	$C_{13}H_{28}$	No activity reported	
4	Phenol, 2,4-bis(1,1-dimethylethyl)-	884	45.1	20.769	6.89	$C_{14}H_{22}O$	Inhibitor	Kim et al., 2017
5	Benzene, 1,2,3-trimethoxy-5-(2-propenyl)-	740	37.4	21.332	1.08	$C_{12}H_{16}O_3$	Antibacterial	Rossi et al., 2007
6	Hexadecane	843	17.7	22.093	0.73	$C_{16}H_{34}$	No activity reported	
7	Cyclohexane,(4-methylpentyl)-	784	15.5	22.858	1.26	$C_{12}H_{24}$	No activity reported	
8	9-Heptadecanone	801	79.1	25.213	0.94	$C_{17}H_{34}O$	No activity reported	
9	Benzeneprop anoic acid, 3,5-bis(1,1-dimethylethyl)-4-hydroxy-,octadecyl ester	728	93.2	76.351	12.77	$C_{35}H_{62}O_3$	Antimicrobial, Anticancer	Elsayed et al., 2020
10	Nonadecane, 2-methyl-	802	13.2	27.635	4.67	$C_{20}H_{42}$	Antibiofilm	Adnan, 2015
11	2-methyloctaco sane	780	15.4	29.481	2.52	$C_{29}H_{60}$	No activity reported	
12	Phenol, 2,2'-methylenebis[6-(1,1-dimethylethyl)-4-methyl-	866	95.3	30.268	10.22	$C_{23}H_{32}O_2$	Insecticidal	Sun et al., 2007
13	Hexadecanoic acid, 2-hydroxy-1-(hydroxymethyl)ethyl ester	786	55.9	31.434	4.79	$C_{19}H_{38}O_4$	Antioxidant, anti-inflammatory, anthelmintic	Ali et al., 2015
14	Octadecanoi acid, 2-hydroxy-1-(hydroxymethyl)ethyl ester	761	46.1	34.951	4.96	$C_{21}H_{42}O_4$	No activity reported	

Zou et al.

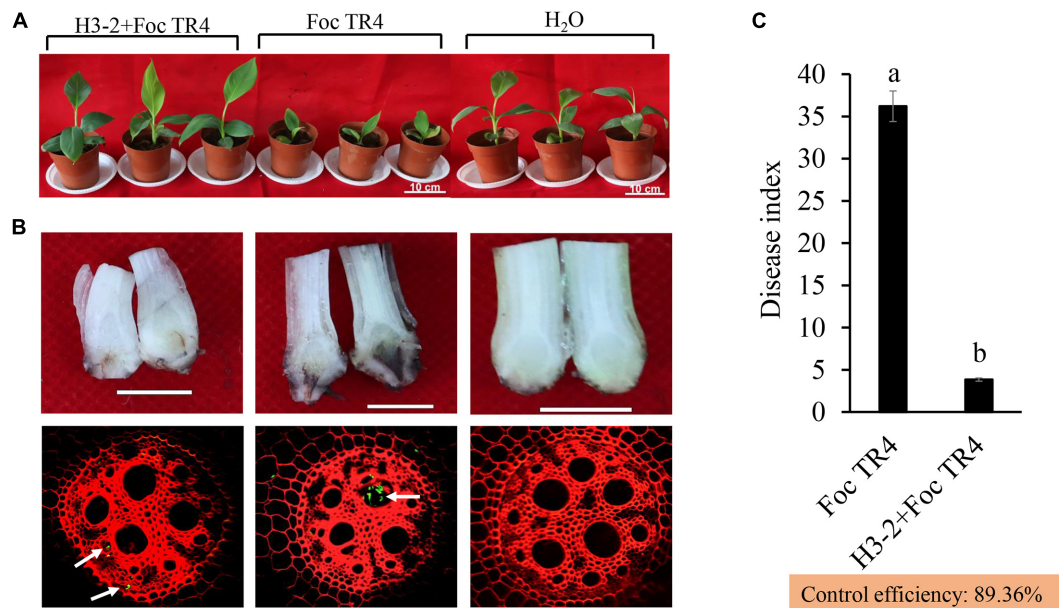Isolation and Identification of *Streptomyces* sp. H3-2

FIGURE 8 | Effects of the strain H3-2 fermentation broth on the growth of banana seedlings and resistance to Foc TR4 in the control (Foc TR4) and the two treatments. **(A)** Chlorotic leaves and growth of banana seedlings were detected 35 days after strain H3-2 treatment. Bars = 10 cm. **(B)** Infection characteristics of Foc TR4 on corms and roots of banana seedlings. The arrows indicate infection sites of Foc TR4. Bars = 1 cm. **(C)** Statistical analysis of disease indexes of banana seedlings 35 days after inoculation with Foc TR4. All experiments were repeated in triplicates. Different lowercase letters indicate a significant difference at the level of $p < 0.05$.
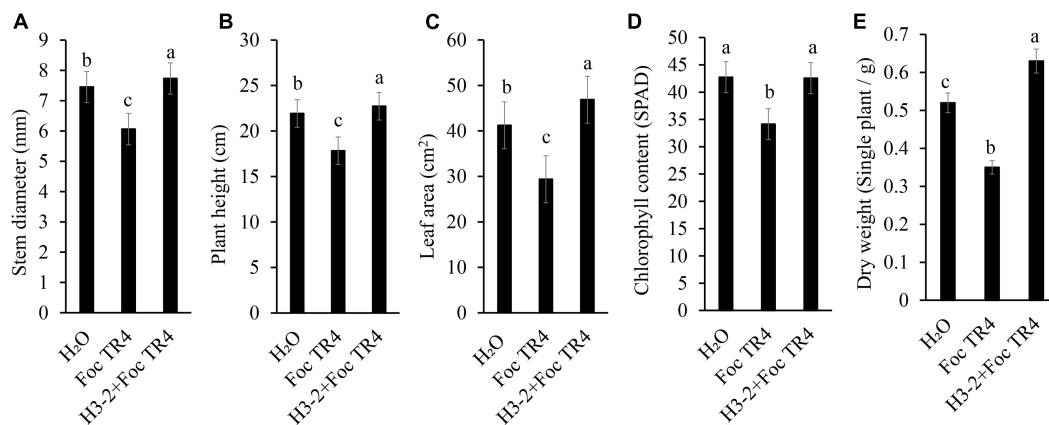

FIGURE 9 | Effect of the strain H3-2 fermentation broth on the growth of banana seedlings. Growth parameters including stem diameter **(A)**, plant height **(B)**, leaf area **(C)**, chlorophyll content **(D)**, and dry weight **(E)** were measured. Different lowercase letters indicate a significant difference at the level of $p < 0.05$.

(Chen et al., 2018; Wei et al., 2020; Li et al., 2021b). In the present study, an actinomycete, named as *Streptomyces* sp. strain H3-2, was isolated from the banana rhizosphere soil. Strain H3-2 and its secondary metabolites effectively inhibit the growth of Foc TR4 and the selected seven phytopathogenic fungi *in vitro*. The EC_{50} value of strain H3-2 extracts against Foc TR4 was 8.83 µg/ml, while EC_{50} values of *Streptomyces* sp. JBS5-6, *Streptomyces* sp. H4, and *Streptomyces* sp. YYS-7 against Foc TR4 were 136.9, 32.6, and 21.1 µg/ml, respectively (Jing et al., 2020; Wei et al., 2020; Li et al., 2021b). Notably, no inhibition activity was observed against endophytic bacteria isolated from banana roots (**Supplementary**

Figure 2), suggesting that *Streptomyces* sp. strain H3-2 has the great potential in controlling banana Fusarium wilt.

Accumulated evidence indicated *Streptomyces* sp. as a biological agent against plant pathogenic fungi mainly because it produced a large number of secondary metabolites with antimicrobial activity (Chen et al., 2018; Yun et al., 2018; Jing et al., 2020; Wei et al., 2020; Li et al., 2021b). *Streptomyces* is also widely used in the medicine industry. More than half of clinical antibiotic drugs and their precursors are produced by *Streptomyces* (Emerson et al., 2012). We found that the inhibition efficiency of extracts isolated using 100% concentration of

methanol was the strongest against Foc TR4 (**Figure 2**). A similar result was demonstrated in our previous studies (Li et al., 2021b). However, extracts of *Streptomyces* sp. JBS5-6 and *Streptomyces* sp. SCA3-4 isolated by ethyl acetate showed more effective antifungal activity (Qi et al., 2019; Jing et al., 2020). It suggested that different kind of compounds were extracted using different solvents, and molecular weights of bioactive metabolites were also distinct in different *Streptomyces* isolates. In this study, inhibitory efficiency was positively correlated with the extract concentration. Mycelial growth was completely inhibited under treatment with more than 200 μg/ml of extracts (**Figure 3A**). It could be supported that Foc TR4 spores could not germinate after treated with $8 \times EC_{50}$ of extracts. Similar results showed that spore germination of *F. oxysporum* was inhibited by extracts of *Streptomyces* sp. WP-1 (Peng et al., 2020).

In addition, the colonial tops of Foc TR4 treated with strain H3-2 extracts became swelling and the mycelia abnormally branched. Similarly, abnormal morphology of *F. oxysporum* fungal mycelia were observed after treatment with extracts of *Streptomyces* sp. JBS5-6 (Jing et al., 2020). Extensive degradation of the cell wall and membrane was also observed, and some cellular contents gradually disappeared. This finding supported the phenomenon of the increase of liposomes and formation of transparent electronic density area. Antifungal ability of *Streptomyces* may be involved in nutrient competition, degradative enzyme biosynthesis, response of fungal defenses, antibiosis, nitrous oxide production, and quorum quenching (Cohen and Mazzola, 2006; Dan et al., 2010). However, the underlying mechanisms of strain H3-2 against Foc TR4 require further studies.

Using GC-MS, some important secondary metabolites of antifungal activity of strain H3-2 were identified. Two phenolic compounds, phenol,2,4-bis(1,1-dimethylethyl)- and phenol,2,2′-methylenebis[6-(1,1-dimethylethyl)-4-methyl- were detected in strain H3-2 extracts, which were reported as antimicrobial agents due to its ability to remove free radicals (Pintać et al., 2019). Recently, phenolic compounds extracted from grape leaves had an obvious inhibitory effect on oral microorganisms, such as *S. aureus*, *E. coli*, and *S. mutans* (Moldovan et al., 2020). In addition, the ester compounds were also detected in our study. The highest level of benzeneprop anoic acid,3,5-bis(1,1-dimethylethyl)-4- hydroxy-,octadecyl ester in the GC-MS fractions showed antimicrobial and anticancer activity (Elsayed et al., 2020). Hydrocarbon exhibited antagonistic ability on various pathogens (Mothana et al., 2011). The alkane (4,6-dimethyldodecane) and olefin (benzene,1,2,3- trimethoxy-5-(2-propenyl)-) detected in the present study have been reported to have antimicrobial activity (Rossi et al., 2007; Geethalakshmi and Sarada, 2013). Some acid compounds also showed antimicrobial activity (Himaman et al., 2016). Hexadecanoic acid,2- hydroxy-1-(hydroxymethyl) ethyl ester extracted from medicinal plants (*Melia azedarach* leaves) had antioxidant, anti-inflammatory, and anthelmintic activities (Ali et al., 2015). Thus, we speculated that these compounds play a key role in the broad-spectrum antifungal activity of *Streptomyces* sp. H3-2 (**Figure 7**).

The pot inoculation experiment demonstrated strong biocontrol efficiency of *Streptomyces* sp. H3-2 on banana Fusarium wilt disease. Notably, the fermentation broth of

Streptomyces sp. H3-2 also significantly promoted the growth of banana seedlings including stem diameter, plant height, leaf area, chlorophyll content, and dry weight in comparison to the Foc TR4 treatment group. Similarly, *Streptomyces* sp. FS-4 not only significantly reduced banana Fusarium wilt, but also promoted the growth of banana seedlings (Duan et al., 2020). Rungin et al. (2012) reported that *Streptomyces* sp. GMKU 3100 stimulated the growth of rice and mungbean plants by producing siderophores. Verma et al. (2011) screened three *Streptomyces* sp. strains promoting plant growth and inhibiting the growth of *Alternaria alternata*, a causal agent of early blight disease in tomato plants. Although the application of *Streptomyces* in field trials was limited due to the complex external environments, antifungal activity of *Streptomyces* sp. H3-2 was confirmed in both pot inoculation experiment and plate culture experiment. Our previous study found that the inhibition activity stability of *Streptomyces* extracts can be kept to some extent under different treatments with temperature, pH, and ultraviolet (UV) (Li et al., 2021a). In addition, *Streptomyces* sp. H3-2 isolated from tropical and subtropical regions with high temperature and strong UV has proven its ability to overcome the complex growth environments, like other species and of *Streptomyces*. Hence, antifungal activity of *Streptomyces* sp. H3-2 may be more stable in agriculture application.

CONCLUSION

Streptomyces sp. H3-2 exhibits a strong antifungal activity against Foc TR4 and its extracts and effectively inhibited the mycelial growth and spore germination of Foc TR4. Mycelial cells of Foc TR4 become deformed and ultrastructure disappeared after treatment with strain H3-2 extracts. Strain H3-2 and its crude extracts exhibited broad-spectrum antifungal activity against the tested seven phytopathogenic fungi. Moreover, the fermentation broth of strain H3-2 significantly improved plant resistance to Foc TR4 infection and promoted the growth of banana seedlings. Fourteen chemical constituents in strain H3-2 extracts were identified with most of them having antimicrobial activity. Our study demonstrated that *Streptomyces* sp. strain H3-2 has the potential as a biocontrol agent for preventing banana plants from the infection of Foc TR4.

DATA AVAILABILITY STATEMENT

The raw data supporting the conclusions of this article will be made available by the authors, without undue reservation.

AUTHOR CONTRIBUTIONS

NZ, MW, DZ, WW, and JX developed the ideas and designed the research plans. MW, WW, and JX supervised the research work and provided funding support. NZ, DZ, PL, and YuC were involved in soil sampling, observation of SEM, and pot experiment of banana seedlings. NZ, DZ, MW, WW, and JX analyzed the data. NZ, MW, and WW prepared the manuscript. YiC helped in revision. All authors contributed to the article and approved the submitted version.

SUPPLEMENTARY MATERIAL

The Supplementary Material for this article can be found online at: https://www.frontiersin.org/articles/10.3389/fmicb.2021.706647/full#supplementary-material

Supplementary Figure 1 | Total ion current chromatograms of strain H3-2 extracts.

Supplementary Figure 2 | Symbiotic experiment of strain H3-2 with endophytic bacteria isolated from banana roots. Different numbers below the pictures represent the diverse endophytic bacteria. Strain H3-2 is first cultured on the YE medium for 2 days, and then each endophytic bacterium is inoculated using a cross method. After co-culture for 24 h, the symbiotic result is observed. The experiment is performed in triplicates.

Supplementary Table 1 | Growth characteristics of strain H3-2 on different solid culture media.

Supplementary Table 2 | Physiological and biochemical characteristics of strain H3-2.

Supplementary Table 3 | Carbon and nitrogen source utilization of strain H3-2.

REFERENCES

Abbas, E., Osman, A., and Sitohy, M. (2020). Biochemical control of *Alternaria tenuissima* infecting post-harvest fig fruit by chickpea vicilin. *J. Sci. Food Agric.* 100, 2889–2897. doi: 10.1002/jsfa.10314

Adnan, H. (2015). Studies on the activity of selected plants against biofilms of *Pseudomonas aeruginosa* strain PA14. *Univ. Of Strathclyde.* 105–157. Available online at: http://oleg.lib.strath.ac.uk/R/?func=dbin-jump-full&object_id=25789

Ali, H. A. M., Imad, H. H., and Salah, A. I. (2015). Analysis of bioactive chemical components of two medicinal plants (*Coriandrum sativum* and *Melia azedarach*) leaves using gas chromatography-mass spectrometry (GC-MS). *Afr. J. Biotechnol.* 14, 2812–2830. doi: 10.5897/ajb2015.14956

Barka, E. A., Vatsa, P., Sanchez, L., Gaveau-Vaillant, N., Jacquard, C., Klenk, H.-P., et al. (2016). Taxonomy, physiology, and natural products of actinobacteria. *Microbiol. Mol. Biol. Rev.* 80, 1–43. doi: 10.1128/mmbr.00019-15

Chen, Y., Zhou, D., Qi, D., Gao, Z., Xie, J., and Luo, Y. (2018). Growth promotion and disease suppression ability of a *Streptomyces* sp. CB-75 from banana rhizosphere soil. *Front. Microbiol.* 8:2704. doi: 10.3389/fmicb.2017.02704

Cohen, M. F., and Mazzola, M. (2006). Resident bacteria, nitric oxide emission and particle size modulate the effect of *Brassica napus* seed meal on disease incited by *Rhizoctonia solani* and *Pythium* spp. *Plant Soil* 286, 75–86. doi: 10.1007/s11104-006-9027-1

Dale, J., James, A., Paul, J. Y., Khanna, H., Smith, M., Peraza-Echeverria, S., et al. (2017). Transgenic cavendish bananas with resistance to Fusarium wilt tropical race 4. *Nat. Commun.* 8:1496. doi: 10.1038/s41467-017-01670-6

Dan, Y., Liu, H. Y., Gao, W. W., and Chen, S. L. (2010). Activities of essential oils from *Asarum heterotropoides* var. *mandshuricum* against five phytopathogens. *Crop Prot.* 29, 295–299. doi: 10.1016/j.cropro.2009.12.007

Dita, M., Barquero, M., Heck, D., Mizubuti, E. S. G., and Staver, C. P. (2018). Fusarium wilt of banana: current knowledge on epidemiology and research needs toward sustainable disease management. *Front. Plant Sci.* 9:1468. doi: 10.3389/fpls.2018.01468

Duan, Y., Chen, J., He, W., Chen, J., Pang, Z., Hu, H., et al. (2020). Fermentation optimization and disease suppression ability of a *Streptomyces* ma. FS-4 from banana rhizosphere soil. *BMC Microbiol.* 20:24. doi: 10.1186/s12866-019-1688-z

Elsayed, T. R., Galil, D. F., Sedik, M. Z., Hassan, H. M. M., and Sadik, M. W. (2020). Antimicrobial and anticancer activities of actinomycetes isolated from egyptian soils. *Int. J. Curr. Microbiol. Appl. Sci.* 9, 1689–1700. doi: 10.20546/ijcmas.2020.909.209

Emerson, D., Silva, I., Martins, M. K., Azevedo, J. D., and De Araújo, J. M. (2012). Antibiotics produced by *Streptomyces. Braz. J. Infect. Dis.* 16, 466–471. doi: 10.1016/j.bjid.2012.08.014

Feduchi, E., Cosin, M., and Carrasco, L. (1985). Mildiomycin: a nucleoside antibiotic that inhibits protein synthesis. *J. Antibiot.* 38, 415–419. doi: 10.7164/antibiotics.38.415

Geethalakshmi, R., and Sarada, D. V. L. (2013). Evaluation of antimicrobial and antioxidant activity of essential oil of *Trianthema decandra* L. *J. Pharm. Res.* 6, 101–106. doi: 10.1016/j.jopr.2012.11.022

Himaman, W., Thamchaipenet, A., Pathom-aree, W., and Duangmal, K. (2016). Actinomycetes from eucalyptus and their biological activities for controlling eucalyptus leaf and shoot blight. *Microbiol. Res.* 18, 42–52. doi: 10.1016/j.micres.2016.04.011

Huang, L., Wei, P., Fan, L., Ye, D., Zhu, X., and Xu, Z. (2010). The biosynthesis and bioactivity evaluation of the cytosine-substituted mildiomycin analogue (MIL-C) for controlling powder mildew. *World J. Microbiol. Biotechnol.* 26, 649–655. doi: 10.1007/s11274-009-0218-9

Jing, T., Zhou, D., Zhang, M., Yun, T., Qi, D., Wei, Y., et al. (2020). Newly isolated *Streptomyces* sp. JBS5-6 as a potential biocontrol agent to control banana *Fusarium* wilt: genome sequencing and secondary metabolite cluster profiles. *Front. Microbiol.* 11:602591. doi: 10.3389/fmicb.2020.602591

Jose, P. A., Maharshi, A., and Jha, B. (2021). Actinobacteria in natural products research: progress and prospects. *Microbiol. Res.* 246:126708. doi: 10.1016/j.micres.2021.126708

Kanini, G. S., Katsifas, E. A., Savvides, A. L., and Karagouni, A. D. (2013). *Streptomyces rochei* ACTA1551, an indigenous greek isolate studied as a potential biocontrol agent against *Fusarium oxysporum* f. sp. *lycopersici. Biomed. Res. Int.* 2013:387230. doi: 10.1155/2013/387230

Kim, C. R., Choi, S. J., Kim, J. K., Park, C. K., Gim, M. C., Kim, Y. J., et al. (2017). 2,4-Bis(1,1-dimethylethyl)phenol from Cinnamomum loureirii improves cognitive deficit, cholinergic dysfunction, and oxidative damage in TMT-treated mice. *Biol. Pharm. Bull.* 40, 932–935. doi: 10.1248/bpb.b16-00997

Kurniawati, N., Meryandini, A., and Sunarti, T. C. (2016). Introduction of actinomycetes starter on coffee fruits fermentation to enhance quality of coffee pulp. *Emir. J. Food Agric.* 28, 188–195. doi: 10.9755/ejfa.2015-05-192

Li, X., Jing, T., Zhou, D., Zhang, M., Qi, D., Zang, X., et al. (2021a). Biocontrol efficacy and possible mechanism of *Streptomyces* sp. H4 against postharvest anthracnose caused by *Colletotrichum fragariae* on strawberry fruit. *Postharvest Biol. Technol.* 175:111401. doi: 10.1016/j.postharvbio.2020.111401

Li, X., Li, K., Zhou, D., Zhang, M., Qi, D., Jing, T., et al. (2021b). Biological control of banana wilt disease caused by *Fusarium oxyspoum* f. sp. Cubense using *Streptomyces* sp. H4. *Biol. Control* 155:104524. doi: 10.1016/j.biocontrol.2020.104524

Zou et al.

Isolation and Identification of *Streptomyces* sp. H3-2

Mak, C., Mohamed, A. A., Liew, K. W., and Ho, Y. W. (2004). "Early screening technique for Fusarium wilt resistance in banana micropropagated plants," in *Banana Improvement: Cellular, Molecular, Biology, and Induced Mutations*, eds S. M. Jain and R. Swennen (Enfield, NH: Science Publishers, Inc.), 219–227.

Moldovan, M. L., Carpa, R., Fizeşan, I., Vlase, L., Bogdan, C., Iurian, S. M., et al. (2020). Phytochemical profile and biological activities of tendrils and leaves extracts from a variety of *Vitis vinifera* L. *Antioxidants* 9:373. doi: 10.3390/antiox9050373

Mothana, R. A. A., Hasson, S. S., Schultze, W., Mowitz, A., and Lindequist, U. (2011). Phytochemical composition and in vitro antimicrobial and antioxidant activities of essential oils of three endemic soqotraen *Boswellia* species. *Food Chem.* 126, 1149–1154. doi: 10.1016/j.foodchem.2010.11.150

Omura, S., and Crump, A. (2014). Ivermectin: panacea for resource-poor communities? *Trends Parasitol.* 30, 445–455. doi: 10.1016/j.pt.2014.07.005

Omura, S., and Crump, A. (2017). Ivermectin and malaria control. *Malar. J.* 16:172. doi: 10.1186/s12936-017-1825-9

Peng, C., An, D., Ding, W. X., Zhu, Y. X., Ye, L., and Li, J. (2020). Fungichromin production by *Streptomyces* sp. WP-1, an endophyte from *Pinus dabeshanensis*, and its antifungal activity against *Fusarium oxysporum*. *Appl. Microbiol. Biot.* 104, 10437–10449. doi: 10.1007/s00253-020-10996-z

Pintać, D., Četojević-Simin, D., Berežni, S., Orčić, D., Mimica-Dukić, N., and Lesjak, M. (2019). Investigation of the chemical composition and biological activity of edible grapevine (*Vitis vinifera* L.) leaf varieties. *Food Chem.* 286, 686–695. doi: 10.1016/j.foodchem.2019.02.049

Qi, D., Zou, L., Zhou, D., Chen, Y., Gao, Z., Feng, R., et al. (2019). Taxonomy and broad-spectrum antifungal activity of *Streptomyces* sp. SCA3-4 isolated from rhizosphere soil of *Opuntia stricta*. *Front. Microbiol.* 10:1390. doi: 10.3389/fmicb.2019.01390

Rossi, P. G., Bao, L., Luciani, A., Panighi, J., Desjobert, J. M., Costa, J., et al. (2007). (E)-methylisoeugenol and elemicin: antibacterial components of *Daucus carota* L. essential oil against *Campylobacter jejuni*. *J. Agric. Food Chem.* 55, 7332–7336. doi: 10.1021/jf070674u

Rungin, S., Indananda, C., Suttiviriya, P., Kruasuwan, W., Jaemsaeng, R., and Thamchaipenet, A. (2012). Plant growth enhancing effects by a siderophore-producing endophytic Streptomycete isolated from a Thai jasmine rice plant (*Oryza sativa* L. cv. KDML105). *Antonie Van Leeuwenhoek Int. J. G.* 102, 463–472. doi: 10.1007/s10482-012-9778-z

Saravanan, T., Muthusamy, M., and Marimuthu, T. (2003). Development of integrated approach to manage the Fusarial wilt of banana. *Crop Prot.* 22, 1117–1123. doi: 10.1016/S0261-2194(03)00146-7

Sun, M. L., Song, Z. Q., and Fang, G. Z. (2007). Insecticidal activity and active components of alcohol extract from Juglans mandshurica Maxim leaves. *Chinese J. Appl. Ecol.* 18, 2910–2914. Available online at: https://www.mysciencework.com/publication/show/insecticidal-activity-active-components-alcohol-extract-from-juglans-mandshurica-maxim-leaves-fc8c35be

Uyeda, M., Mizukami, M., Yokomizo, K., and Suzuki, K. (2001). Pentalenolactone I and Hygromycin A, Immunosuppressants produced by *Streptomyces filipinensis* and *Streptomyces hygroscopicus*. *Biosci. Biotechnol. Biochem.* 65, 1252–1254. doi: 10.1271/bbb.65.1252

Vanewijk, P., and Hoekstra, J. (1993). Calculation of the EC50 and its confidence interval when subtoxic stimulus is present. *Ecotoxicol. Environ. Saf.* 25, 25–32. doi: 10.1006/eesa.1993.1003

Verma, V. C., Singh, S. K., and Prakash, S. (2011). Bio-control and plant growth promotion potential of siderophore producing endophytic *Streptomyces* from *Azadirachta indica* A. Juss. *J. Basic. Microbiol.* 51, 550–556. doi: 10.1002/jobm.201000155

Wang, W., Hu, Y., Sun, D., Staehelin, C., Xin, D., and Xie, J. (2012). Identification and evaluation of two diagnostic markers linked to *Fusarium* wilt resistance (race 4) in banana (*Musa* spp.). *Mol. Biol. Rep.* 39, 451–459. doi: 10.1007/s11033-011-0758-6

Wei, Y., Zhao, Y., Zhou, D., Qi, D., Li, K., Tang, W., et al. (2020). A newly isolated Streptomyces sp. YYS-7 with a broad-spectrum antifungal activity improves the banana plant resistance to *Fusarium oxysporum* f. sp. cubense tropical race 4. *Front. Microbiol.* 11:1712. doi: 10.3389/fmicb.2020.01712

Xu, Z., Wang, M., Du, J., Huang, T., Liu, J., Dong, T., et al. (2020). Isolation of *Burkholderia* sp. HQB-1, a promising biocontrol bacteria to protect banana against Fusarium wilt through phenazine-1-carboxylic acid secretion. *Front. Microbiol.* 11:605152. doi: 10.3389/fmicb.2020.605152

Yun, T. Y., Feng, R. J., Zhou, D. B., Pan, Y. Y., Chen, Y. F., Wang, F., et al. (2018). Optimization of fermentation conditions through response surface methodology for enhanced antibacterial metabolite production by *Streptomyces* sp. 1-14 from cassava rhizosphere. *PLoS One* 13:206497. doi: 10.1371/journal.pone.0206497

Zhang, L., Cenci, A., Rouard, M., Zhang, D., Wang, Y., Tang, W., et al. (2019). Transcriptomic analysis of resistant and susceptible banana corms in response to infection by *Fusarium oxysporum* f. sp. cubense tropical race 4. *Sci. Rep.* 9:8199. doi: 10.1038/s41598-019-44637-x

Zhao, G., Chen, C., Xiong, W., Gao, T., Deng, Z., Wu, G., et al. (2016). Structural basis of the substrate preference towards CMP for a thymidylate synthase MilA involved in mildiomycin biosynthesis. *Sci. Rep.* 6:39675. doi: 10.1038/srep39675

Zhou, D., Jing, T., Chen, Y., Wang, F., Qi, D., Feng, R., et al. (2019). Deciphering microbial diversity associated with Fusarium wilt-diseased and disease-free banana rhizosphere soil. *BMC Microbiol.* 19:161. doi: 10.1186/s12866-019-1531-6

Publisher's Note: All claims expressed in this article are solely those of the authors and do not necessarily represent those of their affiliated organizations, or those of the publisher, the editors and the reviewers. Any product that may be evaluated in this article, or claim that may be made by its manufacturer, is not guaranteed or endorsed by the publisher.

Advantages of publishing in Frontiers

OPEN ACCESS
Articles are free to read for greatest visibility and readership

FAST PUBLICATION
Around 90 days from submission to decision

HIGH QUALITY PEER-REVIEW
Rigorous, collaborative, and constructive peer-review

TRANSPARENT PEER-REVIEW
Editors and reviewers acknowledged by name on published articles

Frontiers
Avenue du Tribunal-Fédéral 34
1005 Lausanne | Switzerland

Visit us: www.frontiersin.org
Contact us: frontiersin.org/about/contact

REPRODUCIBILITY OF RESEARCH
Support open data and methods to enhance research reproducibility

DIGITAL PUBLISHING
Articles designed for optimal readership across devices

FOLLOW US
@frontiersin

IMPACT METRICS
Advanced article metrics track visibility across digital media

EXTENSIVE PROMOTION
Marketing and promotion of impactful research

LOOP RESEARCH NETWORK
Our network increases your article's readership